Experimental investigations of pile behaviour using instrumented field piles

by

Barry Lehane

B.E.

(May 1992)

A thesis submitted to the University of London
(Imperial College of Science, Technology and Medicine)
in partial fulfillment of the requirements for the degree
of Doctor of Philosophy in the Faculty of Engineering.

BIBL. LONDIN. UNIV.

ABSTRACT

ABSTRACT

This Thesis describes a series of field experiments with a heavily instrumented displacement pile. In all, 14 piles were installed in three soil types: medium dense sand, glacial till and soft sensitive clay. The *effective stresses* acting at a number of levels on the pile shafts were measured during pile installation (by fast-jacking), equalisation and load testing. Specific parameters affecting load test capacities were investigated. These included the length of the equalisation period, the direction of loading (tension or compression), the rate of pile loading (drained/ undrained), the pile slenderness ratio and the jacking rate.

Part I of the Thesis reviews and evaluates existing design and theoretical approaches for displacement piles and provides a full description of previous instrumented pile test programmes. Part II first summarises the soil properties at the respective test sites and then presents the results from each pile test programme. Part III assimilates these results and identifies common trends. New design methods are proposed that are based on these trends and those shown by previous instrumented pile test programmes and theoretical approaches.

The main conclusions are as follows:

(i) Shaft capacities of displacement piles are controlled by a complex series of stress changes that take place during installation, equalisation and loading.

(ii) The local shaft friction (τ_f) that can be developed may be described by the simple Coulomb failure criterion: $\tau_f = \sigma'_{rf} \tan \delta$.

(iii) In sands, σ'_{rf} can be described as a function of the initial stress state & relative density, the pile diameter and the distance from the pile tip, but also depends on the direction of loading.

(iv) In clays, σ'_{rf} depends most strongly on the material's initial consistency and sensitivity, the degree of equalisation and the distance from the pile tip.

(v) Interface friction angles (δ) may be estimated with high precision from appropriate direct shear interface tests.

ACKNOWLEDGEMENTS

ACKNOWLEDGEMENTS

The experimental work described in this Thesis was sponsored by:

- The Science and Engineering Research Council (through MTD Ltd.)
- The central and regional divisions of the Laboratoires des Ponts et Chaussées
- AMOCO (UK) Exploration Co.
- The Building Research Establishment
- CONOCO (UK) Ltd.
- Exxon Production Research Co.
- The Health & Safety Exec.
- Mobil Research and Development Corp.
- Shell (UK) Ltd.

Their support, and that of their representatives, is gratefully acknowledged.

I would like especially to thank Richard Jardine for his continual guidance, assistance and motivation throughout my years at Imperial. Richard has an unbounded enthusiasm for Soil Mechanics (and particularly for piles) and his technical, literary and organisational expertise have made an indelible impact on the contents of this Thesis.

The success of the field work can be attributed to the great technical skills of Alan Bolsher who had a genuine interest in the project and always managed to find a way around a difficult problem. In addition to Alan, I would like to express my sincere gratitude to all the researchers in the Soil Mechanics Section at Imperial, *all* of whom, at one stage or another, voluntarily left London for a week's hard labour on site. I am also indebted to Andrew Bond (my predecessor) who showed me the 'ropes' and was always free to discuss any queries.

Finally, I would like to thank my family and close friends (especially Susan) for their constant encouragement and interest in my research - most of them know by now that piles are not synonymous with a medical condition.

2.4 INSTRUMENTED DISPLACEMENT PILES IN CLAY..... 50
2.4.1 General 50
2.4.2 Installation 52
2.4.3 Equalisation 54
2.4.4 Load testing 55
2.4.5 Effect of installation on soil fabric 56

Chapter 3

DISPLACEMENT PILES IN SAND: RECENT DEVELOPMENTS

3.1 INTRODUCTION..... 62
3.2 DESIGN METHODS FOR DISPLACEMENT PILES IN SAND 63
3.2.1 Shaft capacity
3.2.1.1 Conventional 'earth pressure' approach 63
3.2.1.2 Correlations with in-situ test parameters 65
3.2.1.3 Average shear stress approach 66
3.2.2 Base capacity 67
3.3 MODEL PILE TESTS 69
3.3.1 Stress distribution and displacement paths 71
3.3.2 Density changes 72
3.3.3 Average shaft shear stress 74
3.3.4 Local radial and shear stress 76
3.4 FIELD MEASUREMENTS 80
3.4.1 Residual stresses 80
3.4.2 Variation of τ_{av} with depth 81
3.4.3 Tension and compression shaft capacities 82
3.4.4 Pile end condition 82
3.4.5 Effect of installation method 83
3.4.6 Pile set-up 84
3.4.7 Definition of failure 84
3.4.8 Measurements of local shear stress 84
3.4.9 Measurements of local radial stress 86
3.4.10 Trends inferred from local measurements 88
3.5 FINAL COMMENTS 89

Chapter 4
EXPERIMENTAL PROCEDURES

4.1 THE IMPERIAL COLLEGE INSTRUMENTED PILE (ICP) 94
4.1.1 Evolution of the ICP 94
4.1.2 General configuration 94
4.1.3 Instrument description 96
4.1.3.1 Axial load cell 97
4.1.3.2 Pore pressure probe 98
4.1.3.3 Surface stress transducer 99
4.2 TEST PROCEDURES 100
4.2.1 Calibration 100
4.2.1.1 Axial load cell 101
4.2.1.2 Pore pressure probe 101
4.2.1.3 Surface stress transducer 102
4.2.2 Pile preparation 104
4.2.3 Data acquisition system 104
4.2.4 Pile loading frame 105
4.2.4.1 Labenne 105
4.2.4.2 Cowden and Bothkennar 106
4.2.5 Installation 107
4.2.6 Equalisation 108
4.2.7 Load testing 108
4.3 INSTRUMENT PERFORMANCE 111

Chapter 5
SOIL PROPERTIES

5.0 INTRODUCTION 129
5.1 SOIL CONDITIONS AT LABENNE 130
5.1.1 The site 130
5.1.2 Geology 131
5.1.3 Borehole investigation 132
5.1.4 Classification tests 135
5.1.5 In-situ tests 136
5.1.5.1 Density 136
5.1.5.2 Stiffness 137
5.1.6 Initial in-situ stresses 139
5.1.7 Mechanical properties from laboratory tests 140
5.1.7.1 Triaxial tests 140
5.1.7.2 Soil on soil shear box tests 143
5.1.7.3 Interface shear tests 144

5.2 SOIL CONDITIONS AT COWDEN 148
5.2.1 The site 148
5.2.2 Geology 150
5.2.3 Site profile 151
5.2.4 Grading, composition and fabric 152
5.2.5 Index tests 152
5.2.6 c_{u0} & q_c profile 153
5.2.7 Behaviour in 1-D compression 154
5.2.8 In-situ stress state 156
5.2.9 Triaxial tests 160
5.2.9.1 Isotropic tests 160
5.2.9.2 Anisotropic tests 161
5.2.9.3 Triaxial stiffness 163
5.2.10 Ring shear interface tests 165
5.3 SOIL CONDITIONS AT BOTHKENNAR 168
5.3.1 The site 168
5.3.2 Geology 170
5.3.3 Site profile 171
5.3.4 In-situ tests 172
5.3.4.1 Cone Penetration and Piezocone tests 172
5.3.4.2 Self-boring pressuremeter tests 174
5.3.5 Grading, composition and fabric 174
5.3.6 Index tests 175
5.3.7 Undrained shear strength 176
5.3.8 Behaviour in 1-D compression 179
5.3.9 In-situ stress state 181
5.3.10 Stress path testing 184
5.3.10.1 Initial yield surface 184
5.3.10.2 Effective stress parameters 186
5.3.10.3 Triaxial stiffness 187
5.3.11 Direct simple shear tests 188
5.3.12 Ring shear tests 189
5.3.12.1 Slow shearing stages 191
5.3.12.2 Fast shearing stages 192

Chapter 6
PILE TESTS AT LABENNE

6.1 OUTLINE..... 198
6.2 PILE CONFIGURATION AND TEST PROGRAMME 198
6.3 INSTALLATION 199
6.3.1 End resistance 199
6.3.2 Pore pressure 200

6.3.3 Radial effective stress 202
6.3.4 Local shear stress 205
6.3.5 Average shear stress 206
6.3.6 Interface friction angles 207
6.4 EQUALISATION 209
6.5 LOAD TESTING 213
6.5.1 Overall load displacement behaviour 213
6.5.2 Local shear stress 214
6.5.3 Local radial effective stress 216
6.5.4 Effective stress paths 218
6.5.5 Pile reload tests 220
6.5.5.1 Tension and compression tests 220
6.5.5.2 Cyclic tests 222
6.6 DISCUSSION 224
6.6.1 General 224
6.6.2 Changes in σ'_r during pile loading 224
6.6.3 Interface friction angles 225
6.6.4 Distributions of τ_{av} and τ_f with depth 226

Chapter 7

PILE TESTS AT COWDEN

7.1 PILE CONFIGURATIONS AND TEST PROGRAMME 234
7.1.1 Phase 1 (piles CW1 & CW2) 235
7.1.2 Phase 2 (piles CW3 & CW4) 236
7.2 INSTALLATION 237
7.2.1 End resistance 237
7.2.2 Shaft resistance 239
7.2.3 Local shear stress 241
7.2.4 Radial total stress 243
7.2.5 Pore pressure 245
7.2.6 Interface friction angles 248
7.3 EQUALISATION 249
7.3.1 Pore pressure 249
7.3.2 Radial total and effective stresses 252
7.3.3 Long term monitoring of pile CW2 254
7.3.4 Radial effective stresses after equalisation 255
7.3.5 Residual pile stresses 257
7.4 LOAD TESTING 260
7.4.1 Introduction 260
7.4.2 Overall pile behaviour 260
7.4.2.1 Shaft capacity 263
7.4.2.2 Shaft displacement characteristics 264
7.4.2.3 Base load 264

7.4.3 Local stress variations 265
7.4.3.1 Shear stress 265
7.4.3.2 Pore pressure 265
7.4.3.3 Radial total stress 267
7.4.4 Effective stress paths 267
7.4.5 Load test summary 272
7.4.5.1 General trends and comparisons with laboratory tests 272
7.4.5.2 Comparison with other pile tests at Cowden 274

Chapter 8

PILE TESTS AT BOTHKENNAR

8.1 PILE CONFIGURATION AND TEST PROGRAMME 282
8.1.1 General 283
8.1.2 Notes on individual piles 284
8.1.2.1 Phase 1 284
8.1.2.2 Phase 2 285
8.2 INSTALLATION 286
8.2.1 End resistance 286
8.2.2 Shaft resistance 288
8.2.3 Local shear stress 291
8.2.3.1 Rate effects on shear stress 292
8.2.4 Radial total stress 294
8.2.5 Pore pressure 297
8.2.6 Radial effective stress 300
8.3 EQUALISATION 301
8.3.1 General 301
8.3.2 Pore pressure 302
8.3.3 Radial total stress 305
8.3.4 Radial effective stress 306
8.3.4.1 Changes in σ'_r prior to load testing 306
8.3.4.2 Long term variations in σ'_r 309
8.3.4.3 Equalised σ'_r values 310
8.3.5 Residual pile stresses 312
8.4 LOAD TESTING 315
8.4.1 Introduction 315
8.4.2 Overall pile response 315
8.4.2.1 Shaft capacity 318
8.4.2.2 Shaft displacement characteristics 319
8.4.2.3 Base load 319

8.4.3 Local stress variations 320
8.4.3.1 Pore pressure 320
8.4.3.2 Radial stress 322
8.4.3.3 Shear stress 323
8.4.4 Effective stress paths 323
8.4.4.1 Behaviour up to peak shear stress 323
8.4.4.2 Post-peak behaviour 328
8.4.4.3 Comparison with laboratory tests 330

Chapter 9
CORRELATIONS FOR DISPLACEMENT PILES IN SAND

9.1 INTRODUCTION 338
9.2 REDUCTIONS IN RADIAL STRESS WITH DISTANCE FROM THE TIP..... 338
9.3 EQUALISED RADIAL EFFECTIVE STRESS 340
9.3.1 Relationship between σ'_{rc} and pile end resistance 340
9.3.2 Relationship between σ'_{rc} and relative density 344
9.4 CHANGES IN RADIAL EFFECTIVE STRESS DURING PILE LOADING 346
9.4.1 General characteristics 346
9.4.2 Factors causing σ'_r changes 347
9.4.2.1 Reductions in σ'_r 347
9.4.2.2 Increases in σ'_r 348
9.4.3 Empirical correlations for σ'_r changes 351
9.4.4 General comments on relationships for $\Delta\sigma'_r$ 354
9.5 INTERFACE FRICTION ANGLES 355
9.6 IMPLICATIONS OF CORRELATIONS FOR σ'_{rc} AND $\Delta\sigma'_r$ 358
9.7 COMPARISONS WITH RESULTS FROM OTHER FIELD TESTS 360
9.7.1 Shaft capacities in compression 360
9.7.2 Shaft capacities in tension 362
9.7.3 Comparison with other pile design methods 365
9.8 FINAL COMMENTS 366

Chapter 10
SUMMARY OF ICP TESTS IN CLAY

10.1 INTRODUCTION..... 372
10.2 PILE INSTALLATION..... 372
10.2.1 Radial and shear stresses 372
10.2.2 Pore pressure 375
10.2.3 Radial effective stress 377
10.3 EQUALISATION 378
10.3.1 Radial total stress 378

10.3.2 Pore pressure dissipation 379
10.3.2.1 Radial distribution after installation 380
10.3.2.2 Permeability 381
10.3.2.3 Coefficient of consolidation 382
10.3.3 Radial effective stress 385
10.3.3.1 Short term minimum 386
10.3.3.2 Set-up after full equalisation 387
10.3.4 Equalised radial effective stress 387
10.4 LOAD TESTING 390
10.4.1 Overall shaft displacement behaviour 390
10.4.2 Local shear stress variations 392
10.4.3 Loading effective stress paths 394
10.4.3.1 General 394
10.4.3.2 Stress path shapes 395
10.4.3.3 Angles of interface friction 397
10.5 THE 'h/R' EFFECT' 399
10.5.1 General observations 400
10.5.1.1 Radial total stress 400
10.5.1.2 Pore pressure 402
10.5.1.3 Equalised radial effective stress 403
10.5.2 Factors causing the 'h/R effect' 403
10.5.2.1 Instantaneous installation of a frictionless pile 403
10.5.2.2 The effects of time 405
10.5.2.3 The influence of cyclic loading 408
10.5.3 Summary 411

Chapter 11

CORRELATIONS FOR DISPLACEMENT PILES IN CLAY

11.1 INTRODUCTION 416
11.2 THE DATA BASE 416
11.2.1 Clay types 416
11.2.2 Pile configurations 419
11.3 INSTALLATION 420
11.3.1 Radial total stress 420
11.3.2 Pore pressure 423
11.3.3 Radial effective stress 424
11.4 EQUALISATION 425
11.4.1 Relaxation of radial total stress 425
11.4.1.1 Analytical predictions 426
11.4.1.2 Empirical correlation for K_c/H_1 427
11.4.2 Pore pressure dissipation 429
11.4.3 Equalised radial effective stress 430

11.5 ULTIMATE LOCAL SHAFT FRICTION 433
11.6 IMPLICATIONS OF EFFECTIVE STRESS APPROACH FOR EXISTING DESIGN METHODS 434
11.6.1 The α method 434
11.6.2 The β method 438
11.7 CONCLUSIONS 439

Chapter 12
CONCLUSIONS

12.0 OUTLINE 444
12.1 PRINCIPAL CHARACTERISTICS OF DISPLACEMENT PILES 444
12.1.1 Jacked pile installation 444
12.1.2 Equalisation 446
12.1.3 Load testing 448
12.2 PROPOSED DESIGN METHODS 450
12.3 THEORETICAL PREDICTIONS 451
12.4 SUGGESTIONS FOR FURTHER RESEARCH 453

APPENDIX A
INSTRUMENT PERFORMANCE

A1.0 GENERAL..... 458
A1.1 Measurement range 458
A1.2 Instrument drift 459
A2.0 PORE PRESSURE PROBES..... 460
A2.1 General 460
A2.2 Long term performance 461
A2.2.1 Background 461
A2.2.2 Performance at Cowden 462
A2.2.3 Performance at Bothkennar 463
A2.2.4 Conclusion 465
A2.3 Measurements at high pile velocities in clays 466
A2.3.1 During installation in ICP tests 466
A2.3.3 During load tests in ICP tests 467
A2.3.3 Measurements in other pile tests 471
A2.3.4 Conclusion 473
A2.4 Influence of filter stone 473
A3.0 SURFACE STRESS TRANSDUCERS 476
A3.1 General 476
A3.2 Shear stress measurements 476
A3.2.1 General trends 476
A3.2.2 Factors affecting the τ_{rz} and f_s data 478
A3.3 Elastic cell action effects 482

APPENDIX B
INSTRUMENTED DISPLACEMENT PILE TESTS IN CLAY

B1.0 INTRODUCTION 494
B2.0 EXPERIMENTS BY BOND (1989) 494
B2.1 Soil conditions 494
B2.2 Installation 497
B2.3 Equalisation 498
B2.4 Load testing 498
B2.5 Trial pit investigations 501
B2.6 Quality of data 502
B3.0 EXPERIMENTS WITH THE PIEZO-LATERAL STRESS CELL 503
B3.1 Instrumentation 503
B3.2 Soil profiles 503
B3.3 Installation and equalisation 504
B3.4 Load testing 506
B4.0 EXPERIMENTS BY COOP (1987) 507
B4.1 Operation and instrumentation 508
B4.2 Installation 510
B4.3 Equalisation 512
B4.4 Load testing 512
B5.0 EXPERIMENTS BY NGI 515
B5.1 Site properties 515
B5.2 Instrumentation 515
B5.3 Installation and equalisation 517
B5.4 Load testing 517
B5.5 Trial pit investigations 518
B6.0 FIELD TESTS AT ST-ALBAN 518
B6.1 Instrumentation 518
B6.2 Installation 519
B6.3 Equalisation 521
B6.4 Load testing 522
B6.5 Trial pit investigations 522
B7.0 EXPERIMENTS IN TOKYO CLAY 523
B8.0 EXPERIMENTS BY BOGARD & MATLOCK (1990) 523
B9.0 EXPERIMENTS AT COWDEN 525
B10.0 LABORATORY TESTS BY FRANCESCON (1983) 525
B11.0 OTHER PILE TESTS 526

APPENDIX C
SPM/MIT-E3 PREDICTIONS FOR THE ICP TESTS AT BOTHKENNAR

C1.0 INTRODUCTION 542
C2.0 MIT-E3 PARAMETER SELECTION 542
C3.0 COMPARISON OF MEASUREMENTS WITH PREDICTIONS 545
C3.1 General 545
C3.2 Predictions for installation & equalisation 546
C3.3 Predictions for load testing 549
C3.4 Discussion 550
C4.0 CONCLUSION 551

APPENDIX D
DIRECT SHEAR INTERFACE TESTS

D1.0 INTRODUCTION 556
D2.0 RESEARCH USING THE RING SHEAR APPARATUS..... 557
D2.1 The ring shear apparatus 557
D2.2 Shearing modes 558
D2.3 Research by Lemos & Tika 559
D3.0 TEST PROCEDURES 562
D3.1 Sample preparation 562
D3.2 Interfaces 563
D3.3 Ring shear procedures 563
D4.0 RING SHEAR INTERFACE TESTS ON LABENNE SAND 564
D5.0 RING SHEAR INTERFACE TESTS ON COWDEN TILL 567
D5.1 Slow shearing steps 567
D5.2 Fast shearing steps 567
D5.3 Sample inspection 569
D6.0 RING SHEAR TESTS ON BOTHKENNAR CLAY 570
D6.1 Slow shearing steps 570
D6.2 Fast shearing steps 573
D7.0 SHEAR BOX TESTS ON LABENNE SAND 575
D7.1 Soil-interface tests 575
D7.2 Soil on soil tests 577

REFERENCES..... 593

LIST OF FIGURES AND PLATES

Chapter 1

Figure 1.1 Four stages in the life of a displacement pile 5

Chapter 2

Figure 2.1 Variation of α with c_{u0} 19
Figure 2.2 Shear stress distribution in a strain-softening soil 20
Figure 2.3 α variation with c_{u0}/σ'_{v0} 21
Figure 2.4 β variation with pile length in low OCR clays 23
Figure 2.5 Variation of K_c with OCR (Azzouz et al 1990) 25
Figure 2.6 Variation of K_c with OCR and h/R (Bond 1989) 26
Figure 2.7 Predicted deformations around a 'simple pile' 30
Figure 2.8 Strain paths followed during penetration of a 'simple pile' 32
Figure 2.9 Pore pressures and radial effective stresses predicted for pile installation in Bothkennar clay, BC(A) 37
Figure 2.10 Predicted $\Delta u/\Delta u_{shaft}$ v r/R variations 38
Figure 2.11 Predicted variations of H_i and $\Delta u_i/\sigma'_{v0}$ with OCR 40
Figure 2.12 Predicted stress changes during equalisation 43
Figure 2.13 Predicted dependence of K_c/H_i and K_c on I_v^{100} and OCR 45
Figure 2.14 Predicted pile loading stress paths 47

Chapter 3

Figure 3.1 τ_{av} variation with relative density (Toolan et al 1990) 66
Figure 3.2 Berezantsev's (1961) bearing capacity factor, N_q 68
Figure 3.3 Observations of Allersma (1988) 71
Figure 3.4 Density measurements of Chong (1988) 73
Figure 3.5 τ_{av} variation with pile length (Robinsky et al 1964) 74
Figure 3.6 τ_{av} variation with relative density and pile radius (Lebègue 1964) 75
Figure 3.7 Wersching's (1987) data for after installation and during load tests 77
Figure 3.8 Correlation of Robertson (1982) based on CPT data 79
Figure 3.9 Distribution of ultimate shear stresses at Drammen and Hoogzand 85
Figure 3.10 Radial total stresses at Drammen 87

Chapter 4

Figure 4.1 Configuration of the ICP and instrument cluster 95
Figure 4.2 The axial load cell on the ICP 97
Figure 4.3 The pore pressure probe on the ICP 98
Figure 4.4 The surface stress transducer on the ICP 99
Figure 4.5 Notation used for load tests 111
Figure 4.6 Apparent dependence of δ_{ult} on pile rate 114
Plate 4.1a Set-up at Labenne 119
Plate 4.1b Pile installation at Labenne 119
Plate 4.2a Set-up at Cowden 121
Plate 4.2b Arrangement at the pile head at Cowden and Bothkennar 121
Plate 4.3a Set-up at Bothkennar 123
Plate 4.3b Monitoring pile head displacement 123

Chapter 5

Labenne

Figure 5.1 Location of Labenne 131
Figure 5.2 Borehole logs near ICP locations 133
Figure 5.3 Index properties shown by piston samples 134
Figure 5.4 In-situ tests at Labenne 137
Figure 5.5 Shear stiffness moduli measured in PP tests 138
Figure 5.6 CK_0U tests on Labenne sand 141
Figure 5.7 Secant shear moduli measured in CK_0U tests 143
Figure 5.8 Soil on soil friction angles measured in shear box tests 144
Figure 5.9 Typical direct shear soil on soil and soil-steel interface data 145
Figure 5.10 Peak and constant volume interface friction angles measured in direct shear soil-steel interface tests 147

Cowden

Figure 5.11 Cowden location and site plan 148
Figure 5.12 Plan of Tension Pile Test area at Cowden 149
Figure 5.13 Borehole log and index properties near ICP tests 151
Figure 5.14 q_c and c_{u0} profiles for the TPT area at Cowden 153
Figure 5.15 Oedometer tests on Cowden till 155
Figure 5.16 Apparent OCR and K_0 profiles for the TPT area 159
Figure 5.17 CK_0U tests on reconstituted Cowden and Magnus till 162
Figure 5.18 Shear stiffness of Cowden till in triaxial compression 164
Figure 5.19 Ring shear soil-steel interface tests on Cowden till 166

Bothkennar

Figure 5.20 Bothkennar location 168
Figure 5.21 Site plan 169
Figure 5.22 Piezocone data near locations of ICP tests 173
Figure 5.23 Index properties at Bothkennar 176
Figure 5.24 Peak undrained shear strength profiles at Bothkennar 177
Figure 5.25 1-D compression characteristics of Bothkennar clay 180
Figure 5.26 OCR and K_0 profile at Bothkennar 182
Figure 5.27 Stress paths followed in CK_0U tests (Smith 1992) 185
Figure 5.28 Shear stiffness values in CK_0U tests (Smith 1992) 187
Figure 5.29 Direct simple shear tests on intact Bothkennar clay 189
Figure 5.30 Peak and ultimate residual angles for Bothkennar clay in soil on soil and soil-steel interface tests 190
Figure 5.31 Rate dependence of the interface shearing resistance of Bothkennar clay 193

Chapter 6

Figure 6.1 Configuration of piles LB1 and LB2 at Labenne 199
Figure 6.2 End resistance during jacking 200
Figure 6.3 Pore pressures recorded during installation of LB1 201
Figure 6.4 σ'_r values recorded by LB1 in between jacking stages 202
Figure 6.5 Comparison of σ'_{rs} data with PP data 203
Figure 6.6 Variation of σ'_{rs}/q_b with h/R 204
Figure 6.7 Shear stresses mobilised during jacking of LB2 205
Figure 6.8 Average shaft shear stresses mobilised during jacking 206
Figure 6.9 Data recorded during equalisation of LB1 210
Figure 6.10 Residual stresses in the piles at Labenne 211
Figure 6.11 Variation of σ'_{rc} with L/R 212
Figure 6.12 Local shear stress variations with d_p 215
Figure 6.13 Profiles of shear stress and radial effective stress 217
Figure 6.14 τ_{rz} v σ'_r paths at z=1.45m in Test LB2/L1C 218
Figure 6.15 τ_{rz} v σ'_r paths in Tests LB1/L1C and LB2/L1T 219
Figure 6.16 Loading schedule & load displacement curves for LB1 227
Figure 6.17 Loading schedule & load displacement curves for LB2/L1C 228
Figure 6.18 Loading schedule & load displacement curves for LB2 (at a penetration of ≈6m) 229

Chapter 7

Figure 7.1 Pile configurations for Phase 1 234
Figure 7.2 Pile configurations for Phase 2 235

Figure 7.3 End resistances during pile jacking 238
Figure 7.4 Average shaft shear stresses during jacking of CW3 239
Figure 7.5 Rate dependence of installation shear stresses 241
Figure 7.6 Local shear stresses during jacking 242
Figure 7.7 Envelope for σ_{ri} and dependence of σ_{ri} on h/R 244
Figure 7.8 Pore pressures recorded by following probes on CW4 245
Figure 7.9 Envelopes for installation pore pressures (fast-jacking) 247
Figure 7.10 Interface friction angles measured during fast-jacking 248
Figure 7.11 Pore pressures recorded during equalisation of CW4s 250
Figure 7.12 Envelopes for pore pressure ratios and U_d factors 251
Figure 7.13 Equalisation data for CW3 253
Figure 7.14 Normalised stress changes during equalisation of CW2 255
Figure 7.15 Equalised radial effective stress profiles 256
Figure 7.16 Residual stress profile at Cowden 258
Figure 7.17 Shaft load - displacement curves 262
Figure 7.18 Variations of local stresses with d_p in tension and compression 266
Figure 7.19 τ v σ'_r paths in Tests CW2/L1C and CW3/L1T 268
Figure 7.20 Stress paths in Tests CW2/L1C and CW2/L2C, and 'corrected' post-peak paths for Test CW2/L1C 269
Figure 7.21 Stress paths in other primary load tests at Cowden 271

Chapter 8

Figure 8.1 Pile configurations at Bothkennar 283
Figure 8.2 End resistance mobilised during jacking 287
Figure 8.3 Average shear stresses mobilised by BK2 during jacking 288
Figure 8.4 τ_{av} minima measured during jacking 289
Figure 8.5 Effect of time on peak installation τ_{av} values 290
Figure 8.6 Typical local shear stresses developed during jacking 291
Figure 8.7 Rate effect on local shear stresses 293
Figure 8.8 Radial total stresses recorded during installation 295
Figure 8.9 Comparison of σ_{ri} with q_b, q_c, p_{lim} and σ_{h0} 296
Figure 8.10 Installation pore pressures recorded by BK2 298
Figure 8.11 Envelopes for installation pore pressures 299
Figure 8.12 Mean σ'_r values recorded during installation 300
Figure 8.13 Pore pressures recorded during equalisation 303
Figure 8.14 Mean variations of U_d with time at each h/R position 304
Figure 8.15 Normalised radial total stress variation during equalisation 305
Figure 8.16 σ'_r traces during equalisation (1) 307
Figure 8.17 σ'_r traces during equalisation (2) 308
Figure 8.18 Profiles of σ'_{rl} and σ'_{rc} with depth 311
Figure 8.19 Residual pile stresses at Bothkennar 313

Figure 8.20 Shaft load - displacement curves at Bothkennar 317
Figure 8.21 Variations of local stresses with d_p (1) 321
Figure 8.22 Variations of local stresses with d_p (2) 322
Figure 8.23 τ_{rz} v σ'_r paths followed in load tests (1) 324
Figure 8.24 τ_{rz} v σ'_r paths followed in load tests (2) 325
Figure 8.25 τ_{rz} v σ'_r paths followed in 'first-time' testing and re-testing of pile BK4s 328
Figure 8.26 Stress paths in DSS tests on Bothkennar clay & comparison of DSS and pile test stress paths 332

Chapter 9

Figure 9.1 Correlation between σ'_{rc}, q_b and h/R at Labenne 341
Figure 9.2 Predictions for Wersching's σ'_{rc} data 342
Figure 9.3 Predictions for σ'_{rc} data recorded at Drammen 343
Figure 9.4 Stress paths followed during load testing of the ICP at Labenne and laboratory model piles of Wersching 346
Figure 9.5 Measured variation of $\Delta\sigma'_r$ with R, D_r and $\sqrt{\sigma'_{v0}}$ 353
Figure 9.6 Variation of δ_{cv} with D_{50} for sand sheared against a 'rough' steel interface 356
Figure 9.7 Predicted variation of β_{av} with D_r, R and L/R 359
Figure 9.8 CPT q_c profiles at test sites 361

Chapter 10

Figure 10.1 Mean variations of σ_{r1}/q_b with h/R 373
Figure 10.2 Relative changes in radial total stresses during equalisation 379
Figure 10.3 Estimated radial distribution of excess pore pressures induced by pile installation 380
Figure 10.4 Pore pressure dissipation at h/R=53 382
Figure 10.5 Pore pressure dissipation at h/R=5 383
Figure 10.6 Radial effective stress variation during equalisation 385
Figure 10.7 Predicted and measured σ'_{rc} profiles 388
Figure 10.8 Predicted and measured τ_{rz} v d_p variations 391
Figure 10.9 Variations of τ_{rz} with d_p and d at h/R=8 and z=5.5m 393
Figure10.10 Typical effective stress paths measured during load testing of fast-jacked piles after equalisation 395
Figure10.11 Dependence of H_1 on h/R 401
Figure10.12 Dependence of $\Delta u_{max}/\sigma'_{v0}$ on h/R 402
Figure10.13 Typical τ_{rz} v σ'_r paths followed during installation 409

Chapter 11

Figure 11.1 In-situ void indices for materials in case histories 419
Figure 11.2 H_1 variation with apparent OCR for h/R ≥20 421
Figure 11.3 $\Delta u_{max}/\sigma'_{v0}$ variation with apparent OCR 423
Figure 11.4 K_c/H_1 variation with I_v^* 428
Figure 11.5 Dependence of t_{90} on pile diameter 429
Figure 11.6 K_c variation with apparent OCR and I_v^* 431
Figure 11.7 Comparison of predicted 'α v OCR' variation with API (1989) recommendations 437

Appendix A

Figure A1 Long term monitoring of pore pressures at Cowden 464
Figure A2 Data recorded during rate experiment at Bothkennar 468
Figure A3 Rate dependence of pore pressure reductions in load tests at Bothkennar 469
Figure A4 Apparent dependence of δ_{ult} on rate at Bothkennar 470
Figure A5 Apparent dependence of δ_{ult} on rate at Cowden 471
Figure A6 Pore pressures recorded during installation and load testing by probes with steel and ceramic filters 475
Figure A7 Comparison of installation τ_{rz} and f_s data at Cowden 477
Figure A8 Typical τ_{rz} and f_s variations in load tests at Cowden 478
Figure A9 Typical effective stress paths followed during load tests at Cowden 480

Appendix B

Figure B1 Installation radial total stresses and shear stresses in London Clay 495
Figure B2 Equalisation data in London Clay 496
Figure B3 Local stress variation with d_p in load tests in London Clay 499
Figure B4 τ_{rz} v σ'_r paths during load tests in London Clay 501
Figure B5 Configuration of the PLS cell 504
Figure B6 Typical data recorded by PLS cell during installation, equalisation and load testing 505
Figure B7 Configuration and instrumentation of the IMP 509
Figure B8 Radial total stresses recorded by the IMP during installation 511
Figure B9 Equalisation data recorded by the IMP 513
Figure B10 Data recorded by the IMP during load tests 514
Figure B11 Pile configuration and instrumentation at Haga 516

Figure B12 Contours of excess pore pressure ratios at St-Alban 520
Figure B13 Normalised radial distributions of pore pressure at St-Alban 521
Figure B14 Pore pressure dissipation curves measured by Bogard & Matlock (1990) 524

Appendix C

Figure C1 Predicted and measured trends during equalisation 548
Figure C2 Predicted and measured trends for undrained pile load tests 550

Appendix D

Figure D1 The Imperial College ring shear apparatus 557
Figure D2 Dependence of residual stress ratio on e_g 559
Figure D3 Correlation between δ_p & δ_{ult} and PI for disp. piles 561
Figure D4 Ring shear interface tests on Labenne sand 566
Figure D5 Trends shown by Cowden till in soil-steel shear 568
Figure D6 Peak and residual angles measured in soil-soil and soil-steel interface tests on Bothkennar clay 572
Figure D7 Rate dependence of Bothkennar clay in soil-steel interface tests 573
Figure D8 Shear box arrangement for interface tests 575
Figure D9 Friction angles measured in soil-soil and soil-steel shear box tests 576
Figure D10 RSI test on Cowden till, Steps 1 to 11 578
Figure D11 RSI test on Cowden till, Steps 12 to 15 579
Figure D12 RSI test on Cowden till, Steps 16 & 17 580
Figure D13 RS fast shearing steps on Bothkennar clay (1) 581
Figure D14 RS fast shearing steps on Bothkennar clay (2) 582
Figure D15 RS slow shearing steps on Bothkennar clay 583
Figure D16 Shear box interface tests on Labenne sand 584
Figure D17 Shear box tests on Labenne 585

LIST OF TABLES

Chapter 1

Table 1.1 Programme of ICP tests 7

Chapter 2

Table 2.1 Input parameters for SPM/MIT-E3 analyses 36
Table 2.2 Interpretations for the coefficient of friction 49
Table 2.3 High quality instrumented pile tests in clay 51
Table 2.4 Fair/good quality instrumented pile tests in clay 52
Table 2.5 Zones surrounding a displacement pile (Bond & Jardine 1991) 57

Chapter 3

Table 3.1 Design values for cohesionless siliceous soils (API RP2A 1989) 64
Table 3.2 Design values for τ_f in sands based on q_c data (Bustamante & Gianeselli 1982) 65
Table 3.3 Model pile tests in sand 70
Table 3.4 The effects of assuming zero residual pile loads in sands (Briaud & Tucker 1984) 81

Chapter 4

Table 4.1 Mean instrument zero drifts 112

Chapter 5

Table 5.1 Supplementary site investigation performed specifically for the ICP research programme 130
Table 5.2 Stratigraphy at Labenne 137
Table 5.3 In-situ stresses at Labenne 139
Table 5.4 Geological succession at Cowden 150
Table 5.5 In-situ stresses at Cowden 160
Table 5.6 Geological succession at Bothkennar 170
Table 5.7 Stratigraphy at ICP test locations at Bothkennar 172
Table 5.8 Mean peak undrained shear strengths at Bothkennar 178
Table 5.9 In-situ stresses at Bothkennar 184

Chapter 6

Table 6.1	Mean δ values during pile jacking	208
Table 6.2	Details of first-time load tests at Labenne	213
Table 6.3	Summary of all load tests at Labenne	221

Chapter 7

Table 7.1	Average shear stresses during installation	240
Table 7.2	Ranges for installation pore pressures	246
Table 7.3	Equalisation data at Cowden	259
Table 7.4	Primary load tests at Cowden	261
Table 7.5	Tension tests at Cowden	274
Table 7.6	Effective stress failure parameters in load tests at Cowden	277
Table 7.7	Load test summary: Cowden	278

Chapter 8

Table 8.1	Pile details at Bothkennar	282
Table 8.2	Instruments operating for Test BK1/L1T	284
Table 8.3	Installation α values	291
Table 8.4	Normalised σ_{ri} values	296
Table 8.5	Equalisation times at Bothkennar	301
Table 8.6	Long term monitoring of BK2	309
Table 8.7	K_c values at Bothkennar	312
Table 8.8	Equalisation data at Bothkennar	314
Table 8.9	Primary load tests at Bothkennar	316
Table 8.10	Effective stress failure parameters in load tests	327
Table 8.11	Load test summary: Bothkennar	334

Chapter 9

Table 9.1	Illustration of how K_c may vary with h/R and D_r in a normally consolidated sand	345
Table 9.2	Predictions for $\Delta\sigma'_r$ using Eqn. 6	350
Table 9.3	Measured radial stress increases ($\Delta\sigma'_r$) during pile loading in sands	352
Table 9.4	Predictions for compressive shaft capacities	363
Table 9.5	Predictions for tensile shaft capacities	364
Table 9.6	Ratios of predicted to measured shaft capacities for four methods	367

Chapter 10

Table 10.1	Correlations for σ_{r1} data	374
Table 10.2	'Corrected' K_1 values	378
Table 10.3	Approximate relationships for σ'_{rc}	389
Table 10.4	Mean values of $\sigma'_{rf}/\sigma'_{r1}$	396
Table 10.5	Comparison of ring shear data with pile test results	397
Table 10.6	The effect of pause periods at Bothkennar	406

Chapter 11

Table 11.1	Average parameters at test sites	417

Appendix A

Table A1	Range of loads measured by instruments on the ICP	458
Table A2	Average zero drifts of instruments	459
Table A3	Long term pore pressures at Bothkennar	465
Table A4	Pore pressures during installation in ICP tests	467
Table A5	Instrument layout and zero drifts at Labenne	485
Table A6	Zero drifts of pore pressure probes at Labenne and instrument layout at Cowden	486
Table A7	Instrument zero drifts at Cowden	487
Table A8	Pore pressure probe performance at Cowden	488
Table A9	Instrument layout and axial load cell zero drifts at Bothkennar	489
Table A10	Instrument zero drifts at Bothkennar	490

Appendix B

Table B1	Load test parameters measured in London Clay	500
Table B2	PLS cell load test results	507
Table B3	Soil types investigated by Coop (1987)	508
Table B4	Zones adjacent to piles at Haga	518
Table B5	Pile tests in London Clay (Bond 1989)	527
Table B6	Soil properties at PLS sites (Saugus, MIT & Empire)	528
Table B7	PLS cell data at Saugus, MIT and Empire	529
Table B8	Pile tests at Madingley (Coop 1987)	530
Table B9	Pile tests at Huntspill (Coop 1987)	531
Table B10	Pile tests at Gt. Yarmouth and Canons Park (Coop 1987)	532
Table B11	Pile tests at Haga (Karlsrud & Haugen 1985)	533
Table B12	Pile tests at St-Alban (Roy et al 1981)	534

Table B13 Pile tests at Tokyo (Koizumi & Ito 1967) 535
Table B14 Pile tests at Louisiana (Bogard & Matlock 1990), Lab. pile tests in Kaolin (Francescon 1983) 536
Table B15 Pile tests at Cowden (Ponniah 1989) 537
Table B16 Pile tests in Rio de Janeiro, San Francisco & Beaumont clays 538

Appendix C

Table C1 MIT-E3 input parameters for Bothkennar clay 543
Table C2 Laboratory tests used for parameter selection 544
Table C3 Notation 545
Table C4 Pile installation and equalisation results 547
Table C5 Failure parameters in load tests 549

Appendix D

Table D1 Ring shear testing programme (1) 586
Table D2 Ring shear testing programme (2) 587
Table D3 Ring shear test results (1) 588
Table D4 Ring shear test results (2) 589
Table D5 Shear box tests on Labenne sand 590

SYMBOLS AND ABBREVIATIONS

ALC	Axial load cell
API	American Petroleum Institute
BH	Borehole
BKx/Ly	Load test specification for Bothkennar; x = no. of pile, y = load test number (see Chap. 4)
BRE	Building Research Establishment
CEM	Cavity Expansion Method
$CK_0U(x)$	K_0 consolidated undrained test; x=C for triaxial compression, x=E for triaxial extension, x=ss for simple shear test
CLA	Centre line average
CPT	Cone Penetration Tests
CPTU	Piezocone tests
c_u	Undrained shear strength
c_{u0}	Quick undrained (UU) shear strength in triaxial compression
c_{uss}	Undrained strength in simple shear
c_{u0}/σ'_{v0}	Undrained strength ratio
c_h	Horizontal coefficient of consolidation
C_c	Compression index
C_s	Swelling index
C_c^*	Compression index of intrinsic material
CC	Clay content
CWx/Ly	Load test specification for Cowden; x = no. of pile, y = load test number (see Chap. 4)
d	Displacement
d_p	Pile head displacement
D	Pile diameter
D_r	Relative density
DSS	Direct simple shear
e	Void ratio
e_g	Granular void ratio
e_i	Initial void ratio
e_{ss}	Steady state void ratio
e_L	Void ratio at liquid limit
$e_{\sigma r}$	Under-registration of σ_r due to cell action effects
e_τ	Under-registration of τ_{rz} due to cell action effects
e_{100}^*	Void ratio of intrinsic material at σ'_v =100kPa
e_{100}	Void ratio at σ'_v =100kPa
e_{max}	Maximum void ratio
e_{min}	Minimum void ratio
f_c	Shear stress on friction sleeve in CPT and CPTU tests
f_r	Pile plunging rate post-peak in load tests
f_s	Shaft shear stress acting between instrument clusters

$f_{\sigma r}$	Radial compliance of SST
f_{τ}	Shear compliance of SST
FEM	Finite Element Method
FSO	Full scale output
GCG	Geotechnical Consultancy Group, London SW7
G_p	Pressuremeter shear modulus
G_s	Specific gravity
G_{sec}	Secant shear modulus
h	Vertical upward distance from the pile tip
H	Radial total stress coefficient acting on pile [= $(\sigma_r - u_0)/\sigma'_{v0}$], subscripts i,c, f denote values at installation, after equalisation and at peak local shear stress in load tests (τ_f)
$(H_1)_{ref}$	Reference value of H_1 (normally at h/R=8)
I_v	Void index $(e- e_{100}^*)/C_c^*$
I_{v100}	Void index at σ'_{v0} =100kPa
$(I_v)_{ICL}$	Void index of intrinsic material
I_v^*	$I_v - (I_v)_{ICL}$
I_p	Alternative symbol for plasticity index (PI)
I_r	Rigidity index (= $(G/c_{u0})^{0.5}$)
IC	Imperial College
ICL	Intrinsic compression line
ICP	Imperial College instrumented Pile
IMP	Oxford Univ. model pile
J	Length of jack stroke
k_h	In-situ horizontal permeability
K	Radial effective stress coefficient acting on pile (σ'_r/σ'_{v0}), subscripts i,c, f denote values at installation, after equalisation and at peak local shear stress in load tests (τ_f)
K_a	Active coefficient of earth pressure
K_0	In-situ lateral stress coefficient ($=\sigma'_{h0}/\sigma'_{v0}$)
K_{0nc}	K_0 for normally consolidated soil
K_p	Passive coefficient of earth pressure
L	Pile embedded length
L_r	Pile loading rate in load tests (kN/min)
LBx/Ly	Load test specification for Labenne; x = no. of pile, y = load test number (see Chap. 4)
LI	Liquidity index
LL	Liquid limit
L/R	Slenderness ratio
LPC	Laboratoire des Ponts et Chaussées
m_v	1-D volumetric compressibility (subscript h used for 1-D compressibility in radial direction)
MCC	Modified Cam Clay

MIT	Massachusetts Institute of Technology
MIT-E3	E3 soil model developed at MIT
MPM	Menard pressuremeter
N_k	Cone factor (= $(q_c - \sigma_{v0})/c_{u0}$))
N_q	Bearing capacity factor
NGI	Norwegian Geotechnical Institute
OCR	Apparent overconsolidation ratio
OCR_m	Mechanical overconsolidation ratio
P	Pile load
P_{atm}	Atmospheric pressure
P_{max}	Maximum applied pile load
p'	Mean effective stress
p'_0	In-situ mean effective stress
P_{lim}	Pressuremeter limit pressure
P_L	Pressuremeter inflation pressure at 50% volumetric strain
p'_s	Suction
PI	Plasticity index
PL	Plastic limit
PLS cell	Piezo-lateral stress cell
PPU	Pore pressure unit
PP	Pressio-penetrometer
Q_{sc}	Shaft load in compression
Q_{st}	Shaft load in tension
q_b	Pile end bearing
q_c	End resistance measured in CPT and CPTU tests
r	Radial distance from pile centreline
R	Pile radius
R_1	Centre line average roughness
RS	Ring shear
RSI	Ring shear interface
s	$0.5\ (\sigma'_1+\sigma'_3)$
s_t	Sensitivity parameter used by the MIT-E3 soil (see Appendix C)
S_r	Degree of saturation
S_t	Sensitivity
SBP	Self-boring pressuremeter
SPM	Strain Path Method
SST	Surface stress transducer
t	Time
t'	$0.5\ (\sigma'_1 - \sigma'_3)$
t_f	Time to load pile to peak capacity
t_{90}	Time for 90% excess pore pressure dissipation
T	Time factor (= $c_h t/R^2$)
T_p	Alternative time factor [= $(k_h p'_0 t)/(\gamma_w R^2)$]
t_{eq}	Equalisation time

u	Pore pressure
u_c	Pore pressure in CPTU tests
u_{cyc}	Cyclic induced excess pore pressure
u_m	Pore pressure recorded during pile jacking
u_{max}	Maximum pore pressure
u_0	Ambient pore pressure
u_s	Maximum pore pressure recorded in between jacking stages
u_{sh}	Shear induced excess pore pressure
u_{ts}	Excess pressure due to increase in mean total stress
Δu_{shaft}	Excess pore pressure at the pile shaft
$\Delta u_i/\sigma'_{v0}$	Installation pore pressure ratio
$\Delta u_{max}/\sigma'_{v0}$	Maximum pore pressure ratio
Δu_{rate}	Post-peak pore pressure reduction in load tests
U	Pore pressure consolidation factor [= $(u_{max}-u)/(u_{max}-u_0)$]
U_d	Pore pressure dissipation factor [= $(u-u_0)/(u_{max}-u_0)$]
UU	Unconsolidated undrained
VCL	Virgin consolidation line
w	Water content
z	Depth; Note : plots produced by MIT use this symbol to represent the distance from the pile tip (h)
α	average alpha ($=\tau_{avp}/c_{u0}$)
α_L	local alpha (τ_f/c_{u0})
$(\alpha_L)_{av}$	Average local α
β_{av}	average beta ($=\tau_{avp}/(\sigma'_{v0})_{av}$)
β_L	local β ($=\tau_f/\sigma'_{v0}$)
γ_b	Bulk unit weight os soil
γ_{rz}	Shear strain in the vertical plane
γ_w	Unit weight of water
δ	Angle of interface friction (= $\tan^{-1}(\tau/\sigma'_n)$)
δh	Displacement perpendicular to shearing plane (+ve if dilation, -ve if contraction)
δl	Displacement parallel to shearing plane
δ_{cv}	Constant volume δ
δ_f	δ at peak local shear stress (τ_f)
δ_p	Peak δ
δ_{ult}	Post-peak residual δ
ε_c	Cavity strain
ε_s	Shear strain
κ	Slope of 1-D swelling line (e v $\log_e \sigma'_v$ space)
κ_0	Small strain κ value
λ	Slope of 1-D compression line (e v $\log_e \sigma'_v$ space)
μ	Coefficient of friction ($=\tau/\sigma'_n$)
ν	Angle of dilation
ν_{max}	Maximum angle of dilation
ρ	Skin friction coefficient ($=\tau_f/\sigma'_{nc}$)

σ'_n	Normal effective stress
σ'_{nc}	Consolidation σ'_n (also called σ'_{vc})
σ'_v	Vertical effective stress
σ'_{ve}	Vertical effective stress on the virgin consolidation line at the same void ratio as the in-situ material
σ'_{vy}	Vertical yield stress (also called σ'_{vm} or σ'_{vp})
σ'_{h0}	In-situ horizontal effective stress
σ'_{v0}	In-situ vertical effective stress
σ'_r	Radial effective stress
σ'_{rc}	Equalised radial effective stress
σ'_{rf}	Radial effective stress at peak local shear stress
σ'_{ri}	Installation radial effective stress
σ'_{rl}	Pre-loading radial effective stress
σ'_{rm}	Radial effective stress during jacking stages
σ'_{rs}	Radial effective stress between jacking stages
σ'_θ	Hoop effective stress, further subscripts as for σ'_r
σ'_1	Major principal stress
σ'_3	Minor principal stress
τ	Shear stress
τ_{avp}	Peak average shaft shear stress (often referred to as τ_{av})
τ_{avu}	Post-peak τ_{av}
τ_f	Peak local shear stress
τ_{rz}	Shear stress acting on pile shaft
τ/σ_n	Total stress ratio
ϕ'	angle of friction
ϕ'_{cv}	ϕ' at constant volume conditions
ϕ'_p	Peak angle of friction
ϕ'_{ps}	ϕ' in plane strain
ϕ'_r	Residual friction angle (also called ϕ'_{res})
ϕ'_{rp}	Peak residual friction angle
ϕ'_{tc}	ϕ' in triaxial compression
ψ	State parameter ($e - e_{ss}$)

CHAPTER 1

INTRODUCTION

CONTENTS OF CHAPTER 1

1.1 BACKGROUND..... 4
1.2 OUTLINE OF THESIS..... 6
1.2.1 Scope of experimental work 6
1.2.2 Contents of Thesis 7

1.1 BACKGROUND

Displacement piles have been used as foundations for structures since the Neolithic age, about 7000 years ago (Kérisel 1985). These early piles were in the form of timber posts and were pushed manually into soft sedimentary soils to provide support for the platforms of houses built adjacent to lakes and rivers. These types of structures can still be found in many parts of the world today. With time, machines were developed to install piles. Kérisel suggests that the first of these machines was similar to the battering ram devices used by the Greeks (≈800 B.C.) to break down gates and walls.

It is likely that the axial capacity of a pile was rated in accordance with the degree of effort required for its installation. The number of piles needed for a given structure would then estimated from previous knowledge of what had worked and what didn't work under similar conditions. With the advent of soil mechanics, this 'degree of effort' was related to a benchmark parameter which expressed a measure of the strength or consistency of the soil. Typical parameters include the undrained shear strength of a clay and the resistance measured during penetration of a device smaller than a full scale pile (e.g. a cone penetrometer or a Standard Penetration Test tool). Most design methods for piles, in use to this day, are based on correlations which have related the pile capacities measured in controlled load tests to one of these parameters.

The axial capacity of a pile is usually separated into the resistance at the base and the skin friction along the shaft. Historically, most displacement piles were driven until the base reached a competent stratum. In these situations, a large component of the total capacity was derived from the base resistance and the pile design was often controlled by the ability of the pile itself to carry the load. However, as larger structures were demanded and prime sites became less abundant, it became necessary to design longer piles that also relied on shaft friction. For example, the shaft capacity of piles supporting offshore structures often represents more than 90% of their total capacity in clays and more than 50% of their capacity in sands.

With the new requirements for longer and larger piles, it became clear (particularly to the offshore industry) that more soundly based design methods had to be developed and that this could only be achieved with a knowledge of the fundamental mechanics of piles, interpreted within a scientific framework. Soil behaviour is governed by effective stresses (Terzaghi 1936) and therefore a rational theory for pile behaviour must be able to predict the effective stresses in the soil surrounding the pile and particularly at the pile-soil interface. As illustrated on Figure 1.1, predictions must take account of the changing conditions associated with the four stages in the life of the pile :(a) prior to installation, (b) during installation, (c) equalisation (consolidation) after installation and (d) during the static/dynamic loading applied by the structure (shearing).

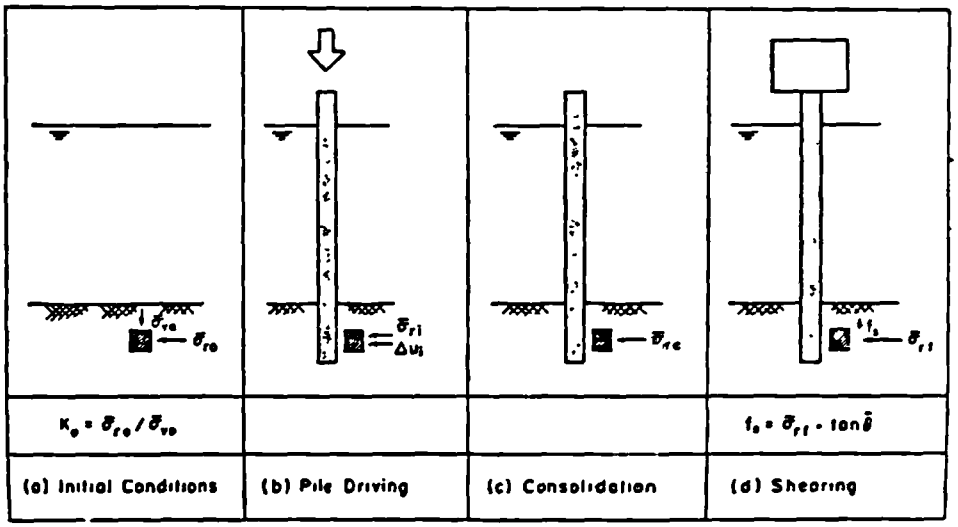

Figure 1.1 Four stages in the life of a displacement pile

Experimental data for each of these stages are required to test and develop any theoretical approach. There is however a great shortage of reliable measurements of the effective stresses developed on displacement piles in clay and virtually no data for piles in sand and, although some encouraging theoretical advances have been made, design methods have

remained purely empirical. It is worthy of note that, in a survey of practising engineers, Focht and O' Neill (1985) found that less than 10% professed to ever using an effective stress approach for pile design; most designers preferred to rely on local experience and static load tests. Briaud & Tucker (1988), amongst others, suggest that existing design methods cannot be expected to consistently predict pile capacities to an accuracy closer than ±50% of the actual capacity.

1.2 OUTLINE OF THE THESIS

1.2.1 Scope of field work presented

Because of the great sparsity of measurements of the effective stresses developed on displacement piles, the primary aim of my research was to extend the existing data base, as far as possible, using piles equipped with high quality instrumentation. This was to be achieved using the Imperial College instrumented Pile (ICP), which is 102mm in diameter and closed-ended, and contains a number of heavily instrumented segments at various positions along its (steel) shaft. The ICP had reached its final stages of development in 1988 and was employed successfully in the London Clay at Canons Park, North London, by Dr. Andrew Bond at Imperial College (Bond 1989).

The series of tests undertaken is outlined in Table 1.1; this programme involved experiments at three carefully selected sites, for each of which reasonably comprehensive site investigations had already been performed. Further site investigation work was carried out , where necessary, to aid interpretation of the test results.

Each test programme allowed a full study of the development of stresses on the piles, allowing for potential variations in soil conditions and possible instrument malfunctions. The number of tests was sufficiently large to allow specific parameters affecting pile behaviour in 'first-time' load tests to be investigated separately. These parameters included pile depth, direction of loading (i.e. tension/compression), equalisation period, rate of pile installation and rate of pile loading (drained /undrained). Secondary tests were performed after initial failure and

these provided further information on the effects of pre-shearing and cyclic loading on pile performance.

Test site	Date	Soil type	No. of 'first-time' load tests
Labenne S.W. France	Jan-Feb 1989	Loose-medium dense SAND	3
Cowden N.E. England	Oct-Dec 1989 Feb-Apr 1990	Stiff glacial TILL	5
Bothkennar Scotland	Oct-Dec 1990 Mar-Apr 1991	Soft sensitive silty CLAY	6

Table 1.1 Programme of ICP tests

1.2.2 Contents of the thesis

While the field work performed with the ICP form the backbone of the data presented in this thesis, further comparative studies with existing theoretical methods for displacement piles and with laboratory test data are presented which help to identify the factors controlling pile behaviour. The findings from these studies, used in conjunction with the trends shown by previous (good quality) instrumented pile test programmes, are used to develop rational design methods for evaluating the shaft capacities of closed-ended displacement piles in clays and sands.

At this point, it is important to emphasise that this Thesis is concerned only with investigations of closed-ended displacement piles. Evidence from limited data on the effect of the pile end condition indicates that the mechanism of pile penetration of an open-ended pile (particularly if its diameter is large) can be such that stresses mobilised on the pile shaft are less than those developed on closed-end piles. Of course, if an open-ended pile plugs (i.e. the amount of soil within the pile does

not vary with pile penetration), then one would expect similar behaviour between the two pile types.

The contents of each chapter are summarised below:

Chapter 2: reviews the recent developments in the study of the behaviour of *closed-ended* displacement piles in clay and discusses existing design approaches, some theoretical advances and the trends shown by previous instrumented pile tests. The sub-section devoted to the instrumented tests is supplemented by Appendix B which describes the most successful of these in detail. Many PhD theses have reviewed displacement pile behaviour in clays, most notably Morrison (1984), Jardine (1985), Coop (1987) and Bond (1989). Instead of simply updating these reviews, I have endeavoured to present an evaluation, rather than an account, of previous research and have concentrated on aspects which were shown in later chapters to be of particular importance in furthering our understanding of pile behaviour in clays.

Chapter 3: presents a review of previous research on displacement pile behaviour in sand and provides a background with which to judge and interpret the findings from the ICP tests. Design approaches used to evaluate pile capacities are discussed before examining the relatively small amount of relevant fundamental research.

Chapter 4: describes the ICP and its instruments and then details the laboratory and field procedures followed for the ICP tests. The general performance of the instrumentation is summarised. A full discussion of this performance is provided in Appendix A.

Chapter 5: presents a summary of the soil properties at each of the three sites studied: Labenne, Cowden and Bothkennar. Attention is focused on those properties that are vital for a thorough interpretation of the pile tests. Additional investigations (performed specifically for this research programme) are also reported. These included ring shear and shear box interface tests which are described in more detail in Appendix D. The data presented in this chapter may also be used to determine the

necessary parameters for any future theoretical examinations of the pile tests.

Chapters 6, 7 & 8: present the results from the ICP tests in the Labenne sand, Cowden till and Bothkennar clay respectively. These chapters form the main body of the Thesis and share a common format for data presentation.

Chapter 9: discusses the characteristics of displacement piles in sand. This discussion centres around the main observations made in the ICP tests at Labenne and the review presented in Chapter 3, and explores the general mechanisms of shaft friction in sands.

Chapter 10: summarises and discusses the trends observed in the ICP tests in Cowden till and Bothkennar clay and also discusses the data obtained in the pile tests performed by Bond (1989) so that the general characteristics of ICP tests in clays may be examined.

Chapter 11: assimilates trends shown by displacement piles in clay from those deduced in Chapter 10 and from the results of previous (good quality) instrumented tests (Appendix B) and theoretical predictions (Chapter 2 and Appendix C).

Chapter 12: presents a brief summary of the main conclusions of the Thesis and makes suggestions for further research.

Supplementary information is provided in the appendices:

Appendix A: Instrument performance
Appendix B: Review of instrumented pile tests in clays
Appendix C: Evaluation of Strain Path Method predictions for the ICP tests at Bothkennar
Appendix D: Ring shear and shear box interface tests on Labenne sand, Cowden till and Bothkennar clay

CHAPTER 2

DISPLACEMENT PILES IN CLAY: RECENT DEVELOPMENTS

CONTENTS OF CHAPTER 2

2.1 INTRODUCTION 14

2.1.1 General 14

2.1.2 Notation and normalisation of measurements 14

2.2 EMPIRICAL METHODS 16

2.2.1 General 16

2.2.1.1 Shaft capacity 16

2.2.1.2 End bearing 17

2.2.1.3 Difficulties with empirical methods 17

2.2.2 Correlations with undrained strength 18

2.2.3 Correlations with σ'_{v0} 22

2.2.4 Semi-empirical methods 24

2.2.4.1 Method proposed by Azzouz et al (1990) 24

2.2.4.2 Method proposed by Bond (1990) 25

2.2.5 Discussion 27

2.3 THEORETICAL DEVELOPMENTS 28

2.3.1 General 28

2.3.2 The Strain Path Method 30

2.3.2.1 Principle 30

2.3.2.2 Procedure 31

2.3.2.3 Predicted strain paths 32

2.4.2.4 Discussion 33

2.3.3 The MIT-E3 soil model 34

2.3.4 Predictions for pile installation 36

2.3.5 Predictions for equalisation 41

2.3.5.1 General 41

2.3.5.2 Linear analysis 41

2.3.5.3 Non-linear analysis 42

2.3.6 Predictions for pile loading 46

2.3.6.1 Analytical predictions 46

2.3.6.2 Predictions using DSS tests 47

2.3.6.3 Coefficients of friction 48

2.4 INSTRUMENTED DISPLACEMENT PILES IN CLAY 50

2.4.1 General 50

2.4.2 Installation 52

2.4.3 Equalisation 54

2.4.4 Load testing 55

2.4.5 Effect of installation on soil fabric 56

2.1 INTRODUCTION

2.1.1 General

This chapter reviews and evaluates the latest developments in the study of the behaviour of *closed-ended* displacement piles in clay and is divided into three sections:

- Section 2.2 assesses the most popular empirical procedures currently in use for conventional pile design.

- Section 2.3 examines various theoretical approaches applied to the prediction of pile behaviour but concentrates on the Strain Path Method (SPM), which is the only analytical technique available that provides a moderately realistic description of the pile installation process. Theoretical predictions depend critically on the constitutive soil model adopted and attention is focused on predictions made using the MIT-E3 model, which is one of the most comprehensive models available for clay soils. The results from a parametric study of documented SPM/MIT-E3 predictions are presented. Trends are identified that reveal the soil properties which may have the strongest influence on pile performance.

- Section 2.4 summarises the general trends evident from the relatively small number of field tests that have measured the effective stresses developed on displacement piles to an acceptable accuracy. This section is supplemented by Appendix B, which provides a detailed review of the soil properties, instrumentation and measurements made in each of the successful test programmes.

2.1.2 Notation and normalisation of measurements

In order to compare data from different sites, obtained with different pile sizes, it is necessary to use a consistent and rational set of normalised parameters. The same parameters may then be used when comparing measurements made in the ICP tests with those of other test programmes and with theoretical predictions.

In this Thesis, the ground stresses are normalised by the free field vertical effective stress (σ'_{v0}). The reasons for this choice are:

- Measurements made in instrumented pile tests indicate that stresses induced by pile installation in a uniform soil of constant overconsolidation ratio increase linearly with depth and in proportion to σ'_{v0} (see Figure B6, Appendix B).
- σ'_{v0} is relatively easy to determine accurately and does not suffer from the uncertainties and scatters associated with the measurement of other possible normalising parameters such as the initial undrained shear strength (c_{u0}), the Cone Penetration Test (CPT) end resistance (q_c) or the pressuremeter limit pressure (p_{lim}).

The following notation is used for the normalised stresses. This is the same as that used to present theoretical predictions made using the Strain Path Method (SPM).

- Normalised radial total stress $H = (\sigma_r - u_0)/\sigma'_{v0}$
- Excess pore pressure ratio $\Delta u/\sigma'_{v0} = (u - u_0)/\sigma'_{v0}$
- Lateral stress coefficient $K = \sigma'_r/\sigma'_{v0}$
- Local beta $\beta_l = \tau_f/\sigma'_{v0}$

In these expressions, σ_r is the radial total stress, τ is the vertical shear stress acting on the pile shaft, u is the pore pressure and u_0 is the ambient pore pressure. Subscripts i, c and f are used to denote values at the completion of installation, after full equalisation and at peak capacity in load tests respectively. For example, H_i is the value of H after installation, K_c is the value of K at the end of equalisation and K_f/K_c is the ratio of K at peak local shear stress to the equalised K value. Note in particular that $H = K + \Delta u/\sigma'_{v0}$ and $H_c = K_c$.

Based on the SPM predictions for the strain paths followed by elements of soil during pile installation (Section 2.3), it is assumed tentatively that scale effects can be removed by normalising distances with respect to the pile radius (R) i.e. stresses and displacements at a given normalised distance from a pile are independent of the pile radius. This normalisation is in keeping with observations made in pile tests such as

the dependence of the rate of excess pore pressure dissipation on the pile radius squared (e.g. Bogard & Matlock 1990 and many others) and the dependence of the unit shaft capacity on the pile slenderness ratio (L/R) (e.g. Semple & Ridgen 1984).

To compare measurements made at the start and finish of a particular phase in the life of a pile (e.g. equalisation), use is made of the following coefficients which express the ratio between these two measurements.

- Set-up coefficient $=K/K_c$ (=1 after equalisation)
- Load test coefficient $=K_f/K_c$
- Relaxation coefficient $=H/H_i$ (=1 after installation)
- Pore pressure factor $=\Delta u/\Delta u_i$ (=1 after installation)

These coefficients allow the effective stresses changes during the life of a pile to be separated into the changes that take place during installation, equalisation and load testing. For example, the peak local shear stress (τ_f) mobilised during a load test after full equalisation may be written as:

$$\tau_f = \sigma'_{rf} \tan \delta_p \qquad (\tan \delta_p = \text{coefficient of friction})$$
$$= \tan \delta_p \, [K_f/K_c] \; K_c \, \sigma'_{v0}$$
$$= \tan \delta_p \, [K_f/K_c] \; [H_c/H_i] \; [H_i] \, \sigma'_{v0} \quad = \beta_1 \, \sigma'_{v0}$$

2.2 EMPIRICAL METHODS

2.2.1 General

2.2.1.1 Shaft capacity

Shaft capacities are most often assessed using empirical correlations which relate ultimate capacities measured in pile load tests to a measurable initial soil parameter. The most commonly used parameters are the undrained shear strength of the clay (c_u) or the in-situ vertical effective stress (σ'_{v0}). The average shaft shear stress (τ_{av}) is then given by:

$$\tau_{av} = \alpha \, (c_u)_{av} \quad (\alpha \text{ is called the adhesion factor})$$
$$\text{or} \quad \tau_{av} = \beta \, (\sigma'_{v0})_{av}$$

Other methods relate τ_{av} with:

- the pressuremeter limit pressure (p_{lim}), e.g. Baguelin et al (1986)
- the Cone Penetration Test (CPT) end resistance (q_c), e.g. Bustamante & Gianeselli (1982)
- $(\sigma'_{v0} + 2c_u)_{av}$ (or the λ method), Vijayvergia and Focht (1972)

Correlations for α and β are discussed in Sections 2.2.2 and 2.2.3.

2.2.1.2 End bearing

The proportion of the total compressive capacity that is carried in end bearing by piles in clay is typically less than 10%, provided that L/R exceeds ≈30 (Fleming et al 1985). The relatively minor contribution of the unit end resistance (q_b) is generally taken from bearing capacity theory i.e.

$$q_b = N_c\, c_{u0} + \sigma_{v0}$$

where c_{u0} =UU triaxial compression strength at pile base

σ_{v0} =Total vertical stress at pile base

N_c =Bearing capacity factor

A bearing capacity factor (N_c) of 9 is usually adopted (Skempton 1951), although N_c can be as low as 5 for large diameter piles and up to ≈20 for small diameter piles; see Jardine & Christoulas (1991). These N_c values apply only to closed-ended piles.

2.2.1.3 Difficulties with empirical methods

A number of points should be borne in mind regarding the principles of the standard empirical methods currently in use.

- A large number of factors are known to affect pile shaft capacity. These include soil type, pile type and geometry, installation method, set-up time, loading history, loading direction and load

test procedure. Because of the large number of influential variables and the relatively sparse data base of well documented pile tests, the empirical rules represent little more than trend lines drawn through poorly correlated scatter diagrams.

- The empirical shaft resistance factors (e.g. α and β) are backfigured from data bases which are composed mainly of results from relatively short and small diameter onshore piles. It is not certain that these factors can be extrapolated to the design of long, large diameter offshore piles.
- Because few piles have been instrumented to measure the variation of local shear stresses along pile shafts, the backfigured α and β values are average values for the complete shaft. The use of these expressions for multi-layered deposits must therefore be in considerable doubt, as would correlations which incorporate empirical factors backfigured from tests in such deposits.
- The methods cannot be used to assess the stresses acting on the pile shaft. Without knowledge of these stresses, prediction of pile behaviour under service loads and more complicated load sets is not possible.

2.2.2 Correlations with undrained strength

The most popular method for determining the shaft capacity of piles in clay is the "α method" which relates the average ultimate shaft shear stress to the average undrained shear strength of the clay by a factor α:

$$\tau_{av} = \alpha \, (c_u)_{av}$$

It became apparent from an early stage (e.g. Tomlinson 1957) that the values of α backfigured from load tests reduced with increasing shear strength. c_u was also known to depend on the sample quality and the test method. Dennis & Olsen (1983) concluded that the inconsistency of the procedures used to determine c_u was the primary reason for the large scatter in α values deduced in previous correlations and proposed the following expression for τ_{av} based on 84 selected pile tests where full equalisation after installation was believed to have been achieved:

$$\tau_{av} = \alpha \, F_c \, F_L \, (c_u)_{av}$$

F_c corrects the measured undrained strength to the equivalent UU triaxial compression strength of high quality samples[1] i.e. $F_c\ c_u = c_{u0}$, and F_L is a correction that was used to fit the correlation with results from tests on piles that were over 30m in length[2]. The variation of α with c_{u0} proposed for design is shown on Figure 2.1 and suggests that α reduces from 1.0 at $c_{u0} \approx 30$kPa to a minimum value of 0.3 for $c_{u0} \geq 250$kPa.

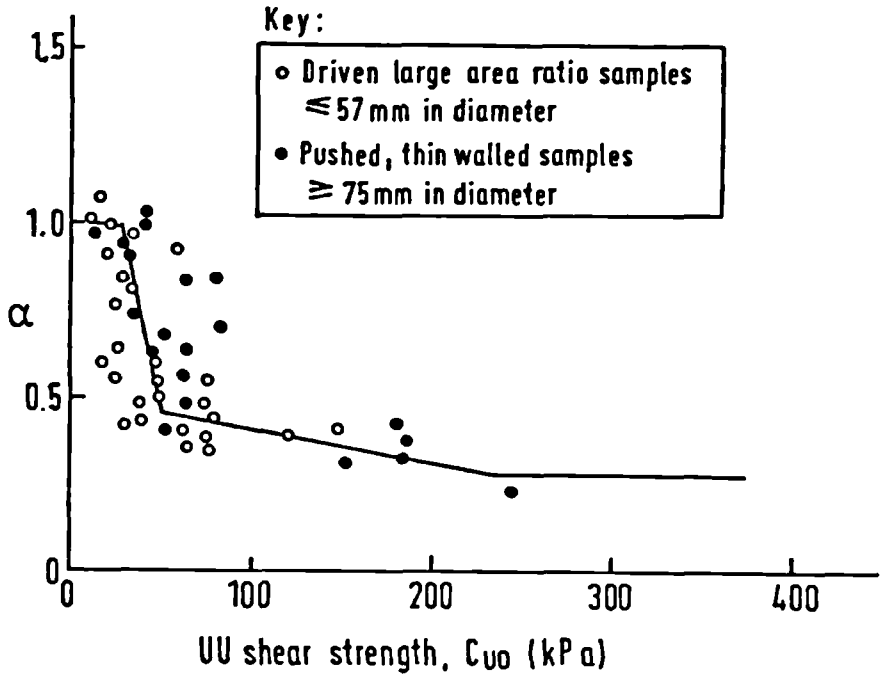

Figure 2.1 Variation of α with c_{u0} (Dennis & Olsen 1983)

In a review of 105 pile tests, Kraft et al (1981) examined the dependence of α on pile length (L) and concluded that α reduces with L (given in metres) as follows:

$$\alpha = 1.34 - 0.126 \ln (L) \qquad \text{for } c_{u0}/\sigma'_{v0} \leq 0.4,$$

$$\alpha = 0.89 - 0.103 \ln (L) \qquad \text{for } c_{u0}/\sigma'_{v0} > 0.4$$

[1]High quality samples were defined as those retrieved by thin wall pistons with a diameter of ≥75mm. However, it is well known that c_{u0} values of larger diameter samples can be considerably different to the c_{u0} values of 75mm diameter samples (e.g. see Section 5.3.7).

[2]F_L increases from 1.0 for a pile length of 30m to 1.8 for pile lengths of ≥50m.

These relationships showed an unacceptable degree of scatter and it was not clear whether the inclusion of different pile types with varying set-up times in the data base had contributed to this trend (Morrison 1984). Kraft et al (1981), Morrison (1984) and others speculated on a number of reasons on why α should reduce with pile length. Two major factors were identified:

(i) Strain softening response of the soil.

Piles are expected to fail progressively, as shown on Figure 2.2 (Kraft 1981), in materials which strain soften. The effect of progressive failure is most pronounced in very compressible piles as the relative movement required for mobilisation of peak local shear stress near the pile base will be such that the soil closer the pile head will experience considerably larger relative movements. These movements may be sufficient for local shear stresses to reach constant ultimate/residual values. It follows that in a 'homogeneous strain softening deposit', α will reduce with pile length (see Randolph 1983 for further discussion).

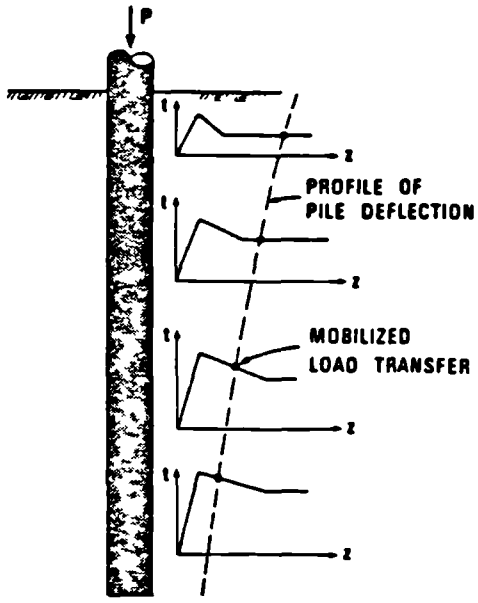

Figure 2.2 Shear stress distribution in a 'strain-softening' soil

(ii) Varying material properties with depth (e.g. OCR)

The most commonly used recommendations for offshore pile design are those produced by the American Petroleum Institute (API). Until recently, these recommendations followed a similar form to those proposed by Dennis & Olsen (1983) on Figure 2.1. However, parametric studies by Semple & Ridgen (1984) and Randolph & Murphy (1985) showed a better fit to the available data base could be obtained by relating α with the undrained strength ratio c_{u0}/σ'_{v0}; this ratio is approximately proportional to $OCR^{0.8}$ (Ladd et al 1977)[1].

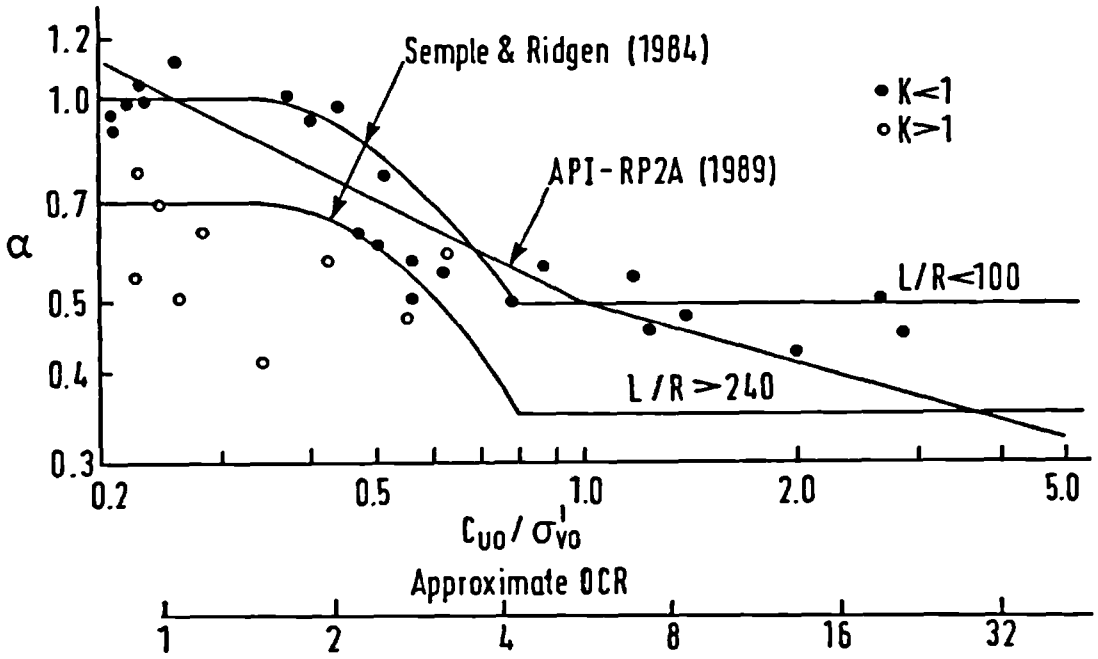

Figure 2.3 α variation with c_{u0}/σ'_{v0}

The variations of α with c_{u0}/σ'_{v0} proposed by Semple & Ridgen (1984) and the latest API code (1989) are shown on Figure 2.3. The Semple & Ridgen trend line differs moderately from that proposed by API as it was based

[1] $c_{u0}/\sigma'_{v0} = (c_{u0}/\sigma'_{v0})_{nc}\ OCR^{0.8}$. $(c_{u0}/\sigma'_{v0})_{nc}$ is the undrained strength ratio at OCR=1 and is virtually constant at 0.3 ±0.05 for most clays (Hight et al 1987).

on a smaller data base (shown on figure) and used the shear strengths measured in *unconfined* triaxial compression tests as opposed to the UU strength (c_{u0}), preferred by API. Semple & Ridgen allow for the anticipated effects of strain softening in their correlation by proposing an α variation for short and long piles (L/R <100 and L/R > 240) and a linear interpolation of α between these two limits. The API method does not (as yet) take the effects of pile compressibility into account but points out in the commentary that these effects should be evaluated.

A statistical study of the API (1989) recommendations by Tang (1988) showed that this α method is a significant improvement on previous API α methods. Furthermore, the method reflects *some* trends of behaviour which have been measured in high quality instrumented pile tests (see Section 2.2.4).

2.2.3 Correlations with σ'_{v0}

A major difficulty of the α method is that c_{u0} is very sensitive, amongst other things, to the degree of sample disturbance. The β method overcomes this difficulty by relating τ_{av} to the average initial in-situ vertical effective stress $(\sigma'_{v0})_{av}$, which is relatively simple to determine accurately i.e.

$$\tau_{av} = \beta \ (\sigma'_{v0})_{av}$$

Several expressions for β have been proposed, each of which assumes that β can be expressed as:

$$\beta = \quad (K_s/K_0) \ K_0 \tan \delta$$

The factor K_s/K_0 represents the increase in radial effective stress caused by pile installation (after equalisation and ignoring any changes in σ'_r during pile loading) and $\tan\delta$ is the coefficient of friction, which may be estimated from the assumed pile failure mechanism.

Burland (1973) showed that assuming $K_s \approx K_0$ provides a lower bound estimate of β for piles installed in normally consolidated clay and Meyerhof (1976) estimated that K_s/K_0 =1.5 ± 0.5 for piles installed in stiff (overconsolidated) clay.

These assumptions lead to the following formulae for β[1]:

$$\beta = \beta_{nc} = (1-\sin\phi')\tan\phi' \qquad \text{Burland (1973)}$$

$$\beta = (1.5 \pm 0.5)\ \beta_{nc}\ OCR^{0.5} \qquad \text{Meyerhof (1976)}$$

The β values backfigured by Meyerhof (1976) from pile tests in lightly overconsolidated materials are shown on Figure 2.4.

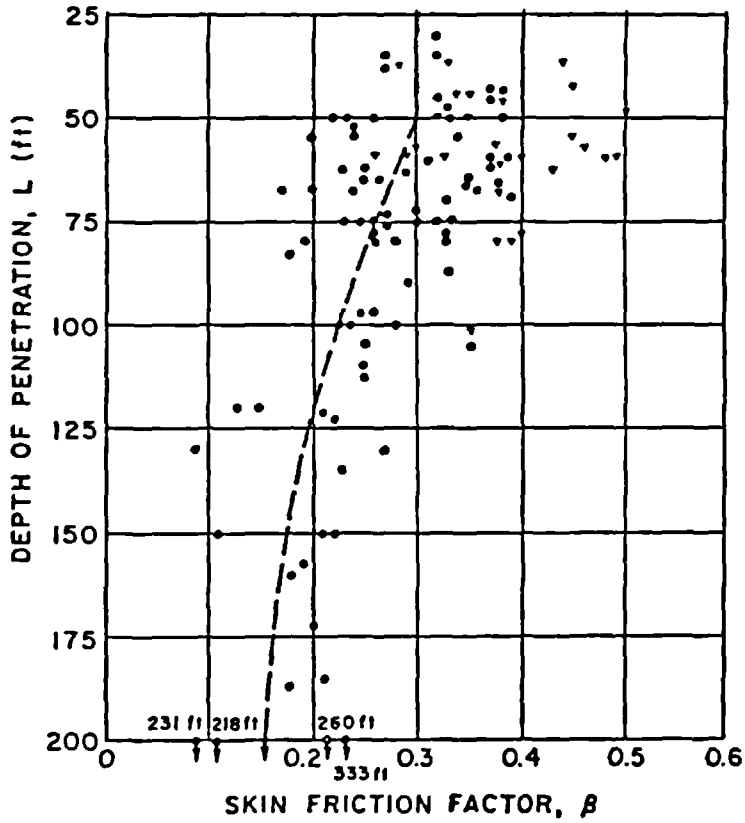

Figure 2.4 β variation with pile length in low OCR clays

The scatter in the data on Figure 2.4 is no better than that seen in the 'α plots' on Figures 2.1 and 2.3. This figure indicates that β reduces with pile length (L). Flaate & Selnes (1977) incorporated an empirical correction for this length effect in their expression for β and, based on over 40 pile tests[2] in normally and moderately overconsolidated clays, obtained the following best fit relationship:

[1]These assume $\delta = \phi'$ and $K_0 = (1-\sin\phi')OCR^{0.5}$

[2]Note that over half of these piles were tapered.

$$\beta = (0.4 \pm 0.1) \frac{(L+20)}{(2L+20)} OCR^{0.5} \qquad \text{(L in metres)}$$

An examination of the data base used by Meyerhof and Flaate & Selnes suggested that the observed reduction of β with pile length cannot be explained solely by the OCR profiles at the sites and strain softening effects. Further advances with the β method can only be made when this length effect can be explained rationally and then quantified.

2.2.4 'Semi-empirical' approaches

As discussed in Chapter 1, a knowledge of the magnitudes of the stresses developed on piles (and the factors that control them) is vital to the development of a rational design method. To this end, the offshore industry has recently funded a number of high quality instrumented pile test programmes (including the work described in this Thesis) and already, based on only a small number of tests and parallel theoretical studies, two tentative 'semi-empirical' design methods have been proposed. These methods are discussed in this section.

2.2.4.1 Method proposed by Azzouz et al (1990)

Azzouz at al (1990) suggested the following procedure to estimate the peak local shear stress (τ_f) for piles installed in lightly overconsolidated materials (OCR ≤ 4). This procedure is based on a review of data from instrumented pile tests and theoretical predictions made using the Strain Path Method (discussed in Section 2.3):

(i) The equalised radial effective stress (σ'_{rc}) may be estimated from the relationship between K_c (= $\sigma'_{rc}/\sigma'_{v0}$) and OCR, shown on Figure 2.5. This figure indicates that σ'_{rc}, referred to as σ'_{hc}, may also be moderately dependent on clay plasticity (I_p).

(ii) The friction ratio (ρ), defined as the maximum shear stress divided by the equalised stress (σ'_{rc}), is measured in constant volume direct simple shear (DSS) tests on <u>intact</u> clay at an OCR of 1.2 ± 0.1. The peak local friction in undrained pile load tests is then

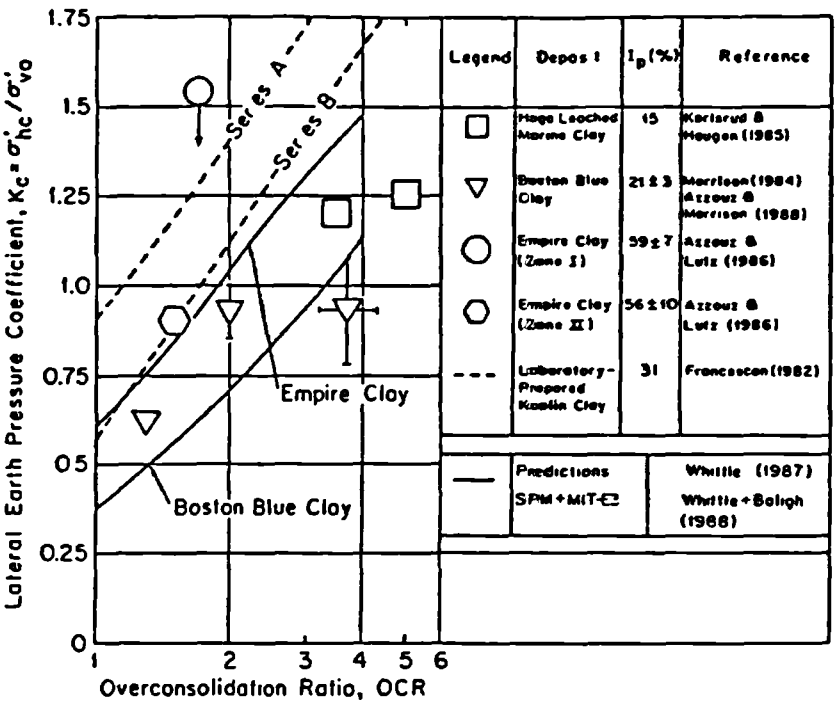

Figure 2.5 Variation of K_c with OCR (Azzouz et al 1990)

given by $\tau_f = \rho\ \sigma'_{rc}$; for "smooth" piles, direct shear interface tests are required to estimate ρ.

Karlsrud & Nadim (1990) propose a similar approach except that they recommend that τ_f should be estimated from ρ values measured in DSS tests on <u>remoulded</u> clay. These ρ values (ρ_{DSS}) are corrected (approximately) as follows to account for the difference between the K_0 stress conditions operating in the DSS apparatus and the stress conditions adjacent to a pile before load testing:

$$(\tau_f/\sigma'_{rc}) = \rho_{DSS} \times [1 + 1/K_c + K_{0nc}]/\ [\ 1 + 2\ K_{0nc}],$$

where K_{0nc} is the K_0 value at OCR=1.

2.2.4.2 Method proposed by Bond (1989)

Bond reviewed the available instrumented pile test data over the full OCR range (up to ≈40) and came independently to the conclusion that σ'_{rc} depends strongly on OCR. His experiments in heavily overconsolidated London Clay suggested that σ'_{rc} acting in any soil horizon is also strongly dependent on the distance of that horizon from the pile tip. This feature was *not* incorporated into the design approaches proposed by

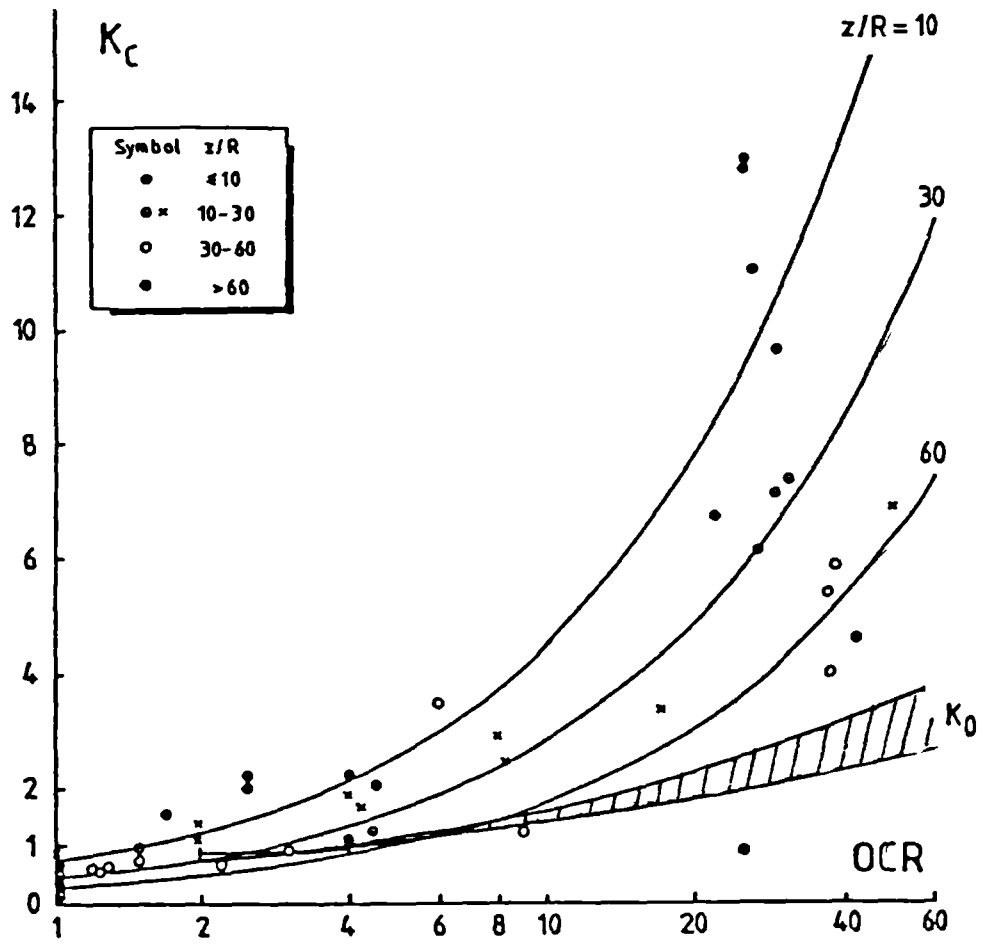

Figure 2.6 Variation of K_c with OCR and z/R (=h/R), Bond (1989)

Azzouz et al (1990) and Karlsrud & Nadim (1990). Bond proposed that K_c ($=\sigma'_{rc}/\sigma'_{v0}$) could be described as a function of OCR and the distance from the pile tip (h) normalised by the pile radius (R) i.e.

$$K_c = \sigma'_{rc}/\sigma'_{v0} = f_1\ (h/R)\ f_2\ (OCR)$$

Little independent data was available to allow the precise form of the function f_1 to be determined. Nevertheless Bond found that following functions provided a good fit to the available data base of measurements (the ± figures indicate 95% confidence limits):

$$f_1\ (h/R) = 0.35 + 0.865\ [1 - (h/R)/60]^2 \qquad f_1 \geq 0.35$$

$$f_2\ (OCR) = (0.82 \pm 0.16)\ OCR^{0.83 \pm 0.11}$$

These functions are plotted with Bond's data base on Figure 2.6.

The peak local shear stress is then obtained from the equation:

$$\tau_f = \sigma'_{rf} \tan\delta = (K_f/K_c)\ K_c\ \sigma'_{v0} \tan\delta$$

Based on the tests in the London Clay, Bond suggested that $K_f/K_c \approx 1$ for piles in heavily overconsolidated clay but, because of the sparsity of reliable load test data in instrumented tests, could not specify a value for lightly overconsolidated materials. Ring shear interface (RSI) tests on London clay indicated that δ could be assessed to a high degree of accuracy from these tests when the installation procedure was simulated correctly. It is noteworthy that RSI tests performed by Lemos (1986) and Tika (1989) showed that δ can vary from 7° to 30° depending, amongst other things, on the clay fraction of the soil, the history of relative displacement and the properties of the interface.

2.2.5 Discussion

Empirical correlations which relate the total shaft capacity to an average measurable or quantifiable parameter over the length of the pile shaft cannot easily accommodate specific variations in the large range of parameters which are known to influence pile capacity. The effective stress methods, discussed in Section 2.2.4, represent a significant improvement on these correlations. These methods are based on physical measurements of the local effective stresses acting on pile shafts and consequently reflect more closely the basic mechanics of pile behaviour. In addition, they are broadly compatible with theoretical methods which attempt to model the pile installation process using a realistic soil model (see Section 2.3).

A comparison of these effective stress methods with the trends shown by the α and β approaches shows that

- The apparent anomalies of α and β reducing with pile length would be explained by the reduction of the equalised radial effective stress with distance from the pile tip (h/R), if this was a general feature of displacement piles.
- The latest API recommendations, which relate α with c_{u0}/σ'_{v0}, and

the β methods which relate β with OCR are generally consistent with the dependence of σ'_{rc} on OCR deduced from instrumented pile tests.

- Although the general trend of available data suggests that σ'_{rc} can be described as a function of [a x OCR^b], where a and b are constants, the sparsity of measurements has led to significantly different values for these constants. These differences are such that the correlations of Azzouz et al (1990) and Karlsrud & Nadim (1990) predict that α reduces with c_{u0}/σ'_{v0} whereas Bond's correlation suggests that α may be relatively independent of c_{u0}/σ'_{v0}.

It is clear that considerably more measurements of σ'_{rc} acting on displacement piles are required if the precise relationship (if indeed there is one) between σ'_{rc} ,OCR and h/R can be established.

2.3 THEORETICAL DEVELOPMENTS

2.3.1 General

Any rational theoretical method for the design of piles must start from an effective stress perspective and model installation, equalisation and load testing separately. Although the process of installation is the most difficult to model, the stress regime surrounding the pile after installation is critical to its subsequent performance.

Much success has been achieved in the solution of boundary value problems in geotechnical engineering using the Finite Element Method (FEM). However, because of the vast number of calculation stages that would be required by the FEM to simulate the intense stress gradients and the changing boundary conditions associated with pile installation, prediction of the effects of installation with the FEM is presently considered to be impractical (e.g. see Baligh 1985). Some attempts using the FEM have been made by Kiousis et al (1988) and others, but these have not helped the study of pile installation as they, in effect, introduce the pile into a pre-bored hole and need to make an assumption about the changes in the stress state of the surrounding soil that preceded this introduction.

Two approximate theoretical methods have been proposed which attempt to simulate the installation process:

(i) Cavity Expansion Method (CEM): This method assumes that during pile installation, the soil (away from the influence of the pile tip and the ground surface) is displaced in a similar manner to the soil adjacent to an expanding cylindrical cavity. The stress changes are predicted using either cylindrical cavity expansion closed-form solutions (e.g. Butterfield & Bannerjee 1970 and Randolph & Wroth 1979), numerical FEM solutions for cavity expansion (e.g. Randolph et al 1979 and Whittle 1987) or the results from in-situ pressuremeter tests.

(ii) Strain Path Method (SPM): This method assumes that the soil moves relative to the pile tip in the same way that an incompressible, inviscid fluid would flow around the tip and that this flow pattern is independent of the shearing resistance of the soil. The flow streamlines are used to determine strain paths for all elements surrounding the pile; these may then be used to calculate effective stresses using an appropriate constitutive model for the soil.

The relative merits of these methods are discussed in detail in PhD theses by Morrison (1984), Jardine (1985), Coop (1987) and Bond (1989). Based on theoretical and experimental studies, two major conclusions emerge:

- The CEM does not provide a realistic description of the installation process and it is necessary to consider the two dimensional nature of pile installation.
- Prediction of stresses induced by pile installation necessitates the use of a constitutive soil model which takes proper account of pre-yield non-linearity, strain softening and soil anisotropy.

For these reasons, it has become evident that the most promising existing theoretical approach for the design of displacement piles is the SPM used in conjunction with a realistic constitutive law, such as the MIT-E3 soil model.

General aspects of the SPM and MIT-E3 model are discussed first below, before typical SPM/MIT-E3 predictions for pile installation, equalisation and load testing are presented.

2.3.2 The Strain Path Method (SPM)

2.3.2.1 Principle

Laboratory observations of soil deformation patterns caused by undrained penetration of model piles in a number of saturated clays led Baligh (1975) to the conclusion that, due to the severe kinematic constraints associated with pile installation, soil deformations and strains are essentially independent of the shearing resistance of the soil and can be estimated with reasonable accuracy without the need to consider the soil's constitutive relations.

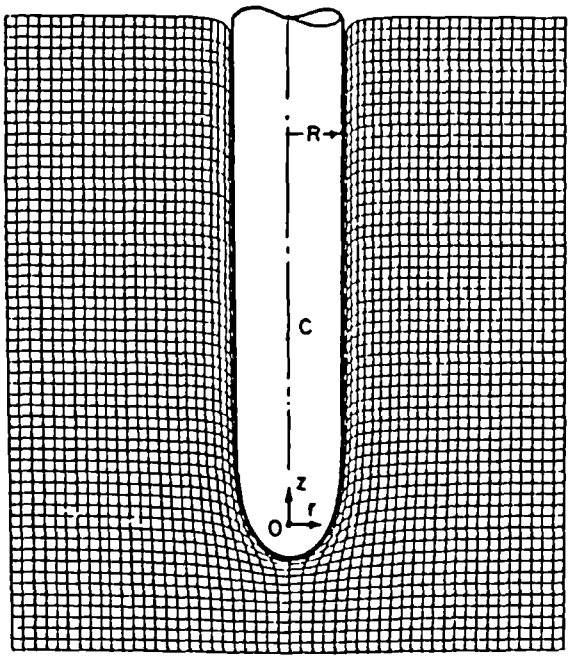

Figure 2.7 Predicted deformations around a 'simple pile'

The Strain Path Method (SPM) changes the frame of reference by viewing the undrained penetration of a pile as a steady state flow of soil past a static pile. Stream lines of 'soil-flow' are then estimated using incompressible inviscid flow theory.

The first pile analysed using the SPM was referred to by Baligh (1984) as the 'simple pile'. The configuration of this pile and its associated deformation pattern (or pattern of streamlines and equi-potentials) are shown on Figure 2.7. These were generated by introducing a single spherical source which discharges an incompressible material at a steady rate into a field of uniform velocity in the vertical (z) direction[1]. More complicated pile geometries have been analysed (e.g. 18° & 60° cone pile tips, sampling tubes) by adding further sources and sinks at the appropriate locations. An open-ended pile is modelled by replacing the spherical flow source by an annular source.

2.3.2.2 Procedure

The principal steps followed in the SPM are as follows:

1. Generate the streamline pattern and calculate the soil velocities.
2. Differentiate the soil velocities with respect to the spatial co-ordinates to obtain strain rates and integrate the velocities with respect to time to obtain the soil deformations.
3. Integrate the strain rates *along* streamlines to determine the strain histories for individual soil elements around the pile.
4. Estimate effective stress fields from the strain histories (paths) using a generalised effective stress soil model to characterise the constitutive behaviour of the soil.
5. Calculate pore pressures from either the vertical or radial equilibrium equation. It is generally found that when one equation is satisfied, the stresses do not obey the other equation precisely[2]. This discrepancy reflects the errors in initial flow field, which was derived from potential theory and cannot be expected to be exactly compatible with the soil model used in (4).

Closed-form solutions may be derived for the stresses in the far field

---

[1]Baligh and his co-workers define 'z' as the vertical upward distance from the pile tip (This Thesis uses the term 'h' to denote this distance).

[2]Whittle & Aubeny (1990) have used an 'averaged approach' by solving equilibrium in the form of a Poisson equation.

(away from the high strain levels close to the pile). It is recommended for the reader wishing to gain a better appreciation of the above steps to refer to Baligh's derivation of these solutions (Baligh 1985).

2.3.2.3 Predicted strain paths

A clear picture of the process of pile installation, as predicted by the SPM, is shown on Figure 2.8. This figure plots the variations of the vertical strain (E_1), the cavity expansion strain (E_2) and the simple shear strain (E_3) experienced by three soil elements (A,F,G) as each passes the pile tip during installation. Several interesting features are apparent:

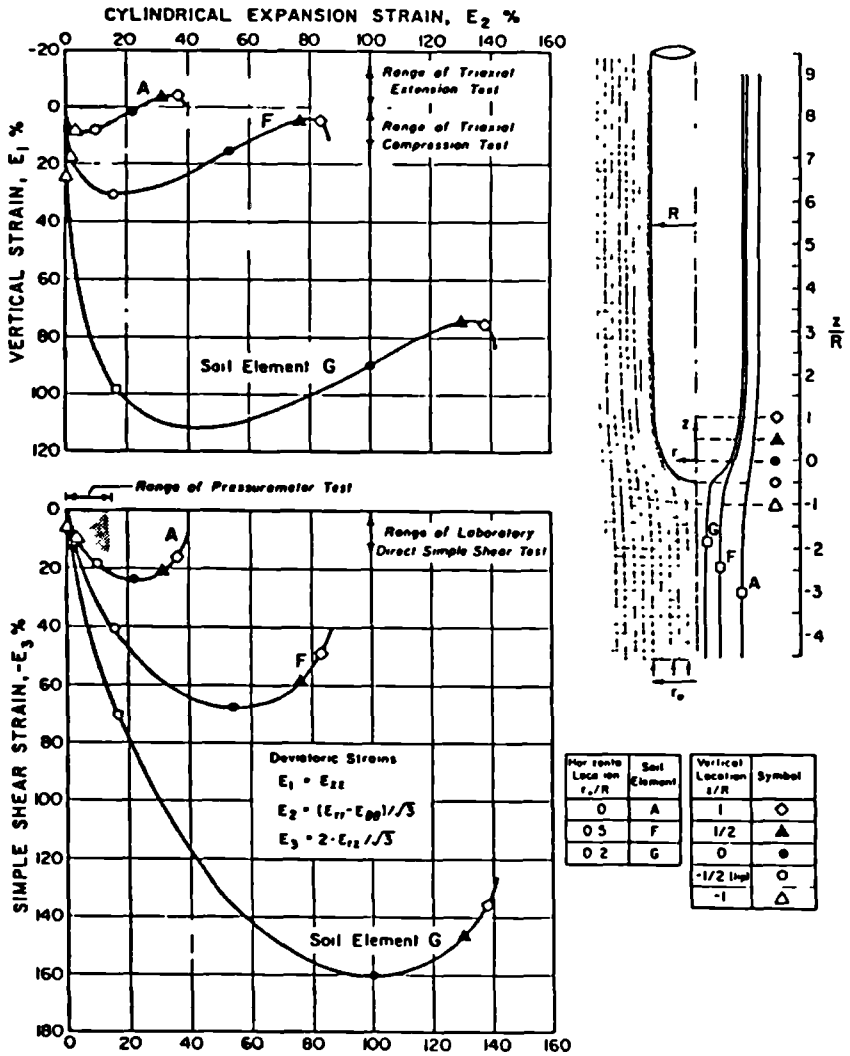

Horizontal Location r_o/R	Soil Element
0	A
0.5	F
0.2	G

Vertical Location z/R	Symbol
1	◇
1/2	▲
0	●
-1/2	○
-1	△

Figure 2.8 Strain paths followed during penetration of a 'simple pile'

(i) Each component of strain has a maximum when the soil element is at a different location relative to the pile tip; vertical strains are a maximum below the pile tip, whilst cavity expansion strains reach a maximum near the shoulder of the pile tip.

(ii) The soil elements are not strained monotonically. Simple shear and vertical strains increase monotonically until the soil elements are at or close to the pile tip but with continued penetration, as the pile tip advances to deeper levels, the sign of the incremental strains reverse and can even reverse again after further penetration. Cavity expansion strains may also show strain reversals for piles with different tip geometries (e.g. 60° cone, Levadoux & Baligh 1980).

(iii) Post-peak behaviour of the soil has a powerful influence on installation behaviour, because of the very large strain levels to which the soil elements in the vicinity of the pile are subjected to.

These predictions suggest that any method which does not incorporate the correct strain history of soil elements (e.g. the CEM which assumes that soil elements experience a monotonic increase in cavity expansion strain only) will not evaluate non-linear effects adequately.

2.3.2.4 Discussion

Some particular features of, and tentative assumptions made in, the SPM should be borne in mind before examining theoretical predictions:

(i) An important consequence of the soil flow analogy is that scale effects can be removed by normalising distances with respect to the pile radius (R). For example, the stresses or displacements evaluated at a given normalised radial distance from the centreline (r/R) and height from the tip (h/R or 'z'/R) are independent of the pile radius.

(ii) The shearing resistance of the soil is ignored in the calculation of soil velocities during installation but is invoked for the calculation of stresses. These assumptions lead to anomalies, particularly with regard to the shear stresses developed at the

pile shaft[1].

(iii) The SPM assumes implicitly that a pile is installed to its final penetration depth instantaneously and conditions are fully undrained. Real piles are, however, installed in a series of discrete hammer blows or jack pushes and therefore subject the soil to quite severe load cycles. Partial equalisation may also take place during the pause periods between hammer blows.

2.3.3 The MIT-E3 soil model

Predictions of pile behaviour using the Cavity Expansion and Strain Path methods have shown that the constitutive model used for the soil has a critical influence on evaluated behaviour (e.g. see Morrison 1984, Whittle 1987).

Initial studies with the SPM and other theoretical approaches for evaluating the performance of embankments on soft ground, led to the development of a range of soil models at the Massachusetts Institute of Technology (MIT), the most recent of which is called MIT-E3. MIT-E3 was designed to model the following aspects of soil behaviour which were expected to have an important influence on pile predictions:

- Anisotropic hardening
- Undrained brittleness in lightly overconsolidated materials
- Non-linearity in undrained shear at small strains
- Irrecoverable (plastic) strains pre-yield

These features are not incorporated in Modified Cam Clay (MCC) - the best known of the elasto-plastic (effective stress) soil models.

A full description and discussion of MIT-E3 and its validation (for OCR's <8) is given in Whittle (1987). While the model appears to be a considerable improvement on existing models, the following limitations

---

[1]Houlsby & Teh (1988) have attempted to correct for the effects of pile surface roughness and a finite shear strength at the pile surface by applying a set of correction forces to the SPM solution in a finite element analysis. This approach appears very promising.

are worthy of note:

- 15 input parameters are required for MIT-E3, compared to 5 for the simplest version of MCC. The selection of these parameters is often made difficult by the variability or shortage of test data (see Appendix C).
- Ultimate conditions are reached on the critical state line and the possibility of residual sliding on shear surfaces is neglected.
- The potential effects of initial structure on the compressibility and strength characteristics of clay cannot be accounted for. The model assumes implicitly that behaviour is normalisable i.e. there is a unique state boundary surface.
- The SPM predicts extremely high shear strain rates close to the pile during installation. These decay rapidly with distance from the pile. However MIT-E3 takes no account of the strain rate dependent properties shown by most clays.
- Other phenomena which are known to have an effect on the behaviour of soils, such as bonding or ageing effects, are not included.

The key MIT-E3 parameters used in documented SPM analyses are summarised in Table 2.1. These analyses have predicted pile behaviour in the following materials for a range of overconsolidation ratios.

- The ICP tests in Bothkennar Clay. 'Class A' & Class C calculations were performed and are referred to as BC(A) & BC(C) respectively; see Appendix C.
- Boston Blue Clay (BBC); Whittle & Baligh (1988) & Azzouz et al (1990)
- Haga clay; Whittle (1991)
- London clay (LC); Bond (1990)
- Empire clay (Emp); Whittle & Baligh (1988)

The reader wishing to study the MIT-E3 model in detail is referred to Whittle (1987).

Parameter		BC(A)	BC(C)	BBC	Haga	LC	Emp
e_{100}	Void ratio at σ'_v =100kPa on VCL	1.75	1.55	1.12	1.08	1.21	1.26
C_c	Compressibility of virgin clay at OCR=1	1.11	0.84	0.42	0.34	0.40	0.63
h	Irrecoverable plastic strain	2.5	1.0	0.2	0.2	0.1	0.2
C_r	Non-linear vol-	2.4	10.0	22.0	22.0	65.0	24.0
n	umetric swelling coefficients	3.0	1.75	1.6	1.6	1.75	1.75
ϕ'_{tc}	Critical state friction angle in triax. comp.	42°	35°	33°	33°	22°	24°
s_t	strain softening in undrained triax. comp.	10.0	4.2	4.5	4.5	3.9	3.0
ω	Non-linearity at small strains	0.5	0.1	0.07	0.07	0.2	0.2
κ_0	Small strain compressibility	0.002	0.005	0.001	0.001	0.001	0.0035

Table 2.1 Input parameters for SPM/MIT-E3 analyses

Predictions made by these SPM/MIT-E3 analyses for pile installation, equalisation and load testing are discussed in the following three sub-sections. The results are presented in terms of the normalised parameters defined in Section 2.1.2.

2.3.4 Predictions for pile installation

A typical example of the stresses predicted just after pile installation in a contractant material (BC(A)) is shown on Figure 2.9 (Whittle 1991).

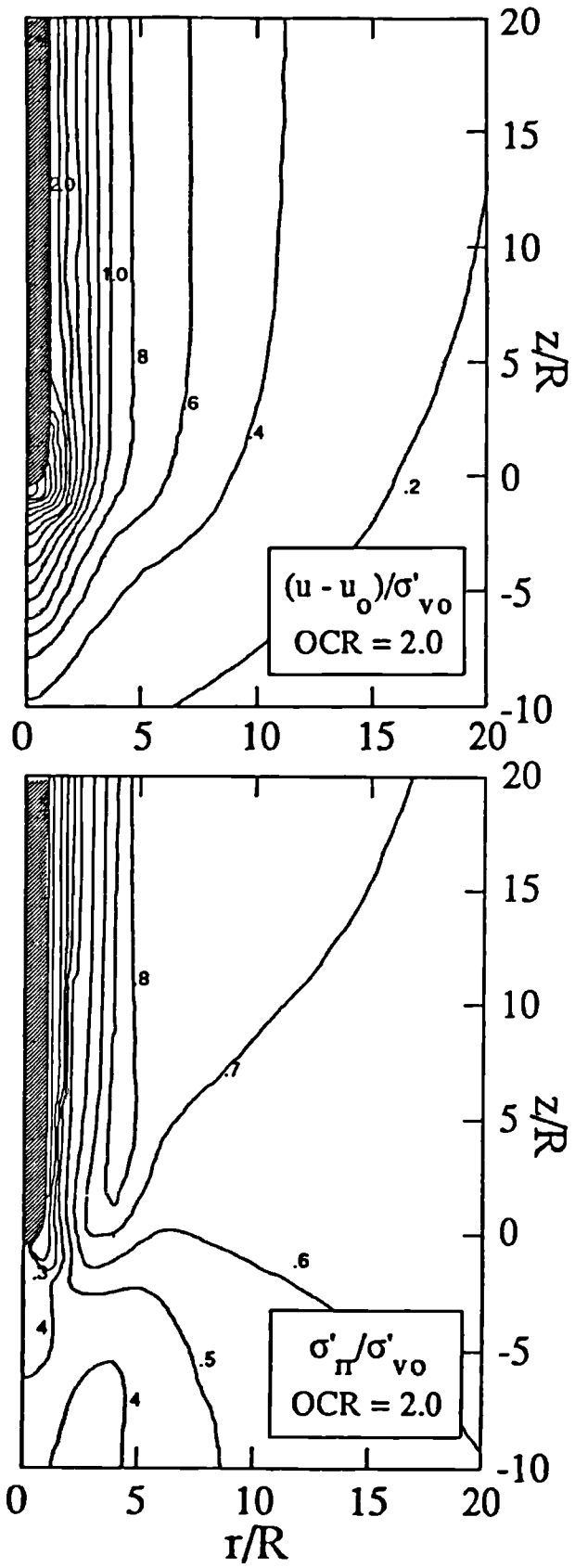

Figure 2.9 Pore pressures and radial effective stresses predicted for pile installation in Bothkennar clay [BC(A)]

Points to note include:

- There are significant gradients of radial effective stress and excess pore pressure close to the pile tip, but at distances greater than 10-15 pile radii above the tip, these stresses are relatively insensitive to the position of the pile tip.
- At locations above the pile tip, pore pressure ratios remain constant from r/R=1 to r/R≈2 and then reduce to about 20% of these values at r/R ≈10.
- Radial effective stresses (σ'_r) at the pile shaft are about five times *lower* than the initial undisturbed horizontal stress (σ'_{h0}) which is $=0.7\sigma'_{v0}$ for the case analysed on Figure 2.9. σ'_r increases with r/R and is comparable to σ'_{h0} at r/R≈5.

The predictions for the excess pore pressures developed in low OCR materials indicate that the OCR and the small strain compressibility of the material (κ_0) (see Table 2.1) have the greatest effect on the computed radial distribution of pore pressures. This is illustrated on Figure 2.10, which plots the *normalised* excess pore pressures ($\Delta u/\Delta u_{shaft}$) against log (r/R) for a range of OCR and κ_0 values. A more dramatic reduction of ($\Delta u/\Delta u_{shaft}$) with distance from the pile is evident in materials of higher small strain compressibility (e.g. high plasticity clays) and higher OCR. However, all predictions suggest that significant excess pore pressures extend to over 10 radii from the pile shaft.

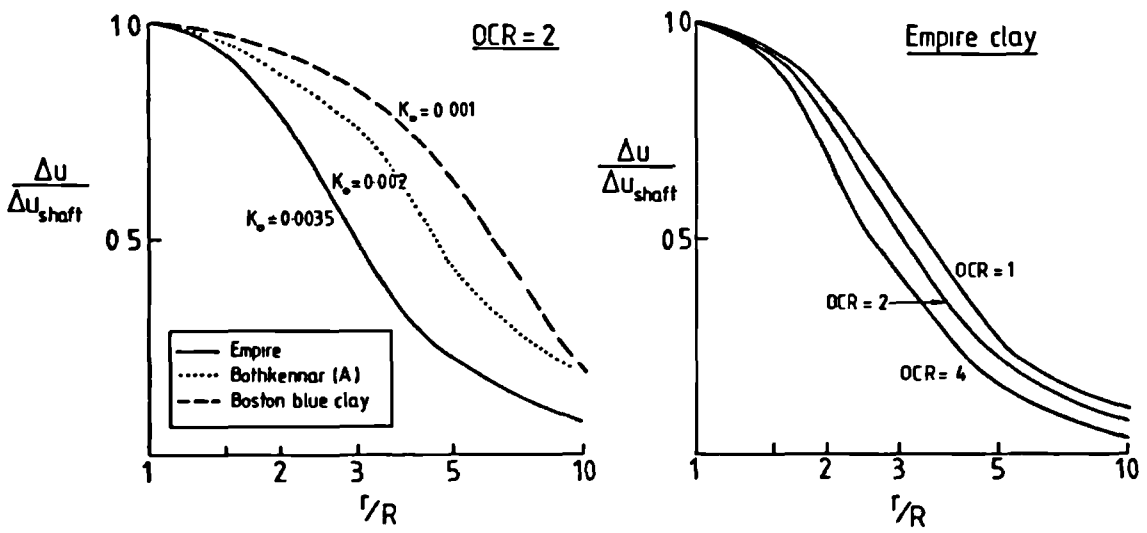

Figure 2.10 Predicted $\Delta u/\Delta u_{shaft}$ v r/R variations

SPM/MIT-E3 analyses of pile installation in heavily overconsolidated (dilatant) London Clay suggest that the maximum pore pressure occurs remote from the pile shaft at $r/R \approx 1.5$ and is about 50% higher than that at the shaft. Bond (1990) attributes this pattern to the *negative* shear induced excess pore pressures predicted for this material.

The predictions for the radial total stresses and excess pore pressures (in normalised form) developed on piles following installation in the materials listed in Table 2.1 are summarised on Figure 2.11 for points on the shaft *at least 20 radii above the pile tip*. Presented in this format, the data illustrate important features of SPM/MIT-E3 predictions.

(i) The radial total stress parameter, H_1 [$= (\sigma_{r1}-u_0)/\sigma'_{v0}$], appears to be most strongly dependent on OCR and follows the trend line $H_1 = 1.3\ OCR^{0.55}$ very closely for all analyses, despite significant differences between the soil properties specified for each material.

(ii) Assuming that the in-situ K_0 value ($\sigma'_{h0}/\sigma'_{v0}$) is given by $K_0 = (1-\sin\phi')OCR^{\sin\phi'}$ (after Mayne & Kulhawy 1982), then for a typical ϕ' value of 25°, $K_0 = 0.580CR^{0.42}$ and predicted H_1/K_0 ratios vary between 2.2 and 3.5 for OCR's between 1 and 30.

(iii) Excess pore pressure ratios ($\Delta u_1/\sigma'_{v0}$) increase with OCR in a similar fashion to the H_1 values, but show a greater dependence on soil properties.

Inspection of the input parameters used for each material suggested that, in addition to OCR, the sensitivity (as described by the MIT-E3 parameter s_t) and the soil stiffness control the magnitudes of the excess pore pressure ratios and radial effective stresses, (note that $H_1 = K_1 + \Delta u_1/\sigma'_{v0}$; see Section 2.1.2). For the materials analysed, the sensitivity and stiffness values specified are such that H_1 is almost constant for a given OCR.

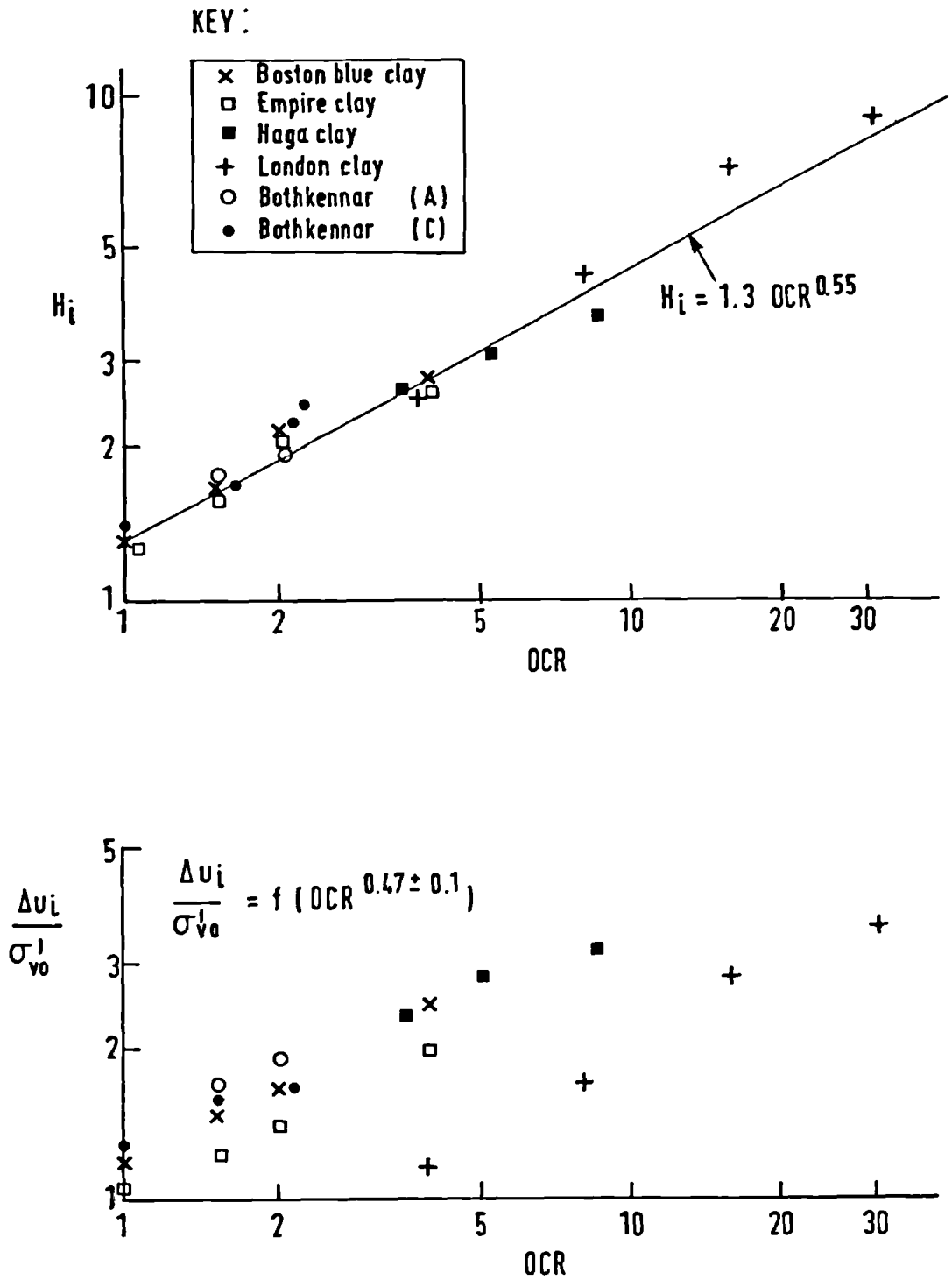

Figure 2.11 Predicted variations of H_i and $\Delta u_i/\sigma'_{vo}$ with OCR

2.3.5 Predictions for equalisation

2.3.5.1 General

The effective stresses in the soil surrounding a pile change after installation, as excess pore pressures dissipate. Levadoux & Baligh (1980), amongst others, have shown that pore water migrates primarily in the radial direction and that the rate of dissipation depends on the soil permeability (k_h), the pile radius (R), the soil 1-D compressibility (m_h) and the radial extent and distribution of the excess pressures.

Sills (1975) showed that radial total stresses remain constant for a linear-elastic, isotropic material undergoing radial consolidation around a pile shaft, so that changes in radial effective stress during equalisation would match the changes in pore pressure exactly. However, experimental observations have shown that radial total stresses do not remain constant (see Section 2.4), indicating that the soil's response is non-linear. Use of a comprehensive soil model and a consolidation theory that models the interaction of the soil skeleton and pore water during dissipation is therefore vital to the prediction of effective stress changes during equalisation. The accuracy of predictions is also of course strongly dependent on the stress regime assumed to exist after installation.

2.3.5.2 Linear analysis

Linear consolidation analyses assume that the pore pressure dissipation process is independent of the effective stress changes taking place during equalisation. A 2-D analysis can be performed relatively easily using the finite difference method to solve the governing differential equation, assuming that the horizontal coefficient of consolidation (c_h), defined as $k_h/m_h\gamma_w$, remains constant[1]. Published solutions for excess pore pressures existing at any time 't' after installation are presented in terms of a time factor T, usually defined at $T = c_h t/R^2$.

The simplicity of linear analyses is partly offset by the difficulty in

[1]The governing equation is derived assuming both k_h and m_h remain constant.

selecting an appropriate value of c_h, which is known to depend on stress history, stress level and stress increment. Based on considerations of the stress state in the soil following installation, Levadoux & Baligh (1986) proposed that the pore pressure dissipation process in both contractant and dilatant materials can be approximated using a linear analysis and the small strain swelling or recompression c_h value of the soil. This hypothesis is supported by data recorded in instrumented pile tests (see Section 2.4).

Parametric studies by Levadoux & Baligh (1980, 1986) and Houlsby & Teh (1988), using linear analyses, revealed the following characteristics of the dissipation process:

- Consolidation is controlled by the horizontal coefficient of consolidation (c_h) and is not affected significantly by different permeabilities in the horizontal and vertical directions.
- Pore pressure dissipation at the pile shaft is faster close to the tip, due to the more three dimensional nature of pore water flow at this location. Dissipation rates are typically over three times faster at the pile tip than at 10 pile radii above the tip.
- Materials with a higher rigidity index [$I_r = \sqrt{(G/c_u)}$] exhibit slower dissipation rates. (Note that I_r generally reduces with increasing OCR, Jardine 1985)
- Time factors for a given degree of dissipation are higher for more extensive initial pore pressure fields (Typical SPM/MIT-E3 predictions for pore pressure fields are shown on Figure 2.10).

2.3.5.3 Non-linear analysis

Non-linear analyses incorporate the dependence of soil stiffness on strain level and stress state. The permeability (k_h) is usually assumed constant but may also be allowed vary as a function of void ratio or stress level. The analyses require a finite element code and, because of their complexity, are one dimensional (i.e. radial axisymmetric analyses). Solutions for both pore pressures and effective stresses are presented for time factors $T_p = k_h p'_0 t/\gamma_w R^2$, where p'_0 is the initial undisturbed mean effective stress.

Examples of the stress changes predicted at the pile shaft in a non-linear analysis using MIT-E3 and initial stresses from the SPM are shown on Figure 2.12, which compares predictions for piles installed in lightly overconsolidated Bothkennar Clay (OCR=2) and heavily overconsolidated London Clay (OCR =24).

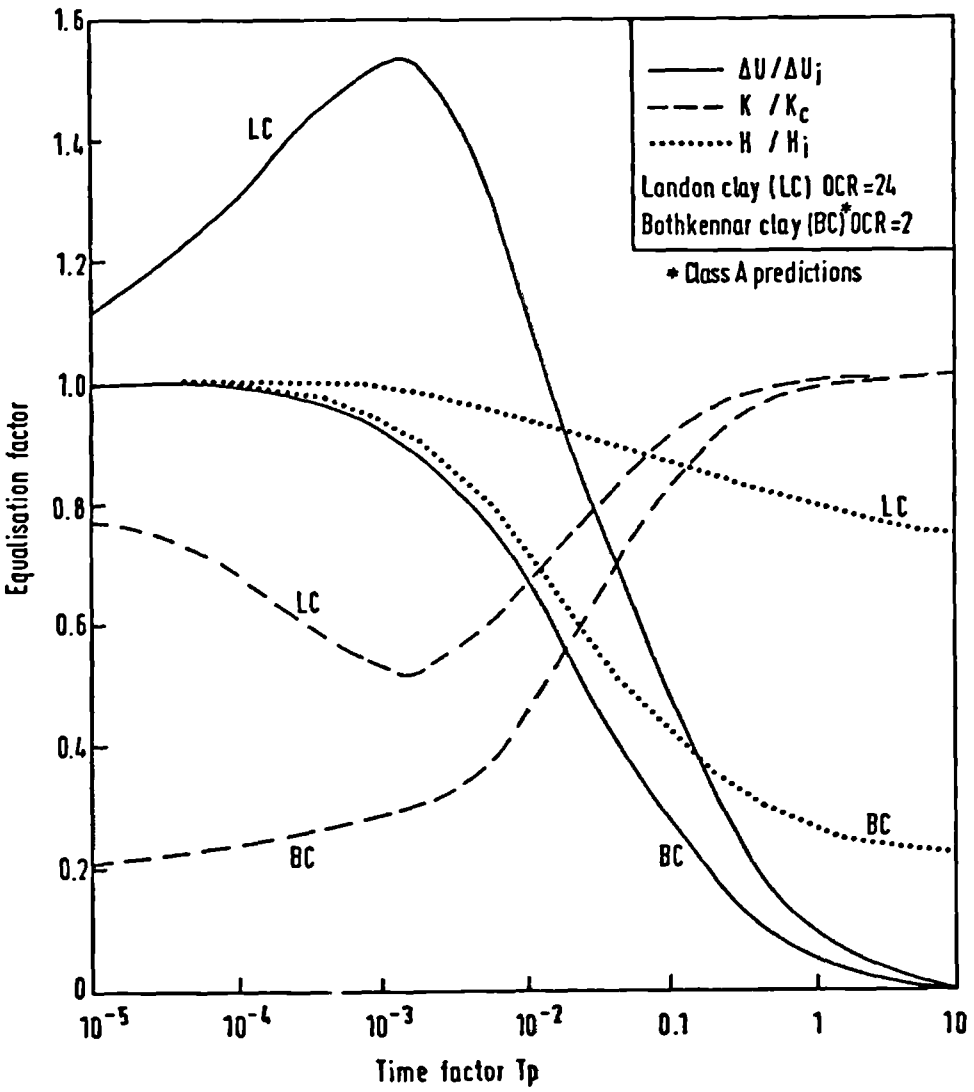

Figure 2.12 Predicted stress changes during equalisation

It can be noted that:

- The pore pressure factors ($\Delta u/\Delta u_i$) in London Clay show an initial rise before falling. This response is due to the large *negative* shear induced excess pore pressures predicted close to the pile

during installation in this material. The increase in pressure after installation arises because the higher initial pressures remote from the shaft (see Section 2.3.4) cause water to flow radially towards the shaft over the early stages of equalisation

- In the lower OCR Bothkennar Clay, shear induced pressures are positive and add to those induced by the increase in mean stress, leading to a monotonic decrease of $\Delta u/\Delta u_1$ during equalisation.
- Radial total stresses, [$H = (\sigma_r - u_0)/\sigma'_{v0}$], reduce during equalisation. This reduction is far more significant in the low OCR, sensitive Bothkennar Clay.
- Radial effective stresses ($K = \sigma'_r/\sigma'_{v0}$) reduce during the early stages of equalisation in the London Clay (as pore pressures increase) and then increase to final values that are about 20% higher than those measured during installation. The increase in radial effective stress is much larger in Bothkennar Clay, where equalised stresses (K_c) are about five times larger than installation stresses.

Examination of the trends shown by SPM/MIT-E3 predictions for the clays listed in Table 2.1 suggested that the clay sensitivity and OCR had the most significant effect on the magnitude of the relaxation coefficient (K_c/H_1); this parameter has a critical influence on the shaft capacity mobilised after equalisation.

The MIT-E3 model expresses sensitivity in terms of a parameter (s_t) which has no direct physical meaning and is derived using computer aided techniques which 'curve-fit' the triaxial test data of a given material. MIT-E3 does, however, use the void ratio at σ'_v =100kPa (e_{100}) on the virgin compression line (VCL) as an input parameter and this ratio may be used to calculate the void index at 100kPa (I_v^{100}) which provides a good measure of the clay sensitivity prescribed in the analyses (see Burland 1990). I_v^{100} is defined as $(e_{100} - e_{100}^*)/C_c^*$, where e_{100}^* is void ratio at σ'_v =100kPa of the intrinsic (normally consolidated, reconstituted) material and C_c^* is the compressibility of the intrinsic material.

The dependence of the predictions for the relaxation coefficient (K_c/H_1)

on I_v^{100} and OCR for the cases listed in Table 2.1 is shown on Figure 2.13. The intrinsic properties were estimated using correlations with the void ratio at liquid limit proposed by Burland.

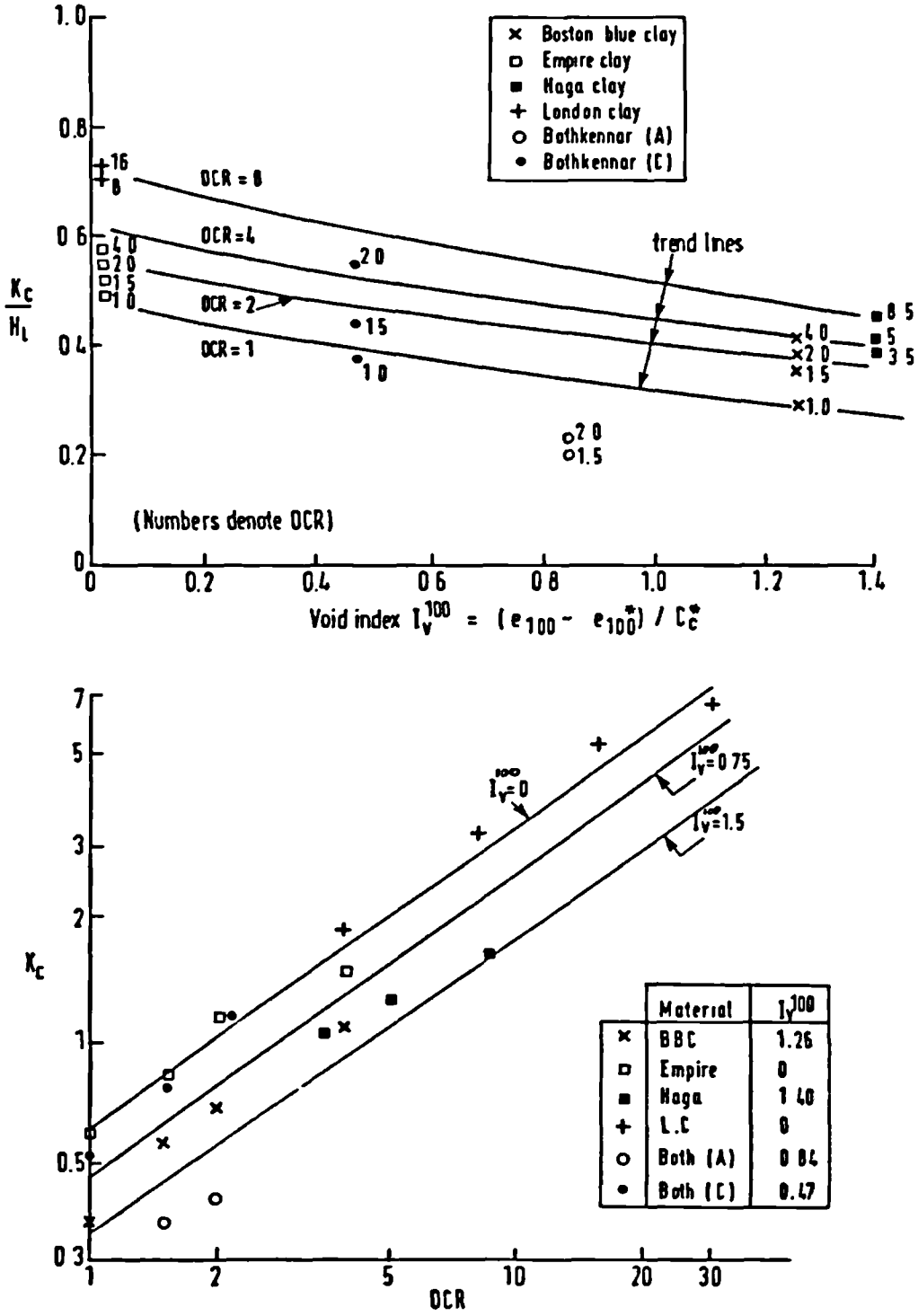

Figure 2.13 Predicted dependence of K_c/H_i and K_c on I_v^{100} and OCR

It is seen that K_c/H_1 decreases with I_v^{100} (i.e. decreases with increasing sensitivity) and increases with OCR. The relatively small scatter in the data suggests that other specified factors controlling the equalisation process such as the clay compressibility, small strain stiffness and friction angle may have had some systematic and compensating relationships with regard to the prescribed soil sensitivity.

The equalised lateral stress coefficient K_c ($=\sigma'_{rc}/\sigma'_{v0}$) is given by the product of H_1 and the relaxation coefficient and is therefore strongly dependent on OCR and sensitivity (or I_v^{100}). This dependence is confirmed on Figure 2.13, which plots mean regression lines of equal void index (I_v^{100}) through the 'K_c v OCR' predictions.

2.3.6 Predictions for pile loading

2.3.6.1 Analytical predictions

Whittle & Baligh (1988) and other workers at MIT have made predictions for the stress paths followed during undrained loading of a rigid pile using the Finite Element Method and assuming the initial stresses derived in SPM/MIT-E3 analyses. The analyses discounted two dimensional effects close to the pile tip and the ground surface and assumed that stresses varied in the radial direction only.

Predictions for the variation of shear stress with radial effective stress (τ_{rz} v σ'_r) during pile loading (up to peak shear stress) are shown on Figure 2.14 for Boston Blue Clay (BBC), Bothkennar Clay (BC) and London Clay (LC). These paths have been normalised by the pre-loading (equalised) radial effective stress (σ'_{rc}) and indicate:

- significant reductions in radial effective stress in the low OCR Bothkennar and Boston Blue clays, giving a ratio $K_f/K_c = (\sigma'_{rf}/\sigma'_{rc})$ of 0.68 ± 0.08. Little change in σ'_r is predicted for pile loading in London Clay ($K_f/K_c \approx 1.0$)
- very high residual shear stresses locked into piles in the London Clay.
- obliquities at peak shear stress (δ_p) of ≈24° for all materials, apart from the London Clay at OCR=24 which gave $\delta_p \approx 19°$.

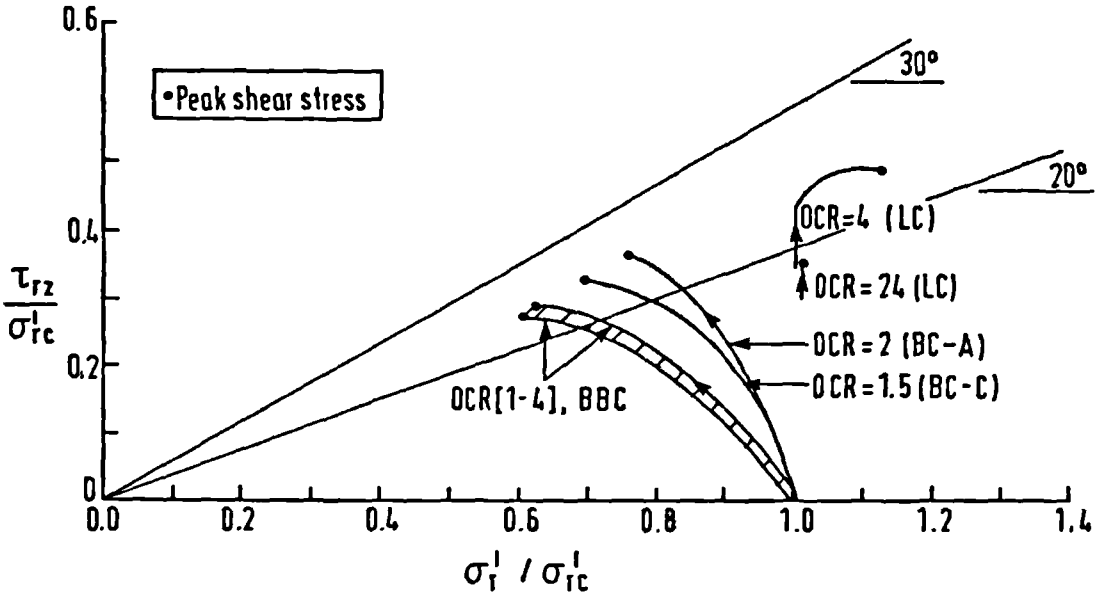

Figure 2.14 Predicted pile loading stress paths

Post-peak, the analyses predict that σ'_r continues to reduce, while the obliquity increases to reach an ultimate value equivalent to the critical state friction angle of the material (ϕ'_{cv}).

Jardine & Potts (1988) predicted the stress paths to failure followed during loading of piles supporting the Hutton tension leg platform in the North Sea. This analysis (i) employed a non-linear elasto-plastic constitutive model for the soil[1], (ii) specified failure characteristics at the pile-soil interface using data from ring shear interface tests and (iii) assessed the pre-loading stresses from the available data base of stress measurements made by displacement piles. Virtually no change (either pre- or post-peak) in σ'_r during loading was predicted, although the in-situ material was in a lightly overconsolidated stress state.

2.3.6.2 Predictions using the Direct Simple Shear (DSS) tests

The kinematic boundary constraints imposed on soil elements adjacent to a rigid pile at locations remote from the pile tip and ground surface are such that, for a no slip condition, these elements are subjected to pure shear during undrained loading i.e. the shear strain is the only non-zero

[1]This was a variant of MCC.

strain component. For this reason, Randolph & Wroth (1981) proposed that constant volume Direct Simple Shear (DSS) tests on (K_0) normally consolidated clay might be used to predict the variation of σ'_r during pile loading (taken to be equivalent to changes in the normal effective stress in DSS tests) and the obliquity at peak shear stress.

Studies by Whittle & Baligh (1988), using MIT-E3, and Potts & Martins (1982), using MCC, have suggested that the pile loading stress paths will differ from those measured in DSS tests at OCR=1. Although SPM/MIT-E3 analyses predict that the clay is in a normally consolidated state after equalisation, the studies have shown that, because of the differences between the consolidation stress conditions in the DSS apparatus and those (predicted) adjacent to a pile, the results from DSS tests performed on (very) lightly overconsolidated samples will match the pile loading stress path more closely. Azzouz, Baligh & Whittle (1990) concluded from analyses of this type that, in low OCR materials (OCR ≤4), the loading stress path is approximately equivalent to that measured in DSS tests on intact material at an OCR=1.2 ±0.1.

In a parametric study on the effect of the pre-loading stresses on the pile loading paths followed in Boston Blue Clay, Whittle & Baligh (1988) found that when the prescribed pre-loading ratio of the vertical to radial effective stress ($\sigma'_{zc}/\sigma'_{rc}$) was increased from 0.48 to 1.54, predictions for δ_p rose from 19.1° to 32.4°. The ratios $\sigma'_{\theta c}/\sigma'_{rc}$ and $(\tau_{rz})_c/\sigma'_{rc}$ were also seen to affect the value of δ_p, but to a lesser extent than the $\sigma'_{zc}/\sigma'_{rc}$ ratio.

2.3.6.3 Coefficients of friction ($\mu = \tan\delta_p$)

While the *changes* in the stress state during pile loading can only be predicted using a numerical analysis, coefficients of friction ($\mu = \tan\delta_p$) may be assessed by assuming a given failure mode of the soil adjacent to the pile shaft. Some of the most popular of these assumptions are summarised in Table 2.2.

μ	Values of μ for $\phi'=25°$	Assumption
1. $\tan \delta$	0-0.47	Failure controlled by slippage at pile-soil interface (angle depends on soil composition, shearing mode, pile surface properties etc.)
2. $\tan \phi'$	0.47	Failure on a vertical surface within the soil, inclined at $(45 - \phi'/2)$ to σ'_1 direction
3. $\sin \phi'$	0.42	Max τ on a vertical surface within the soil, pile axis at 45° to σ'_1 direction
4. $\frac{\sin\phi' \cos\phi'}{1 + \sin^2 \phi'}$	0.32	Failure is initiated on horz. planes within the soil, inclined at $(45 + \phi'/2)$ to the σ'_3 direction (OCR=1) (see Randolph & Wroth 1981)
5. Depends on ϕ' + initial stresses	0.32-0.47	Simple shear SPM/MIT-E3 analysis (Whittle & Baligh 1988)

Table 2.2 Interpretations for the coefficient of friction

The assumed failure criterion can only be validated or discounted by the results from instrumented pile tests which measure values of μ. An important feature of displacement piles, which was demonstrated by Chandler & Martins (1982) and Bond (1989), amongst others, is that installation process can lead to the formation of low strength residual surfaces either at the pile surface or within the soil. The drained strength of these surfaces can be well below the critical state strength (ϕ'_{cv}) of the material and is best measured using the ring shear apparatus (e.g. see Tika-Vassilikos 1991).

2.4 INSTRUMENTED DISPLACEMENT PILES IN CLAY

2.4.1 General

The measurement of stresses acting on piles requires the use of instrumentation which is both robust and sensitive. Careful attention to design detail is required to ensure that sensors have good linearity characteristics, respond quickly to a change in applied stress and are both stiff enough to ensure minimal under-registration and compliant enough that stresses are recorded to an acceptable accuracy (see Appendix A). Many attempts to instrument piles have been unsuccessful because of large shifts in zero outputs and calibration coefficients of sensors. These have occurred due to moisture ingress, high accelerations during pile installation and other effects.

A review of the literature revealed 10 case histories where high success has been achieved with the instrumentation of displacement piles in the field and a further 10 case histories where fair/good quality data was measured. This section summarises the general trends observed in these tests. Tables 2.3 lists the case histories where the measurements obtained are considered to be of a sufficiently high quality to develop correlations for displacement piles in clay, whilst those listed in Table 2.4 have not been included in this data base for the reasons given.

The characteristics of displacement piles presented in this section have been summarised from the detailed review given in Appendix B, which considered the soils encountered, the instrumentation used and the measurements made at each site. This appendix also provides a data base of measurements (using normalised parameters defined in Section 2.1.2) with which the results from the ICP tests at Cowden and Bothkennar may be compared. Further use will be made of these data in Chapters 10 & 11.

No.	Site	Soil type	Reported by
1	Canons Park, London	London Clay	Bond (1989), Bond & Jardine (1990), Coop (1987)
2	Madingley (Cambridgeshire)	Gault Clay	Coop (1987), Coop & Wroth (1989)
3	Huntspill (Somerset)	Alluvium	Coop (1987), Coop & Wroth (1989)
4	Gt Yarmouth (E. Anglia)	Alluvium	Coop (1987)
5	MIT & Saugus (Mass. USA)	Boston blue Clay	Morrison (1984), Azzouz & Morrison (1988)
6	Empire (Louis. USA)	Empire Clay	Azzouz and Lutz (1986)
7[1]	St-Alban (Québec, Can)	Champlain Clay	Roy et al. (1981), Roy & Lemieux (1986), Konrad & Roy (1987)
8	Haga (Norway)	Haga Clay	Karlsrud & Haugen (1985)
9	Otemachi (Tokyo)	Tokyo Clay	Koizumi and Ito (1967)
10	Rio de Janeiro	Soft clay	Soares & Dias (1990)
11	Cowden (N.E. Eng)	Cowden Till	This thesis, Lehane & Jardine (1992)
12	Bothkennar (Scotland)	Bothkennar alluvium	This thesis, Lehane & Jardine (1992)

[1] only pore pressure measurements

TABLE 2.3 High quality instrumented pile tests in clay

No.	Soil type	Reported by	Remarks
A	Cowden Till	Ponniah (1989)	superseded by (12)
		McAnoy at al (1982)	(open-ended piles)
B	Alluvium	Bogard & Matlock (1990)	'fair' quality
C	Empire Clay	Bogard & Matlock (1990)	Case (7) preferred
D	Beaumont Clay	O' Neill et al (1982)	primarily pile group measurements
E	Kaolin	Francescon (1983)	high quality lab. tests
F	London Clay	Johnston (1972)	superseded by (1)
G	London Clay	Jardine (1985)	superseded by (1)
H	San Francisco bay mud	Kirby & Roussel(1980), Reese & Seed (1955)	poor inst. drift
I	Quick Clay	Kenney (1967)	pile did not plug
J	Soft Clay	Nauroy et al (1985)	poor inst. drift

TABLE 2.4 Fair/good quality instrumented pile tests in clay

2.4.2 Installation

In all the tests listed in Tables 2.3 and 2.4, piles were *jacked* to their final penetration in a series of pushes equivalent to the stroke of the jack. The main characteristics of the measurements made are as follows:

1. In almost all cases, the radial total stresses (σ_{ri}) developed on the pile shaft during installation (σ_{ri}) are considerably less than the stress required to expand a cylindrical cavity in-situ (p_{lim}), but are greater than the initial undisturbed horizontal stress (σ_{h0}).

2. Higher values of σ_{ri} are mobilised in clay strata of stronger consistency. The consistency of the clay stratum can be expressed in terms of the undrained strength (c_{u0}), CPT end resistance (q_c) or overconsolidation ratio and initial vertical effective stress (OCR and σ'_{v0}).

3. The radial and shear stresses measured at fixed depths appear to reduce as the pile tip penetrates to deeper levels (i.e. they reduce with increasing height from the pile tip). This trend was clearest in the ICP tests in the London Clay (Bond 1989), but further data are required to check if it is a general feature of displacement piles.

4. The pore pressures developed during pile installation in lightly overconsolidated and sensitive materials are comparable in magnitude to the radial total stresses (σ_{r1}). Radial effective stresses (σ'_{r1}) are therefore close to zero and usually less than the initial undisturbed horizontal effective stresses (σ'_{h0}).

5. In heavily overconsolidated clays, pore pressures reduce during jacking stages. These reductions are thought to be due to strong dilation of the material close to the pile shaft. Negative pore pressures are often measured and these may cause cavitation of the fluid of the pore pressure sensors and hence reduce their response time considerably. Calculated radial effective stresses (σ'_{r1}) in these materials are usually larger than σ'_{h0}.

6. Pore pressure reductions during penetration were noted in some low OCR materials. Coop & Wroth (1989) attribute these reductions to "measurements at the pile shaft (being) unrepresentative of those on the failure plane which may be at a small distance from the shaft". In these instances, pore pressures rose rapidly to high positive values at the completion of the pile push.

7. Excess pore pressures in contractant materials decrease with distance from the pile shaft in approximate proportion to the logarithm of the normalised radius (i.e. with log (r/R)) and extend to r/R >20. However, radial distributions of pore pressure inferred by Bond & Jardine (1991) from pore pressures recorded at the shafts of piles installed in London Clay indicated that excess pore pressures may only have extended to 4 radii from the piles.

8. In materials which are susceptible to the formation of low strength residual surfaces, the rate of pile installation can have a significant effect on the clay fabric induced close to the pile. The partial dis-ordering of the particle fabric can affect the subsequent pile capacity considerably. Bond (1989) found that the fabric created by fast-jacking in London Clay (at rate of 500mm/min) was similar to that induced by conventional pile driving.

9. The coefficients of friction ($\mu = \tan\delta_p = \tau_f/\sigma'_r$) measured during installation appear, in most cases, to be lower than coefficients measured at the slower rates of displacement used in pile load tests. This may imply, as suggested by Coop & Wroth (1989), that the measurements made during installation at the pile shaft are not representative of those acting on the principal displacement shear.

2.4.3 Equalisation

The data recorded as stresses equalised after pile installation show the following trends:

1. Pore pressures rise rapidly after installation in heavily overconsolidated clays and some low OCR materials (see point 6 above). This rise in pressure is accompanied by a corresponding reduction in radial effective stress (σ'_r). The minimum σ'_r value usually develops shortly after installation and may imply a minimum in pile capacity (Jardine & Bond 1989, Coop & Wroth 1989)

2. The pore pressure dissipation process is controlled primarily by radial drainage. Dissipation times are proportional to the square of the pile radius and backfigured coefficients of consolidation (c_h) lie within the range $0.2mm^2/s$ to $4.4mm^2$ (Bond 1989).

3. Radial total stresses generally *reduce* during equalisation. The total reductions in low OCR and sensitive materials may amount to over 50% of the radial stress measured at the end of installation (σ_{ri}). Total reductions in high OCR materials are less than $0.25\sigma_{ri}$.

4. The equalised radial effective stresses (σ'_{rc}) in low OCR and sensitive materials are significantly higher than σ'_r values measured immediately after installation, whilst, in high OCR materials, σ'_r may reduce throughout equalisation.

5. Equalised radial effective stresses appear to display a similar dependence on the distance from the pile tip to that shown by the installation radial total stresses, although no conclusive proof of this dependence has been established in any previous test.

2.4.4 Load testing

Very few measurements have been made showing how stresses vary during pile loading. It is believed that ICP tests in the London Clay (Bond 1989) are the only experiments where these changes have previously been measured to an acceptable accuracy. The London clay tests showed that:

- Radial effective stresses remained virtually constant up to peak shear stress (i.e. $\sigma'_{rf} \approx \sigma'_{rc}$)
- The obliquity at peak shear stress (δ_p) was the same as the peak residual angle measured in ring shear interface tests which simulated the displacement history of soil elements adjacent to the pile during installation.
- σ'_r generally increased post-peak (by ≈10%) as the obliquity reduced to an ultimate residual value (δ_{ult}).
- Piles re-loaded in the same direction mobilised a peak obliquity equivalent to the ultimate residual value (δ_{ult}) measured in first-time tests and as a result had a lower shaft capacity than in first-time loading.

The data from other instrumented pile test programmes (bearing in mind that these are less reliable) showed that:

- Undrained pile loading in the contractant Haga and Boston Blue clays led to reductions in σ'_r up to peak local shear stress of ≈20% and ≈50% respectively, but no equivalent change in σ'_r was measured in Huntspill clay which is also a contractant material.

- The δ_p values mobilised in the Gault and Huntspill clays were comparable to δ values measured in appropriate ring shear interface tests. No such tests were performed for other clays in the data base.
- In contrast to the trends shown by the ICP tests in the London Clay, piles in Haga Clay (tested after full equalisation) mobilised higher capacities in reload tests than in first-time tests. This was seen to be partly because smaller reductions in σ'_r took place during re-loading and δ values were marginally higher.

These observations indicate that a knowledge of factors affecting the clay behaviour at large strains (i.e. the residual strength) is vital to the prediction of pile capacity. Further reliable data concerning the pre- and post-peak changes in σ'_r is clearly required.

2.4.5 Effect of installation on soil fabric

Trial pits excavated adjacent to the piles installed in the Haga and London clays allowed the shear strains (γ_{rz}) that were induced in the soil by installation and load testing to be inferred from the orientation of bedding planes. Bond & Jardine (1991) showed that the reduction of γ_{rz} with radial distance from the pile (r/R) was similar at both sites and suggested that the pattern of shear distortion around a displacement pile is insensitive to the properties of the clay (this is the central assumption of the Strain Path Method). It was proposed that the soil adjacent to a pile could be classified into three zones, as summarised in Table 2.5.

The trial pit investigations showed that the response of the soils to the high shear strains imposed on the inner zone ($r/R < 1.5$) was dependent on the clay type. Bond & Jardine (1991) demonstrated (using X-ray photographs of thin sections) that these strains led to the formation of vertical low strength residual surfaces in the London clay, whereas Karlsrud & Haugen (1985) suggested that they caused complete "remoulding" of the (sensitive) clay at Haga (at $r/R \leq 1.1$). In pits excavated adjacent to piles in the sensitive St-Alban clay, Roy & Lemieux (1986) concluded

that the material close to the pile shaft was "destructured" but that the "destructuration" was not as severe as complete remoulding.

Zone	Extent	Properties
A	$r/R \leq 1.5$	Shear strains (γ_{rz}) have magnitudes larger than 50% and the soil may be sheared to critical state conditions.
B	$1.5 < r/R \leq 4$	The strains are high enough to cause the soil to dilate or contract but not sufficient for it to reach critical state conditions ($\gamma_{rz} < 50\%$)
C	$r/R > 4$	The soil behaves quasi-elastically

Table 2.5 Zones surrounding a displacement pile (Bond & Jardine 1991)

Measurements of the radial variations of soil properties in these trial pits showed the following characteristics (Note that the pits were excavated after equalisation and load testing):

- The water content (w) of the clays at $r/R \leq 2$ at Haga & St-Alban clays were lower than the undisturbed in-situ water content; no systematic radial variation of w in the London Clay was apparent.

- The undrained strength of the clay close to the pile shaft at Haga (measured using a fall cone) was almost double that of the undisturbed clay, whereas at St-Alban, the shear strength of the clay close to the pile shaft (measured using a field vane) was ≈30% less than that of the undisturbed clay. Pocket penetrometer measurements in the London Clay suggested that undrained shear strengths did not vary with r/R.

- Mean effective stresses (p'), estimated from suction measurements, reduced with r/R in the London clay and were equivalent to the undisturbed mean effective stresses (p'_0), at $r/R \approx 4$. The p' values close to the pile shaft were about four times p'_0, but only ≈35% of

the p' value expected at the critical state. Bond & Jardine (1991) stated these measurements proved conclusively that the London Clay was in an *overconsolidated* state after full equalisation.

CHAPTER 3

DISPLACEMENT PILES IN SAND: RECENT DEVELOPMENTS

CONTENTS OF CHAPTER 3

DISPLACEMENT PILES IN SAND: RECENT DEVELOPMENTS

3.1 INTRODUCTION 62

3.2 DESIGN METHODS FOR DISPLACEMENT PILES IN SAND 63

3.2.1 Shaft capacity

3.2.1.1 Conventional 'earth pressure' approach 63

3.2.1.2 Correlations with in-situ test parameters 65

3.2.1.3 Average shear stress approach 66

3.2.2 Base capacity 67

3.3 MODEL PILE TESTS 69

3.3.1 Stress distribution and displacement paths 71

3.3.2 Density changes 72

3.3.3 Average shaft shear stress 74

3.3.4 Local radial and shear stress 76

3.4 FIELD MEASUREMENTS 80

3.4.1 Residual stresses 80

3.4.2 Variation of τ_{av} with depth 81

3.4.3 Tension and compression shaft capacities 82

3.4.4 Pile end condition 82

3.4.5 Effect of installation method 83

3.4.6 Pile set-up 84

3.4.7 Definition of failure 84

3.4.8 Measurements of local shear stress 84

3.4.9 Measurements of local radial stress 86

3.4.10 Trends inferred from local measurements 88

3.5 FINAL COMMENTS 89

3.1 INTRODUCTION

Skempton et al (1953) remarked that the contribution of the shaft friction to the total capacity of a pile in sand is sufficiently small that it may be neglected completely. However, with the new demands for larger structures, it has become necessary to design longer piles that rely on shaft friction. Discounting this friction would not only be very uneconomical, but also unsound, as the performance of the structure under service loads depends almost entirely on the shaft characteristics.

There is, however, a dearth of information available on the stresses developed on displacement piles in sand. No theoretical method for design has been proposed (yet alone validated) and design at present is based on purely empirical methods. Poulos (1989) in his Rankine lecture stated:

"A number of significant aspects of pile behaviour lack a proper theoretical framework of understanding including..... the behaviour of piles in sand. There is substantial scope for further research into such aspects so that those aspects of pile design which are still empirical may ultimately be replaced by more soundly-based approaches."

As seen in Chapter 2, the development of a theoretical framework for piles in clay has made significant advances over the past 20 years. However far less comparable research has been carried out for piles in sand. The reasons for this include:

- Until recently, the shaft capacity of a pile in sand represented a small fraction of the total capacity.
- The development of a theoretical model is complicated by the particulate and free draining characteristics of sand. The results from some of the first laboratory model pile tests showed that the installation process causes apparently random changes in the in-situ density and associated changes in the frictional and stiffness properties of the material.
- It is almost impossible to retrieve undisturbed samples in sand and reliance has to be placed on in-situ tests and reconstituted laboratory samples.

- There has been virtually no instrumented field pile tests in sand where reliable measurements of radial stress, pore pressure and shear stress developed on the pile shaft have been recorded. In contrast, at least 20 good quality instrumented pile test programmes have been performed in clays.

Our understanding of the processes that govern pile behaviour in clays has been improved considerably through the use of high quality instrumented piles. The tests performed with the Imperial College Pile (ICP) in the sand site at Labenne (Chapters 5,6 & 9) demonstrate that such high quality tests can also allow the principal patterns of pile behaviour in sands to be identified and aid the development of rational design methods.

The review presented in this chapter discusses existing design methods for displacement piles in sand and then examines the trends shown by laboratory model piles and field piles. Attention is focused on those trends which may assist the interpretation and extrapolation of the results from the ICP tests at Labenne.

3.2 DESIGN METHODS FOR DISPLACEMENT PILES IN SAND

This section discusses some of the more popular design methods used to evaluate the shaft and base capacity of a displacement pile in sand. All of these methods are empirical.

3.2.1 Design methods for shaft capacity

3.2.1.1 Conventional 'earth pressure' approach

The most common design methods for shaft capacity assume that the local radial effective stress (σ'_{rf}) acting on the pile shaft at peak local shear stress (τ_f) is proportional to σ'_{v0} i.e.

$$\sigma'_{rf} = K\,\sigma'_{v0} \quad \text{and}$$

$$\tau_f = \sigma'_{rf} \tan \delta \qquad (\delta = \text{angle of interface friction})$$

Correlations for K are based on <u>mean</u> values [$=\tau_{av}/(\sigma'_{v0})_{mean}$] backfigured from load tests using measured[1] or assumed angles of interface friction. Meyerhof (1951) recommended K values for design of 0.5 and 1.0 for piles driven into loose and dense sands respectively, but wide variations in suggested K values can be found in the literature. For offshore piles, the most popular design method of this form is that proposed by the American Petroleum Institute (API 1989), which assumes K=1.0 for closed-ended piles and specifies the values of δ and maxima for the local shear stresses (denoted as f_{lim}) given in Table 3.1. (Note 1 ksf ≈48 kPa)

Relative Density	Soil Description	δ deg	f_{lim} ksf	N_q	q_{lim} ksf
very loose loose medium	sand sand-silt silt	15	1.0	8	40
loose medium dense	sand sand-silt silt	20	1.4	12	60
medium dense	sand sand-silt	25	1.7	20	100
dense very dense	sand sand-silt	30	2.0	40	200
dense very dense	Gravel sand	35	2.4	50	250

Table 3.1 Design values for cohesionless siliceous soils (API RP2A 1989)

It will be shown in Chapters 6 & 9 that the dependence of δ on relative density, implied by Table 3.1, is not realistic. However, as Briaud & Audibert (1990) remind us, the API procedure is a "design method and not a predictive method". The experimental evidence, discussed in Sections 3.3 & 3.4, suggests that the values of δ have been selected to compensate for the choice of a constant K value.

Shaft capacities predicted using the API method have been compared with measured capacities by many workers e.g. Lings (1985), Briaud & Tucker (1988), Toolan & Ims (1988). Lings reviewed the data from the tension

[1]From laboratory direct shear interface tests. It is surprising, however, to find that few results from such tests are reported.

piles included in the API data base and therefore, for the reasons outlined in Section 3.4.1, did not need to assess the effects of the residual loads in the piles after driving. He concluded that the API method:

- becomes progressively less conservative with increasing pile length and over-predicts capacities for piles longer than ≈30m.
- provides reasonable predictions for the shaft capacities of piles of moderate length (10-20m) in medium dense and dense sands, but over-predicts capacities in loose sand and under-predicts capacities in very dense sands. This trend reflects the bias in API's data base towards conventional onshore piles in medium to dense sands.

3.2.1.2 Correlations with in-situ test parameters

Briaud & Tucker (1988) reviewed 13 of the more popular existing pile design methods (including API) against an independent data base and concluded that the most successful of these methods was the 'LPC cone method', proposed by Bustamante & Gianeselli (1982). This method relates the local ultimate shear stress (τ_f) to the Cone Penetration Test (CPT) end resistance (q_c), as outlined in Table 3.2.

Pile type	Sand density	τ_f	$(\tau_f)_{max}$
Concrete	Loose	$q_c/60$	35kPa
	Medium-dense	$q_c/100$	80kPa
Steel	Loose	$q_c/120$	35kPa
	Medium-dense	$q_c/200$	80kPa

Table 3.2 Design values for τ_f in sands based on q_c data (Bustamante & Gianeselli 1982)

Other methods relate τ_f with the pressuremeter limit pressure (e.g. Baguelin et al 1986) and with the blowcount measured in Standard Penetration tests (e.g. Canadian Geotechnical Society 1985). The review of Briaud & Tucker and another independent review by Bustamante et al

(1991) suggest that, while the correlations with q_c may be more reliable, predictions for a given pile are generally only satisfactory if it has similar characteristics to the piles included in data base from which the design method was derived (as is the general case for all empirical methods).

3.2.1.3 Average shear stress approach

Field and laboratory pile tests, discussed in Sections 3.3 and 3.4, have shown that the average ultimate shaft shear stress (τ_{av}) mobilised on a pile installed in a uniform sand deposit is virtually independent of its length (L), if L is greater than ≈20 times the pile diameter. This trend prompted design methods that relate the value of τ_{av} to the initial consistency of the sand.

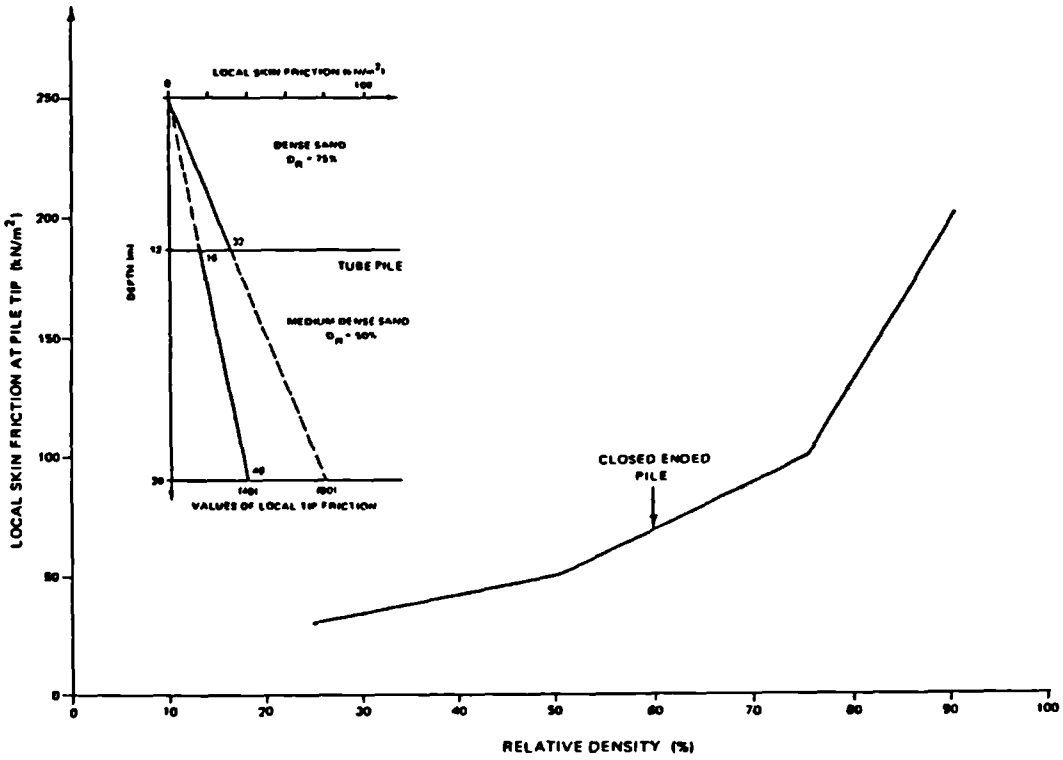

Figure 3.1 Dependence of the ultimate shear stress at the pile tip (=$2\tau_{av}$) on relative density (Toolan et al 1990)

Meyerhof (1976), Vesic (1977), Coyle & Castello (1981) and Lings (1985) proposed correlations of this form, using either interpreted values of the soil's friction angle or relative density (D_r) as a measure of the initial consistency. These correlations indicate that τ_{av} varies from ≈20 ± 10 kPa for piles in loose sand to ≈80 ± 20kPa in medium dense to dense sand. Toolan et al (1990) proposed the most recent correlation between τ_{av} and D_r, based on the results of 24 carefully selected tension pile tests[1], and in addition, suggested how this approach could be extended to estimate shaft capacities in layered sand deposits. They assumed that, in each test considered, the local ultimate shear stress (τ_f) increased linearly with depth and, consequently, the τ_f value developed at the pile tip was inferred to be twice the backfigured value of τ_{av}. The design curve for the τ_f value at the pile tip ($=2\tau_{av}$) is given on Figure 3.1 which also shows how, by using a "sliding triangle" procedure, these τ_f values may be used to evaluate the capacities in layered deposits. This method was shown to provide reasonable predictions for a large range of sand densities and pile lengths.

Potential problems and errors which can arise from using an average shear stress approach have been discussed in Section 2.2 for piles in clay. A further difficulty with using this approach for piles in sand is that τ_{av} is related to *interpreted* parameters such as relative density or friction angle. It is more desirable that correlations are made directly with measurable parameters such as the CPT q_c value to avoid the rather subjective assessment of relative density or sand friction angle. In addition, it should be borne in mind that correlations for τ_{av} which are based on the results from tension pile tests may not be applicable to compression piles.

3.2.2 Base capacity

Conventional methods for determining the unit ultimate pile end bearing resistance (q_b) in a sand use modified forms of Terzaghi's bearing capacity theory applied to deep foundations. These methods assume q_b is independent of pile diameter and can be related to the free field

[1]thereby avoiding problems associated with indeterminate residual stresses (see Section 3.4.1).

vertical effective stress (σ'_{v0}) by a bearing capacity factor N_q i.e.

$$q_b = N_q \, \sigma'_{v0}$$

One of the most popular correlations for N_q, shown on Figure 3.2, was developed by Berezantsev (1961) who suggested that the value of N_q reduced with the ratio of the pile penetration into the bearing stratum (D) divided by the pile width (B)[1]. Nordlund (1963) and Vesic (1964) showed that this correlation provided reasonable predictions for q_b values mobilised by "standard end-bearing piles" , for which D/B is typically less than 20. The N_q values recommended by API (1989), listed in Table 3.1, are seen to be more conservative than Berezantsev's values.

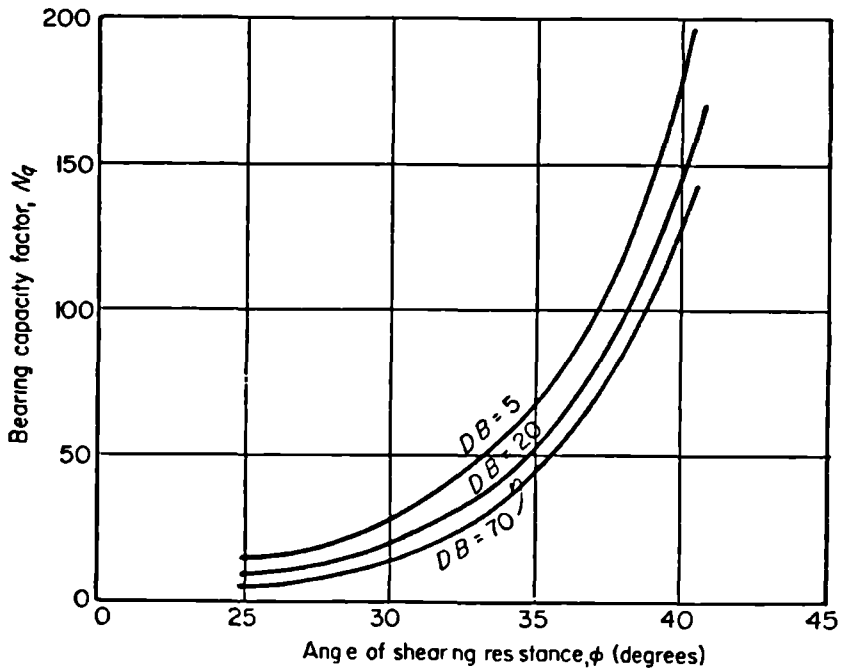

Figure 3.2 Berezantsev's (1961) bearing capacity factor, N_q

Experiments by Kérisel (1964), Vesic (1970) and Tavenas (1971), amongst others, have shown that q_b in a uniform material attains a relatively constant value below a certain 'critical depth' of between 10 and 20 pile

[1]This is a consequence of assuming that the failure surface extends from the pile base up to the top of the bearing stratum.

diameters. For this reason and to restrict pile settlements, a limiting maximum value of q_b is normally specified. The limiting values of q_b recommended by API (1989) are given in Table 3.1 (referred to as q_{lim}).

The variable trends of q_b with depth have prompted more recent approaches which relate q_b to the CPT end resistance (q_c). Meyerhof (1976) and Schmertmann (1978) suggested that q_b was equivalent to an average lower bound value of q_c in the vicinity of the pile tip. However, additional experimental data indicated that q_b reduced with pile diameter. This was thought to be due to the development of narrow shear bands at the pile base which interfere with the conventional bearing capacity mechanism. Meyerhof (1983) therefore revised his approach and proposed that q_b, for piles of greater than 500mm in diameter, should be taken as ≈2/3 and ≈1/3 of the average q_c value in loose and dense sands respectively. In the LPC cone method (see Section 3.2.1.2), a correction factor of 1/2 is applied to the averaged q_c value.

Open-ended piles may give a significantly different dependence on pile diameter to that shown by closed-ended piles (e.g. see Jardine & Christoulas 1991). Hight & Lawrence (1992) have demonstrated that the end bearing resistance of these piles is complicated further by dilation phenomena at the pile's inner wall.

3.3 MODEL PILE TESTS

Despite the great shortage of instrumented field pile tests in sand, insight into the basic mechanics of pile behaviour in sands can be obtained from the relatively large number of investigations made with model pile tests in the laboratory. The principal findings of these tests are discussed by making reference to five high quality instrumented laboratory test programmes, described in Table 3.3. The probable effect of the chamber size (and other scale effects, discussed below) on the results from these tests should be borne in mind.

D (mm)	$(L/R)_{max}$	Tank size BxL (m)	Soil props.	Features
Robinsky & Morrison (1964) and Robinsky et al (1964)				
29-36	34	0.6x0.81	Ottawa sand d_{50} ≈0.35mm D_r =[17-37]%	Disp. from radiographs of lead shots, density derived from disp., strain gauges for τ_{rz}.
Lebègue (1964)				
35-215	34	0.8x0.2	Leucate sand d_{50} ≈0.5mm D_r ≈[20-70]%	Measurement of τ_{av} for large range of pile diameters.
Wersching (1987)				
114	32	3.0x3.0	Leighton Buzzard, d_{50}≈0.45mm D_r ≈16%	τ_{rz} & σ_r measured at various levels on shaft Remote from shaft:- measured vert. disp. (with electro -levels), density (using sand /plaster method) and stresses (with diaphragm transducers).
Allersma (1988)				
50	12	0.6x0.7	Crushed glass d_{50} ≈2.5mm D_r =[10-30]%	Stresses from photoelastic props of glass, disp. from markers and camera.
Chong (1988)				
36.6	40	1.2x1.1	Leighton Buzzard, d_{50}≈0.35mm D_r =[35-95]%	Densities at and remote from pile shaft using thermocouple needle probes.

Table 3.3 Model pile tests in sand

3.3.1 Stress distribution and displacement paths

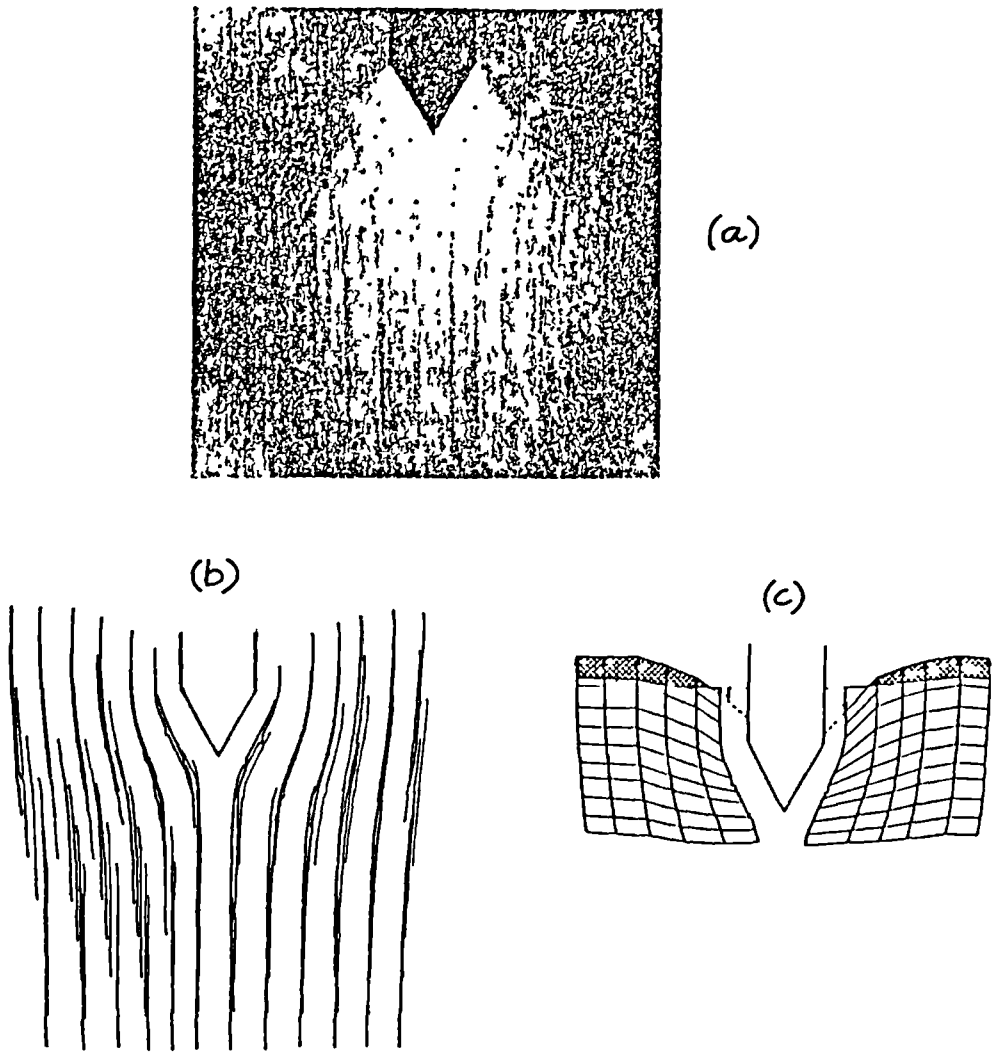

Figure 3.3 Observations of Allersma (1988)

The experiments of Allersma (1988) provide a good insight into the mechanics of pile penetration in a granular medium, but it should be noted that the piles were installed to a maximum slenderness ratio (L/R) of only 12. Allersma made use of the photoelastic properties of glass to visualise stresses during installation of a cone penetrometer (R=25mm) into crushed glass with a particle size of 2-3mm. A photograph in circularly polarised light during penetration of the cone is shown on Figure 3.3a and indicates that the areas of higher stress (or brighter areas) are concentrated around the cone tip and emanate downwards from

the tip at an angle of ≈45°. Stresses above the cone shoulder are evidently much smaller than those at the tip and friction on the pile shaft provides a relatively minor contribution to the penetration resistance.

The deformation pattern measured for a cone displacement of ≈4R is shown on Figure 3.3c and indicates a pattern reminiscent of the Prandtl bearing capacity failure mechanism for shallow foundations: close to the pile tip, the soil moves downwards and radially outwards, whereas at larger radial distances, an upward component of motion is observed as the soil accommodates the rotation of material from the tip. Similar patterns of movement were measured by Wersching (1987).

The displacements of the marked particles relative to the cone tip are shown on Figure 3.3b. It is evident that these 'flow' around the pile tip in a similar way to the 'flow paths' observed during *undrained* penetration of piles in saturated clays (Baligh 1975, see Section 2.3.2). One important difference to the paths observed in clays is that the (free draining) material immediately adjacent to the pile shaft moves downwards relative to the pile tip as large compression volume changes take place at the pile toe. Robinsky & Morrison (1964) measured a similar pattern of displacements and suggested that this downward movement leads to the formation of a loose sand zone next to the shaft, which is surrounded by a cylinder of denser sand that was compacted originally by the pile toe. These conditions promote *arching* of the radial stresses.

3.3.2 Density changes

Changes in density within a sand mass are very difficult to determine accurately because of the indeterminate effect of the monitoring system on the measurements. One of the more recent attempts to measure such changes during pile installation was made by Chong (1988) using a pile of radius 18mm in a tank of Leighton Buzzard sand. Sand densities were measured both *at the surface* of the pile and within the soil mass using thermocouple needle probes. These probes were calibrated to provide a direct (and repeatable) relationship between the thermal conductivity of sand and the sand density.

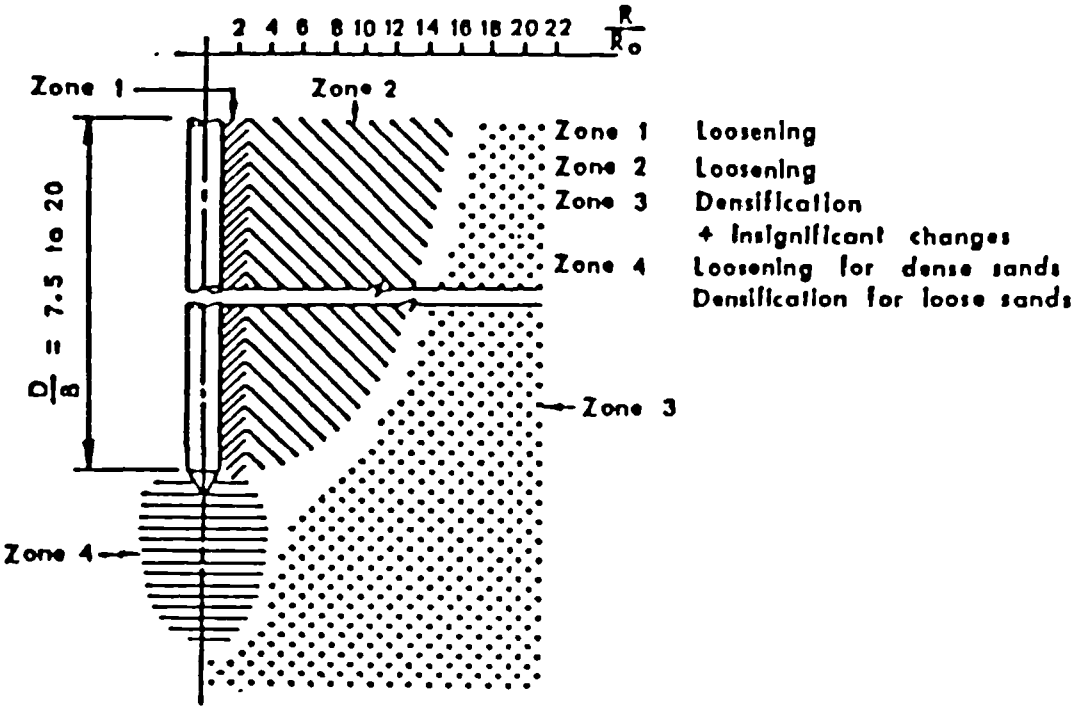

Figure 3.4 Density measurements by Chong (1988)

Chong identified the four zones surrounding a displacement pile, shown on Figure 3.4. Of particular importance is the zone of "significant sand loosening" (Zone 1) adjacent to the pile shaft for piles installed in both loose and dense sands. This zone had previously been postulated by Robinsky & Morrison (1964).

Density changes induced by pile installation have also been measured by Wersching (1987), Davidson et al (1981) and Robinsky & Morrison (1964). These experiments showed seemingly random and complex patterns of high and low sand density. No measurements were made immediately adjacent to the shaft, but all displayed a general trend for an increase in density with proximity to the pile shaft in Zone 2 (Figure 3.4)[1].

[1]Chong measured a random variation of density in Zone 2 but concluded that there was generally less densification than loosening within this zone.

3.3.3 Average shaft shear stresses

Because of problems associated with determining the magnitudes and distributions of the residual loads existing in field piles after driving (discussed in Section 3.4.1), there is little information available on how the local shear stresses acting on piles in sand vary with depth. A common assumption, as discussed in Section 3.2.1, is that the local ultimate shear stress (τ_f) is proportional to the free field vertical effective stress (σ'_{v0}) i.e. $\tau_f = K\,\sigma'_{v0} \tan\delta$, where K = constant and δ = angle of wall friction. This assumption implies that, for a constant value of $K\tan\delta$ in a deposit where σ'_{v0} increases linearly with depth, the average shaft shear stress [$\tau_{av} = (1/L) \int^L \tau_f \, dz$] must also increase linearly with depth. However, all the tests listed in Table 3.3 showed that τ_{av} remained relatively constant for pile penetrations below a certain critical depth (typically between 20 and 60 pile radii). It thus appears that $K\tan\delta$ must vary with pile penetration.

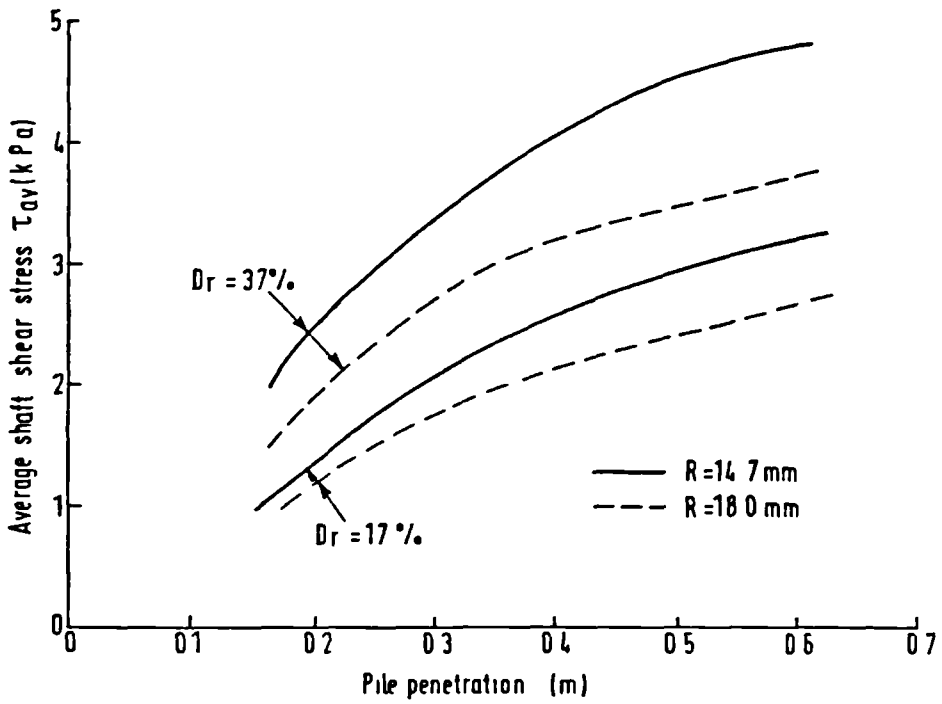

Figure 3.5 τ_{av} variation with pile length in model tests of Robinsky et al (1964)

The variations of τ_{av} with pile length measured by Robinsky et al (1964) are shown on Figure 3.5 and illustrate three important general characteristics seen in laboratory pile tests:

- τ_{av} does not increase linearly with depth but tends to a constant value as the pile penetration increases. It can be inferred that the 'critical depth' in this case is at ≈0.7m (≈50R).
- The value of τ_{av} is dependent on the initial relative density (D_r) of the sand; higher values of τ_{av} are mobilised in sand with a higher D_r value.
- Larger values of τ_{av} are mobilised on piles with a smaller radius.

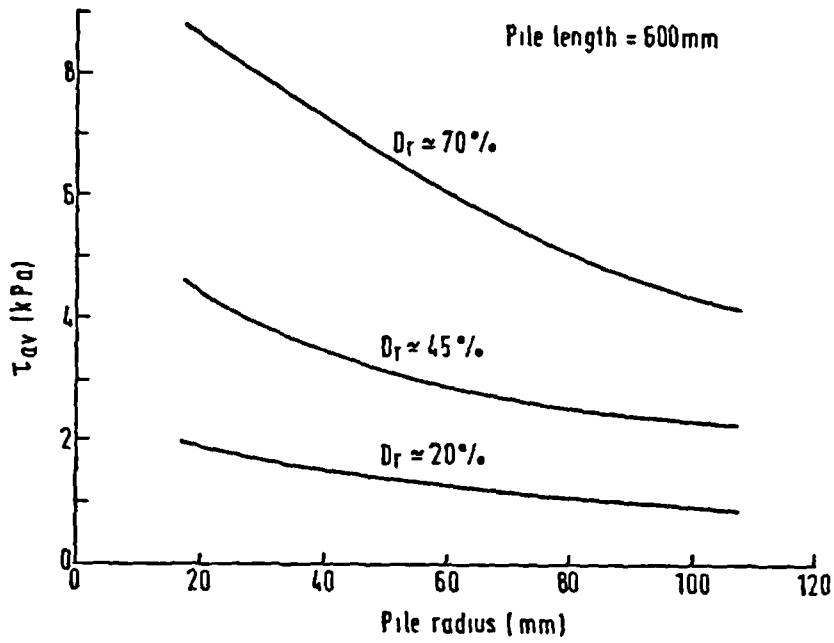

Figure 3.6 τ_{av} variation with relative density and pile radius (Lebègue 1964)

The dependence of τ_{av} on pile radius was investigated by Lebègue (1964) who carried out a number of tension tests on model piles of constant length (600mm) but with radii ranging from ≈18mm to 108mm. The reduction of τ_{av} with pile radius measured in these tests at three initial sand relative densities is shown on Figure 3.6. Despite the large range of L/R

values in this data base (which varied from 5 to 35), the results illustrate the strong influence of pile radius as well as relative density on the values of τ_{av} that are mobilised. For example, at $D_r \approx 70\%$, τ_{av} reduces from 8.6kPa for R=20mm to 4.2kPa for R=110mm. A similar dependence on pile radius has been inferred by Hettler (1982) in a review of further laboratory model pile test data.

Hettler (1982) and Boulon & Foray (1986), amongst others, suggested that the dependence of τ_{av} on pile radius arose because of dilation of the sand adjacent to the pile shaft during loading. They postulated that this dilation causes an increase in radial stress acting on the pile and that this increase is inversely proportional to the pile radius. It follows that, as laboratory piles operate under low stress levels (when more dilation is expected) and have a small radius, the relative contribution of dilation to the unit shaft capacity of a full scale pile may be far less significant than seen in laboratory tests.

3.3.4 Local radial and shear stresses

The instrumented pile used in laboratory tests by Wersching (1987) (see Table 3.3) was equipped to obtain simultaneous measurements of radial and shear stresses acting at various levels along the shaft during pile loading. To my knowledge, no other tests where similar measurements were made in sand have been reported. The instruments used were of a similar design to the surface stress transducers mounted on the ICP (see Chapter 4).

The radial effective stresses measured after two pile installations (S1 and S2) to L/R=32 are shown on Figure 3.7a, where they are seen to increase almost linearly with depth and lie within the range $0.5\sigma'_{v0}$ and $1.0\sigma'_{v0}$. These stresses are between 50 and 100 times less than the base pressures mobilised during installation. This high concentration of stress at the pile tip was observed in the experiments of Allersma (Figure 3.3).

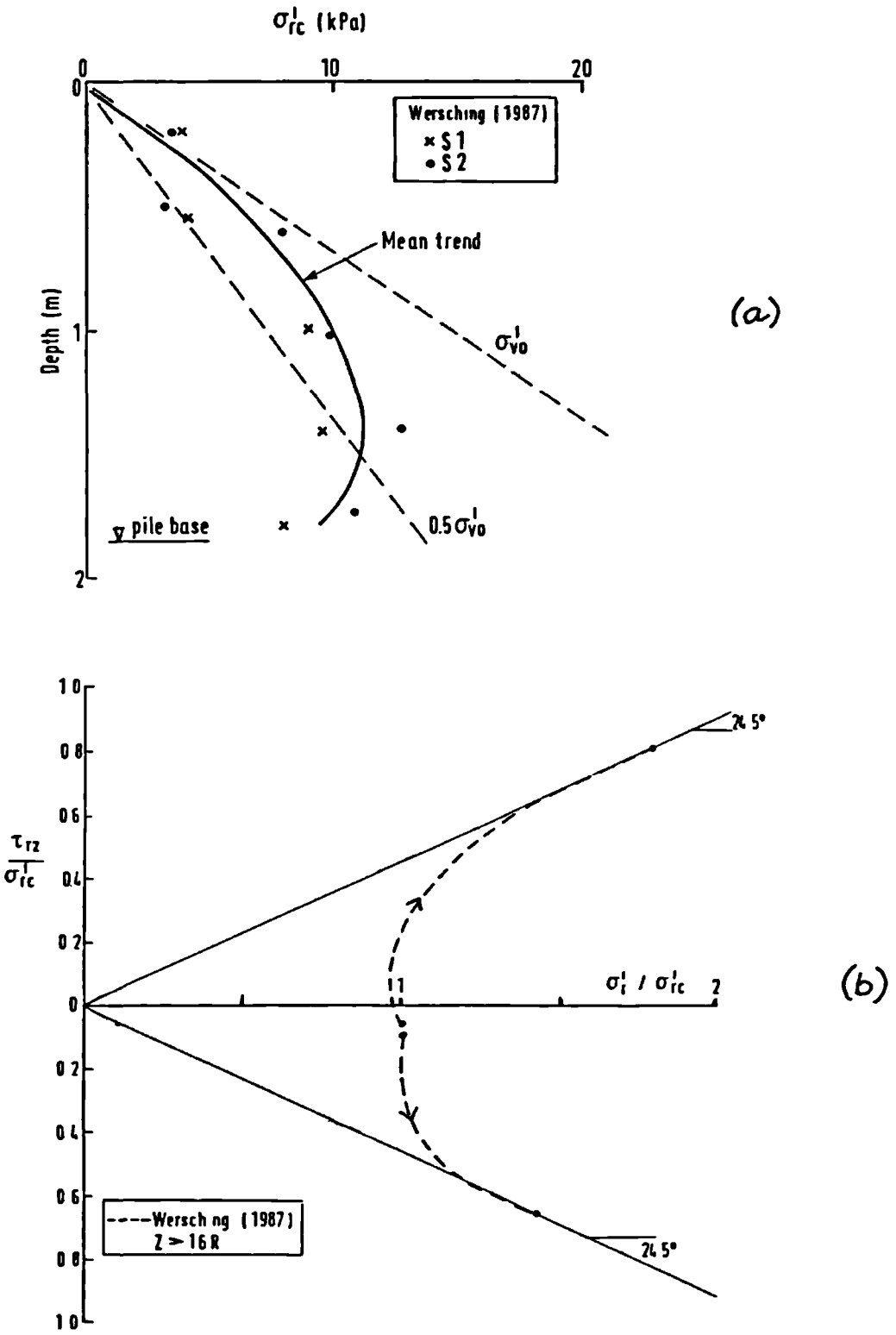

Figure 3.7 Wersching's (1987) data after pile installation (a) and during load tests (b)

Wersching's load test data is summarised on Figure 3.7b by plotting typical variations of the radial effective stress (σ'_r) with shear stress (τ_{rz}) measured during compression and tension loading. These 'stress paths' are normalised by the pre-loading radial effective stress (σ'_{rc}). Points to note include:

- σ'_r increases as the piles are loaded. These increases suggest that the sand adjacent to the shaft dilates.
- The interface friction angle, $\delta = \tan^{-1}(\tau_{rz}/\sigma'_r)$, reaches a maximum value of 24.5 ± 4° before the maximum shear stress is mobilised. No significant difference between values of δ measured in compression and tension tests was observed.
- Maximum shear stresses (τ_f) are mobilised when there are no further increases in σ'_r (perhaps indicating the end of dilation). At this point σ'_r had increased by ≈80% in the compression tests and by ≈50% in the tension tests[1].
- Wersching observed that the tensile shaft capacity was always less than the compressive shaft capacity of an equivalent pile. This appears to be due primarily to the smaller increases in σ'_r recorded during tension loading.

A useful contribution to the study of the factors affecting the magnitudes of radial stresses developed on small diameter piles was by Robertson (1982) by inference from friction sleeve measurements made during cone penetration tests in Ticino sand[2]. By assuming an angle of interface friction (δ) of 30° between the friction sleeve and the sand, Robertson deduced that the ratio of the ultimate radial effective stress to the initial horizontal stress ($\sigma'_{rf}/\sigma'_{h0}$) increased with sand density and reduced with increasing stress level. A consistent relationship was found between the value of $\sigma'_{rf}/\sigma'_{h0}$ and the maximum dilation angle of the sand (ν_{max}). This correlation is shown on Figure 3.8 and suggests that σ'_{rf}

---

[1]At shallower depths (z < 800mm), significantly larger increases in σ'_r were observed and σ'_{rf} often exceeded $3.0\sigma'_{rc}$.

[2]Cone penetrometers which make direct measurements of the radial stresses acting behind the tip have been developed by Huntsman (1985) and Amar et al (1982). The device developed by Amar et al (the LPC pressio-penetrometer) was used to measure radial stresses at the Labenne test site and is discussed in Chapters 5 & 6.

at the friction sleeve location may be over six times σ'_{h0} in a dense sand but that as the stress level increases (and ν_{max} becomes smaller), the ratio $\sigma'_{rf}/\sigma'_{h0}$ will reduce. In loose sands σ'_{rf} is comparable to σ'_{h0}.

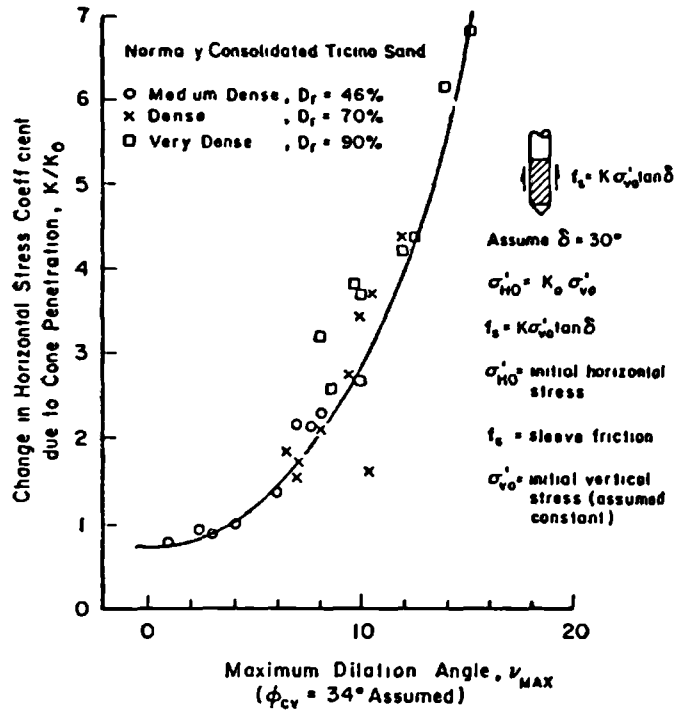

Figure 3.8 Correlation of Robertson (1982) based on CPT data

No clear pattern emerges from model pile tests concerning the distribution of the ultimate shear stresses (τ_f) developed along the pile shaft. In deposits of uniform relative density, some tests show that τ_f remains relatively constant with depth (e.g. Wersching 1987) whereas other tests show τ_f generally increasing with depth (Robinsky et al 1964). The experiments of Wersching suggest that these unsystematic trends may be associated with large and variable increases in radial effective stresses during pile loading. If the increases in radial effective stress are dependent on pile diameter, as discussed in Section 3.3.3, then the τ_f distributions measured in laboratory tests may differ significantly from the distributions on full scale piles.

3.4 FIELD MEASUREMENTS

Few firm conclusions can be made from the existing data base of field piles regarding the factors controlling the behaviour of displacement piles in sand, as relatively few piles have been instrumented and, of these, only a handful achieved moderate success with the instrumentation.

This section discusses some general aspects observed in field tests and presents the available data on the distributions of local stresses developed on piles.

3.4.1 Residual stresses

Many driven piles have been instrumented with a view to determining the contribution of the shaft and base loads to the pile capacity, as well as determining the distribution of the local shear stresses. However, the instrumentation employed has not been capable of withstanding the large accelerations imposed during driving and large shifts of the zero readings of the instruments were experienced. It was conventional practice to re-zero all instruments prior to load tests and to assume (implicitly) that residual loads existing in the piles after driving were negligible.

Hunter & Davisson (1969) investigated the effects of re-zeroing instruments after driving instrumented piles at Arkansas River. By estimating the residual base load after installation from the apparent base tension measured at peak capacity in tension tests, they deduced that the true shaft load in compression tests was only 70% of that implied from the measurements taken after re-zeroing of instruments.

In a series of model pile experiments, Hanna & Tan (1973) showed that a parabolic distribution of the local ultimate shear stresses (τ_f) would be deduced if the residual loads in the piles prior to load tests were

assumed to be zero, whereas the correct τ_f values increased linearly with depth. Although the piles used were not displacement piles[1], these experiments highlight the severe effect of re-zeroing instruments on the interpreted τ_f profile.

Typical effects of re-zeroing instruments after pile installation in sand on the measurements obtained during compression and tension tests are summarised in Table 3.4 (after Briaud & Tucker 1984).

	Compression test	Tension test
Local shear stress	steeper gradient with depth	smaller gradient with depth
Base load	under-estimated	Apparent large base tension
Shaft load	over-estimated	O.K., if zero base load is assumed

Table 3.4 The effects of assuming zero residual pile loads in sands.

3.4.2 Variation of τ_{av} with depth

Despite the difficulties associated with residual loads, discussed above, field tests reported by Vesic (1970), Tavenas (1971), Gregersen et al (1973) and others have confirmed the tendency seen in laboratory tests for the average shaft shear stress to remain 'quasi-constant' below a critical depth of about 10 and 30 pile diameters.

This trend contradicts the conventional assumption that the local shear stress is a constant (K) times the free field vertical effective stress (Section 3.2.1). The following possible explanations for the phenomenon have been proposed:

[1]Piles were suspended in an empty container before placing the sand. The residual load distribution was, therefore, probably not typical of displacement piles.

- rapidly reducing K_0 value with depth (Kulhawy 1984)
- friction fatigue processes (Toolan et al 1990)
- reduced sand dilation at depth (Hettler 1982, Toolan et al 1990)
- errors in the assumed or measured residual stress distribution (Kraft 1991)

Reliable measurements of the local effective stresses developed on piles provide the only means of testing these hypotheses.

3.4.3 Tension and compression shaft capacities

Many tests on displacement piles in sand, both in the laboratory and the field, have shown a tendency for the tension shaft capacity (Q_{st}) to be less than the compression shaft capacity (Q_{sc}) and, up to 1984, the American Petroleum Institute (API) recommended that for closed-ended piles, Q_{st} should be assumed to be a half of Q_{sc}.

Re-zeroing of instrumentation prior to load tests, with the assumption that residual stresses in the piles are negligible, generally leads to an over-estimate of Q_{sc} (see Table 3.4). Based on a recognition of this effect and a larger data base, API recommendations since 1984 have assumed that the tension and compression capacities are equal.

However, in a review of 11 pile tests which could be corrected for residual loads, Briaud & Tucker (1984) showed that tensile capacities were generally between 5% and 30% smaller than compressive shaft capacities. The tendency for smaller tensile capacities was most pronounced in loose sands, where in one case, Q_{st} was only half of Q_{sc}. This data base is too small to allow any firm conclusions to be made and further research into the factors that influence the relative magnitudes of Q_{sc} and Q_{st} is required.

3.4.4 Pile end condition

Although this review is concerned with closed-ended displacement piles, it should be borne in mind that open-ended piles show consistently lower shaft and base capacities than closed-ended piles (e.g. see Figure 3.9).

API (1989) acknowledges this trend and suggests that the shaft capacity of an open-ended pile should be taken as 80% of that of an equivalent closed-ended pile.

3.4.5 Effect of installation method

There is very little information available on how the capacity of a jacked pile compares with that of a driven pile.

One comparison was made by Jolly (1963) using laboratory model piles. The shaft capacity of driven piles (installed using a drop hammer with a hammer to pile weight ratio ranging from one to five at 40-60 blows per minute) was typically about 20% greater than that of equivalent jacked piles and it was inferred that the vibration caused by the action of driving destroyed some of the conditions promoting arching, postulated by Robinsky & Morrison (1964); see Section 3.3.1.

Driving techniques vary widely and it is difficult to come to a conclusion as to how these techniques may affect capacity. Two general comments may be made:

- Provided that the driving method imparts a significant vibration to the soil mass, driving is likely to cause more compaction than jacking, particularly in loose sands. This compaction may result in higher radial stresses and therefore higher shaft capacities.
- Although the pile installation rate has a significant effect on the capacity of displacement piles in clays that form low strength residual shear surfaces, such as London clay (see Section 2.4.5), the installation rate is unlikely to have significant effect on ultimate interface friction angles mobilised by piles in sands.

The available evidence suggests that the shaft capacity of a jacked pile in sand is the same or somewhat less than a driven pile[1]. Further research on this subject is required although it is not certain that clear and consistent trends would be forthcoming because of the erratic

[1]Meyerhof (1976) suggests that the shaft capacity of a jacked pile in sand can be a little as one third of that of an equivalent driven pile. There is however little evidence to support this claim.

and random nature of driving in the field.

3.4.6 Pile set-up

It is generally assumed that conditions during pile installation and load testing in sand are near to being fully drained and therefore that there is no set-up effect, characteristic of piles installed in clay. However, Tavenas & Audy (1972) found that the capacity of concrete piles tested in compression in a fine to medium sand increased with time after installation. In one case, the capacity of a pile tested 12 hours after installation was only half of that measured in a reload test performed 20 days after installation. This was attributed to ageing/strain hardening effects but could also have been the result of physical changes in the shaft roughness due to chemical and other effects.

3.4.7 Definition of failure

Compression piles in sand generally do not fail in a brittle manner and relatively large displacements are required to mobilise full base resistance. Consequently, workers have used different definitions of failure and these have complicated the comparison of capacities at different sites. For example, Vesic (1970) assumed ultimate capacity was attained when the displacement rate of the pile first reached its maximum, whilst Gregersen et al (1973) defined pile capacity as that load at which the settlement was double the settlement at 90% of the load. The development of consistent design methods requires the use of a standard definition of failure. The definition adopted in this Thesis is that used by API, which defines the pile capacity as the load at which the settlement of the pile reaches one tenth of the pile diameter, excluding compression of the pile itself.

3.4.8 Measurements of local shear stress

Two instrumented pile test programmes, reported by Gregersen et al 1973 and Beringen el 1979, had reasonable success in correcting for the zero shifts of strain gauges induced during pile driving. The tests therefore took proper account of residual stresses and allowed a reasonable

assessment of the variations of the local ultimate shear stresses with depth.

The tests reported by Gregersen et al were performed on 280mm diameter precast concrete piles in a *loose* sand site at Drammen, Norway, and those reported by Beringen et al used 457mm diameter steel pipe piles in a *dense* sand deposit at Hoogzand, Holland. The shear stress distributions measured at peak load at the two sites are shown on Figures 3.9.

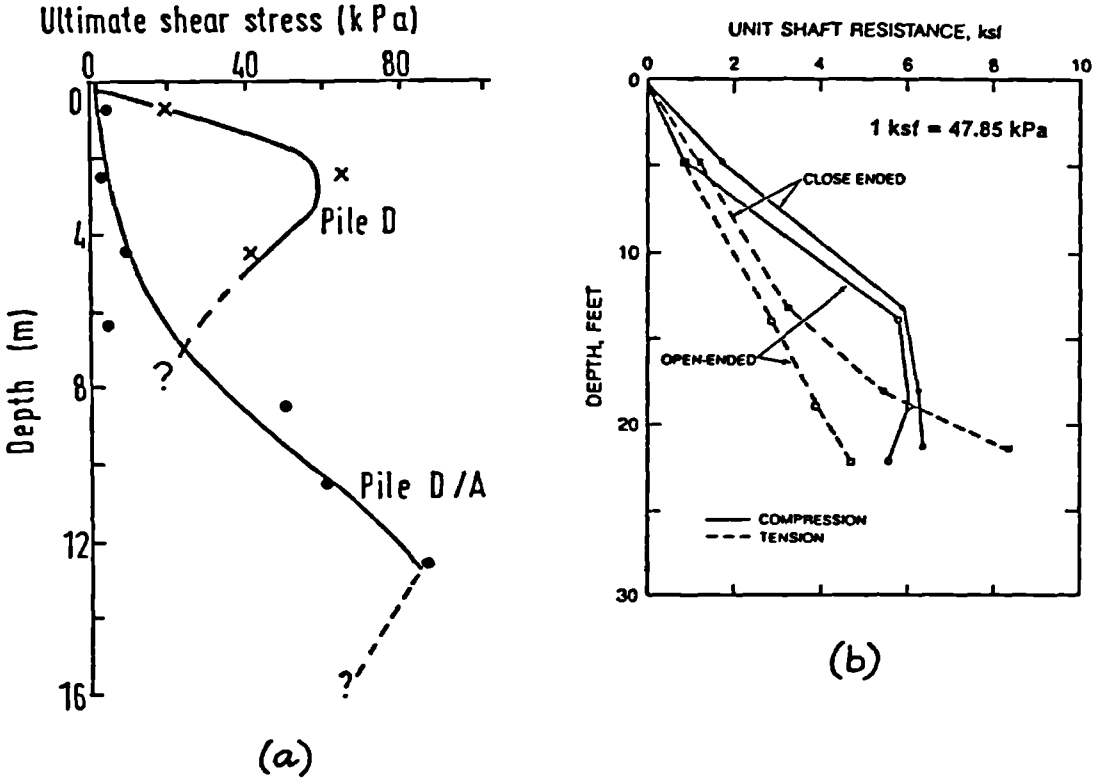

Figure 3.9 Distribution of ultimate shear stresses at (a) Drammen (in compression tests) and (b) Hoogzand

The followings observations may be made:

(i) The shear stress acting at a given depth on the shorter pile at Drammen is significantly larger than the shear stress mobilised at the same depth on the longer pile.

(ii) Shear stresses developed on piles tested in compression increase linearly with depth but close to the pile tip appear to either

remain constant or reduce with depth. Kraft (1991) suggested that the profile near the tip is associated with loosening of the sand adjacent to the shaft (because of large compression volume changes at the pile tip).

(iii) Lower peak shear stresses are mobilised in tension tests and there is no tendency for the stresses to reduce close to the pile tip.

It is interesting to note the following comments of Olsen (1990) regarding the measurements at Drammen:

"Detailed examination of their data, however, shows some strange effects. For example, a pile driven to a depth of 8m transferred about 21 tons of load in side shear, but when the pile was driven to 16m of penetration, the load transfer in the top 8m dropped to about 5 tons."

Although Olsen regarded these measurements as "strange", it will be shown in subsequent chapters that they are characteristic of trends exhibited by all displacement piles (in both sands and clays). The reduction in shear stresses mobilised at any fixed depth, as the pile penetrates to deeper levels, is compatible with the relative independence of the *average* shaft shear stresses (τ_{av}) on pile length observed at Drammen.

3.4.9 Measurements of local radial stress

The test programme in the loose sand at Drammen (Gregersen et al 1973) is one of only a few examples of where radial stresses acting on field displacement piles in sand have been reported. No distinction was made between the stresses recorded after pile installation and during load testing but it is reported that "measured changes were relatively small throughout". The full range of measurements are shown on Figure 3.10.

It is evident that stresses developed at a given level on the shorter pile are greater than those acting on the longer pile i.e. stresses reduce as the relative depth of the pile tip increases. This trend matches that shown by the corresponding shear stress profiles on Figure 3.9. The magnitudes of the radial effective stresses (σ'_r) range from an

average value of $\approx 0.5\sigma'_{v0}$ on the short pile to only $\approx 0.2\sigma'_{v0}$ on the long pile. These σ'_r values are the same or less than the initial undisturbed horizontal effective stresses, σ'_{h0}, ($= K_0\ \sigma'_{v0} \approx 0.5\sigma'_{v0}$).

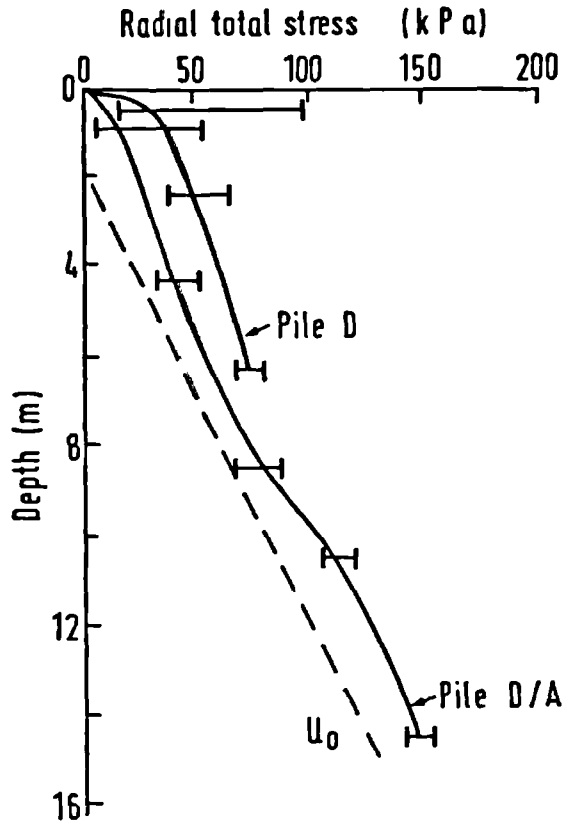

Figure 3.10 Radial total stresses at Drammen

Puech et al (1982) measured the radial effective stresses (σ'_r) developed on a 273mm diameter pile which was driven through loose silty sand into a clay deposit at 9m depth. The pre-loading σ'_r values (reported for depths less than 5.5m) were $\approx 0.39\sigma'_{v0}$ and these increased to $\approx 0.46\sigma'_{v0}$ on first-time loading in tension. Puech et al also report data for a "cast-in-place" model pile (D=55mm, L=1.6m) and found that σ'_r (measured at 1.2m depth) increased during tension loading by ≈20% in loose sand and by ≈150% in dense sand. These relatively large increases, which were also observed in the model pile tests of Wersching (Figure 3.7), were attributed to dilation of the sand at the pile-soil interface. It is surmised that the (reported) small changes in σ'_r during pile loading at Drammen may be associated with (a) a more contractant behaviour of the sand and (b) a larger pile diameter.

3.4.10 Trends inferred from local measurements

Based on the data presented by Wersching (1987), Robertson (1982) and Puech et al (1982), it appears that the magnitude of the local radial effective stress at peak shear stress (σ'_{rf}) is larger than the pre-loading radial effective stress and depends primarily on the:

1. initial undisturbed sand density (D_r)
2. stress level
3. pile diameter
4. distance from the pile tip
5. direction of loading

Toolan et al (1990) proposed an alternative approach to their method described in Section 3.2.1, which took the effects of (1) and (2) into account by relating σ'_{rf} to the maximum angle of dilation of the undisturbed sand (ν_{max}). Two main assumptions were made:

(i) The ratio of the ultimate radial effective stress to the initial horizontal stress ($\sigma'_{rf}/\sigma'_{h0}$) varies with ν_{max} in the manner shown on Figure 3.8. This trend had been deduced by Robertson (1982) from friction sleeve measurements made in cone penetration tests.

(ii) ν_{max} can be approximated by the expression proposed by Bolton (1986) (for plane strain conditions):

$$\nu_{max} = 6.25\ D_r\ (10 - \ln p'_0) - 1\ ;$$

D_r = relative density
p'_0 = initial mean effective stress

As ν_{max} reduces with increasing stress level (p'_0), the trend line on Figure 3.8 implies that the *local* earth pressure coefficient, K, ($=\sigma'_{rf}/\sigma'_{v0}$) reduces with depth (z) when D_r is constant. Consequently, Toolan et al predicted that[1], if the local shaft friction (τ_f) is given by [K tanδ σ'_{v0}], the *average* ultimate shaft shear stress (τ_{av}) acting on a pile of length L increases in approximate proportion to $L^{0.7}$. (Note that

[1]assuming δ is constant, σ'_{v0} = 10 z (kPa) and K_0 =0.4. p'_0 is then given by :σ'_{v0} $(1+2K_0)/3$ = 6 z (kPa)

conventional earth pressure theory suggests that τ_{av} increases linearly with L). The assumptions in (i) & (ii) also lead to a strong dependence of σ'_{rf} and τ_f on relative density (as ν_{max} increases with D_r) and suggest that, at D_r =90%, these stresses are about six times those at D_r =30%.

Therefore based purely on trends inferred from cone penetration tests, Toolan et al predicted two characteristic features of displacement piles in sand: (a) the partial stabilisation of τ_{av} with pile depth and (b) the strong dependence of τ_{av} on the in-situ relative density. However, the validity of this approach must be in some doubt because of:

- the dependence of local stresses on the diameter (discussed in Section 3.3.3); stresses developed on cone penetrometers may consequently be less than those acting on full scale piles.
- the dependence of stresses on the distance from the pile tip seen at Drammen; stresses acting along most of the shaft length of a pile may therefore be less than those recorded at the friction sleeve of a cone penetrometer.

A rational design method must take the effect of all the major influential factors into account; the preceding sections suggest that these may be the factors 1 to 5 listed above.

3.5 FINAL COMMENTS

Laboratory experiments have provided some insight into the factors controlling the behaviour of displacement piles in sand. While the findings from these tests have not been generally accepted as being applicable to full scale pile behaviour (because of the unknown scale and boundary effects in the laboratory), the tests have shown that the conditions around displacement piles in sand are far more complex than the simple theory ($\sigma'_{rf} = K\sigma'_{v0}$) would suggest. For this reason and the great shortage of successfully instrumented piles, design methods have remained purely empirical.

Pile instrumentation systems have generally not been sufficiently robust

to obtain reliable measurements of the residual stresses existing in piles after driving. Consequently, only a small number of tests have been reported where the compressive shaft capacity has been measured to an acceptable accuracy. As a result, the empirical design approaches have had to ignore the influence of several key parameters and the methods have a poor reliability in practice (see Briaud & Tucker 1988).

Contrary to experimental evidence, most designers assume that the specific soil properties (e.g. grading, stress state etc.) and the pile diameter, length and material properties have no effect on unit capacities. Arbitrary assumptions have had to be made regarding the influence of the direction of loading (i.e. tension or compression) and no account is taken of the potential influence of the driving procedure or set-up time. Because of the number of assumptions involved in the development of existing design methods, the superior predictive performance of one method compared to another is probably coincidental.

Carefully designed instrumented field pile tests, which provide reliable measurements of the local shear and radial effective stresses acting on piles, play a key role in furthering our understanding of the mechanisms that govern pile behaviour and advancing current design approaches. The dearth of reliable data of this nature prompted the instrumented pile tests at Labenne presented in this Thesis.

CHAPTER 4

EXPERIMENTAL PROCEDURES

CONTENTS OF CHAPTER 4

EXPERIMENTAL PROCEDURES

4.1 THE IMPERIAL COLLEGE INSTRUMENTED PILE (ICP) 94

4.1.1 Evolution of the ICP 94

4.1.2 General configuration 94

4.1.3 Instrument description 96

4.1.3.1 Axial load cell 97

4.1.3.2 Pore pressure probe 98

4.1.3.3 Surface stress transducer 99

4.2 TEST PROCEDURES 100

4.2.1 Calibration 100

4.2.1.1 Axial load cell 101

4.2.1.2 Pore pressure probe 101

4.2.1.3 Surface stress transducer 102

4.2.2 Pile preparation 104

4.2.3 Data acquisition system 104

4.2.4 Pile loading frame 105

4.2.4.1 Labenne 105

4.2.4.2 Cowden and Bothkennar 106

4.2.5 Installation 107

4.2.6 Equalisation 108

4.2.7 Load testing 108

4.3 INSTRUMENT PERFORMANCE 111

4.0 EXPERIMENTAL PROCEDURES

This chapter describes the pile instrumentation used at each of the three field programmes reported in this Thesis i.e. Labenne, Cowden and Bothkennar. General laboratory and field procedures used to conduct each test are summarised. Specific details concerning the programme of work and pile configurations employed at each site are provided in Sections 6.1, 7.1 and 8.1.

4.1 THE IMPERIAL COLLEGE INSTRUMENTED PILE (ICP)

4.1.1 Evolution of the ICP

The Imperial College instrumented Pile (ICP), used in the field tests, evolved from an instrumented pile which was designed at Southampton University to study the effects of electro-osmosis on the behaviour of piles (Johnston 1972, Butterfield & Johnston 1973). Jardine (1985) refurbished this pile and added some new instruments including pore pressure sensors. A 'pilot test' performed in the London Clay at Canons Park, North London, met with reasonable success, but it was clear that considerable changes to the instruments were required if the quality of the data retrieved was to be improved. Bond (1989) carried out a complete re-design of all instruments, with notable attention to detail, finally creating what is now known as the ICP. The steps involved in this design process are described in his PhD Thesis and by Bond et al (1991). Four tests with the 'new' ICP were performed at Canons Park; these have been reported widely (Jardine & Bond 1989, Bond & Jardine 1989, 1990, 1991).

4.1.2 General configuration

The ICP is a 101.6mm (4") diameter steel tubular pile which is assembled in segments to give a typical total length of ≈7m (Figure 4.1). Two piles have been manufactured and each contains stainless steel instrumented sections (or clusters) which are interconnected by molybdenum steel casings with a wall thickness of ≈9.5mm. A solid 60° cone is fitted at the pile tip.

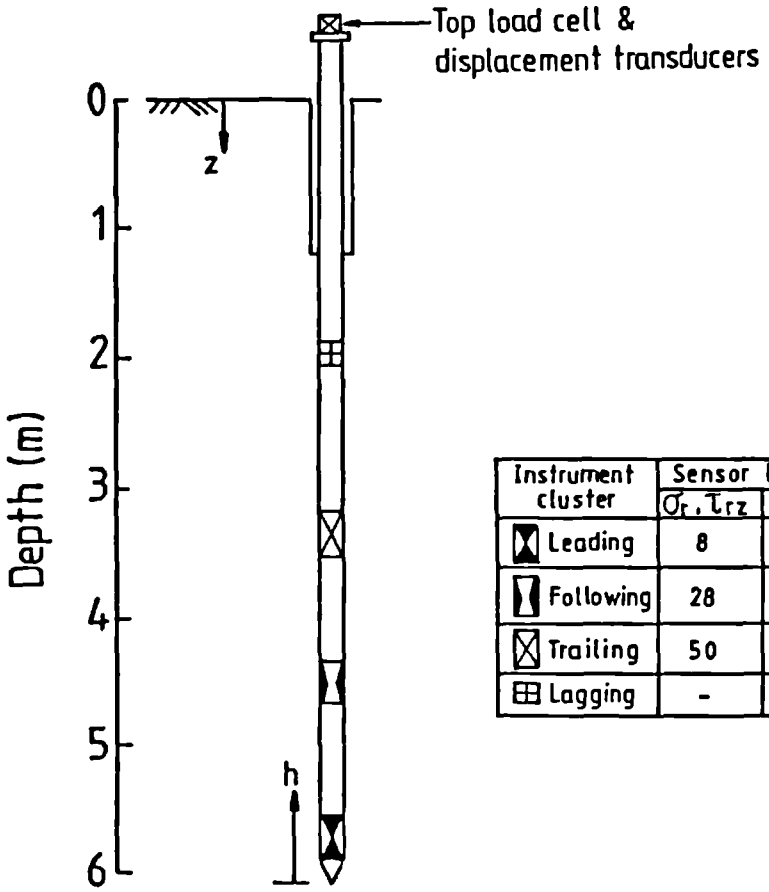

Instrument cluster	Sensor location (h/R)		
	σ_r, τ_{rz}	u	P
Leading	8	5	3
Following	28	30	32
Trailing	50	53	55
Lagging	-	-	77

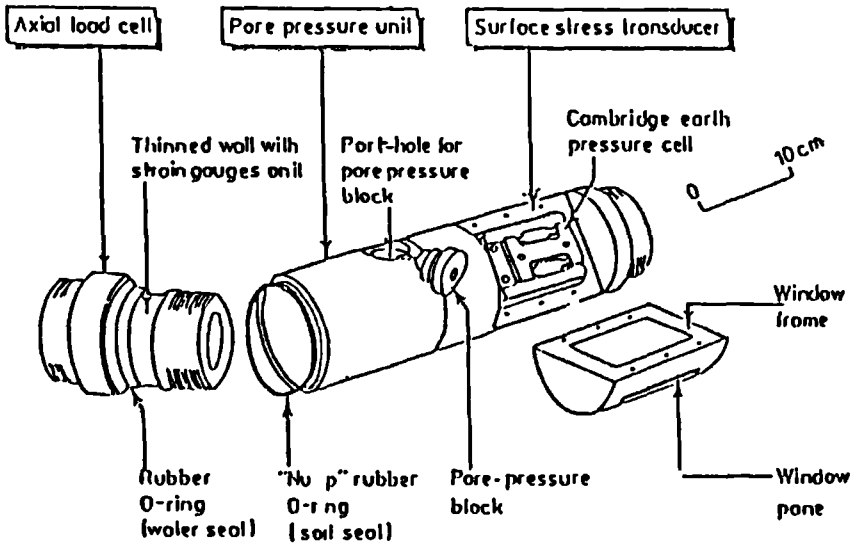

Figure 4.1 Configuration of the ICP and instrument cluster

Three instrument clusters (referred to as the leading, following and trailing clusters) are positioned over the lower 3m length of the piles. As shown on Figure 4.1, each cluster contains:

- an axial load cell (ALC)
- a surface stress transducer (SST) which measures the radial total stress (σ_r) and shear stress (τ_{rz})
- a pore pressure unit (PPU) which houses two diametrically opposite pore pressure probes
- a temperature sensor within each SST

Measurements made by each device are referred to by their distance from the pile tip (h) normalised by the pile radius (R) (i.e. h/R)

The cables from each instrument run through the core of the pile to a data logger at the ground surface. Severe space restrictions on the waterproof cables (and associated plugs) now used precludes the use of more than three SST's to be mounted on any one pile[1]. An additional axial load cell, positioned at about 4m from the pile tip, has been used in most of the piles used in the current research.

Two independent axial load cells at the pile head are used to measure the applied load and three displacement transducers and a dial gauge measure the pile head movement during load tests.

4.1.3 Instrument description

All instruments use Electrical Resistance Strain (ERS) gauges which are fixed to a given element in the instrument and are energised by an input voltage of 5 Volts. A force applied to instrument strains this element and causes the resistance of the gauge to change, hence altering its output voltage. The ratio of the output to the input voltage is calibrated against known applied forces.

[1]Some of earlier tests used four instrument clusters.

Each instrument is described below. Design details are provided by Bond (1989).

4.1.3.1 Axial load cell

The axial load cell is the least complex of all instruments on the pile and is shown on Figure 4.2. Loads bearing on the instrument are directed via a well protected, short, thinned-wall section (7mm in length, 2.25mm thickness) on which strain gauges are mounted. These gauges are arranged in a Poisson bridge configuration (4 gauges in axial direction and 4 in circumferential direction) and convert the load into an electrical signal. The dimensions of the thinned-wall section are such that it will yield rather than buckle and the nominal capacity is 209kN (at 0.2% axial strain).

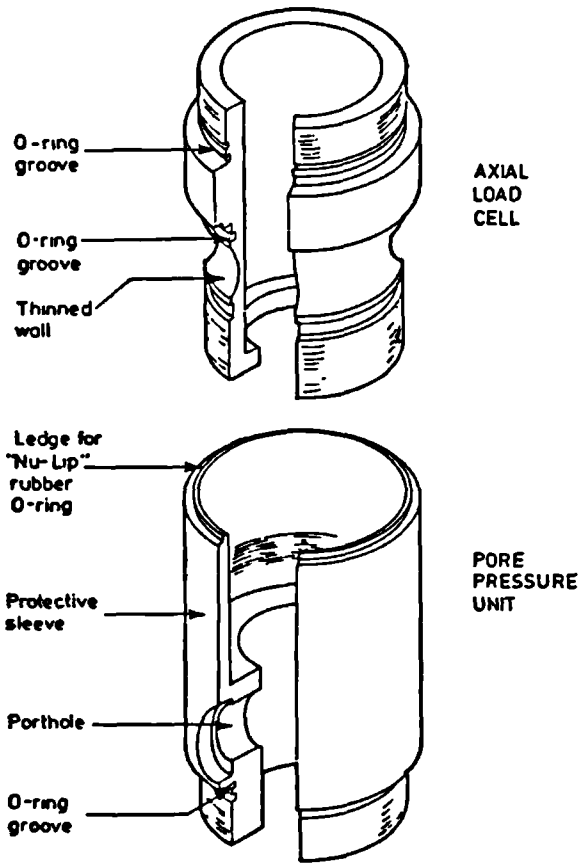

Figure 4.2 The axial load cell on the ICP

4.1.3.2 Pore pressure probe

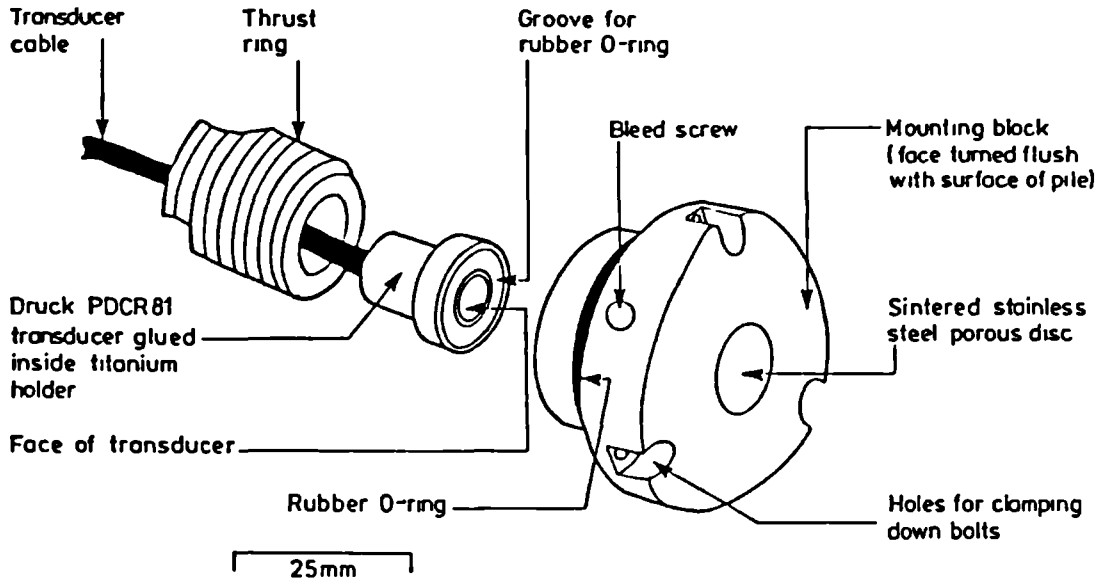

Figure 4.3 The pore pressure probe on the ICP

The pore pressure probe, shown on Figure 4.3, consists of a plastic mounting block (43mm in diameter) at the centre of which a sintered stainless steel filter stone (12.7mm diameter, 3.18mm thick) is fixed by heat shrinking. Pressures are measured using a Druck PDCR81 semi-conductor transducer which is housed in a titanium holder. A thrust ring screws into the back of the block and clamps the flange of the titanium holder in position behind the filter stone, leaving a small gap which is sealed by an O-ring. The filter stone and gap are saturated in de-aired silicone oil[1]. This oil is used in preference to water because its high viscosity allows it to recover quickly from cavitation (see Lunne et al 1986).

The extremely small internal volume (291mm^3) of this probe makes it very fast-acting, provided that this volume is fully de-aired. However, the response time can be affected severely if air enters the device. Bond (1989) suspected that this occurred after 4-8 days in the tests at Canons

[1]Dow Corning 200 fluid, which has a viscosity ≈25 times higher than water.

Park and designed a flushable probe with a large internal volume to measure long term pore pressures. Use of these 'slow-acting' probes were not required for the tests performed in the current research (see Section 4.3).

4.1.3.3 Surface stress transducer

The surface stress transducers (SST's) are the most complex of the instruments used on the ICP. They consist of four main elements, as shown on Figure 4.4.

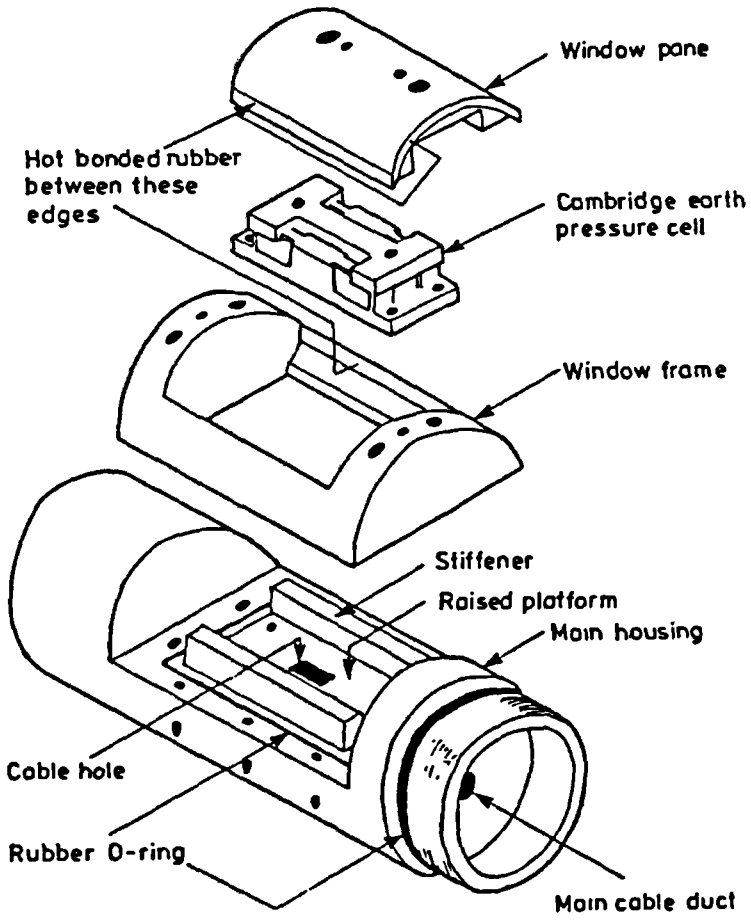

Figure 4.4 The surface stress transducer on the ICP

Any loads that bears on the window pane/loading platen (measuring 97.5mm x 77.5mm) is transmitted directly to a Cambridge 'dogbone' load cell[1].

[1]This name originates from the shape of its top plate.

This cell comprises 4 strain gauged webs oriented in the longitudinal direction to sense the applied shear load and four other webs in the normal direction to sense the radial load. The dimensions of these webs (typically 1mm thick and 10mm long) were selected to ensure minimal compliance, whilst retaining the sensitivity required for adequate resolution of the stress measurements in the tests at Canons Park. The radial and shear stress capacities (for an axial web strain of 0.2%) are 870kPa and 262kPa respectively.

The strain gauges (two per web) are arranged in three Wheatstone bridge configurations to give two radial compression circuits (one for each side of the 'dogbone') and one shear circuit. The temperature sensor is an integrated circuit device and is located on the base of the Cambridge cell. This cell is bolted to a raised platform between stiffeners (designed to increase the resistance of the instrument to bending) and is wedged between the window pane and the main housing. The window pane is fixed to the window frame by a 2.5mm wide layer of hot bonded rubber. One large O-ring between this frame and the main housing completes the sealing of the instrument.

4.2 TEST PROCEDURES

4.2.1 Calibration

The calibration procedures employed were in general similar to those set out by Bond (1989).

All instruments were calibrated fully prior to each pile installation over a range of loads compatible with that expected at each site. Almost no dependence of the calibration coefficients on the loading range was observed and, unless instruments had been over-loaded during their previous service on site, calibrations coefficients remained virtually unaltered throughout the entire research programme.

New or repaired instruments were subjected initially to 100 load cycles (up to design capacity), maintained at a load equivalent to half their design capacity for ≈1 day and finally subjected to a further 100 load

cycles before being calibrated. This 'bedding-in' procedure was essential if drift, non-linearity and hysteresis were to be minimised.

4.2.1.1 Axial load cell

The axial load cells were calibrated in tension and compression using an *Amsler* loading machine which had a resolution of 0.1kN. Calibrations which compared the output from one load cell with another were also performed on site to check any apparent anomalies or instrument malfunction.

4.2.1.2 Pore pressure probe

The pore pressure probes were assembled in two steps:

- The porous stones and mounting block were first positioned in sealed brass chambers. After thoroughly evacuating these chambers, de-aired silicone oil was forced through the stone under an applied positive pressure of 200kPa on one side of the stone and a full vacuum suction on the other side. A new stone was employed with each use of the probe.
- After removing the bottom cover of the brass chamber, the pressure transducer was fixed in position in a bath of de-aired silicone oil.

The probes were calibrated using a *Budenberg* dead weight tester and retained in the brass chambers until their imminent use on site.

The poor long term performance of these probes at Canons Park (Bond 1989) prompted the use of ceramic stones in three of the six probes mounted on one pile at Cowden. These stones had an air blow-through pressure six times higher than the 'standard' stainless steel stones and were expected to slow down potential diffusion of air into the probes. Saturation of these stones showed them to be ≈600 times less permeable to silicone oil than the stainless steel discs and a positive pressure of 500kPa was used to speed up the saturation procedure.

4.2.1.3 Surface stress transducer

The SST's were calibrated in a rig, described by Bond (1989), which allowed shear and compression loads to be applied simultaneously to the window pane by application of dead weights to a series of hangers. Various combinations of shear and normal load were used because of the (small) cross-sensitivities of the signals from the shear and compression circuits. Checks on these calibrations were performed by subjecting the SST, positioned in a sealed chamber, to a range of water pressures. Air pressures were used initially to check the watertightness of the instrument.

The SST's were designed specifically for use in tests in the London Clay at Canons Park. Radial stress measurements at Canons Park were, however, typically ten times larger than those measured at Labenne and Bothkennar and therefore secondary factors affecting the signal output, which were not significant at Canons Park, had to be examined carefully. Two of the most important of these factors, which became apparent from the first test programme at Labenne, were the effects of temperature and axial load on the signals from the radial compression circuits[1].

(i) Temperature sensitivity

The radial stress circuits are arranged in a 'half-active' Wheatstone bridge configuration and the arrangement employed is such that no compensating gauges can be used to correct for when the webs expand due to an increase in temperature. This expansion leads to an apparent reduction of radial stress, amounting to a shift in output of ≈2kPa per 1°C increase in temperature (when measured in the laboratory). Each SST gave a linear and repeatable temperature calibration between 5°C and

[1]The output signals from the shear stress circuits, axial load cells and pore pressure probes were relatively insensitive to temperature because the temperature compensating strain gauges used in their bridge configurations were fully effective. Field measurements and calibration tests showed that pore pressures and shear stresses were independent of the axial load.

25°C. These calibrations greatly assisted in selecting a precise initial zero reading.

The effects of temperature may also affect the in-situ radial stress measurements. However, the correction applied was usually small as the SST temperature prior to installation rarely differed by more than 5°C from its final temperature in the ground.

(ii) Sensitivity to axial load

The centroid of the SST does not lie along the central axis of the pile and consequently an axial load applied along this axis causes the main housing to bend and the Cambridge load cell to deform. For this reason, all SST's were calibrated for (tension and compression) axial load in the *Amsler* machine used for calibration of the axial load cells. The SST's were tested with the remainder of the instrument cluster attached in order to simulate the end restraints as representatively as possible. The output from the compression circuits indicated an apparent reduction in σ_r of typically ≈0.4kPa per kN increase in compressive axial load, but the response was often not completely linear and exhibited some hysteresis.

A bi-linear dependence of radial stress to axial load was specified for each SST at all sites. Despite the hysteretic nature of the response, it was believed that, based on the trends shown by many calibration checks, this specification would ensure that the error in the σ_r measurements due to the axial load sensitivity would be limited to a maximum of ±2kPa. This correction was only significant for the pile tests at Labenne, where the axial loads were high (up to 100kN) and the radial stresses were low (typically ≈50kPa). It could be argued that, after the pile enters the ground, the radial stresses developed will serve to reduce the bending of the instrument and hence reduce its sensitivity to axial load. However, careful examination of the data at Labenne indicated that application of the full correction was justified as it explained anomalies such as apparent *negative* radial stresses and inconsistent (and unrealistic) coefficients of friction.

4.2.2 Pile preparation

After completing calibrations, the instrumented sections of the piles were assembled in the laboratory. Particular attention was paid to ensuring that the pile was fully watertight (this had proved to be a particular problem in the early stages of the development of the ICP). Hylomar gasket sealant, in addition to an O-ring, was positioned at each joint and bags of silica gel were housed within the pile to assist in absorbing any moisture.

The consequences of slight variations in pile surface roughness had not been fully appreciated until after the first phase of tests at Cowden had been performed (see Section 4.3)[1]. Therefore in all subsequent tests, the piles were shotblasted to a *uniform* centre line average roughness of 8-9μm, which is a typical value for an industrial steel pile (Tika-Vassilikos 1991).

After transporting the piles to site, the instruments were energised for at least one day prior to installation. Indents on the pile shafts, such as at bolt locations (on instruments) and lug positions (on the steel casings), were filled with in-situ clay at Cowden and Bothkennar and a sand/polyfilla mixture at Labenne.

4.2.3 Data acquisition system

All instruments were monitored during the four phases of the pile's lifetime i.e. installation, equalisation, load testing and extraction. The data were acquired by a Solatron 3530A Orion data logger which digitised the output voltages of the instruments and recorded them on magnetic tape. This logger was also used for calibrations.

The logger could be programmed to record the readings for any instrument or set of instruments at a range of time intervals. These time intervals were specified to match the expected rate of change of data and varied

---

[1]For the first test series (at Labenne), the centreline average roughness values varied from between ≈4μm to ≈8μm (In real terms, this does not represent a significant roughness variation).

from 3 secs[1] during pile jacking stages to ≈20 mins for long term monitoring. The facility of the data logger to print some data onto paper tape proved invaluable as a means of site control.

A vast amount of data was recorded for each pile installed and tested. These data were transferred from magnetic tape to a Prime mini-computer and processed using a series of computer programs which were written as part of the Canons Park test series. These programs required relatively minor modifications and additions to suit the data recorded in this research.

4.2.4 Pile loading frame

Photographs of the pile loading frames and the installation & load testing arrangements used at each site are provided in Plates 4.1-4.3 at the end of this Chapter.

4.2.4.1 Labenne

The experimental site at Labenne had been developed by the Laboratoire des Ponts et Chaussées (LPC) to investigate the performance of shallow pad foundations in sands. LPC installed a series of ground anchors, encircling a central anchor, and manufactured a reaction beam which could rotate about this central anchor and connect to one of the perimetric anchors. This system allowed a number of footings to be tested with relative ease.

On completion of the footing tests, the site was excavated to a depth of 1.5m below the original ground level and the footings were removed. The site layout after this excavation, shown on Plate 4.1a, provided a ready made set-up for the ICP tests.

---

[1]A period of 0.1 secs was required to achieve an accurate measurement of the output signal from each transducer circuit. As ≈28 separate readings were generally required to monitor all instruments, a period of 3 secs was the minimum interval than could be specified.

The reaction beam was constructed from two I-beams which were welded together with plates. Piles were installed through the gap between the beams by a jack connected to the pile head. The jack pushed upwards against a plate which was connected by high yield steel bars to the reaction beam (Plate 4.1b). Guides on the beam helped to maintain verticality.

4.2.4.2 Cowden and Bothkennar

The same pile loading frame that was used for the ICP tests at Canons Park was also used at Cowden and Bothkennar and is described in more detail in Bond (1989). This frame was the property of the Building Research Establishment (BRE).

The set-up used at Cowden and Bothkennar is shown on Plates 4.2a and 4.3a. The reaction beam, as at Labenne, was constructed from two I-beams, on top of which a movable frame was mounted. Piles were installed through the gap between the beams by jacking against a crosshead located near the top of this frame (Plate 4.2b). Reaction for compression loading was provided by kentledge positioned on grillages, which were clamped to either end of the beams. The movable frame allowed a number of pile installations to be performed without re-locating the entire set-up. However, as the clear working space between both stacks of kentledge was ≈6m, only two pile installations per location were permitted to ensure a minimum distance between piles of 2.5m (or 50 pile radii).

Higher axial loads were anticipated for pile tests at Cowden and the loading frame used at Canons Park was modified by BRE. The modifications included:

- bracing the two I-beams
- incorporating additional clamps at either end of the beams
- reducing the span from ≈8.5m to 6.5m

If these improvements had not been made, it is likely that the reaction beam would have suffered severe distortions when, due to an obstruction encountered during a pile installation at Cowden, the applied load increased dramatically from 100kN to 300kN.

Timber railway sleepers provided a foundation for each grillage at Cowden. However, because of the much softer material at Bothkennar, it was decided to construct 2.2m x 2.2m concrete foundations within the upper crust at this site (with a formation level at 0.3m depth) to help spread the reaction load and reduce ground settlements. The reaction beam and kentledge were positioned on these footings 4 to 5 months before each phase of the ICP tests was performed so as to minimise any potential effects on the experiments[1]. Measurements of ground stresses, strains and pore pressures beneath other footings at the site (Jardine, Lehane, Smith & Gildea 1993) suggested that their zone of influence would not encroach on that of the piles.

4.2.5 Installation

The pile installations at Cowden and Bothkennar proceeded from the base of pre-bored holes, with depths ranging from 0.55m to 2.7m. These holes eliminated the effects of the superficial material and were either hand augered or drilled by BRE using a power auger.

All, but two, of the piles were installed by jacking at the relatively fast rate of 500mm/min. The two other piles, one at Cowden and the other at Bothkennar, adopted a slower jacking rate of ≈80mm/min to investigate rate effects. Pile depths were measured using graduations marked on the pile and the jacking rate was monitored using a stop watch.

Jacking was not continuous due to the need to reset the jack (which had a stroke of ≈225mm) and add additional lengths of pile casing as installation progressed[2]. Pause periods between jacking stages were in most cases between 3 and 6 mins but, occasionally, were up to 45 mins long when pile casings and pore pressure probes were added. All instruments were monitored both during and between jacking stages.

---

[1]The static bearing pressure on each footing at Bothkennar was ≈10kPa and led to a total settlement of 10mm up to the beginning of the pile testing. 7mm of this settlement took place in the first two months.

[2]The pile length above the ground was restricted to ≈2.5m to avoid excessive bending of the pile.

4.2.6 Equalisation

After installation, attempts were made to limit the amount of moisture within the piles by:

- attaching bags of silica gel crystals at the top of the pile and then sealing it with numerous layers of polythene and tape.
- trickling nitrogen gas to the top of the pile and extracting it using a vacuum pump connected to a line extending to the pile base.

The instruments were monitored at progressively longer intervals as equalisation progressed. Piles were generally load tested when radial effective stresses had reached stable, fully equalised values. This took about 4 days for the piles installed in the clays at Cowden and Bothkennar but was almost immediate in the sand at Labenne. Other tests were performed before full equalisation in the clays to investigate the effects of time on pile capacity.

4.2.7 Load testing

Piles were load tested in tension and compression and all instruments were monitored at intervals of ≈10 secs. Some cyclic load tests were performed *after* first-time load tests with a (one way) load cycle taking ≈1 min.

For tension tests (and pile extraction), a steel bar, which was bolted to the pile head (Plate 4.3b), was passed through the centre of the jack. The jack applied a tension load by pushing against a plate fixed at the top of this bar and reacting against either the reaction beam (at Labenne) or crosshead (at Cowden and Bothkennar). The same set-up to that employed for installation was used to load test piles in compression (Plate 4.2b).

The load applied at the pile head was measured using a standard axial load cell (Figure 4.2) and the pile head displacement was measured by displacement transducers mounted on arms fixed to the base of this load

cell (Plate 4.3b). Three transducers were used so that the precise vertical movement at the pile axis could be resolved. The supports for the transducers were clamped to a reference beam which was supported at either end by blocks or driven stakes positioned about 2.5m (50 pile radii) from the pile. Another load cell at the pile head, which gave direct output of load to a digital meter, and a dial gauge mounted adjacent to one of the displacement transducers, facilitated site control of load and displacement.

The 'standard' loading testing procedure used at all sites was the same at that adopted at Canons Park by Bond (1989) and is a modified version of the procedure used by Les Ponts et Chaussées (Bustamante 1982). The applied load was increased in a series of small increments (typically 5-10% of the maximum expected load). These increments were maintained for a set holding period of ≈5 mins, during which movement of the pile was monitored. When the creep curves (plots of pile displacement versus time for each holding period) indicated approaching failure, load increments were reduced and holding periods were increased so that the failure load could be defined accurately. Failure occurred when the creep curves showed an increasing rate of pile settlement with time. At this stage, attempts were made to maintain the maximum load by continuous pumping of the loading ram or, if this is not possible, loading was continued at a controlled rate of plunging.

The main characteristics of this procedure were:

- Failure of the pile was always attained in less than 2 hours.
- The loading rate led to essentially undrained failures in clays. (Pore pressures did not vary during holding periods in the tests at Cowden, Bothkennar and Canons Park).
- The creep curves provided a good indication of incipient pile failure.
- For piles that failed in a brittle manner, the energy within the loading system was such that the piles typically failed at a rate of ≈5mm/min.

- With ductile failures, creep rates did not generally exceed 1mm/min. In some instances, the load continued to reduce very slowly and the peak capacity was defined as the load mobilised after a pile head displacement of 10mm (10% of pile diameter).

The procedure allowed consistent and accurate measurements of peak pile capacity. However, the post-peak response of 'brittle piles' was less easily assessed because the piles were moving rapidly.

Some anomalous features of post-peak behaviour were observed in tests at Cowden and Bothkennar. It was considered important to compare measurements in these tests with those obtained using another loading method, which was slow enough to ensure both drained conditions and an accurate definition of post-peak conditions. One load test (at Bothkennar) was carried out specifically for this comparison and adopted the following procedure:

- The initial load increments were applied as in the 'standard' method, but were maintained for holding periods which were typically 20 times longer (100 mins). These intervals were sufficient to allow dissipation of all incremental excess pore pressures at the pile shaft between loading stages.
- As failure was approached, the loading procedure was switched from being load controlled to displacement controlled. A slow displacement rate was adopted (0.02mm/min) so that loading was fully drained (i.e. no excess pore pressures were generated).
- The test was terminated after ≈24 hours, at a pile head displacement of 13mm, when ultimate conditions were clearly established (and I needed some sleep).

The notation used to describe each load test is given in Figure 4.5. This notation is essentially the same as that adopted by Bond (1989) and incorporates the pile site, the rate of pile installation, the number of the load test (1 for first-time loading) and the type of load test.

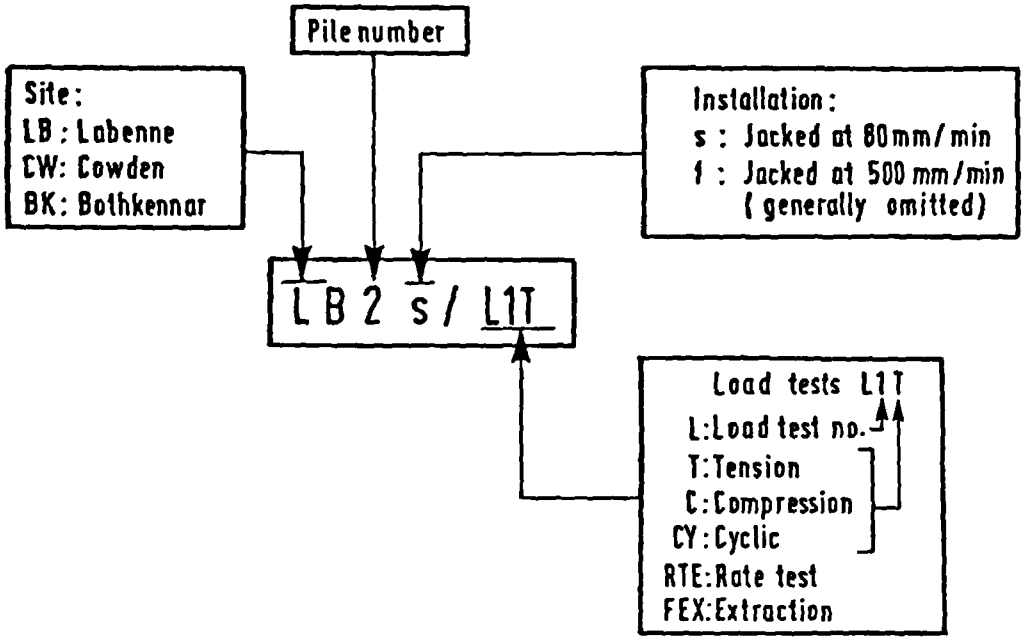

Figure 4.5 Notation used for load tests

4.3 INSTRUMENT PERFORMANCE

The performance of the instrumentation at all sites is discussed in detail in Appendix A. This section provides a short summary of the principal features.

1. All of the instrumentation remained operational throughout each testing programme, with the following exceptions:

   - A minor leak in the rubber bonding surrounding the window pane of one SST at Labenne caused one of the two radial compression circuits to become unstable after installation. (Fortunately, one circuit is sufficient to measure σ_r).
   - Three of the six pore pressure probes mounted on the first pile installed at Cowden did not operate properly because of faulty plug connections.

- A leak through a minor fracture in a steel casing in the first pile installed at Bothkennar rendered about half of the instruments unstable shortly after installation.

Given that 14 successful first-time load tests were performed, these incidents were relatively insignificant. The in-built redundancy in both the pile and the testing programmes ensured that they did not affect the overall success of the project.

2. The radial and shear stresses measured at Labenne and Bothkennar were typically less than 10% of the full scale output (FSO) of the SST. However, the high resolution and linearity of the devices and the comprehensive calibration procedures adopted ensured that consistent (and credible) data were obtained.

3. Typical ranges for the drift in zero instrument readings from before pile installation to after pile extraction are listed in Table 4.1.

Instrument	Labenne	Cowden	Bothkennar
Axial load cell (kN)	± 0.6	± 0.5	± 0.7
Pore pressure probe (kPa)	± 3.5	± 4.0	± 3.0
Radial stress sensor (kPa)	± 3.0	± 4.0	± 4.0
Shear stress sensor (kPa)	± 0.4	± 1.0	± 0.8

Table 4.1 Mean instrument zero drifts

These drifts are small in comparison to the measured stresses (see Table A1, Appendix A) and are indicative of the robustness and reliability of the instruments. It is anticipated that their effects were furthered reduced by assuming a constant drift rate. In some cases, as noted in Appendix A, drifts exceeded acceptable limits, but these could be tolerated due to the redundancy in the experiments.

4. All measurements were repeatable. Measurements recorded by instruments on different piles at the same depth and distance from the pile tip generally agreed to within 10% at each site. Such differences could be accounted for by considerations of site variability alone.

5. The combined measurements of radial stress (σ_r), shear stress (τ_{rz}) and pore pressure (u) led to angles of interface friction, $\delta = \tan^{-1}[\tau_{rz}/(\sigma_r - u)]$, in load tests that were consistent for all instrument clusters at each site. The fact that these angles were also closely comparable to values measured in appropriate direct shear interface tests gave additional confidence in the measurements.

6. The output signals from the pore pressure probes in the ICP tests in the London Clay exhibited large and erratic jumps after ≈4 days and the readings after this period were deemed unreliable. However, little evidence of this phenomenon was observed in the current research and the outputs from the probes at Labenne, Cowden and Bothkennar remained stable throughout the monitoring periods. Possible causes for the problems experienced in the London Clay are discussed in Appendix A.

These six points highlight the success of the instrumentation. However two main problems, which were related to the interpretation of measurements, became apparent during the course of the research. These required an understanding of:

(i) the unusual pore pressure measurements made at fast rates of displacement at Cowden and Bothkennar.

(ii) the incompatibility, in some instances, of the local shear stresses measured by the SST's (τ_{rz}) and the average shear stresses acting between instrument clusters, derived from the axial load cell data (f_s).

(i) Pore pressures at fast rates of displacement in clays

When the piles were stationary, or moving at a slow rate - as in load tests, the pore pressure probes gave consistent and repeatable measurements of pore pressure (u). Pressures registered by the two probes in the same instrument cluster were in good agreement with each other and with equivalent measurements made on other piles. The values of radial effective stresses ($\sigma'_r = \sigma_r - u$) calculated just prior to failure in load tests were consistent with the measured shaft capacities and the interface shearing characteristics of the materials.

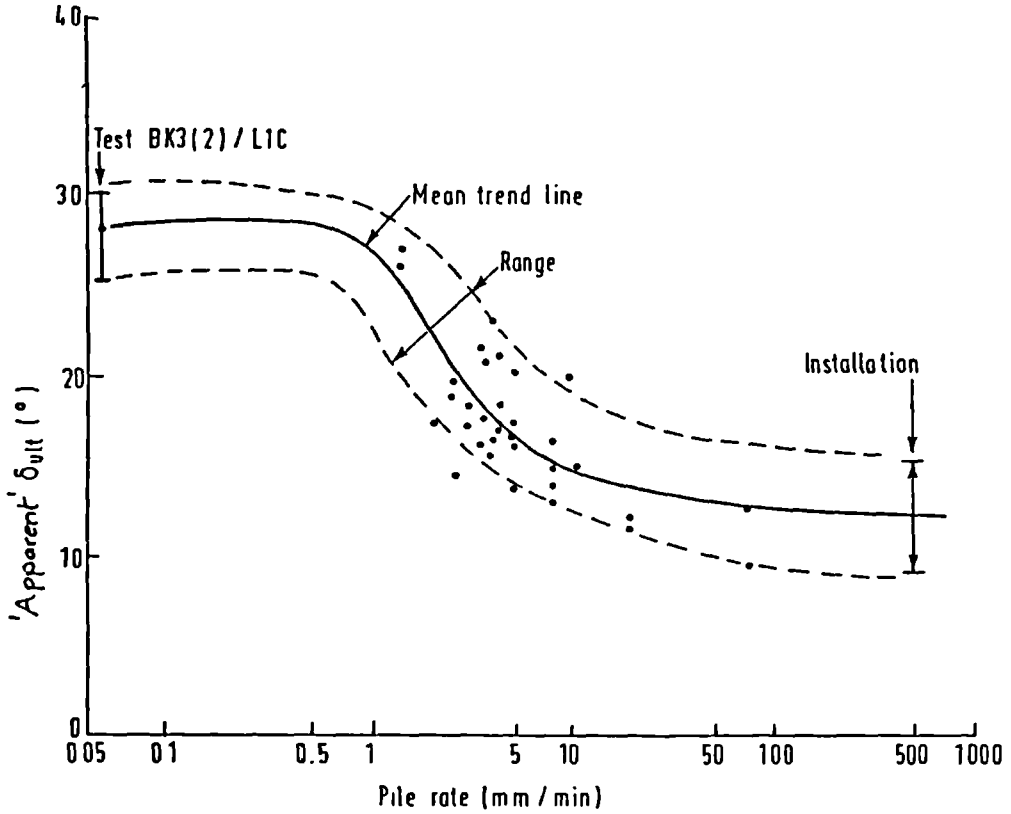

Figure 4.6 Apparent dependence of δ_{ult} value on rate

However, when the pile displacement rate exceeded a threshold value (≈1mm/min), pore pressures began to reduce significantly and these reductions became more accentuated as the rate was increased. No corresponding change in shear stress (τ_{rz}) or radial total stress (σ_r) was

measured, so that the calculated ultimate interface friction angle, [$\delta_{ult} = \tan^{-1} (\tau_{rz}/\sigma'_r)$], apparently reduced with increasing rate. At very fast rates (e.g. during installation), calculated δ_{ult} values were about half of those measured at slow rates of displacement.

The apparent variation of δ_{ult} with displacement rate measured at Bothkennar is shown on Figure 4.6. At rates less than ≈1mm/min, δ_{ult} is within the range expected from the slow drained shearing characteristics of the material but at rates greater than ≈5mm/min, δ_{ult} attains a steady value of only 15°; a transition zone exists between these two rates in which δ_{ult} reduces sharply with rate. This reduction is completely reversible and δ_{ult} returns to the high values measured in slow tests if the rate is decreased to below 1mm/min. The low δ_{ult} values are therefore not associated with the development of a low strength residual fabric.

Based on observations made in all the pile tests, it is concluded in Chapters 7 & 8 and Appendix A that the pore pressures measured on *fast moving* piles are anomalous (although relatively consistent) and probably not representative of the pressures acting on the principal displacement shear, which may have existed at a short distance from the pile. An examination of measurements made in other instrumented pile tests (Appendix A) showed that the pore pressure trends were not unique to Cowden and Bothkennar, or to the instrumentation on the ICP. Indeed the trends appear be a characteristic of all pore pressure measurements made on displacement piles at high pile velocities. Possible reasons for these trends are discussed in Appendix A, but it is clear that further research is required into the effective stresses developed in clay soils at fast rates of displacement.

(ii) Local and average shear stress measurements.

The average values of shaft shear stress acting between adjacent instrument clusters (f_s) may be derived from the difference between the respective axial load measurements. At Bothkennar (and Canons Park), these f_s values were within ≈5% of the average value of the local shear stresses (τ_{rz}) measured by these instrument clusters. However, at Cowden, the average of the local measurements were *in some cases* up to 30% less

than the f_s values. Differences of up to 15% were observed at Labenne at fast rates of displacement.

Factors which may explain this anomaly are discussed in Appendix A. The available evidence suggests that it was due to moderate differences in the surface properties (e.g. roughness, hardness & texture) of the stainless steel SST's and the molybdenum steel of the interconnecting pile casings. It is evident from observations made in laboratory interface shear tests (described in Appendix D) that small differences in surface properties could have a significant effect on the interface shearing characteristics of Cowden till and Labenne sand but would not unduly influence the interface shear behaviour of Bothkennar or London clay.

While the mobilisation of lower peak shear stresses at the instrument positions does not present any problem to the interpretation of the test results, it should be borne in mind that the global pile behaviour is governed by the shearing characteristics of the material against the pile casings which make up the majority of the pile shaft.

PLATES

Plate 4.1a Set-up at Labenne ---------->

Plate 4.1b Pile installation at Labenne ------>

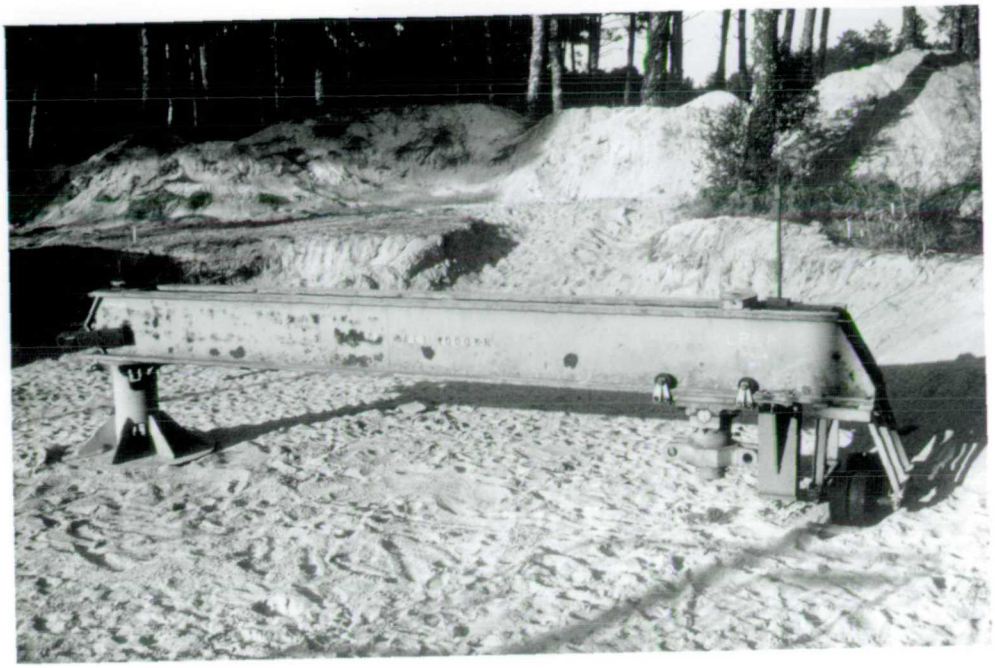

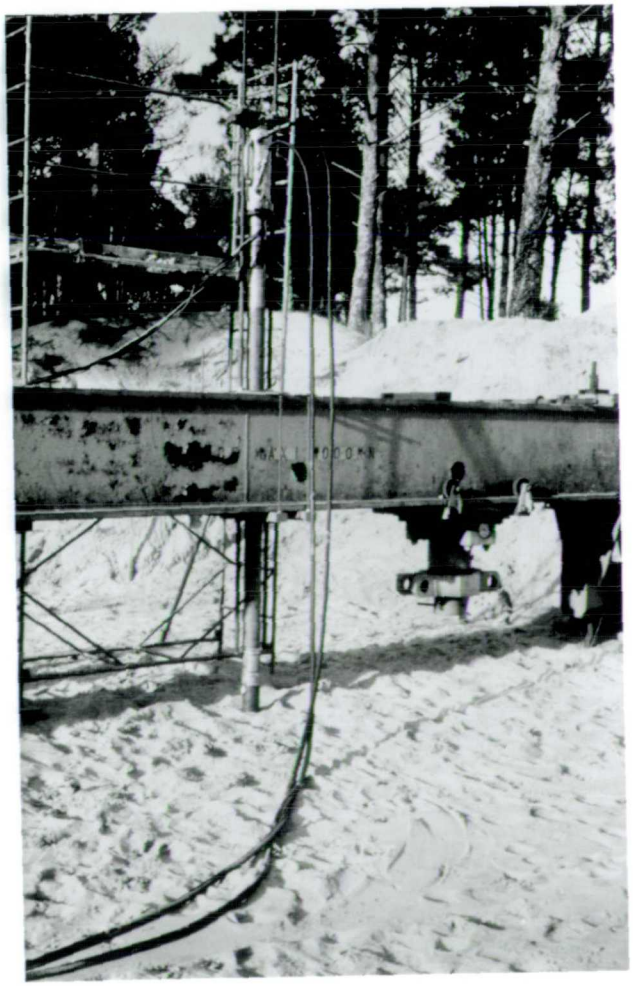

Plate 4.2a Set-up at Cowden ----------›

Plate 4.2b Arrangement at the pile head

at Cowden and Bothkennar ----------›

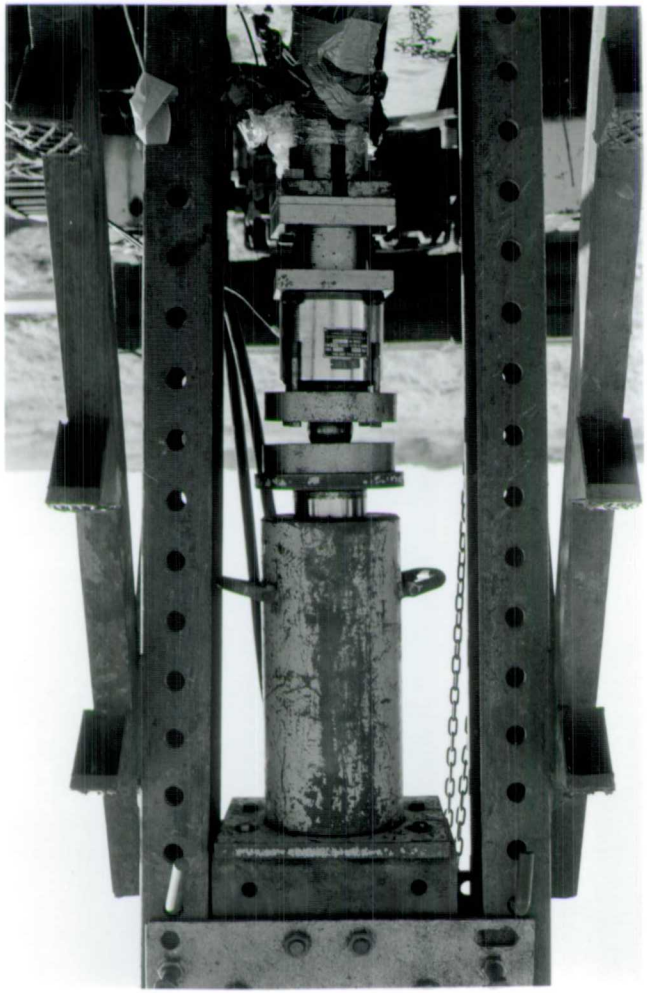

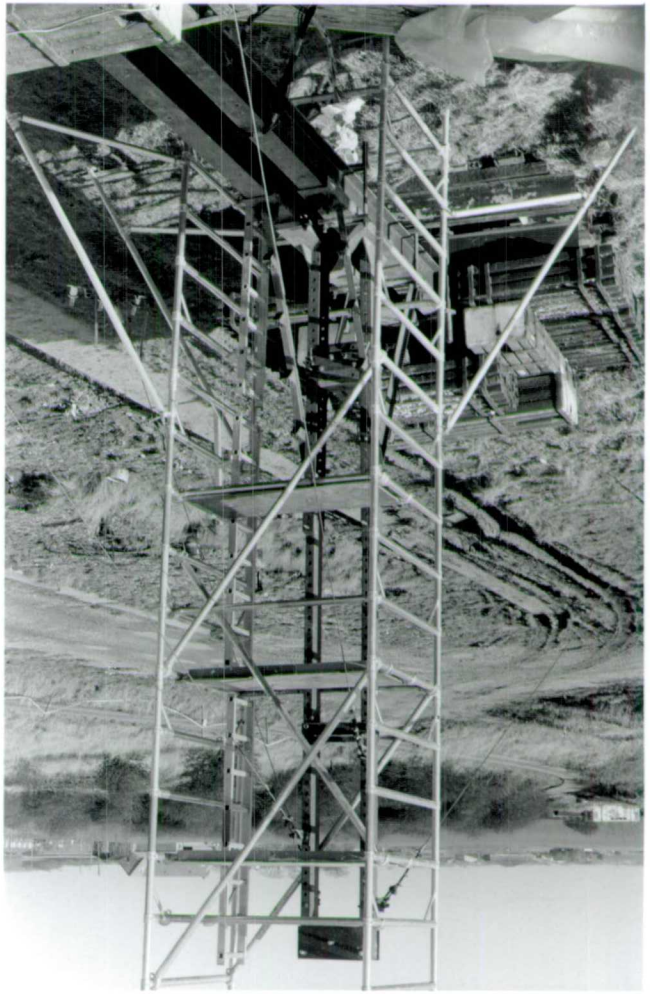

Plate 4.3a Set-up at Bothkennar ---------->

Plate 4.3b Monitoring pile head displacement ---------->

G
H
D

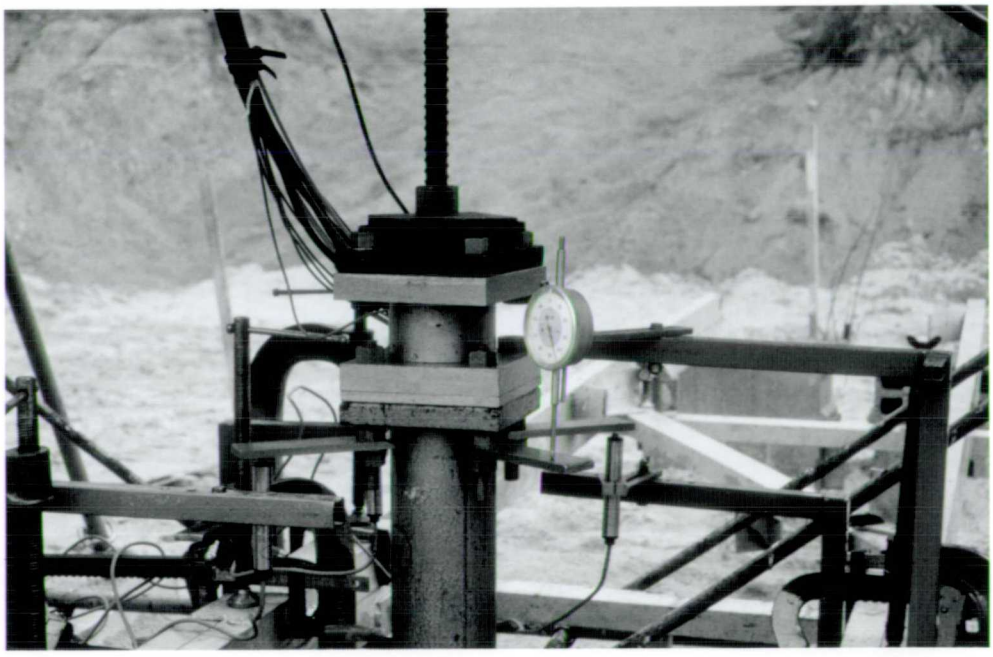

CHAPTER 5

SOIL PROPERTIES

CONTENTS OF CHAPTER 5

SOIL PROPERTIES

5.0 INTRODUCTION 129

5.1 SOIL CONDITIONS AT LABENNE..... 130

5.1.1 The site 130

5.1.2 Geology 131

5.1.3 Borehole investigation 132

5.1.4 Classification tests 135

5.1.5 In-situ tests 136

5.1.5.1 Density 136

5.1.5.2 Stiffness 137

5.1.6 Initial in-situ stresses 139

5.1.7 Mechanical properties from laboratory tests 140

5.1.7.1 Triaxial tests 140

5.1.7.2 Soil on soil shear box tests 143

5.1.7.3 Interface shear tests 144

5.2 SOIL CONDITIONS AT COWDEN 148

5.2.1 The site 148

5.2.2 Geology 150

5.2.3 Site profile 151

5.2.4 Grading, composition and fabric 152

5.2.5 Index tests 152

5.2.6 c_{u0} & q_c profile 153

5.2.7 Behaviour in 1-D compression 154

5.2.8 In-situ stress state 156

5.2.9 Triaxial tests 160

5.2.9.1 Isotropic tests 160

5.2.9.2 Anisotropic tests 161

5.2.9.3 Triaxial stiffness 163

5.2.10 Ring shear interface tests 165

5.3 SOIL CONDITIONS AT BOTHKENNAR 168

5.3.1 The site 168

5.3.2 Geology 170

5.3.3 Site profile 171

Continued.....

5.3.4	In-situ tests		172
	5.3.4.1	Cone Penetration and Piezocone tests	172
	5.3.4.2	Self-boring pressuremeter tests	174
5.3.5	Grading, composition and fabric		174
5.3.6	Index tests		175
5.3.7	Undrained shear strength		176
5.3.8	Behaviour in 1-D compression		179
5.3.9	In-situ stress state		181
5.3.10	Stress path testing		184
	5.3.10.1	Initial yield surface	184
	5.3.10.2	Effective stress parameters	186
	5.3.10.3	Triaxial stiffness	187
5.3.11	Direct simple shear tests		188
5.3.12	Ring shear tests		189
	5.3.12.1	Slow shearing stages	191
	5.3.12.2	Fast shearing stages	192

5.0 SOIL CONDITIONS

This Chapter summarises the soil conditions at the three sites where ICP tests were performed: Labenne (Section 5.1), Cowden (Section 5.2) and Bothkennar (Section 5.3).

Extensive site investigations have been carried out, independently of the ICP research, at each of the three sites. The large body of data from these investigations has been collated and supplemented by additional field and laboratory tests, performed as part of the current research project. These additional tests, which are summarised in Table 5.1, allowed a full interpretation of the pile tests and clarified any anomalies of the existing data.

The aim of this Chapter is to present a summary that focuses on those soil characteristics which are most likely to have a significant bearing on the performance of the piles. This information is vital to the interpretation of the test results and may also be used to determine the necessary parameters for any future theoretical predictions of the pile tests using, for example, the Strain Path or Finite Element methods.

The following aspects are considered:

(i) General site properties (geology, site profile, soil composition and index tests).
(ii) In-situ stress state.
(iii) Drained one-dimensional compression and swelling behaviour.
(iv) Undrained stress-strain and strength properties under triaxial and direct shear conditions.
(v) Behaviour in interface shear at varying displacement rates.

Labenne (field)	•	2 fully sampled boreholes drilled by Laboratoire des Ponts et Chaussées
Labenne (lab.)	•	Extensive measurements of physical properties
	•	CK_0U triaxial tests (by Dr. V. Georgiannou)
	•	Ring shear interface (RSI) tests (by Dr. T. Tika-Vassilikos)
	•	Shear box soil on soil and soil-interface tests
Cowden (lab.)	•	Index properties determination
	•	Oedometer tests
	•	RSI tests (supervised by Dr. T. Tika-Vassilikos)
Bothkennar (field)	•	Piezocone tests (performed by Fugro-McClelland Ltd.)
Bothkennar (lab.)	•	Ring shear soil on soil and soil-interface tests

Table 5.1 Supplementary site investigation performed specifically for the ICP research programme

5.1 SOIL CONDITIONS AT LABENNE

5.1.1 The site

The Laboratoire des Ponts et Chaussées (LPC) foundation test site is located just outside the village of Labenne, in the province of Landes, south west France. Labenne is 150km south of Bordeaux, 5km north of Bayonne and about 7km from the Atlantic coastline (Figure 5.1).

The site was selected for the ICP tests as it provided a deep deposit of uniform sand that had been investigated extensively by LPC. These investigations were supplemented by additional field and laboratory work, as outlined in Table 5.1, which provided some key parameters that were required for the interpretation of the ICP tests.

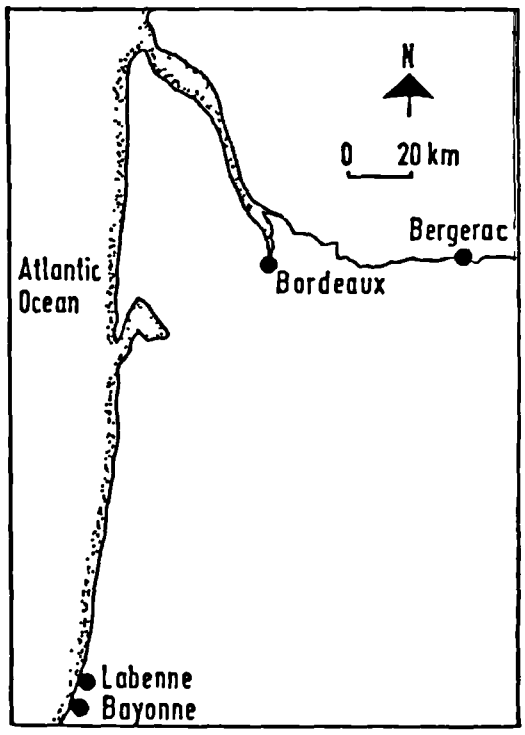

Figure 5.1 Location of Labenne

As discussed in Section 4.2.4, the experimental area was excavated by LPC to a depth of 1.5m below the original ground level prior to the pile tests (see Plate 4.1a). All depths quoted herein are depths below the excavated level.

5.1.2 Geology

The soils in the Landes province were deposited within the last 10,000 years and are erosion products (by sea and wind) of material that was laid down by glaciers which descended from the Pyrenées and the Massif Central during the Quaternary period (Famechon 1963). Strong westerly winds swept these sands inland and formed large dunes that extend a distance of 10km from the Atlantic coastline. The test site is within

this dune zone and is underlain by sands of marine origin at about 12m depth.

As described below, sand with a high organic content was encountered at 3.3m depth during the borehole investigations. This material is thought to be the remains of plants that grew during wet periods, when wind transportation of the sand was not possible. Such organic deposits are often seen in coastal dune deposits; e.g. see Jelgersma (1966).

5.1.3 Borehole investigation

The Bordeaux division of LPC was commissioned by IC to carry out a borehole (BH) to 7m depth at the location of the pile tests (BH IC1, Figure 5.2). Samples were obtained by jacking 80mm diameter, 1m length, plastic sample tubes from within a steel casing which housed a piston. The piston remained fixed in position at the top of the sample during penetration of the sample tube. The LPC drillers were unable, initially, to retrieve any samples from below 3.6m depth (about 1m below the water table) but in a second attempt, ≈10m north of the preferred location (BH IC2), succeeded in obtaining samples to the desired depth (see Figure 5.2).

The samples were extruded at the LPC laboratory in Bordeaux and immediately weighed, described and photographed. The borehole logs, given on Figure 5.2, confirmed the presence of relatively uniform sand to 7m depth, except for a layer with a high organic content at 3.3m depth in BH IC1. This 'organic' deposit was not present in BH IC2, indicating that it is not continuous across the site.

The bulk density (γ_b) and water content (w) of the sand samples, as determined after extrusion, are plotted on Figure 5.3. Void ratios (e), saturation coefficients (S_r) and relative densities (D_r) derived from these measurements are also plotted[1].

---

[1]The specific gravities (G_s) of the sand and organic material were assumed equal to 2.65 and 0.6 respectively. The void ratio (e) was calculated from $e = \gamma_w G_s (1+w)/\gamma_b - 1$, the degree of saturation (S_r) from $S_r = wG_s/e$ and the relative density (D_r) from e_{max} and e_{min} values, given in Section 5.1.4.

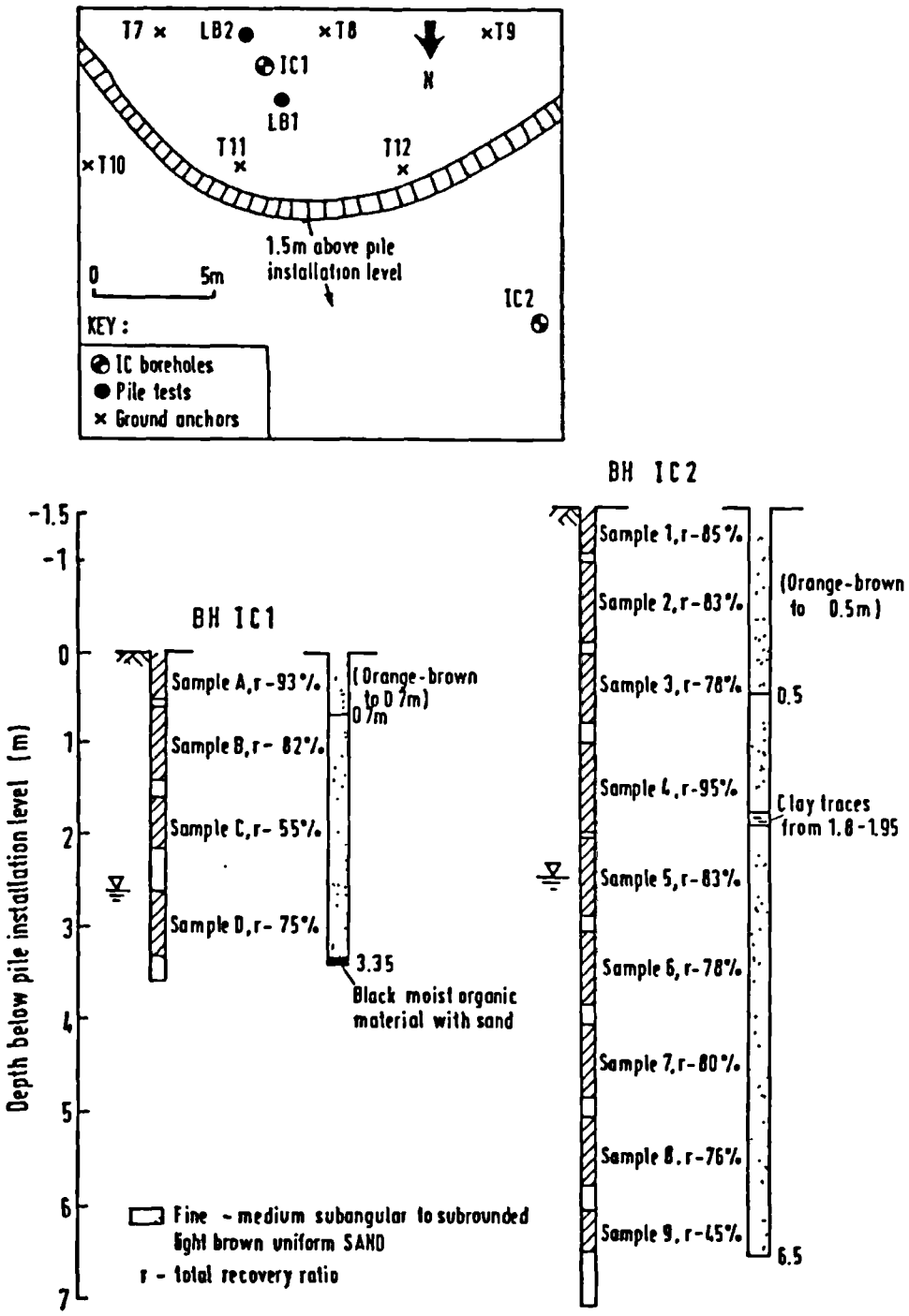

Figure 5.2 Borehole logs near ICP locations

Marcuson & Franklin (1979) suggest that conventional piston sampling does not cause significant disturbance of medium dense sands. If this were the case at Labenne, then the average in-situ properties of the sand to 2m

are: γ_b = 16.7kN/m3, e= 0.62, w = 4%, S_r = 17% and D_r ≈ 55%. Below 2m, the water content and bulk density increase to the fully saturated values at the water table level (≈2.5m).

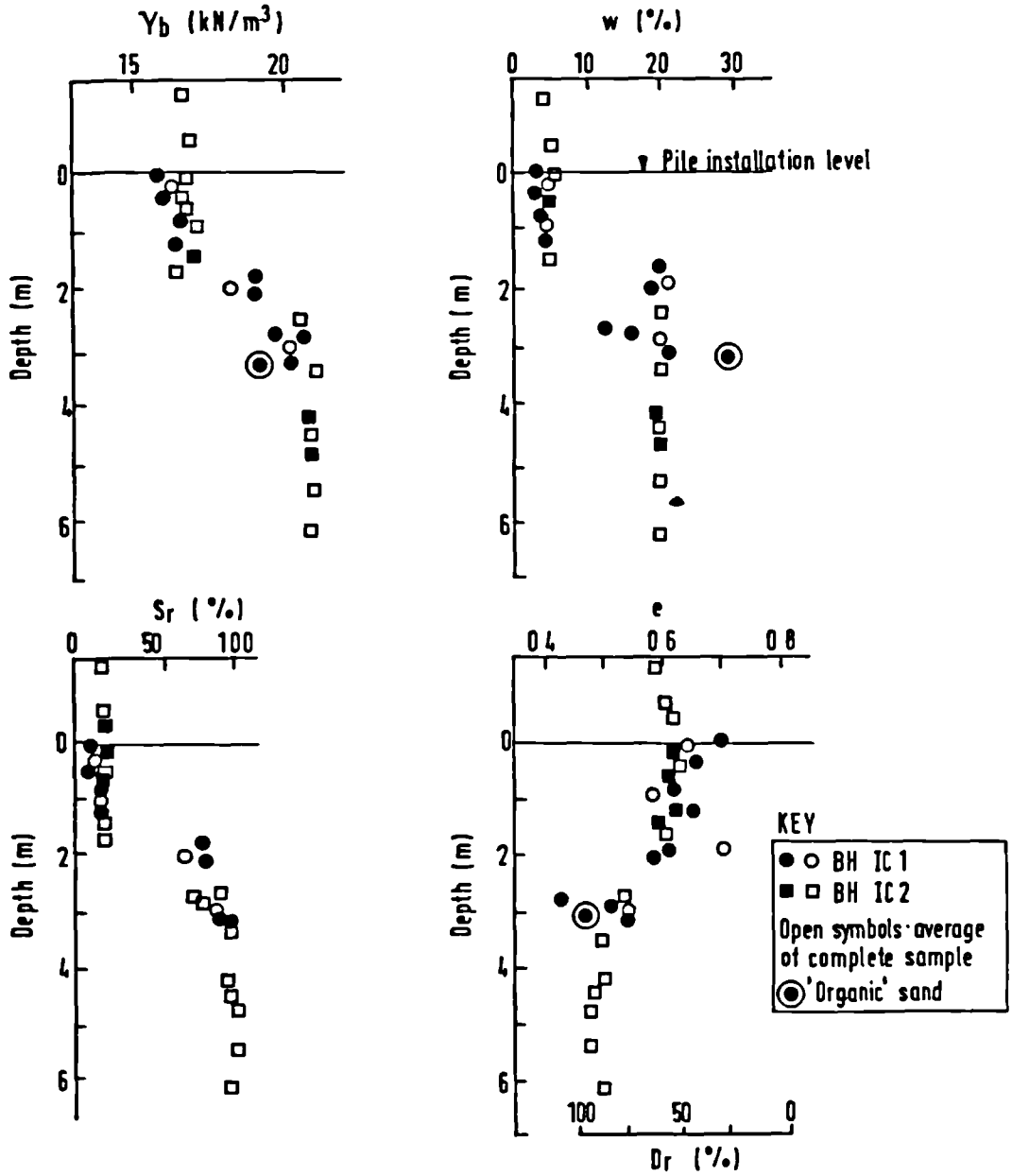

Figure 5.3 Index properties shown by piston samples

The boreholes did not remain open below the water table and it was necessary to jack the piston through the collapsed spoil to reach the desired start depth for the next sample. This procedure caused large

disturbance, which was apparent on extrusion of the samples. For this reason, the measurements plotted below the water table on Figure 5.3 are not considered representative of the in-situ material. The results from in-situ tests (Section 5.1.5) suggest that the sampling procedure *densified* the sand.

A comparison of the depth to water encountered in BH's IC1 & IC2 with LPC records showed that there are seasonal variations of up to 0.5m in the water table level. The pore pressure probes mounted on the piles proved that this level was at 2.9m during the pile tests.

5.1.4 Classification tests

The parameters used to describe the physical properties of sand include the mineralogy, roundness, grading, maximum & minimum void ratio limits and static angle of repose. Laboratory tests on the material retrieved from BH's IC1 & IC2 were carried out by the author to determine these properties and their variability with depth.

Mineralogy: Five determinations of the specific gravity (G_s) of the sand particles at different depths were performed in accordance with BS1377. The mean value of G_s measured was 2.645, with a maximum deviation of 0.005. These measurements and microscopic examination of the samples supported the contention of Famechon (1963) that *quartz* is the predominant mineral. The organic content of the sand encountered at 3.3m depth in BH IC1 was measured using the ignition method, as outlined in BS1377. The contents measured varied between 2.22% and 4.28% by weight and between 9.9% and 16.5% by volume (assuming the specific gravity of the organic (wood-like) material is 0.6).

Roundness: The roundness of the particles, as defined by Powers (1953), varied from subangular for particles with a mean size of ≈150μm to subrounded for 420μm diameter particles. In general, over 90% of the sand particles fell between these grain sizes.

Grading: Samples were wet sieved initially to determine the percentage of particles smaller than 63μm but as this was always less than 1%, the

samples were subsequently dry sieved. The results of these sieve analyses indicated that the soil could be described as a fine to medium uniformly graded sand with D_{50} = 0.32mm, D_{10} = 0.19mm, D_{60} = 0.35mm and a uniformity coefficient (D_{60}/D_{10}) of 1.8. The deviation from these properties was less than 10% in all cases and no systematic variation with depth was observed. The grading curves for the 'organic sand' showed the sand to be slightly finer with a D_{50} value of 0.23mm. The average size of the organic particles was of similar size.

Void ratio limits: A minimum void ratio (e_{min}) of 0.45 and maximum void ratio (e_{max}) of 0.81 were measured using the methods recommended by BS1377. These limits are consistent with the uniformity and roundness of the sand (see Youd 1973).

Static angle of repose: The static angle of repose, determined using the procedure set out by Cornforth (1973), was found to be 33.5° ± 0.5° for all samples. Cornforth suggests that this angle is a good approximation of the ultimate friction angle (ϕ'_{cv}) of the sand in direct shear.

5.1.5 In-situ tests

5.1.5.1 Density

Because of the inevitable disturbance caused to samples retrieved in sand, an estimate of the in-situ density is best obtained from the results of in-situ tests. Typical measurements made in Cone Penetration Tests (CPT), Standard Penetration Tests (SPT) and pressuremeter tests are shown on Figure 5.4[1]. These traces indicate that the relative density of the sand varies with depth. A particularly loose layer is apparent between 2.8m and 3.8m, which includes the organic sublayer referred to above.

---

[1] q_c= CPT end resistance, f_c= CPT sleeve friction, p_l= pressuremeter pressures measured at a volumetric cavity strain of 50% (and not 100%, which would represent the ultimate limit pressure (p_{lim}); see Mair and Wood 1987), N = SPT blows/300mm.

The laboratory classification tests and standard correlations (e.g. Jamiolkowski et al 1988, Baguelin et al 1978 and Thorburn 1963) which relate sand properties to q_c, p_L and N suggest that the stratigraphy at Labenne can be defined by three layers with the properties listed in Table 5.2.

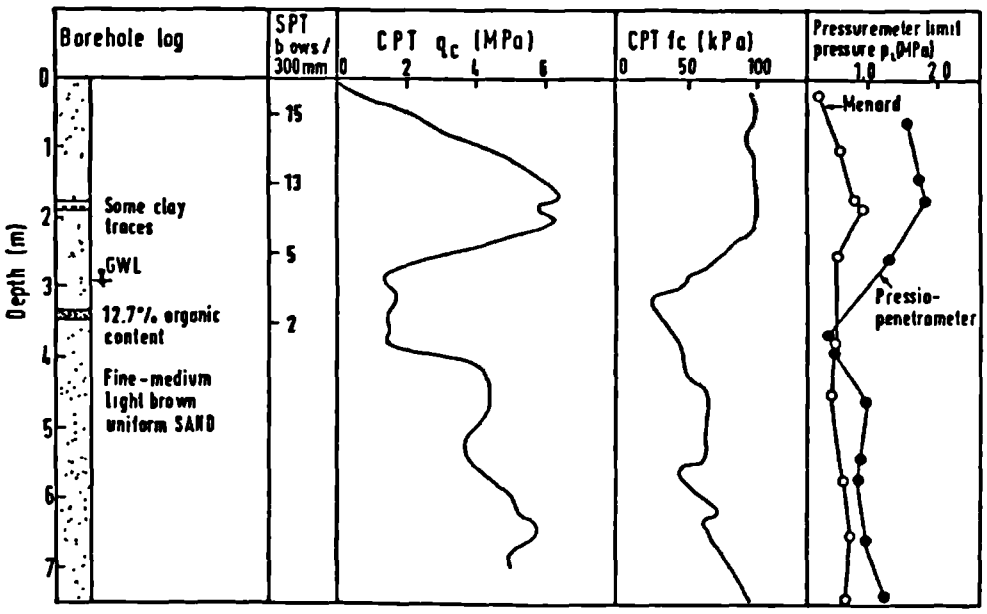

Figure 5.4 In-situ tests at Labenne

Stratum No.	Depth (m)	D_r (%)	e	γ_b (kN/m^3)
1	0-2.2	60	0.60	16.9
1A	2.2-2.8	(transition zone from stratum 1 to 2)		
2	2.8-3.8	25	0.72	19.2
3	3.8-6.0	40	0.67	19.5

Table 5.2 Stratigraphy at Labenne

5.1.5.2 Stiffness

A series of tests to determine the in-situ stiffness was performed at Labenne with the LPC pressio-penetrometer (PP). This device has a diameter of 89mm and its membrane (300mm in length) is positioned ≈300mm

from a conical tip (see Amar et al 1982). The instrument is jacked into the ground and then inflated, as in a standard pressuremeter test. Given its similarity to the ICP, both in terms of diameter and installation method, it is suggested that the inflation pressure-cavity strain curves can provide a good indication of the radial soil stiffness appropriate to the load testing stage of the ICP.

Nine PP tests were performed by LPC within a 20m radius of the pile test area and the shear moduli derived from the *initial* loading stage of each test (assuming elastic conditions) are plotted against cavity strain (ε_c) on Figure 5.5. G_p values are normalised by the square root of the initial undisturbed mean effective stress (p'_0), in keeping with the trends, reported by Seed & Idriss (1970) and others, regarding the stiffness properties of sands at small strains[1].

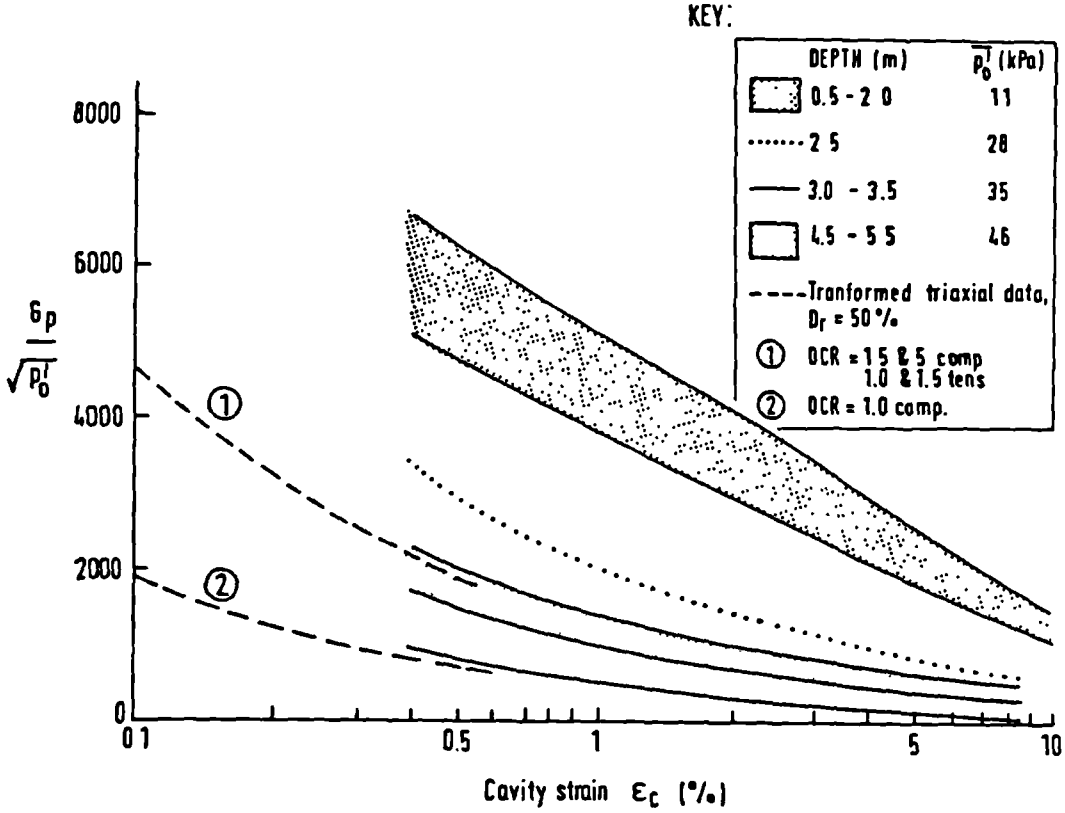

Figure 5.5 Shear stiffness moduli measured in PP tests

[1]Note that other workers, such as Tatsuoka & Shibuya (1991), suggest that G values should be normalised by p'_0 over most of the strain range that can be resolved in the these tests.

$G_p/\sqrt{p'_0}$ is seen to show a marked dependence on depth. This dependence is consistent with the inferred variation of in-situ relative densities at the site (as summarised in Table 5.2) e.g. the normalised stiffness measured in the sand at 2m (with an in-situ D_r ≈60%) is six times that in the loose layer at ≈3m (in-situ D_r ≈25%). It thus appears that installation of the PP did not alter the layered characteristic of the profile significantly.

5.1.6 Initial in-situ stresses

The estimated initial in-situ stresses at Labenne are summarised in Table 5.3. The free field vertical effective stress (σ'_{v0}) is calculated from the bulk density variation given in Table 5.2 and the water table is assumed to be at 2.9m below ground level (see Section 5.1.3). The in-situ horizontal effective stress σ'_{h0} (= $K_0\ \sigma'_{v0}$) is estimated assuming K_0 = (1-sin ϕ')$OCR^{\sin\phi'}$ (Mayne & Kulhawy 1982) with ϕ'=33°. The sand was assumed to be normally consolidated prior to the general (1.5m) excavation at the site.

Depth (m)	u_0 (kPa)	σ_{v0} (kPa)	σ'_{v0} (kPa)	OCR	K_0	σ'_{h0} (kPa)	σ_{h0} (kPa)
1.0	0	17	17	2.5	0.75	13	13
2.0	0	34	34	1.8	0.62	21	21
3.0	1	51	50	1.5	0.57	28	29
4.0	11	70	60	1.4	0.55	33	44
5.0	21	90	69	1.4	0.54	38	58
6.0	30	110	79	1.3	0.53	42	72

Table 5.3 In-situ stresses at Labenne

5.1.7 Mechanical properties from laboratory tests

The mechanical properties of the Labenne sand were investigated in a programme of laboratory tests undertaken at IC which included:

- Undrained triaxial compression and extension tests on K_0 consolidated samples
- Shear box tests
- Ring shear and shear box interface tests.

The shear box and ring shear tests are discussed in detail in Appendix D.

5.1.7.1 Triaxial tests

Five K_0 consolidated undrained (CK_0U) triaxial tests were performed Dr. V. Georgiannou on pluviated samples of Labenne sand, prepared at a 'typical' in-situ relative density of 50%. These tests incorporated local strain instrumentation to ensure that the shear stiffness characteristics at small strains were measured accurately.

Figure 5.6 shows the stress-strain curves (with the strain axis to a logarithmic scale) and stress paths observed in compression and extension tests for samples taken to overconsolidation ratios (OCR's) of between 1 and 5. Samples were sheared at an axial strain rate of 0.1% per minute to a maximum strain of between 4% and 9%.

Points to note include:

- The samples tested in compression 'dilate' from very small strains, and the mean effective stress continues to increase until critical state conditions are attained. In contrast, the extension samples 'contract' markedly, generating positive pore pressures until the stress ratio (t/s') approaches sin ϕ'_{cv}. From this point onwards, samples tested in extension also dilate.

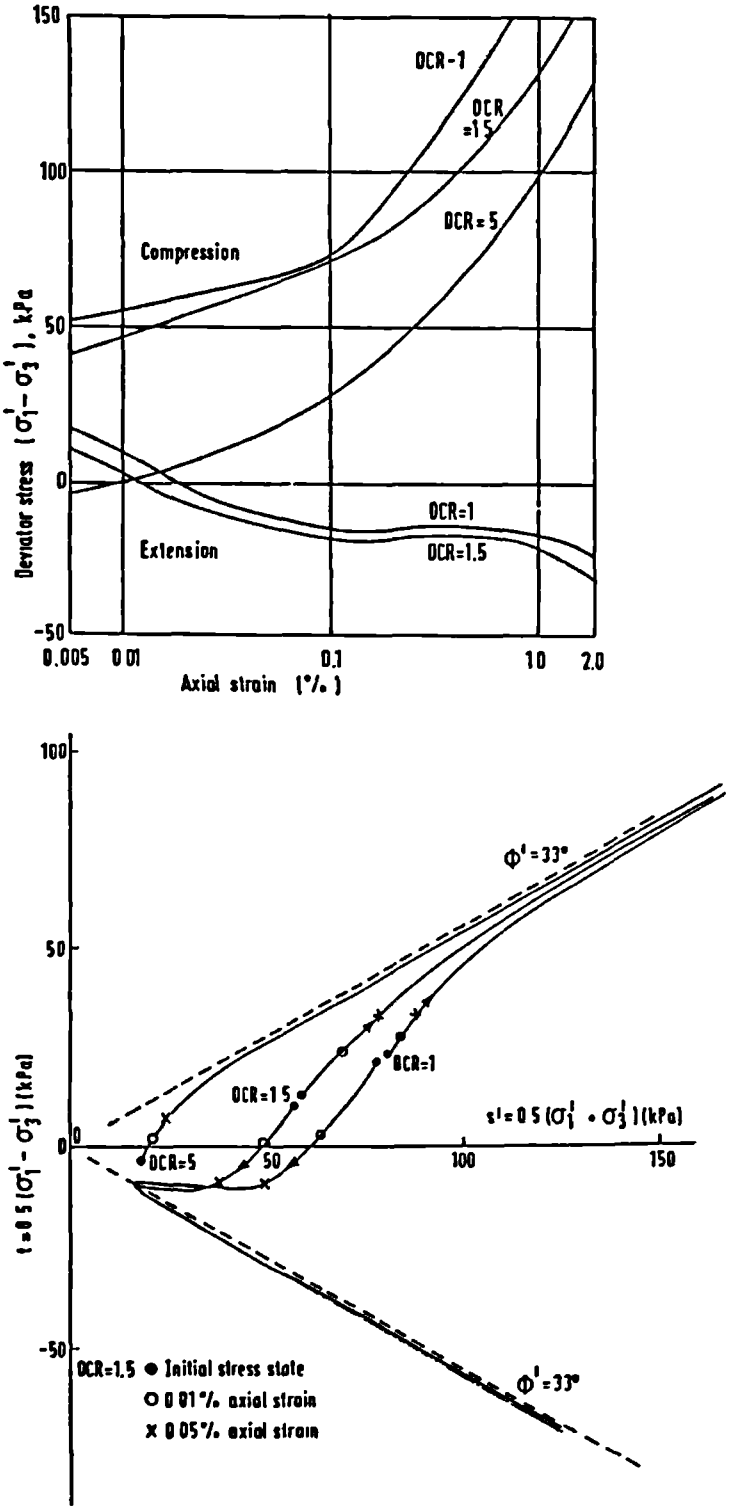

Figure 5.6 CK_0U tests on Labenne sand

- The deviator stress increases monotonically with axial strain in the compression tests. However, the extension tests display a quasi-peak deviator stress at an axial strain of about 0.05% and then show slight strain softening until dilation starts after tensile strains of ≈1%.
- Both extension and compression samples tend to an ultimate ϕ'_{cv} of 33°.

It is evident that the comparatively large strains experienced by samples during K_0 consolidation lead to a soil fabric which is particularly resistant to loading in the same direction (i.e. in compression tests when the major principal stress acts in the same direction as during consolidation). However, when the principal stress directions are rotated through 90°, as in the extension tests, the sand's response changes from dilatant and strain hardening to contractive and gently strain softening. Arthur at al (1977) and others have observed similar effects of 'induced anisotropy' on the behaviour of sands.

Secant shear stiffness values (G_{sec}) were calculated from the stress-strain curves on Figure 5.6 and values of ($G_{sec}/\sqrt{p'_0}$) are plotted against shear strain (ε_s) on Figure 5.7. At strains larger than about 0.05%, the data from all tests, except for the normally consolidated sample tested in compression, fall within a relatively narrow band. The magnitudes and trends of these data are in general agreement with the findings of Georgiannou (1988).

Also shown on Figure 5.7 are estimates of the equivalent pressuremeter moduli (G_p) assessed from the mean G_{sec} values. These moduli were derived using a procedure set out by Jardine (1992) who showed that, for constant volume conditions, G_p is approximately equivalent to G_{sec}, when

$$\varepsilon_c/\varepsilon_s = 1.2 + 0.8\log_{10}(\varepsilon_c/10^{-5}), \text{ where } \varepsilon_c = \text{cavity strain}$$

This approach was developed for the analysis of undrained tests in clays, but also provides a useful approximation for pre-yielding conditions in sand. The transformed G_p values are compared with G_p values measured in pressio-penetrometer tests on Figure 5.5 and are seen to be compatible

(except for curve 2) with values measured in the loose to medium dense material (D_r ≈40%) at ≈5m.

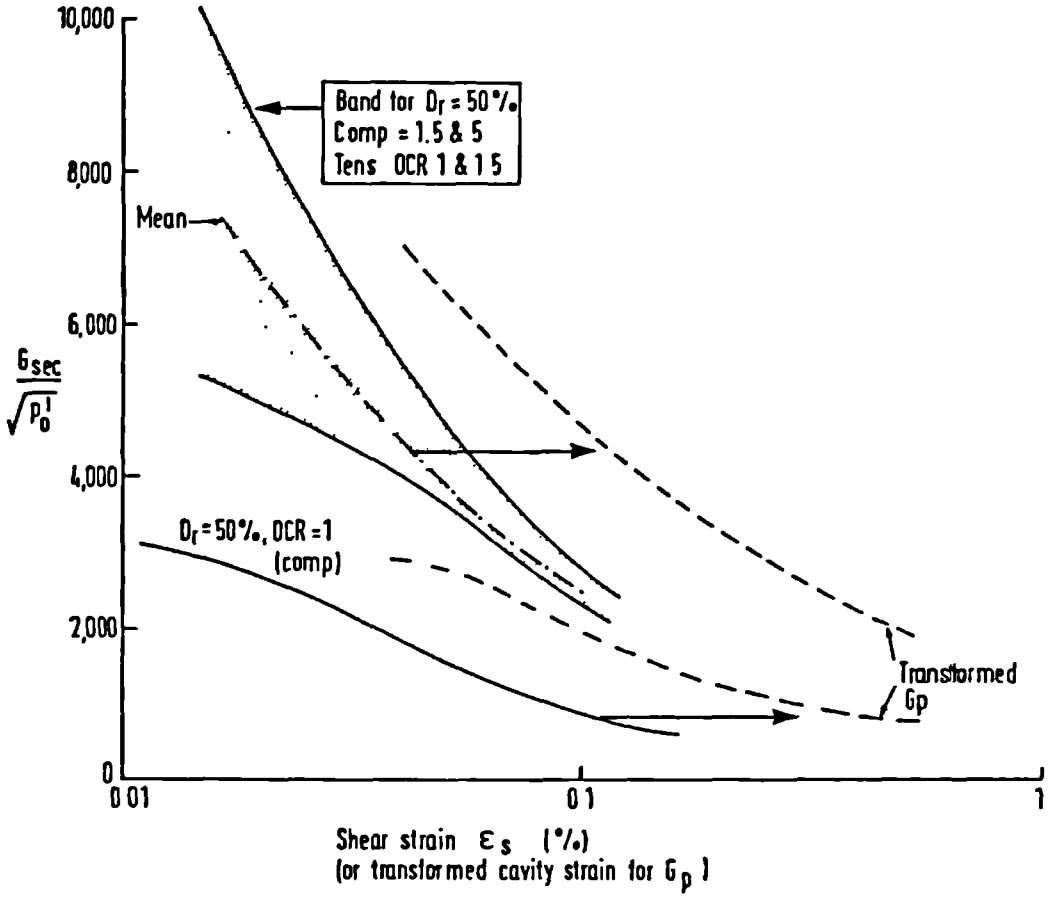

Figure 5.7 Secant shear moduli (G_{sec}) measured in CK_0U tests (estimated G_p values are also shown)

5.1.7.2 Soil on soil shear box tests

Shear box tests were carried out on samples prepared to a range of relative densities at normal stresses (σ'_n) between 30kPa and 120kPa. The peak and constant volume angles of friction recorded (where $\phi' = \tan^{-1}(\tau/\sigma'_n)$) are summarised on Figure 5.8. These angles give trends typical of subrounded sands (Bolton 1986, Cornforth 1973) and indicate a constant volume angle (ϕ'_{cv}) close to that observed in the triaxial compression and extension tests (33°).

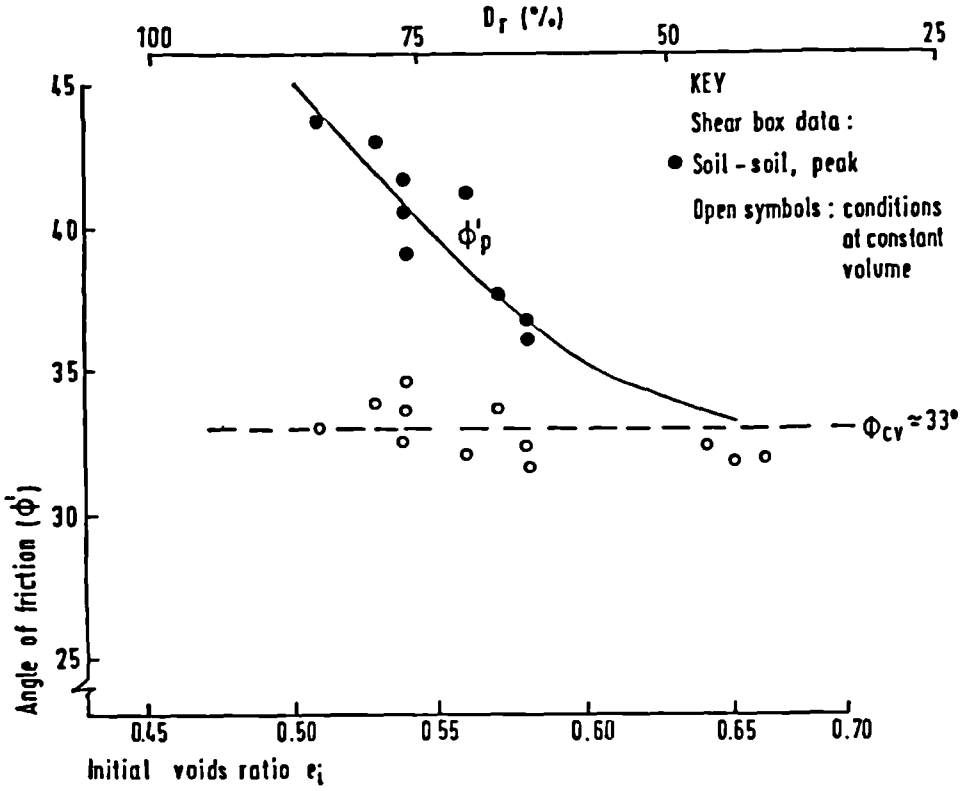

Figure 5.8 Soil on soil friction angles measured in shear box tests

5.1.7.3 Interface shear tests

Shear box and ring shear *soil-steel* interface tests were performed to investigate the behaviour of (fully saturated) Labenne sand in interface shear. The three interfaces used had centre line average (CLA) roughness values (R_1) compatible with the R_1 range of the pile shafts (7 ± 2.5μm) and normal stresses were comparable to the radial effective stresses measured in the pile tests (60 ± 40kPa). The interface used in the ring shear tests was made from stainless steel (i.e. the same material as the SST's), but mild steel was used in the shear box tests.

Typical interface-shear test data for loose and dense samples (as measured in shear box tests) are shown on Figure 5.9, where they are compared with data from equivalent soil on soil shear box tests.

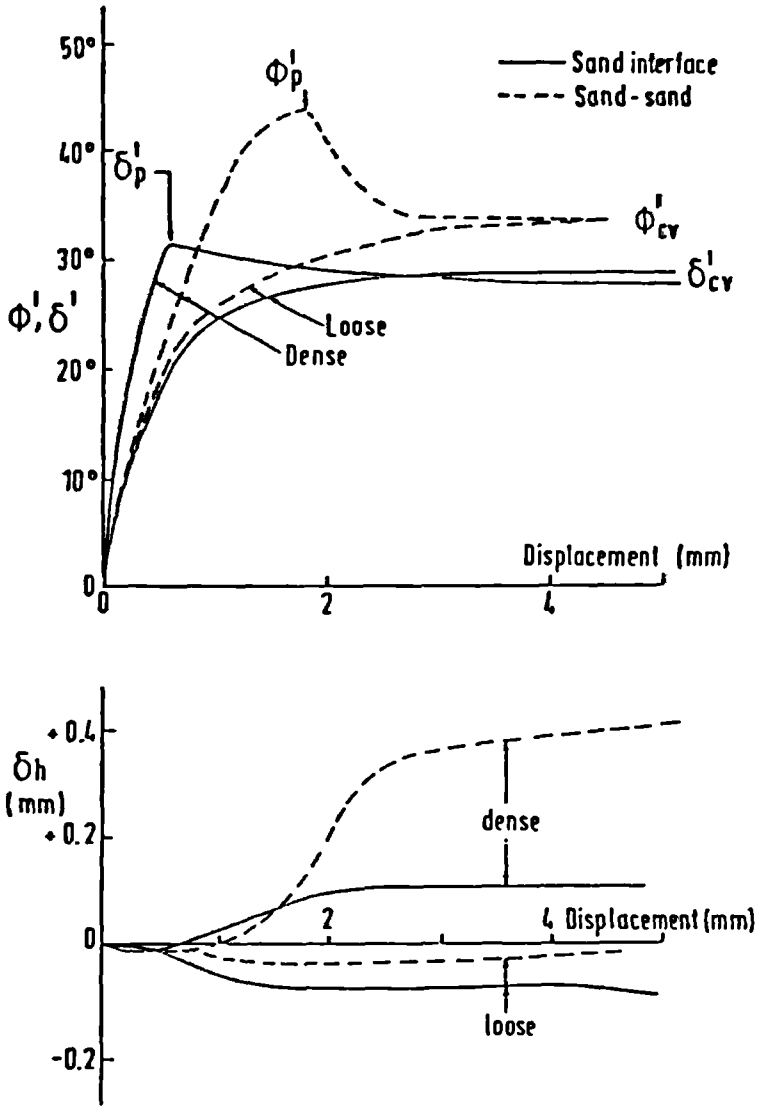

Figure 5.9 Typical direct shear soil on soil and soil-steel interface data

It is apparent that:

- As with the soil on soil tests, soil-interface tests on dense samples display a peak angle of friction (δ_p) and tend, after moderate displacements (3-4mm), to a constant volume interface friction angle (δ_{cv}).
- The friction angles mobilised in interface tests (δ_p & δ_{cv}) are significantly smaller than the equivalent ϕ' values determined in soil on soil tests.

- The dilation shown by dense sand in interface shear results in smaller normal displacements (δh) than in equivalent soil on soil tests.
- Loose sand contracts in both soil on soil and soil-interface shear, so that peak and ultimate conditions coincide.

These observations suggest that, in the presence of an interface (which is effectively 'smoother' than a sand interface), less over-riding and rolling of sand particles is required in order to achieve a critical density[1]. The interface friction angles are controlled primarily by the properties of the interface and the mineralogy of the sand.

Two ring shear interface tests investigated if the shearing history had an effect on the interface-shear behaviour. Samples were subjected initially to a relative displacement of ≈2.5m in 8 shearing pulses at a rate of 530mm/min. This stage simulated the displacement history of a soil element located adjacent to the shaft of a pile which was installed with its tip 2.5m below the soil element. The samples were subsequently sheared at a slow drained rate of displacement (as in shear box tests). The friction angles mobilised during fast shearing pulses showed little dependence on the magnitude or rate of displacement and were typically only 2° less than the angles measured in slow shear. The difference of 2° may be due to (i) a slight difference between the 'dynamic' and 'static' shearing mode of the sand and/or (ii) the generation of small positive excess pore pressures at fast rates of displacement.

The trends of the peak and ultimate angles of friction observed during slow shear in ring shear and shear box interface tests are shown on Figure 5.10. It is evident that both roughness and relative density affect the value of δ_p, but the variation is small (29° to 33°) in comparison with the corresponding range measured for ϕ'_p (45° to 33°). The ultimate interface friction angle (δ_{cv}) is 5° less than ϕ'_{cv}; δ_{cv} and ϕ'_{cv} appear to be *independent* of relative density.

---

[1]A similar mechanism is presumed to operate when the sand is dry as the δ values (at these R_1 values) measured in the wet and dry states are comparable (see Everton 1991 and Section 9.5).

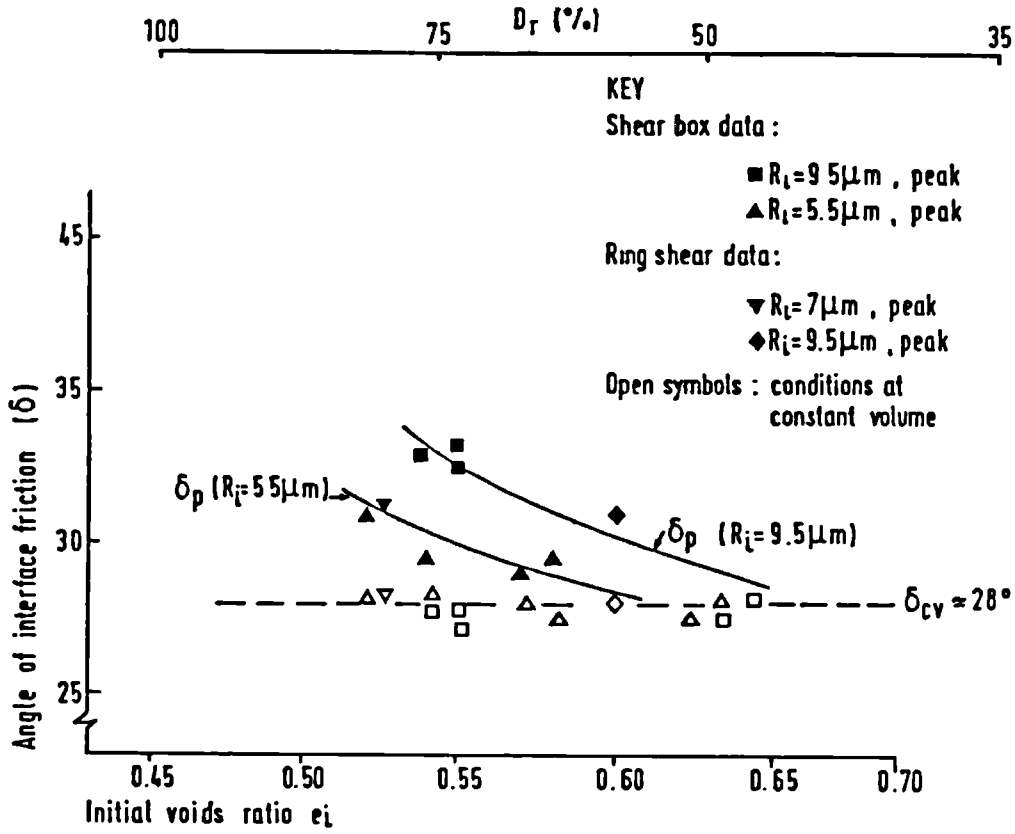

Figure 5.10 Peak and constant volume interface friction angles measured in direct shear soil-steel interface tests.

The shear box and ring shear interface tests exhibit comparable trends, suggesting that δ values are relatively insensitive to the displacement history of the sand. Shear box tests therefore appear to be an expedient way of assessing the magnitudes of interface friction angles appropriate to displacement piles.

Two samples of the 'organic sand', retrieved at a depth of 3.3m in BH IC1, were tested in the shear box against a rough steel interface (R_i=9.5μm). Both samples contracted during shear and mobilised a δ_{cv} value of 27°, which is only slightly less than δ_{cv} values shown by pure sand (28°). It should be noted, however, that it was not possible to control the quantity of organic material at the interface in these tests.

5.2 SOIL CONDITIONS AT COWDEN

5.2.1 The site

The Building Research Establishment (BRE) test site at the RAF base in Cowden, North Humberside (Figure 5.11), was set up in 1976 to provide facilities for research into the engineering properties of glacial clay tills. These tills cover large areas of England and the southern North Sea.

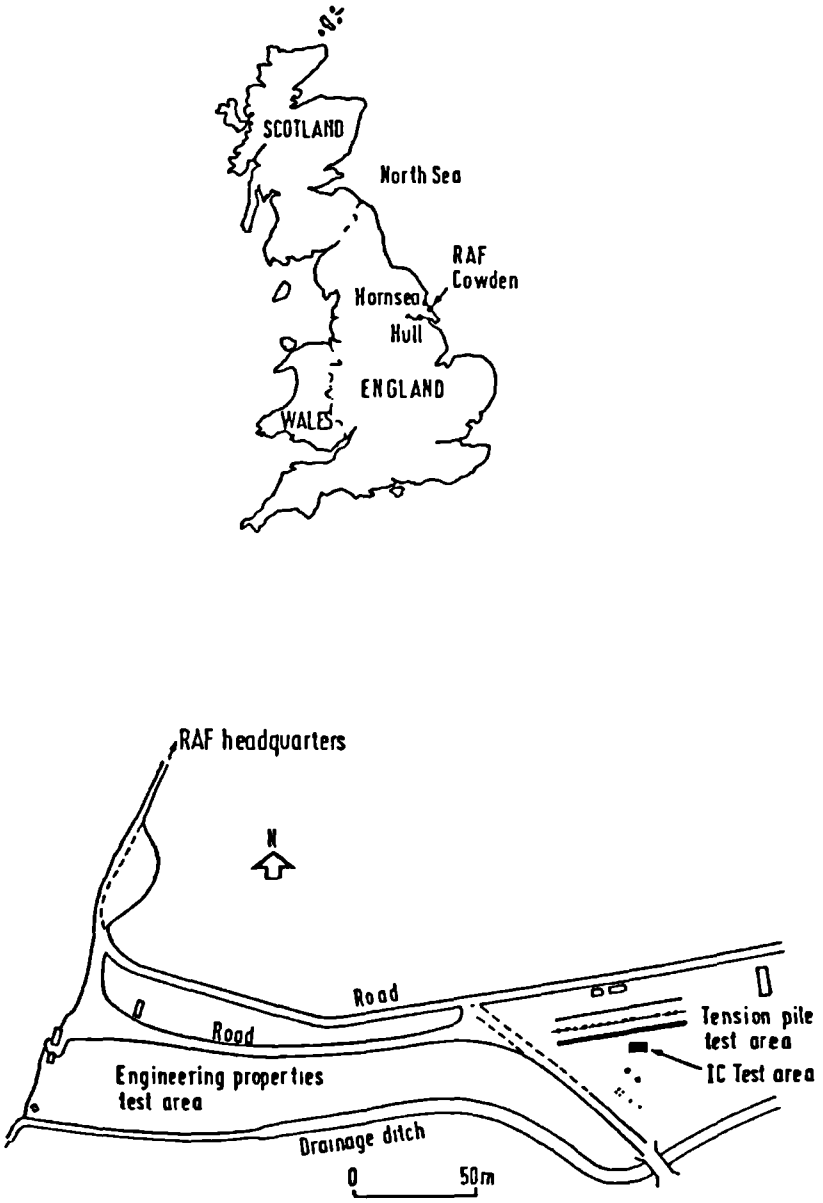

Figure 5.11 Cowden location and site plan

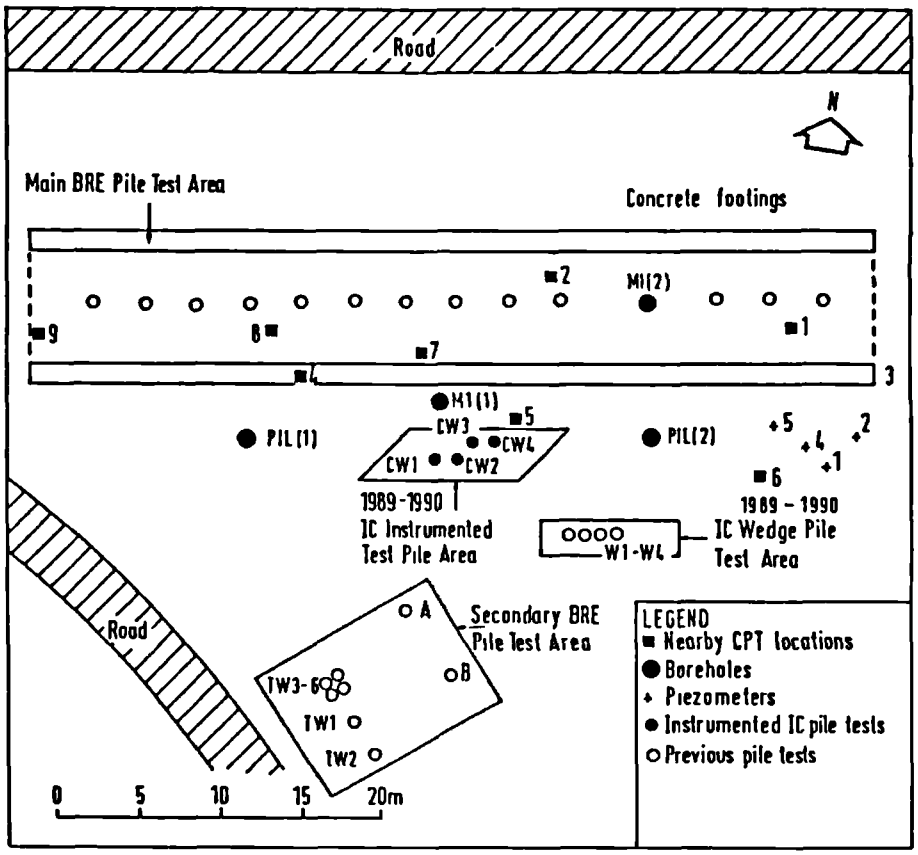

Figure 5.12 Plan of Tension Pile Test (TPT) area at Cowden

The site covers an area of about 2.5 hectares and lies 800m west of the coastal cliffs. Many different in-situ tests and pile tests were performed at the site and these have been supplemented by an extensive laboratory testing programme. All previous investigations have been reported comprehensively (e.g. see Marsland & Powell 1985 and Robson 1988).

The site is nominally divided into :

(i) The engineering properties (EP) test area

(ii) The tension pile test (TPT) area

The ICP tests (designated CW1 to CW4) were carried out in the TPT area and their locations relative to other site investigation and pile test locations in this area are shown on Figure 5.12. The TPT area was dedicated originally to a project, sponsored by the UK Dept. of Energy,

which examined some of the factors affecting the performance of piles subjected to tensile loads. This project used over 20 steel 10m long piles, ranging in diameter from 193mm to 457mm, and investigated (a) the influence of the pile end condition (i.e closed-ended or open-ended), (b) the performance of pile groups and (c) the effects of grouting piles after installation. The general trends that emerged from the tests on single (ungrouted) piles are compared with the ICP results in Chapter 7.

5.2.2 Geology

The Cowden area was glaciated during each of the three major ice advances on to lowland Britain during the late Quaternary period (Anglian - 200,000 years before present (b.p.), Wolstonian - 125,000 b.p. and Devensian 75,000 b.p.). A detailed geological study by Madgett & Catt (1978) suggested that the succession in the top 20m was deposited by lodgement from a single two tiered ice sheet during the Devensian period. This ice sheet was a combination of ice fronts originating in the Pennines and Scotland and led to the classification of strata given in Table 5.4. Cretaceous chalk underlies the glacial deposits (referred to as till) at a depth of ≈40m.

Stratum	Depth[1] (m)	Origin
Withernsea TILL	0-10	Ice front from Pennines
Englacial SAND	10-12	Fluvial-glacial material between ice fronts
Skipsea TILL	12-19	Ice front from Scotland

Table 5.4 Geological succession at Cowden

The well graded nature of the till (see below) has been the result of thorough mixing in a relatively wet state in the thin (≈0.5m) layer of regelation ice immediately above the base of the glacier (Marsland 1985).

[1]Depth in the vicinity of the pile tests. Variations of up to 4m from these depths exist across the site.

Since the retreat of the ice fronts, weathering in the top 5m of the Withernsea till, due to the effects of permafrost/surface moisture deficiencies, has led to the creation of fissures, to decalcification and to increased shear strength. Oxidation of the pyrite and siderite minerals has led to colour changes.

5.2.3 Site profile

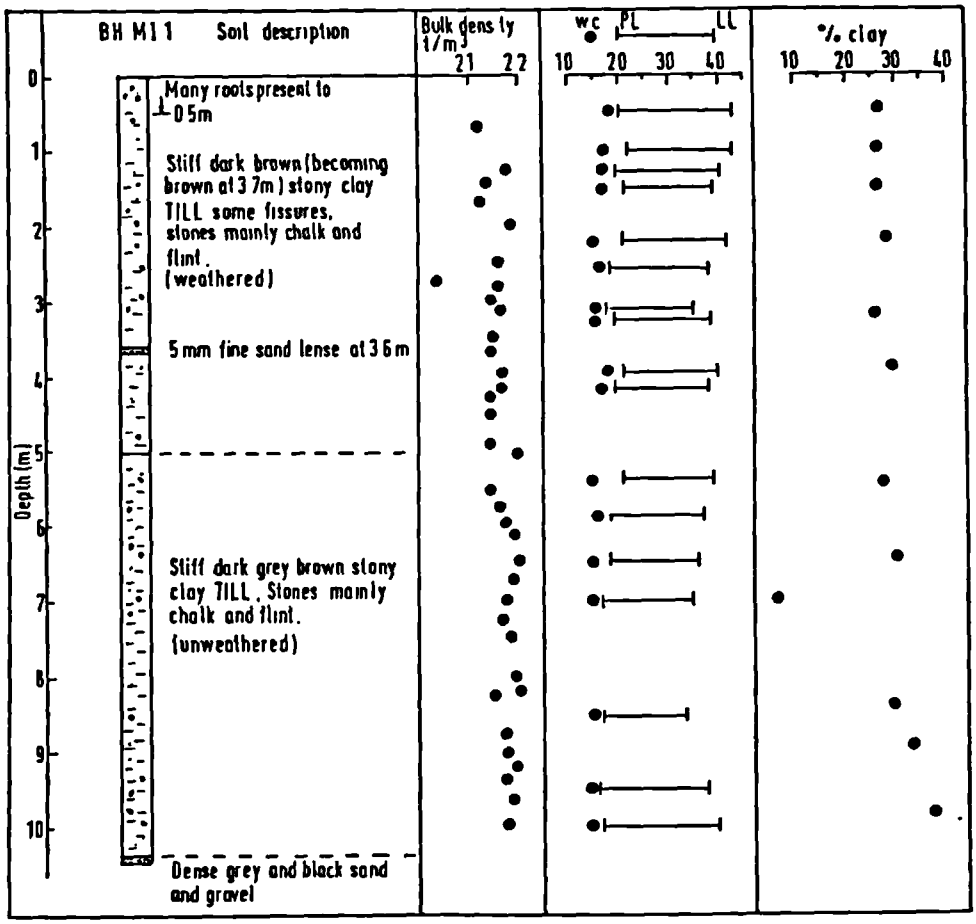

Figure 5.13 Borehole log and index properties near ICP test locations

The log for the borehole closest to the ICP tests (BH M1(1), Figure 5.12) is shown on Figure 5.13. The upper till (Withernsea) extends to 10.5m and is underlain by a layer of dense sand and gravel (englacial layer). The colour change observed at 5m has been interpreted as the boundary between the weathered and unweathered material. Nearby Cone Penetration tests suggest that the englacial layer is slightly deeper (≈11m) at the

location of the pile tests and is ≈1m thick. The underlying (Skipsea) till extends to ≈19m.

The depth to the water table measured during the pile tests was 0.8m. In-situ pore water pressures were measured by a series of piezometers installed at various depths at a location 20m east of these tests (Figure 5.12) and showed that the upper till is under-drained by the englacial sand layer (presumably to a buried river channel or exposures on the cliff face). This under-drainage leads to an average pore pressure gradient of ≈8.4kN/m^2 per metre depth within the strata penetrated by the piles (i.e. to ≈6m)

5.2.4 Grading, composition & fabric

Grading analyses of samples from Borehole M1(1) showed that the material is uniform and well graded, comprising ≈30% clay, 50% silt and 20% sand & gravel. The granular fraction comprises ≈60% chalk; the remaining 40% includes flint, sandstone, limestone and quartzite. X-ray diffraction analyses (BRE 1986) showed that the clay fraction consisted of kaolinite and mica. These minerals were reported to be less crystallised within the weathered material.

Studies of the fabric of Cowden till have been reported by Derbyshire & Love (1981). Macro-fissures were only identified at shallow depths and were generally near vertical, planar, of moderate size (0.01-1.0m^2) and low intensity (less than 3m^2 per cubic metre). One such fissure, coated with grey silt, was observed in Borehole M1(1) at 4m depth. Fabric studies have also shown that the granular fraction of both the weathered and unweathered till is separated by clay and silt sized particles; parallel clay particles along micro-shears (typically 0.05-0.2mm long) are very common and these usually terminate against grain boundaries of the larger material. This well ordered, 'clay matrix dominated' form is typical of a lodgement till (Marsland 1985).

5.2.5 Index tests

The variations with depth of the bulk density, water content, index properties and clay content are shown on Figure 5.13 and may be summarised as follows (for material to 7m depth):

- The bulk unit weight (γ_b) remains relatively constant at 2.16±0.02 t/m^3.
- The liquid and plastic limits reduce slightly with depth; liquid limits (LL) reduce from ≈42% near the surface to ≈36% at 7m and the plastic limits (PL) reduce correspondingly from ≈21% to ≈18%.
- The plasticity indices (PI) vary from about 21 ±2% in the top 2.5m to ≈19% below this level.
- The water contents vary between 15% and 18% and imply liquidity indices (LI) of -0.17 ± 0.08.
- The clay content (CC) varies between 27% and 30%, except for a sandy lense at 7m.

5.2.6 c_{u0} & q_c profile

The UU shear strength (c_{u0}) and CPT q_c profiles[1] measured for the TPT area of the site are shown on Figure 5.14.

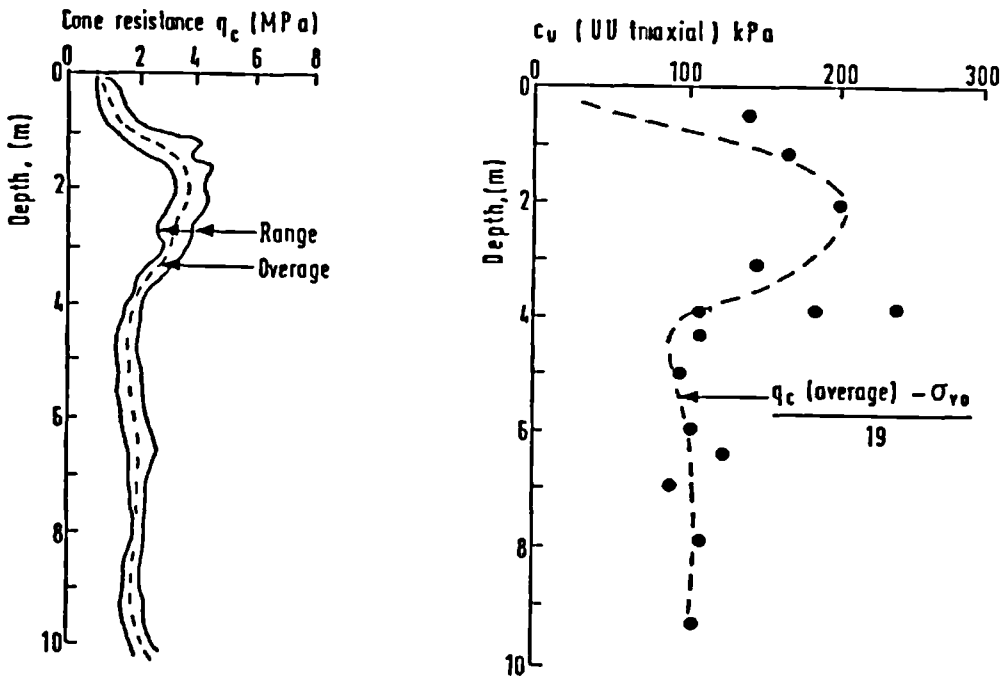

Figure 5.14 q_c and c_{u0} profiles for the TPT area at Cowden

Considerable variability in the q_c values is apparent in the top 3.5m, where the resistance increases to a maximum of about 4MPa at 2m. Below

[1]This figure ignores the 'blips' in the CPT traces caused by the presence of stones in the till.

3.5m, the q_c values are relatively constant at 2MPa. The c_{u0} values follow the same trend and are compatible with a cone factor N_k) of ≈19. The upper 3.5m may be classified as a stiff to hard till; below this level, the material is of stiff to very stiff consistency (BS1377).

Two notable features of the c_{u0} and q_c measurements were observed:

- Gens & Hight (1979), and others, have shown that c_{u0} values of intact, remoulded and reconstituted samples with the same matrix water content and mean effective stress are very similar. This <u>insensitive</u> characteristic is in sharp contrast to the behaviour observed in triaxial tests on Bothkennar clay (see Section 5.3).
- Powell & Quarterman (1989) showed that the q_c value is rate dependent; q_c values reduce by about 10% for each log cycle reduction in penetration rate (between 1mm/min and 1000mm/min).

5.2.7 Behaviour in 1-D compression

16 oedometer tests were carried out by BRE on *intact* samples from between 3m and 9m depth (LL≈36%). The conventional e v log σ'_v plots of these data showed continuous changes in curvature with increase in stress level and therefore no clear indication of yield (Robson 1988). An improved identification of a vertical yield stress (σ'_{vy}) can be found by plotting log (1+e) in place of e on the vertical axis (Butterfield 1979). Data from three tests are shown in this form on Figure 5.15a and all show a distinct change in curvature (or yield) at σ'_{vy} ≈550kPa. This yield stress is compatible with apparent overconsolidation ratios estimated from strength and in-situ stress measurements (Section 5.2.8). The average compression index (C_c), measured at σ'_v=1500kPa, is ≈0.15 and the swelling index (C_s) is ≈0.037.

The compression curve measured in an oedometer test, performed at IC, on *reconstituted* Cowden till from 2m depth (LL=40%, PL=20%)[1] is shown on Figure 5.15b.

---

[1]The fraction greater than 0.6mm was removed and the sample was then reconstituted at a water content of 1.5 times the liquid limit. All load increments were maintained for 24 hours.

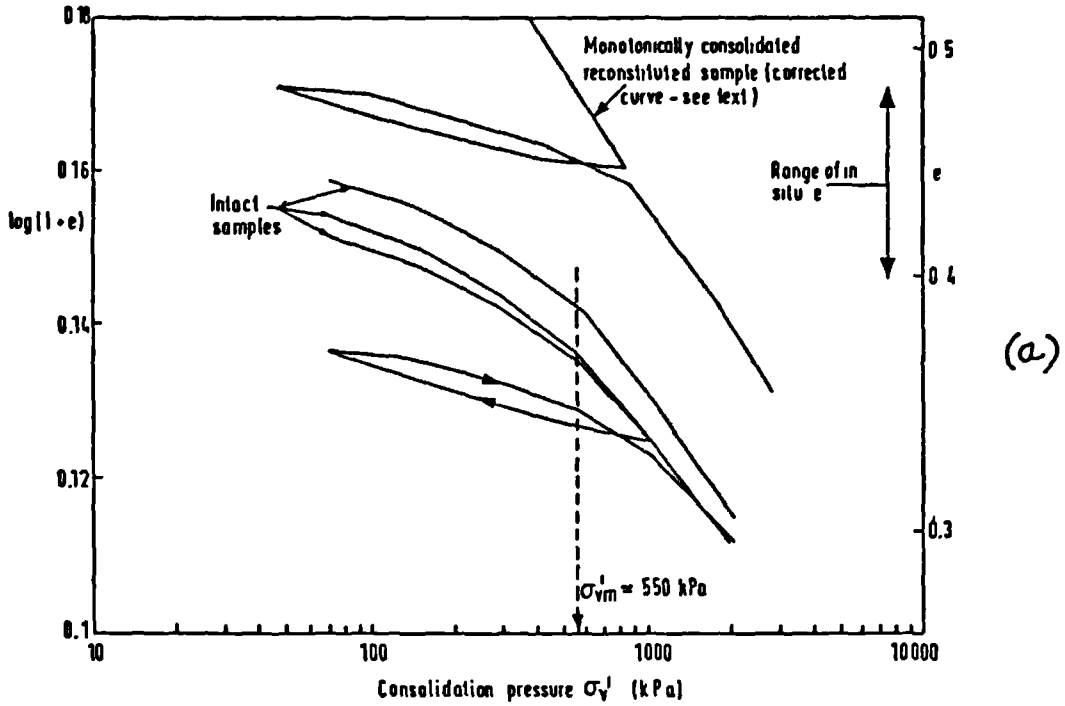

(a)

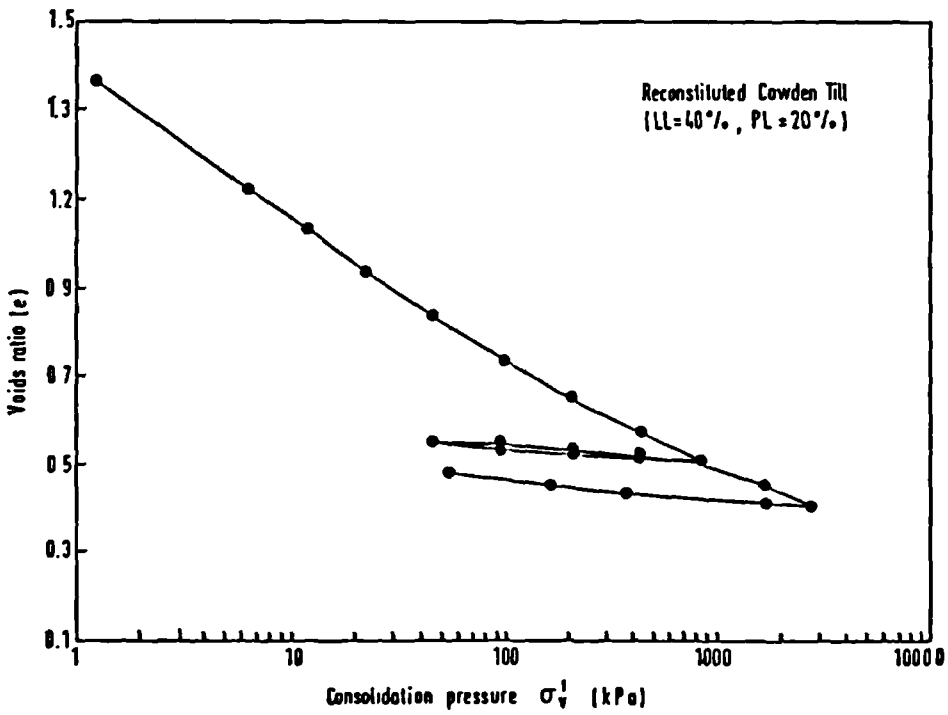

(b)

Figure 5.15 Oedometer tests on Cowden till

The reconstituted sample had the following properties:

- Compression index (C_c^*) = 0.24 (stress range 200kPa-1000kPa)
- Void ratio at σ'_v =100kPa (e_{100}^*) =0.736
- Swelling index (C_s^*) ≈ 0.046 (OCR=10)

The values of C_c^* and e_{100}^* are in good agreement with correlations between these parameters and the liquid limit (Burland 1990), but are ≈30% higher than those of the intact soil. This discrepancy may be partly because the sample had a higher liquid limit than most of the intact soil and also had its gravel content (amounting to 6%) removed. Approximate corrections[1] to the reconstituted data for these two effects have been made to allow the comparison with intact behaviour, shown in Figure 5.15a.

The 'corrected' trace for the reconstituted till clearly lies above those of the intact material. There is no evidence that the two sets of data converge at high stresses, despite apparent yield of the samples at σ'_{vy} ≈550kPa. The complex depositional history of Cowden till, which probably involved many cycles of loading and unloading over different stress ranges, may have caused this effect.

5.2.8 In-situ stress state

Attempts to obtain direct measurements of the in-situ horizontal stresses (σ_{h0}) in the 'EP area' at Cowden (Figure 5.11) were made using Menard and self-boring pressuremeters, spade cells and dilatometers. However, the indeterminate degree of disturbance caused by the respective instruments led to a wide range in the estimated profile of σ_{h0}. Even the measurements made by the self-boring pressuremeter, which is generally considered the most suitable of the above instruments, showed an unacceptable degree of scatter with poor repeatability (Powell & Uglow 1985).

---

[1]The correction for LL was based on the correlations proposed by Burland (1990). The correction for the gravel fraction (which is primarily composed of chalk) was made using the value of the saturation water content of this fraction reported by Gens & Hight (1979).

Given the apparent failure of the in-situ devices, Marsland & Powell (1985) interpreted a more consistent 'best' estimate of σ_{h0} for the EP area using suction test measurements and estimates of apparent OCR (from oedometer tests). The 'best estimate' profile lay near the average line interpreted from the Menard pressuremeter and spade cell tests.

Estimates of in-situ stress state (σ_{h0},K_0,OCR) for the TPT area are made in the following using the results of undrained triaxial tests, suction tests and oedometer tests. The relationships between OCR, c_{u0} and K_0, outlined below, assume the simple process of mechanical consolidation followed by unloading with no subsequent reloading. Although the geological history of Cowden till is far more complicated than this simple process, the formulae should help to provide (upperbound) estimates of K_0 and OCR, which are critical parameters governing subsequent behaviour of the till.

(i) Undrained triaxial tests

14 UU triaxial compression tests were carried out on samples from the TPT area, giving the profile with depth shown on Figure 5.14. These data may be used to deduce the variation of apparent OCR with depth using a relationship of the kind proposed by Ladd et al (1977) who showed that data from six sedimentary clays which had undergone K_0 consolidation and monotonic swelling fitted the expression[1]:

$$c_u/\sigma'_{v0} = (c_u/\sigma'_{v0})_{nc}\ OCR^{(0.8\pm0.05)}$$

A similar formula was found to fit the behaviour of monotonically overconsolidated Magnus till, which has similar index properties to Cowden till (Jardine 1985)[2]:

$$c_u/\sigma'_{v0} = 0.325\ OCR^{0.71} \qquad \text{(a)}$$

---

[1]The subscript 'nc' denotes normally consolidated. The ratio $(c_u/\sigma'_v)_{nc}$, for triaxial compression (peak strengths), is expected to be in the range 0.3 to 0.33 for clay of PI≈19% (Hight et al. 1987).

[2] Magnus till : CC =35%, LL =32%, PL =15%, PI =17%
Cowden till : CC =30%, LL =38%, PL =19%, PI =19%

The most widely accepted expression relating K_0 with OCR for simple mechanical overconsolidation is that proposed by Mayne & Kulhawy (1982): $K_0 = (1-\sin\phi')\ OCR^{\sin\phi'}$, which for $\phi' = 26°$ (see Section 5.2.9) gives:

$$K_0 = 0.56\ OCR^{0.44} \qquad \text{(b)}$$

Profiles of apparent OCR and K_0, derived from the c_{u0} profile (Figure 5.14) using expressions (a) and (b), are shown on Figure 5.16.

(ii) Suction tests

16 soil suction tests were carried out by BRE under triaxial conditions within 2hrs of sampling. The cell pressure was increased to ≈600kPa in each case and pore pressures were measured via a porous stone (with a low air entry value) positioned at the base of the sample. Equilibrium was generally attained after 1 hour and the suction (p'_s) noted as the difference between the cell pressure and the pore pressure. If it is assumed that (a) the sample was fully saturated and (b) sampling consists only of an elastic unloading of deviator stress, then the measured suction is equal to the mean effective stress in the ground prior to sampling. If drainage does not occur, then

$$K_0 = \sigma'_{h0}/\sigma'_{v0} = (3p'_s - \sigma'_{v0})/2\sigma'_{v0} \qquad \text{(c)}$$

Values of K_0 derived using this expression, and apparent OCR using expression (b), are plotted on Figure 5.16.

Tube sampling of real soils can, however, alter the mean effective stress considerably from its in-situ value. For heavily overconsolidated clays $|p'_s| > p'_{in\text{-}situ}$, whilst the reverse is true for low OCR samples. We might therefore expect the OCR and K_0 profiles to be over-predicted by this method for the uppermost layers at Cowden.

(iii) Oedometer tests

The vertical effective yield stresses (σ'_{vy}) were most easily identified from oedometer tests by plotting the (e,σ'_v) data on logarithmic axes, as described in Section 5.2.7. The values of σ'_{vy} varied between 480kPa and

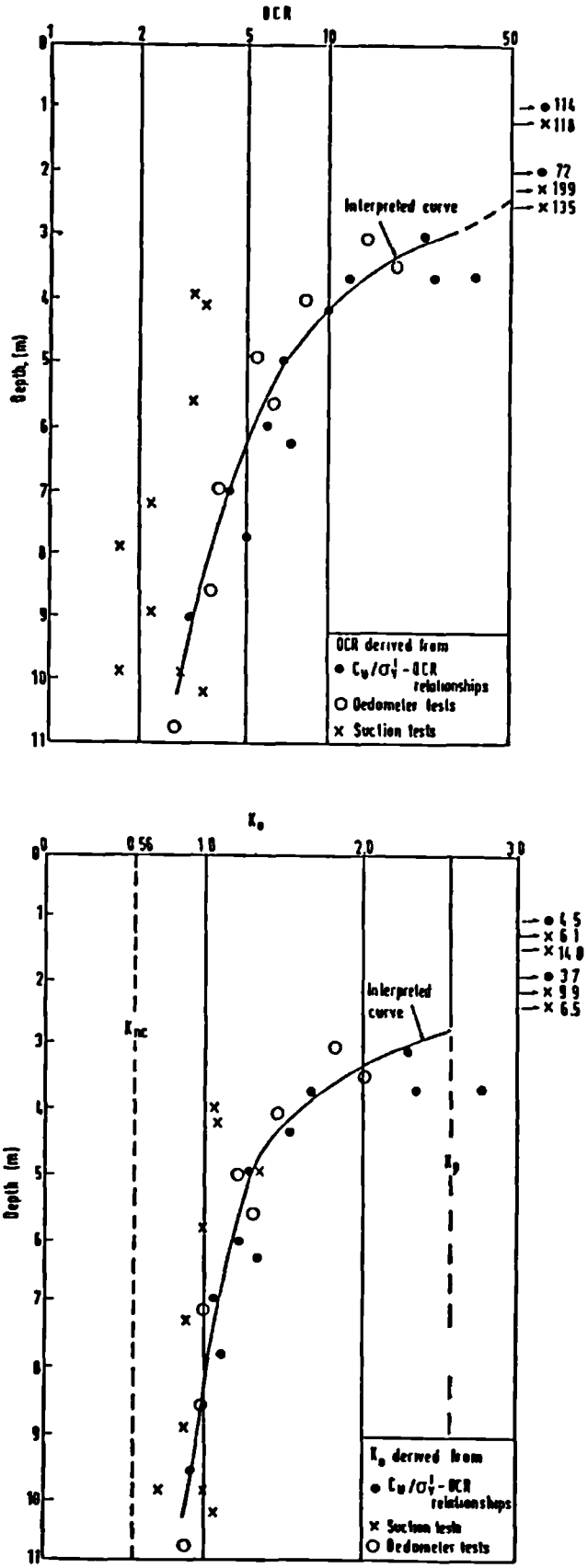

Figure 5.16 Apparent OCR and K_0 profiles for the TPT area at Cowden

630kPa and showed no systematic variation with depth. The apparent OCR values ($\sigma'_{vy}/\sigma'_{v0}$), calculated assuming σ'_{vy} =550kPa, are shown on Figure 5.16; the corresponding K_0 values were determined from expression (b).

Summary profile

Interpreted lines are shown through the calculated data on Figure 5.16 which take account of the limitations of the various test methods, the trends of the in-situ tests and the constraint that K_0 should not greatly exceed the limiting passive pressure coefficient K_p[1]. The co-ordinates of the interpreted lines are listed in Table 5.5.

Depth (m)	u_0 (kPa)	σ_{v0} (kPa)	σ'_{v0} (kPa)	OCR	K_0	σ'_{h0} (kPa)	σ_{h0} (kPa)
1.0	2	22	20	>50	2.60	52	54
2.0	12	44	32	50	2.60	83	95
3.0	21	64	43	30	2.50	108	129
4.0	29	85	56	11	1.60	90	119
5.0	36	106	70	6.8	1.30	91	127
6.0	44	127	83	5.4	1.17	97	141
7.0	51	150	99	4.6	1.10	109	160
8.0	59	170	111	3.7	1.00	111	170
9.0	59	191	132	3.3	0.95	125	184
10.0	54	212	158	2.9	0.90	142	196

Table 5.5 In-situ stresses at Cowden

5.2.9 Triaxial tests

5.2.9.1 Isotropic tests

Marsland & Powell (1985) reported results from isotropically consolidated undrained (CIU) triaxial extension and compression tests on piston

[1]Where $K_p = (1+\sin \phi'_{cv})/(1-\sin \phi'_{cv}) = 2.6$.

samples taken from between 2m and 10m. The samples were consolidated to initial stresses ranging from 140kPa to 1000kPa. The tests showed that:

- All samples tended to yield when the mobilised ϕ' approached its peak value and then began to *dilate* towards an ultimate state. No clear peak value of deviator stress was attained and dilation continued at strains in excess of 15%.
- The ultimate strength was typically 25% larger in compression than in extension (for the same initial consolidation pressure).

The average effective stress parameters were as follows:

Compression :	c'=10kPa, ϕ'=28.5°	(at peak obliquity)
	ϕ'=26°	(at peak deviator stress)
Extension:	c'=12kPa, ϕ'=32°	(at peak obliquity)
	ϕ'=32°	(at peak deviator stress)

5.2.9.2 Anisotropic tests

Hight et al (1985), and others, have suggested that in the absence of high quality undisturbed samples, the pre-failure behaviour of the intact material may be assessed from tests using reconstituted samples that are consolidated anisotropically (i.e. CK_0 tests).

Only a limited study of the undrained behaviour of anisotropically consolidated reconstituted Cowden till has been carried out (Gens & Hight 1979, De Campos 1984). The results from these studies can, however, be supplemented using the results from tests performed on reconstituted Magnus till (Jardine 1985) which has similar index properties to Cowden till. The stress paths for the series of CK_0U tests on Magnus and Cowden tills are shown on Figure 5.17.

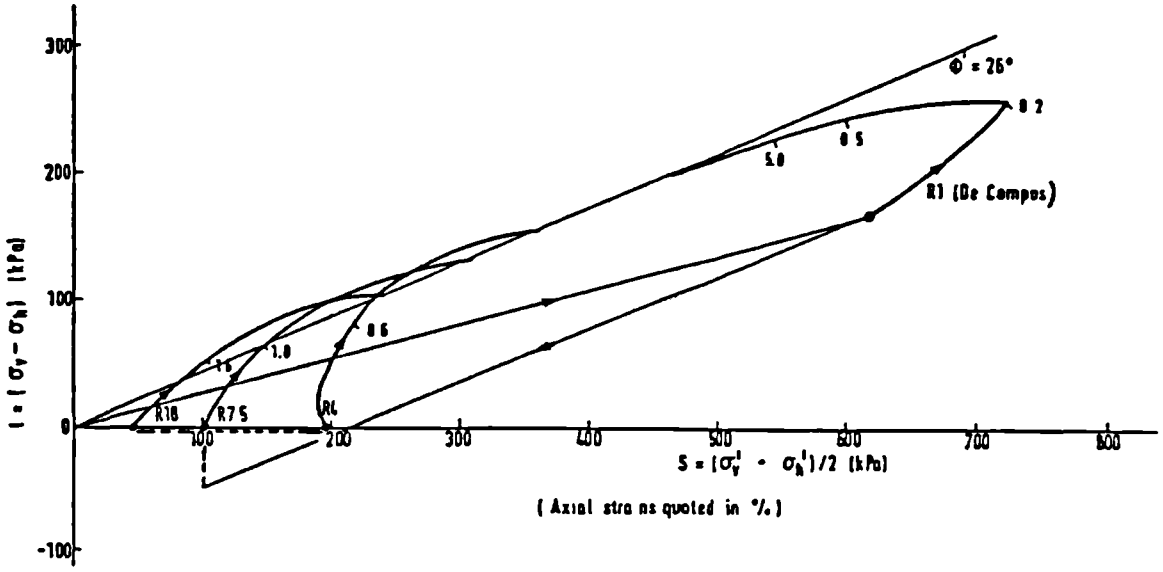

COWDEN TILL (GENS AND HIGHT 1979)

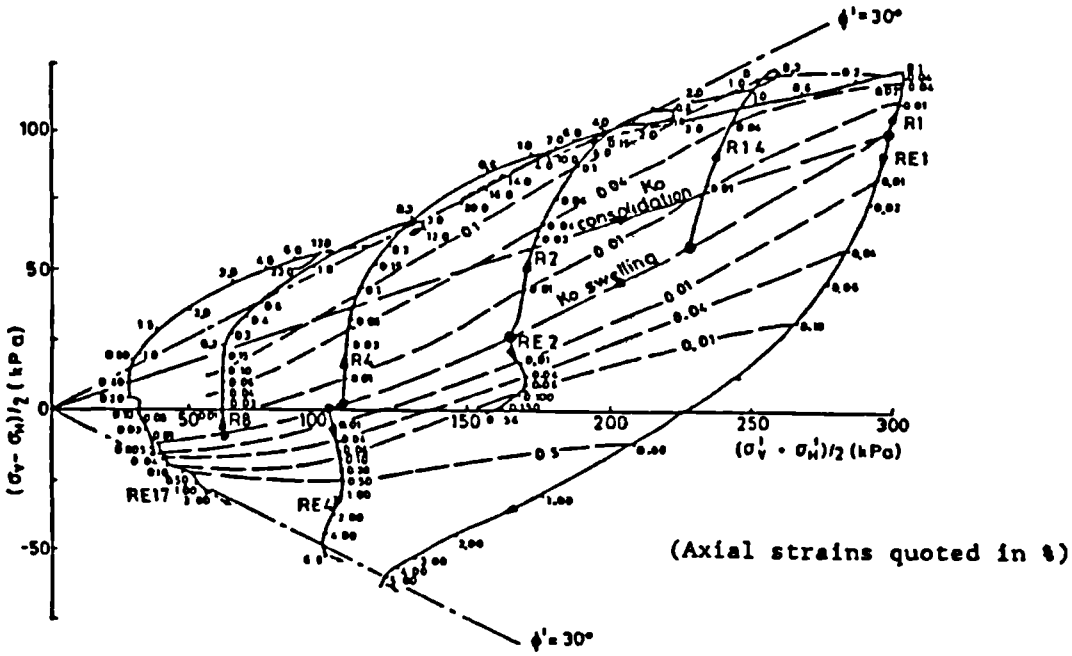

MAGNUS TILL (JARDINE 1985)

Figure 5.17 CK_0U tests on reconstituted Cowden and Magnus till

Both tills show comparable trends:

- The normally consolidated reconstituted soil[1] exhibits pronounced undrained brittleness in compression. This brittleness reduces with increasing OCR and is absent in triaxial extension. (Note that brittleness was not apparent in any of the *isotropically* consolidated tests.)
- There is anisotropy of ultimate strength and stiffness, both being lower in triaxial extension.
- Strains to mobilise peak strengths in compression increase from very small values (≈0.1%) for normally consolidated soil to 10%-20% at high OCR.

5.2.9.3 Triaxial stiffness

The stiffness measurements made in the CK_0U tests on Cowden till, referred to above, are not considered reliable as they did not measure strains locally on the samples. Triaxial compression tests which did incorporate local small strain instrumentation have, however, been performed on *unconsolidated* and *isotropically* consolidated samples of Cowden till (Hird et al 1991). The variations of shear stiffness with shear strain measured in these tests are plotted on Figure 5.18.

Jardine et al (1991) reviewed the factors affecting the small strain stiffness measured in triaxial tests and suggested that tests which do not recover the in-situ stress state, such as those of Hird et al, are unlikely to give representative stiffness values for the intact soil. The importance of stress history is illustrated using two CK_0U tests on reconstituted Magnus till which subjected samples to the following stress paths prior to shearing:

(a) K_0 consolidation followed by swelling back to an OCR=7.4

(b) As (a) but with the removal of shear stress

---

[1]This test was carried out by De Campos (1984) at a initial $s'=0.5(\sigma'_1+\sigma'_3)$ of 275kPa and its data have been factored by the ratio 626/275=2.28 to facilitate comparison with the tests of Gens & Hight (1979) who consolidated the samples to s'=626kPa.

The stress path followed by sample (b) is the theoretical path followed by a sample during K_0 consolidation and swelling, which is then sampled 'perfectly' i.e. the sample only experiences a removal of shear stress. The stiffness of this sample during subsequent shearing is however considerably lower than that of sample (a). This is attributed to the traversing of part of the small strain region during the removal of shear stress.

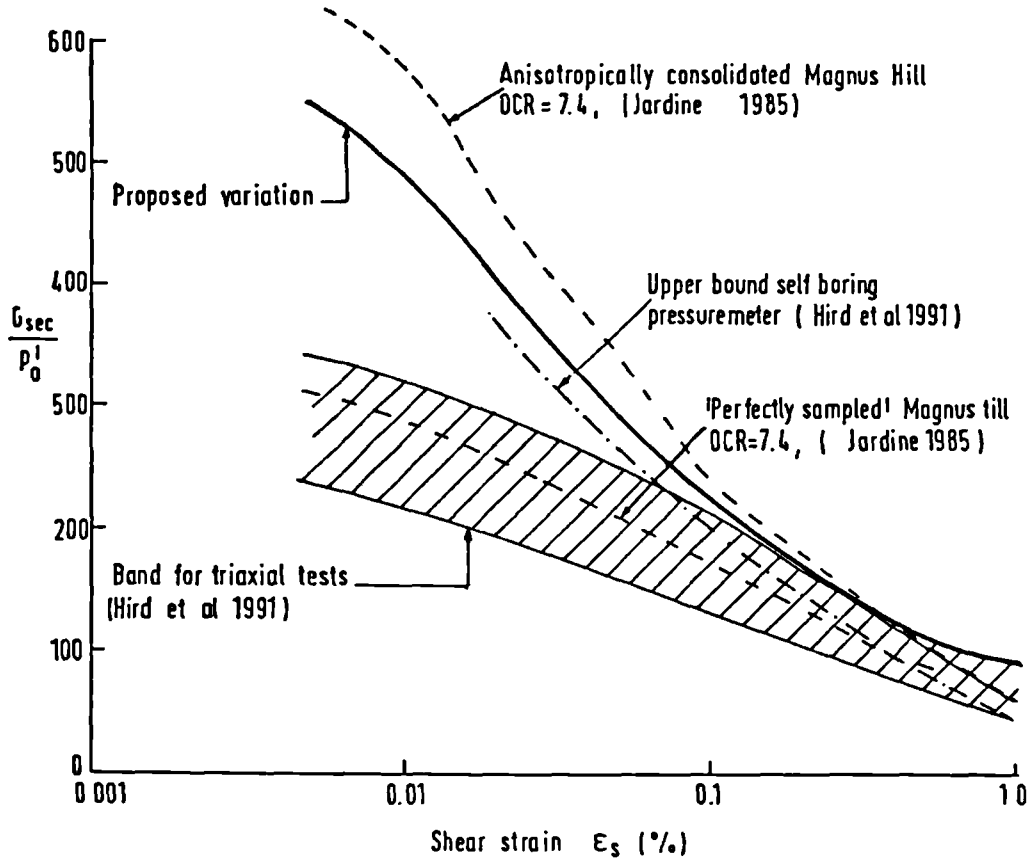

Figure 5.18 Shear stiffness of Cowden till in triaxial compression

The stress paths involved in tube sampling and subsequent extrusion are far more complex than in perfect sampling. In general, it has been found that the 'true' triaxial stiffness of intact samples, at intermediate OCR's (such as below 3.5m depth at Cowden), is slightly less than the stiffness measured on reconstituted samples that have been K_0 consolidated and then swelled back to the in-situ OCR (Hight et al 1985).

Based on these observations, the proposed G/p'_0 variation for undrained triaxial compression of the intact soil, shown on Figure 5.18, is biased

in favour of the CK_0U tests on Magnus till (Test a), which has been shown to have similar index properties to Cowden till. This variation is comparable to the upperbound stiffness measured in reloading stages of self-boring pressuremeter tests at Cowden (Hird et al 1991). Other tests on reconstituted Magnus till suggest that the stiffness in triaxial extension may be only 50% of that in triaxial compression.

5.2.10 Ring shear interface tests

The interface shearing characteristics of Cowden till were investigated in a ring shear interface experiment which used a stainless steel interface of similar roughness to that of the SST's (centre line average roughness ≈8.5μm) and a normal stress range comparable to the range of radial effective stresses measured in the ICP tests at Cowden.

After initial consolidation to a normal stress (σ'_{nc}) of 375kPa, the sample was sheared to a relative displacement of 2m in a series of shearing pulses performed at 530mm/min. This process modelled the displacement history of soil elements adjacent to the piles during installation. After a reduction in σ'_{nc} to 255kPa and a pause period of ≈24 hours, the sample was sheared again, but at a rate designed to ensure full drainage (0.004mm/min) and simulate the load testing stage of the piles. The displacement rate was varied between 0.004mm/min and 1020mm/min in 15 subsequent shearing stages, allowing pause periods of 24 hours after stages where the shearing rate exceeded 0.004mm/min.

The experiment is described fully in Appendix D. The main conclusions are outlined below and summarised on Figure 5.19.

- During fast shearing[1], the total stress ratios (τ/σ'_{nc}) increased with displacement and typically required between 50mm and 300mm to attain a steady (maximum) value. As shown by Figure 5.19, at a displacement rate of 1000mm/min, this maximum resistance is ≈55%

[1]Pore pressures acting at the interface were not measured. Therefore, any excess pore pressures (Δu_{sh}) that may have been generated by fast shearing are not known. Consequently, the normal effective stresses ($= \sigma'_{nc} - \Delta u_{sh}$) are also unknown.

greater than that at 1mm/min. A comparison of these data with the response seen in subsequent slow shearing stages, suggests that most of this rate dependence is related to transient phenomena such as pore pressure changes and viscous effects.

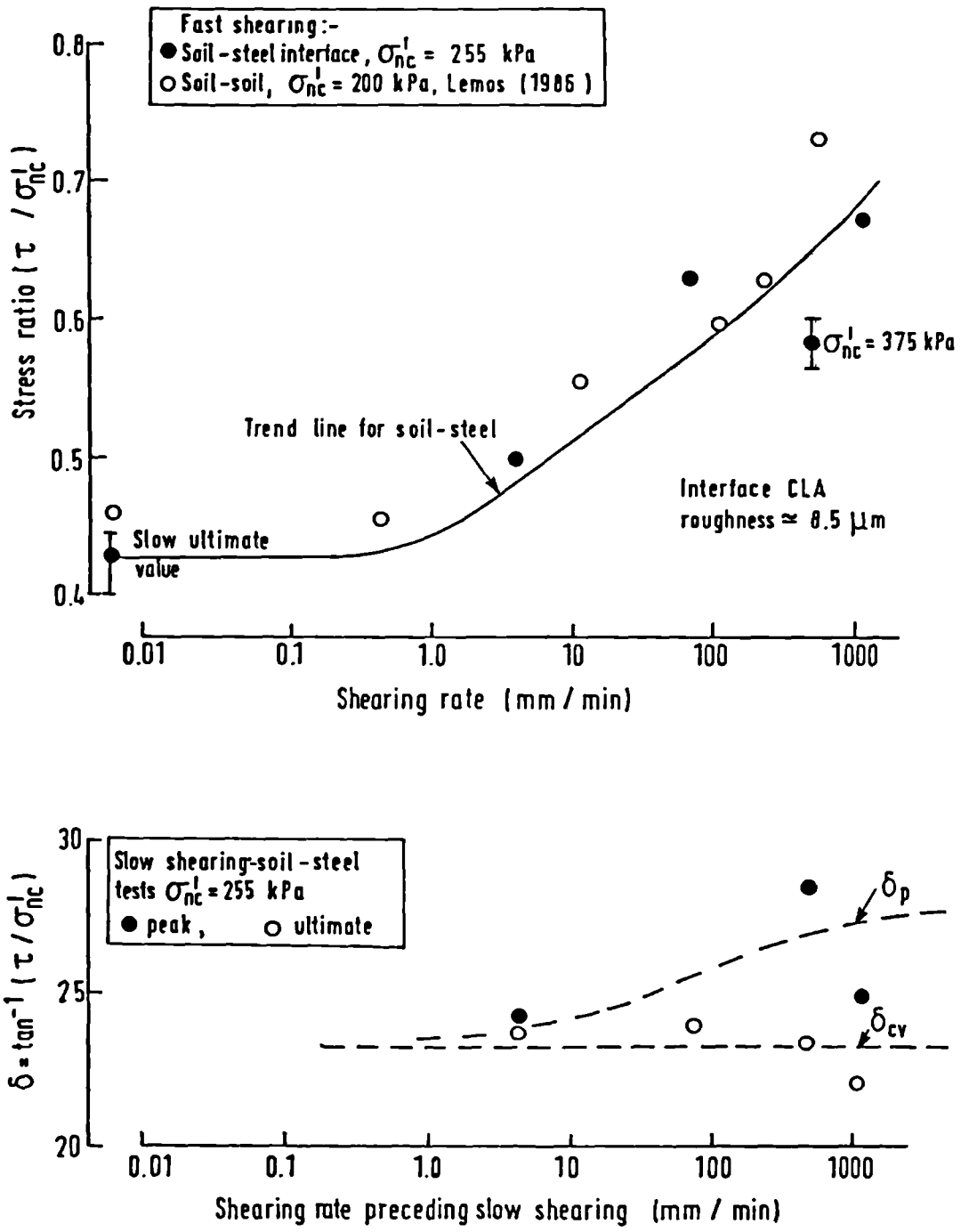

Figure 5.19 Ring shear soil-steel interface tests on Cowden till

- Peak angles of interface friction (δ_p) of between 25° and 28° were observed during slow (drained) shearing stages that were preceded by a shearing stage performed at ≥100mm/min. These peak angles are believed to reflect the dis-ordering of the material within the shear zone during fast shearing (Lemos 1986).
- The ultimate (post-peak) interface friction angles (δ_{ult}) developed in slow tests were between 22° and 24° and showed no dependence on the magnitude or rate of displacement adopted in the preceding fast shearing stage. These angles may be compared with the ultimate residual soil on soil angle (ϕ'_{res}) of 25° (measured at the same normal stress level; see Lupini et al 1981).

The values of δ_{ult} are only slightly smaller than ϕ'_{res}. No polished slip surfaces were identified on examination of the sample after testing and failure appeared to occur within the soil close to the interface. It may therefore be concluded that the roughness and type of interface did not permit a shearing mechanism that required appreciably less energy than the soil on soil shearing mechanism.

Although this ring shear experiment indicated little difference between the soil on soil and soil-steel resistances, extensive research at Imperial College (e.g. Lemos 1986, Tika 1989) has shown that the shearing resistance of materials of low-medium plasticity, such as Cowden till, are sensitive to (a) the properties of the interface and (b) minor changes in the composition of the material. For example, in experiments with Cowden till, Lemos (1986) measured δ_{ult} values of less than 15° when the till was sheared against a 'smooth' glass interface and Ove Arup & Partners (1986) report a δ_{ult} value of 19° for a mill varnished steel interface. Lemos also found that the shearing resistance fell by ≈15% when the clay content was increased from 26% to 30%.

Factors affecting the interface shear characteristics of clays are discussed in Appendix D.

5.3 SOIL CONDITIONS AT BOTHKENNAR

5.3.1 The site

In 1989, the Science and Engineering Research Council (SERC) set up the UK soft clay test bed site at Bothkennar, Scotland, to provide facilities for research into the engineering properties of low OCR, high plasticity clays. This site was selected after preliminary investigations at a range of potentially suitable sites, details of which are summarised by Hawkins et al (1989).

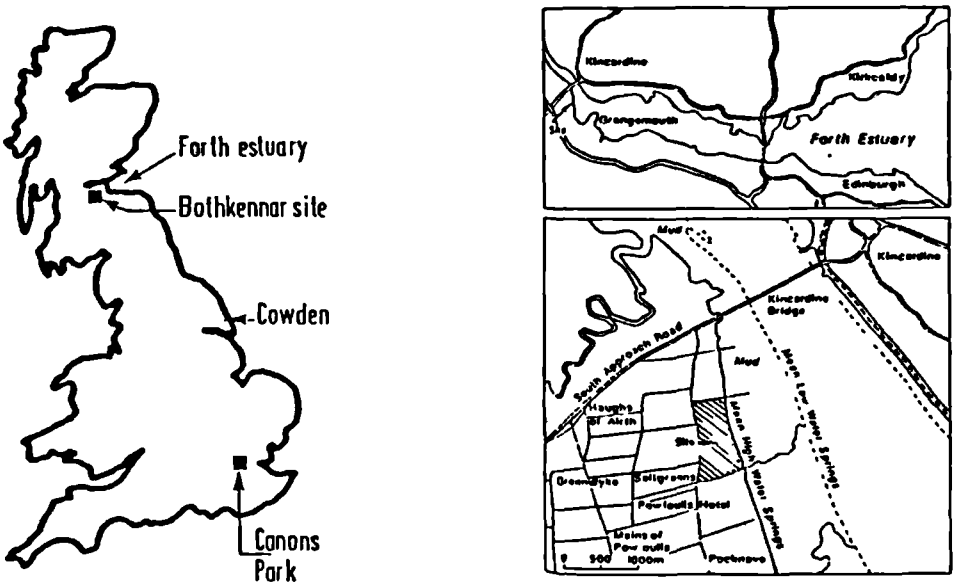

Figure 5.20 Bothkennar location

Bothkennar is located on the bank of the Forth estuary about 1 km south of Kincardine village (Figure 5.20). Only a small proportion of the total site area, measuring 1000m by 500m, has been used by research projects to date. These areas are shown in relation to the area selected for the ICP tests on Figure 5.21.

SERC have coordinated an extensive site investigation programme which used state-of-the-art sampling and in-situ test techniques. This programme was performed by the Building Research Establishment (BRE)

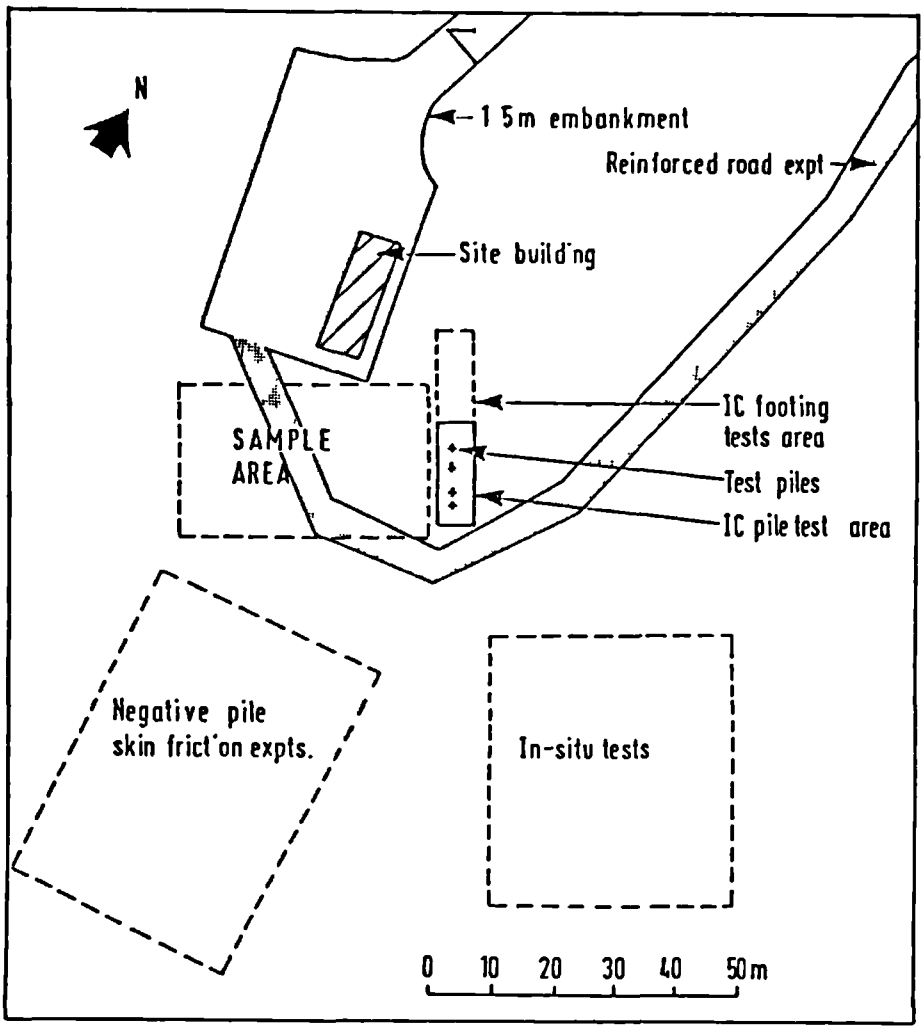

Figure 5.21 Site plan

and a range of British Universities and Polytechnics. The site is acknowledged to be one of the most comprehensively investigated in Britain and findings from these investigations are now being made available e.g. Geotechnical Consultancy Group (1991), Smith (1992) and a Geotechnique Symposium in Print (June 1992).

Most of the boreholes were excavated in the 'sample area', shown on Figure 5.21, which lies adjacent to the ICP test area. The sampling methods included conventional 66mm & 100mm diameter piston techniques as well as the more sophisticated Laval (La Rochelle et al 1981) and Sherbrooke techniques (Lefebvre & Poulin 1979). It was anticipated that

the Sherbrooke 'block' samples and the Laval piston samples (200mm diameter) would experience the least disturbance.

The majority of in-situ tests at the site were performed in the 'in-situ test area' which is about 40m from the ICP test area.

5.3.2 Geology

The general geological succession in the area around Bothkennar, interpreted from research by Gostelow & Browne (1986), Hawkins et al (1989) and Paul et al (1991), is summarised in Table 5.6.

	Material	Thickness (m)	Depth to top of stratum (m)	Geological Unit
1.	Desiccated silty clay	≈1	0	Recent tidal mudflats & Claret beds
2.	Post-glacial silty clay & clayey silt	15-20	≈1	Claret beds
3.	Shelly clayey silts + gravels	1-3	≈19	Letham beds and Bothkennar gravels
4.	Late glacial silts & clays	15-25	≈22	Abbotsgrange clays
5.	Sands & gravels	3-10	≈42	Abbotsgrange sands
6.	Late glacial laminated clay	≈15	≈50	Loanhead beds
7.	Boulder clay	15-30	≈65	Glacial till
8.	Sandstone	-	≈90	Bedrock

Table 5.6 Geological succession at Bothkennar

The last major glaciation in the Firth of Forth area took place about 13,000 before present (b.p.). Since then, the patterns of deposition have been shaped by the interaction between (a) the rises in land level following the removal of ice loads and (b) the associated local and

worldwide rises in sea level. Based on faunal evidence and a study of the variation of shoreline levels, the uppermost 20m of the Bothkennar profile (predominantly the Claret Beds) is believed to have accumulated in a stable shallow marine environment under 10 to 20m of water between 8500 b.p. and 6500 b.p. (Hawkins et al 1989, Paul et al. 1991). This environment led to the formation of very soft to soft black silty clay and clayey silt, with some laminations of fine sand.

The surface of the Claret beds was raised above sea level around 6500 b.p. and an upper crust developed due to the action of weathering. Hawkins et al (1989) suggested that part of this crust, which may also include desiccated material from the more recent deposits of mudflats, has been eroded by flood tides with the result that its thickness (≈1m) is 1-2m less than the crust of the surrounding hinterland. This erosion and fluctuations of the water table level has caused minor mechanical overconsolidation of the site.

The Claret beds are underlain by shelly clayey silt and a glacio-fluvial gravel layer (the Letham beds and Bothkennar gravels respectively), both of which were deposited following a minor glaciation (the Loch Lomond ice sheet re-advance) around 11,000 b.p.. These in turn are underlain by more late glacial silts and clays (Abbotsgrange beds).

5.3.3 Site profile

Detailed descriptions of the material encountered by boreholes in the uppermost 20m at Bothkennar are given by Hawkins et al. (1989) and Paul et al. (1991). These logs indicate that layers of soft silty clay (1-2m thick) alternate in an irregular fashion with clayey silt layers and occasional silt laminae.

The material within the depths penetrated by the piles (1.2m-6m is primarily within a 'mottled silty clay facies' (see Paul et al 1991). In this facies, the sedimentary structures have been partially or totally destroyed by burrowing organisms. Mottles at scales from ≈3mm to 1-2cm occupy 20-50% of the surface in a vertical section. Immediately below the crust, the logs reveal a more silt rich stratum. This is part of the

'laminated' facies, which evolved during more energetic depositional conditions.

Augered holes near the pile locations indicated that the weathered crust extends to a depth of about 1.0m and is underlain by a thin shell layer (≈0.3m in thickness). This shell layer represents the boundary between the Claret beds and the overlying clayey silts of the tidal mudflats. The water table level in these holes remained constant at 1m depth during the pile test programme. Although some underdrainage by the 'Bothkennar gravels' at ≈20m depth is thought to occur, a hydrostatic distribution with depth to 6m can be reasonably assumed.

The soil profile interpreted at the ICP test locations is given in Table 5.7. This profile is based on the data outlined above and on the results from in-situ tests and soil classification tests, discussed below.

Stratum	Depth(m)	Soil type
A	0-1	Weathered clayey SILT (CRUST)
B	1-1.3	Shell layer
C	1.3-2.2	Soft clayey SILT with some shell fragments (Laminated facies)
D	2.2-7	Soft black silty CLAY with fine mottling and occasional silt laminae (Mottled facies)

Table 5.7 Stratigraphy at ICP test locations

5.3.4 In-situ tests

5.3.4.1 Cone Penetration and Piezocone tests

Cone Penetration (CPT) and piezocone (CPTU) tests have been performed at three stages of the Bothkennar site investigations. The first series of tests were included in the initial survey, described by Hawkins et al.

(1989). Cone resistances were in good agreement with those discussed below, apart from in tests conducted in the south east corner of the site, which revealed silt rich material to a depth of up to 5m. This material is considered to be an infill meander of the Forth and extends to within ≈100m of the ICP test area.

BRE carried out CPTU tests in the 'in-situ test area' and investigated the influence of rate on the CPTU parameters. These tests showed that both the end resistance (q_c) and pore pressure (u_c) increased by about 8% for each log cycle increase in the penetration rate between 10mm/min and 1000mm/min (Powell 1992).

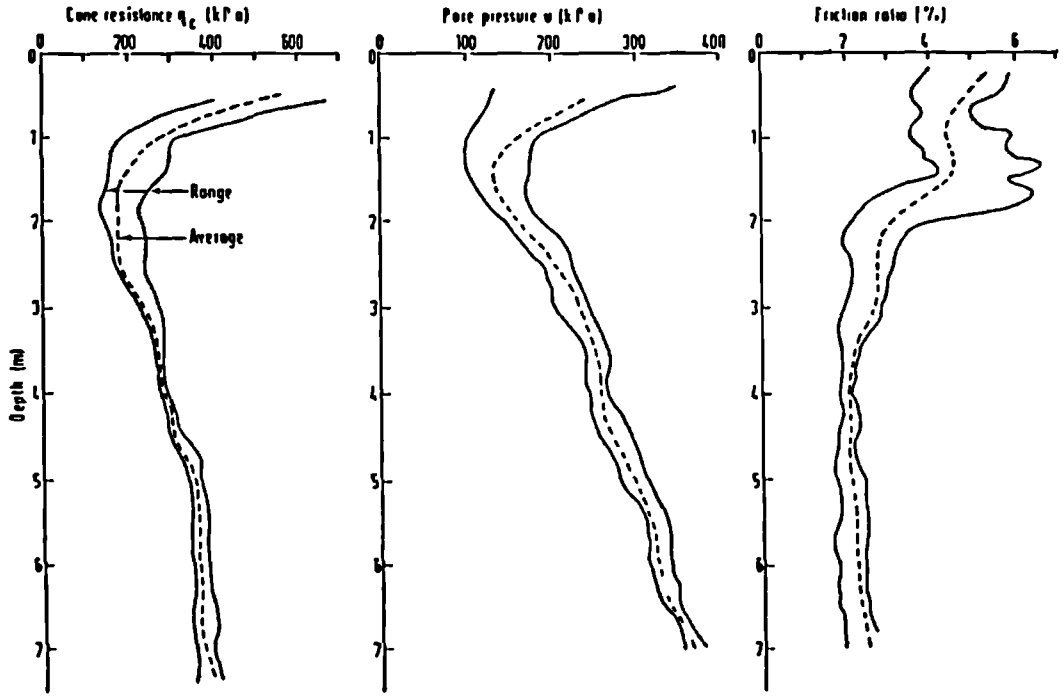

Figure 5.22 Piezocone data near locations of ICP tests

To assess the specific variability in the pile test area, Fugro McClelland Ltd. were requested to perform 8 CPTU tests (at the standard rate of 1200mm/min) within a 20m radius of the ICP locations. The range and average of the measurements made are shown on Figure 5.22. Points to note include:

- The end resistance (q_c) and pore pressure traces below ≈2m are very consistent. Both increase linearly with depth, suggesting that there are no significant changes in soil properties with test location and depth[1].
- The variability of the traces to 2m is consistent with the presence of silt laminae and the shell layer beneath the crust (see Table 5.7).
- Index tests (Section 5.3.6) suggest that the higher friction ratios at shallow depths are related to the lower sensitivity of this material (see Searle 1979).

5.3.4.2 Self-boring pressuremeter tests

Self-boring pressuremeter tests were performed by P-M In-Situ Ltd. at one metre intervals in the 'in-situ test area' of the site. The horizontal effective stresses (σ'_{h0}) measured in these tests are compared with values interpreted from laboratory tests in Section 5.3.9. Limit pressures (p_{lim}), extrapolated from the inflation curves, are compared with radial stress measurements made by the ICP in Figure 8.9 (Chapter 8), where they are seen to follow a similar variation with depth to the q_c traces. p_{lim} typically varies from 150kPa at 2m to 250kPa at 6m.

5.3.5 Grading, composition and fabric

Grading analyses of the main strata (C & D; Table 5.7) indicated a clay fraction between 15% and 45%; less than 10% of the particles were sand-sized. The large range in the clay fraction is typical of alluvial deposits (Smith 1992).

X-ray analyses suggest that the clay fraction comprises kaolinites, illites and *rock flour* (composed of quartz, feldspars and micas). The proportion of rock flour in the clay fraction has not been established. Quartz is the principal mineral in the silt fraction (50-75%), although

---

[1]The excess pore pressure ratio ($\Delta u/\sigma'_{v0}$), measured at the cone face, remained constant at ≈6 below 2m.

feldspars, micas and various ferro-magnesian minerals have also been identified.

The organic fraction is typically 2-3% of the dry weight[1] in the mottled facies and 1-1.5% in the laminated facies and is present in the form of residues (e.g. oils and fats) bound to the clay minerals. These residues evolved from the soft bodied organisms which produced the mottled fabric.

The mottled facies has a uniform micro-fabric which is 'clay matrix dominated'. Post-depositional chemical alterations which have been observed include local *bonding* between silt particles (based on alumino-silicates and iron compounds) in the laminated facies and parts of the mottled facies.

5.3.6 Index tests

The variation with depth of the water contents, unit weights, Atterberg limits and clay contents are shown on Figure 5.23, which may be summarised as follows:

- The average water content increases from ≈40% at 1m to ≈70% at 7m, and the unit weights reduce correspondingly from 17.6kN/m^3 at 1.0m to 15.4kN/m^3 at 7m.
- The plastic limit remains constant at ≈30% within the profile but the liquid limit tends to increase with depth, ranging from about 50-65% to 4m and 80% below 4m. The variation of the plasticity index (PI) with depth therefore matches that of the liquid limit. PI values are in the range 25-40% to 4m and ≈50% below 4m.
- Clay contents (determined using British Standard procedures) also show a trend to increase with depth, varying from about 15% at 2m to about 40% at 7m.
- The liquidity index ranges from about 0.5 to 0.9 showing no specific pattern with depth. A typical average value for the profile is ≈0.75.

---

[1]as determined by the 'hydrogen peroxide' procedure (Paul et al. 1991). The organic content by the ignition method is about 2% higher.

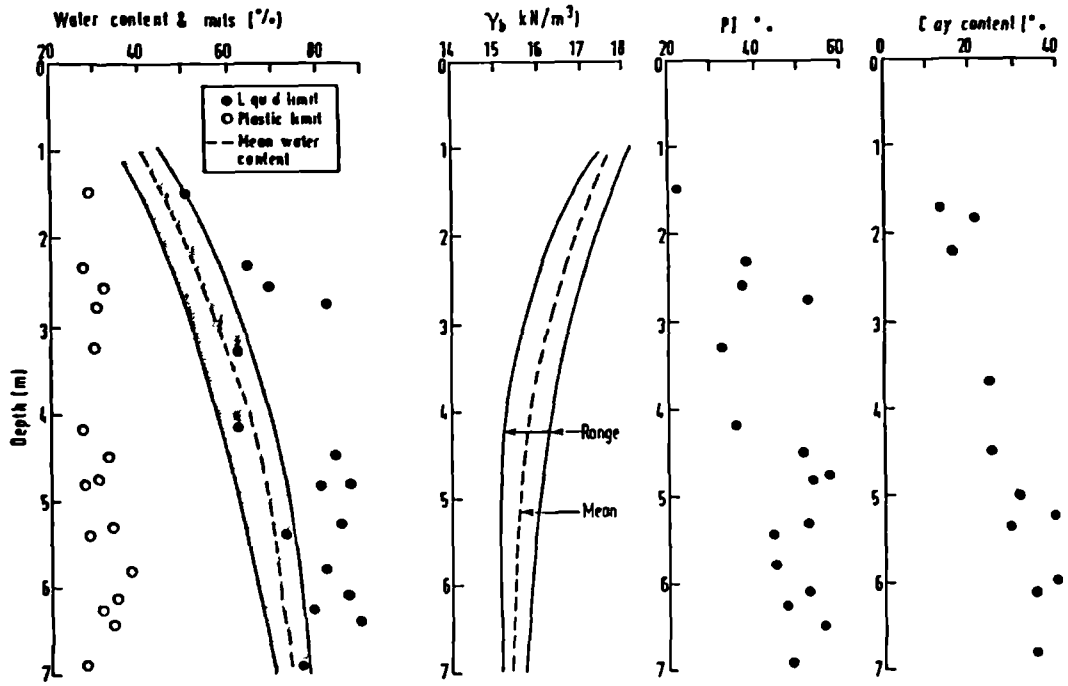

Figure 5.23 Index properties at Bothkennar

The measured plasticity indices (typically 40-50%) are higher than would be expected from the mineralogy of the deposit. Paul et al. (1991) have shown that the plasticity is enhanced by the organic material; the plasticity indices measured on samples from all depths, after the organics were removed, varied between 20% and 25%.

5.3.7 Undrained shear strength

The undrained shear strength of Bothkennar clay has been measured by the following methods:

- Unconsolidated undrained triaxial compression tests (UU)
- K_0 consolidated undrained triaxial compression and extension tests (CK_0UC and CK_0UE)
- K_0 consolidated constant volume direct simple shear tests (DSS)
- Field vane tests (at 6°/min)
- Cone penetration tests at 1200mm/min (indirectly).

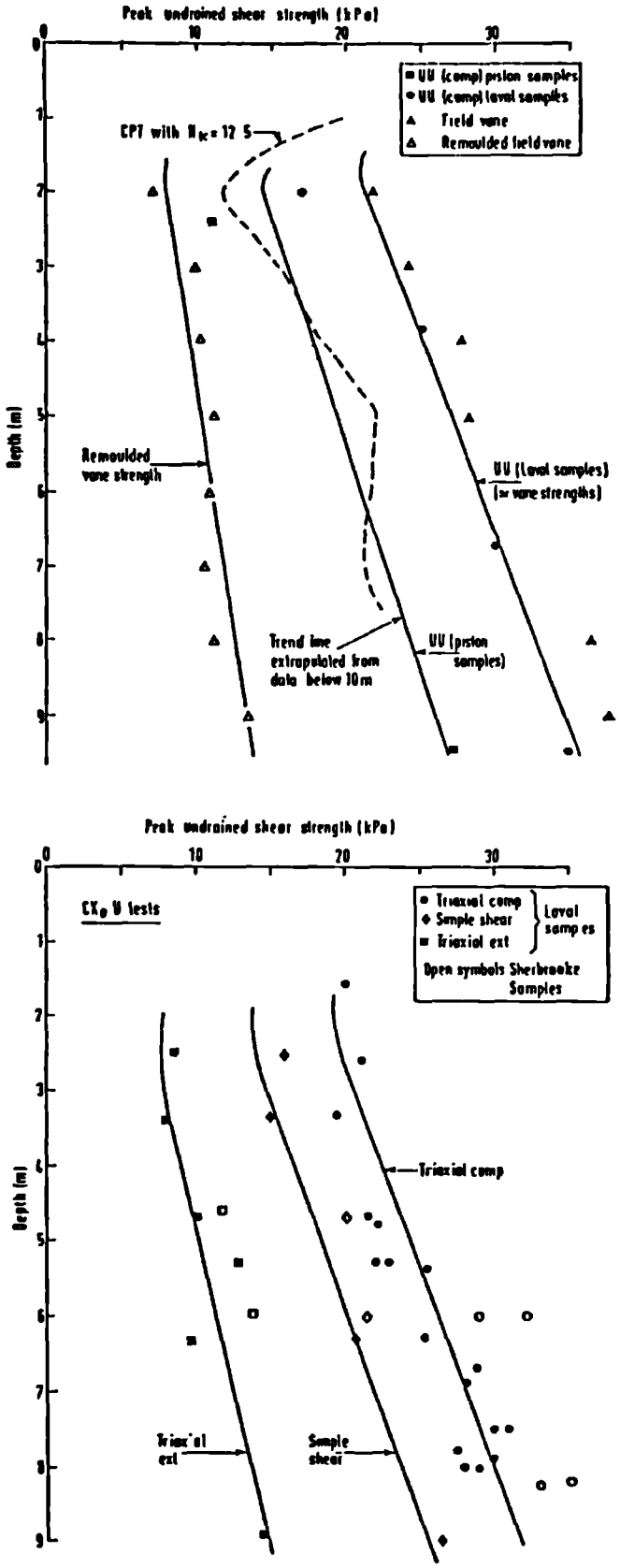

Figure 5.24 Peak undrained shear strength profiles at Bothkennar

Peak strengths measured by each of these methods[1] are plotted on Figure 5.24. It is evident that, while all strengths increase linearly with depth below ≈2m, there are significant differences between each data set. These differences occur primarily because of the well known dependence of 'undrained strength' on (a) the mode of deformation imposed by different testing procedures and (b) sampling disturbance. For this reason, the peak UU strength of conventional samples, which are typically between 75mm and 100mm in diameter, is generally selected as the 'standard' strength when using an '$\alpha\ c_u$' approach for pile design (see Section 2.2). This strength, referred to as c_{u0}, is compared with other peak strengths in Table 5.8.

Test	Sample	Average strength from 2-6m (kPa)	Proportion of c_{u0}
UU	Conventional piston (D=100mm)	17.5	1.0
UU	Laval	25.0	1.4
CK_0UC	Laval	22.5	1.3
CK_0UE	Laval	8.8	0.5
CK_0UC	Sherbrooke	26.0	1.5
CK_0UE	Sherbrooke	10.5	0.6
DSS	Laval	16.3	0.9
DSS	Sherbrooke	18.0	1.0
Field vane		25.0	1.4
CPT (N_k =12.5)		17.5	1.0

Table 5.8 Mean peak undrained shear strengths at Bothkennar

These measurements indicate a number of interesting features:

- Strengths depend on the sample type and test method and vary between $0.5c_{u0}$ and $1.5c_{u0}$.

[1] The shearing stages of the triaxial tests (on 38mm diameter samples) were generally carried out at an axial strain rate of ≈5% per day. Some of the CK_0U tests subjected the samples to an initial load-unload loop to simulate the stress history of the material (see Section 5.3.10).

- Peak strengths of Laval samples are ≈15% lower than those measured on Sherbrooke samples. This is believed to be caused by the greater damage to the natural bonded structure of the material induced by the Laval sampler (Smith 1992).
- The strengths of conventional piston samples are even lower than those of Laval samples, illustrating the strong influence of the sampling method in sensitive clays.
- Ultimate shear strengths[1] measured in UU, CK_0UC and DSS tests on all sample types were comparable and gave a mean strength between 2m and 6m of ≈13kPa. More severe shearing leads to a further reduction in strength such as measured post-peak in field vane tests which gave a mean remoulded strength of ≈9.5kPa i.e. a vane sensitivity of 2.6.
- Peak and ultimate strengths measured in triaxial extension are significantly less than the equivalent strengths in triaxial compression.
- The average value of N_k which inter-relates the triaxial c_{u0} and CPT q_c value is 12.5, $[N_k = (q_c-\sigma_{v0})/c_{u0}]$. This ratio is within the range of 10 to 16 generally expected for lightly overconsolidated clays (Nader & Lunne 1988).

5.3.8 Behaviour in 1-D compression

The 1-D compression characteristics of the Bothkennar clay are illustrated on Figure 5.25a, using tests performed by Bristol University. As described by Burland (1990), the compression behaviour of natural clays differs considerably from that shown by reconstituted samples. It can be seen that when the vertical yield stress (σ'_{vy}) is exceeded, the trace for the intact sample leaves the sedimentary compression line (SCL) and (with increasing stress) approaches the 1-D characteristic for the reconstituted material (i.e. its intrinsic compression line or ICL). The post-yield compressibility (C_c) is initially significantly higher than the intrinsic compressibility (C_c^*), but approaches C_c^* as the natural fabric of the clay is destroyed with increasing stress.

[1]At 15% axial strain in triaxial tests and 20% shear strain in DSS tests.

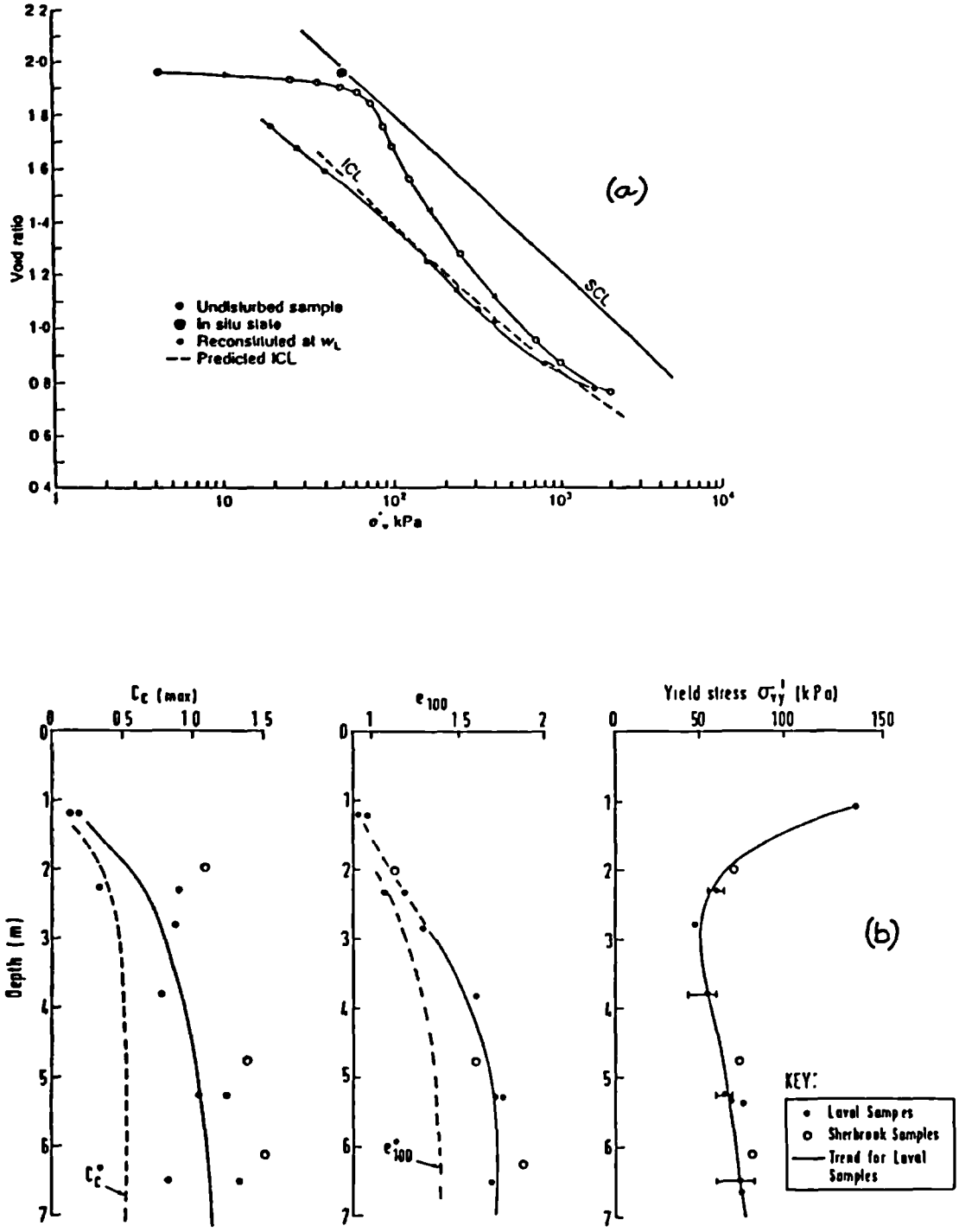

Figure 5.25 1-D compression characteristics of Bothkennar clay

Profiles with depth of $(C_c)_{max}$, e_{100} and (σ'_{vy}) are shown on Figure 5.25b. Points to note include[1]:

- C_c and e_{100} increase with depth, following the trend of the liquid limits.
- $(C_c)_{max}$ is typically twice the intrinsic compressibility C_c^*.
- The yield stresses and compressibilities shown by the Sherbrooke 'block' samples are higher than those of the Laval samples.
- The material between 1 and 2m is at a much higher OCR than the underlying material (see Section 5.3.9)

The swelling index (C_s) of the intact material over the OCR range 1-5 lies between 0.02 and 0.045.

5.3.9 In-situ stress state

Yield stresses (and hence apparent OCR's) deduced from tests on soft clay are affected significantly by sample quality as well as strain rate and ageing effects. The apparent OCR variation with depth at Bothkennar, shown on Figure 5.26a, was estimated for Laval samples, using two 'standard' approaches:

(a) Oedometer tests, where load increments were applied for a period of 24 hours. The yield stresses (σ'_{vy}) were identified using the procedure proposed by Butterfield (1979) and are plotted on Figure 5.25b; OCR was calculated as $\sigma'_{vy}/\sigma'_{v0}$.

(b) Peak undrained compression strengths in UU and CK_0U tests (for samples tested at ≈5% axial strain per day) and the relationship proposed by Ladd et al (1977):

$$c_u/\sigma'_{v0} = (c_u/\sigma'_{v0})_{nc}\ OCR^{0.8},$$ where $(c_u/\sigma'_v)_{nc}$ is assumed =0.35 (see Section 5.3.10)

---

[1]where the standard incremental load procedure was followed and each load increment was applied for 24 hours. Notation: $(C_c)_{max}$ = C_c measured in first post-yield load increment, e_{100}= void ratio at σ'_v =100kPa, σ'_{vy}= yield stress deduced from data plotted in log(1+e):log σ'_v space.

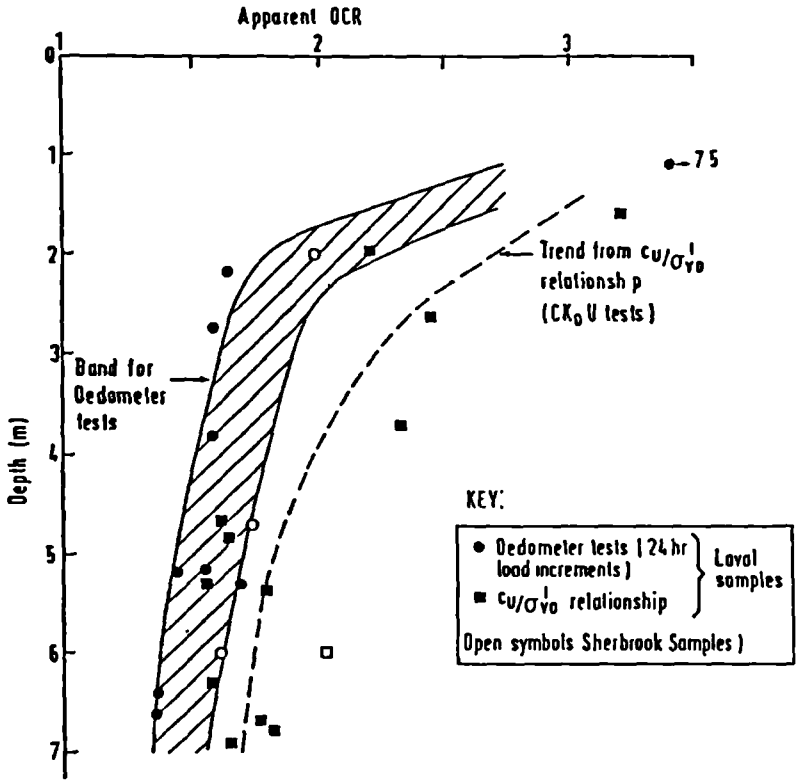

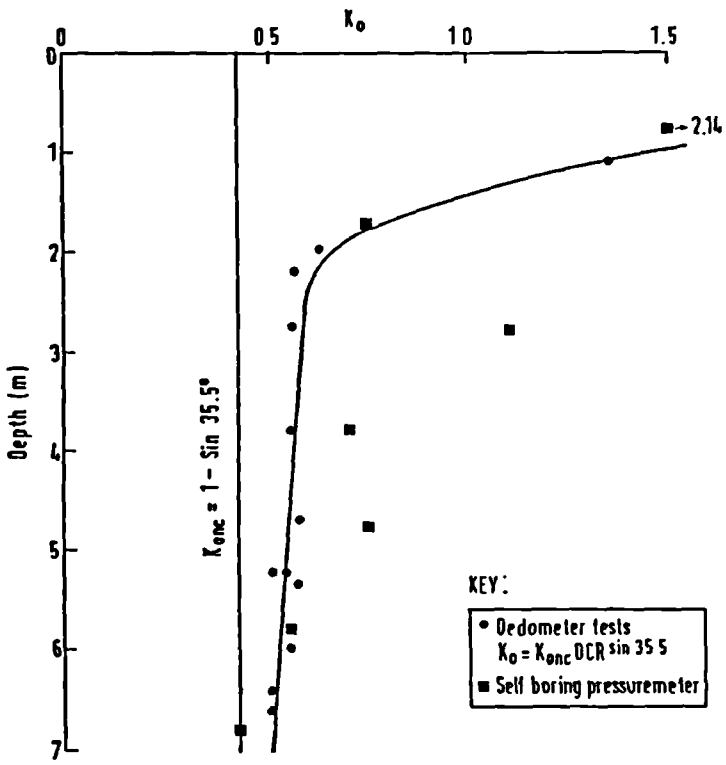

Figure 5.26 OCR and K_0 profile at Bothkennar

Given the empirical nature of Ladd's expression, good general agreement between the two data sets is observed. Apparent OCR values of as high as 7.5 are measured in the material to 2m but, below this depth, they show little variation, reducing from ≈2 at 2m to ≈1.5 at 6m.

Due to small degree of cementation/bonding in the Bothkennar clay, OCR estimates would be about 20% higher than the mean trend shown by Laval samples, if the results from tests on Sherbrooke samples were adopted using the above methods. Conversely, because of the sensitivity of the material, the undrained strengths of conventional 100mm diameter piston samples suggest OCR values that are ≈30% lower than those indicated by Laval samples (see Table 5.8).

The K_0 profiles for Bothkennar can be assessed from both the direct measurements of the in-situ horizontal effective stress (σ'_{h0}) and the relationship proposed by Mayne & Kulhawy (1982):

$$K_0 = (1-\sin\phi')OCR^{\sin\phi'}$$
$$= 0.42\ OCR^{0.58} \text{ for } \phi'=35.5° \quad \text{(see Section 5.3.10)}$$

The values of K_0 derived using this formula are also plotted on Figure 5.26b and are seen to be in reasonable agreement with the direct measurements of K_0 obtained using the self-boring pressuremeter in the 'in-situ test area' of the site[1].

Summary profile

The data on Figures 5.23 and 5.26 is used to summarise the in-situ stress state given in Table 5.9. The OCR values listed are those derived from oedometer tests on Laval samples and are seen to be in reasonable agreement with the mechanical overconsolidation ratio (OCR_m) calculated on the basis of a pre-consolidation pressure (σ'_{vm}) of 20kPa.

[1]More scatter is seen in the pressuremeter data because of the inevitable disturbance caused by installation of this instrument. The high values of K_0 at 2.8m and 4.8m were attributed to sand lenses in this area of the site.

A σ'_{vm} value of 20kPa is an upperbound estimate which was assessed from a review of the geological history (Section 5.3.2). Of course, there is no reason to expect that the OCR deduced as outlined above (i.e. the apparent OCR) will be the same as the mechanical OCR. Apparent OCR's are generally higher than OCR_m values due to post-depositional processes such as ageing, desiccation and chemical alterations.

Depth (m)	u_0[1] (kPa)	σ_{v0} (kPa)	σ'_{v0} (kPa)	OCR	OCR_m	K_0	σ_{h0} (kPa)	σ'_{h0} (kPa)
1.0	0	18.2	18.2	8.0	2.10	1.8	32.8	32.8
2.0	10	35.5	25.5	2.0	1.78	0.65	26.6	16.6
3.0	20	52.1	32.1	1.73	1.62	0.58	38.6	18.6
4.0	30	68.2	38.2	1.64	1.52	0.56	51.4	21.4
5.0	40	83.9	43.9	1.56	1.45	0.54	63.7	23.7
6.0	50	99.4	49.4	1.48	1.40	0.52	75.7	25.7
7.0	60	124.8	54.8	1.42	1.36	0.50	87.4	27.4

Table 5.9 In-situ stresses at Bothkennar

5.3.10 Stress path testing

5.3.10.1 Initial yield surface

The general behaviour of the Bothkennar clay under triaxial conditions can be summarised using the series of tests performed by Smith (1992) on Sherbrooke samples from 6.1m depth[2] (Figure 5.27). The tests can be divided into the following three groups.

---

[1] γ_w = 10kN/m^3 for water with a salt content of 20g/l.

[2] Except for sample T3, which was a Laval sample from 5.4m depth. K_0 consolidation and swelling were performed at an axial strain rate of 1% per day. Prior to swelling, the samples were allowed age until the strain rate had fallen to 0.05% per day. This ageing step often took ≈1 week for samples consolidated outside the volumetric yield surface.

Group (a) :Drained tests on 'intact' soil: After re-consolidation along path A-B-C-F to recover the in-situ stress conditions, eight drained probing tests were carried out to identify the volumetric yield surface, shown on Figure 5.27. This surface, which is skewed about the K_0 line, represents the transition from very stiff to soft behaviour. However, unload-reload tests showed that plastic straining had started long before this surface was reached. Non-linear behaviour within the volumetric yield surface is described and discussed by Smith et al (1992).

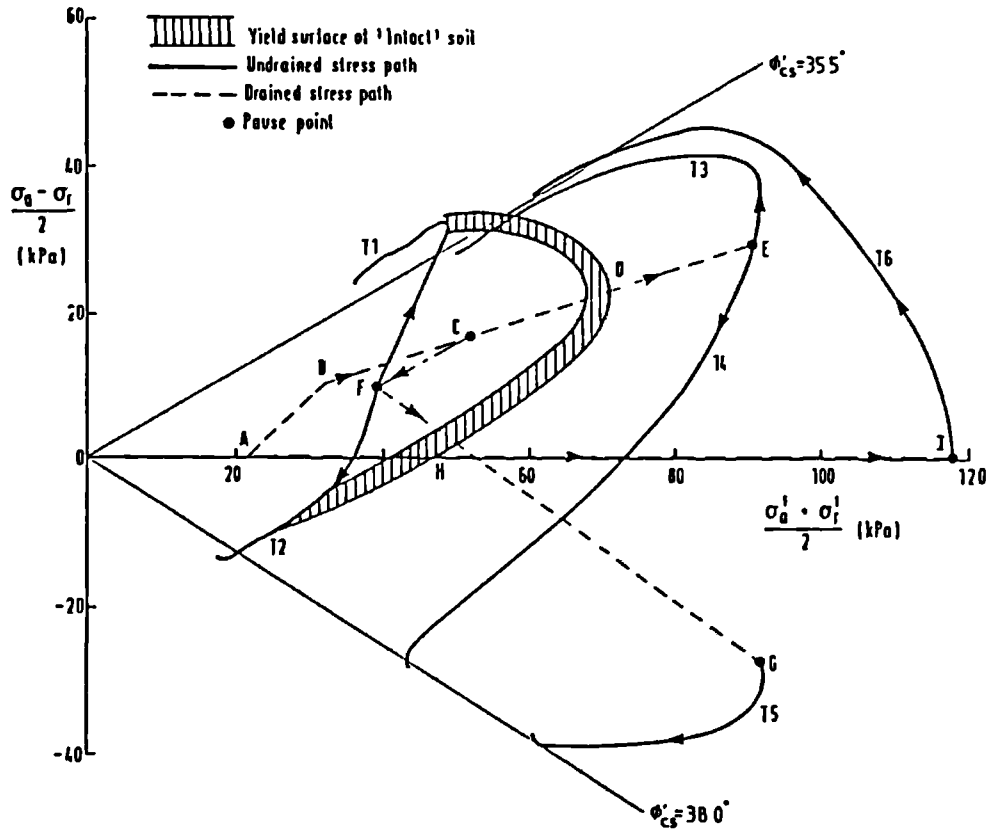

Figure 5.27 Stress paths followed in CK_0U triaxial tests (Smith 1992)

Group (b) :Undrained test on 'intact' soil: Undrained tests T1 and T2 (compression and extension respectively) were carried out after reconsolidation along path A-B-C-F. Small pore pressure reductions (in T1) and increases (in T2) were observed prior to yield. Post-yield, T1 exhibits marked brittleness as the mean stress reduces and the sample approaches critical state conditions. This brittleness was less pronounced in compression tests on Laval samples, where sampling is

thought to have destroyed some of the material's natural bonding. No brittleness was observed in the extension test (T2).

Group (c) :Undrained tests at OCR=1: The re-consolidation paths for these tests (T3 to T6) are shown dotted on Figure 5.27. The tests (called modified SHANSEP tests; see Smith 1992) gave undrained strength ratios (c_u/σ'_{v0}) of 0.35 in compression and 0.24 in extension.

After normalising these tests for the effects of water content variations, Jardine & Smith (1991) showed that no unique state boundary surface exists for the Bothkennar clay. This is because of the high sensitivity of the material. Only at high stresses, when the natural clay fabric has been broken down, will the material's behaviour be normalisable in terms of water content. This occurs at a mean effective stress (p') of ≈1MPa; for example the intact and reconstituted oedometer curves converge at such a stress level.

5.3.10.2 Effective stress parameters

Triaxial compression tests on Laval samples re-consolidated to in-situ stress conditions, and SHANSEP tests on Sherbrooke and Laval samples gave ϕ'_{cv} values of between 33° and 36.5°, with a mean value of 35.5°. Peak values of ϕ' of up to 42° were measured in tests on Sherbrooke samples[1] tested at in-situ stresses, which also gave higher ϕ'_{cv} values of ≈38°. This is most probably due to the presence of bonding, which was destroyed during the Laval sampling and SHANSEP procedures.

Values of ϕ'_{cv} measured in triaxial extension showed considerable scatter (35°± 9°). This was attributed to measurement inaccuracies associated with sample necking and membrane stretching at low stress levels (Smith 1992).

Given that the stress conditions at ultimate conditions are less certain in triaxial extension, a mean ϕ'_{cv} for the material of 35.5° under triaxial conditions is proposed. Bonding in the material will be destroyed during the process of pile installation and the very high peak

[1]Assuming a cohesion intercept c'= 0. The peak strengths measured in these tests are, however, better represented by c'≈4kPa and ϕ'=35.5°.

(and ultimate) strengths of the Sherbrooke samples are only likely to be applicable for points far from the shaft.

It is suggested that the relatively high value of ϕ'_{cv} may be associated with the significant proportion of rock flour in the clay fraction and the material's organic content. Standard correlations relating ϕ'_{cv} with plasticity index (e.g. Kenney 1959) suggest far lower values ϕ'_{cv} (of between 20° and 25°), indicating that this index alone is an unreliable guide to soil behaviour for soils with an unusual mineralogy and organic fraction (see Smith 1992).

5.3.10.3 Triaxial stiffness

The variation of the shear stiffness with shear strain measured in the suite of tests carried out by Smith (1992) is shown on Figure 5.28.

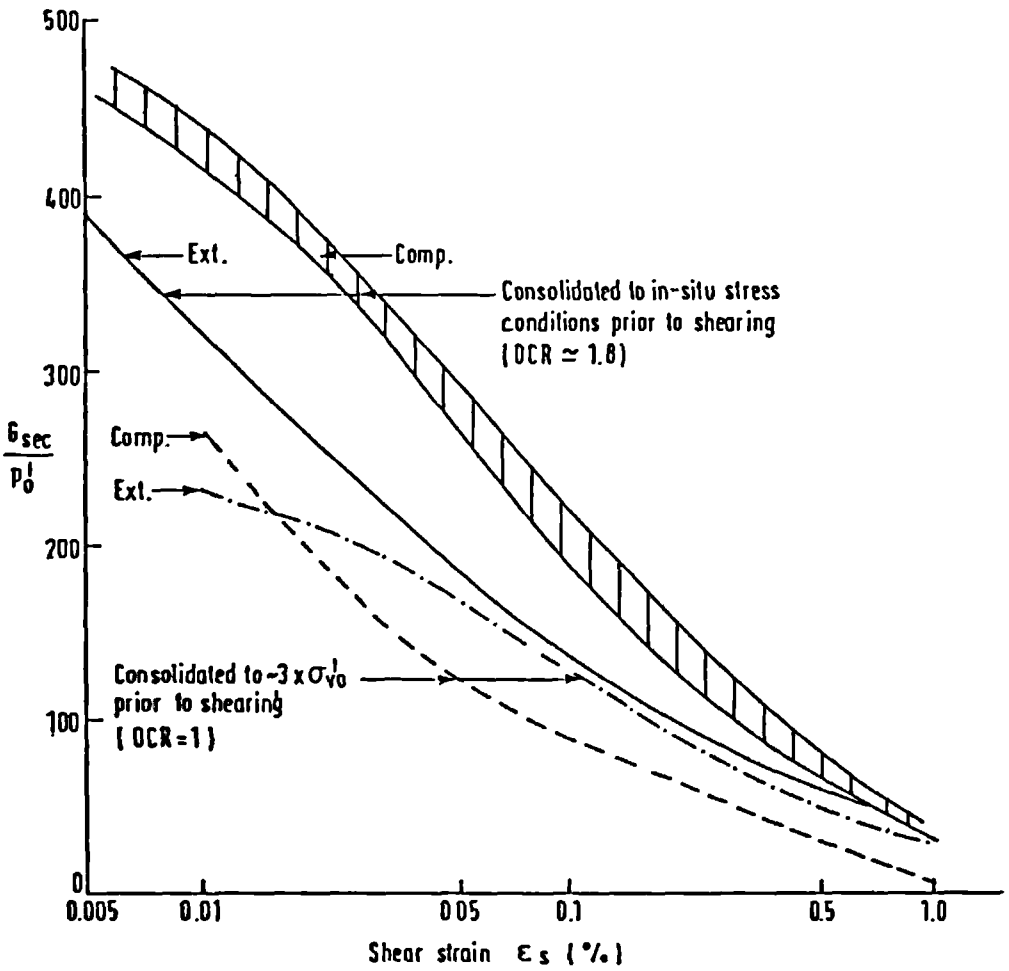

Figure 5.28 Shear stiffness values in CK_0U triaxial tests (Smith 1992)

Figure 5.28 shows:

- A similar variation of G_{sec}/p'_0 with shear strain (ε_s) for Sherbrooke and Laval samples. G_{sec}/p'_0 reduces by a factor of two when ε_s increases from 0.01% to 0.1%.
- Samples which recovered their (overconsolidated) in-situ stress conditions (by consolidation along path A-B-C-F , see Figure 5.27) have significantly higher G_{sec}/p'_0 values than those which have been normally consolidated outside the yield surface.
- The stiffness in extension for samples at in-situ stress conditions is typically about 30% less than that measured in compression. However, the reverse trend is apparent for samples normally consolidated outside the yield surface.
- Smith (1992) suggested that the stiffness characteristics of the Bothkennar clay are more in keeping with the trends shown by other clays if its plasticity index is assumed to be that measured when the organic fraction is removed (i.e. ≈20% compared to 25-50% for the natural soil).

5.3.11 Direct simple shear (DSS) tests

Data from a set of constant volume DSS tests performed on horizontally orientated Laval samples[1] consolidated to in-situ stresses are shown on Figure 5.29a. The variations of the applied horizontal shear stress (τ_h) with vertical effective stress (σ'_n) show consistent trends when normalised by the consolidation stress ($\sigma'_{nc} = \sigma'_{v0}$) used in each test (Figure 5.29b):

- The vertical effective stress reduces as τ_h increases. This reduction amounts to ≈20% of σ'_{nc} at peak shear stress, giving an obliquity at this stage ($\tan^{-1}(\tau_h/\sigma'_n)$) of ≈29.5°.
- Significant reductions in σ'_n are observed post-peak. By the end of the test (at a shear strain of 20%), τ_h reduced by ≈25% and σ'_n reduced to $\approx 0.4\sigma'_{nc}$.
- The obliquity at the end of the test, as critical state conditions are approached, is ≈38.7°. This angle is slightly larger than the mean ϕ'_{cv} measured in triaxial tests (35.5°).

---

[1]Except for a Sherbrooke sample at 6.1m. Note also that the tests did not include any swelling stage in their consolidation stress paths.

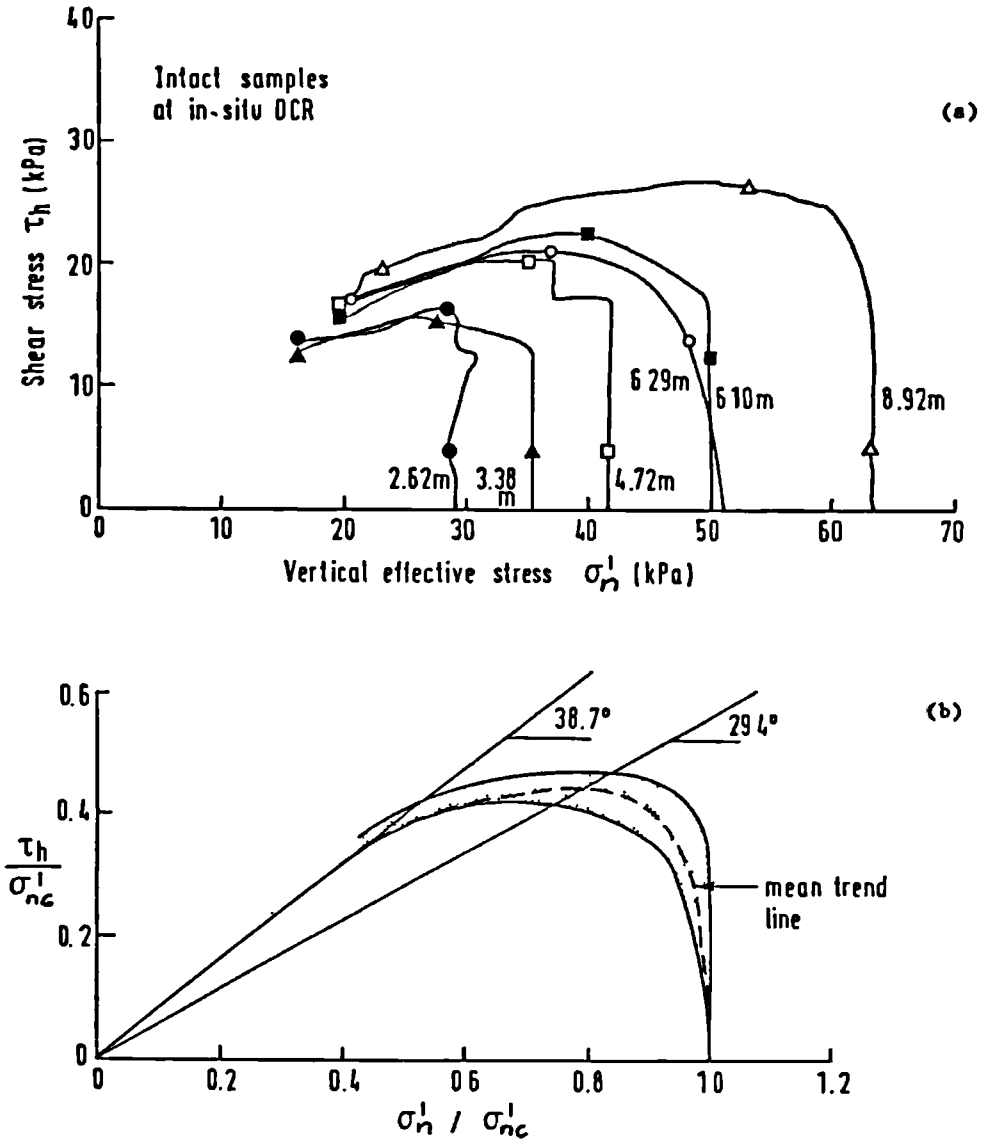

Figure 5.29 Direct simple shear tests on intact Bothkennar clay

5.3.12 Ring shear tests

A series of soil on soil and soil-steel interface ring shear experiments was performed on Bothkennar soil to aid interpretation of the pile test results. The experiments were similar (but more extensive) to those performed for Labenne sand and Cowden till and are described fully in Appendix D and in Lehane & Jardine (1992).

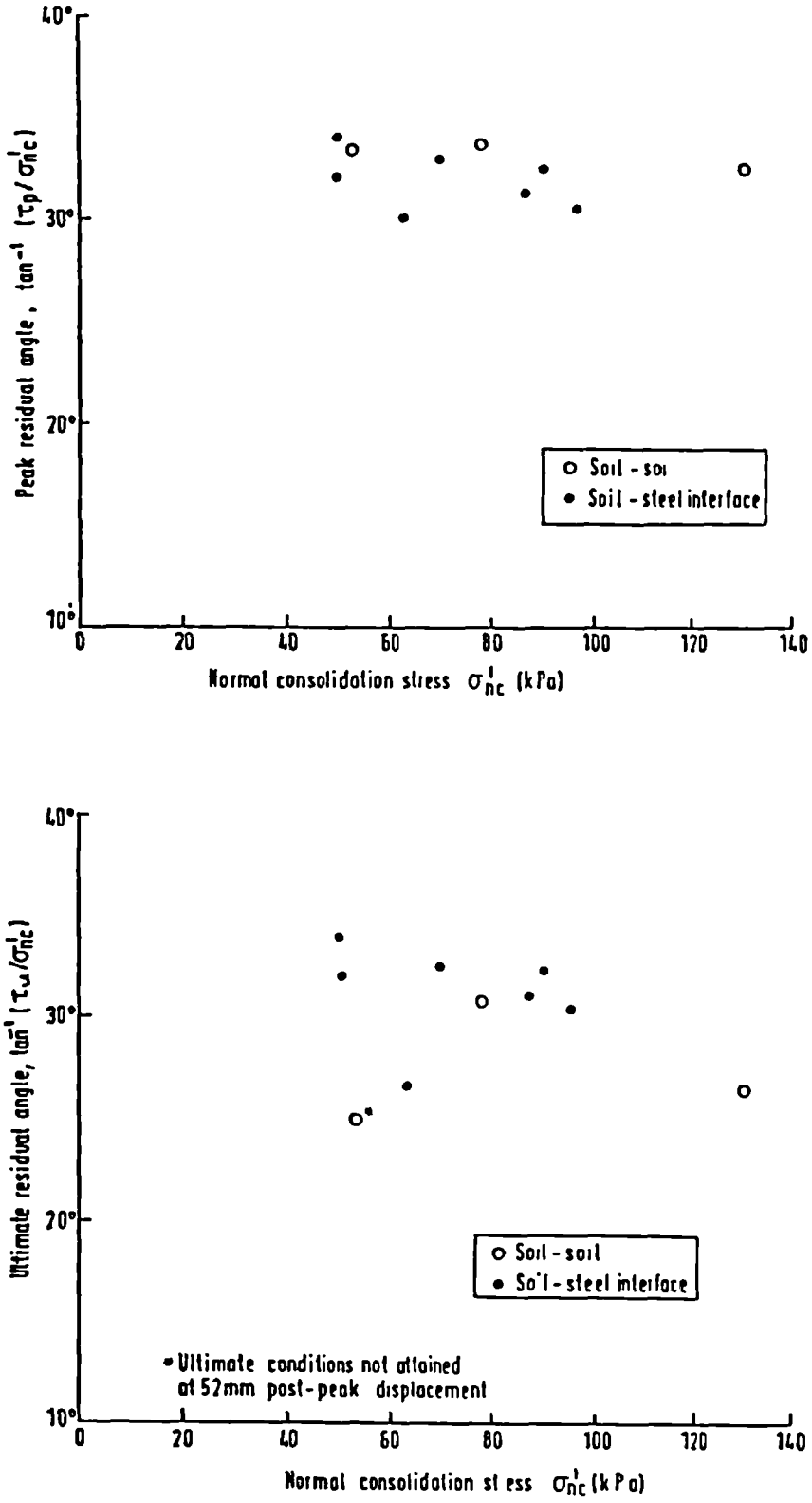

Figure 5.30 Peak and ultimate residual angles for Bothkennar clay in soil on soil and soil-steel interface shear

As in the earlier tests, the displacement history of soil elements adjacent to a pile during installation and load testing was modelled by subjecting all samples to an initial relative displacement of more than 1.2m in a series of pulses at 500mm/min; slow (drained) tests were performed on the following day. Subsequent shearing stages varied the displacement rate and the normal stress (σ'_{nc}). The normal stress range was of the same order as the radial effective stresses acting on the ICP's at Bothkennar and the interfaces were of the same material and roughness as those of the instruments.

The main trends of the data during slow (drained) and fast shearing stages are outlined below.

5.3.12.1 Slow shearing stages

Peaks in shearing resistance were observed in all slow shearing stages, giving the friction angles shown on Figure 5.30a. The range of angles measured is very narrow, despite large differences between the displacement histories of samples[1] in each stage and the range of normal stresses (σ'_{nc}). Soil on soil and soil-steel angles fall within 33° ± 1° and 31° ± 2° respectively.

Considerable post-peak brittleness was seen in approximately one third of all slow shearing tests, whilst little or no loss of strength was observed in the remaining two thirds. This inconsistency led to the unexpected wide span of ultimate residual angles shown on Figure 5.30b. It is interesting that, in the cases where brittleness was observed, subsequent slow tests (performed after changes in σ'_{nc} or intervals of faster shearing) indicated ultimate angles which were closer to the peak values.

The resistances in soil on soil and soil-interface shear were comparable and visual inspection of the samples after testing showed no evidence of polished shear surfaces or interface slippage. It could therefore be concluded that the shearing mode in soil on soil shear had not been

[1]given that all samples experienced an initial relative displacement of ≥1200mm (at 500mm/min).

altered by the presence of an interface and failure in the interface tests probably occurred within the soil mass.

The comparable peak and ultimate resistances and their relative insensitivity to the displacement and normal effective stress history are indicative of a turbulent mode of shearing. Whilst brittle characteristics were seen in some shearing stages, indicating a degree of particle sorting, it seems that the resulting lower strength soil fabric was meta-stable and reverted to a turbulent unsorted fabric when re-sheared after changes in stresses or rates had been applied. A turbulent shearing mode is generally only seen in low plasticity clays, but this anomaly may be explained by the lean and rock flour rich composition of the material and the enhancement of its plasticity index by the organic fraction.

5.3.12.2 Fast shearing stages

All fast shearing steps were characterised by an initial peak in shearing resistance which was followed by a reduction to an ultimate condition. Figure 5.31 summarises the data by plotting the peak and ultimate stress ratios (τ/σ'_{nc}) against displacement rate[1].

For velocities less than ≈100mm/min, peak resistances increase by ≈6% per log cycle increase in rate. Ultimate resistances show no apparent rate dependence, giving ratios comparable to those measured in fully drained shearing stages. The moderate positive rate effect of peak resistances is typical of many soils and has been ascribed to viscous phenomena, combined with variable degrees of particle sorting within the shear zone; see Lemos (1986) and Tika (1989).

However, both the peak and ultimate resistances reduce when the velocity exceeds ≈100mm/min: increasing the rate to 500mm/min almost halves the ultimate shearing resistance. This negative rate effect rate is in sharp contrast to that obtained in ring shear tests on Cowden till performed over a similar rate interval (Figure 5.19) and, at first, suggests that

[1]For fast shearing stages that were preceded, where necessary, by a period to allow for full consolidation (see Appendix D).

positive excess pressures were developed within the shear zone at these rates. It is interesting in this regard to note that the minima for ultimate stress ratios (τ/σ'_{nc}) exceed the large strain value appropriate for Bothkennar clay in slow constant volume DSS tests (for which $\tau/\sigma'_{nc} \approx 0.2$, see Figure 5.29). However, evidence presented by Lemos (1986) and Tika (1989) indicate that the phenomenon may in fact be related to a transition from turbulent shearing to a dynamic mode which dissipates less energy and involves the creation of a particularly high void ratio in the shear zone. Lemos & Vaughan (1992) postulate that this mechanism can only apply when, as in the ring shear apparatus, the shear zone has free access to water.

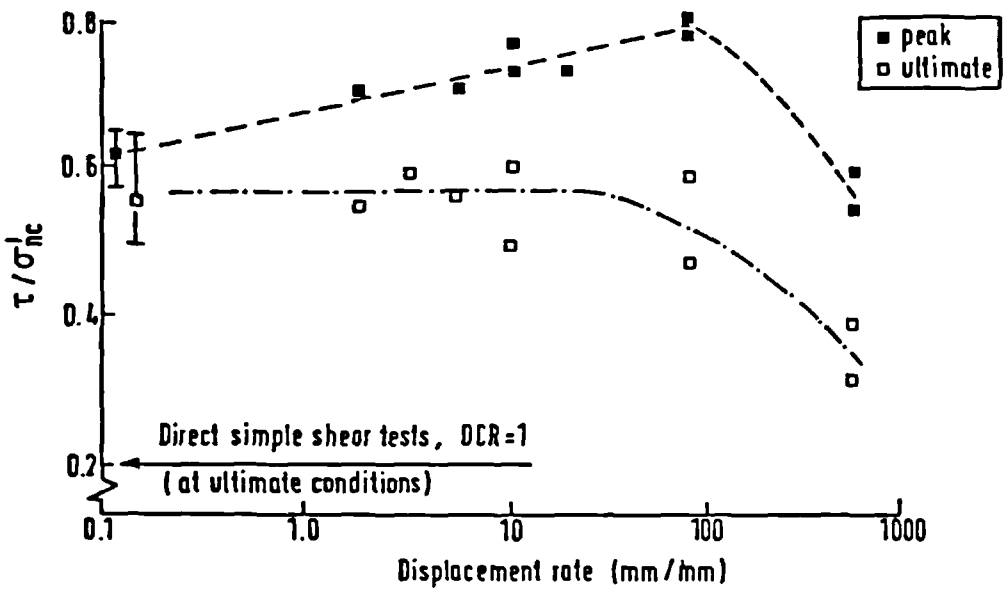

Figure 5.31 Rate dependence of the interface shearing resistance of Bothkennar Clay

CHAPTER 6

PILE TESTS AT LABENNE

CONTENTS OF CHAPTER 6

PILE TESTS AT LABENNE

6.1 OUTLINE 198

6.2 PILE CONFIGURATION AND TEST PROGRAMME 198

6.3 INSTALLATION 199

- 6.3.1 End resistance 199
- 6.3.2 Pore pressure 200
- 6.3.3 Radial effective stress 202
- 6.3.4 Local shear stress 205
- 6.3.5 Average shear stress 206
- 6.3.6 Interface friction angles 207

6.4 EQUALISATION 209

6.5 LOAD TESTING 213

- 6.5.1 Overall load displacement behaviour 213
- 6.5.2 Local shear stress 214
- 6.5.3 Local radial effective stress 216
- 6.5.4 Effective stress paths 218
- 6.5.5 Pile reload tests 220
  - 6.5.5.1 Tension and compression tests 220
  - 6.5.5.2 Cyclic tests 222

6.6 DISCUSSION 224

- 6.6.1 General 224
- 6.6.2 Changes in σ'_r during pile loading 224
- 6.6.3 Interface friction angles 225
- 6.6.4 Distributions of τ_{av} and τ_f with depth 226

6.1 OUTLINE

This Chapter presents the results of the ICP tests performed in the loose to medium dense sand at Labenne. The experimental procedures used and the soil conditions at the site are described in Chapters 4 and 5.

The data obtained during pile installation, equalisation and load testing are first discussed separately (Sections 6.3-6.5). Trends identified during each of these stages are summarised in Section 6.6 and compared in Chapter 9 with previous research on the behaviour of displacement piles in sand.

6.2 PILE CONFIGURATION AND TEST PROGRAMME

The field tests at Labenne were carried out over a two week period in January & February 1989. Two ICP's, designated LB1 and LB2, were jacked from ground level to a final penetration of ≈6m. The piles were subsequently load tested after an equalisation period of ≈15 hours (Tests LB1/L1C and LB2/L1T). Installation of pile LB2 was halted temporarily for ≈2.5 hours at a depth of 1.83m to allow a preliminary load test to be performed (Test LB2/L1C). Further secondary load tests, including cyclic load tests, were carried out after the initial load tests.

The arrangement of instrumentation on both piles was identical and is shown on Figure 6.1. Each pile contained three standard instrument clusters (i.e. the leading, following and trailing clusters) over the lower 3m length of the pile shaft. These clusters measured radial stress, shear stress, axial load and temperature, as detailed in Chapter 4.

All instruments remained stable and showed negligible zero drift or change in sensitivity throughout the testing programme (see Appendix A)[1].

---

[1]One radial compression circuit in the leading SST on pile LB1 became unstable due to moisture ingress shortly before load testing. Fortunately, radial stresses could be resolved from the second circuit.

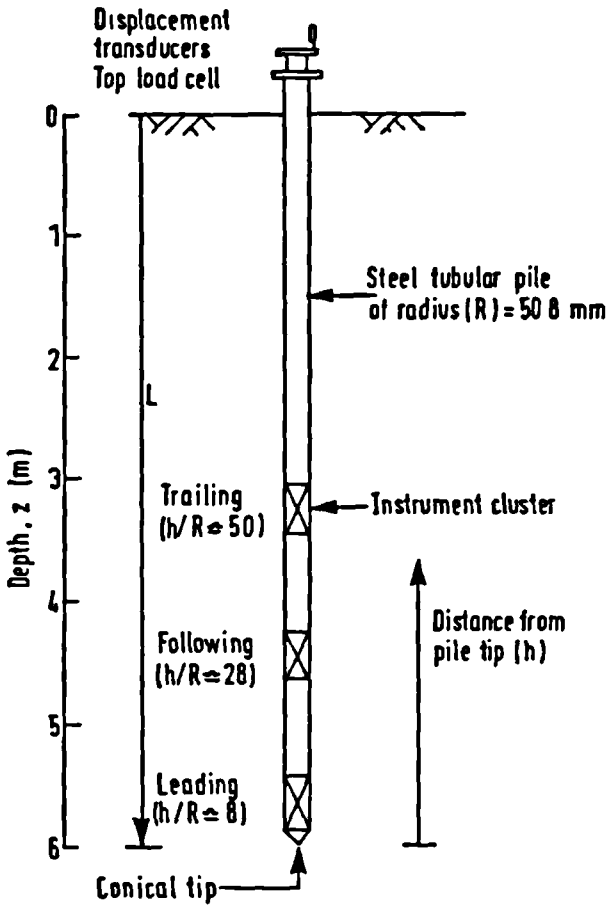

Figure 6.1 Configuration of piles LB1 and LB2 at Labenne

6.3 INSTALLATION

The piles required about 25 jack pushes to reach final penetrations of 6m. The data recorded during jacking, and while the piles were stationary in between jacking stages, are presented in this section.

6.3.1 End resistance

The variation with depth of the end resistance (q_b) met by each pile during jacking is shown on Figure 6.2. A comparison of the respective profiles indicates:

- q_b for both piles is almost identical to about 2m depth, but below 3m, q_b values for LB2 are up to 20% greater than those of LB1.
- There are appreciable differences in the loose sand at ≈3m.

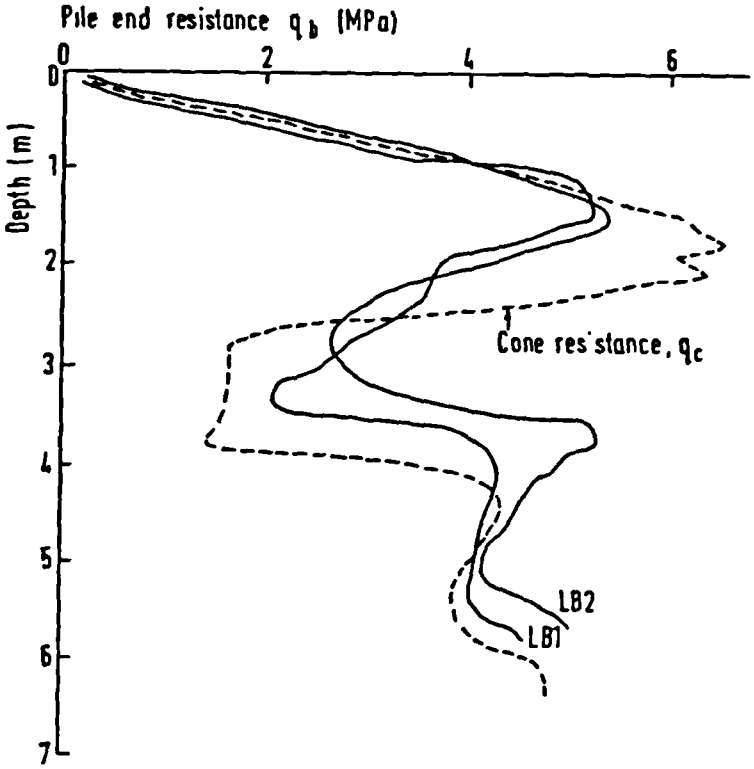

Figure 6.2 End resistances during jacking

A typical Cone Penetration Test (CPT) end resistance (q_c) profile at Labenne is also shown on Figure 6.2 and is seen to be in reasonable agreement with q_b. However, stratum boundaries appear to be defined less sharply by the q_b traces, suggesting that the zones of influence of the two 'penetrometers' are in proportion to their diameters (the CPT tool has a diameter of 36mm). This observation is in keeping with design methods which propose that q_b may be derived by averaging the q_c variation in the vicinity of the pile tip over distances proportional to the pile diameter (e.g. Bustamante & Gianeselli 1982, Schmertmann 1978).

6.3.2 Pore pressure

The variations of pore pressure measured during pile installation are illustrated on Figure 6.3, using data recorded by the three instrument clusters on pile LB1. The pore pressures recorded while the pile is stationary are indicated by horizontal spikes - where depth is constant,

but pore pressures can change. Allowing for the difficulty in selecting a precise calibration zero offset for the probes, the stationary pressures correspond to, on average, a hydrostatic distribution of pore pressure from ≈2.9m below ground level.

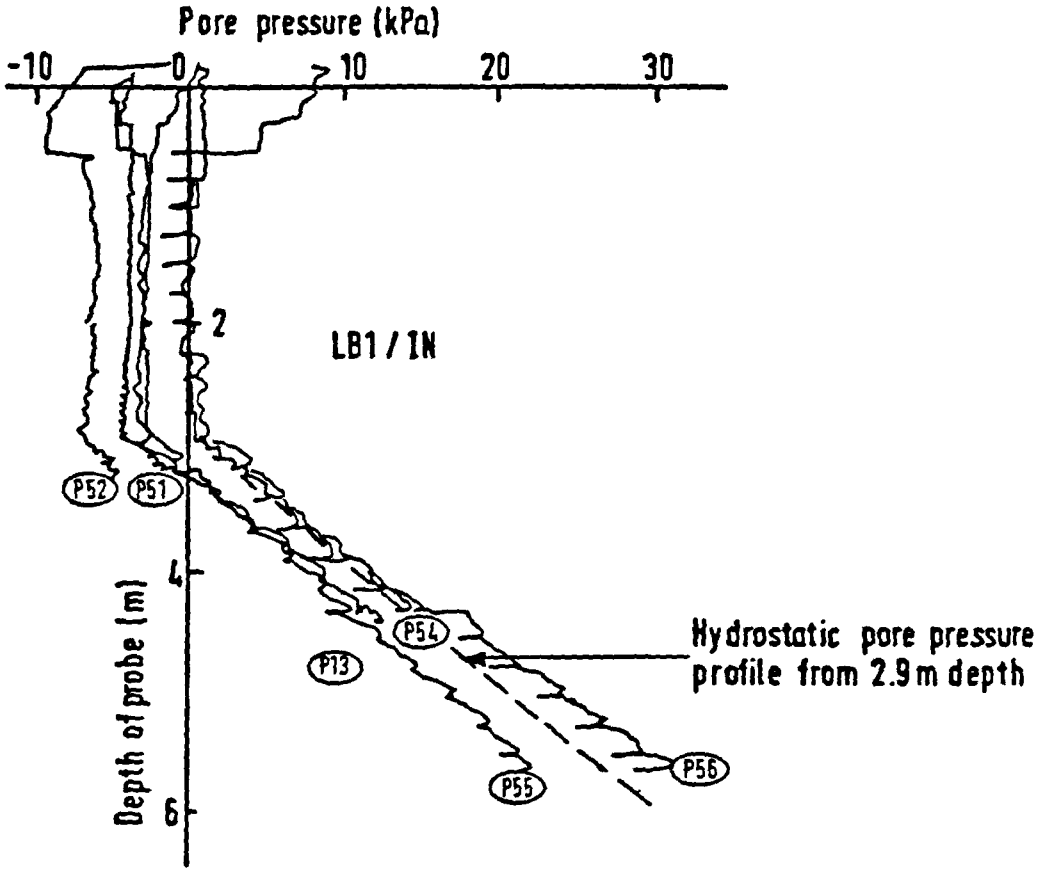

Figure 6.3 Pore pressures recorded during installation of LB1

Pore pressures recorded while the piles were moving varied by about ±2kPa from the hydrostatic distribution but these (small) excess pressures dissipated within one minute of the completion of a jacking stage. To simplify the interpretation of the tests, it was decided to neglect these small deviations and to assume that pile installation and load testing are *drained* processes with hydrostatic pressures acting throughout.

The records for both piles showed the water table level to be at ≈2.9m depth.

6.3.3 Radial effective stress

Radial effective stresses (σ'_r) tended to increase at the beginning of a jacking stage, so that the stationary profiles of σ'_r (referred to as σ'_{rs}) differ from those recorded whilst the pile was moving (σ'_{rm}). These increases ranged from ≈5kPa in the loose sand at ≈3m to up to 25kPa in the medium dense sand at shallow depths. This phenomenon will be discussed later, but at present attention will be focused on the values recorded between the jacking stages.

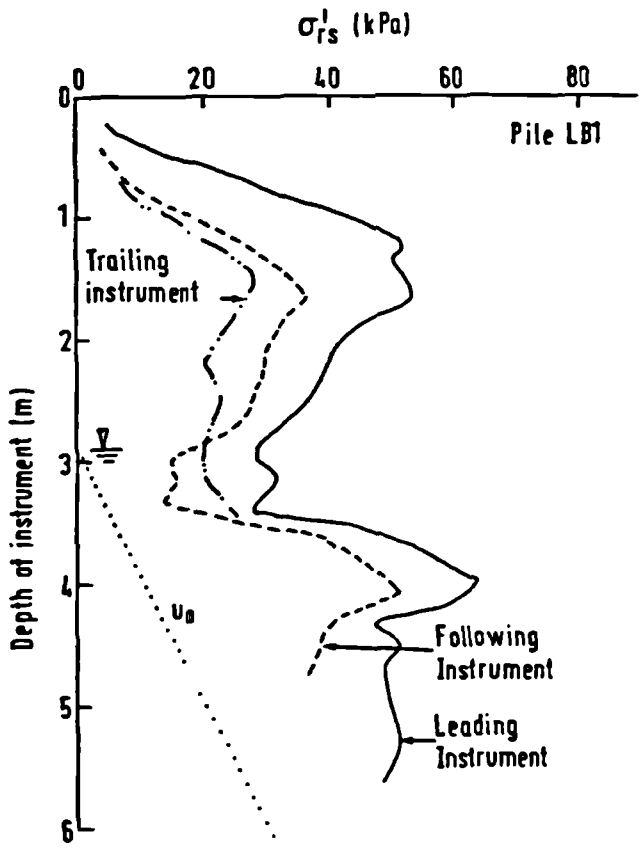

Figure 6.4 σ'_r values recorded by LB1 in between jacking stages

Typical σ'_{rs} data (recorded by pile LB1) are shown on Figure 6.4. Points to note include:

- The σ'_{rs} values are at least an order of magnitude less than the pressure required to expand a cylindrical cavity (i.e. the pressuremeter limit pressure; see Figure 5.4). It is thus clear

that cavity expansion analogies (see Section 2.3.1) are not applicable to piles in sand.

- The σ'_{rs} profiles resemble closely the q_b and q_c traces shown on Figure 6.2, indicating the strong dependence of these stresses on the relative density of the strata through which a pile is installed.
- Values of σ'_{rs} recorded at fixed depths in the soil profile tend to reduce as the relative depth of the pile tip (h/R) increases. For example, at the 2m level, σ'_{rs} reduces from ≈40kPa when h/R=8 to ≈22kPa when the tip penetrates a further 42 radii to give a h/R value of 50.
- Equivalent σ'_{rs} values recorded by instrument clusters on pile LB2 were within 10kPa of the stresses plotted for LB1 on Figure 6.4[1]. This narrow range of measurements can be explained by local ground variability and is indicative of the high repeatability of the instrumentation.

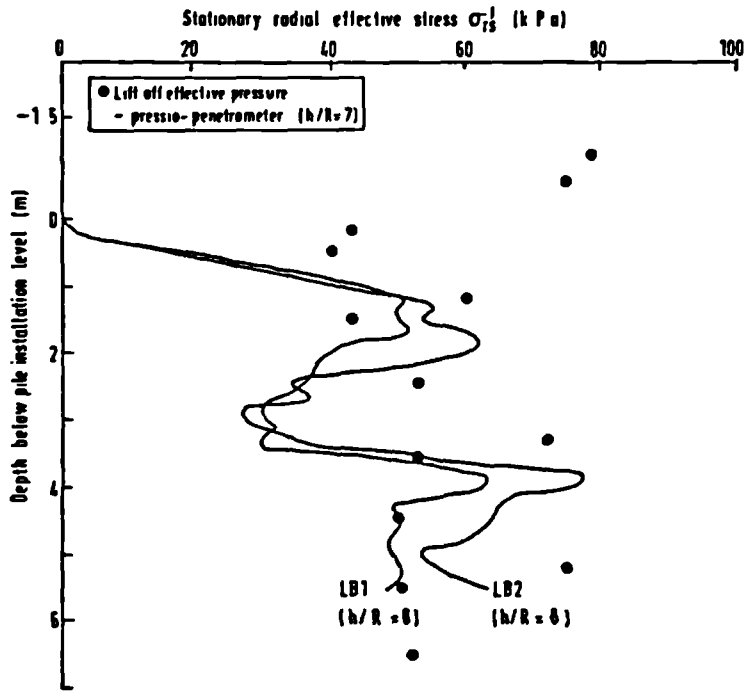

Figure 6.5 Comparison of σ'_{rs} data with PP data

[1]Except for the SST at h/R=28 on this pile, which, for no ascertainable reason, registered negative (i.e inadmissable) radial total stresses in the loose sand at ≈3m. A correction of +15kPa was applied to all subsequent σ_r data presented for this SST to ensure that all its σ_r records were positive. This correction resulted in good compatibilty with data from all other SST's.

The σ'_{rs} values recorded at h/R=8 on both piles are compared on Figure 6.5 with the *lift-off* effective pressures (measured at h/R=7) in pressiopenetrometer (PP) tests at Labenne (see Section 5.1.5). Good agreement between both data sets is observed, despite the fact that the PP results were obtained prior to the (1.5m) general excavation at the site. This comparison reveals that, for a given h/R value, radial effective stresses are most strongly controlled by the in-situ relative density.

The separate effects of q_b ($\approx q_c$) and h/R on σ'_{rs} are investigated in Figure 6.6, which shows the envelopes established from approximately 30 individual σ'_{rs} measurements on both piles. Plotting the ratio σ'_{rs}/q_b against the h/R values at which the radial effective stresses were measured brings the data set into a relatively narrow band and demonstrates the strong dependence of σ'_{rs} on the relative position of the pile tip (h/R): normalised stresses are seen to reduce by approximately 50% as the pile tip moves from 8 radii below a given soil horizon to 50 radii below it.

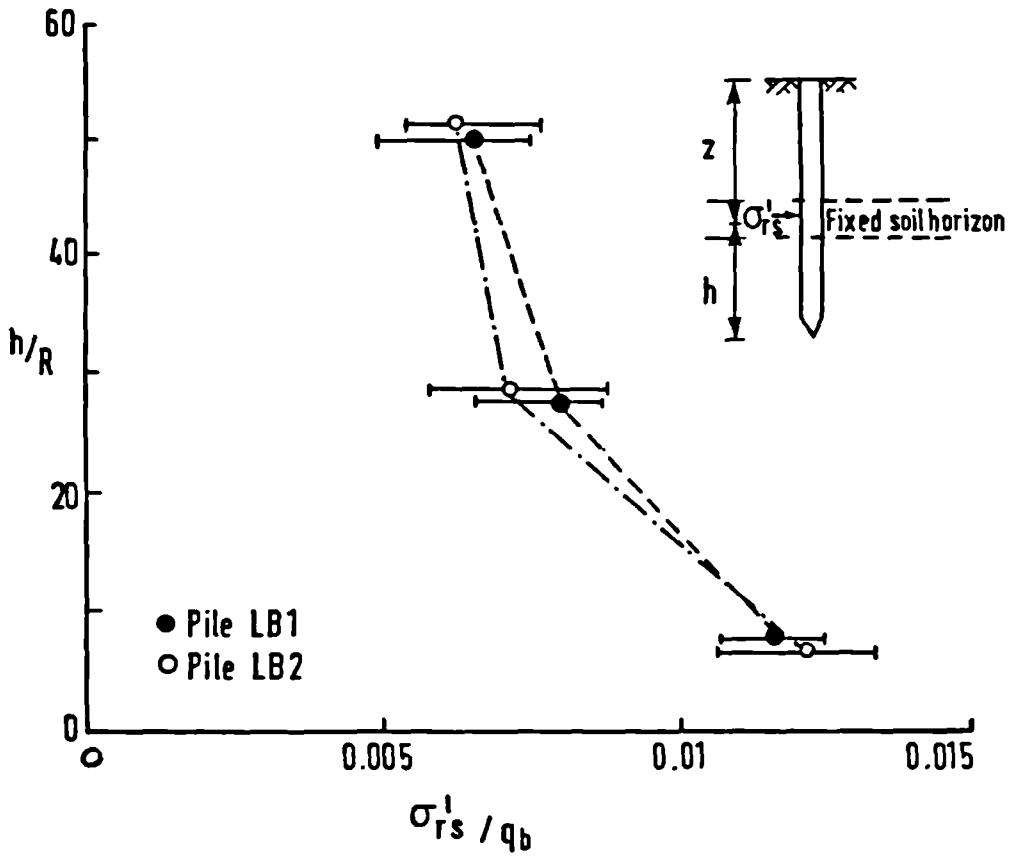

Figure 6.6 Variation of σ'_{rs}/q_b with h/R

6.3.4 Local shear stress

Figure 6.7 plots the shear stresses developed on the shaft of pile LB2 during jacking. Local values of the shear stresses (τ_{rz}) were measured directly by the SST's (τ_{rz}) and average values acting between instrument clusters (f_s) were derived from the axial load cell data.

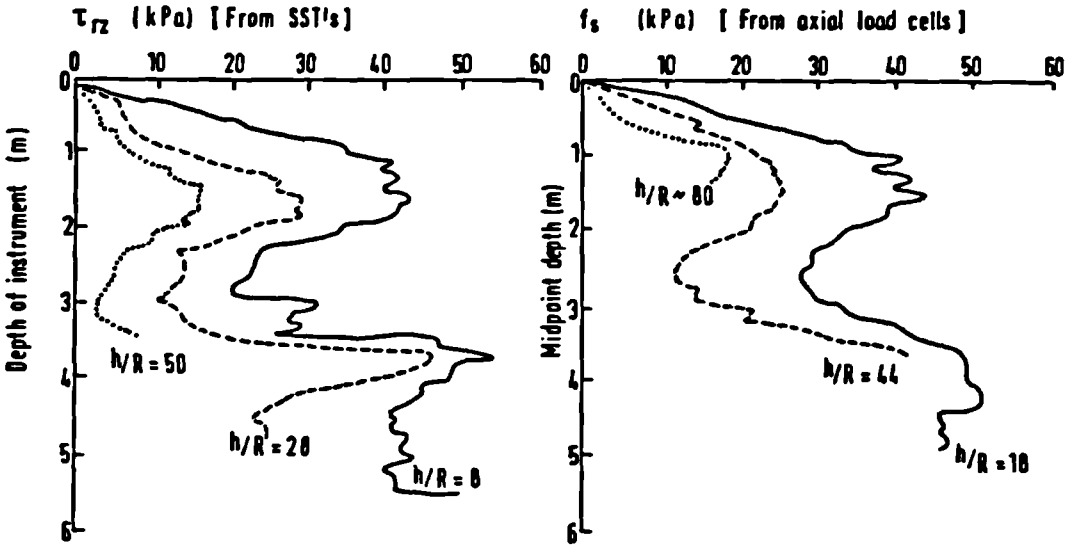

Figure 6.7 Shear stresses mobilised during jacking of LB2

It is apparent that, as for the σ'_r records:

- the τ_{rz} and f_s profiles at each instrument position show a strong dependence on the initial relative density, as expressed by the end resistance (q_b).
- τ_{rz} and f_s, measured at fixed depths, reduce as h/R increases

Closer examination of the τ_{rz} and f_s data, bearing in mind their dependence on h/R, revealed that the τ_{rz} records were typically 15% lower than equivalent f_s values. This apparent incompatibility was also observed during some load tests and is discussed in Section 6.5.

The general trends of all the installation shear stress data suggest that the τ_{rz} measurements made by the leading SST (at h/R=8) on pile LB1 were under-registered by ≈15%. This may have been due to the slightly smoother

surface finish of this SST[1], although such a high sensitivity to slight variations in surface roughness was not shown by the other SST's on the piles or observed during the laboratory interface shear test programme.

6.3.5 Average shear stress (τ_{av})

Pile installation is effectively drained and, as will be shown in Section 6.4, the stress conditions stabilise rapidly between jacking stages. Therefore each individual jacking stage can be considered as a separate load test which has been preceded by full equalisation.

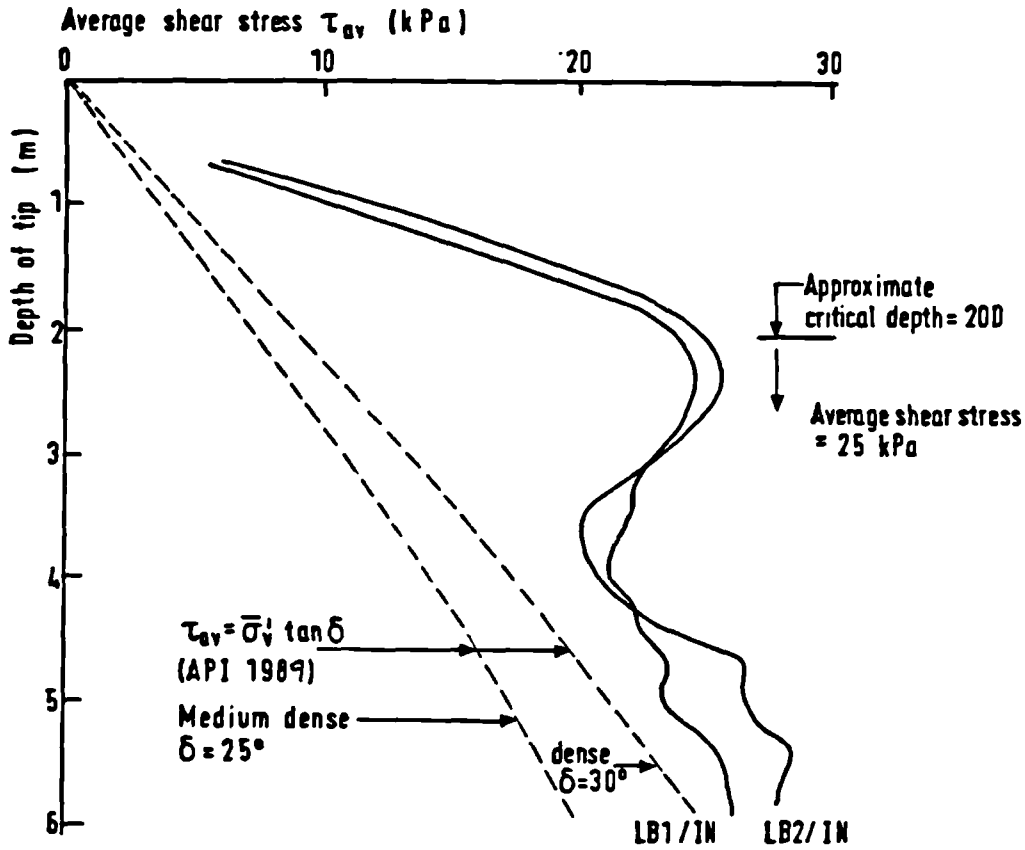

Figure 6.8 Average shaft shear stresses mobilised during jacking

[1]The centre line average roughness of this instrument after pile extraction was ≈5.0μm. This value is towards the lower end of the range of 4.5μm to 7.0μm shown by the other SST's.

The variations of the peak average shear stress measured over the full shaft length (τ_{av}) with the depth of the pile tip, for all jacking stages, are shown on Figure 6.8. τ_{av} is seen to increase linearly with depth up to 2m penetration but thereafter remains quasi-constant varying between 20kPa and 28kPa, albeit with a slight tendency to increase with depth. This trend is consistent with measurements made in load tests on other displacement piles in sand, discussed in Chapter 3, which showed that τ_{av} tended to a relatively constant value below a 'critical depth'. The 'critical depth' for the Labenne tests appears to be at ≈2m (20 pile diameters).

The stabilisation of the average shear stress with depth is not recognised explicitly in the API(1989) recommendations (see Section 3.2) which, as shown on Figure 6.8, assumes a quite different relationship to that found experimentally. Recalling that the Labenne sands are loose to medium dense, the API recommendations can be seen to be conservative over the depth penetrated by the ICP's. However, if the results are extrapolated to deeper levels, it appears that the API rules would over-predict shaft capacities for penetrations greater than about 7.5m (75 pile diameters).

6.3.6 Interface friction angles

The interface friction angles (δ) mobilised during jacking may be calculated from the local stress measurements as : $\delta = \tan^{-1} (\tau_{rz}/\sigma'_{rm})$. The angles, so obtained, fell within ± 3° of the mean values listed in Table 6.1. For the pile casings, the angles were calculated using (i) the shear stresses derived from the axial loads in adjacent instrument clusters (f_s) and (ii) the average of the σ'_r values measured by these two clusters.

	h/R	LB1	LB2
Leading SST	8	25°[1]	28°
Leading pile casing	18	32°	30°
Following SST	28	28°	29°
Following pile casing	44	29°	32°
Trailing SST	50	20°	22°

Table 6.1 Mean δ values during pile jacking

δ values did not show any systematic variation with depth, apart from in the loose sand at ≈3m, where values were generally 3-5° lower than average.

Far fewer measurements are recorded per unit displacement during installation than during load tests and therefore these δ values are less reliable than those presented in Section 6.5. Nevertheless some preliminary observations may be made:

- δ values are in good agreement with the range expected from laboratory interface shear tests (see Section 6.6.3)
- values measured by the SST's are typically ≈3° less than those mobilised at the pile casings. This difference is consistent with the discrepancy, noted in Section 6.3.4, between the τ_{rz} and f_s records.

The low angles recorded by trailing instrument (at h/R ≈50) and by all instruments at ≈3m depth may be due to the sensitivity of the calculations to small inaccuracies in the measurements at low stress levels; e.g. for typical measurements at h/R ≈50, an over-estimate of just 4kPa in σ'_{rm} and under-estimate of 2kPa in τ_{rz} would cause the calculated δ value to reduce from 30° to 22°.

[1]This SST registered uncharacteristically low shear stresses (see Section 6.3.4).

6.4 EQUALISATION

The variations of σ_r, u and τ_{rz} recorded after a typical pile installation (LB1) are shown on Figure 6.9. A logarithmic time scale is used so that variations during the last push (0.1m in length) can also be included. Both σ_r and τ_{rz} reduce immediately when the pile comes to rest and it is evident that equilibrium conditions are achieved (constant σ_r, u and τ_{rz}) within one minute. Slight apparent fluctuations of pore pressures after about 500 mins are attributed to instrument drift.

It can be seen on Figure 6.9 that the equilibrium (residual) τ_{rz} values are negative (i.e. they act downwards on the pile shaft). The distribution of these stresses is shown on Figure 6.10 where they are observed to remain relatively constant along the shaft, giving an average value of ≈7.5kPa. This average value is compatible with the distribution of the pile axial loads, which increase linearly from zero at the ground surface to ≈14kN at the pile base.

As discussed in Chapter 3, because of the large zero shifts generally experienced by instruments during driving in previous testing programmes, it is common practice to re-zero the instruments after installation, with the implicit assumption that the residual loads in piles are negligible. It is apparent from the load tests results presented in Section 6.5 that, if this procedure was followed at Labenne, the compressive shaft capacities would be over-estimated by ≈25%, as the initial base load (of 14kN) would have been discounted.

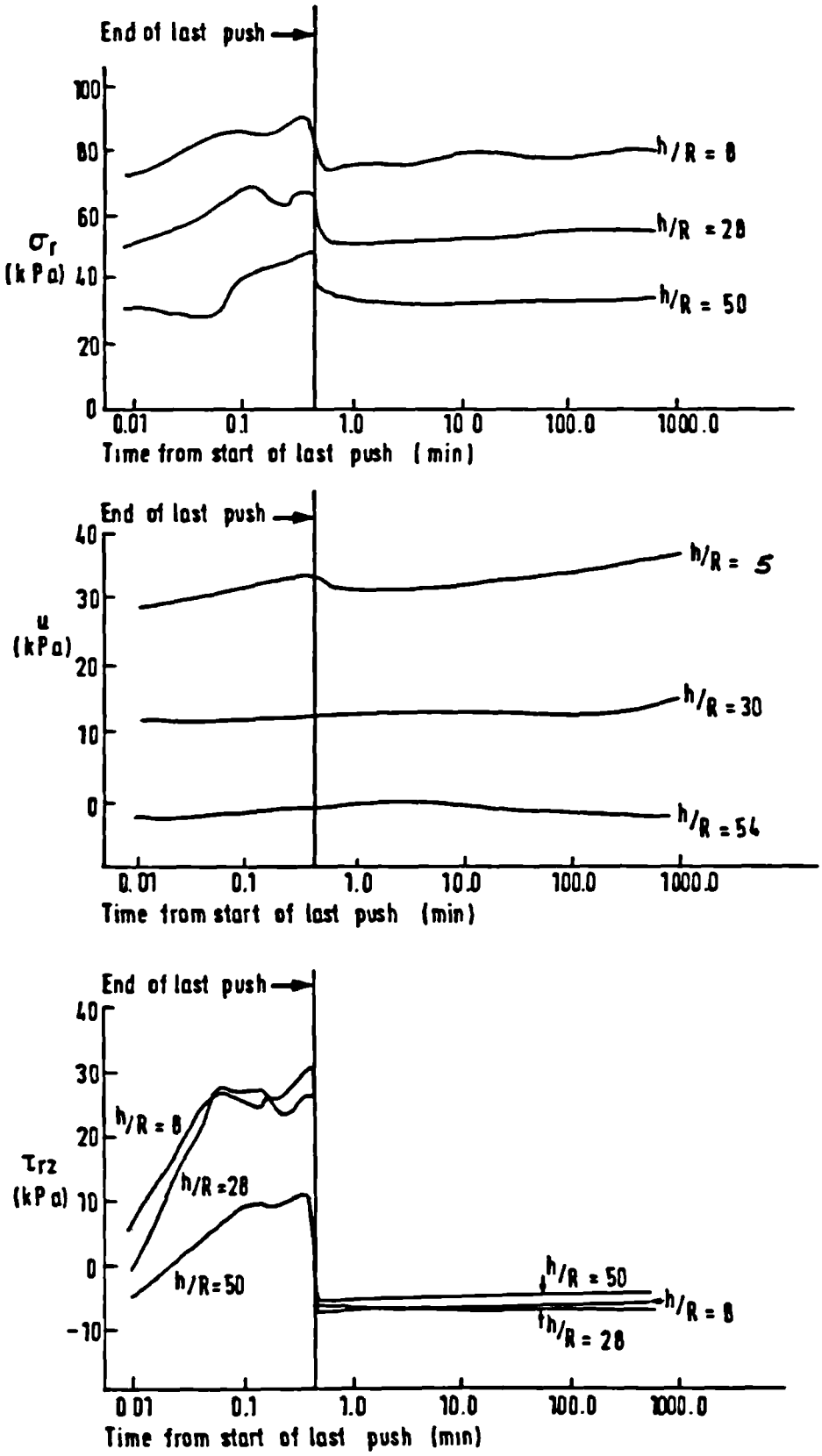

Figure 6.9 Data recorded during equalisation of LB1

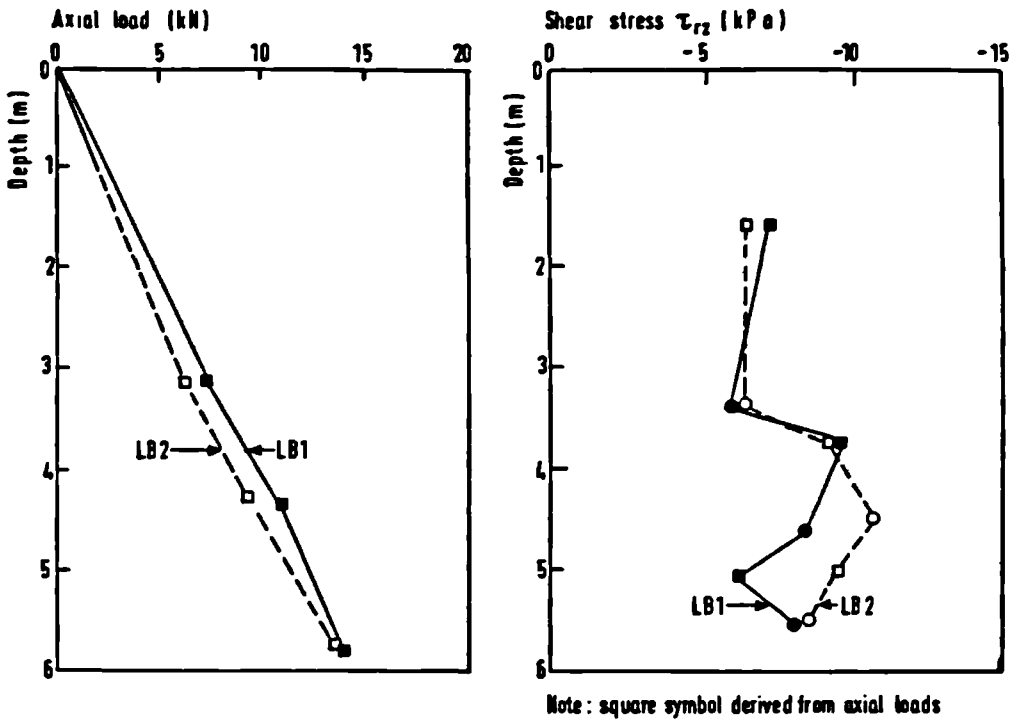

Figure 6.10 Residual stresses in the piles at Labenne

Because of the observed rapid equalisation of stresses, the stationary radial effective stresses recorded during installation pause periods are equivalent to the long term equalised values (σ'_{rc}) for a pile that had penetrated to the same tip depth, but no further. The data base of σ'_{rc} measurements can therefore be expanded greatly as the distribution with depth of $\sigma'_{rs} \approx \sigma'_{rc}$ for all pile penetrations up to 6m can be assessed. This is illustrated on Figure 6.11 for embedded pile lengths (L) ranging from 50 to 116 pile radii (R), using the mean values of σ'_{rs} measured by piles LB1 and LB2. Equalised radial effective stresses developed at any sub-layer are seen to depend not only on the local initial properties and state of the sand at that depth, but also on the position of the pile tip in relation to that sub-layer. Values of σ'_{rs} range from about $0.5\sigma'_{v0}$ to $1.1\sigma'_{v0}$, depending on the depth and h/R value. It is interesting that at large h/R ratios, σ'_{rs} values tend to values close to the estimated initial undisturbed horizontal stress (σ'_{h0}).

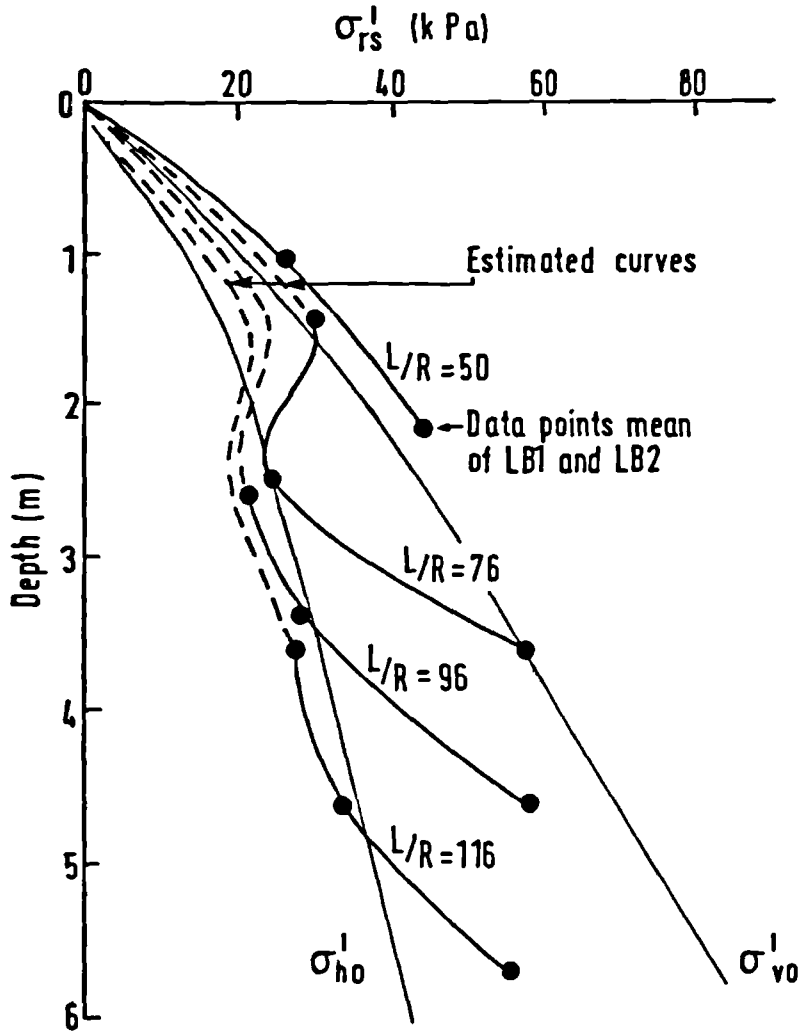

Figure 6.11 Variation of σ'_{rs} ($=\sigma'_{rc}$) with pile slenderness ratio (L/R)

It is apparent from the data on Figure 6.11 that the mean value of σ'_{rs} acting on a pile of given length remains relatively constant at ≈30kPa for L/R >40. This trend is compatible with the stabilisation of τ_{av} with depth seen on Figure 6.8 and it may be inferred that, as the *local* values of radial effective stress and shear stress generally increase with depth, the trend for τ_{av} to attain a quasi-constant value arises, primarily, because of the dependence of these local stresses on the relative depth of the pile tip (h/R).

6.5 LOAD TESTING

The general results from the complete Labenne load testing programme are summarised in Table 6.3 on page 221 and Figures 6.16-6.18 on pages 227-229. This section focuses on the results from the three 'first-time' load tests: Tests LB1/L1C, LB2/L1C & LB2/L1T.

6.5.1 Overall load-displacement behaviour

Key measurements made in each of the three first-time load tests are given in Table 6.2.

Test	LB1/L1C	LB2/L1C	LB2/L1T
Depth of pile tip (m)	5.95	1.83	5.92
Test type	Comp.	Comp.	Tens.
Set-up period (hrs)	15	2	15
Peak load (kN)	97	51	-50.0
Peak τ_{av} (kPa)	32	24	-26.5
Displacement at peak τ_{av} (mm)	3.6	20	-13.5
Ultimate[1] τ_{av} (kPa)	29	24	-26.5
Ultimate q_b (kPa)	4.7	4.3	0
Response	Stiff, slightly brittle	Initially stiff, ductile	Soft, ductile

Table 6.2 Details of first-time load tests at Labenne

It is evident that there are considerable differences between the overall shaft characteristics of piles tested in compression and tension. For piles installed to ≈6m:-

- The peak shaft capacity (τ_{av}) in tension is about 20% less than in compression, even though the sand may have been in a slightly

[1]At a pile head displacement of 20mm.

denser initial state at the location of the tension test (see Section 6.3.1)

- The pre-failure tensile response is considerably softer than the response in compression.
- The tension failure is ductile[1], whilst the compression test shows a post-peak reduction in capacity of 10%; the ultimate compression and tensile capacities differ by ≈10%.

The q_b and ultimate τ_{av} values measured in two first-time compression tests are comparable to those values measured during the last jacking stage at installation. This observation supports the inference made from the equalisation data that there is no significant set-up effect in this material.

The following sections discuss detailed results obtained with the local pile instrumentation.

6.5.2 Local shear stress

The variations of shear stress (τ_{rz} and f_s) with pile head displacement (d_p) during the two first-time load tests on piles installed to ≈6m (i.e Tests LB1/L1C and LB2/L1T) are shown on Figure 6.12. These variations illustrate the remarkable differences between tension and compression loading, referred to above, and are consistent with the trends shown by the load displacement curves on Figures 6.16 & 6.18.

The residual (pre-loading) shear stresses act in the opposite direction to the ultimate shear stresses (τ_f) developed in the compression test and in the same direction as τ_f in the tension test. Given that these residual stresses amount to between 20% and 40% of the τ_f values, it is not surprising that the initial stiffness values in tension loading are considerably less than those in compression loading (e.g. see Poulos 1989). However, the compression pile maintains a much higher stiffness

[1]The base load represented 75% of the total capacity of the short pile (Test LB2/L1C). The ductile response seen in this test is typical of that shown by 'end-bearing' piles (e.g. see Tomlinson 1963).

value up to peak shear stress and it is clear that other factors such as the anisotropic characteristics of sand control the stiffness characteristics (c.f. differences between triaxial compression and extension tests on Labenne sand; Figure 5.6) .

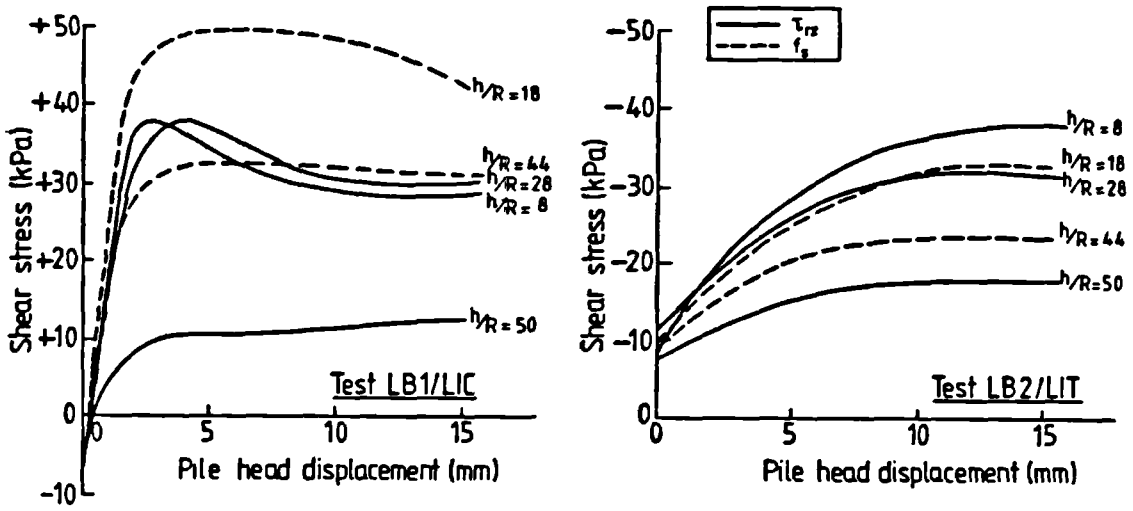

Figure 6.12 Local shear stress variations with pile head displacement

Two unusual features of the data recorded in Test LB1/L1C are apparent from Figure 6.12:

- Shear stresses recorded by the SST's (τ_{rz}), particularly at large post-peak displacements, are smaller than the values that would be inferred from the f_s records[1].
- The post-peak reductions of τ_{rz} values are generally more pronounced and occur at lower pile head displacements than reductions in the f_s measurements.

Data from all the load tests at Labenne indicated that the discrepancies between τ_{rz} and f_s values were most pronounced after piles had failed in

[1]Note that τ_{rz} values measured by the SST at h/R=8 on this pile were untypically low (see Section 6.3.4).

a brittle fashion (i.e. as they accelerated into the ground)[1]. Ring shear tests on Labenne sand (Section 5.1.7) suggest that the 'dynamic' interface friction angle (at 500mm/min) may be up to 3° less than the 'static' angle (at <1mm/min). It thus appears possible that the different post-peak characteristics of the τ_{rz} and f_s seen in Test LB1/L1C and implied by the installation data, may be due to differences between the static and dynamic frictional characteristics of the sand when sheared against the stainless steel SST's and the interconnecting molybdenum steel casings. In addition, it must be borne in mind that f_s values may reflect un-measured erratic variations of radial effective stresses in between instrument clusters. Such variations over very short distances were observed following unloading of piles after each load test (see Section 6.5.5).

The profiles with depth of the local shear stresses (τ_{rz} & f_s) measured at different pre-peak pile head displacements (d_p) are shown on Figure 6.13 for Tests LB1/L1C and LB2/L1T. It is noted that:

- The (pre-peak) τ_{rz} and f_s values are generally in good agreement.
- Both distributions reflect the layered profile at the site.
- The rate at which τ_{rz} is mobilised is relatively constant at all levels in the tension test but appears to be slightly faster at depth in the compression test i.e. pile LB1 fails progressively from the pile tip.
- Lower local peak shear stresses are measured at all depths (except at ≈3.4m) in the tension test.

6.5.3 Local radial effective stress

The variations with depth of the radial effective stresses prior to loading (σ'_{rc}) and at peak pile capacity (σ'_{rf}) are also shown on Figure 6.13 for Tests LB1/L1C and LB2/L1T.

---

[1]Ductile (slow) pile failures occurred in all tension tests and in the compression re-test of pile LB1 (Test LB1/L2C).

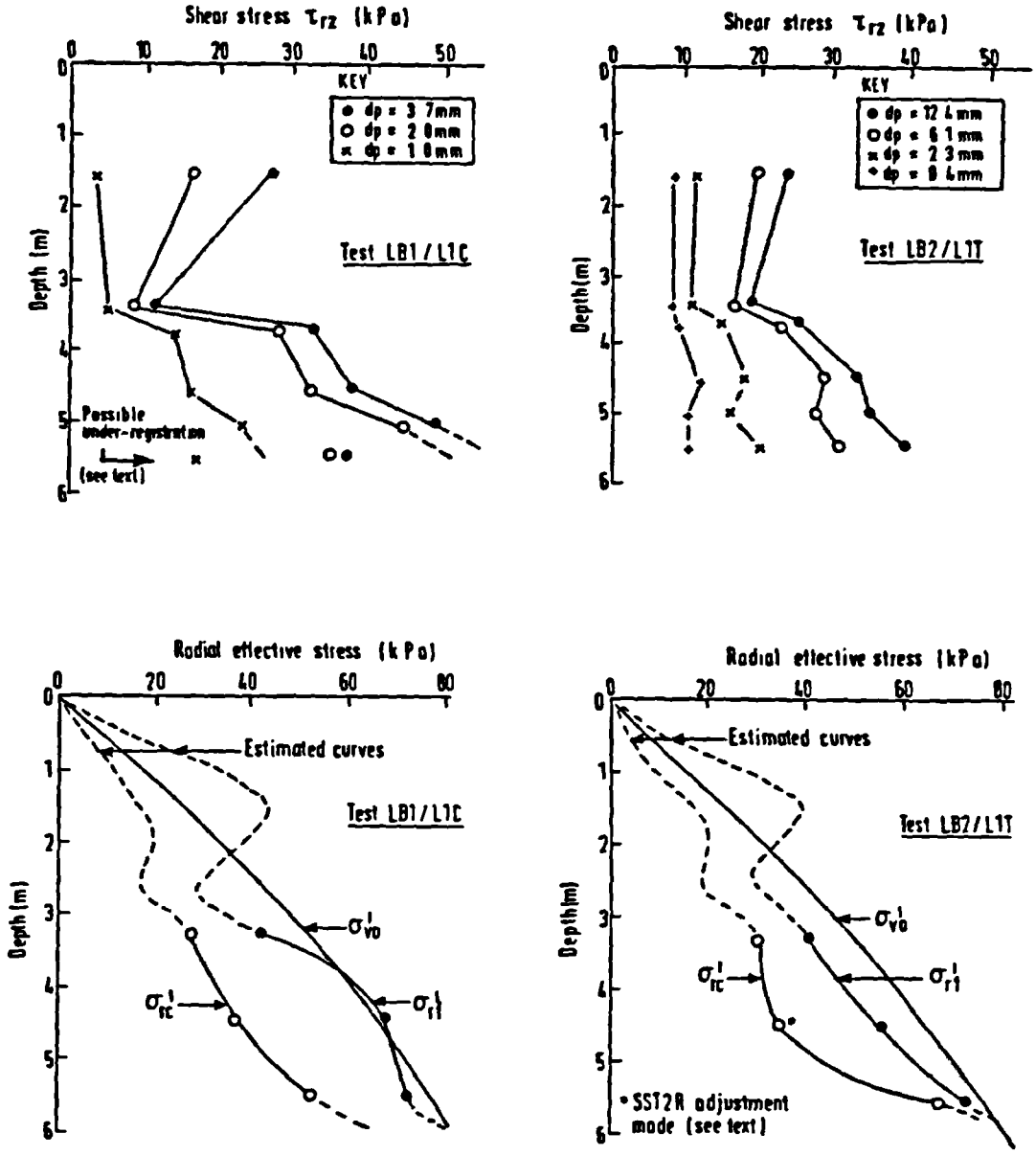

Figure 6.13 Profiles of shear stress and radial effective stress

Two notable features are:

- σ'_{rf} is typically between 20% and 50% greater than σ'_{rc} i.e. σ'_r shows a large overall increase during pile loading.
- higher values of σ'_{rf} are mobilised by the compression pile.

At depths below 3m, σ'_{rf} values vary between 0.8-1.0σ'_{vo} and are in reasonable agreement with API (1989) which recommends that σ'_{rf} may be

assumed equivalent to σ'_{v0} for full displacement piles. However, the values of σ'_{rf} at shallow depths (which were inferred from the measured shaft capacities and the trends shown by Figure 6.11), exceed σ'_{v0} considerably. The tendency for σ'_{rf} to exceed σ'_{v0} at shallow depths was confirmed in Test LB2/L1C, where $\sigma'_{rf}/\sigma'_{v0}$ was found to equal 4 at a depth of 1.45m (and h/R value =8).

6.5.4 Effective stress paths

The pile tests at Labenne provided the unique opportunity to study the detailed variations of shear stress (τ_{rz}) and radial effective stress (σ'_r) during load testing in sand. The data are presented most succinctly by plotting the paths followed during loading in (τ_{rz} ,σ'_r) co-ordinates. This is illustrated for Test LB2/L1C in Figure 6.14, using data from the leading instrument cluster (h/R=8) in the medium dense sand at 1.45m depth.

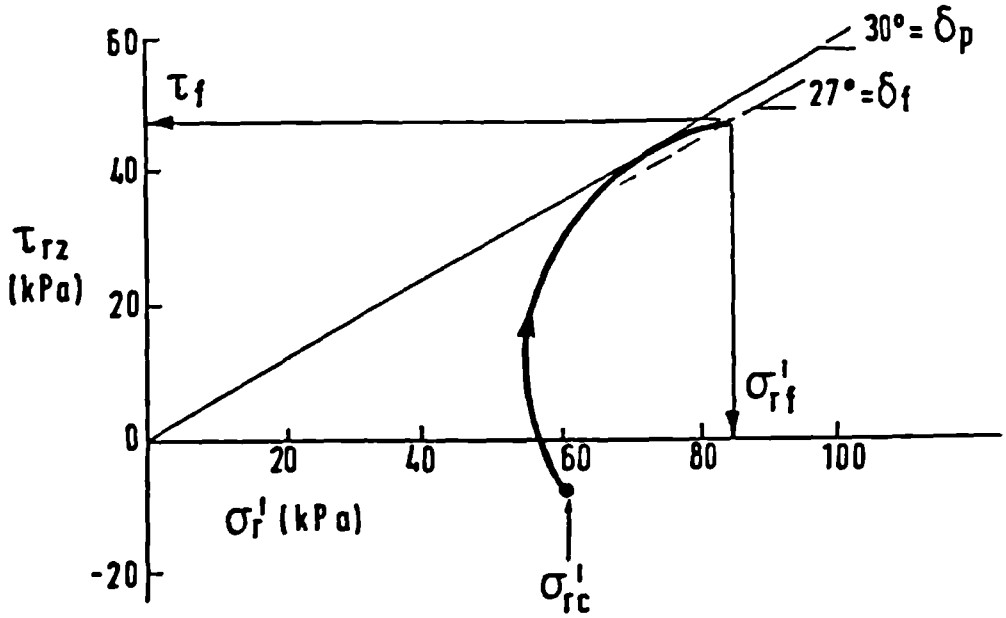

Figure 6.14 τ_{rz} v σ'_r paths at z=1.45m in Test LB2/L1C

Points to note include:

- The effective stress path shows an initial slight reduction in σ'_r but continued displacement leads to a large increase in σ'_r. At

peak shear resistance (τ_f), the radial effective stress (σ'_{rf}) is ≈1.4 times its stationary equilibrium value (σ'_{rc}).

- Local failure at the shaft occurs when τ_{rz} and σ'_r reach their maxima and the stress obliquity δ [= $\tan^{-1}(\tau/\sigma'_r)$] equals its ultimate angle (δ_f) of 27°. However, the stress obliquity shows its maximum value (δ_p) of 30° at an earlier stage.

The stress paths measured during the first-time load tests on piles at full penetration are shown on Figure 6.15.

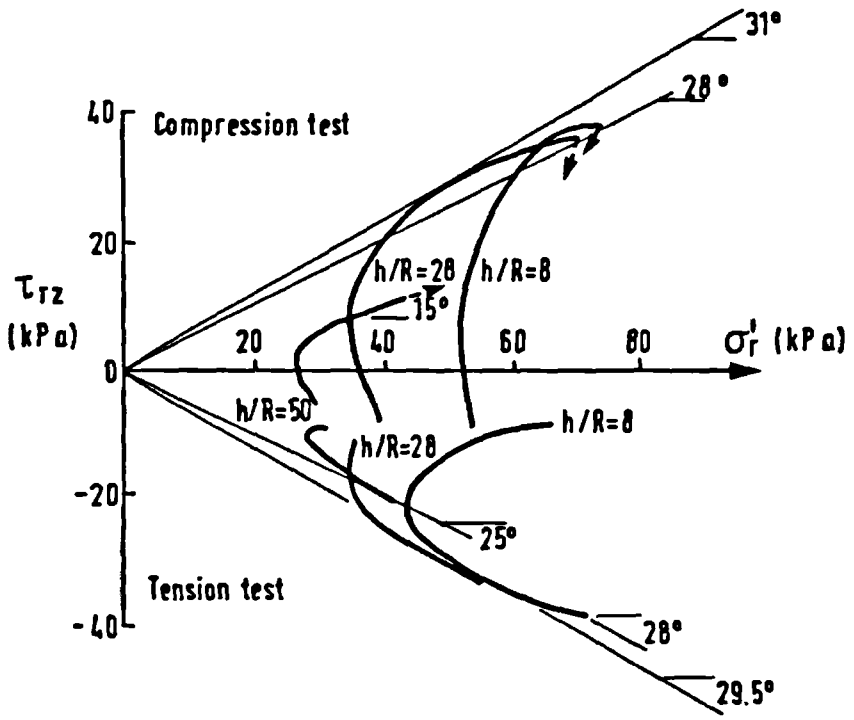

Figure 6.15 τ_{rz} v σ'_r paths in Tests LB1/L1C and LB2/L1T

Figure 6.15 displays similar trends to those seen in Test LB2/L1C and allows some additional observations to be made:

- Comparable values of δ_p and δ_f are developed in the tension and compression tests. Therefore, the lower shaft capacity in the tension test must be primarily due to the lower values of σ'_{rf} mobilised on this pile (compare profiles of σ'_{rf} on Figure 6.13).

- The lower σ'_{rf} values developed by the tension pile appear to be due to larger initial reductions in σ'_r during the early stages of tension loading.

- The instruments at h/R=50 show low values of δ, particularly in Test LB1/L1C. This was probably partly due to the loose organic sub-layer which was later proven at this instrument's level in a fully sampled borehole (Figure 5.2). When pile LB1 was re-jacked a further 0.25m and re-tested (Test LB1/L2C), the value of δ_f rose from 15° to 23.5°.

- Pile LB1 accelerated into the ground after peak capacity was mobilised. The stress paths measured during this stage of the test are shown by the dashed arrows on Figure 6.15 and indicate that the post-peak brittleness of τ_{rz} observed in this test (see Figure 6.12) is related to a further small reduction in δ. Based on observations made in ring shear interface tests performed at fast and slow rates of displacement (Section 5.1.7), it is surmised that this reduction (≈3°) represents the difference between the ultimate static and dynamic interface friction angles.

6.5.5 Pile reload tests

6.5.5.1 Tension and compression tests

Table 6.3 lists the relevant effective stress parameters measured in the 8 load tests performed at Labenne (including the 3 first-time tests, discussed above). The load displacement curves for these tests are given in Figures 6.16-6.18.

The values of obliquity recorded by the leading and following instrument positions at peak local shear stress (δ_f) do not differ, in any test, by more than 1.5° (or 5%) from the mean value of 28.5°. Values measured at the trailing instrument position (at ≈3.5m depth) were typically 25° ± 2°, but these were most probably affected by the organic sub-layer at

Test	L (m)	τ_{av}[1] (kPa)	d_{pm}	h/R	σ'_{rl} (kPa)	σ'_{rf} (kPa)	K_f/K_l	τ_f (kPa)	δ_f (°)
Pile LB1									
L1C	5.95	31.8	3.6	8	53.4	71.0	1.33	37.0	27.5
				28	39.0	68.0	1.74	37.2	28.5
				50	29.0	42.0	1.45	11.1	14.8
L2C	6.20	28.0	2.1	8	74.5	91.0	1.22	48.4	28.0
				28	40.2	63.9	1.59	33.5	27.7
				50	39.0	56.0	1.43	24.3	23.5
FEX[2]	6.22	21.0	15.0	8	71.8	79.0	1.10	42.0	28.0
				28	42.6	40.2	0.94	20.7	27.3
				50	42.5	50.7	1.19	22.7	24.1
Pile LB2									
L1C	1.83	24.0	20.0	8	60.0	83.0	1.38	43.0	27.4
L1T	5.92	26.5	13.5	8	68.0	73.0	1.07	38.5	28.0
				28[3]	38.0	57.2	1.50	32.5	29.5
				50	32.0	40.6	1.27	19.0	25.0
L2T	5.90	27.3	0.80	8	62.5	75.5	1.21	41.0	28.5
				28[3]	48.3	77.3	1.60	32.5	27.5
				50	32.0	42.0	1.31	18.0	23.2
LCY	5.89	26.5	0.50	8	71.3	76.5	1.07	44.0	29.9
				28[3]	53.4	57.3	1.07	33.0	29.3
				50	34.0	27.2	0.80	17.0	27.2
FEX	5.87	26.7	2.06	8	61.0	81.1	1.32	43.2	28.0
				28[3]	46.0	63.8	1.38	35.3	29.0
				50	29.0	35.6	1.22	17.1	25.7

[1] at peak pile capacity (Note: tension tests have negative τ_{av} and τ_f values)
[2] performed after unsuccessful cyclic load test (see Figure 6.16)
[3] +15kPa added to all σ_r measurements for this instrument (see text)

Table 6.3 Summary of all load tests at Labenne

this depth and inaccuracies associated with δ measurements at low stress levels (see Section 6.3.6).

Given the high consistency of the measurements, it may be concluded that δ_f values are insensitive to (a) the initial relative density of the sand, (b) the previous shearing history of the pile and (c) the degree of saturation of the sand.

As δ_f values are virtually constant, differences between the radial effective stresses at failure (σ'_{rf}) in each test must be the primary reason for the wider relative span found for the unit shaft capacities (27kPa ± 15%). The differences between respective σ'_{rf} values may be understood more easily by viewing each value as a combination of the pre-loading radial effective stress (σ'_{r1}) and the load test coefficient K_f/K_1 ($=\sigma'_{rf}/\sigma'_{r1}$). These data are listed in Table 6.3 and show:

- The mean K_f/K_1 values for first-time compression and tension loading are 1.45 and 1.2 respectively.

- A second tension test performed after initial tension failure results in a much stiffer pile response, a larger K_f/K_1 value and a slightly higher capacity.

- The values of σ'_{r1} do not vary with depth in a well ordered fashion. For example, re-jacking of pile LB1 by a further 250mm after its first load test caused σ'_{r1} at the leading instrument position to increase from 53.4kPa to 74.5kPa. Such erratic variations in radial effective stress should be borne in mind when inspecting the interpreted profiles of σ'_{rs} ($=\sigma'_{rc}$) on Figure 6.11.

6.5.5.2 Cyclic tests

The Labenne tests included cyclic loading experiments. Loads were applied to both piles in one way cycles with a period of one minute after the reload tests LB1/L2C and LB2/L2T had been completed. Pile LB1 was

subjected initially to 25 compression cycles[1], whereas 40 tension cycles were applied to pile LB2. The observations from these tests may aid a more detailed research programme into the cyclic behaviour of piles in sand.

The load cycles varied the applied shaft shear stress on pile LB1 from 15% to 55% of the ultimate compressive shaft capacity, and on pile LB2 from 40% to 70% of the ultimate tensile shaft capacity (see Figures 6.16 and 6.18). The cyclic amplitude of pile head displacement was similar for both piles (≈0.3mm). However, while LB1 did not accumulate displacement, LB2 suffered a permanent displacement of 0.3mm after 40 cycles. This observation is consistent with tests performed by Wong & Arthur (1986) in the directional shear cell which showed that a minimum principal stress ratio (or degree of strength mobilisation) exists above which displacement accumulates continuously. The subsequent load test to failure gave a lower than average load test coefficient of ≈1.0.

The load cycles did not cause an accumulation of excess pore pressures, illustrating the free draining nature of the sand. Local radial and shear stresses reflected the cyclic variation of the applied load - increasing with an increase in applied compressive <u>or</u> tensile load and reducing for a reduction in applied load, but showed no overall changes from their mean values. The cyclic amplitude of the radial stress variations was ≈2.5kPa at each instrument in tension cycling and between 1kPa and 3kPa in compression cycling.

---

[1]The planned schedule of compression load cycles for LB1 was, however, not achieved as the pile was accidentally overloaded after 30 cycles (see Figure 6.16).

6.6 DISCUSSION

6.6.1 General

The clearest result to emerge from the Labenne tests is that the ultimate shaft shear stress may be described by the simple Coulomb failure criterion:

$$\tau_f = \sigma'_{rf} \tan \delta_f$$

The sensitive earth pressure cells showed how the radial effective stresses on the shaft at failure differ from the equilibrium values (σ'_{rc}) by an amount $\Delta\sigma'_r$:

$$\sigma'_{rf} = \sigma'_{rc} + \Delta\sigma'_r$$

The experiments demonstrate how the equilibrium radial effective stress (σ'_{rc}) is controlled by the combination of the initial in-situ conditions and the process of pile installation. At Labenne, the σ'_{rc} value developed in any soil horizon can be described as a function of the pile end resistance (q_b) in that horizon and the relative position of the pile tip (h/R) i.e.

$$\sigma'_{rc} = f\ (q_b\ ,\ h/R)$$

where f is the function shown on Figure 6.6.

As q_b ($\approx q_c$) is a measure of the relative density (D_r) of the sand, σ'_{rc} may also be related by

$$\sigma'_{rc} = f_1\ (D_r,\ \sigma'_{v0},\ h/R)$$

Relationships of this type are explored in Chapter 9 and compared with data from other instrumented pile tests in sand.

6.6.2 Changes in σ'_r during pile loading

Significant changes in σ'_r were observed during pile loading. It is suggested these changes may be separated into components due to:

(i) principal stress rotation ($\Delta\sigma'_{rp}$) in the sand and

(ii) dilation due to slip at the interface ($\Delta\sigma'_{rd}$)

These aspects are discussed in more detail in Chapter 9 using the ICP data in conjunction with measurements made in previous pile tests in sand.

(i) Principal stress rotation component ($\Delta\sigma'_{rp}$)

It is possible that the principal stress rotations associated with pile loading caused the reductions in σ'_r noted over the early stages of the Labenne pile tests. The reductions were small for compression loading but were more significant in tension tests. This anisotropy may be analogous to that seen in triaxial tests (Figure 5.6), where a large rotation (90°) of the major principal stress direction, from that applied during consolidation, led to a more contractant response.

(ii) Interface slip dilation ($\Delta\sigma'_{rd}$)

Following initial reductions, marked increases in σ'_r were observed as each section of the pile approached local failure. Laboratory studies of sand to steel shear by Uesugi & Kishida (1986) have shown that the shear and volume strains developed between peak and ultimate conditions are concentrated in a narrow band of soil close to the interface. For surfaces with roughnesses of 'typical' steel piles, this dilation consists of a few grains close to the shaft moving radially so that slip may occur. It is likely that the observed increases in σ'_r are due to such radial displacements, although other theoretical interpretations can be made (see Potts & Martins 1982). This effect is discussed in detail in Chapter 9, where it is shown to imply an important scale effect for the Labenne experiments.

6.6.3 Interface friction angles

The tests at Labenne showed that the shear stress obliquity reached a peak value (δ_p) of 30.5° ±1.5° prior to the mobilisation of the maximum shear stress (τ_f). Uesugi & Kishida (1986) suggest that this peak represents the transition from continuum behaviour to interface sliding. δ values reduced subsequently as the piles approached failure and τ_f was attained when σ'_r reached its maximum value at an obliquity (δ_f) of 28.5°

±1.5°. It thus appears that local failure at the shaft occurs when dilation stops and it is the *constant volume* interface friction angle that controls shaft capacity.

δ_f values may be compared with the ultimate (constant volume) interface friction angles (δ_{cv}) measured in direct shear interface tests. The results from ring shear and shear box interface tests on Labenne sand are presented in Section 5.1.7 and in more detail in Appendix D. These tests suggested that δ_{cv} was *independent* of the initial relative density of the sample and fell in the range 27° to 29° for steel interfaces of similar roughness to the SST's. These laboratory δ_{cv} values (measured under comparable conditions to those adjacent to the pile) are in excellent agreement with the field measurements of δ_f.

Although the exact agreement between the field δ_f values and laboratory δ_{cv} values may be partly fortuitous, the ICP tests have shown that shear box interface tests, which are relatively inexpensive to perform, are an expedient way of determining the approximate friction angles mobilised on piles in sand. Factors controlling the magnitude of δ_{cv} are discussed in Chapter 9.

6.6.4 Distributions of τ_{av} and τ_f with depth

The Labenne experiments help to resolve long standing questions concerning the variations with depth of the average and local shaft friction. The trend for τ_{av} to remain relatively constant below a certain critical depth led Vesic (1967) to postulate that the *local* shear stress diminishes with depth below a certain level, whilst Kulawhy (1984) argued that the trends of the field tests could be explained by reductions in K_0 due to OCR declining with depth (see Section 3.4.2). The Labenne data show that *highest* stresses (τ_f) are mobilised near the pile tip and that stabilisation of τ_{av} with pile depth results from the tendency for σ'_{rc} to reduce at all levels as the relative depth of the pile tip (h/R) increases. In addition to this h/R effect, the non-linear relationship between τ_{rz} and σ'_{v0} depends on the interface shear characteristics and the soil properties. These aspects are discussed in Chapter 9.

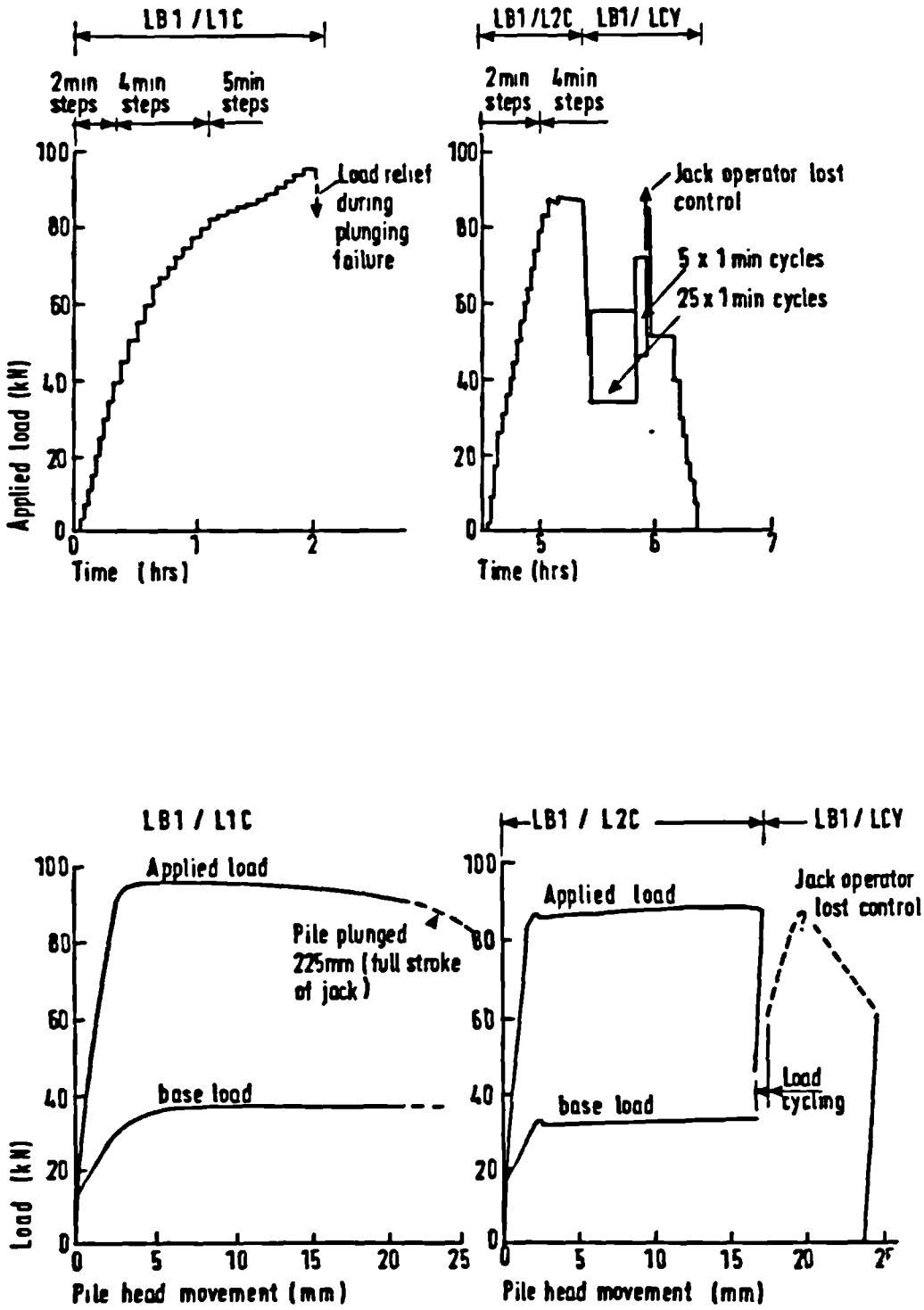

Figure 6.16 Loading schedule and load displacement curves for pile LB1

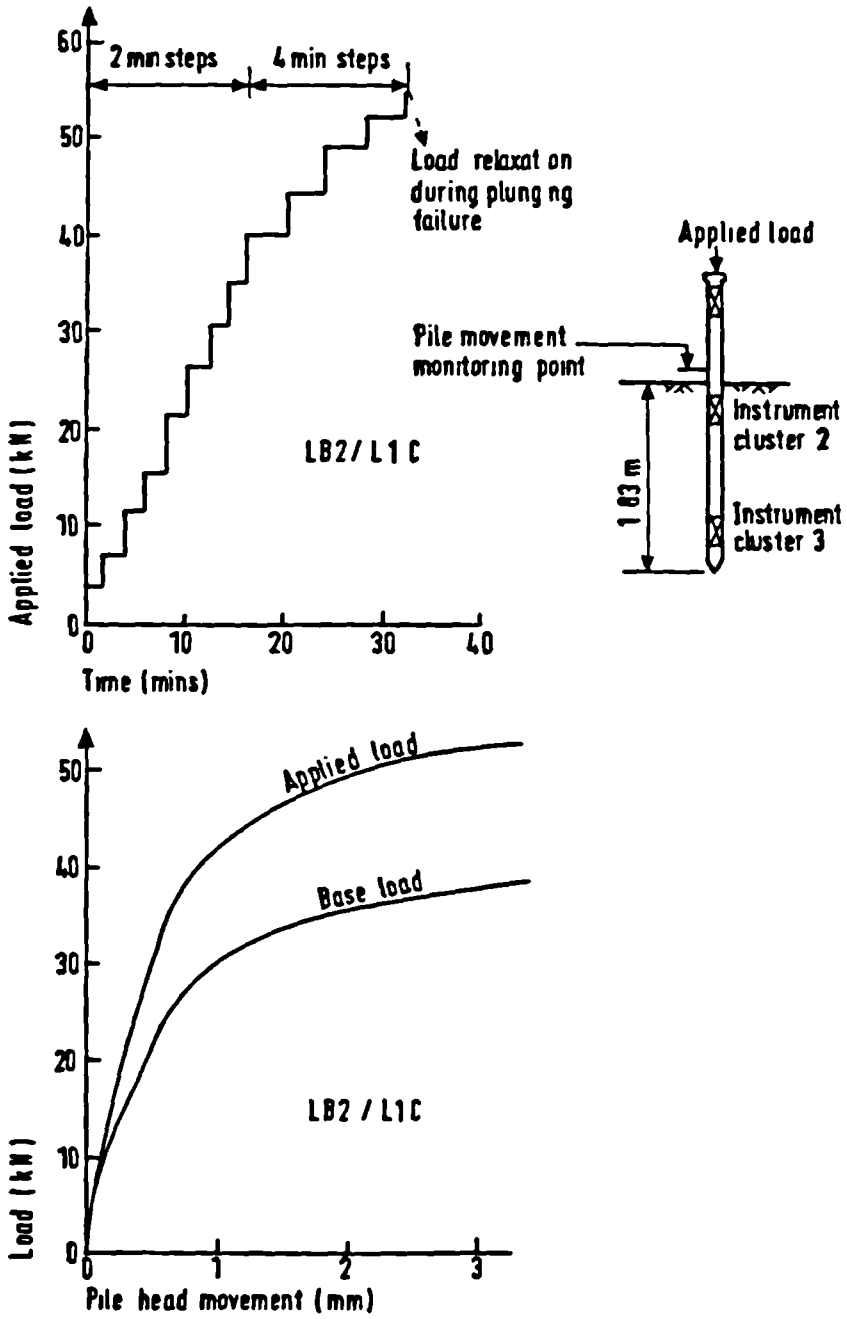

Figure 6.17 Loading schedule and load displacement curves Test LB2/L1C

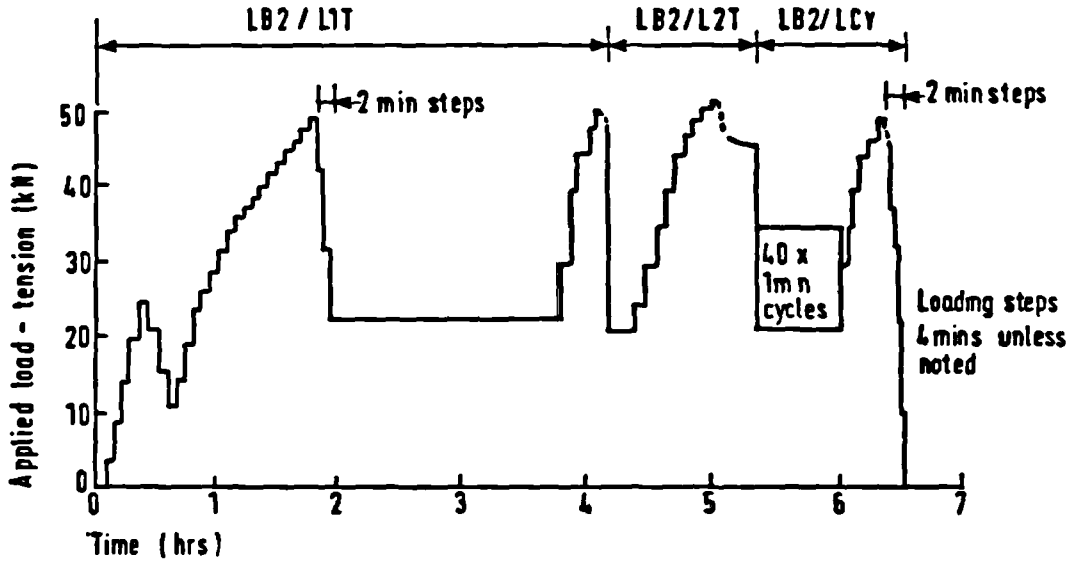

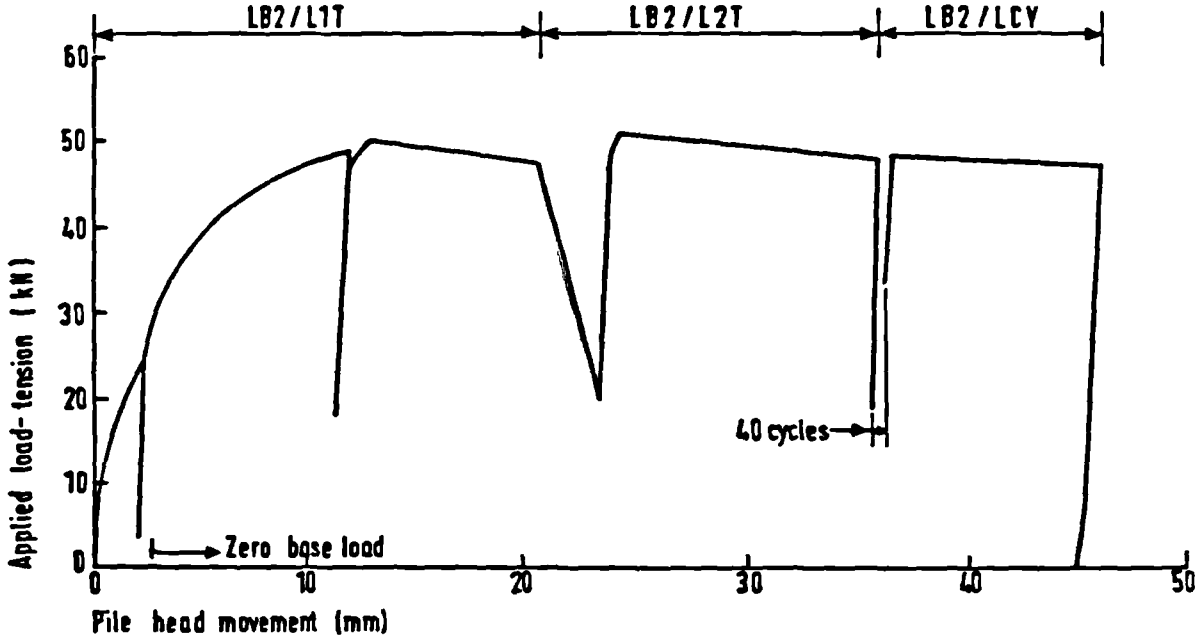

Figure 6.18 Loading schedule and load displacement curves for LB2 (at a penetration of ≈6m)

CHAPTER 7

PILE TESTS AT COWDEN

CONTENTS OF CHAPTER 7

PILE TESTS AT COWDEN

7.1 PILE CONFIGURATIONS AND TEST PROGRAMME 234
7.1.1 Phase 1 (piles CW1 & CW2) 235
7.1.2 Phase 2 (piles CW3 & CW4) 236
7.2 INSTALLATION 237
7.2.1 End resistance 237
7.2.2 Shaft resistance 239
7.2.3 Local shear stress 241
7.2.4 Radial total stress 243
7.2.5 Pore pressure 245
7.2.6 Interface friction angles 248
7.3 EQUALISATION 249
7.3.1 Pore pressure 249
7.3.2 Radial total and effective stresses 252
7.3.3 Long term monitoring of pile CW2 254
7.3.4 Radial effective stresses after equalisation 255
7.3.5 Residual pile stresses 257
7.4 LOAD TESTING 260
7.4.1 Introduction 260
7.4.2 Overall pile behaviour 260
7.4.2.1 Shaft capacity 263
7.4.2.2 Shaft displacement characteristics 264
7.4.2.3 Base load 264
7.4.3 Local stress variations 265
7.4.3.1 Shear stress 265
7.4.3.2 Pore pressure 265
7.4.3.3 Radial total stress 267
7.4.4 Effective stress paths 267
7.4.5 Load test summary 272
7.4.5.1 General trends and comparisons with laboratory tests 272
7.4.5.2 Comparison with other pile tests at Cowden 274

7.1 PILE CONFIGURATIONS AND TEST PROGRAMME

The field tests at Cowden were carried out in two phases. The first phase consisted of installing and testing piles CW1 and CW2 in November 1989. Following a review of the data from these tests, the second phase commenced in March 1990, when two more piles (CW3 and CW4) were installed and tested.

The configurations of the piles are shown on Figures 7.1 and 7.2 and each experiment is described below.

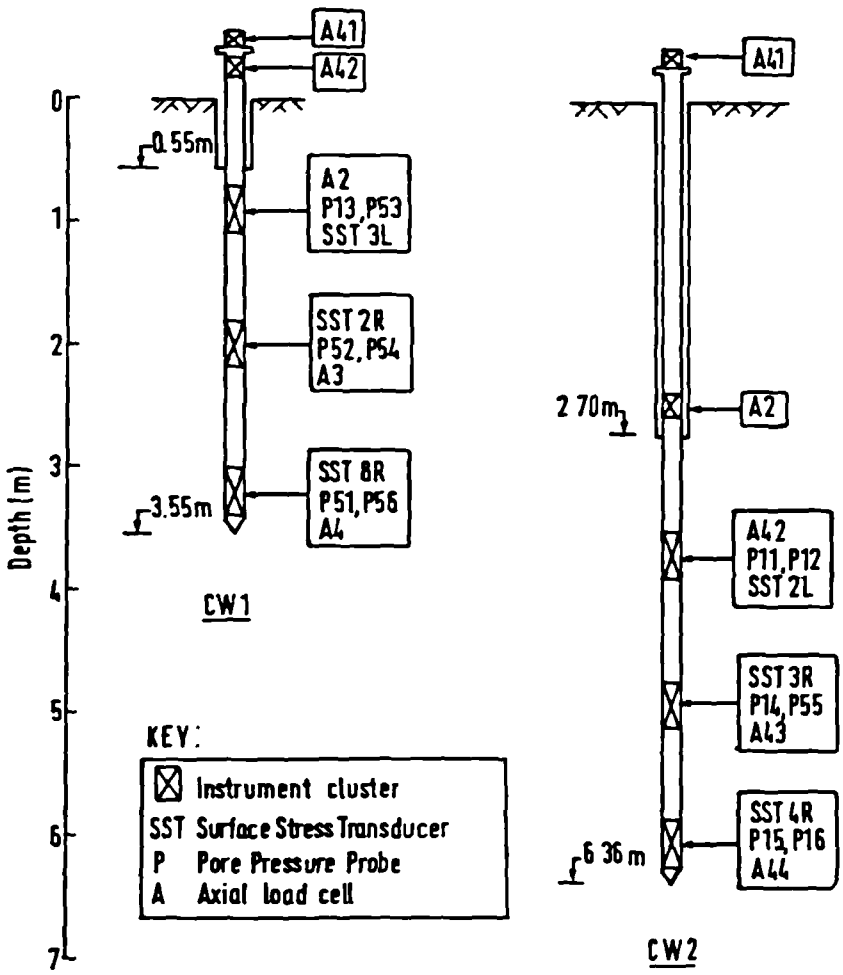

Figure 7.1 Pile configurations for Phase 1

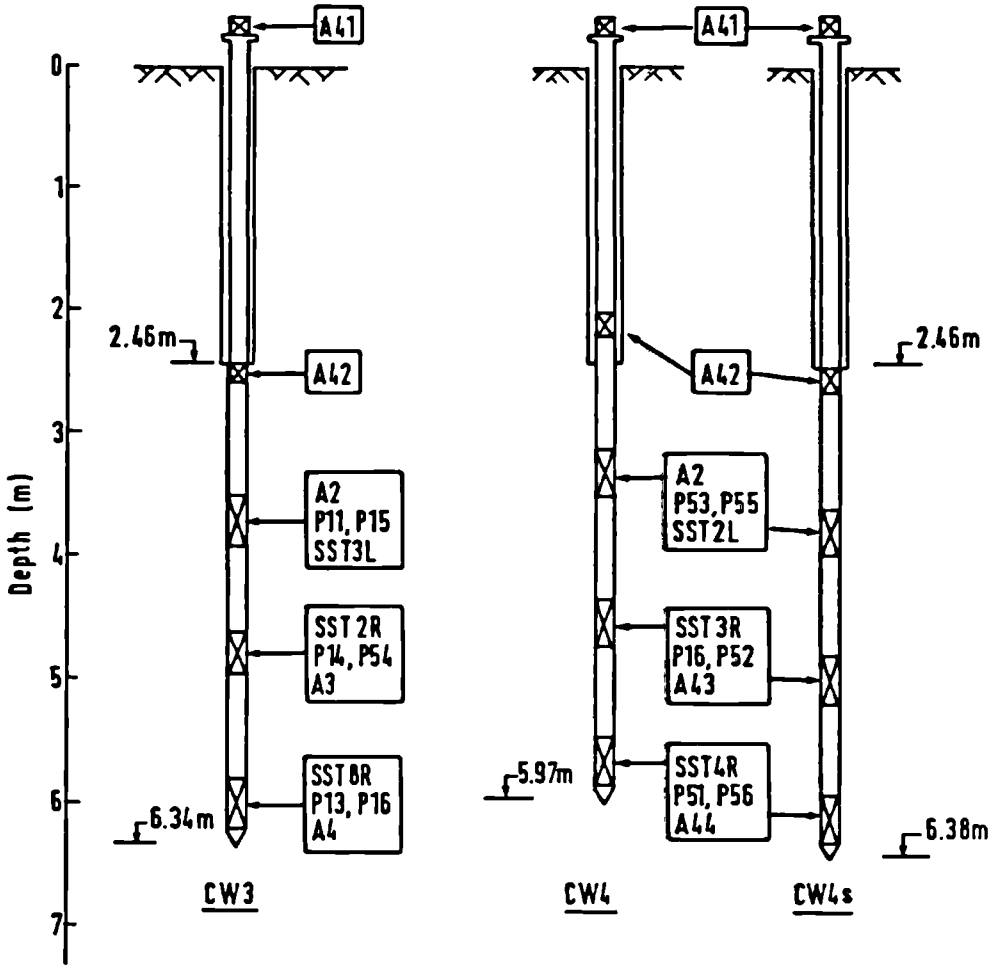

Figure 7.2 Pile configurations for Phase 2

7.1.1 Phase 1 (Piles CW1 & CW2)

(i) Pile CW1

The first pile was installed from a shallower (0.55m) pre-bored hole to that which was used for the subsequent tests. It was the original intention to jack this pile to ≈6m. However, the tip met an obstruction at 3.55m which could not be overcome with the available kentledge (300kN) and installation was terminated at this depth. The pile was subsequently load tested in tension after an equalisation period of ≈ 4days (Test CW1/L1T). It was clear from the blunted pile tip, evident on extraction, that a large cobble had caused the obstruction.

During installation, large shear stresses (up to 250kPa) were developed in the hard weathered till between 1.0m and 2.5m depth; these exceeded the nominal capacity of the SST's[1]. Because of (a) this over-stress, (b) the high reaction loads that would be required to install a pile from the ground surface to 6m depth and (c) the uncertain nature of the properties of the till at shallow depths (see Section 5.2), it was decided to install all subsequent piles (CW2-CW4) from the base of 2.5m deep pre-bored hole. These holes were bored by BRE using a power auger.

Three of the six pore pressure probes mounted on this pile developed faulty connections during installation and, for this reason, no pore pressure measurements were obtained at the following instrument position. Despite the difficult ground conditions, the robustness of the instrument designs ensured that no other fault or calibration shift occurred.

(ii) Pile CW2

The second pile was installed from the base of a 2.7m deep pre-bored hole to a final penetration of 6.35m and was tested in compression after an equalisation period of 4 days (Test CW2/L1C). Monitoring was continued for a period of 3 months, after which the pile was re-tested in compression. The pile was finally extracted in February 1990. All instruments remained operational and no difficulties were experienced.

7.1.2 Phase 2 (Piles CW3 and CW4)

Prior to installation, the window panes of the SST's on these piles were shotblasted to a roughness comparable to that of the interconnecting casings (CLA roughness ≈9μm). This was carried out in an attempt to resolve the disagreement, noted in Phase 1, between the local shear stresses measured by the SST's and the average shear stresses derived from the axial load cell data.

---

[1]The nominal design load of 140kPa leads to a strain of 0.1% in the shear webs of the SST. However, no shift in the zeros of the shear circuits subjected to loads of up to 250kPa was detected.

The piles were jacked to the same final penetration as pile CW2. Pile CW3 was identical in all respects to pile CW2 except that the first load test was a tension test (Test CW3/L1T) rather than a compression test.

Pile CW4 was used to investigate (a) the 'short-term' minimum in radial effective stress observed during equalisation in Phase 1 and (b) potential jacking rate effects. The pile was halted temporarily at ≈6m and load tested in compression after just 2 hours (Test CW4/L1C). Once this test was completed, the pile was re-jacked a further 380mm at the slower rate of 80mm/min[1] to a final penetration of 6.38m. A further compression test was performed four days later (CW4s/L1C), so that the effects of installation rate on static capacity could be assessed.

All instruments operated successfully during this phase of the experiments.

7.2 INSTALLATION

This section presents the data obtained during the installation of the four piles (CW1-CW4). Each pile required about 20 pushes to reach the required penetration and all instruments were monitored continuously both during and between each push.

7.2.1 End resistance

The end resistances (q_b) met by the piles during jacking are shown on Figure 7.3 and compared with the q_c trace measured in the Cone Penetration test closest to the pile tests (CPT5; see Figure 5.12).

[1]The standard penetration rate during jacking stages was 500mm/min.

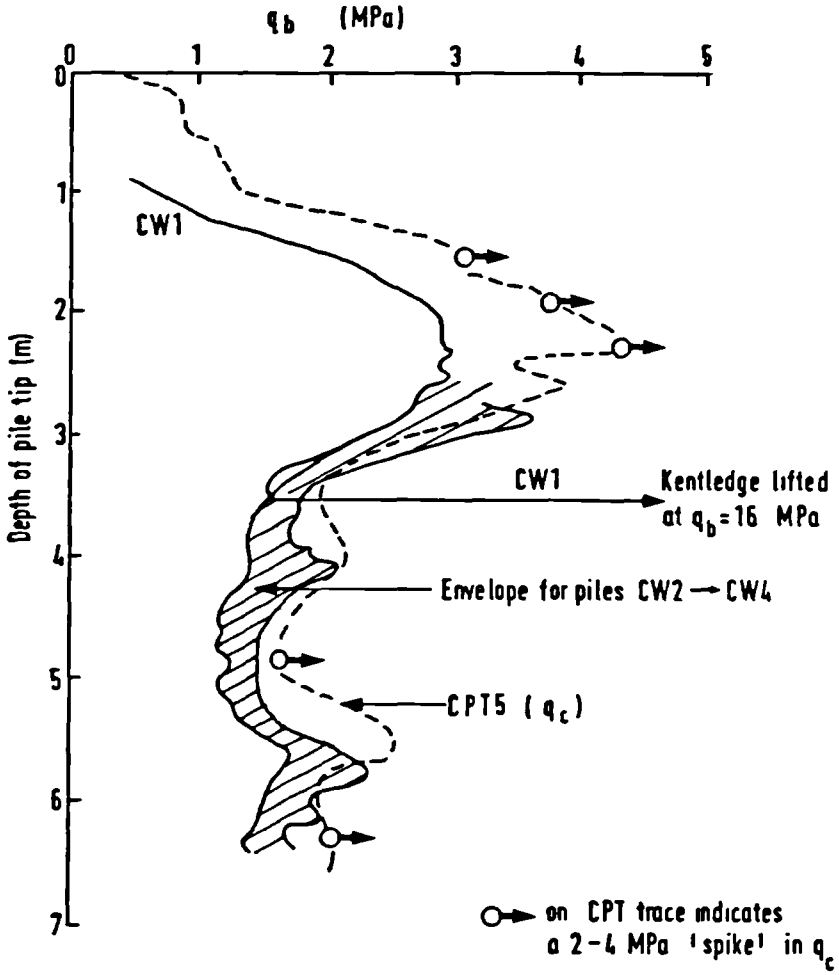

Figure 7.3 End resistances during pile jacking

It is evident that:

- The uppermost 3m of the profile is particularly variable.
- q_b traces for the tests with deep pre-bored holes (CW2-CW4) are continuous with that of CW1, which was installed from 0.55m depth.
- The q_b and q_c profiles are very similar in shape, except for the q_c 'spikes', which may be due to thin sand layers or small cobbles.
- The magnitude of q_b is typically 10% less than q_c. This may be explained by the (a) faster rate used in the cone tests (1200mm/min, see Section 5.2.6), (b) the larger end area of the pile (see De Beer 1977) and/or (c) the variability of the ground.

No discernible difference was observed between the mean q_b profile and that for pile CW4s, which was installed at the slower rate of 80mm/min.

7.2.2 Shaft resistance

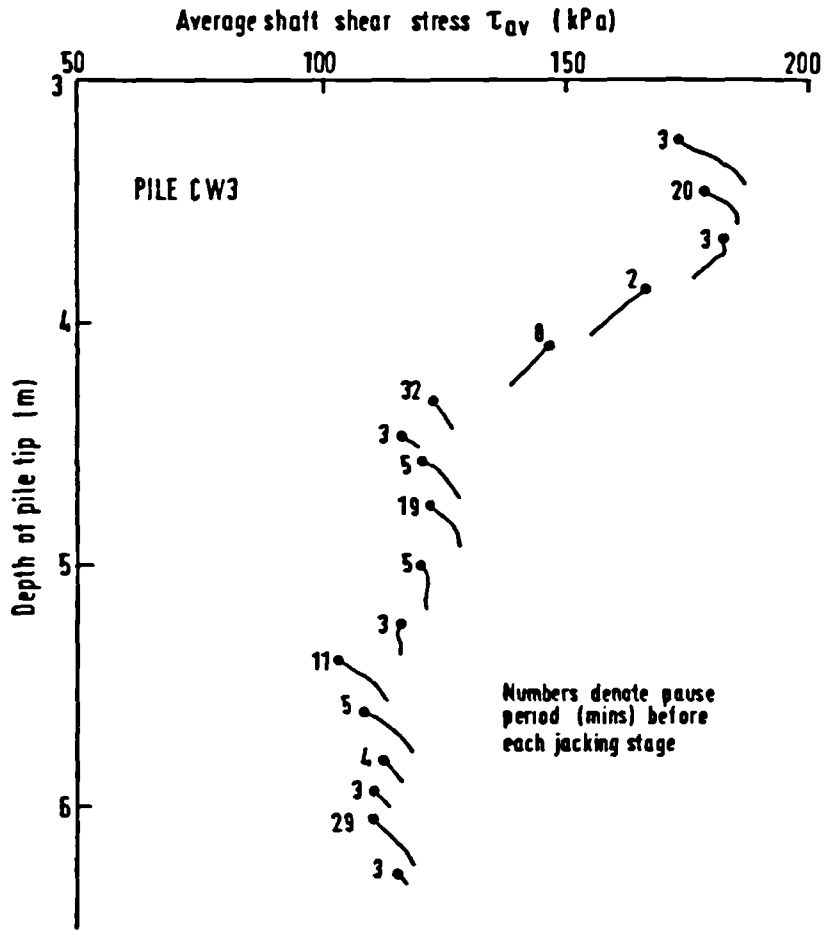

Figure 7.4 Average shaft shear stresses during jacking of CW3

The variation of the average shaft shear stress (τ_{av}) with depth recorded during a typical pile installation (CW3) is shown on Figure 7.4. Two main observations may be made:

- τ_{av} generally increases during a jacking stage in a similar way to the increase in resistance with displacement observed during fast shearing stages in ring shear tests on Cowden till; see Figures D10-D12, Appendix D.

- In 'uniform' strata, the τ_{av} value recorded at the start of any given jacking stage appears to *fall* marginally as the length of the preceding pause period increases.

The mean values of τ_{av} mobilised during installation of all the piles and the associated α values are summarised in Table 7.1.

Pile	Tip depth (m)	τ_{av} (kPa)	c_{u0} (kPa)	α
CW1	2.0	125	140	0.90
	3.0	175	155	1.13
	3.55	125	150	0.83
CW2	4.0	120	157	0.76
	5.0	100	138	0.72
	6.0	100	129	0.77
	6.35	108	126	0.86
CW3	4.0	150	157	0.95
	5.0	122	138	0.88
	6.0	112	129	0.87
	6.35	112	126	0.94
CW4	4.0	136	157	0.87
	5.0	112	138	0.81
	6.0	112	129	0.87
CW4s	6.38	71	126	0.56

Table 7.1 Average shear stresses during installation

α for fast installations varies between 0.72 and 1.13 and has a mean value of 0.87. However, a considerably lower α value is mobilised during the 'slow' installation of pile CW4s. This rate dependence is illustrated on Figure 7.5, which plots the results for all piles and includes data from four other jacked piles at Cowden at similar depths (Ponniah 1989)[1].

[1]It is assumed that pause period of ≈2 hours which preceded test CW4/L1C and the installation of CW4s did not affect the data significantly.

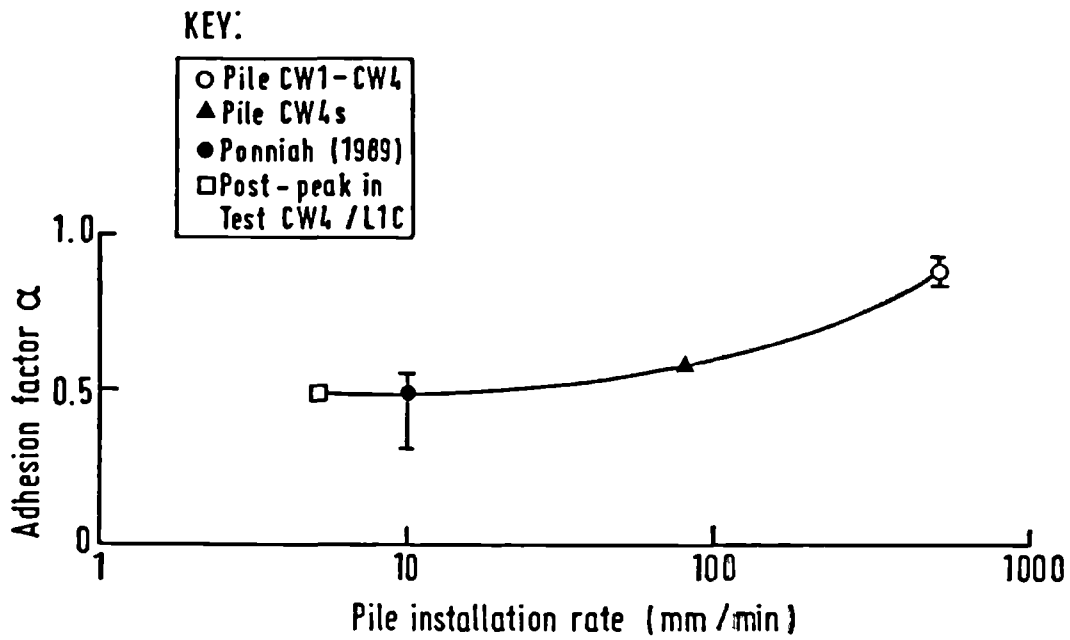

Figure 7.5 Rate dependence of installation shear stresses (pile depth ≈6m)

The rate effect appears to be slight at pile velocities less than about 50mm/min, but, at faster rates, the trend line climbs steeply with a maximum gradient of about 100% per log cycle, matching closely the response measured in the London Clay by Bond (1989). The ring shear experiments on Cowden till showed a smaller rate dependence, amounting to a 15% increase in shearing resistance per log cycle between 1mm/min and 1000mm/min (see Section 5.2.10). This may be due to differences between the drainage conditions in the laboratory and field.

7.2.3 Local shear stress

The envelopes of shear stresses measured by the SST's (τ_{rz}) and those derived from the axial load cell data (f_s), during jacking of all piles, are plotted on Figure 7.6.

The τ_{rz} and f_s profiles reflect the variations in soil consistency shown by the q_c and q_b traces. In particular, the leading instrument (at h/R=8) shows the same sharply defined maximum at ≈2m depth and minimum at ≈4.8m

depth. In addition, as at Labenne, the shear stresses are seen to depend on the relative depth of the pile tip (h/R); stresses recorded by the SST's *in any given soil horizon* reduce by about 60% as h/R increases from 8 to 50.

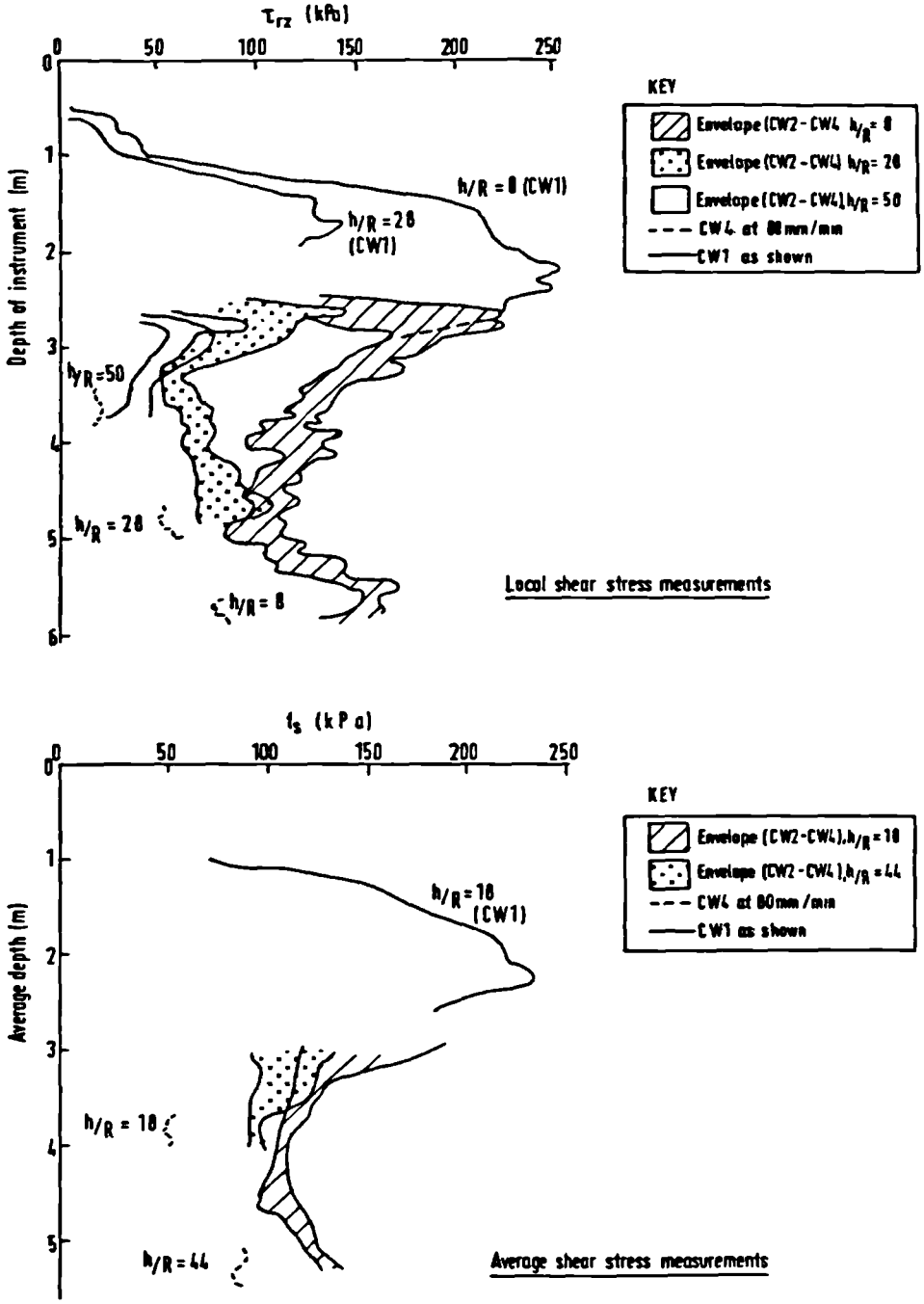

Figure 7.6 Local shear stresses during jacking

The dependence of τ_{rz} and f_s on h/R is comparable. However, τ_{rz} values at the same depth and value of h/R are typically 20% less than the equivalent f_s values inferred at this h/R value. This incompatibility is attributed tentatively to the different characteristics of the till when sheared against the (stainless steel) SST's and the (molybdenum steel) interconnecting casings (see Section 7.4).

Reducing the jacking rate of pile CW4 from 500mm/min to 80mm/min led to reductions in the local shear stresses which were compatible with the strong overall rate effect, illustrated on Figure 7.5.

7.2.4 Radial total stress

The envelopes of the radial total stresses (σ_{rt}) measured during jacking of all piles at Cowden are shown on Figure 7.7a. The following observations are made:

- The measurements are reasonably repeatable: data recorded by instruments at similar depths and h/R agree to within 50kPa (i.e. ≈5% of the σ_{rt} maxima).
- All stresses fall far below the Menard p_{lim} profile (which represents the stresses required to inflate a cylindrical cavity) and above the estimated initial undisturbed horizontal stress (σ_{h0}). σ_{rt} values are typically between three and five times σ_{h0}.
- The σ_{rt} profiles at each instrument position reflect the changes in soil consistency and follow a similar shape to the τ_{rz}, f_s and q_b profiles (see Figures 7.6 and 7.3).
- Radial stresses developed at fixed depths reduce with h/R. This reduction is illustrated graphically on Figure 7.7b, which plots the ratios of σ_{rt} measured by the trailing and following instruments (h/R=28 & 50) to the σ_{rt} values measured by the leading instruments (h/R=8). These ratios fall within narrow limits for all depths and indicate that σ_{rt} reduces by about 50% between h/R=8 and h/R=50. This reduction is comparable to that seen in the ICP tests at Labenne.

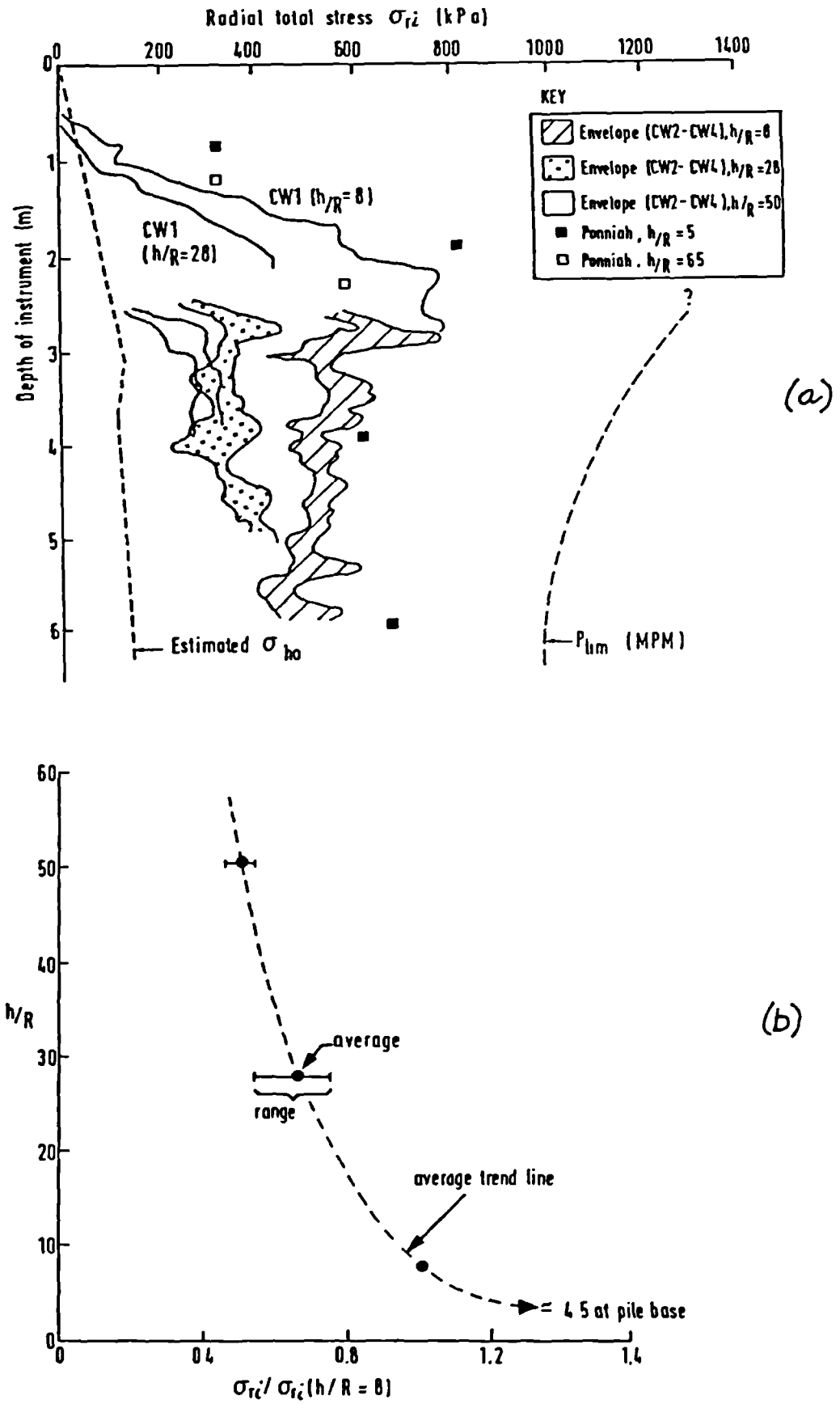

Figure 7.7 Envelopes for σ_{ri} (top); dependence of σ_{ri} on h/R (bottom)

- When the observed h/R effect is accounted for, the measured stresses are in reasonable agreement with those obtained by Ponniah (1989) at Cowden using 193mm diameter *open-ended* jacked piles (see Section B9, Appendix B)
- Reducing the jacking rate of pile CW4 had no discernible effect on the radial stresses measurements.

7.2.5 Pore pressure

The pore pressure measurements recorded by the following probes during installation of pile CW4 are shown on Figure 7.8. These traces exhibit features common to all the probes at Cowden. The overall envelopes of pressure measured by piles CW2-CW4 are shown on Figure 7.9 and summarised in Table 7.2.

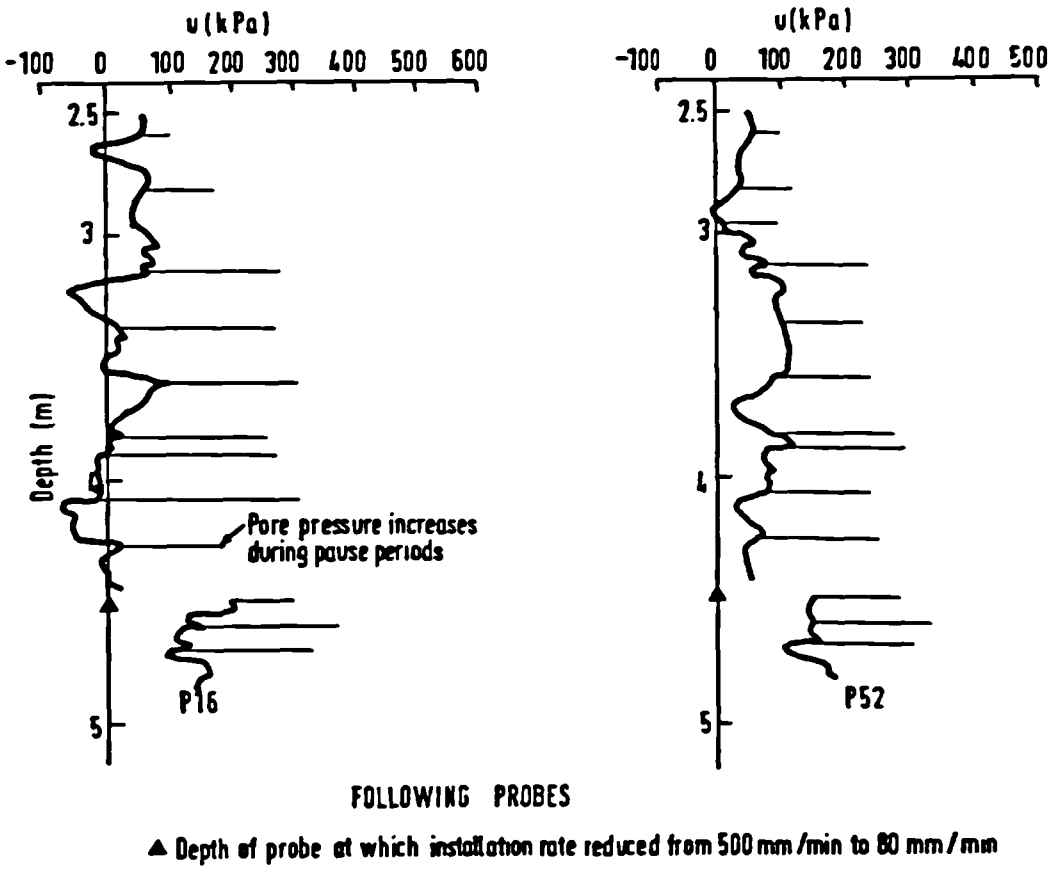

Figure 7.8 Pore pressures recorded by following probes on pile CW4

Instrument position	Pore pressure when pile is moving u_m(kPa)	Pore pressure prior to next pile push u_s(kPa)
Leading (h/R=5)	[-80, 80]	[300, 500]
Following (h/R=30)	[-10, 130]	[200, 350]
Trailing (h/R=54)	[50, 150]	[200, 300]

Table 7.2 Ranges for installation pore pressures

We note:

- Pore pressures reduce significantly at the beginning of a jacking stage. These reductions are largest close to the pile tip.
- During the pause periods in between jacking stages, pressures rise rapidly (typically in less than 3mins) to reach relatively steady large positive values. The greatest pressures develop at the leading instrument position.
- The moving values (u_m) measured by pairs of probes in the same instrument cluster differ, in some cases, by up to 200kPa. These variations may reflect local large variations in pressure due, perhaps, to irregularities on the pile surface and/or a reduced response time of those probes which had previously cavitated.
- In contrast, the stationary pressures (u_s) measured by probes in the same instrument cluster agree to within 20kPa.
- It is clear from Figure 7.8 that values of u_m increased sharply in response to the reduction in the jacking rate of pile CW4. Given the relative independence of the σ_{rt} records to a change in rate, it appears that the rate effect on shear stresses (Figure 7.5) is related to a pore pressure phenomenon.

Attempts to rationalise this complicated pattern of the pore pressure measurements are detailed in Chapter 10.

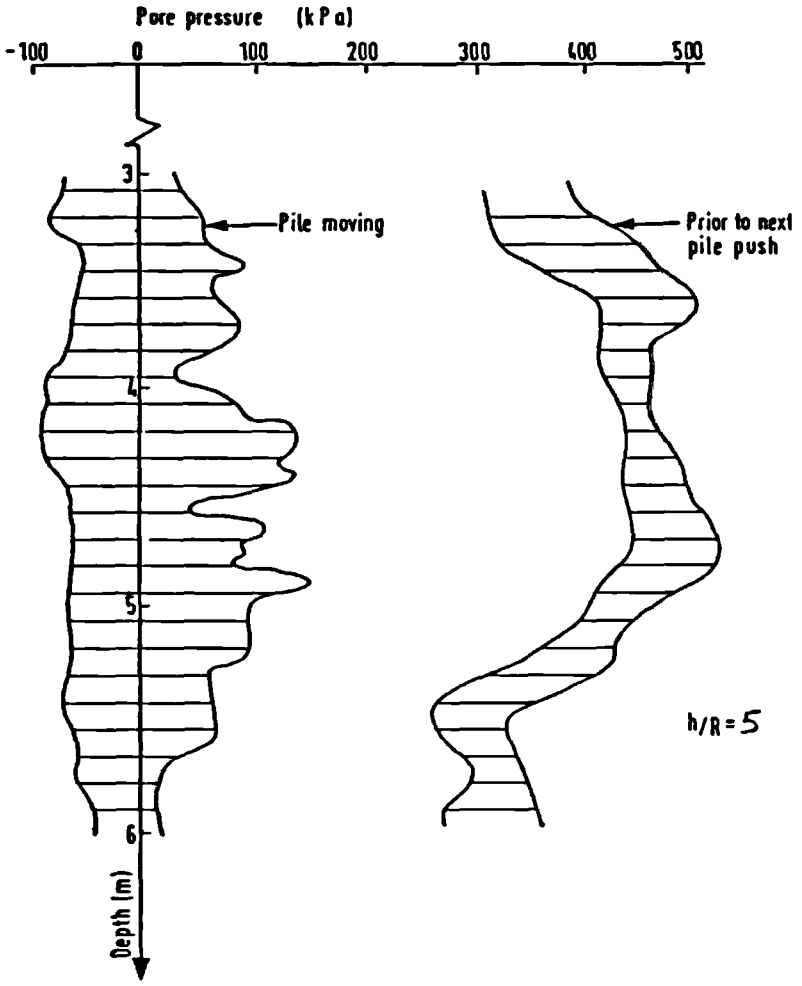

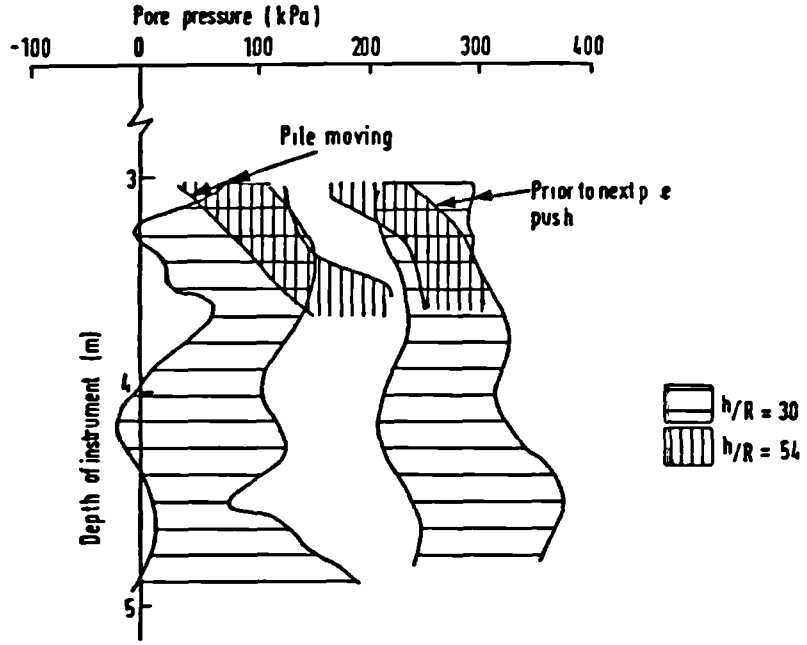

Figure 7.9 Envelopes for installation pore pressures (fast-jacking)

7.2.6 Interface friction angles

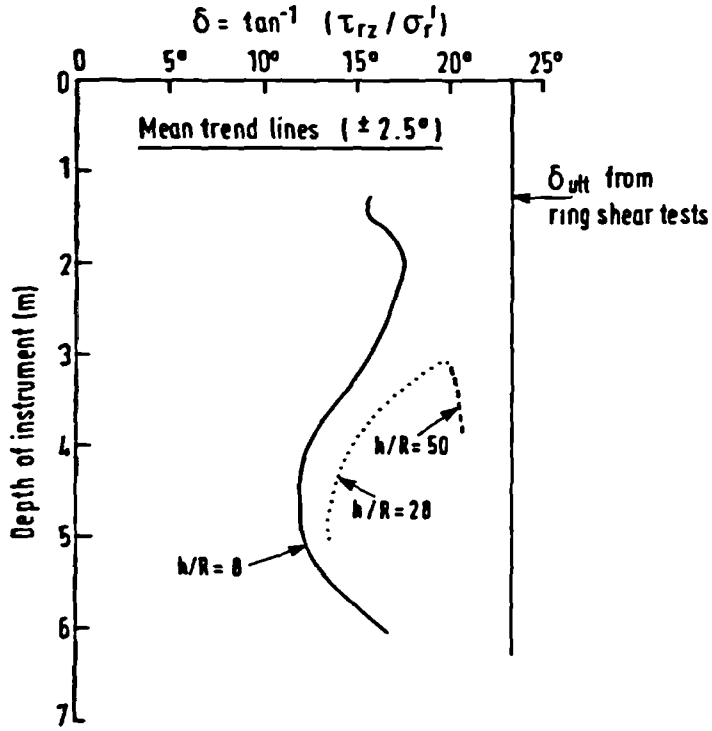

Figure 7.10 Interface friction angles measured during fast-jacking

The mean interface friction angles mobilised during jacking are shown for each instrument position on Figure 7.10. These angles, which were calculated from the local radial effective stress and shear stress measurements as $\delta = \tan^{-1}[\tau_{rz}/(\sigma_{ri} - u_m)]$, are less than the ultimate residual angles (δ_{ult}) measured in drained ring shear experiments and in subsequent (slow) load tests and also show an unexpected dependence on h/R. The load test results (reported in Section 7.4) and a review of data from other instrumented pile tests in Appendix A show that these low values are not indicative of a low strength soil fabric and are due solely to anomalous pore pressures being measured at the pile shaft when displacement rates exceed ≈1mm/min. It is shown that these pressures (i.e. values of u_m) are unlikely to be representative of those acting on the principal displacement shear, which was probably a short distance away from the pile.

More plausible values of pore pressure acting in the failure zone may be estimated from the τ_{rz} and σ_{ri} values by assuming that the interface

friction angles proven at slow rates of displacement during load tests also apply during installation. The pore pressures corrected in this way fall between the recorded values of u_m and u_s (see Table A4, Appendix A).

It is interesting that *apparent* δ values calculated for the faster and slower stages of the installation of pile CW4 were comparable, although the u_m and τ_{rz} values differed significantly. This observation is consistent with the data reported in Appendix A which shows that the *apparent* δ value, although less than the value measured during slow shear, remains relatively constant at pile velocities greater than ≈20mm/min.

7.3 EQUALISATION

With the exception of the first load test on pile CW4, which took place 2 hours after the end of jacking, a period of 4 to 5 days was allowed for ground equalisation prior to load testing. This duration (t_{eq}) was adopted to avoid the possibility of long term drift of the pore pressure measurements (which occurred at Canons Park, Bond 1989) as well as to minimise site mobilisation costs. Long term observations, made after testing of pile CW2, showed that the radial effective stresses were within 10% of equilibrium values at t_{eq} =4 days.

The full set of equalisation data recorded is summarised in Table 7.3 on page 259. Specific trends are discussed in the following sections.

7.3.1 Pore pressure

The pore pressures measured during equalisation of pile CW4s were typical of those measured by the other piles and their variations are shown on Figure 7.11 from the start of the last jacking stage until the first load test.

It is evident that, during the last pile push, pressures recorded by probes in the same instrument cluster differ by up to 200kPa. These differences become negligible shortly after the pile comes to rest, when

the pressures *increase* rapidly to reach a short term maximum[1]. Pore pressures decay, after attaining this maximum, and are generally within ≈50kPa of nominal hydrostatic values within 4 to 5 days of installation. In some cases (particularly at the trailing instrument position), excess pressures of greater than 50kPa existed at this stage.

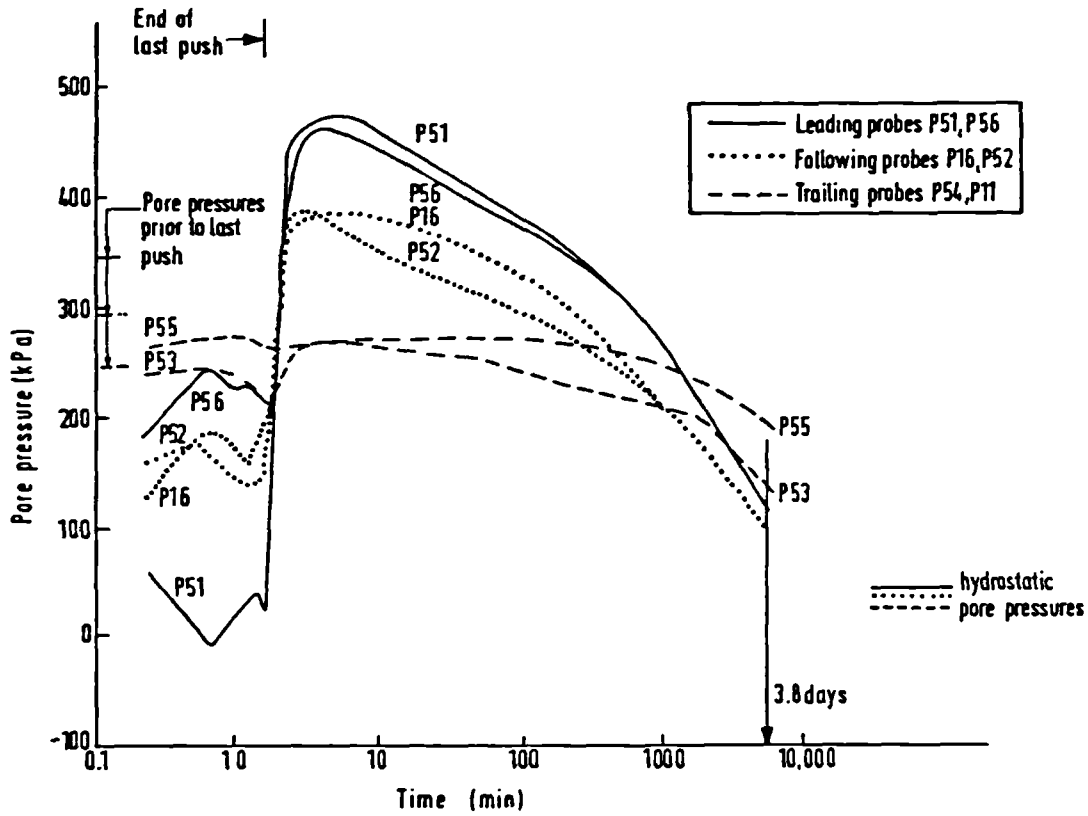

Figure 7.11 Pore pressures recorded during equalisation of CW4s

The envelope and mean trend of the excess pore pressure ratio ($\Delta u/\sigma'_{vo}$) with time after installation are shown in Figure 7.12a for all instruments on piles CW2-CW4. It can be seen that the ratio attains a maximum value of 4.5 ±0.5 before reducing to reach a typical value of ≈0.7 in 4-5 days.

[1]The magnitude of these maxima could be related to the rise time of the instruments; higher values are noted with the more rapidly responding probes. Note, also, that pressures recorded *during* jacking of this pile were higher than those recorded on fast-jacked piles (see Figure 7.8)

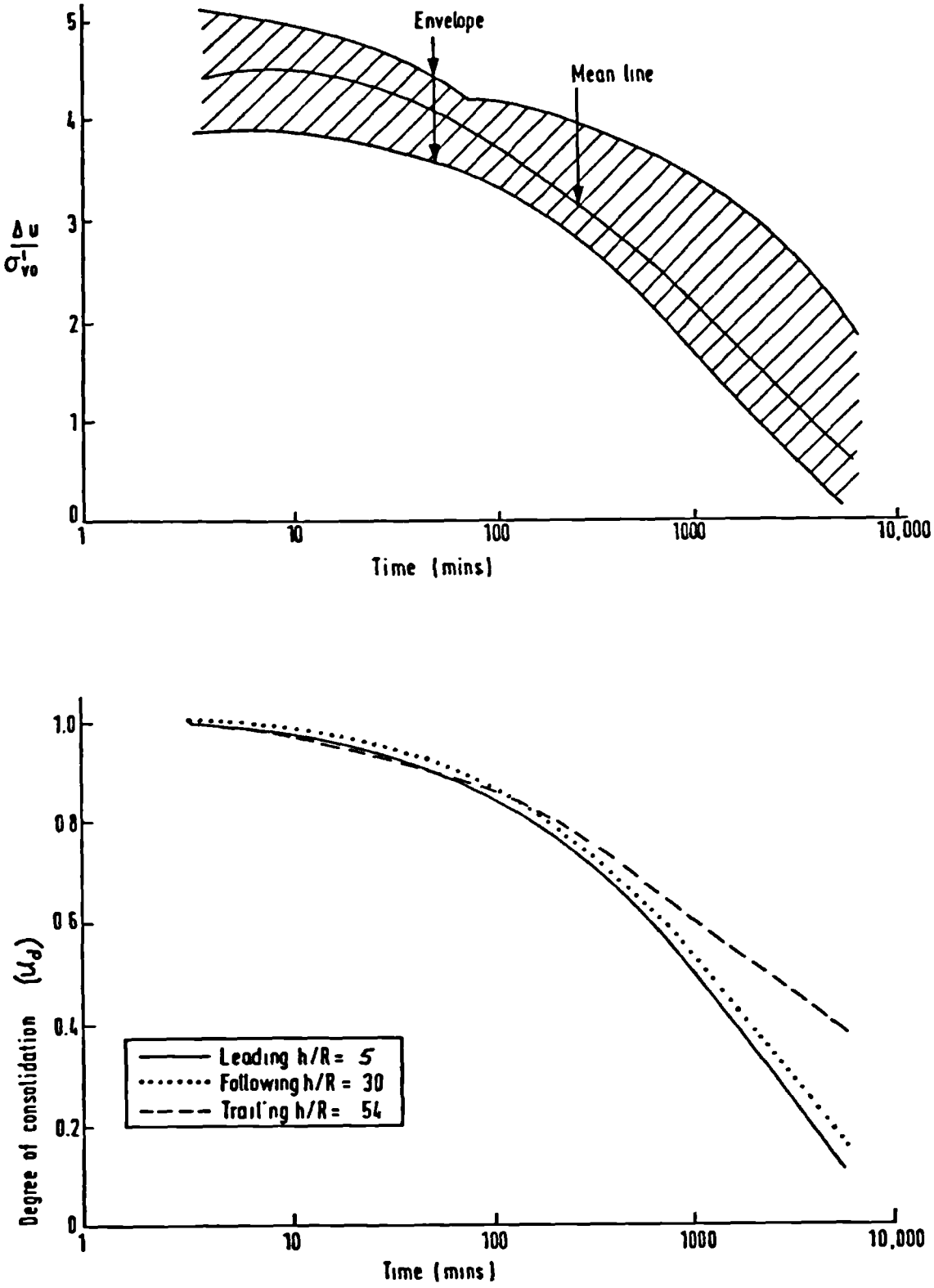

Figure 7.12 Envelope for pore pressures ratios (top) and mean U_d factors (bottom)

While the maximum pore pressure ratio, $(\Delta u/\sigma'_{v0})_{max}$, appears to be relatively insensitive to the location of the instrument, measurements made during the installation pause periods show that $(\Delta u/\sigma'_{v0})_{max}$:

(i) reduces with depth (or OCR) for fixed instrument positions (h/R). Note, for example, that a maximum ratio of ≈11 was measured at h/R=8 on pile CW1 at 2m depth.

(ii) decreases with h/R in any given soil horizon (c.f. u_s values ($=u_0 + \Delta u$) on Figure 7.9)

These two factors combined lead to the relatively constant value of $(\Delta u/\sigma'_{v0})_{max}$, seen on Figure 7.12a.

Average curves for the variation with time of the pore pressure dissipation factor (U_d)[1] at the three instrument positions are shown on Figure 7.12b. The dissipation rate at h/R=54 is seen to be significantly slower than that at h/R ≤ 30, where U_d values reduced to ≈0.15 after 4 days. These records are used in Chapter 10 to estimate the radial distribution of pore pressure after installation and the horizontal coefficients of consolidation (c_h) and permeability (k_h) controlling consolidation.

7.3.2 Radial total and effective stresses

The changes in the radial total and effective stresses that occurred during equalisation at Cowden are summarised using the typical results obtained with pile CW3. These variations are shown with the corresponding pore pressure measurements on Figure 7.13.

A number of characteristic features are evident:

- Radial total stresses show only minor reductions over the first 1000 mins after pile installation, typically amounting to less than 25% of the total reduction measured.

---

[1] $U_d = (u - u_0)/(u_{max} - u_0)$; $U_d = 0.0$ at full dissiaption.

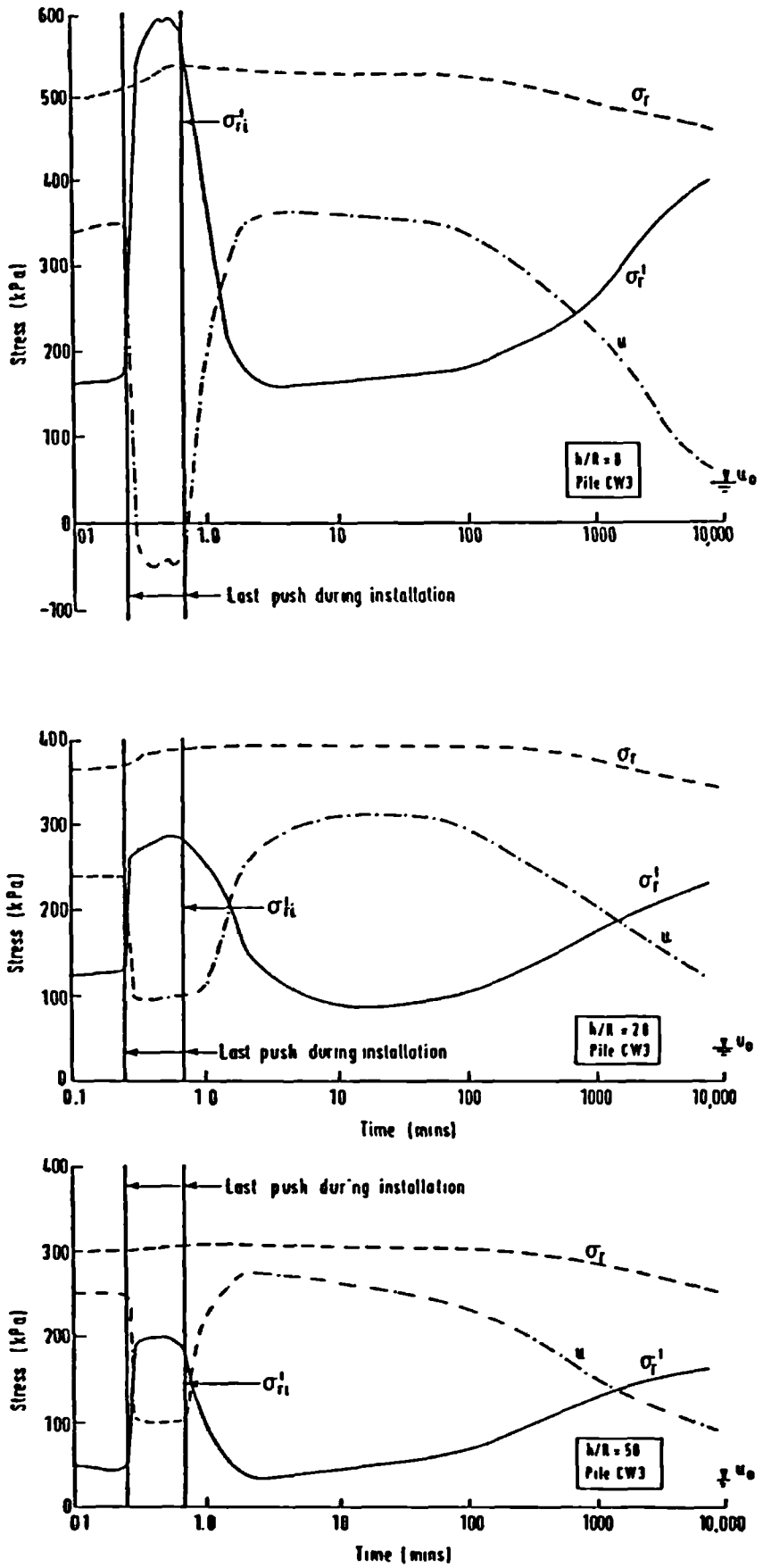

Figure 7.13 Equalisation data for pile CW3

- The rapid increases in pore pressure observed shortly after installation lead to sharp reductions in σ'_r, giving minima that are typically only ≈25% of the apparent maxima recorded during jacking.
- Low values of σ'_r persist for about 100 mins, after which pore pressure dissipation at the pile shaft becomes significant and σ'_r increases steadily. Near equilibrium is reached after 4-5 days, when σ'_r values are typically 2 to 3 times greater than their short term minima.

Also shown on Figure 7.13 are the installation radial effective stresses (σ'_{ri}), which have been corrected, as proposed in Section 7.2.6, for the anomalous pore pressures recorded during pile jacking. These stresses are generally comparable to the final equalised stresses, suggesting that the long term static shaft capacity may be similar to that measured during installation. The 'corrected' σ'_{ri} values for the pile installed at the slow rate (CW4s) were typically ≈20% *less* than the final σ'_{rc} values.

7.3.3 Long term monitoring of pile CW2

Pile CW2 was monitored for 90 days after its initial load tests at t_{eq} ≈4 days. Discounting the 'temporary' changes in stresses that occurred during these tests, it was found that good agreement between the equalisation data recorded at *all* instrument positions was obtained when the stresses were expressed in terms of the non-dimensional coefficients[1] (H/H_i), K/H_i and U_d. The mean trend lines of these coefficients are plotted on Figure 7.14.

It is evident that radial effective stresses (as described by K/H_i) have reached fully equalised values even when ≈10% of excess pore pressures generated during installation are still present (i.e. U_d =0.1); subsequent reductions in pore pressure are matched by equivalent reductions in radial total stress. It is important to emphasise, however, that the load tests to failure performed on this pile at t_{eq} ≈4 days may

---

1 $H/H_i = (\sigma_r - u_0)/(\sigma_{ri} - u_0)$
$K/H_i = \sigma'_r/(\sigma_{ri} - u_0)$

have affected this trend (although σ_r changes during these tests were relatively minor).

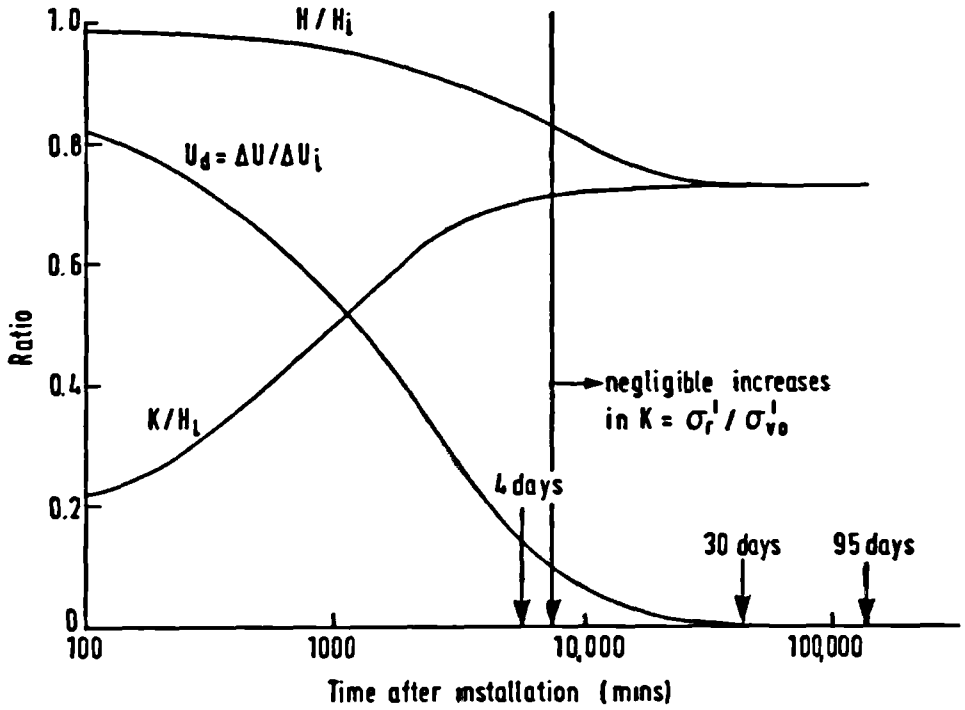

Figure 7.14 Normalised stress changes during equalisation of CW2

Pile CW2 was untypical in that the value of U_d at $t_{eq} \approx$ 4days did not exceed 0.13 at *any* instrument position. However, as seen on Figure 7.12b and Table 7.3, U_d was typically ≈0.3 at the trailing instrument position after 4-5 days. It may be therefore be inferred from Figure 7.14 that the corresponding σ'_r values measured at this stage were approximately 90% of the fully equalised stresses (σ'_{rc}).

7.3.4 Radial effective stresses after equalisation

Fully equalised profiles of radial effective stress (σ'_{rc}) are presented on Figure 7.15. These have been extrapolated, where necessary, from the pre-load test values recorded at t_{eq} ≈4days by applying small corrections (< 10% in all cases; see Table 7.3) on the basis of the long term equalisation data shown on Figure 7.14.

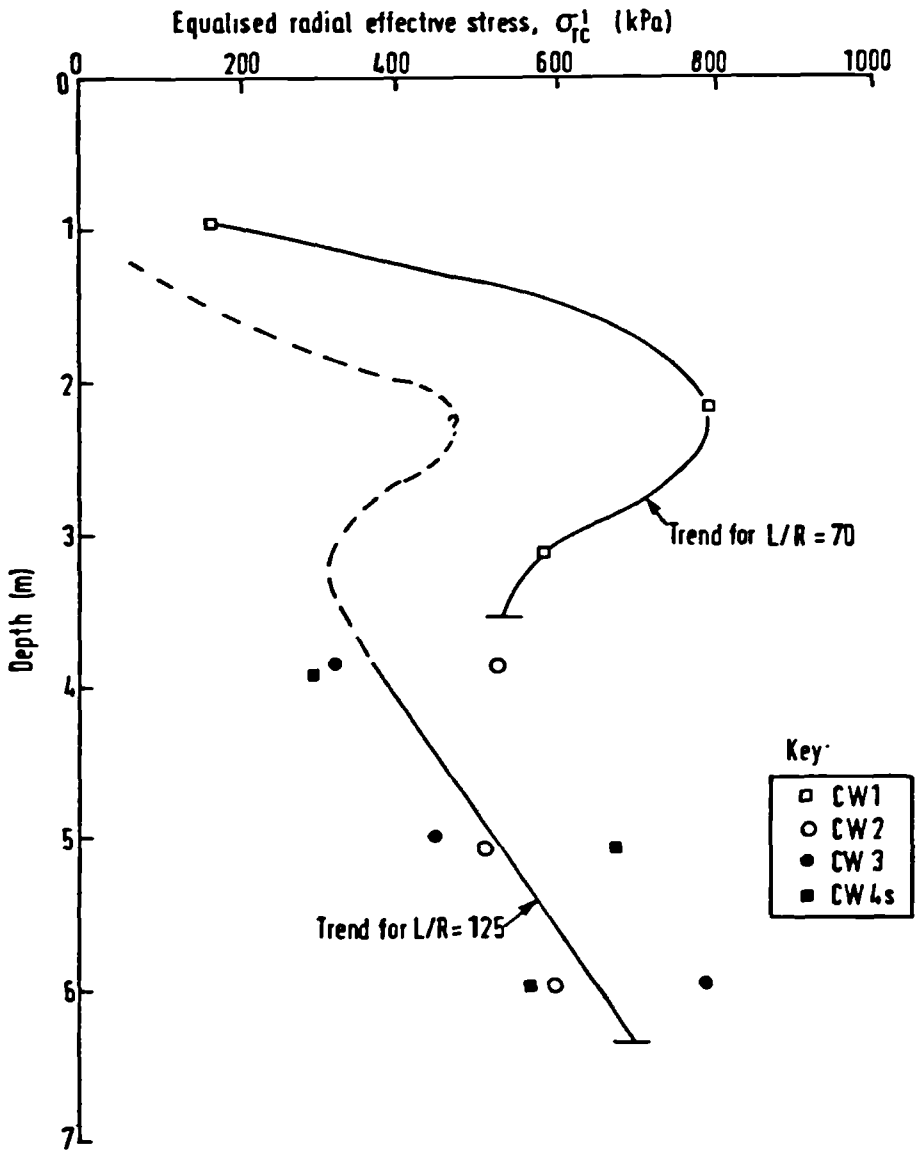

Figure 7.15 Equalised radial effective stress profiles

The main points to note are:

- The measurements show moderate scatter (± 50kPa) from the mean trend lines for σ'_{rc}. This scatter may reflect the inherent variability of Cowden till.

- The stresses developed at a given depth on the shorter pile are higher than those acting on the longer piles, indicating that σ'_{rc} reduces with the distance from the pile tip (h/R).
- The variable σ'_{rc} profile on the shorter pile shows clearly how the equilibrium stresses reflect local changes in the soil consistency (as indicated by the q_c, q_b and c_{u0} traces on Figures 7.3 and 5.14)

These trends are similar to those shown by the radial total stresses recorded during installation (σ_{r1}). This similarity may be expected as the relaxation coefficients, K_c/H_1, [= $\sigma'_{rc}/(\sigma_{r1}-u_0)$] were relatively independent of h/R: of the twelve K_c/H_1 values recorded, all but one differs by no more than 12% from the mean value of 0.75 (see Table 7.3). This trend suggests that profiles of σ'_{rc} for *all* pile lengths up to maximum penetration depth (i.e. 6.4m) may be approximated by applying a factor of 0.75 to the installation (σ_{r1} - u_0) data (see Section 10.3).

7.3.5 Residual pile stresses

The shear stresses derived from the axial load cell data (f_s) following the last push at installation and those after 4-5 days equalisation are shown on Figure 7.16 for piles CW2-CW4. These records showed similar trends to the τ_{rz} data.

It is noted that after installation, a significant downward drag (negative shear stress) is present over the top 1.5m of the piles. This is balanced by a residual base load (typically 6kN) and a positive shear stress over the lower 2m length of the piles. This profile can be explained by the higher stiffness (and strength) of the till to 3.5m depth. The drag over the top of the pile increases during equalisation, presumably as a consequence of the dissipation of excess positive pore pressures caused by installation.

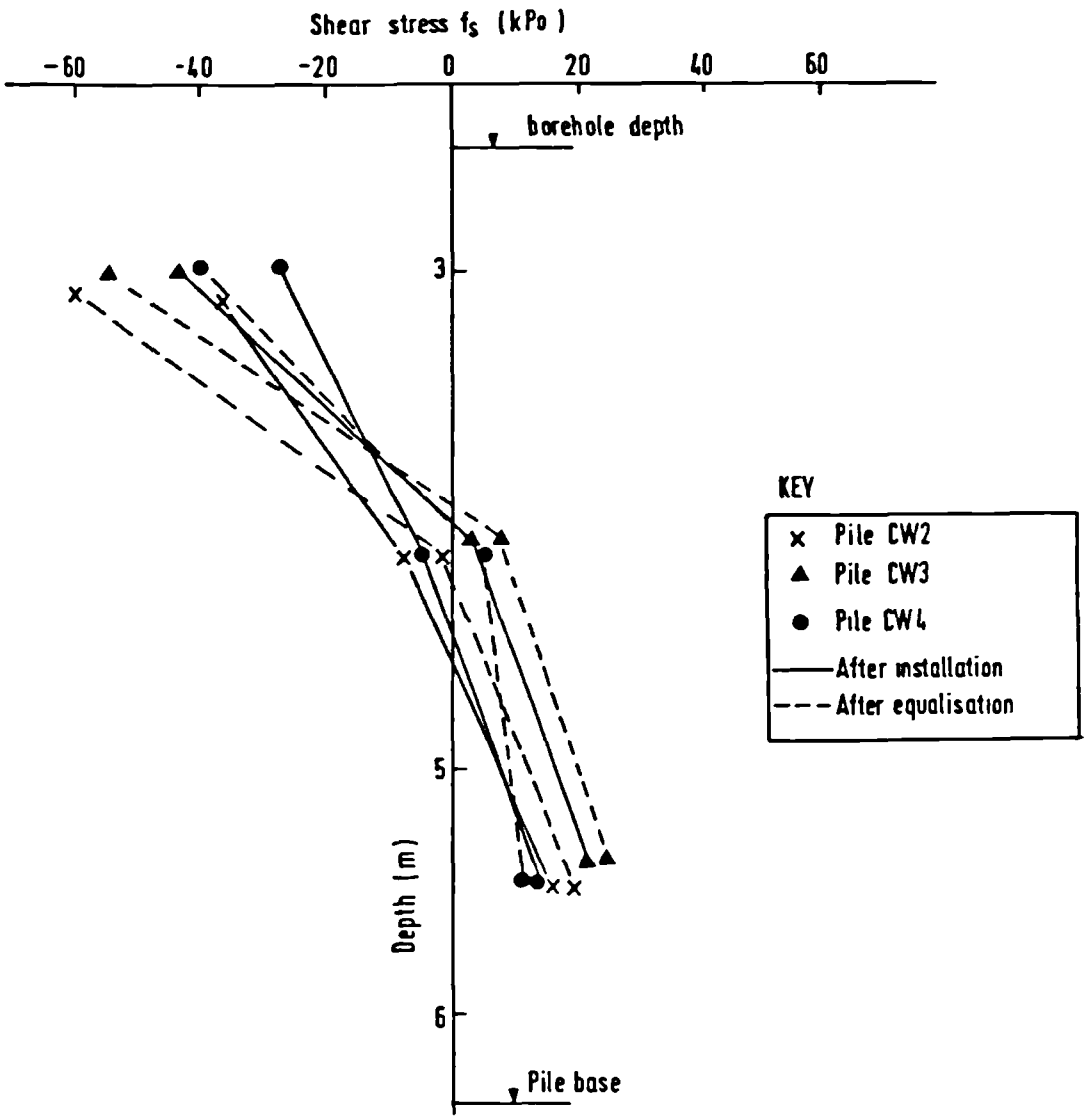

Figure 7.16 Residual stress profile at Cowden

This residual shear stress profile can be contrasted with that measured in the sand at Labenne (Figure 6.10), where all the shear stresses acted downwards on the pile shaft (i.e. negative shear). This situation arose because of the appreciably higher relative stiffness of the pile base in sand.

Pile	z(m)	h/R	σ_{rl}	H_i	u_{max}	u_l	σ'_{rl}	U_d	σ'_{rc}	K_c	K_c/H_i
CW1	3.1	8	432	9.2	256	79	292	0.24	313	7.0	0.76
	2.1	28	523	15.1	450	100	400	0.20	410	12.1	0.80
	1.0	50	95	4.5	36	0	78	0.00	78	3.9	0.82
CW2	5.9	8	450	5.0	360	51	298	0.04	296	3.6	0.72
	5.0	28	380	5.0	360	71	258	0.13	260	3.7	0.74
	3.8	50	372	6.4	330	65	266	0.12	272	4.9	0.76
CW3	5.9	8	528	5.9	365	65	400	0.07	400	4.9	0.83
	4.9	28	389	5.0	310	119	229	0.23	246	3.5	0.70
	3.8	50	301	5.0	275	97	157	0.28	173	3.2	0.64
CW4	5.5	8	420	4.9	375	326	71	0.85	-	-	-
	4.6	28	408	5.8	298	283	122	0.94	-	-	-
	3.4	50	318	6.0	255	232	82	0.90	-	-	-
CW4s	6.0	8	452	4.9	463	111	285	0.16	297	3.6	0.73
	5.0	28	460	6.1	383	92	342	0.16	355	5.1	0.83
	3.8	50	332	5.6	270	128	148	0.41	186	3.4	0.61

Notes:

1. σ'_{rl} and u_l are the radial effective stresses and pore pressures prior to the first load test. This test was performed for all piles except pile CW4 after an equalisation period of 4-5 days; pile CW4 was tested 2 hours after installation.
2. u_{max} is the maximum pressure recorded after installation. This occurred almost instantaneously in most cases but took 30 mins to develop at h/R=8 on pile CW1. Values of U_d are derived using this u_{max} value.
3. σ'_{rc} is extrapolated from σ'_{rl} for piles CW1, CW3 and CW4s on the basis of the long term data recorded by pile CW2 (see text). σ'_{rc} was measured on pile CW2.
4. Values of pore pressure at h/R=28 on pile CW1 are estimated as pore pressure measurements were not made at this location (see Section 7.1).
5. u_l at h/R = 50 on pile CW2 is a corrected value for probe no. P12C, which experienced an unexplainable jump in the signal (see Figure A1, Appendix A).

Table 7.3 Equalisation data at Cowden (stresses given in kPa)

7.4 LOAD TESTING

7.4.1 Introduction

The load testing programme was designed to investigate the influence of four main parameters on pile behaviour in this material:

(a) Initial conditions within the till, particularly its apparent overconsolidation ratio.
(b) Direction of first time loading (i.e. tension or compression).
(c) Duration of the equalisation period.
(d) Rate of installation

Pile CW1 was installed to 3.55m depth within the heavily overconsolidated and un-uniform upper layers, described in Section 5.2. The influence of the initial soil conditions can be examined by comparing the tension test on this pile with the equivalent test on pile CW3 which was sleeved through these layers (to ≈2.5m) and installed to 6.3m within the less overconsolidated underlying till.

Piles CW2 and CW4 were also sleeved to ≈2.5m and installed to ≈6.3m. The first compression load test on pile CW2 (Test: CW2/L1C) is used as a base case with which the other tests are compared in order to assess the effect of parameters (b), (c) and (d).

7.4.2 Overall pile behaviour

Table 7.4 provides details of the six primary load tests performed at Cowden and also lists the measurements characterising the overall pile behaviour observed. This table, in conjunction with Figure 7.17, which shows the variations of the unit shaft capacity (τ_{av}) with pile head displacement (d_p) measured in these tests, are used to deduce the trends summarised in the following sub-sections. Full details of all load tests are provided in Table 7.7 on page 278.

Test description:

Test	Test details	Main objective[1]
CW1/L1T	Installed at 500mm/min to 3.55m (sleeved to ≈0.5m) and tested in tension ≈4 days later	(a)
CW2/L1C	Installed at 500mm/min to ≈6.3m (sleeved to ≈2.5m) and tested in compression after ≈ 4 days	Base case
CW2/L3C	Compression re-load test of pile CW2 after secondary load tests and a further 90 days equalisation	(c)
CW3/L1T	As CW2/L1C but tested in tension	(b)
CW4/L1C	As CW2/L1C but tested after ≈2 hours	(c)
CW4s/L1C	As CW2/L1C but installed from 6m to 6.38m at an installation rate of 80mm/min	(d)

[1] as indexed in Section 7.4.1

Test results:

Test	τ_{avp} (kPa)	α	d_{pm} (mm)	τ_{avu} (kPa)	τ_{avi} (kPa)	q_b (MPa)
CW1/L1T	89	0.60	1.87	82	125	-
CW2/L1C	104	0.82	2.42	83	108	1.87 at 17mm
CW2/L3C	116	0.92	2.25	98	108	2.37 at 14mm
CW3/L1T	72	0.57	4.40	70	118	-
CW4/L1C	62	0.49	1.55	60	112	1.54 at 15mm
CW4s/L1C	75	0.60	1.75	66	71	1.81 at 13mm

Note: τ_{avi} =average shear stress measured during the last push at installation, τ_{avp} =peak average shear stress, τ_{avu} =ultimate (post-peak) average shear stress, d_{pm} =pile head displacement at τ_{avp}, α =adhesion factor at d_{pm} ($=\tau_{avp}/c_{u0}$), q_b =maximum pile end bearing.

Table 7.4 Primary load tests at Cowden

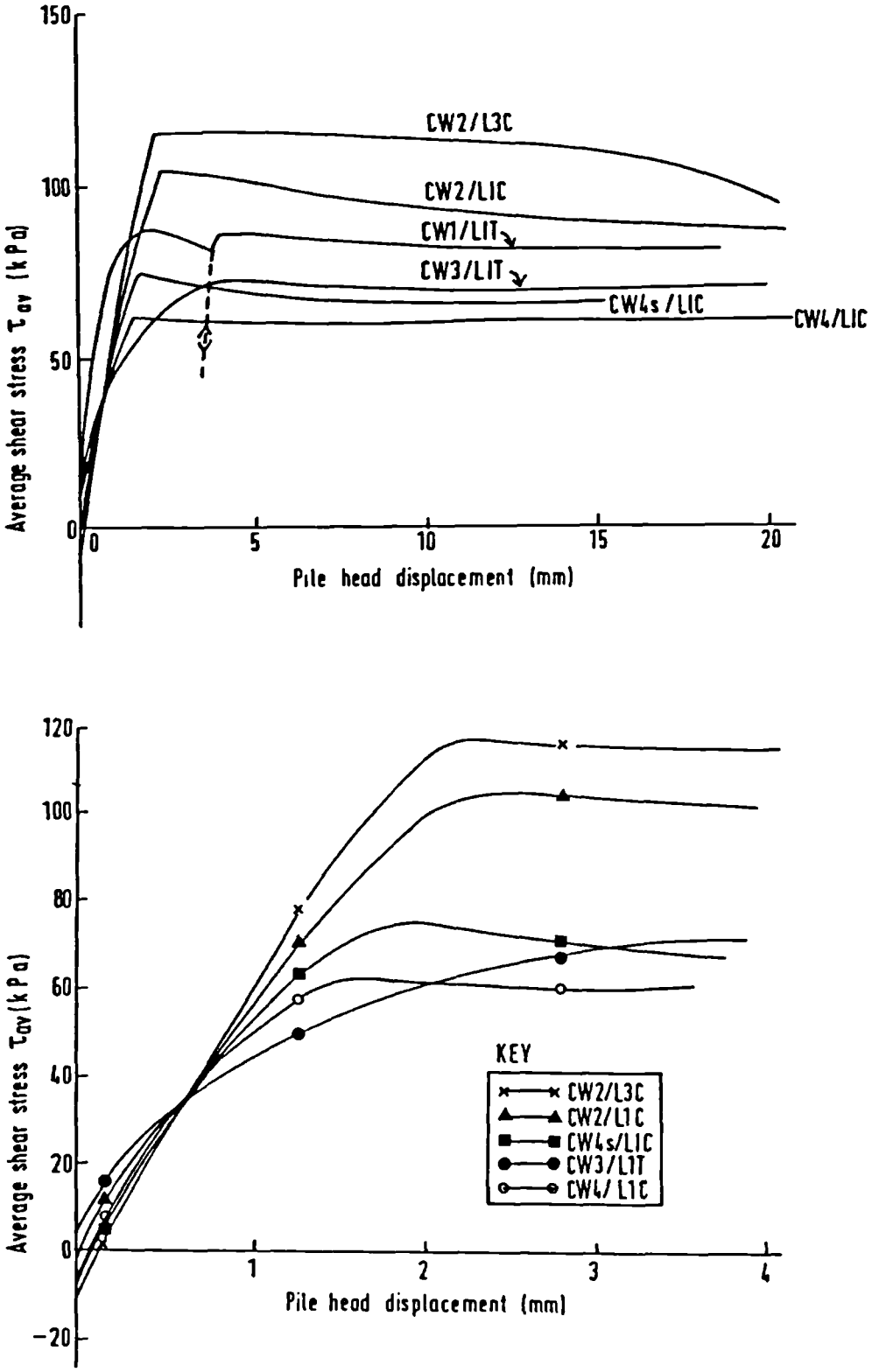

Figure 7.17 Shaft load - displacement curves

7.4.2.1 Shaft capacity

The adhesion factors (α) for 'first-time' load tests on piles, tested 4 days after installation (when equalisation was effectively completed), vary between 0.57 and 0.82. This range is relatively wide, but is in good agreement with the mean value of 0.7 proposed by Weltman & Healy (1978) for driven piles in glacial tills (of the consistency measured at Cowden). The spread in capacities is not believed to be related to ground variability or to instrument scatters as the data recorded by each pile during installation and equalisation were in good agreement. For example, the average shear stresses measured during the final stages of fast installation (τ_{avf}) of piles CW2-CW4 agreed to within 4%.

A comparison of the shaft capacities measured shows that:

- The shaft capacity of a pile initially tested in compression is about 40% *higher* than the tensile capacity of an equivalent pile.
- As might be expected from the variations of σ'_r with time after installation (Figure 7.13), the shaft capacity depends on the duration of the equalisation period (t_{eq}). At t_{eq} ≈4days, the compressive capacity is about 70% *higher* than that of a pile tested at t_{eq} = 2hrs.
- The combined effects of allowing a 2 hour pause period and re-jacking for 380mm at 80mm/min led to a permanent *reduction* in shaft capacity of ≈30% when compared with the capacity of a standard fast-installed pile.
- Although no appreciable changes in the radial effective stresses acting on pile CW2 were observed over the 90 days following its first load test (Figure 7.14), a repeat compression test showed that shaft capacity had *increased* by ≈10% over this period.

The standard degree of 'set-up' may be assessed by comparing the *post-peak* average shaft resistance measured in the first compression test on pile CW2 with that measured during the last stages of fast-jacking. This comparison shows that the pile suffers an overall *loss* of 20% in shaft capacity. A less pronounced loss of resistance was observed for the slow-jacked pile - in keeping with its larger $\sigma'_{rc}/\sigma'_{rf}$ (see Section 7.3.2).

7.4.2.2 Shaft displacement characteristics

The load-displacement curves of compression tests showed similar characteristics up to τ_{av} =50kPa, but their shapes at higher stresses were constrained by the maximum capacity that could be mobilised. However, even from the first load steps, the tension characteristic measured in Test CW3/L1T was distinctly softer than the other (compression) curves. This response is believed to be related to the anisotropy in the soil fabric created by installation.

Piles that showed relatively low peak capacities (due to the effects of time, displacement rate or loading direction) showed less brittle behaviour than high capacity piles (i.e. compression tests on fully equalised fast installed piles). In the cases where the response was brittle[1], τ_{av} showed little change over the initial 2 to 3mm of post-peak displacement: displacements in excess of 15mm were generally required to reduce the shaft resistance to its ultimate value.

7.4.2.3 Base load

Base resistances in compression tests at peak shaft capacity were typically 80% of their ultimate values (q_b). These ultimate values required a pile head displacement of ≈15mm (i.e. 15% of the pile diameter) for full mobilisation.

q_b values were within 5% of the end resistances measured during the last jacking stage at installation and showed no dependence on the length of the equalisation period. However one exception was seen in the re-test of pile CW2 performed after an extended equalisation period (Test CW2/L3C). The q_b value measured in this test was 25% larger than that measured in the initial test performed at t_{eq} ≈4 days. As noted above, the shaft capacity had also benefited from the effects of pre-shearing after full equalisation.

[1]Pile plunging rates are given in Table 7.7 on page 278.

7.4.3 Local stress variations

Typical variations of shear stress, pore pressure and radial total stress with pile head displacement (d_p) are shown on Figure 7.18, using data from tests CW2/L1C and CW3/L1T. These variations are first described separately before examining their combined effect in Section 7.4.4.

7.4.3.1 Shear stress

The local shear stresses vary with d_p in a similar way to the average shaft shear stresses, discussed above. In addition, it may be observed that the value of d_p required to mobilise peak stresses generally increases with depth indicating that piles failed progressively from the top down. This feature is discussed in Chapter 10.

It is also evident that the shear stresses measured by the SST's (τ_{rz}) in Test CW2/L1C are not compatible with those derived from the axial load cell data (f_s). This incompatibility, which was also observed during installation, occurred in 'high capacity' compression piles. Peak τ_{rz} values were ≈20% smaller than those implied by the f_s measurements and were mobilised at a lower value of d_p. However, all tension tests (and some compression tests) showed compatible τ_{rz} and f_s variations (e.g. Test CW3/L1T). An explanation for these trends will become apparent in the next section.

7.4.3.2 Pore pressure

During pile loading, pore pressures at the leading and following instrument positions (h/R=5 and 30) generally increased by between 30kPa and 50kPa pre-peak and then began to fall at post-peak displacements of less than ≈0.5mm; the trailing instruments show a more muted response. Dramatic post-peak reductions in pressure were measured by all piles that failed in a brittle manner (e.g. CW2/L1C), but less severe reductions occurred in tension tests (e.g. CW3/L1T), where post-peak displacement rates were lower.

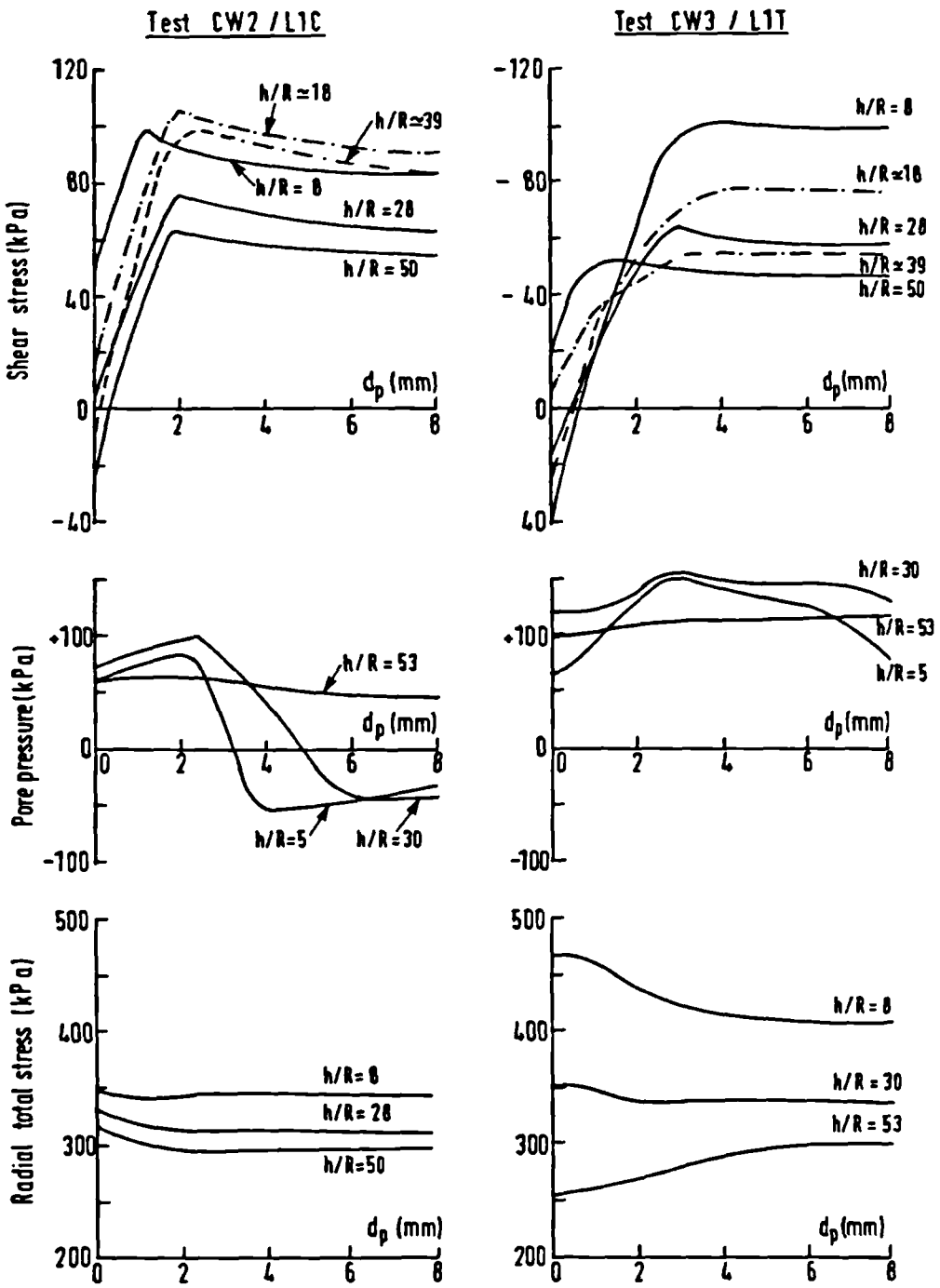

Figure 7.18 Variations of local stresses with d_p in tens. and comp.

Other points of note regarding the pore pressure measurements are:

- The short term test on pile CW4 (with $t_{eq} \approx$ 2hrs) showed uncharacteristic pre-peak *reductions* in pore pressure at all instrument positions.
- Pre-peak increases in pressure were larger in the first test on pile CW2 (CW2/L1C) than in re-tests on the same pile.
- Pressures measured in tests CW2/L1C and CW4s/L1C showed a comparable response, suggesting that the lower capacity of pile CW4s is not related to a pore pressure phenomenon.

7.4.3.3 Radial total stress

Radial total stresses (σ_r) *reduced* pre-peak by between 5% and 10% at all depths in compression tests and below 4m in tension tests (where the till was less overconsolidated). At shallower depths in tension tests, σ_r *increased* pre-peak by between 10% and 15%. Post-peak, σ_r remained virtually constant in all load tests; this neutral response is in sharp contrast to the large post-peak variations in pore pressure.

The changes in σ_r during pile loading showed no clear dependence on the installation rate, loading rate or the period allowed for equalisation.

7.4.4 Effective stress paths

Figure 7.19 presents typical variations of shear stress with radial effective stress measured at each instrument position in first-time compression and tension tests. These 'stress paths' are shown for both the local and average shear stresses (i.e. τ_{rz} and f_s); radial effective stresses plotted in conjunction with the f_s measurements are the average of the values measured by the two instrument clusters from which a given f_s data set was calculated.

It is noted that:

- σ'_r reduces as the pile is loaded and is at a minimum near to the instant of peak local shear stress.

- Larger pre-peak reductions of σ'_r are observed in tension tests, except at the trailing instrument position (h/R=50, z≈3.8m) where σ'_r remained relatively constant.
- The discrepancy between the τ_{rz} and f_s data in the compression tests (Figure 7.18) is seen to be related to the higher peak obliquity (δ_p) shown by the f_s measurements (≈24° compared to ≈19°)
- The maximum f_s and τ_{rz} values are both mobilised at a lower peak obliquity (δ_p) of ≈18° in the tension test.
- Large increases in σ'_r are observed post-peak, while shear stresses remain relatively constant. These increases lead to apparent ultimate obliquities (δ_{ult}) of between 10° and 15° in both tests.

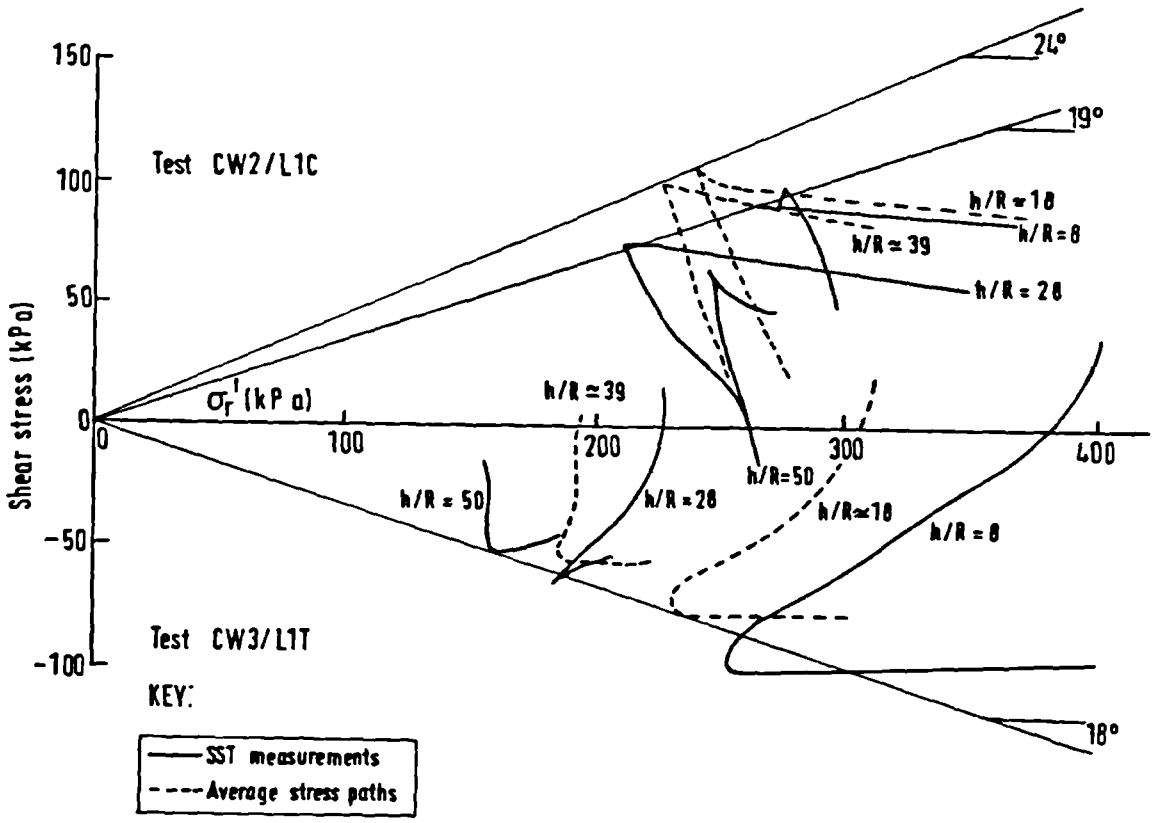

Figure 7.19 τ v σ'_r paths in Tests CW2/L1C and CW3/L1T

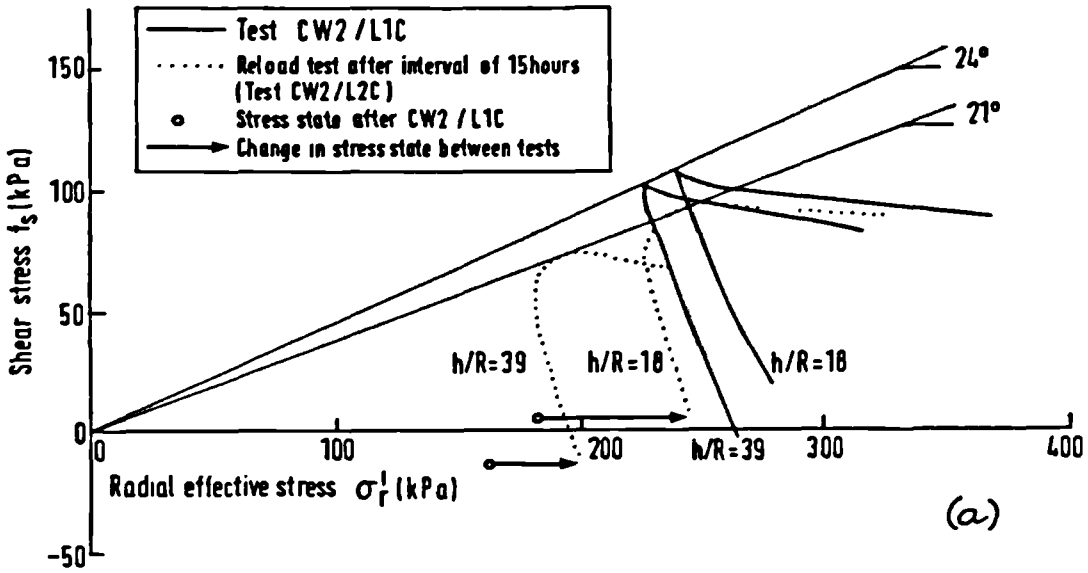

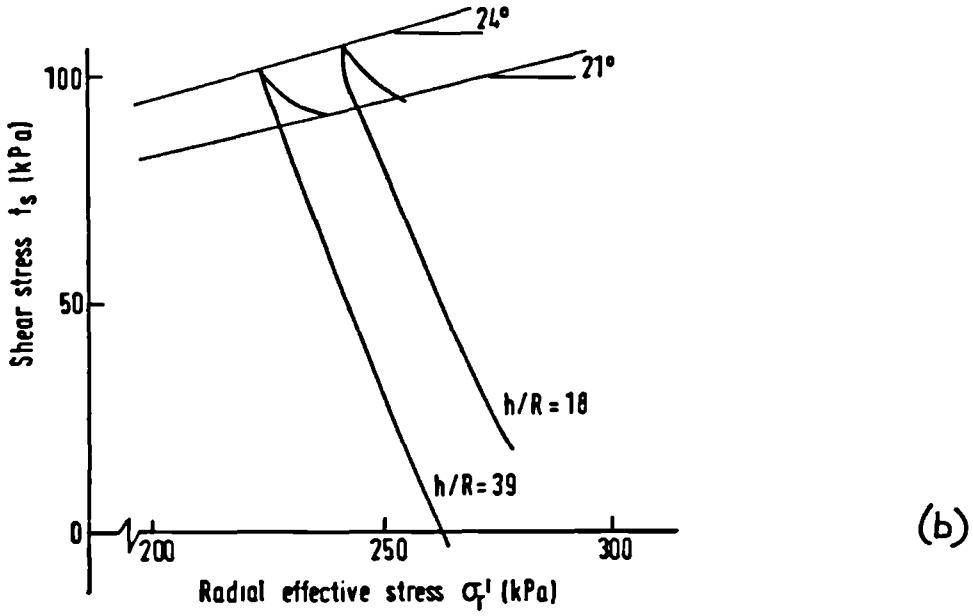

Figure 7.20 Stress paths in tests CW2/L1C and CW2/L2C (top); 'corrected' post-peak stress paths for test CW2/L1C (bottom)

Pile CW2 was re-loaded to failure 14 hours after the initial compression test (Test CW2/L2C). The stress paths measured in both tests are compared on Figure 7.20a and show:

- Unloading of pile CW2 after its first test (CW2/L1C) caused the radial effective stresses to reduce to values ≈40% less than those existing before this test. These stresses increased by about 30% in the period prior to the reload test, as excess pore pressures dissipated.
- Smaller pre-peak reductions of σ'_r occur in the reload test and peak shear stresses are mobilised at δ_p =21°. This angle is less than the value of δ_p measured in the initial test, but much larger than ultimate angle recorded in the same test (10°-15°)
- Large post-peak increases in σ'_r also take place in the reload test and lead to an apparent ultimate obliquity (δ_{ult}) of less than 15°.

Reload tests, such as Test CW2/L2C, show that the low δ_{ult} values measured do not control subsequent pile capacity and therefore do not correspond to permanent changes in the residual soil fabric close to the pile. This conclusion is supported by ring shear interface tests (Section 5.2.10) which gave δ_{ult} values of 23 ± 1° and indicated that peak and ultimate angles should not differ by more than ≈5°. As mentioned in Section 7.2.6 (and discussed in more detail in Appendix A), the under-prediction of the ultimate post-peak angles in load tests and during installation is due to the measurement of anomalous pore pressures at pile velocities in excess of ≈1mm/min. Although pre-peak pile displacement rates in load tests were always less than 1mm/min, 'brittle' piles tended to accelerate after failure, attaining typical post-peak velocities of ≈5mm/min. Pore pressures recorded during such failures therefore suffer from the same phenomenon affecting the pore pressure data during installation jacking stages.

Figure 7.20a may be used to assess a plausible post-peak stress path representing conditions on the principal displacement shear during the first load test on pile CW2 (CW2/L1C). The peak obliquity mobilised in the reload test was 3° less than that measured in Test CW2/L1C. It may therefore be presumed that post-peak shearing (of ≈20mm) during the initial test created a more ordered soil fabric adjacent to the pile and reduced the residual angle from 24° to 21°. As little post-peak brittleness was evident in the reload test, it is suggested that the

operational value of δ_{ult} is ≈21°. Based on these assumptions, the 'corrected' stress paths for Test CW2/L1C, shown on Figure 7.20b, were constructed. These suggest that post-peak increases in σ'_r on the failure shear surface were ≈15kPa and significantly less than the pore pressure measurements imply.

Stress paths measured up to peak shear stress in three further compression load tests are shown on Figure 7.21[1] and compared with the first-time test on pile CW2. These paths add further insight into aspects governing shaft capacity, discussed below.

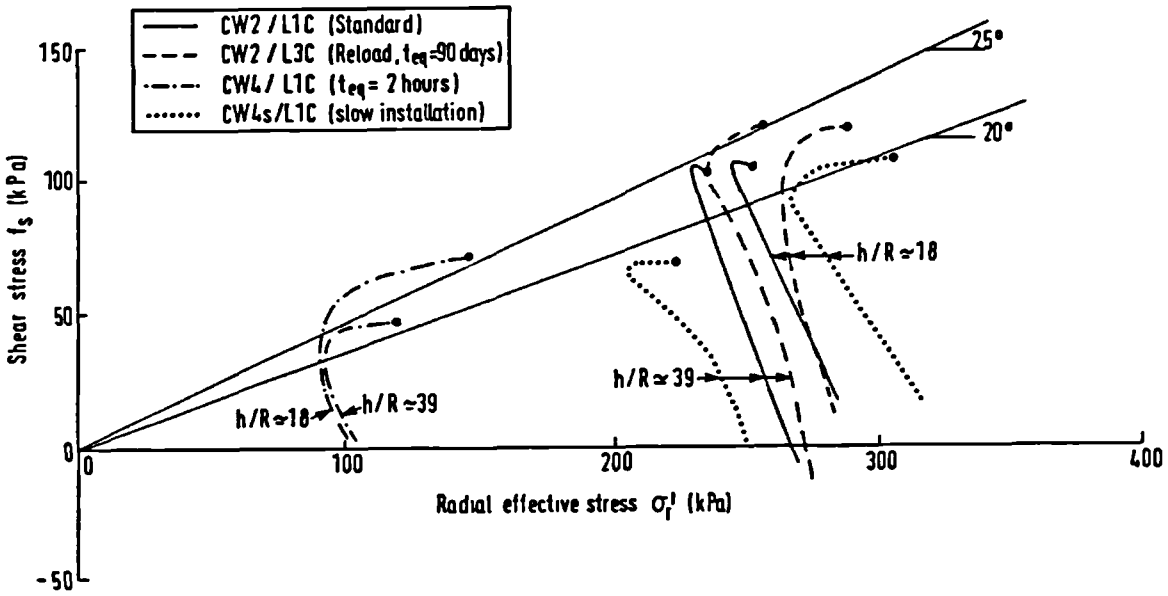

Figure 7.21 Stress paths in other 'primary' load tests at Cowden

[1]These stress paths use the f_s data in preference to the τ_{rz} data as the global pile behaviour is governed by the shearing characteristics of the till against the pile casings, which make up the majority of the pile shaft.

7.4.5 Load test summary

7.4.5.1 General trends and comparisons with laboratory tests

The stress path plots reveal consistent patterns between the tests and confirm that the magnitude of the peak local shear stress is related directly to the local radial effective stress at this stress (σ'_{rf}) through the equation: $\tau_f = \sigma'_{rf} \tan \delta_p$. Alternatively, this equation may be written as $\tau_f = (K_f/K_1)\ \sigma'_{r1} \tan\delta_p$, where σ'_{r1} = pre-loading radial effective stress and $K_f/K_1 = \sigma'_{rf}/\sigma'_{r1}$.

The large range of pile shaft capacities measured at Cowden was reflected by relatively wide variations in the values of K_f/K_1 and δ_p, summarised in Table 7.6 on page 277 at the end of this section. Condensed in this form, the data show the clear trends outlined below:

1. Radial effective stresses generally decrease during pile loading. The K_f/K_1 values, with some exceptions noted below, were typically between 0.8 and 0.9.

2. Large pre-peak increases in σ'_r were observed in the test performed at t_{eq} = 2 hours (Figure 7.21) and K_f/K_1 values of between 1.1 and 1.5 were recorded. These increases suggest that pre-peak dilation is more significant when the till is sheared in a partially equalised condition.

3. Instruments within the more lightly overconsolidated material below 4m give lower values of K_f/K_1 ($\approx$0.75 $\pm$0.05) in tension tests[1]. This more 'contractant' response may reflect the anisotropy induced by installation and is analogous to the tendency seen in CK_0U triaxial tests for stronger contraction to occur after a large rotation of the principal stress directions (c.f. differences between CK_0U triaxial extension and compression tests; Figure 5.17).

---

[1]Similar values were measured at these depths during extraction of all piles.

4. Smaller overall pre-peak reductions in σ'_r are observed in reload tests and K_f/K_1 is close to 1.0. The larger K_f/K_1 ratio is attributed to plastic hardening caused by pre-shearing during the initial load test. It is apparent from the data recorded during the final re-test on pile CW2 (Test CW2/L3C, Figure 7.21) that an extended equalisation period, following pre-shearing, also causes an increase in the obliquity at peak shear stress (from 21° to 24°).

5. The peak angle of interface friction mobilised on the pile casings, in compression tests on fast-jacked piles is typically 25°. This angle lies within the 'peak' range measured in ring shear interface tests (24° to 28°), discussed in Section 5.2.10. However, lower peak values of ≈20° were measured by the SST's, suggesting that local slippage took place at the surface of the SST before an overall shaft failure occurred.

6. The ring shear tests showed that fast pre-shearing at 500mm/min disorders the potential residual shear zone and induces a peak friction angle which is ≈3° higher than the slow ultimate residual angle (≈23°). The tests on pile CW2 showed the same feature with δ (from f_s measurements) reducing post-peak from 24° to an ultimate value (δ_{ult}) of ≈21°.

7. Test CW4s/L1C showed comparable peak and ultimate angles of 20°. It appears that the jacking rate of this pile (80mm/min) was not fast enough to disrupt the ordered soil fabric created by the preceding slow load test (CW4/L1C).

8. The peak and ultimate obliquities were also equal (at ≈18°) in tension. This low angle, which was not anticipated from ring shear tests, accounts for the significant difference between compression and tension shaft capacities. The peak shaft resistance may have been controlled, in this instance, by continuum failure in the soil mass, rather than slippage at the interface or on a residual surface close to the interface.

7.4.5.2 Comparison with other pile tests at Cowden

Driven and jacked steel piles have been installed and tested at Cowden close to the location of ICP tests (see Figure 5.12). In most cases, the piles were tested in tension initially after a period sufficient for full equalisation to take place. Their tensile capacities are compared in Table 7.5 with those measured in Tests CW1/L1T and CW3/L1T. It should be noted that the previous tests followed a variety of load testing procedures (e.g. constant rate of extraction, constant rate of loading, maintained load tests) and cyclic loading experiments often preceded the tension test to failure.

Diam. (mm)	Installation	Depth (m)	No. of piles	End condition	τ_{av} (kPa)	α
102	ICP: Jacked	3.5	1	Closed	89	0.60
	at 500mm/min	6.3	1	Closed	72	0.57
193	Jacked at 10mm/min	9.9	1	Open	86	0.84
203	Driven	9.5	3	Closed	51 ± 7	0.50
203	Driven	9.5	2	Open	54 ± 4	0.53
305	Driven	9.5	2	Closed	43 ± 1	0.42
305	Driven	9.5	2	Open	42 ± 2	0.41
457	Driven	9.9	1	Closed	90	0.88
457	Driven	9.9	1	Open	83	0.82

Table 7.5 Tension tests at Cowden[1]

These tests, while indicating little difference between the shaft capacity of an open and closed-ended pile, exhibit a large range of unit shaft capacities and associated α values. In particular, the unit capacities of the 203mm and 305mm piles are appreciably less than those of other piles installed to the same depth. These low capacities were

[1] References: 193mm pile (Ponniah 1989 and McAnoy et al 1982), 203mm and 305mm piles (Ove Arup & Partners 1986), 457mm piles (Gallagher & St. John 1980).

thought to be due to a smooth coating of mill varnish that was applied to these piles prior to installation (Ove Arup & Partners 1986)[1]. Confirmation of the effect of the mill varnish was obtained from a series of shear box interface tests which indicated that the resistance of the till sheared against a mill varnished steel interface was ≈30% less than that if sheared against a rusted steel interface.

These observations reinforce the importance, noted in the ICP tests, of (a) specifying and measuring the frictional properties of the interface and (b) describing shaft capacity in terms of effective stress parameters.

Additional points to note are:

(i) Based on data from compression tests that were preceded by tension tests, Ove Arup & Partners (1986) concluded that the compressive and tensile shaft capacities at Cowden were comparable. The ICP tests have shown, however, that initial tension testing of a pile to failure affected the soil fabric permanently; the maximum δ value that could be mobilised in a subsequent compression test (e.g. CW3/L2C; see Table 7.6) was only ≈20° compared to a value of ≈25° measured in first-time compression testing of a fast-jacked pile. It thus appears that compressive capacities cannot be deduced from piles that had previously been tested in tension.

(ii) The ICP tests showed the tensile shaft capacity to be about 30% less than the equivalent compressive shaft capacity. A lower (by 12%) shaft capacity in tension was also observed in the tests on the 457mm diameter piles, reported by Gallagher & St John (1980).

(iii) The 193mm diameter pile was installed at a slow jacking rate of ≈10mm/min and gave an initial tensile load capacity 35% greater than the installation (compressive shaft capacity[2]. In sharp

---

[1]The 203mm diameter piles were reported to have a less continuous cover of mill varnish, hence explaining their higher unit capacities.

[2]This pile was equipped with a load cell at the pile tip and was one of a group of four piles installed with a spacing of 3 diameters.

contrast, the tensile capacity of pile CW3 was 40% less than the shaft capacity at installation. This difference may be partly explained by the dependence of the evaluated set-up on the pile installation rate (see Section 7.4.2).

(iv) After a period of about a year, all piles were re-tested to failure and showed a 20% increase in capacity. This gain in capacity with time and pre-shearing, after radial effective stresses had equalised, was also observed in the long term compression test on pile CW2 (Test CW2/L3C).

Test	Description	Average failure parameters		
		K_f/K_1	δ_p (f_s)[1]	$\delta_p(\tau_{rz})$
First time load tests				
CW1/L1T	Fast installation to 3.55m (i.e. within high OCR material), tested in tension after 4 days	0.98	15.5°	16.0°
CW2/L1C	Standard test (fast installation to ≈6.3m tested in compression after 4 days)	0.88	24.0°	18.0°
CW3/L1T	As per standard but tested in tension	0.82	17.5°	18.5°
CW4/L1C	As per standard, but tested after 2 hours	1.30	25.5°	22.0°
CW4s/L1C	As per standard, but slow installation	0.85	19.5°	19.9°
Secondary tests				
CW2/L2C	Reload of pile CW2 after 14 hours	0.98	21.0°	17.5°
CW2/L3C	Reload of pile CW2 after a further 90 days	1.00	24.0°	17.0°
CW3/L2C	Comp. test on CW3, 10 hours after first tension test	0.88	20.0°	20.5°
Pile extractions				
CW2/FEX		0.97	21.0°	20.1°
CW3/FEX		1.04	18.0°	18.2°
CW4/FEX		0.84	17.7°	19.3°

[1] δ_p (f_s) and δ_p (τ_{rz}) are the peak obliquities calculated using the f_s and τ_{rz} data respectively.

Table 7.6 Effective stress failure parameters in load tests at Cowden

Test	Time	Date	t_f (min)	P_{max} (kN)	L_r (kN/min)	d_{pm} (mm)	τ_{avp} (kPa)	f_r (mm/min)	τ_{avu} (kPa)
Pile CW1									
L1T	15:40	18/11/89	84	-82.4	1.0	1.87	-88.7	0.3	-81.5 at 4mm
L2T		18/11/89		-79.0	1.2		-85.0		
L3C	11:08	19/11/89	102	65.7	0.6	1.70	68.9	1.6	68 6 at 6mm
FEX	10:59	20/11/89	1	-74.3	74.0	N/A	-80.0	1.0	76 0 at 10mm
Pile CW2									
L1C	17:12	27/11/89	108	131.0	1.2	2.42	104.0	5.7	83 0 at 21mm
L2C	8:00	28/11/89	24	117.0	4.9	1.59	92.6	0.8	83 0 at 10mm
LCY.	10:00	28/11/89	5	112.0	22.0	0.12	85.8	1.2	84 4 at 5mm
L3C	16:44	27/02/90	60	149.0	2.5	2.25	116.0	4.4	98.0 at 18mm
FEX	13:00	28/02/90	53	-100.4	1.9	1.80	-89.4	1.2	-81.6 at 8mm
Pile CW3									
L1T	17:30	19/03/90	80	-88.3	1.1	4.40	-72.0	2.3	-71.3 at 22mm
L2C	10:10	20/03/90	38	81.3	2.1	5.20	65.4	-	-
FEX	11:40	20/03/90	5	-74.6	15.0	5.00	-61.3	-	-
Pile CW4									
L1C	19:40	22/03/90	32	77.5	2.4	1.55	62.0	5.6	59.5 at 21mm
Pile CW4s									
L1C	16:00	26/03/90	45	102.0	2.3	1.75	75.0	5.4	65.5 at 15mm
FEX	7:30	27/03/90	12	-73.0	6.1	3.82	59.3	-	-

Notes: t_f = time to load to P_{max}, L_r = average loading rate to P_{max}, d_{pm} = pile head displacement at P_{max}, τ_{avp} = average shaft shear stress at P_{max}, f_r = plunging rate after reaching P_{max}, τ_{avu} = final shaft shear stress, LCY. after 50 one minute load cycles between 50kN and 95kN.

Table 7.7 Load test summary: Cowden

CHAPTER 8

PILE TESTS AT BOTHKENNAR

CONTENTS OF CHAPTER 8

PILE TESTS AT BOTHKENNAR

8.1 PILE CONFIGURATION AND TEST PROGRAMME 282
8.1.1 General 283
8.1.2 Notes on individual piles 284
8.1.2.1 Phase 1 284
8.1.2.2 Phase 2 285
8.2 INSTALLATION 286
8.2.1 End resistance 286
8.2.2 Shaft resistance 288
8.2.3 Local shear stress 291
8.2.3.1 Rate effects on shear stress 292
8.2.4 Radial total stress 294
8.2.5 Pore pressure 297
8.2.6 Radial effective stress 300
8.3 EQUALISATION 301
8.3.1 General 301
8.3.2 Pore pressure 302
8.3.3 Radial total stress 305
8.3.4 Radial effective stress 306
8.3.4.1 Changes in σ'_r prior to load testing 306
8.3.4.2 Long term variations in σ'_r 309
8.3.4.3 Equalised σ'_r values 310
8.3.5 Residual pile stresses 312
8.4 LOAD TESTING 315
8.4.1 Introduction 315
8.4.2 Overall pile response 315
8.4.2.1 Shaft capacity 318
8.4.2.2 Shaft displacement characteristics 319
8.4.2.3 Base load 319
8.4.3 Local stress variations 320
8.4.3.1 Pore pressure 320
8.4.3.2 Radial stress 322
8.4.3.3 Shear stress 323
8.4.4 Effective stress paths 323
8.4.4.1 Behaviour up to peak shear stress 323
8.4.4.2 Post-peak behaviour 328
8.4.4.3 Comparison with laboratory tests 330

8.0 PILE TESTS AT BOTHKENNAR

This chapter presents the findings from the series of tests carried out with the ICP in the soft clay at Bothkennar, Scotland. A general summary of the programme of works is described first, before the specific results obtained during pile installation, equalisation and load testing are presented. Further discussion and analyses of these data are provided in Chapter 10.

8.1 PILE CONFIGURATION AND TEST PROGRAMME

8.1.1 General

The field experiments at Bothkennar were carried out in two phases between October 1990 and April 1991 and involved the installation and load testing of four piles, designated BK1-BK4, with the configurations shown on Figure 8.1. The tests utilised the standard instrumentation and site procedures that were described in Chapter 4. Earlier preparatory work had involved the construction and pre-loading of footings for the loading frame (see Section 4.2).

Pile		Phase	Depths penetrated by pile toe (m)	Installation rate (mm/min)	t_{eq}
BK1		1	1.0 - 6.0	500	0.8 days
BK2		1	1.2 - 6.0	500	4 days
BK3					
	BK3(1)	2	1.2 - 3.15	500	115 mins
	BK3(2)	2	3.15 - 5.9	500	4 days
BK4					
	BK4f	2	1.2 - 3.15	500	4 days
	BK4s	2	3.15 - 5.95	75	2 days

Table 8.1 Pile details at Bothkennar

The piles were installed from the base of a 1.0-1.2m pre-bored hole to eliminate the effects of the stiff crust on the measurements made. The

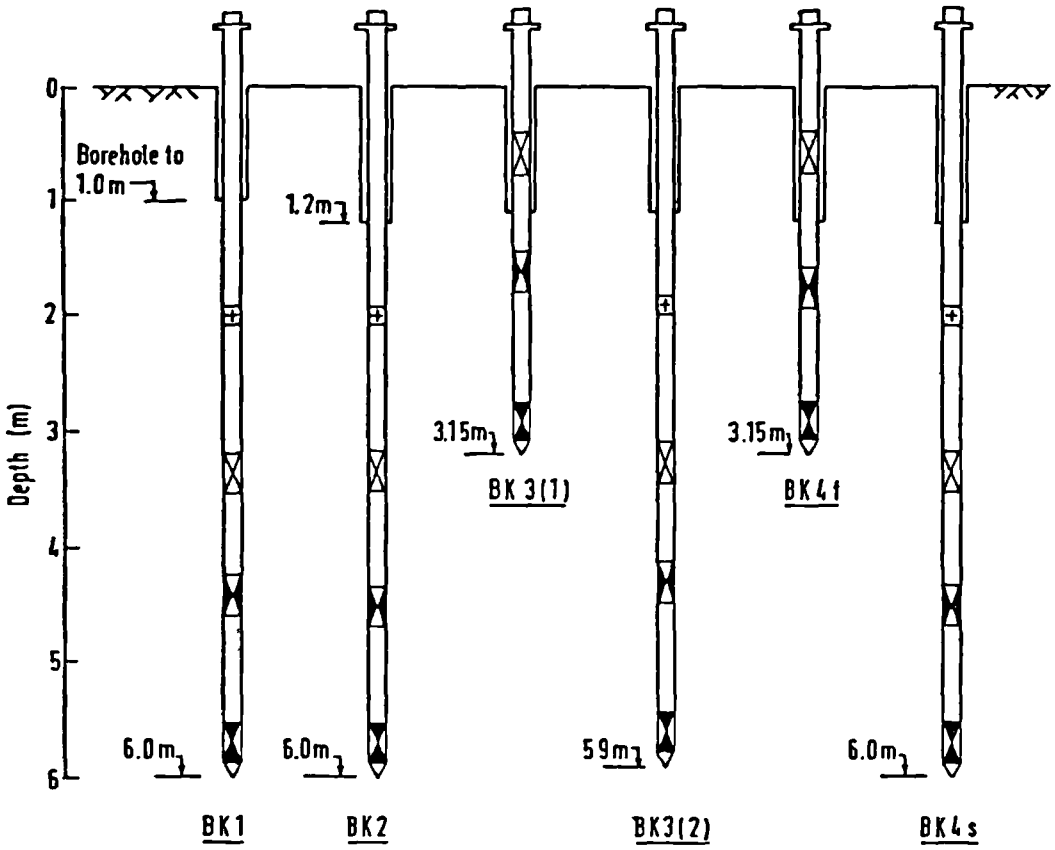

KEY:

	Cluster	Sensor location (h/R)		
		SST	ppu	ALC
	Leading	8	5	3
	Following	~28	~30	~32
	Trailing	50	53	55
	Lagging	-	-	77

NOTATION.

SST : Surface stress transducer
ppu : Pore pressure unit
ALC Axial load cell
h : Distance from pile tip
R : Pile radius = 50.8 mm

Figure 8.1 Pile configurations at Bothkennar

installation of BK3 and BK4 was halted at 3.15m to allow preliminary load tests to be carried out. These piles were installed subsequently to ≈6m, by which stage most of the instruments were within 'fresh' strata that had not been affected by the initial installation stage to 3.15m. The

relevant penetration depths, installation rates and periods allowed for equalisation before load testing (t_{eq}) for all piles are summarised in Table 8.1.

8.1.2 Notes on individual piles

8.1.2.1 Phase 1

The first phase of the experiments used piles BK1 & BK2 and was carried out between October and December 1990.

(i) Pile BK1

Pile BK1 was installed first and it had been the original intention to load test the pile in compression after full equalisation. However, the lowest instrument cluster began to show signs of instability shortly before completing installation to 6m and it was suspected that water was seeping into the pile through a loose joint. In order to minimise instrument damage and maximise the value of data obtained, the pile was tested in tension (Test BK1/L1T) after a shortened equalisation period of 20 hours.

Most instruments performed satisfactorily during installation, but by the time the pile was load tested, only half of the instruments were operational, as outlined in Table 8.2.

Instrument position	Radial stress	Shear stress	Axial load	Pore pressure
Leading	no	no	no	no
Following	yes	yes	no	yes
Trailing	yes	no	yes	yes
Lagging	-	-	yes	-

Table 8.2 Instruments operating for Test BK1/L1T

After extraction, the source of the leak was located at a perforated lug[1] on a steel casing.

(ii) Pile BK2

Pile BK2 was installed successfully to 6m. The post-installation data showed that, by four days, approximately 85% of excess pore pressures had dissipated and radial effective stresses had approached equilibrium values. The pile was then load tested in compression (Test: BK2/L1C). No instruments malfunctioned and a complete set of good quality data was obtained.

The pile was re-tested (again in compression) 32 days later (Test: BK2/L2C). By this time, the compression circuits of one of the three SST's had become unstable due to another (but less serious) leak at a lug in the steel casing immediately above the instrument cluster. The instrument survival rate for this test was 93%.

It had been the intention to monitor the instruments in the period in between these tests. Unfortunately, a site power-cut occurred two days after the first test and the associated power surge switched the data logger off. This was not discovered until the site team returned to site one month later to perform the second load test; the records between the two tests are therefore discontinuous.

8.1.2.2 Phase 2

Phase 2 of the testing programme was carried out in March and April 1990. Preparatory work included repairing the instruments affected by leaks in Phase 1, identifying and sealing all potential leak areas[2], re-calibrating all instruments and re-shotblasting the piles. No instrument malfunctioned at any stage of this phase.

---

[1]Lugs were provided to allow tightening of the steel casings with a C-spanner.

[2]An additional seal was positioned where the main cable loom enter the SST's.

(i) Pile BK3

Pile BK3 was installed to a depth of 3.15m and, as planned, load tested in compression after an equalisation period of just two hours (Test BK3(1)/L1C). The pile was then jacked on to a final penetration of 5.9m and re-tested in compression four days later (Test BK3(2)/L1C). This load test was performed at a rate slow enough to ensure that all excess pore pressures dissipated during loading. The rate of loading necessary to obtain this fully drained condition was about 20 times slower than used in all previous ICP tests. The test took more than 24 hours to complete.

(ii) Pile BK4

About 3 days later, pile BK4 was also installed to an initial depth of 3.15m, but this time the load test was performed after equalisation was essentially completed at $t_{eq} \approx 4$ days (Test BK4f/L1C).

A supplementary test was carried out to investigate the effect of the pile installation rate. The pile was jacked slowly (at a rate of ≈75mm/min[1]) to 5.95m and load tested in compression 2 days later (Test BK4s/L1C). The standard equalisation period of 4 days was not adopted in this case, as site mobilisation costs would have been excessive

A feature of the supplementary test (BK4s/L1C) was the untypical measurements made by instruments installed to depths of less than 4m. These were probably due to the long pause period allowed between the two installation phases (4 days) and are discussed separately in Section 10.5.2.

8.2 INSTALLATION

8.2.1 End resistance

The end resistances (q_b) recorded during jacking are shown on Figure 8.2. These measurements represent only 1% of the full scale output (FSO) of the base load cell and their absolute accuracy may not be sufficient to

[1]The standard jacking rate of 500mm/min was adopted in all other tests.

justify close comparisons between the different tests. However, some general observations may be made:

- q_b values are between 5 and 20 times smaller than those measured at Labenne and Cowden.
- End resistances decrease from ≈400kPa at 1.2m (just below the crust) to a minimum value of ≈275kPa at 2m before increasing slowly to reach ≈400kPa at 6m.
- Pile BK4s (installed at 75mm/min) shows more variability and on average mobilises q_b values that are 20% lower than those of all the other piles (installed at 500mm/min). A rate dependence of CPT end resistances (q_c) at Bothkennar was also observed (Powell 1992), but these tests showed that q_c differed by only ≈7% over the same rate intervals.
- The q_b and q_c profiles are similar, although q_b is typically ≈10% less than q_c. This is illustrated in Figure 8.9.

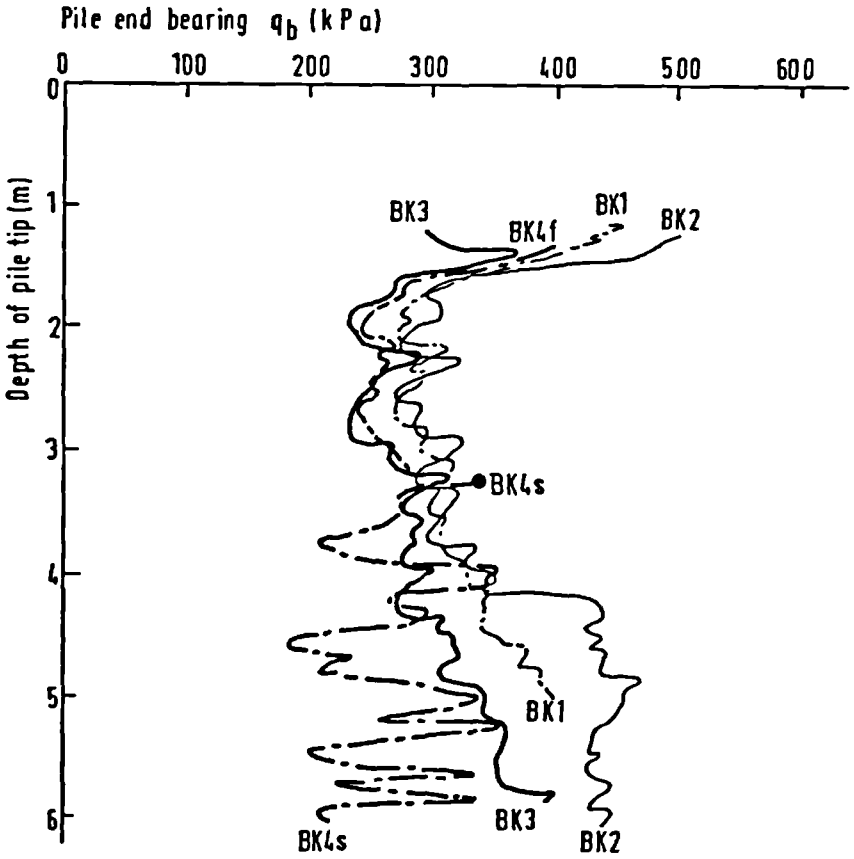

Figure 8.2 End resistance mobilised during jacking

8.2.2 Shaft resistance

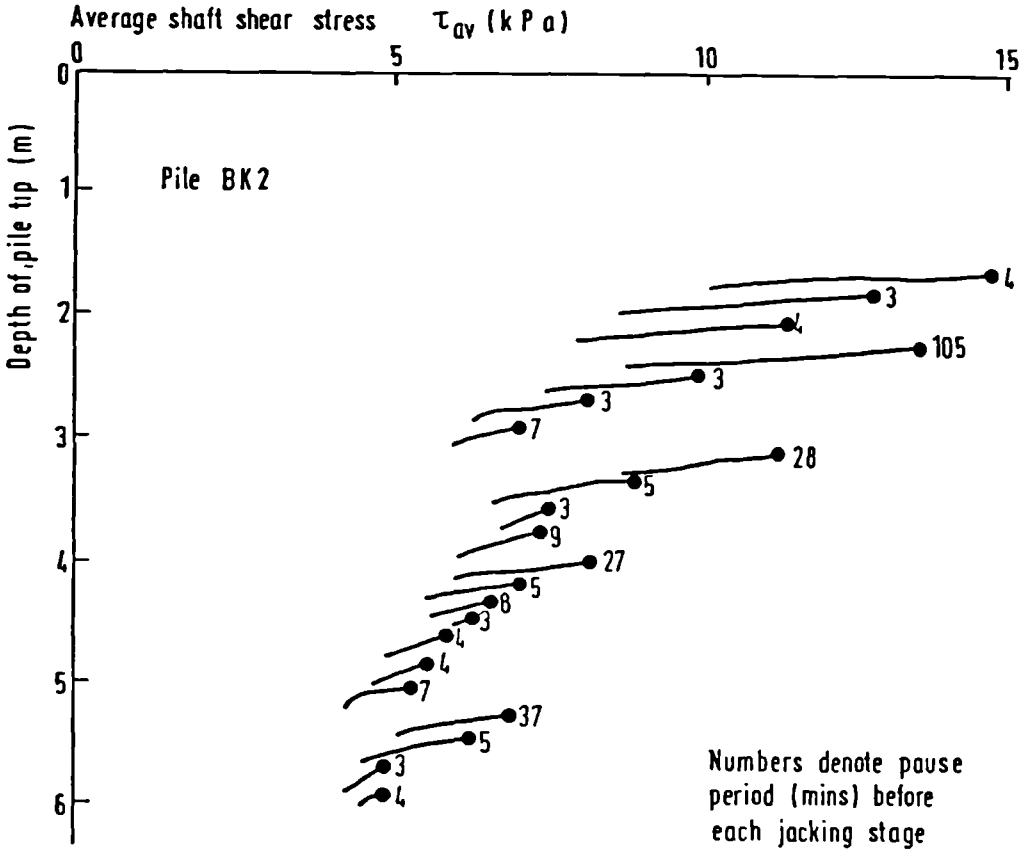

Figure 8.3 Average shear stresses mobilised by pile BK2 during jacking

The average shaft shear stresses (τ_{av}) measured during a typical pile installation (BK2) are shown on Figure 8.3. Two characteristic features, which contrast with those observed during installation at Cowden (see Figure 7.4), are evident:

- The resistance reduces steadily from a maximum at the start of a pile push (τ_{avp}) to a minimum (τ_{avu}) at the end of the push. A similar trend was observed during fast shearing pulses in ring shear tests (see Figures D13-D14, Appendix D).

- Considerably higher values of τ_{avp} are mobilised in jacking stages that were preceded by extended pause periods (of greater than ≈7

mins). Such increases in capacity with time are a well known characteristic of piles in soft clay (e.g. see Konrad & Roy 1987).

Although the peak shear stresses (τ_{avp}) increased with the length of the preceding pause period, the minimum resistances (τ_{avu}) tended towards a consistent lower bound envelope, as shown on Figure 8.4. τ_{avu} is practically constant for tip depths greater than ≈2m and remains within the range 4.5kPa to 6kPa for all pile installations. These data suggest that τ_{av} would tend to a lower limit of ≈4.5kPa if the piles were pushed continuously (with no pause periods) to their final penetration depth. Such a condition of 'steady' penetration is assumed by the Strain Path Method, when modelling the installation process (see Section 2.3)

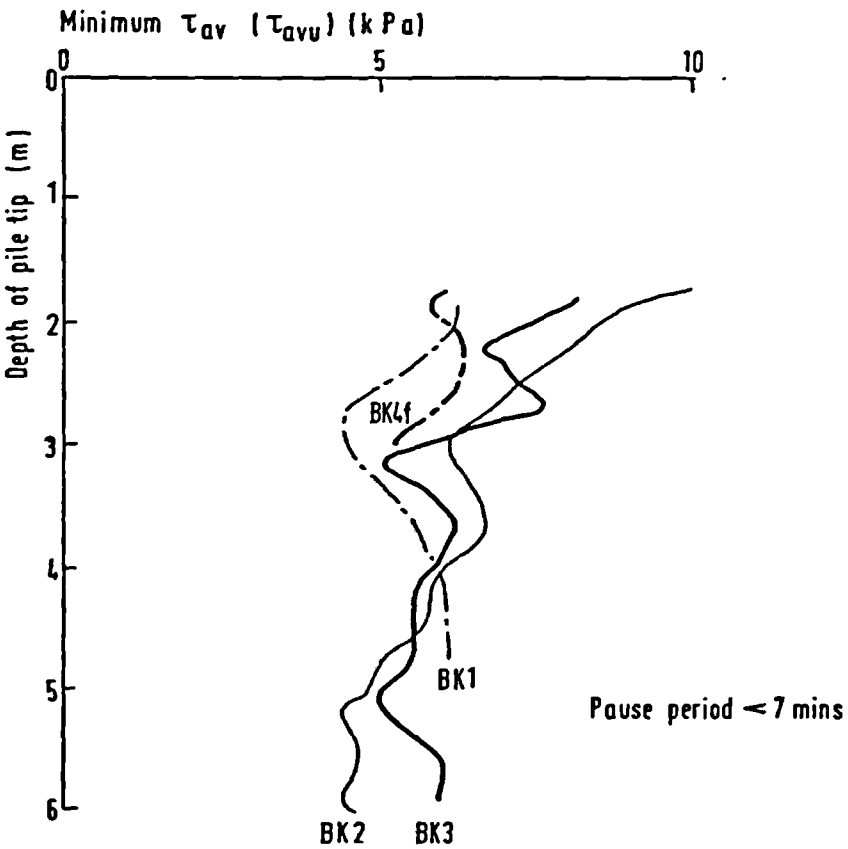

Figure 8.4 τ_{av} minima measured during jacking

The tendency for a strong positive set-up is explored further on Figure 8.5, which plots the variation of the peak shaft shear stress (τ_{avp}) mobilised in each jacking stage (normalised by the 'steady state' value, τ_{avu}) against the length of the pause period preceding that stage[1]. It is apparent that installation capacities increase by a factor of two after only 50 mins and a factor of about 3.5 after 6000 mins.

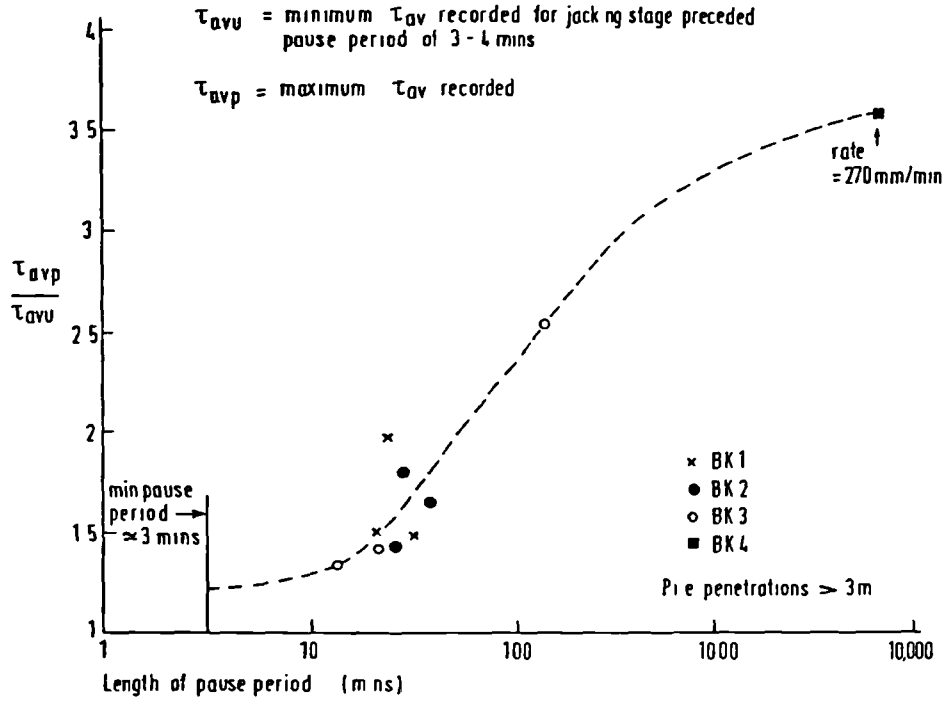

Figure 8.5 Effect of time on peak installation τ_{av} values

The corresponding variation of the mean peak installation α values are summarised in Table 8.3. These values were calculated using the c_{u0} values measured in UU tests on conventional 100mm diameter piston samples and would be ≈30% lower if the UU strengths from Laval samples were used for the calculations (see Table 5.8). α also showed a weak trend to reduce with pile penetration, but this was masked by the strong set-up effect.

[1]The data points plotted at 135 mins and 6000 mins are for the first pushes on piles BK3(2) and BK4s respectively. Note also that although the average jacking rate of pile BK4s was 75mm/min, its first push was carried out at 270mm/min.

Length of pause period (mins)	Installation α (τ_{avp}/c_{u0})
0 (steady state)	0.28
2 < t < 7	0.38
20	0.48
50	0.62
200	0.83
1000	1.01
7000	1.11

Table 8.3 Installation α values

8.2.3 Local shear stress

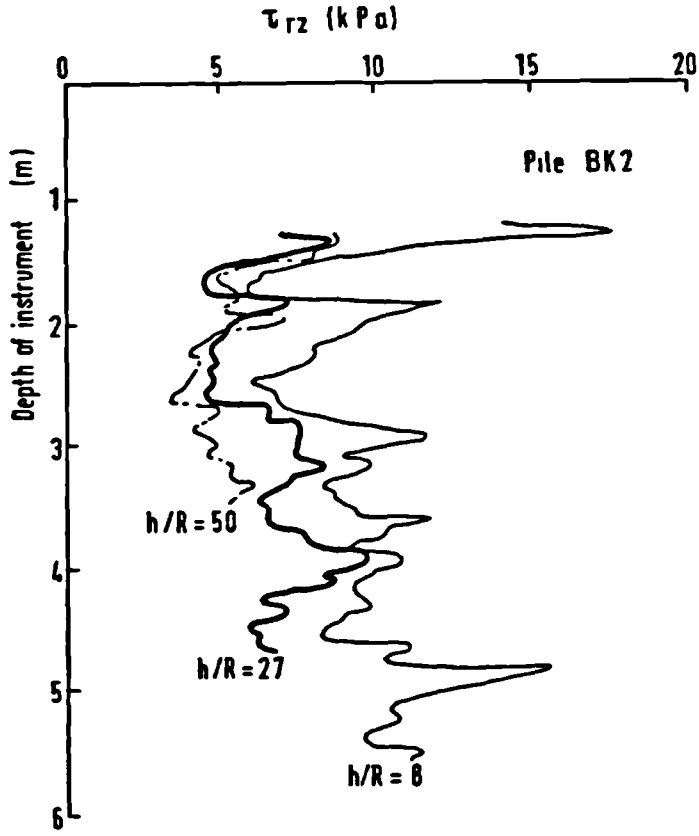

Figure 8.6 Local shear stresses developed during jacking of BK2

The local shear stresses recorded by the SST's (τ_{rz}) during a typical pile installation (BK2) are shown on Figure 8.6. The sharp peaks in the traces

correspond to measurements obtained at the start of jacking stages that were preceded by a pause period exceeding ≈7 mins. When these peaks are discounted, two distinctive features for the remaining 'steady penetration' data become evident:

- Stresses recorded by the leading instrument (h/R=8) are about 20% higher than the corresponding measurements made by the following instrument (h/R=28) *in the same soil horizon*; τ_{rz} values recorded at h/R=50 are comparable to those at h/R=28.
- τ_{rz} measured at each instrument position increases slowly with depth in a comparable fashion to the c_{u0}, q_b and q_c profiles at the site.

8.2.3.1 Rate effects on shear stress

An assessment of the effects of the jacking rate on installation resistance may be made using Figure 8.7 which compares the τ_{rz} values recorded during penetration of pile BK4s (at 75mm/min) with those for the standard rate of 500mm/min. Only stresses below ≈4m (referred to as 'virgin ground') are compared, as the data at shallower depths on BK4s were affected by the 4day equalisation period that preceded its installation from 3.15m (see Table 8.1 & Section 10.5.2).

Inspection of Figure 8.7 shows no clear pattern:

- Close to the tip (at h/R=8), the slow-jacked pile initially mobilises higher τ_{rz} values. However, as installation progressed, the 'slow' and 'fast' data converged.
- Further from the tip (at h/R=27), the 'slow' τ_{rz} values are ≈20% higher than the equivalent measurements at the standard rate.

During installation of the piezo-lateral stress cell in Boston Blue Clay, Morrison (1984) observed that after a long equalisation period, untypically high radial and shear stresses were recorded temporarily as soon as the instruments entered 'virgin' ground. With continued penetration, stresses decreased to values measured during normal steady penetration. Morrison attributed this unexpected response to the

development of a densified 'clay cake' on the pile shaft during the consolidation period and suggested that the subsequent measurements were not representative of those acting on the principal displacement shear.

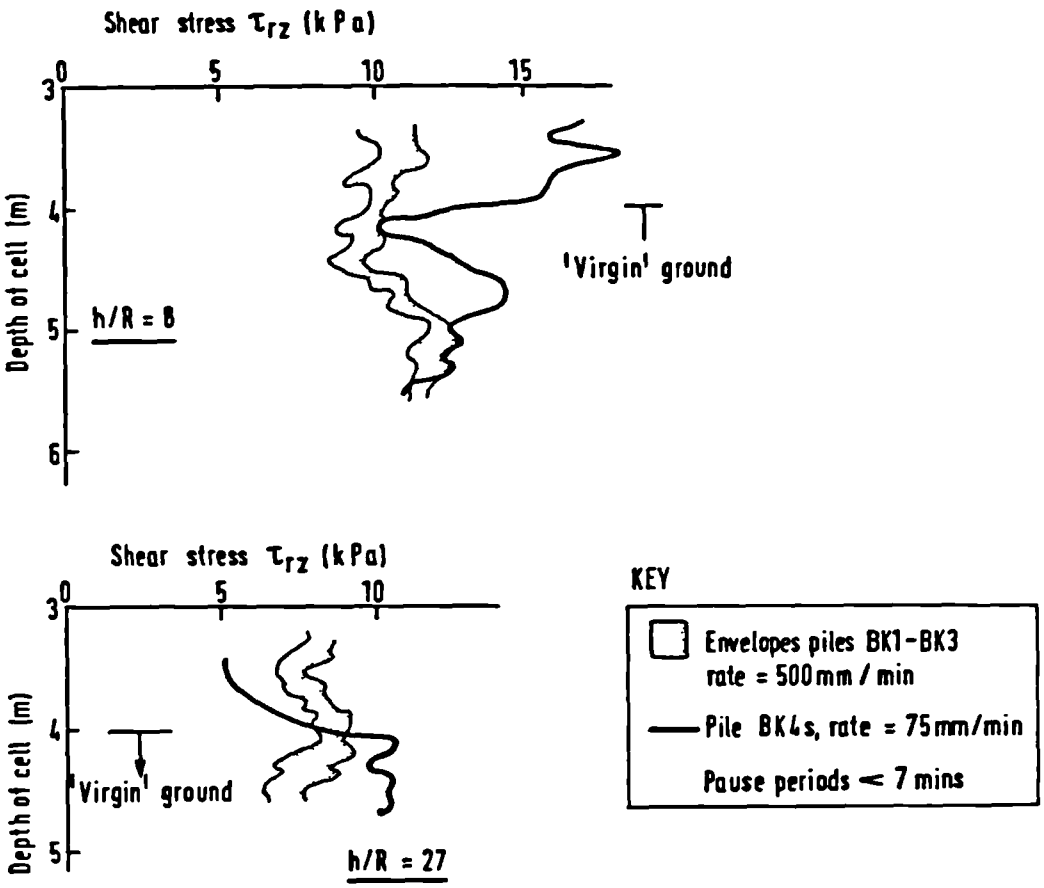

Figure 8.7 Rate effect on local shear stresses

The stresses recorded by pile BK4s also exhibited these features (note also the uncharacteristic σ_{r1} measurements between 4 and 5m on Figure 8.8b) and it seems that an assessment of the rate effects on shear stress can only be made using data recorded below ≈5m, when stresses on pile BK4s appeared to return to 'steady state' penetration values. These stresses are comparable to those measured at the fast installation rate and it is therefore suggested that there is <u>not</u> a strong rate effect on shear stresses at jacking rates between 75mm/min and 500mm/min. This apparently weak rate dependence is in sharp contrast to that seen at Cowden, where τ_{rz} differed by a factor of ≈2 over the same rate interval.

Ring shear tests on Bothkennar clay showed that the shearing resistance almost halved when the rate was increased from 80mm/min to 500mm/min. Lemos & Vaughan (1992) postulated that this *negative* rate effect relies on rapid changes in water content taking place in the shear zone. It is surmised that the absence of a such a strong effect in the pile tests is because the drainage boundary is remote from the shear zone.

8.2.4 Radial total stress

The radial total stresses (σ_{rt}) recorded during a typical pile installation (BK2) are shown on Figure 8.8a and envelopes of the measurements made in all Bothkennar installations are shown on Figure 8.8b. The following observations are made:

- Stresses recorded by instruments at the same depth and distance from the pile tip agree to within 10kPa.

- The σ_{rt} traces increase linearly with depth below ≈2.5m and show a similar dependence on the instrument position (h/R) to the local shear stress records. Measurements made by the following instruments (at h/R=28) are typically 20% less than those measured in the same soil horizon by the leading instruments (at h/R=8). The records at h/R=28 and h/R=50 are comparable, suggesting that σ_{rt} values are relatively insensitive to h/R for h/R ≥28.

- σ_{rt} values between 4 and 5m on pile BK4s are untypically high. As discussed in Section 8.2.3, this response may have been caused by the long pause period (4 days) preceding installation of this pile.

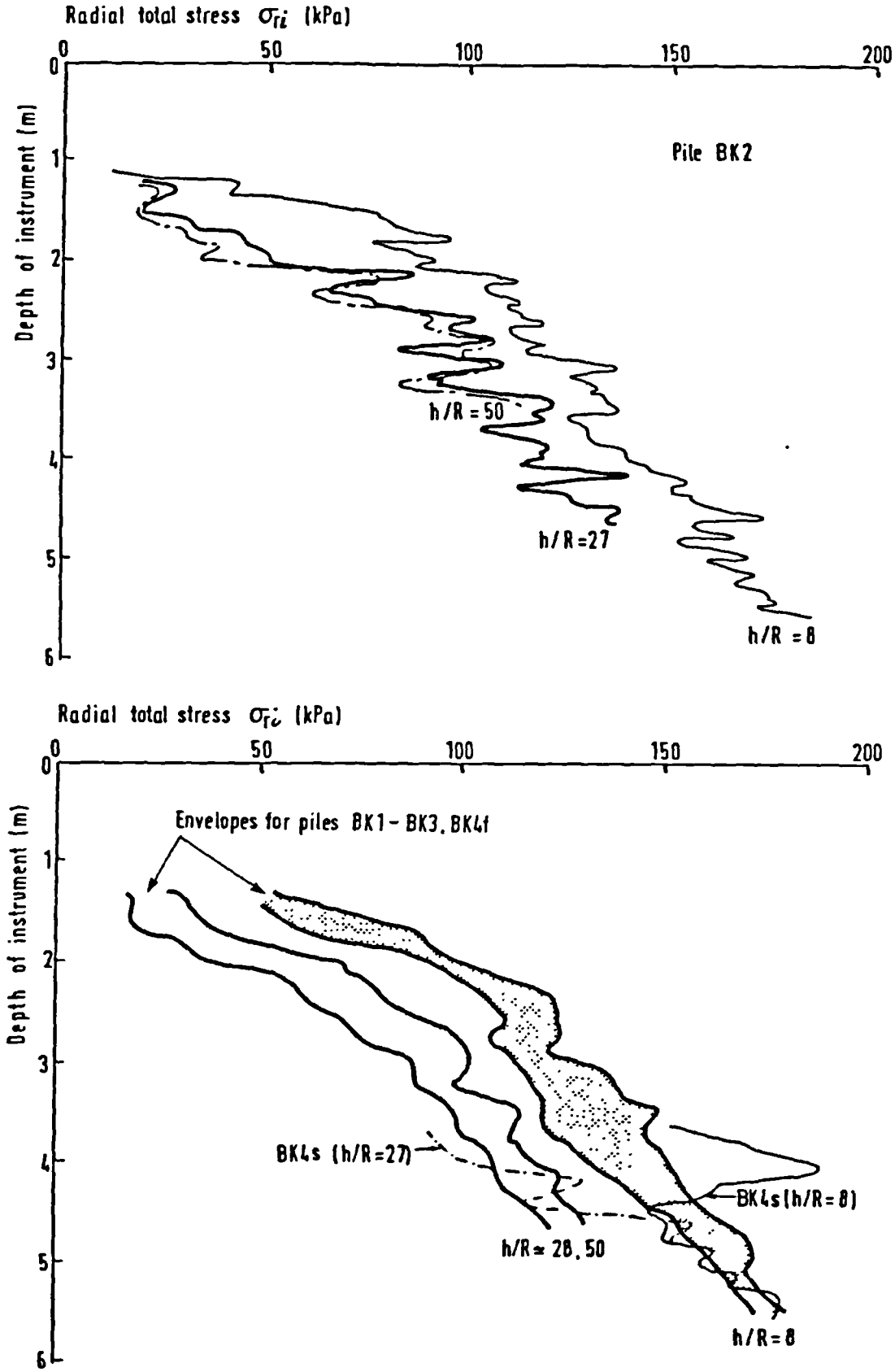

Figure 8.8 Radial total stresses recorded during installation

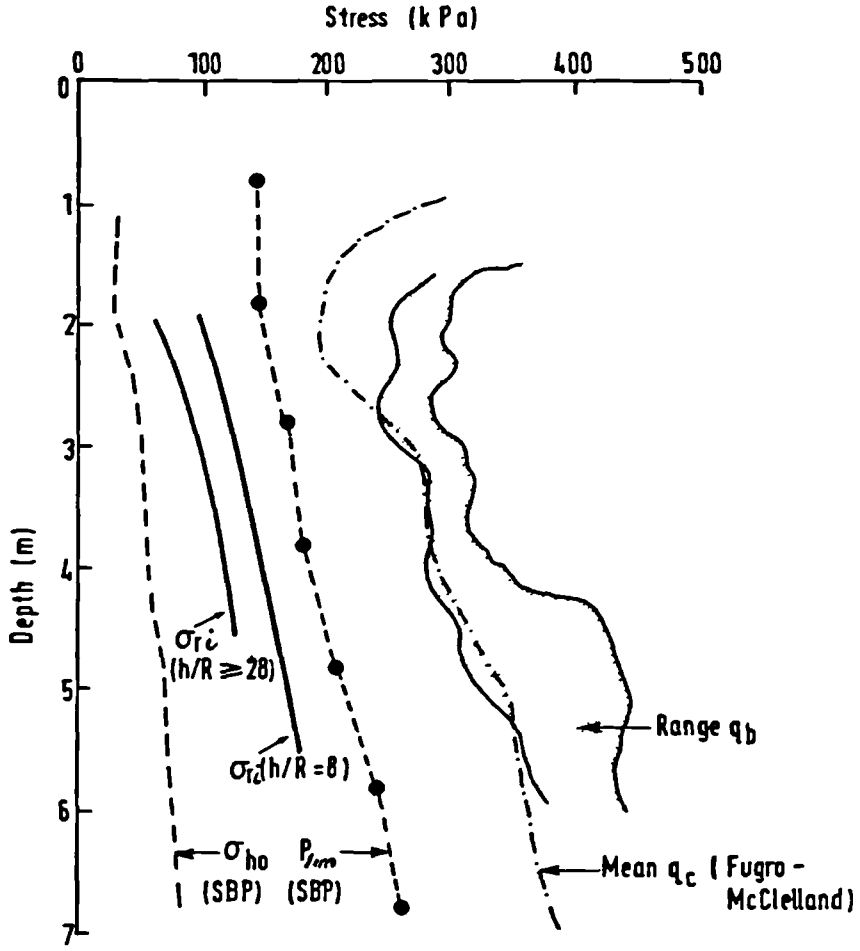

Figure 8.9 Comparison of σ_{ri} with q_b, q_c, p_{lim} and σ_{h0}

As shown on Figure 8.9, the σ_{ri} profiles lie between the initial undisturbed horizontal stress (σ_{h0}) and pressuremeter limit pressure (p_{lim}). The mean ratios of σ_{ri} to σ_{h0}, p_{lim} and the pile end bearing pressure (q_b) are listed in Table 8.4.

h/R	σ_{ri}/q_b	σ_{ri}/p_{lim}	σ_{ri}/σ_{h0}
8	0.44	0.78	2.55
28	0.33	0.60	2.00
50	0.30	0.54	1.85

Table 8.4 Normalised σ_{ri} values

8.2.5 Pore pressure

The individual traces recorded by the pore pressure probes during installation of pile BK2 are shown on Figure 8.10; the results from all the tests are summarised on Figure 8.11.

The records show four main characteristics:

- Pore pressures reduce significantly at the beginning of each pile push. The reductions are typically 50kPa at h/R =5 and 25kPa at h/R ≥ 30 and appear to be more pronounced at depth.

- On the completion of each jacking stage, the pore pressures increase rapidly to reach temporary maxima (u_s) within ≈1 min. This response suggests that steep pore pressure gradients exist between the pile surface and the surrounding soil mass during jacking.

- The u_s measurements are very consistent. The records for instruments at the same depth and h/R all agree to within ≈10kPa. The pore pressures measured when the piles are moving (u_m) show more variability, but generally agree to within 20kPa.

- Both u_s and u_m increase with depth and reduce with h/R, but only up to h/R =30. Strong hydraulic gradients near the pile tip may be inferred from the piezocone tests performed at Bothkennar (Figure 5.22), which recorded pore pressures at h/R=1 that were almost double the values of u_s measured at h/R=5 on the piles[1].

The pore pressures recorded during slow jacking of pile BK4s (at 75mm/min) are compared with the measurements made by fast-jacked piles on Figure 8.11. This comparison reveals no clear rate effect, such as that seen at Cowden.

---

[1]The Strain Path Method predicts that the magnitudes of the pore pressures developed at the shaft of a pile/penetrometer are independent of its radius (see Section 2.3).

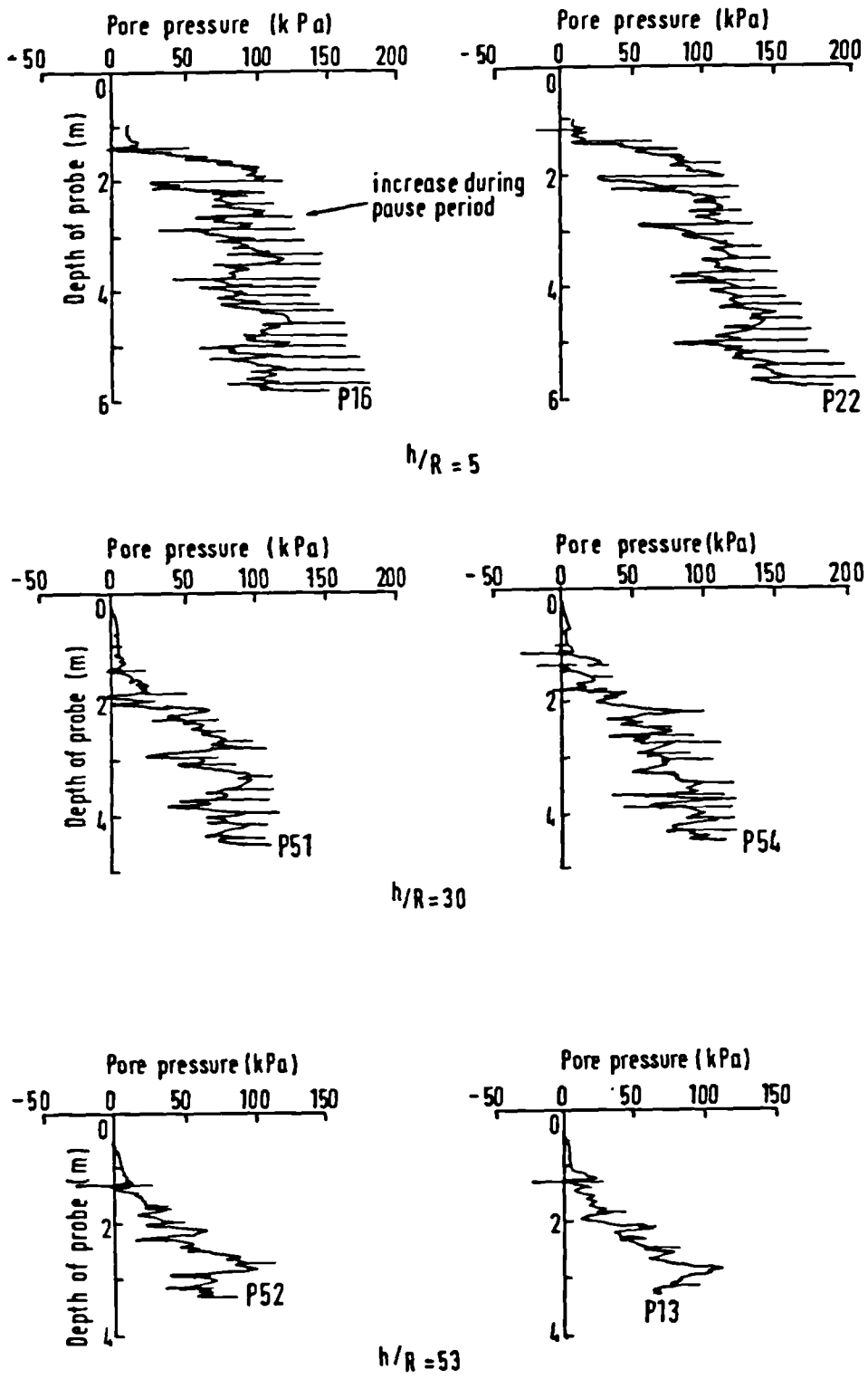

Figure 8.10 Installation pore pressures recorded by BK2

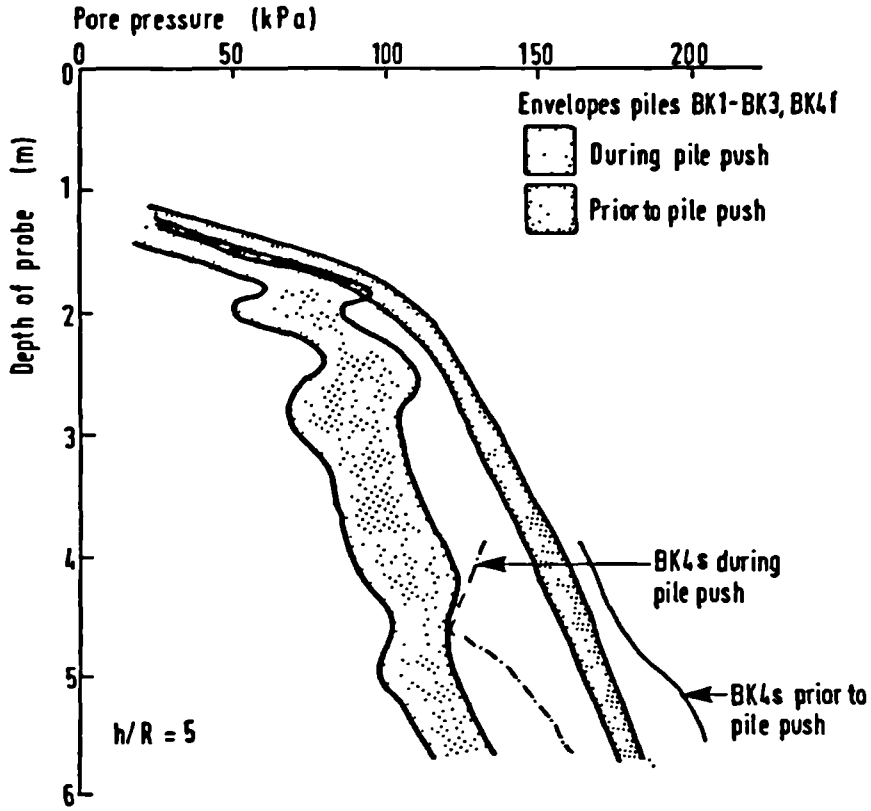

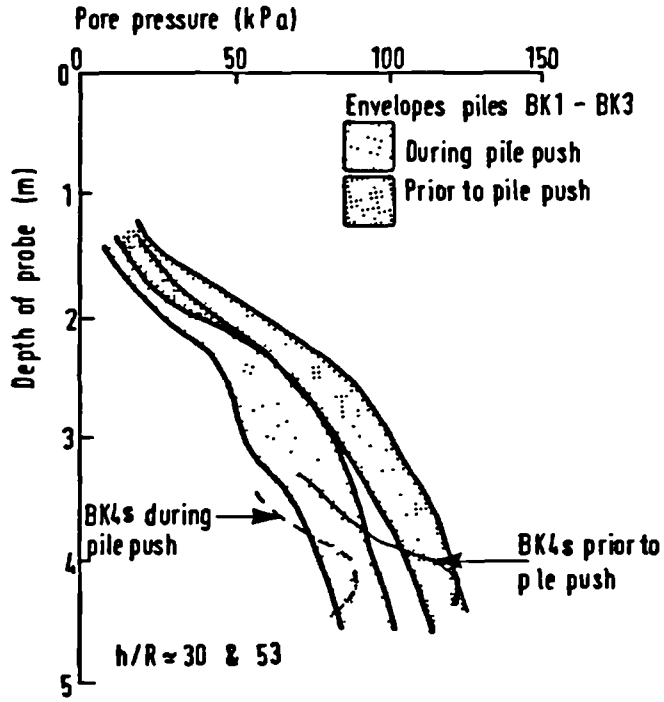

Figure 8.11 Envelopes for installation pore pressures

8.2.6 Radial effective stress

The mean values of the radial effective stresses recorded during installation of all piles are presented on Figure 8.12 in terms of the normalised radial effective stress ratio K_i ($=\sigma'_{ri}/\sigma'_{v0}$).

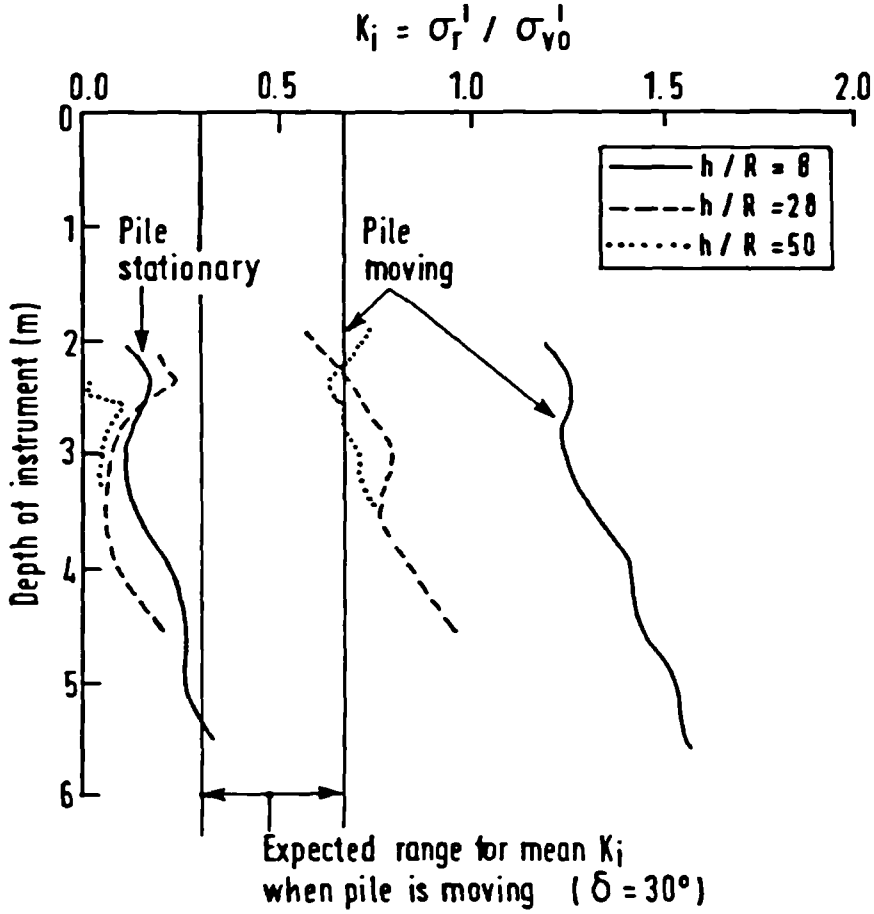

Figure 8.12 Mean σ'_r values recorded during installation

K_i increases moderately with depth and reduces with h/R. Values measured during jacking stages range from 0.5 to 1.55. However, after the pile comes to rest (as pore pressures rise rapidly), K_i reduces to values less than 0.3. These at rest K_i ratios are significantly smaller than the initial undisturbed lateral stress coefficient ($K_0 \approx 0.55$).

Angles of interface friction (δ) of $\approx 30°$ were measured during slow shearing stages in ring shear interface tests (Section 5.3.12) and in pile load tests (Section 8.4). Figure 8.12 shows the expected range for

K_1, assuming that the same angle operates during jacking[1]. This range is compatible with pore pressure values which are *between* those measured when the pile is moving (u_m) and the peak stationary values (u_s); see Table A4, Appendix A.

Anomalous K_1 ratios were also measured at Cowden. Based on evidence presented in Section 8.4 and Appendix A, it is surmised that the discrepancy arises because the pore pressures recorded when the pile is moving at velocities in excess of ≈1mm/min are not representative of those present within the failing shear zone adjacent to the pile.

8.3 EQUALISATION

8.3.1 General

First-time load tests were performed after periods ranging from 2 hours to 4 days. This section presents typical plots showing how pore pressures, radial total stresses, radial effective stresses and residual pile loads varied during these equalisation periods.

Table 8.5 lists the equalisation periods (t_{eq}) and the average degree of excess pore pressure dissipation (U) achieved for each pile. The complete set of equalisation data is summarised in Table 8.8 on page 314.

Pile	Tip depth (m)	t_{eq} (mins)	U (%)
BK1	6.00	1200	60
BK2	6.00	6000	84
BK3(1)	3.15	120	28
BK3(2)	5.90	5600	88
BK4f	3.15	6000	90
BK4s	5.95	2650	79

Table 8.5 Equalisation times at Bothkennar

[1] $K_1 = \tau_{avp} / [(\sigma'_{v0})_{mean} \tan 30°]$

It is evident that the standard 4 day period (5760 mins) allowed ≈87% of excess pore pressures to dissipate; the reasons for load testing before 4 days are given in Section 8.1.

8.3.2 Pore pressure

The detailed pore pressure response during equalisation is illustrated using data for pile BK2. Data recorded during the last jacking stage and over the full equalisation period for this test are shown on Figure 8.13a, whilst the full spread of measurements made with all the piles is summarised on Figure 8.13b.

General points to note include:

- The consistency of the records increased with time after the end of jacking. Traces from opposing probes mounted in the same instrument cluster differed by up to 40kPa while the pile was moving, but generally agreed to ≈10kPa within 10 mins of the end of jacking.
- Pore pressures rise rapidly when the pile stops moving (as they did during installation pause periods), reaching a maximum in typically less than 1 min. These maxima showed the same dependence on depth and h/R as the installation u_s values i.e. they increased with depth and reduced with h/R.
- Significant pore pressure dissipation begins to occur (at the pile shaft) after ≈20 mins. Pressures fall in a systematic fashion and after 4 days are within 20kPa of their nominal hydrostatic values.

The mean variations with time of U_d $[=(u-u_0)/(u_{max}-u_0)]$ for all the piles at the three instrument positions are given on Figure 8.14 and show that the average time for 50% of excess pore pressures to dissipate is ≈750 mins.

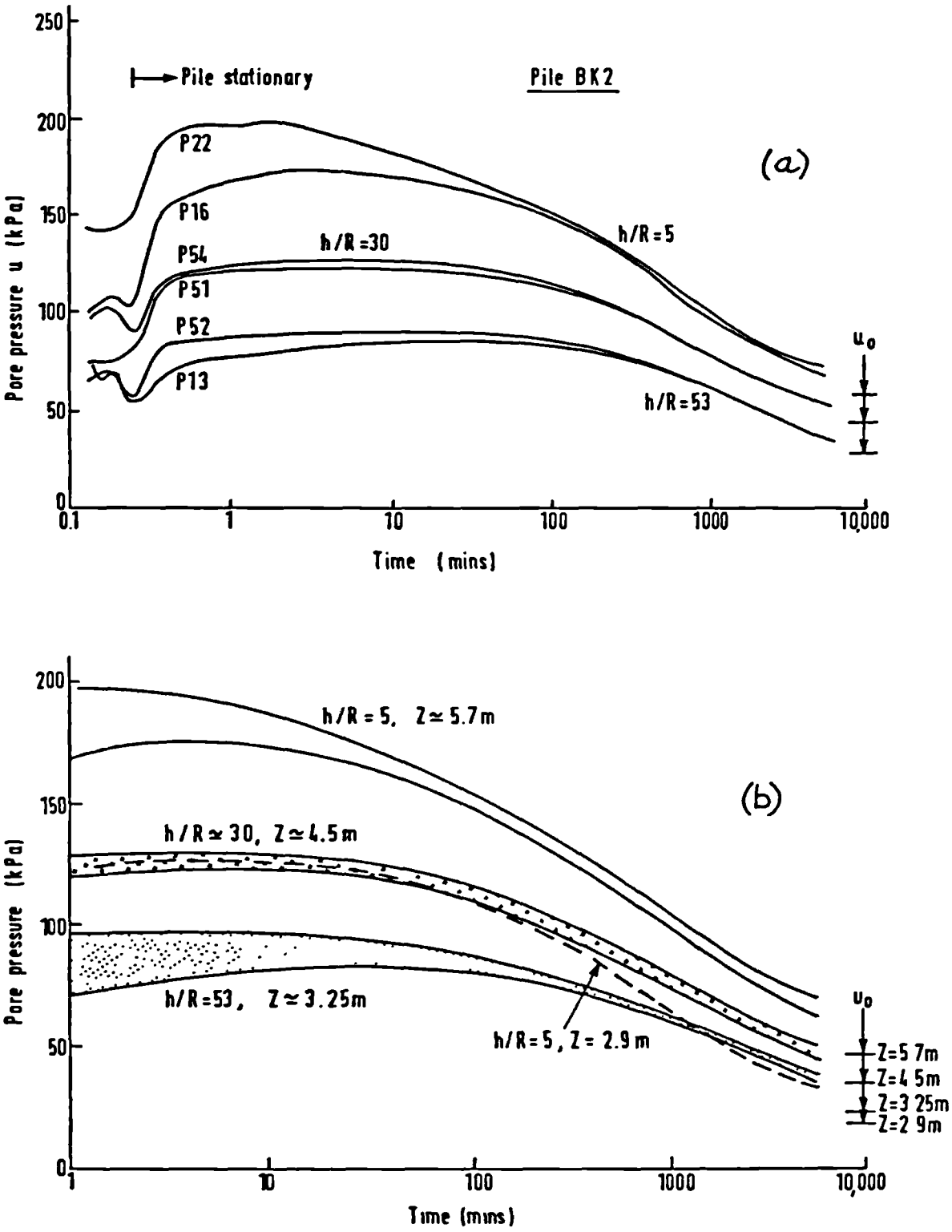

Figure 8.13 Pore pressures recorded during equalisation

Figure 8.14 also shows that:

- Local variations in soil permeability and compressibility are not significant, as similar dissipation curves are measured by instruments positioned at the same distance from the pile tip (h/R=5), but installed to different depths (2.9m and 5.7m).
- Dissipation rates vary with h/R; dissipation at h/R=53 is about twice as slow as that at h/R=5 and about seven times slower than at h/R=1 (i.e. measured in piezocone dissipation tests). This trend reflects the three dimensional drainage conditions near to the tip (e.g. see Houlsby & Teh 1988)

Pore pressure dissipation is discussed further in Chapter 10.

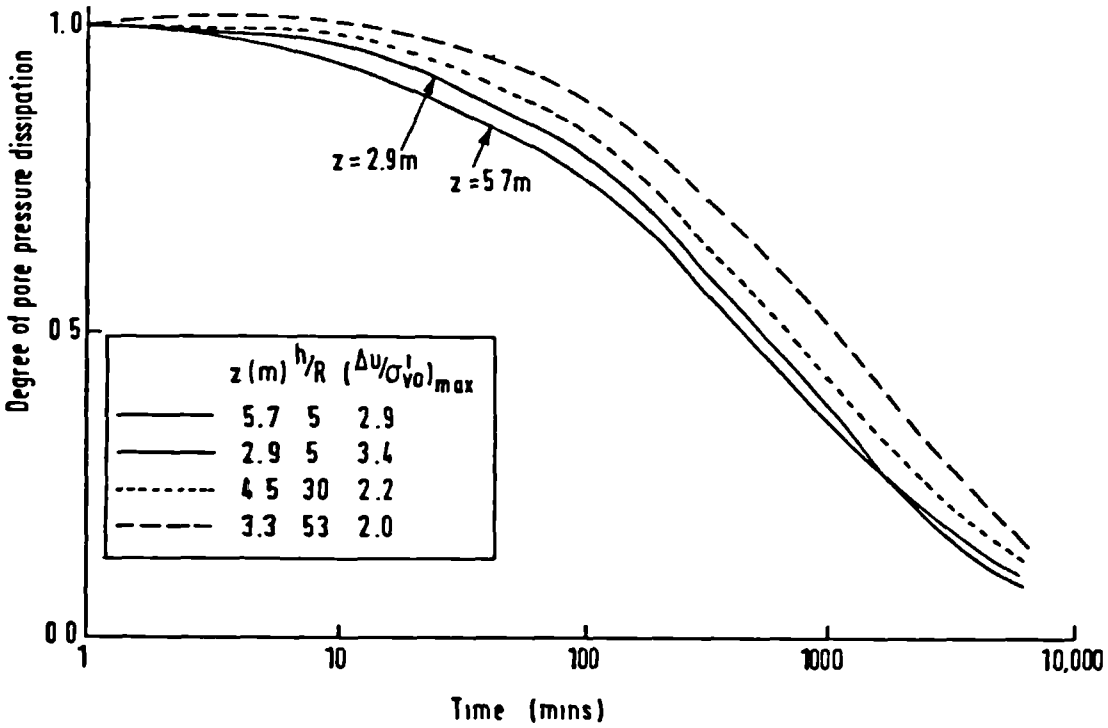

Figure 8.14 Mean variations of U_d at each instrument position (h/R)

8.3.3 Radial total stress

As at Cowden, radial total stresses reduced during equalisation. These reductions are summarised on Figure 8.15 for all piles and instrument positions by plotting the variation of H/H_i $[=(\sigma_r-u_0)/(\sigma_{ri}-u_0)]$ with time.

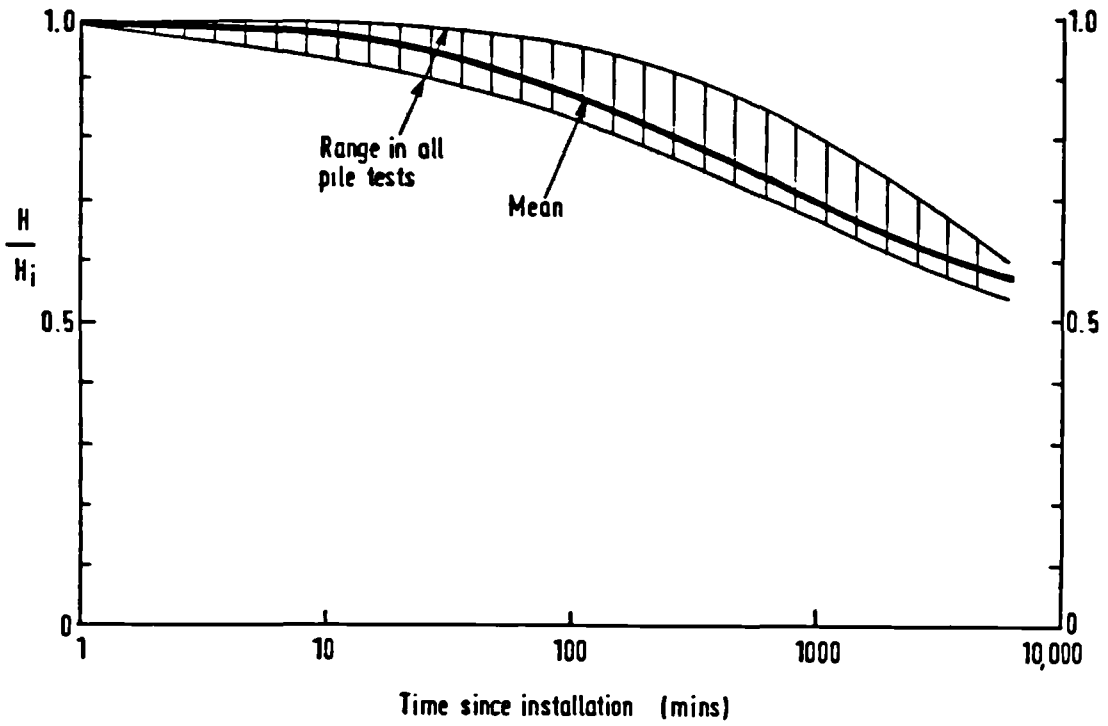

Figure 8.15 Normalised radial total stress variation during equalisation

H/H_i reduced throughout equalisation in a similar way at *all* instrument positions and attained a value of 0.57 ± 0.04 after four days. This H/H_i value is significantly smaller than the corresponding ratio measured at Cowden, but is consistent with observations made in other instrumented pile tests in soft clay e.g. Azzouz & Morrison (1988). As will be seen later, H/H_i reduced to a final value of 0.44 ± 0.04 after *all* excess pore pressures had dissipated (i.e. $H_c/H_i = K_c/H_i = 0.44$)

8.3.4 Radial effective stress (σ'_r)

8.3.4.1 Changes in σ'_r prior to load testing

The changes in pore pressure and radial total stress during equalisation, discussed above, lead to the variations of radial effective stress (σ'_r) with time shown on Figures 8.16-8.17. Each plot summarises the trends seen at a particular instrument position.

σ'_r reduces over the first minute after installation. These reductions are due to the rapid increases in pore pressure observed over the same time period and are such that when the σ_r and u measurements at the leading instrument cluster are combined, apparent σ'_r values of *less than zero* are calculated. As noted in Section 8.2.5, the hydraulic gradients near the tip are particularly steep and this anomaly most probably arose because the pore pressure sensors were located closer to the pile tip (at h/R=5) than were the radial stress sensors (at h/R=8).

The values of σ'_r calculated for the following and trailing clusters were in some instances also less than zero shortly after installation. Karlsrud & Haugen (1985) report similar observations in the sensitive clay at Haga. It thus appears necessary for the accurate evaluation of low radial effective stresses to measure σ_r and u at exactly the same location.

After reaching temporary minima in ≈1 min, radial effective stresses increase with time and tend to constant values after ≈4 days. Most of the significant changes occur within the first 1000 mins after installation.

The uncharacteristic variation of radial effective stress shown at h/R=50 on pile BK4s (Figure 8.17b) was most probably related to the disturbance caused by the earlier installation phase of pile BK4f and is discussed in Section 10.5.2.

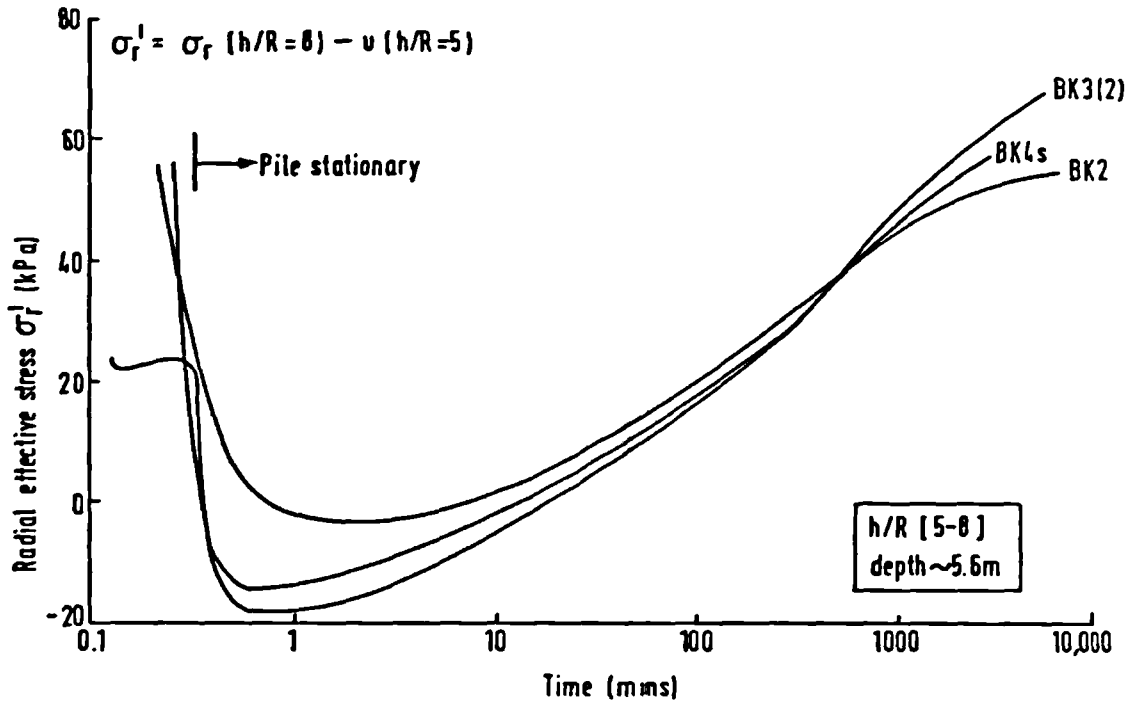

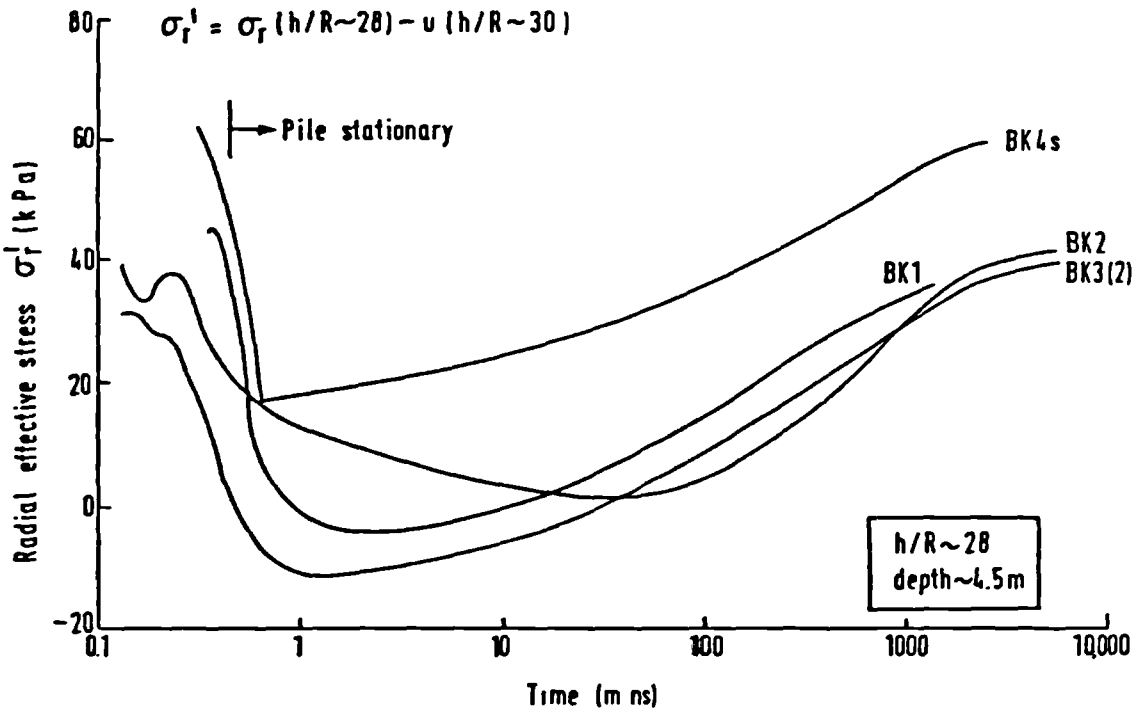

Figure 8.16 σ'_r traces during equalisation (1)

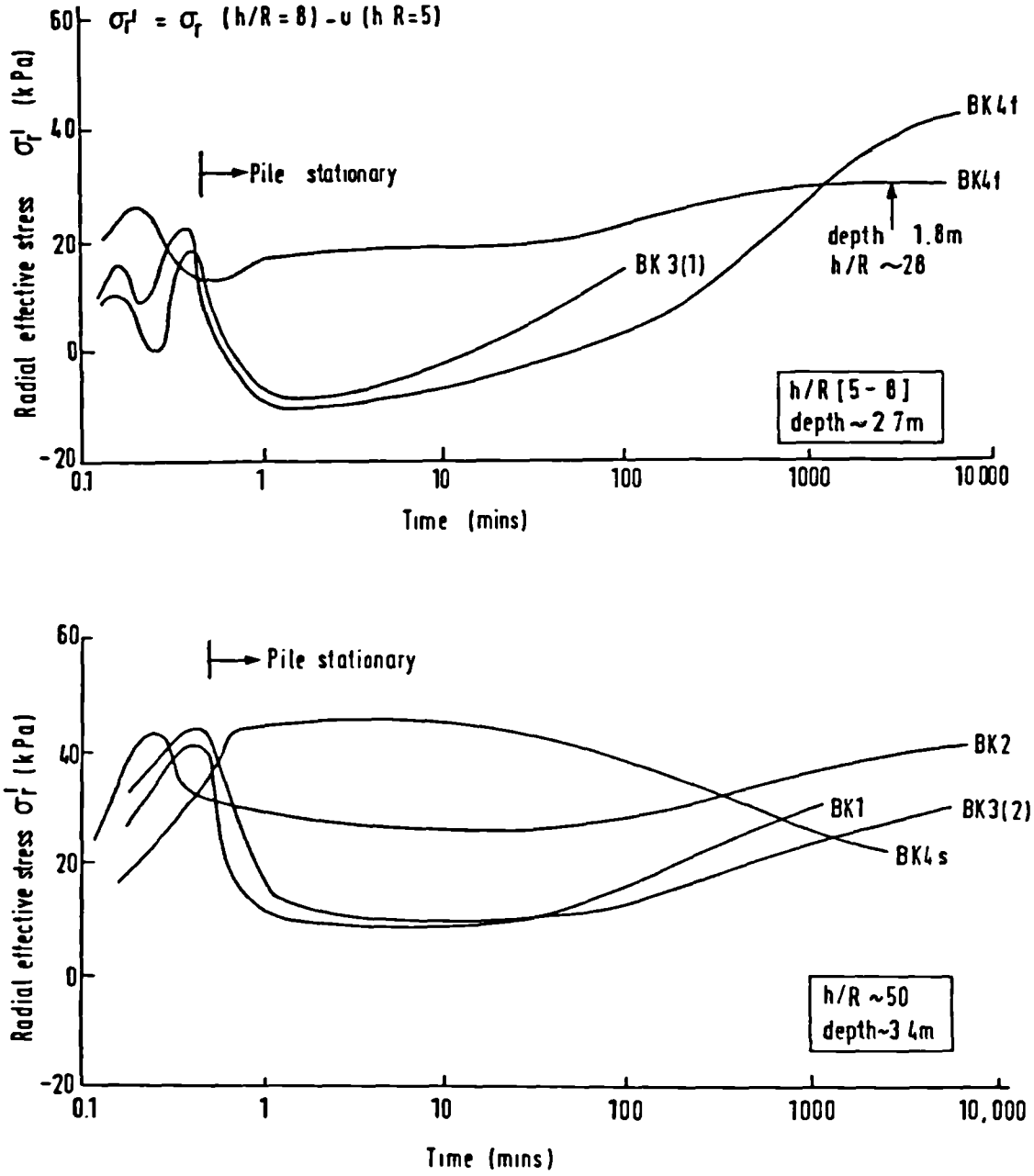

Figure 8.17 σ'_r traces during equalisation (2)

8.3.4.2 Long term variations in σ'_r

Pile BK2 was monitored for 32 days after its initial load test at t_{eq} ≈4 days. The records obtained with this pile may be used to assess the long term characteristics of the equalisation process, if it is assumed that the initial load test did not affect the subsequent long term measurements significantly[1].

The data recorded at t_{eq} =4 days and t_{eq} =36 days are summarised in Table 8.6. Using trends shown in load tests, discussed in Section 8.4, anticipated σ'_r values at t_{eq} = 36 days have been inferred from the shear stresses mobilised in the re-test performed at this time. These 'inferred' σ'_r values are also listed in Table 8.6.

Inst.	t_{eq} = 4days			t_{eq} = 36 days				
	σ_r	u	σ'_r	σ_r	u	σ'_r (meas)	σ'_r (inferred)	u_0
h/R=8	123	67	56	107	53	54	54	46
h/R=28	93	52	41	70	41	31	38	37
h/R=50	74	36	38	NM[2]	28	NM	37	25

Table 8.6 Long term monitoring of BK2 (stresses in kPa)

It may be seen that excess pore pressures reduce from an average of ≈18kPa at t_{eq} ≈4 days to ≈7kPa at t_{eq} ≈36 days. This slow dissipation rate is consistent with the predictions for pile equalisation (using coupled consolidation analyses), which show that surprisingly large time factors are required to restore hydrostatic conditions (e.g. see Whittle 1991).

No significant change in σ'_r occurred at h/R=8 as the pore pressure reduction was matched by a similar reduction in σ_r. However, σ'_r appeared to reduce by 10kPa at h/R=28, although the inferred final σ'_r value is

[1]As will be seen later, load testing of this pile caused the radial total stress to reduce by only ≈2kPa.

[2]This σ_r value was not measured (NM) because of an instrumentation problem (see Section 8.1).

comparable to that at t_{eq} = 4 days. It is suggested that this reduction is due to instrument drift.

In summary, based on (i) the direct measurements of σ'_r, (ii) the trends deduced from the re-test of pile BK2 and (iii) the general shape of the "σ'_r v time" plots on Figures 8.16-8.17, it is concluded that the radial effective stresses were very close to their fully equalised values after 4 days and subsequent reductions in pore pressure were comparable to reductions in radial total stress.

8.3.4.3 Equalised σ'_r values

The profiles of radial effective stresses acting on the piles prior to their first-time load tests (σ'_{r1}) are shown on Figure 8.18a. These traces show a general trend to increase with depth and indicate that higher stresses are developed on the shorter pile (BK4f). However, this plot is complicated by the different equalisation periods (t_{eq}) adopted for each of the piles.

Tests on piles BK1 and BK4s were performed after equalisation periods of ≈0.8 and 1.8 days respectively. The σ'_r measurements for these piles were (tentatively) extrapolated[1] to t_{eq} =4 days from their "σ'_r v time" plots on Figures 8.16-8.17 and shown on Figure 8.18b in conjunction with the σ'_{r1} values recorded at t_{eq} =4 days by the other piles. These profiles may be considered (to an acceptable accuracy) to be equivalent to fully equalised radial effective stress (σ'_{rc}) profiles. It should be noted that the measurements made by pile BK4s between 3.5m and 5m have been excluded from this figure, as these were affected by the 4 day pause period that preceded its installation from 3.15m to 6m (see Section 8.2.3).

[1]As most of the increases in σ'_r occurred in the first 1000mins after installation, these extrapolations amounted to a σ'_r increase of less than $0.2\sigma'_{r1}$ for both piles (see Table 8.8).

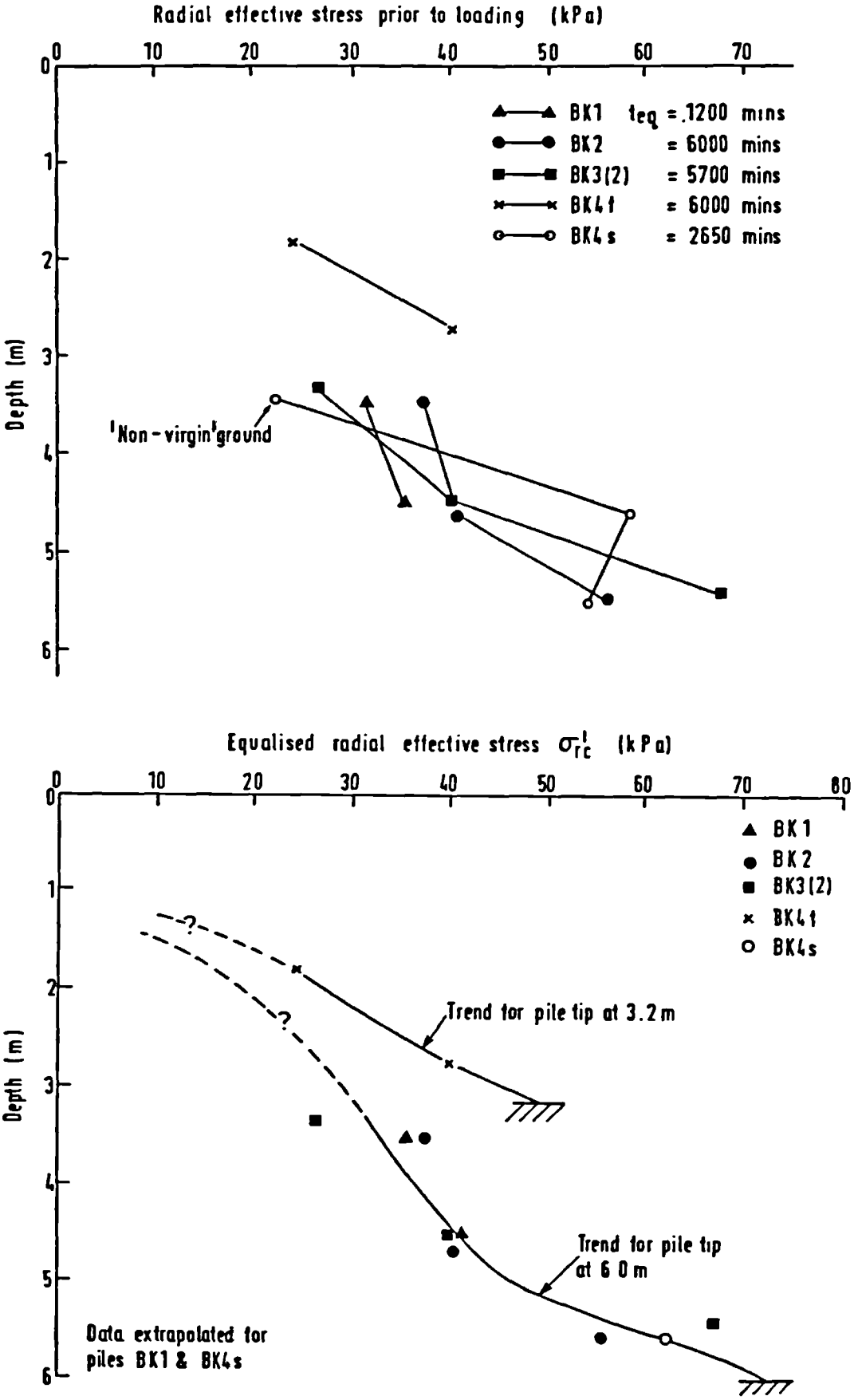

Figure 8.18 Profiles of σ'_{rl} and σ'_{rc} with depth

The σ'_{rc} values are consistent and increase with depth for the two pile lengths considered. In addition, it is evident that stresses developed *in the same soil horizons* on the shorter pile are larger than those acting on the longer pile, indicating that σ'_{rc} reduces with the distance from the pile tip (h/R).

h/R	L/R=120	L/R=64
5	1.41	1.42
10	1.34	1.33
20	1.06	1.12
30	0.98	-
50	0.95	-

Table 8.7 K_c values at Bothkennar

The σ'_{rc} trend lines are summarised in Table 8.7 in terms of the normalised equalised effective stress ratio K_c ($=\sigma'_{rc}/\sigma'_{v0}$) and indicate that K_c is controlled most strongly by the relative depth of the pile tip (h/R). Piles installed to different depths show the same variation of K_c with h/R, even though there are variations in the c_u/σ'_{v0} and OCR profiles over the respective sections of the soil profile (see Figure 5.26). The steepest variations in K_c are found for h/R < 30.

These trends are similar to those shown by the radial total stresses recorded during installation (σ_{ri}). This similarity arises because the relaxation coefficient, K_c/H_i [$= \sigma'_{rc}/(\sigma_{ri}-u_0)$], was virtually independent of h/R. As shown in Table 8.8, K_c/H_i ($=H_c/H_i$) was typically 0.44 ± 0.04.

8.3.5 Residual pile stresses

The local shear stresses (τ_{rz}) measured immediately after installation and at t_{eq} =4 days for piles installed to ≈6m depth are shown on Figure 8.19. Profiles with depth for both sets of measurements are shown; these also incorporate the trends of the axial load cell data.

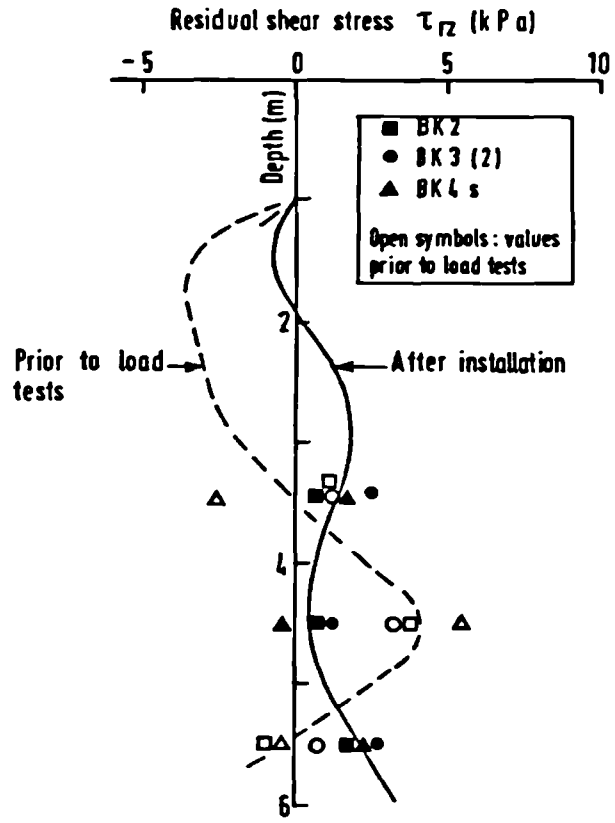

Figure 8.19 Residual pile stresses at Bothkennar

It is evident that, at the end of installation, small residual shear stresses of ≈2kPa acted upwards on the pile shaft to support the weight of the pile and a small amount of negative friction near the pile head. However, during equalisation, negative residual shear stresses of up to 5kPa were developed over the top of the piles. These were probably caused by vertical consolidation of the soil layers, associated with excess pore pressure dissipation, and were opposed by positive shear stresses between 3.5 and 5m. Further negative stresses were developed near the pile base.

These profiles show interesting characteristics which are a function of the relative stiffnesses in the system and the degree of equalisation. Parametric studies performed by Whittle & Baligh (1988) and Whittle (1991) on the effect of residual stresses on pile capacity in low OCR clays suggest that the stresses at Bothkennar were sufficiently low to have no effect on the subsequent static shaft capacity.

Pile	t_{eq} (mins)	z (m)	h/R	H_i	u_{max}	u_l	σ'_{rl}	U_d	σ'_{rc}	K_c	K_c/H_i
BK1	1200	5.6	8	-	-	-	-	-	-	-	-
		4.6	28	2.13	128	73	35.0	0.40	41.3	0.99	0.46
		3.5	50	1.88	85	54	31.0	0.48	36.0	1.02	0.54
BK2	6000	5.6	8	2.83	188	67	56.0	0.14	56.0	1.18	0.42
		4.7	27	2.38	126	52	40.7	0.17	40.7	0.97	0.41
		3.5	50	2.61	89	37	37.6	0.18	36.6	1.06	0.41
BK3/1	114	2.7	8	3.95	120	90	27.4	0.72	-	-	-
		1.7	28	1.30	35	19	17.7	0.43	-	-	-
BK3/2	5650	5.5	8	2.99	190	60	67.5	0.10	67.5	1.43	0.48
		4.5	28	2.01	123	44	39.7	0.11	39.7	0.98	0.49
		3.4	50	1.99	91	36	26.5	0.18	26.5	0.78	0.40
BK4f	6000	2.7	8	3.38	131	29	39.9	0.10	39.9	1.32	0.40
		1.8	27	1.83	40	17	24.2	0.28	24.2	1.00	0.55
BK4s	2600	5.6	8	2.99	205	76	54.2	0.19	62.0	1.32	0.44
		4.7	27	3.06	137	60	58.4	0.23	62.0	1.48	0.48
		3.5	50	1.54	50	43	21.8	0.75	-	-	-

Notes:

1. σ'_{rl} and u_l are the radial effective stresses and pore pressures prior to the first load test.
2. u_{max} is the maximum pressure recorded after installation. This occurred almost instantaneously in most cases. U_d is then assumed = $(u_l - u_0)/(u_{max} - u_0)$
3. σ'_{rc} values were extrapolated from the "σ'_r v time" plots for piles BK1 & BK4s.
4. The records at h/R=50 on pile BK4s were affected by the equalisation of pile BK4f.
5. Pore pressures quoted at h/R =8 on pile BK3/1 are corrected for the large hydraulic gradients close to the tip (note that pore pressures were measured at h/R=5)

Table 8.8 Equalisation data at Bothkennar (stresses in kPa)

8.4 LOAD TESTING

8.4.1 Introduction

The full programme of load tests performed at Bothkennar is summarised in Table 8.11 on page 334. This programme was designed to examine the influence of the following factors on pile behaviour under first-time loading:

(a) Pile depth
(b) Direction of loading (i.e. tension v compression)
(c) Duration of equalisation period
(d) Rate of pile installation
(e) Rate of pile loading

As shown in Table 8.9, each first-time load test examined the separate influence of one of these factors. The first compression test on pile BK2 (Test BK2/L1C) was used as a 'base case' with which to compare the other tests. Secondary load tests examined factors affecting the reload capacity and the post-peak pile behaviour.

All tests followed the 'standard' load testing procedure apart from the test on pile BK3(2) which was loaded at a far slower (drained) rate of displacement. These procedures are described in Section 4.2.7.

8.4.2 Overall pile response

The overall load displacement behaviour determined in the primary Bothkennar tests is summarised by the curves shown on Figure 8.20 and the data summary in Table 8.9. These results allow some preliminary observations to be made before examining the local variations of stresses along the pile shafts.

Test description

Test	Test details[1]	Main objective[1]
BK2/L1C	Installed at 500mm/min to 6.0m and at t_{eq}= 4 days, load tested to failure in compression in ≈1 hour	Base case
BK1/L1T	Tension test at t_{eq} =1200 mins	(b)
BK3(1)/L1C	Installed to 3.15m and tested at t_{eq} =115 mins	(a) & (c)
BK3(2)/L1C	Loaded to failure in 24 hours	(e)
BK4f/L1C	Installed to 3.15m	(a)
BK4s/L1C	Installed at 75mm/min and load at t_{eq} =2 days	(d)

[1]Test details given are those which differed from details of the base case test. Refer to Section 8.4.1 for index of main objectives.

Test results

Test	L (m)	τ_{avp} (kPa)	α	β	d_{pm} (mm)	τ_{avi} (kPa)	τ_{avu} (kPa)	q_b (MPa)
BK2/L1C	6.00	16.7	0.98	0.47	3.75	4.8	14.5	0.35 at 6mm
BK2/L2C	6.01	19.7	1.16	0.55	2.75	4.8	19.0	0.45 at 12mm
BK1/L1T	6.00	15.3	0.90	0.43	12.0	≈7	15.3	-
BK3(2)/L1C	5.90	17.4	1.02	0.49	5.0	6.5	16.3	0.51 at 13mm
BK4s/L1C	5.95	15.8	0.93	0.44	3.8	8.0	15.0	0.35 at 15mm
BK3(1)/L1C	3.15	9.2	0.61	0.34	2.0	5.9	6.5	0.27 at 10mm
BK4f/L1C	3.15	17.8	1.19	0.67	3.7	6.6	16.3	0.25 at 6mm

Note: τ_{avp} =peak average shear stress, τ_{avu} =ultimate (post-peak) average shear stress; τ_{avi} = peak average shear stress measured towards the end of installation (preceded by pause periods < 7mins); d_{pm} =pile head displacement at τ_{avp}; α =adhesion factor at d_{pm} ($=\tau_{avp}/c_{u0}$), where c_{u0} is measured in UU tests on conventional (100mm diam.) piston samples; $\beta = \tau_{avp}/\sigma'_{v0}$, q_b =maximum pile end bearing.

Table 8.9 Primary load tests at Bothkennar

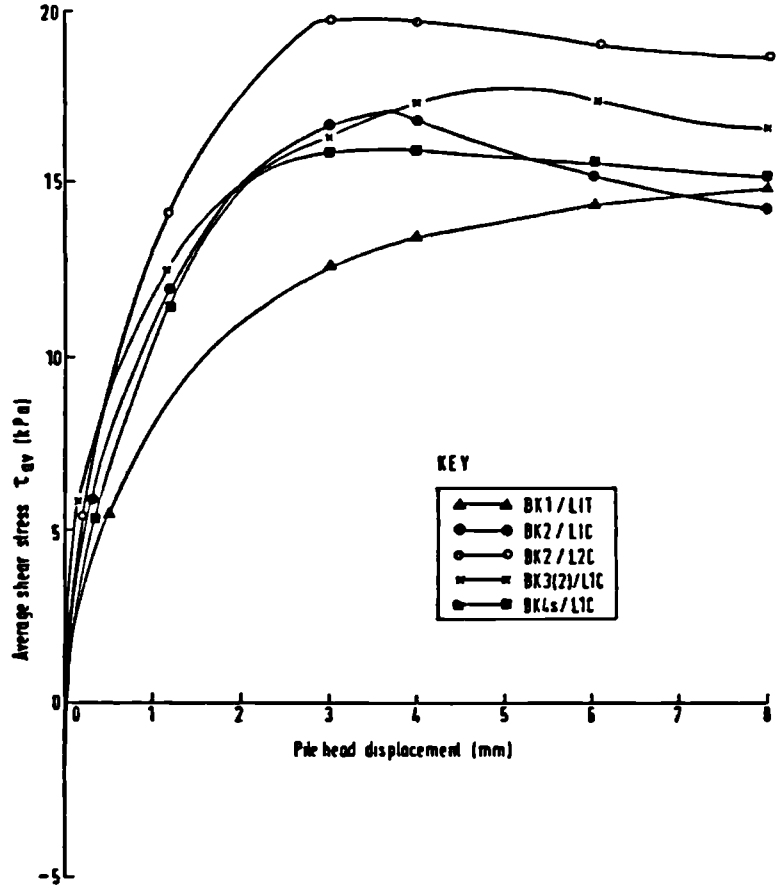

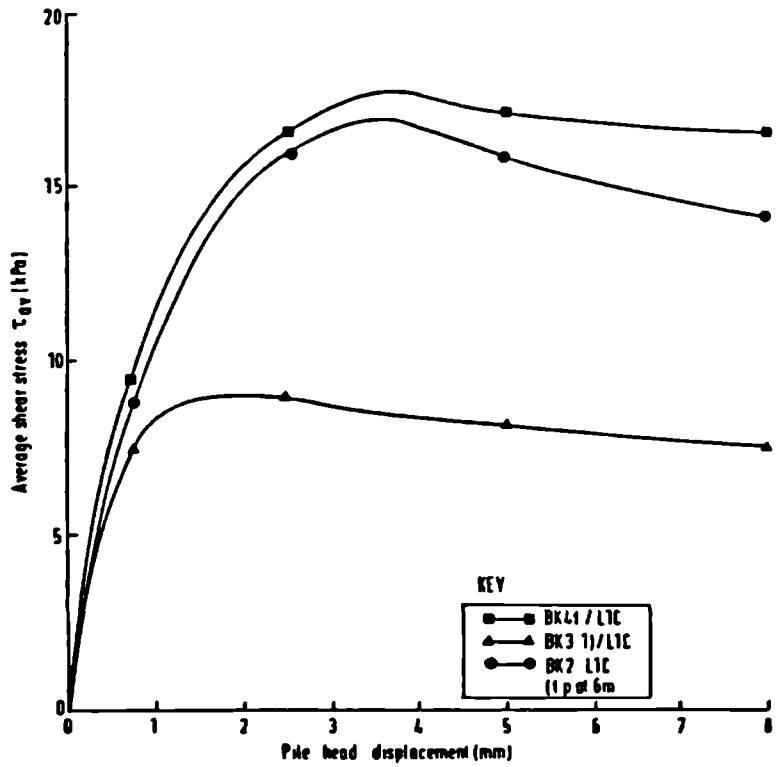

Figure 8.20 Shaft load - displacement curves at Bothkennar

8.4.2.1 Shaft capacity

Excluding the short term test (BK3(1)/L1C), the peak average shaft resistances (τ_{avp}) measured in first-time tests are within 10% of the mean value of 16.6kPa. This narrow range suggests that the unit shaft capacities (mobilised ≈1 day after installation) are relatively insensitive to the:

- pile depth (from 3 to 6m)
- direction of loading
- rate of pile installation (from 75 to 500mm/min)
- pile loading rate (at < 1mm/min)

By comparison, the τ_{avp} values at Cowden varied by ±25% when the same factors were altered by similar amounts.

The average α value for the same group of pile tests is ≈1.0, based on the peak triaxial UU strengths of 100mm diameter piston samples, and ≈0.7 using the UU strengths of (better quality) 200mm diameter Laval samples (see Section 5.3.7). These values are somewhat higher than the range of 0.55 to 0.75 recommended by API (1989)[1].

Further points to note include:

- The decrease of β with pile depth is much more pronounced than that for α, reducing from 0.67 for piles installed to 3.15m depth to ≈0.46 for piles at ≈6m depth. Reductions of β with pile depth are common for piles installed in lightly overconsolidated clays (e.g. see Figure 2.4).
- While the length of the equalisation period has little influence on capacity after one day has elapsed, it has a critical influence over the first few hours. Capacities after full equalisation are typically three times those measured at the end of installation. This strong positive set-up was also shown by installation data and is another distinctive characteristic of piles in low OCR clays.

[1]API (1989) proposes that $\alpha = 0.5\ (c_{u0}/\sigma'_{v0})^{-0.5}$, for $c_{u0}/\sigma'_{v0} \leq 1$

- Although radial effective stresses were very close to fully equalised values prior to the initial load test on pile BK2 (Test BK2/L1C), the shaft capacity was 18% higher, when this pile was re-tested 32 days later (Test BK2/L2C)

- Further re-tests of pile BK2, described in Appendix A, showed that the *peak* shaft capacity increased by ≈6% when the load testing rate was increased from 1mm/min to 10mm/min. This rate effect is comparable to that observed in ring shear tests at similar velocities (see Figure 5.31).

8.4.2.2 Shaft displacement characteristics

The shaft load displacement curves are shown on Figure 8.20. The principal features to note are:

- The non-linear characteristics from the very early stages of loading.
- The narrow spread of curves for all first-time *compression* tests until ≈85% of the respective peak capacities are mobilised; peak capacity is generally attained at a pile head displacement (d_p) of between 3 and 5mm.
- The significantly softer response in *tension*[1] and the stiffer response in reload tests.

Slight brittleness was evident in compression tests, where shaft capacities fell by ≈10% after post-peak displacements of less than ≈6mm. No loss of capacity was observed in tension tests.

8.4.2.2 Base load

The base loads measured during load tests were very small and, as such, because of the relatively low sensitivity of the base load cell, q_b values quoted in Table 8.9 are only considered accurate to about ±15%.

---

[1]This was also observed in secondary tension tests that were preceded by compression tests (see Table 8.11, page 334).

Allowing for this, it appears that the ultimate capacities (which were mobilised fully at a pile head displacement of ≈10mm) are close to those measured during the last installation jacking stage (see Figure 8.2). At peak shaft capacity, the base loads were ≈85% of these ultimate values.

8.4.3 Local stresses variations

The variations of the local pore pressures, shear stresses and radial stresses with pile head displacement observed in six load tests are shown on Figures 8.21-8.22. The general trends of these data are discussed briefly before reviewing their combined effect in the next section.

8.4.3.1 Pore pressure

- In all the load tests that followed the standard loading procedure (i.e. *undrained* tests), pore pressures increase until peak local capacity is mobilised. The increases vary between 2kPa and 14kPa and are largest close to the pile tip and in first-time load tests; no significant difference is observed between compression and tension tests.
- After peak capacity is mobilised, pore pressures reduce dramatically and attain relatively steady values after a post-peak displacement of ≈10mm. Larger pressure reductions were measured in tests that exhibited brittleness.
- On unloading, pore pressures increase to values that are higher than their pre-peak maxima (e.g. Test BK4s/L2C, Figure 8.22). These pressures reduce to their initial pre-loading values after ≈ 1day.
- No changes in pore pressure were observed in Test BK3(2)/L1C which used the *'drained'* loading procedure (see Figure 8.22).
- When pile BK3(2) was unloaded rapidly (after been taken to failure at a drained rate of displacement), pore pressures increased by about 10kPa.

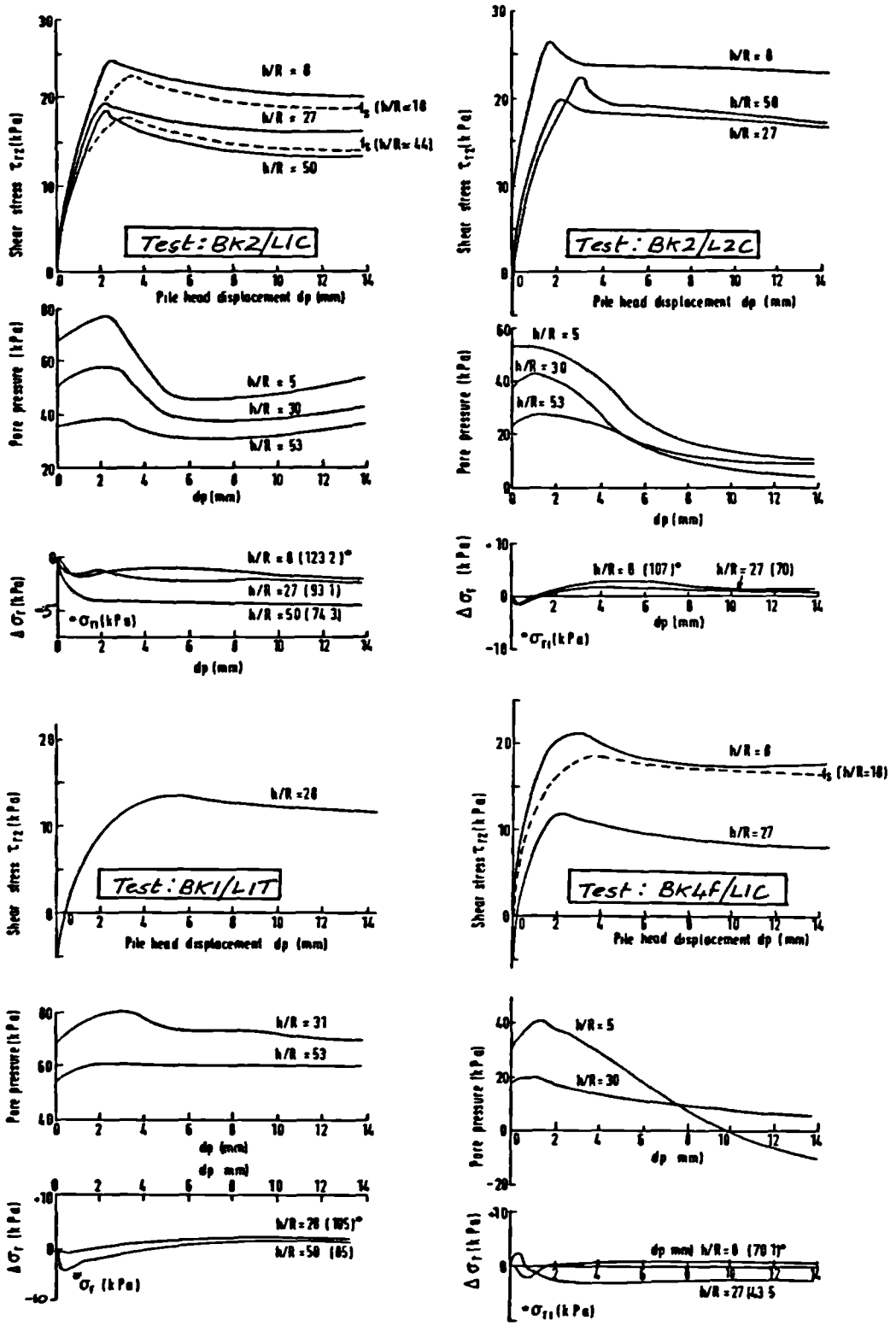

Figure 8.21 Variations of local stresses with d_p (1)

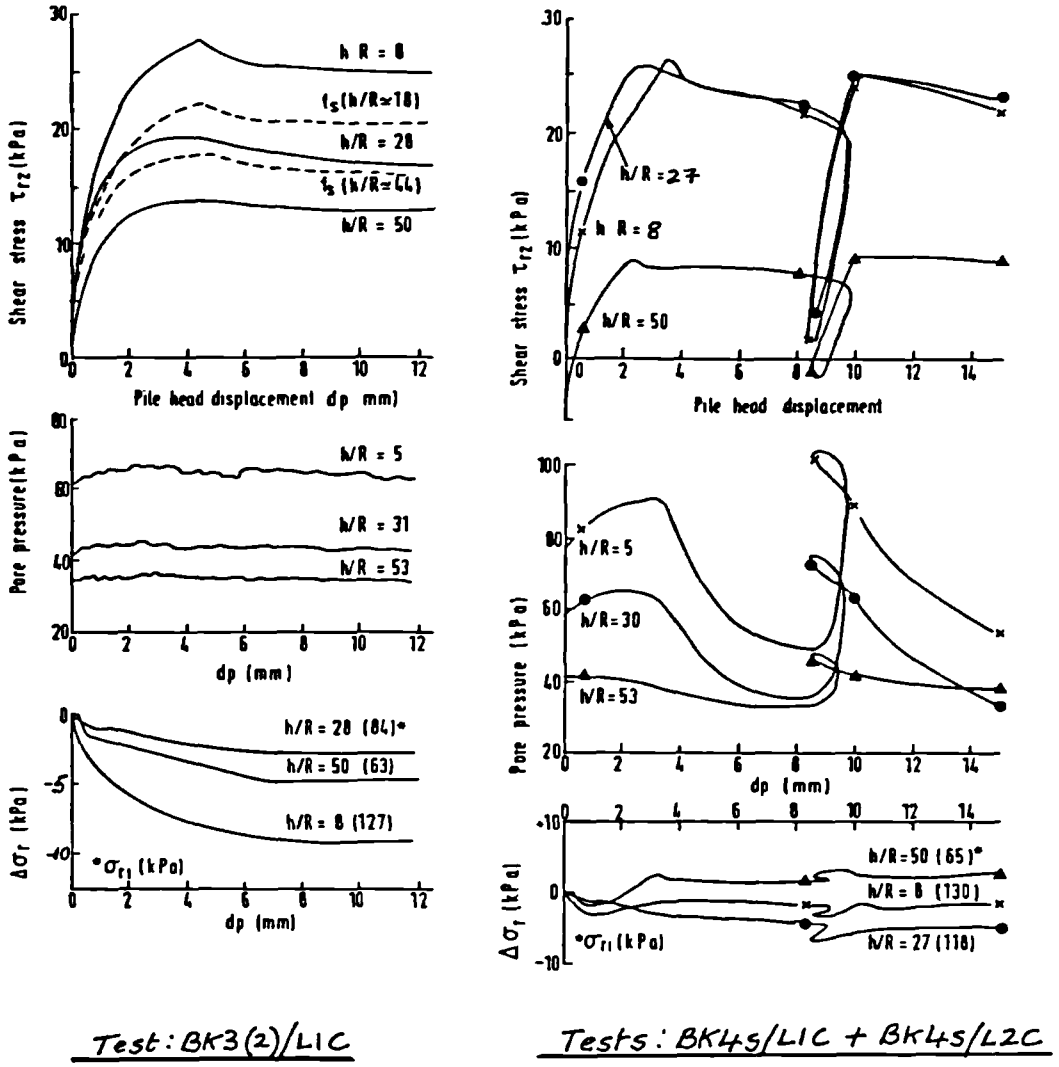

Figure 8.22 Variations of local stresses with d_p (2)

8.4.3.2 Radial stress

In both compression and tension *undrained* tests, the changes in radial stress (pre- and post-peak) were virtually negligible (typically ≈2kPa). However, pre-peak reductions in radial stress of up to 10kPa were observed in the *drained* test.

8.4.3.3 Shear stress

The variations of local shear stresses with pile head displacement exhibit features compatible with the those shown by the total shaft loads (Figure 8.20). These features include a stiffer response (i) in compression compared with tension, (ii) in reload tests and (iii) at locations on the shaft with higher pre-loading radial effective stresses. The pile head displacements required to mobilise peak capacity generally increase with depth and are in proportion to the local radial effective stresses.

It is encouraging that the local shear stresses (τ_{rz} - measured with the SST's) and the average shaft frictions (f_s -derived from the axial load cell data) show good agreement[1] (all of the f_s data are not shown for clarity). In some instances (e.g. Test BK2/L1C, Figure 8.21), peak τ_{rz} values are mobilised prior to corresponding peak f_s records, but both data sets indicate comparable brittleness. The shearing characteristics of the clay adjacent to the pile shaft therefore appear to be relatively insensitive to the properties of the pile surface.

8.4.4 Effective stress paths

This section presents the variations of τ_{rz} with σ'_r measured during each load test. Plotting the results in this format brings together the individual local measurements of σ_r, u and τ_{rz} and allows the underlying factors controlling shaft capacity to be identified.

8.4.4.1 Behaviour up to peak shear stress

The 'stress paths' measured up to peak shear stress[2] in the primary load tests at Bothkennar are shown on Figures 8.23-8.24. Each plot shows the paths followed in two tests so that, by comparison, the effect of a changing each test parameter (see Section 8.4.1) can be identified.

---

[1]This also appeared to be the case during installation. However, no firm conclusion could be made as the resolution of the installation f_s data was not particularly high (because the axial loads were small).

[2]For the reasons outlined in the next section, the post-peak paths for the drained test BK3(2)/L1C are also shown.

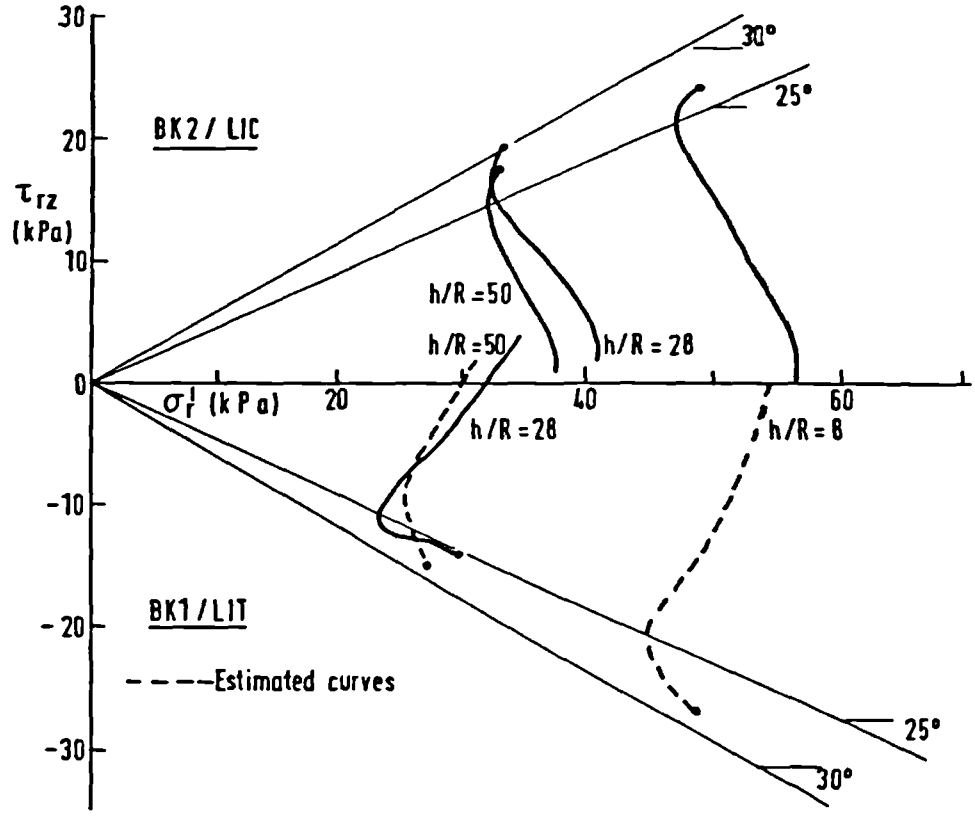

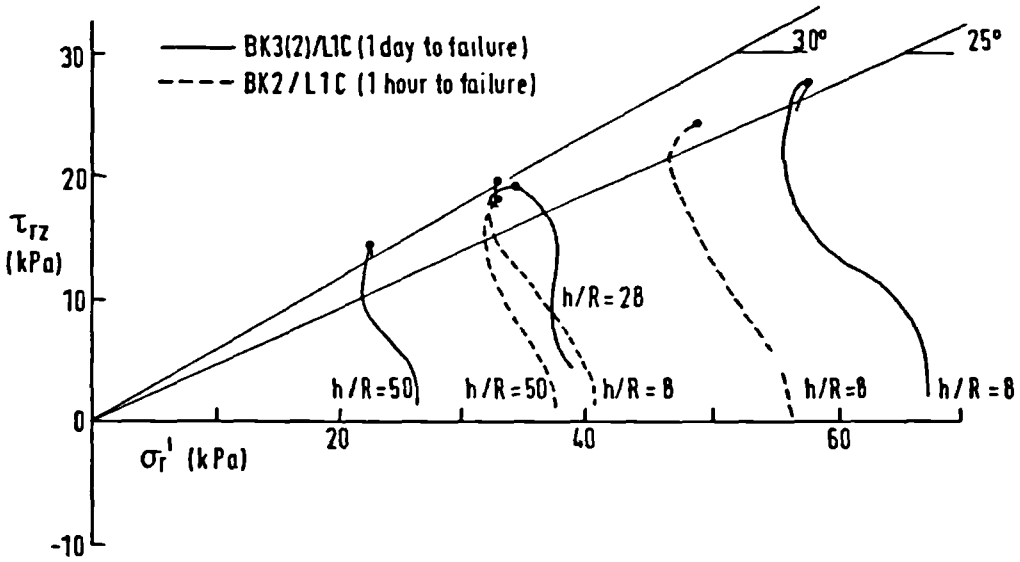

Figure 8.23 τ_{rz} v σ'_r paths followed in load tests (1)

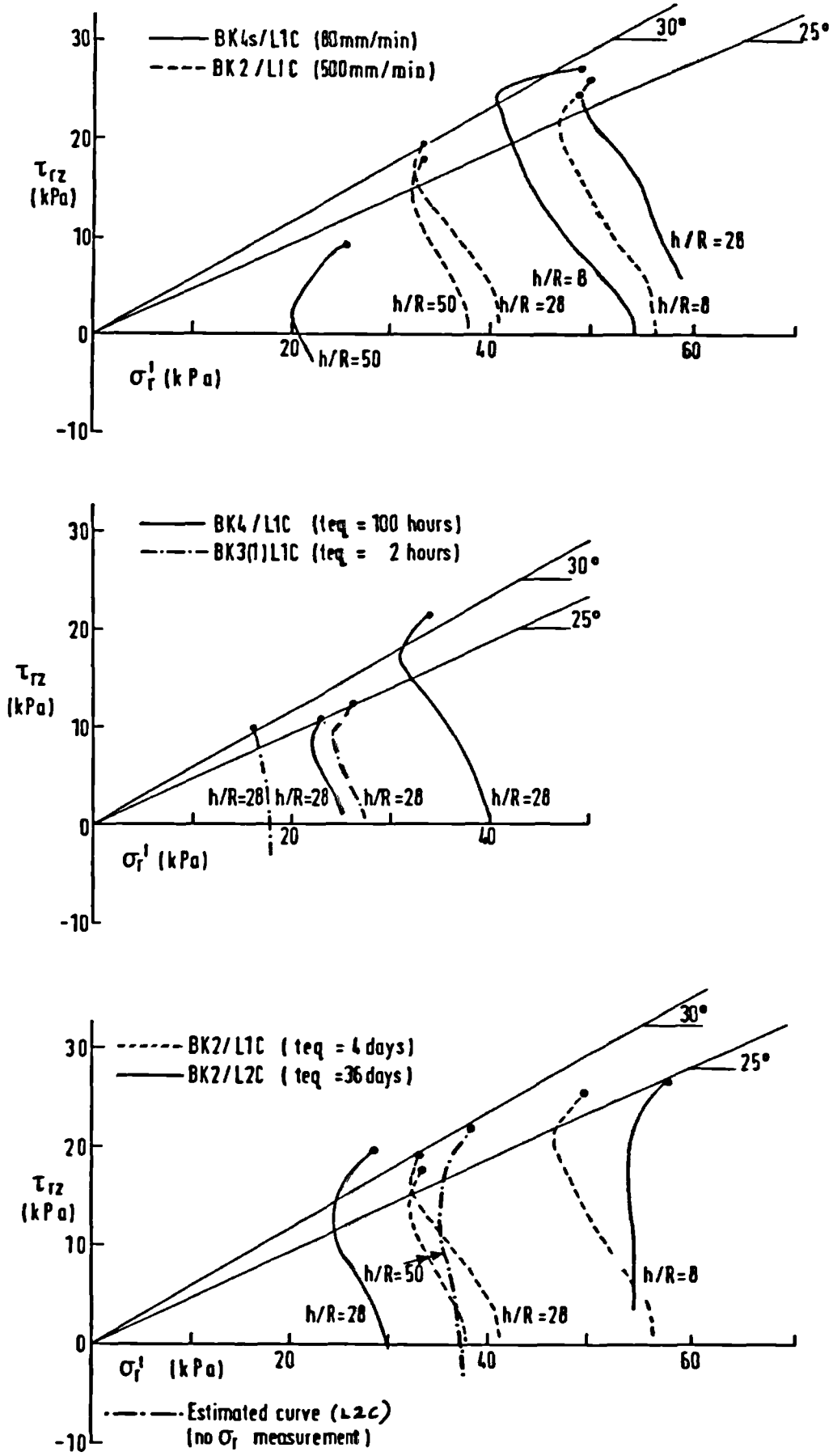

Figure 8.24 τ_{rz} v σ'_r paths followed in load tests (2)

Two consistent characteristics are evident:

(i) As the applied load increases, the radial effective stresses reduce until the shear stresses are within ≈10% of their peak values. For the final increases in τ_{rz}, σ'_r remains constant or increases marginally.

(ii) Peak shear stresses are mobilised at interface friction angles (δ_p) which lie within the relatively narrow range of 25° to 30° at all instrument positions.

The conditions at peak shear stress in each first time-load test and first reload test are summarised in Table 8.10 by <u>mean</u> values of δ_p and the load test coefficient, K_f/K_1 ($=\sigma'_{rf}/\sigma'_{r1}$).

We note:

- K_f/K_1 values in first-time load tests show a deviation of less than 5% from a mean value of 0.87 (except for the test on the partially equalised pile, BK3(1), which gave a slightly higher K_f/K_1 value of 0.95).
- Highly consistent mean values of δ_p are obtained (28.5° ± 1.5°). If δ_p was in fact constant, then this range implies that the individual measurements of τ_{rz}, σ_r and u are accurate to about 2.5kPa.

As both K_f/K_1 and δ_p are effectively constant in all first-time load tests, it appears that their values are independent of the direction of loading, the rate of pile installation, the rate of pile loading and the length of the equalisation period. As the peak shear stress (τ_f) is given by:

$$\tau_f = (K_f/K_1)\ \sigma'_{r1} \tan \delta_p$$

it is clear that differences in capacities at Bothkennar are associated (primarily) with variations in the pre-loading radial effective stresses (σ'_{r1}).

Test	K_f/K_1	δ_p(°)	δ_{ult}(°) (Apparent)	f_r (mm/min)
First-time tests				
BK2/L1C	0.85	29.4	17.3	3.5
BK1/L1T	0.87	27.0	27.0	1.5
BK3(1)/L1C	0.95	28.5	15.0	8.0
BK3(2)/L1C	0.86	29.2	27.8	0.05
BK4f/L1C	0.87	28.6	14.3	4.3
BK4s/L1C	0.87	28.3	15.0	4.5
Reload tests				
BK2/L2C	1.00	≈30	15.0	3.0
BK3/L3T	0.96	29.9	26.0	1.0
BK4s/L2C	1.60	29.0	15.0	4.2

Notes:

1. Average values for BK4s/L1C exclude measurements in the disturbed material at h/R= 50, which showed uncharacteristic trends with K_f/K_1 =1.17 and δ_p =19.3° (see Section 10.5).
2. BK2/L2C was performed 32 days after initial test, but BK4s/L2C was carried out immediately after BK4s/L1C.

Table 8.10 Effective stress failure parameters in load tests

Reload tests gave comparable δ_p values to those measured in first-time tests, suggesting that particle re-orientation does not play an important role during shearing. However, higher values of K_f/K_1 were measured. These varied from 1.6 for a pile in a partially equalised state (Test BK4s/L2C) to 1.0 after full equalisation (Test BK2/L2C). This response may be related to the plastic hardening caused by pre-loading (which was also evident in the overall load displacement behaviour) and the overconsolidated state of the clay surrounding a partially equalised pile.

8.4.4.2 Post-peak behaviour

In all compression tests that used the 'standard' loading procedure, the pile accelerated once failure had started, as attempts were made to maintain the maximum applied load. The pile velocity increased from a typical creep value of ≈0.2mm/min towards a maximum plunging rate (f_r) that varied between 1.0mm/min and 8mm/min.

The plunging conditions towards the end of each test are summarised in Table 8.10. Widely scattered δ_{ult} values are observed (between 14° and 28°) which appear to depend on pile velocity (f_r). As at Cowden, it is believed that these values, when velocities are high, do not reflect accurately the conditions within the soil which is failing close to the shaft. The arguments supporting this assertion for the Bothkennar experiments are given below, using data from first-time and reload tests on pile BK4s (Figures 8.22 & 8.25).

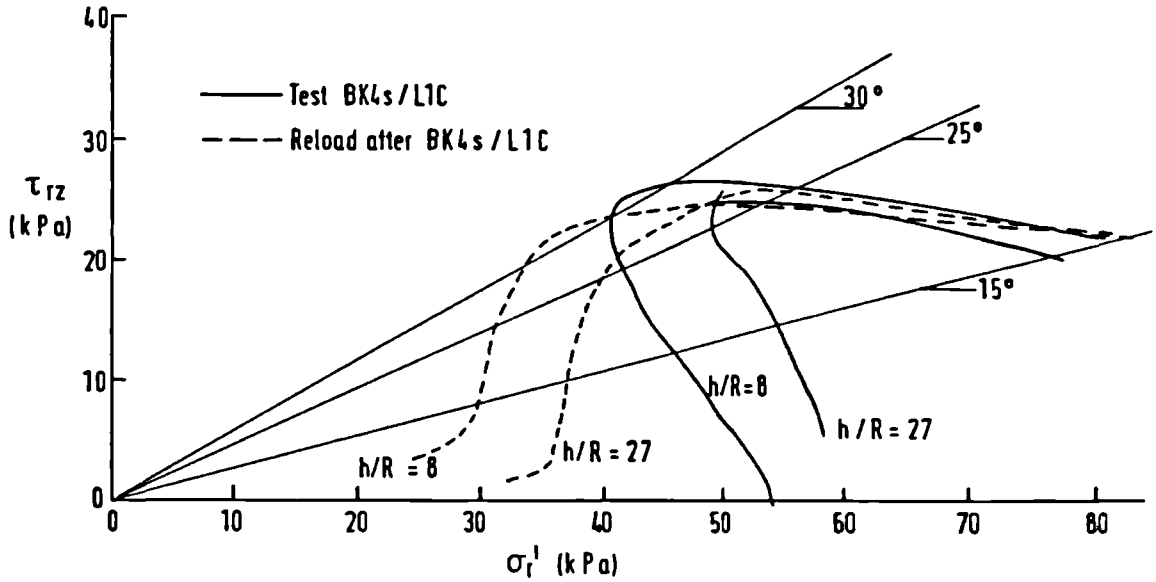

Figure 8.25 τ_{rz} v σ'_r paths followed in 'first-time' testing and re-testing of pile BK4s

First points to note are:

- As the pile plunges post-peak (at ≈4.5mm/min) in Test BK4s/L1C, radial total stresses remain relatively constant and shear stresses

decrease marginally. The apparent halving of the interface friction angle (from 28° to 15°) results purely from the post-peak pore pressure reductions.

- On unloading, pore pressures increase rapidly and the calculated radial effective stresses reduce to values that are about half of those measured before the start of the test. When the pile was reloaded shortly afterwards, the pore pressures decrease and the effective stress paths migrate towards their *previous peak conditions* with $\delta_p \approx 28°$.
- When the pile accelerates post-peak in the re-test ($f_r \approx 4.2$mm/min), further large reductions in pore pressure (and corresponding increases in σ'_r) are observed which lead again to a decrease in δ to an ultimate value of ≈15°.

The large post-peak reduction of the δ (from ≈28° to ≈15°) is completely reversible and disappears as soon as the pile velocity drops to below ≈1mm/min. *It cannot, therefore, be associated with the development of a low strength residual soil fabric.* It follows that the low δ_{ult} values, measured at fast rates, do not control subsequent pile capacity and should not be considered as true failure parameters for the pile-soil system. This contention is further substantiated by the post-peak measurements made in the slow (drained) test (BK3(2)/L1C) and the laboratory ring shear experiments (see Figures 8.23 & 5.30), both of which showed that δ_{ult} was closely comparable to δ_p.

Given the small post-peak changes in radial stress and shear stress, the low and transient δ_{ult} values recorded can, as at Cowden, be attributed to the measurement of anomalous pore pressures at pile velocities in excess of ≈1mm/min. Possible explanations for this effect are offered in Appendix A.

Therefore, the only reliable *post-peak* stress paths recorded were those measured during the drained test :BK3(2)/L1C, where the maximum displacement rate of the pile was maintained at less than 0.05mm/min. This test (Figure 8.23) indicates little post-peak variation in σ'_r and δ_{ult} values that are, at most, 2° less than δ_p. As δ_p values measured in reload tests were comparable to those mobilised in first-time tests, it

is surmised that post-peak variations of σ'_r on the principal displacement shear during 'undrained' pile tests were also negligible.

8.4.4.3 Comparison with laboratory tests

Ring shear tests

A comparison between the results obtained in ring shear interface and displacement pile tests on Bothkennar clay revealed the following similarities:

- The ring shear tests (see Section 5.3.12) showed that interface friction angles were independent of the pre-shearing rate and the history of relative displacement (after an initial displacement of 1.2m). The insensitivity to displacement history was also shown in the pile tests by the independence of the peak δ values (δ_p) on the pile installation rate and the number of previous load tests.
- The ring shear tests gave peak angles of interface friction in the range 29° to 33° and ultimate angles that were typically not more than 1° less than peak angles (i.e. negligible brittleness). These angles are in good agreement with the mean δ_p value measured in the pile tests (28.5°) and the ultimate angles measured in the *drained* pile test (≈28°) and inferred from reload tests (≈ 29 ± 2°).

The results from the soil on soil and soil-steel ring shear tests indicated that the steel interface, which was of the same material and roughness as those of the SST's, did not represent a plane of weakness and that failure in interface tests probably took place within the soil. Given the similarities of the δ values measured in these tests and in the pile tests, it appears that the principal displacement shear was also within the soil in the pile tests.

It is interesting to compare the typical field and laboratory interface friction angle of ≈30° with the critical state friction angle (ϕ'_{cv}) of ≈35.5° measured in triaxial compression tests. Interpreted in the conventional manner, the interface friction angle is ≈5° less than ϕ'_{cv}, despite the turbulent nature of soil shear and the appearance that

slippage did not occur at the interface. If, however, it is assumed from plasticity theory (e.g. see Potts & Martins 1982) that the principal axes of stress and strain increments are coincident and that there is no dilation at peak conditions, then the boundary conditions are such that the principal stresses at failure are inclined at ±45° to pile axis and δ is given by:

$$\delta = \tan^{-1} (\sin \phi'_{cv}) = 30°$$

This interpretation therefore offers a plausible explanation for the measured δ value. However, it should be borne in mind that ϕ'_{cv} in direct shear may be different to that experienced under triaxial conditions.

Direct simple shear (DSS) tests

Analogies between the boundary conditions imposed on samples in constant volume direct simple shear tests (DSS) and the conditions adjacent to a pile during loading were discussed in Section 2.3.6. It may be recalled that Randolph & Wroth (1981), and others, proposed that the changes in radial effective stress during undrained pile loading were equivalent to the changes in the vertical effective stress (σ'_v) measured in constant volume DSS tests on *normally consolidated* clay. Azzouz et al (1990) predicted (using SPM/MIT-E3 analyses) that the directions of the principal stresses after equalisation differ from those present at the start of a DSS test because of the complex stress changes associated with pile installation and equalisation. They suggest that these differences are such that the (normally consolidated) material adjacent to the pile during load testing will appear to behave in a similar way to the same material at OCR =1.2 ±0.1 in a DSS test (see Section 2.3). The applicability of these analogies is examined below.

The DSS tests on Bothkennar clay, discussed in Section 5.3.12, were performed on intact samples, re-consolidated to in-situ stress conditions (i.e. $\sigma'_{vc} = \sigma'_{v0}$, $\sigma'_{hc} = K_0\ \sigma'_{v0}$). Mean variations of the applied shear stress (τ_h) with the vertical effective stress are plotted on Figure 8.26a, where they are normalised by the maximum preconsolidation pressure

(σ'_{vm} = OCR x σ'_{vc})[1]. These data and correlations developed by Ladd & Edgers (1972) suggest that the simple shear peak undrained shear strength (c_{uss}) of Bothkennar clay can be approximated by the expression: (c_{uss}/σ'_{v0}) = 0.325 $OCR^{0.8}$. The behaviour at OCR's of 1 and 1.2 was estimated using this expression and trends exhibited in DSS tests on Boston Blue clay (Azzouz et al 1990).

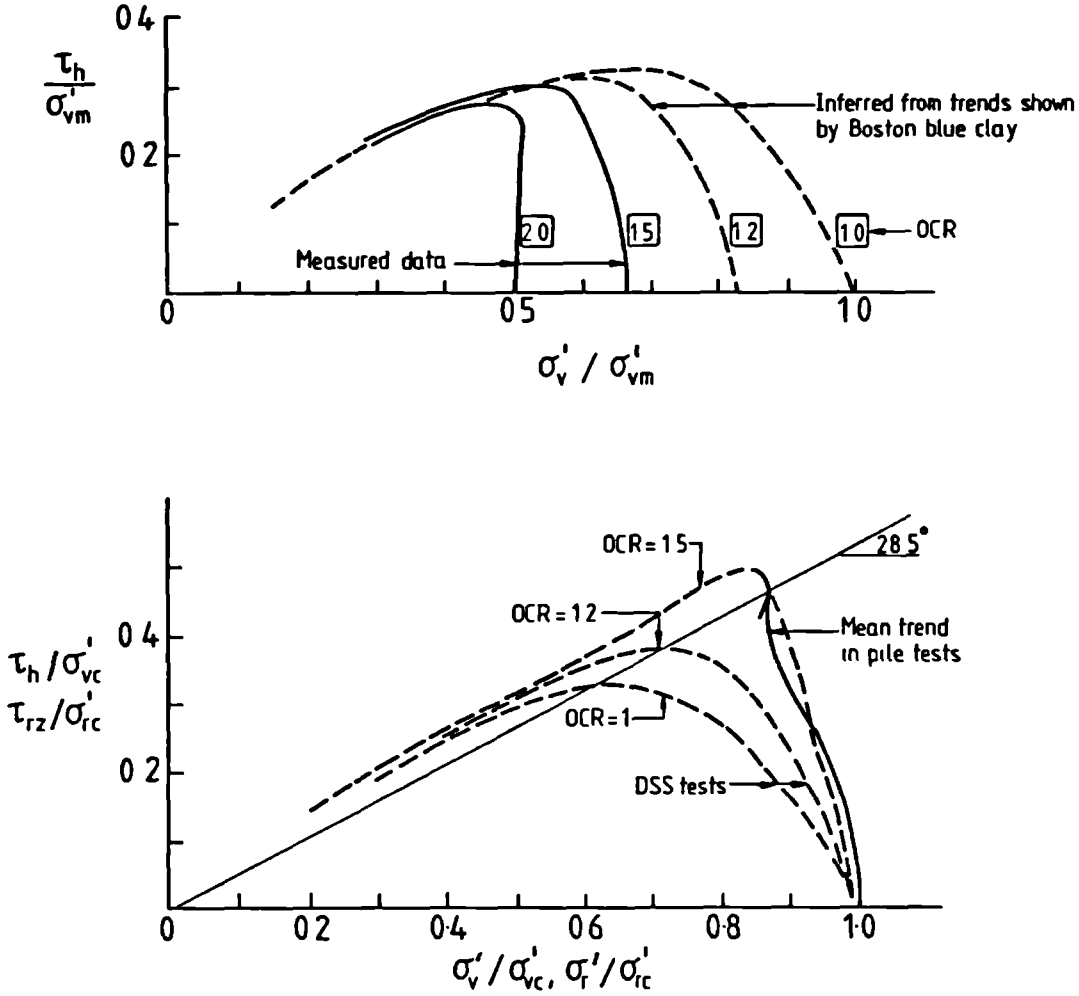

Figure 8.26 Stress paths in DSS tests on Bothkennar clay (top), comparison of DSS and pile test stress paths (bottom)

The DSS characteristics are compared on Figure 8.26b with the mean variation of shear stress with radial effective stress measured in the pile tests. In this figure, the shear and normal stresses have been normalised by the pre-loading normal effective stress. We note:

[1]The OCR of the samples used in each DSS test was estimated from Figure 5.26.

- Pre-peak reductions in σ'_r/σ'_{rc} are smaller than the reductions of σ'_v/σ'_{vc} at OCR=1.2 and significantly smaller than reductions of σ'_v/σ'_{vc} at OCR=1. The pre-peak stress path seen in the pile tests is more compatible with that measured in a DSS test at OCR=1.5.
- The obliquity at peak shear stress in the DSS test at OCR=1.2 is comparable to that measured in the pile tests.
- Post-peak, the DSS tests exhibit a very different response to that shown by the field measurements. Both the drained load test and the undrained load tests (when corrected for anomalous pore pressures) indicate little post-peak change in σ'_r and approximately constant obliquity, whilst the obliquity in DSS tests increases post-peak and σ'_v/σ'_{vc} decreases further.

Three points of note may be inferred from this comparison:

(i) The similarity of the stress paths measured in the drained pile test (Figure 8.23) with those measured in undrained pile tests and pre-peak in DSS tests (at OCR =1.5) suggests that the soil adjacent to the shaft in the drained test is also sheared at approximately constant volume, but with σ_r reductions taking the place of pore pressure increases.

(ii) The difference between the pre-peak pile loading stress paths and those predicted by SPM/MIT-E3 analyses (which suggest that paths should be equivalent to DSS paths at OCR =1.2 ±0.1) may be because (a) the directions of the principal stresses prior to load tests at Bothkennar differ from those predicted in the analyses, (b) the clay adjacent to the piles is not in a normally consolidated state or (c) the analysis of pile loading process is too simplified.

(iii) The clear disagreement between the post-peak field measurements and DSS tests suggests there is a departure from continuum behaviour adjacent to the piles and ultimate conditions are developed either (a) at the pile-soil interface or (b) on a continuous shear surface at a short distance from the pile. In these situations, the ultimate stress obliquity may be obtained from ring shear interface tests.

Test	Time	Date	L (m)	t_{eq} (mins)	t_f (mins)	L_r (kN/min)	d_p (mm)	τ_{av} (kPa)	f_r
BK1/L1T	15:12	19/10/90	6.0	1200	53	0.5	12	15.3	1.5
BK2/L1C	19:30	29/10/90	6.0	6000	48	0.6	3.75	16.7	0.5
							8.0	14.5	3.5
BK2/L2C	9:46	4/12/90	6.0	32days	56	0.6	2.75	19.7	0.5
							8.0	19.0	3.0
BK2/RTE	11:24	4/12/90	6.0	40	8	3.6	2.25	16.7	0.5
							15.0	14.9	4.0
							25.0	15.6	11.0
BK2/FEX	12:50	4/12/90	6.0	0	15	1.9	7.0	18.7	1.0
							16.0	20.0	12.0
BK3-1/1C	13:33	7/3/91	3.15	114	14	0.5	2.0	9.2	2.0
							12.0	6.5	8.0
BK3-2/1C	13:30	11/3/91	5.9	5650	1200	0.02	5.0	17.4	0.02
							8.0	16.3	0.03
BK3/L3T	16:00	12/3/91	5.9	100	98	0.3	10	19.7	1.0
							20	20.4	9.0
BK4f/L1C	17:10	18/3/91	3.15	6000	35	0.35	3.7	17.8	1.4
							8.5	16.6	4.3
BK4s/L1C	8:15	21/3/91	5.95	2600	60	0.4	3.8	15.8	1.0
							9.0	15.0	4.5
BK4s/L2C	9:18	21/3/91	5.95	0	26	1.0	2.0	16.4	1.3
							7.4	15.8	4.2
BK4/FEX	11:05	21/3/91	5.95	90	45	0.5	12.0	15.3	1.0

Notes

1. First-time load tests are shown in bold.
2. Pile BK1 used a pre-bored hole to 1.0m depth. All other piles used a hole drilled to 1.2m.
3. t_{eq} =equalisation time (for secondary tests: time since last load test); t_f =time to reach max shaft capacity; L_r =average loading rate to reach max. shaft capacity; d_p =pile head displacement; τ_{av} =average shaft shear stress; f_r =pile displacement rate at peak capacity and average rate thereafter (mm/min).

Table 8.11 Load test summary: Bothkennar

CHAPTER 9

CORRELATIONS FOR DISPLACEMENT PILES IN SAND

CONTENTS OF CHAPTER 9

CORRELATIONS FOR DISPLACEMENT PILES IN SAND

9.1 INTRODUCTION 338

9.2 REDUCTIONS IN RADIAL STRESS WITH DISTANCE FROM THE TIP..... 338

9.3 EQUALISED RADIAL EFFECTIVE STRESS 340

9.3.1 Relationship between σ'_{rc} and pile end resistance 340

9.3.2 Relationship between σ'_{rc} and relative density 344

9.4 CHANGES IN RADIAL EFFECTIVE STRESS DURING PILE LOADING 346

9.4.1 General characteristics 346

9.4.2 Factors causing σ'_r changes 347

9.4.2.1 Reductions in σ'_r 347

9.4.2.2 Increases in σ'_r 348

9.4.3 Empirical correlations for σ'_r changes 351

9.4.4 General comments on relationships for $\Delta\sigma'_r$ 354

9.5 INTERFACE FRICTION ANGLES 355

9.6 IMPLICATIONS OF CORRELATIONS FOR σ'_{rc} AND $\Delta\sigma'_r$ 358

9.7 COMPARISONS WITH RESULTS FROM OTHER FIELD TESTS 360

9.7.1 Shaft capacities in compression 360

9.7.2 Shaft capacities in tension 362

9.7.3 Comparison with other pile design methods 365

9.8 FINAL COMMENTS 366

9.1 INTRODUCTION

The discussion presented in this chapter centres around the three main observations made with the ICP in the loose to medium dense sand at Labenne:

(i) The equalised radial effective stresses (σ'_{rc}) depend on the initial relative density (D_r) and stress state of the sand and reduce with the vertical distance from the pile tip (h).

(ii) During pile loading, radial effective stresses reduce initially and then increase significantly, reaching a maximum value (σ'_{rf}) at peak shear stress (τ_f).

(iii) Obliquities at peak shear stress, δ_f [$=\tan^{-1}(\tau_f/\sigma'_{rf})$], are closely comparable to the constant volume interface friction angles (δ_{cv}) measured in direct shear interface tests.

This Chapter formulates these observations into a series of expressions which (a) predict the magnitudes and variations of the stresses measured by the piles at Labenne and (b) incorporate the trends observed in other instrumented pile tests and laboratory tests. The expressions are used to predict the shaft capacities of piles at other sites and these predictions are compared with the measured capacities and the predictions made using three popular design methods.

9.2 REDUCTIONS IN RADIAL STRESS WITH DISTANCE FROM THE PILE TIP

One of the most striking observations made in all tests with the ICP has been that stresses acting on the shaft, at any fixed depth, reduced as the pile penetrated to deeper levels. In clays, this reduction may be at least partially explained if it is assumed that, during *undrained* pile installation, the soil moves relative to the pile tip in the same way that an *incompressible* (and inviscid) fluid would flow around the tip. The Strain Path Method (SPM) predicts that these 'flow paths', which are consistent with observations made with laboratory model piles, are such that the radial stresses developed on the shaft reduce with the vertical distance from the pile tip (h) normalised by the pile radius (R) i.e. h/R.

Unfortunately, the SPM cannot be applied to sands because pile installation is *not* undrained and, consequently, the sand will change in volume (i.e. it will not behave like an incompressible fluid). Nevertheless, the pattern of deformations experienced by the soil during pile installation in sands (see Figure 3.3) is comparable, in some respects, to that observed in clays (see Figure 2.7), suggesting that the kinematics of steady pile penetration may explain, or at least contribute, to the stress reductions with h/R observed at Labenne.

As will be shown in Chapter 10, the SPM predicts that stresses are relatively independent of the location of the pile tip at $h \geq 15R$, whereas at both the clay sites and at Labenne, stresses continued to reduce with increasing h/R. One feature which is not modelled by the SPM and may explain some of these observations is the cyclic nature of jacked pile installation[1]. The Labenne tests showed that radial effective stresses (σ'_r) increased from their equilibrium values (σ'_{rc}) during loading but σ'_r (recorded at fixed depths) reduced to values slightly less than the initial σ'_{rc} values after the pile came to rest. It will be shown that the increases in σ'_r are most likely associated with dilation (i.e. loosening) of the sand. When the applied load was removed, it appears that the soil close to the shaft contracted again, as the surrounding soil mass relaxed. This loading cycle was experienced by the sand at every jacking stage and it is possible that each cycle led to progressive loosening of the sand close to the shaft. Alternatively, as suggested by Robinsky & Morrison (1964), such a zone of loosened sand may develop simply because of the large compression volume changes occurring at the pile tip. In either case, this zone may allow arching of the radial effective stresses and cause σ'_{rc} to reduce with the distance from the pile tip. (It may be recalled that Chong (1988) showed that the sand immediately adjacent to a pile is in a looser state than at further radial distances from the shaft; see Section 3.3).

The evidence presented in subsequent sections suggests that the reduction in radial stress with the distance from the pile tip (h) <u>is</u> a general feature of displacement piles in sand. However, virtually no data

---

[1]The relevance of this phenomenon for piles in clay is discussed in Section 10.5.

comparable to that obtained at Labenne exists which can shed light on the factors influencing the form of this reduction. The limited data available indicated that stresses reduced with 'h' in a similar way to that at Labenne, when this distance was normalised by the pile radius (R). It is therefore proposed tentatively that the Labenne data may be generalised by assuming stresses reduce with h/R, but it should be noted that, for the reasons outlined above, stresses may also depend on (a) the absolute distance 'h' and/or (b) the number of load cycles.

9.3 EQUALISED RADIAL EFFECTIVE STRESS

This section explores possible relationships for the equalised radial effective stresses (σ'_{rc}) developed on displacement piles in sand based on the observations at Labenne. These relationships are compared with measurements made in other instrumented pile tests.

9.3.1 Relationship between σ'_{rc} and pile end resistance

It has been seen in Chapter 6 (Figure 6.6) that the equalised radial effective stresses (σ'_{rc}) acting in any soil horizon on the piles at Labenne depended on the pile end bearing measured in that horizon (q_b) and the distance of that horizon from the pile tip (h/R) i.e.

$$\sigma'_{rc} = f\ (q_b,\ h/R)$$

Because of the rapid equalisation of stresses, it has been argued that the stationary radial effective stresses recorded during the pause periods in between jacking stages (σ'_{rs}) are equivalent to the long term equalised values (σ'_{rc}) for a pile length corresponding to depth of the pile during that pause period. A regression analysis of over 30 σ'_{rs} measurements on each of the two piles (LB1 & LB2) gave the following best fit relationship (for $8 \leq h/R \leq 50$):

$$\sigma'_{rs} = \sigma'_{rc} = 0.024\ q_b\ (h/R)^{-0.33} \qquad \text{Eqn. 1}$$

It was noted that the ratio σ'_{rc}/q_b increased slightly with depth and a better fit to the data base was obtained for:

$$\sigma'_{rc} = 0.0114\ q_b\ (\sigma'_{v0})^{0.2}\ (h/R)^{-0.33} \qquad \text{Eqn. 2}$$

(stresses in kPa)[1]

Both of these relationships are plotted on Figure 9.1. Eqn. 2 has a regression correlation coefficient (r^2) of 0.87 and predicts 90% of the measured σ'_{rc} data to within 10%. However, as the maximum vertical effective stress (σ'_{v0}) at Labenne was only ≈80kPa, the apparent dependence of σ'_{rc}/q_b on σ'_{v0} must be viewed as tentative.

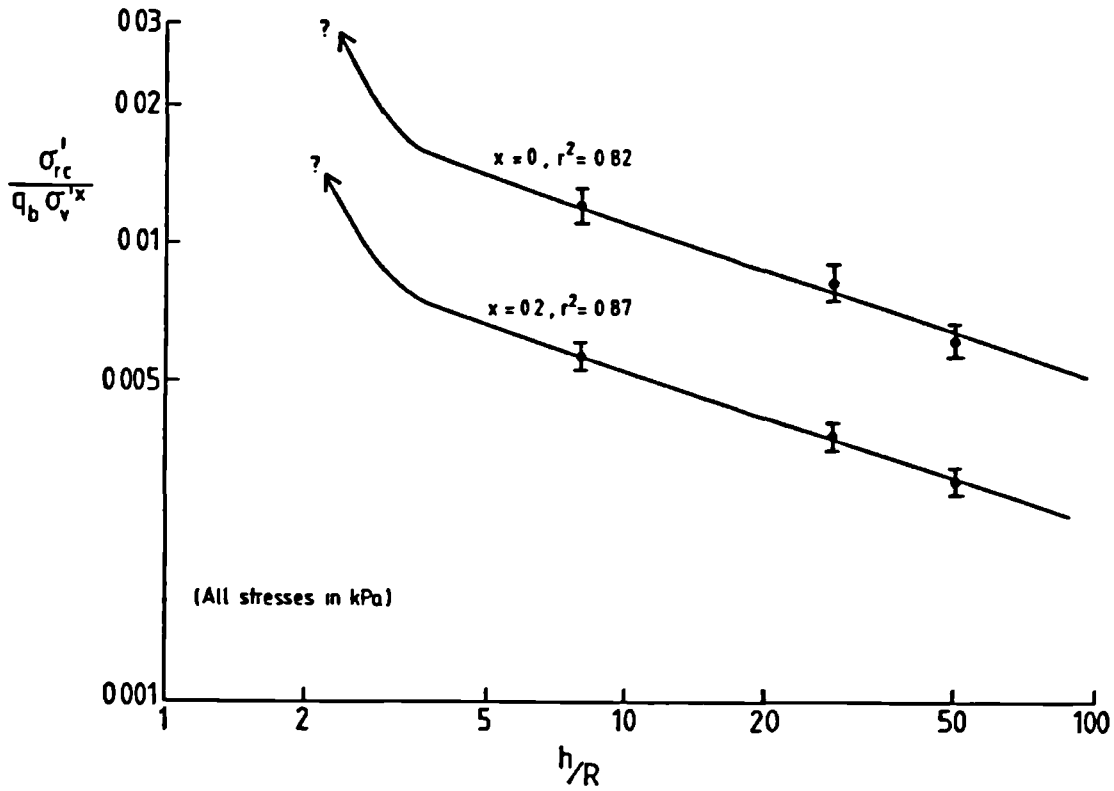

Figure 9.1 Correlation between σ'_{rc}, q_b and h/R at Labenne

As discussed in Chapter 3, there are virtually no reliable measurements

[1]Alternatively, this equation may be expressed in a non-dimensional format as: $\sigma'_{rc} = 0.029\ q_b\ [\sigma'_{v0}/P_{atm}]^{0.2}\ (h/R)^{-0.33}$, where P_{atm} is atmospheric pressure. To simplify presentation, correlations developed in this chapter are not presented in a non-dimensional format.

of the radial effective stresses developed on displacement piles in sand. One notable exception was the series of tests performed by Wersching (1987) using 1.85m long, 114mm diameter piles, which were jacked into a tank of Leighton Buzzard sand. Wersching's σ'_{rc} measurements are shown on Figure 9.2 and compared with the σ'_{rc} values predicted by Eqn.2. It is encouraging to see that the predictions are typically within 10% of the measurements, even though these σ'_{rc} values are over 5 times smaller than those measured at Labenne.

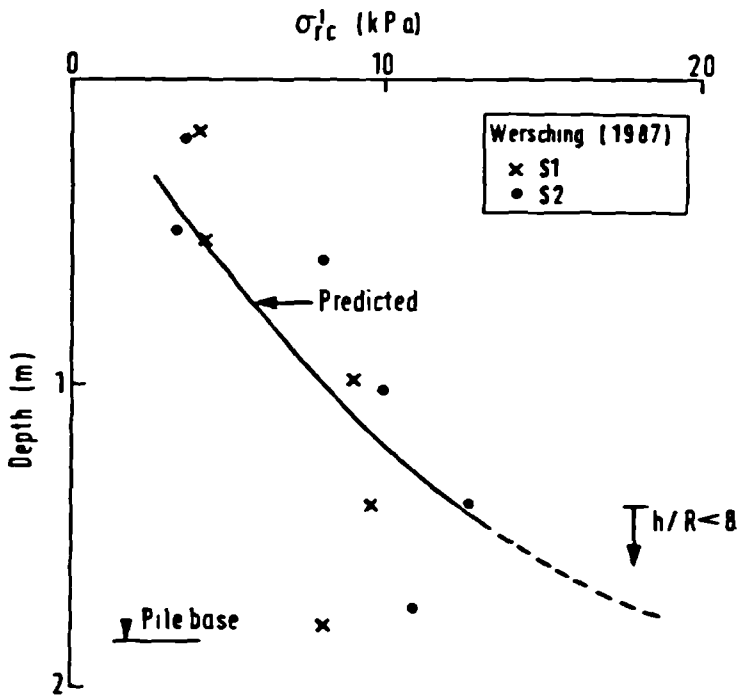

Figure 9.2 Predictions for Wersching's σ'_{rc} data using Eqn. 2

The test programme at Drammen, described by Gregersen et al (1973), is the only field case history, where values of local stresses developed on piles of different lengths in the same sand deposit have been reported. Instrumented, 280mm diameter, precast concrete piles were driven into very loose sand to final depths of 8m and 16m. The σ'_{rc} values recorded are shown on Figure 9.3 and compared with the predictions made using Eqn. 2, assuming that the Cone Penetration test (CPT) end resistance (q_c) can be used in place of q_b. (Relatively minor differences between q_c and q_b were observed at Labenne and it is suggested that the Labenne q_b profiles represent the best estimate of q_c at each pile location).

The σ'_{rc} measurements at Drammen are reported to be "characterised by a good deal of scatter", but nevertheless are in reasonable agreement with the Labenne correlation. Importantly, the Drammen tests show a similar dependence of σ'_{rc} on h/R to that measured at Labenne. This dependence explained why the average shaft shear stresses (τ_{av}) at both sites remained relatively constant[1] for pile lengths (L) greater than about 40 pile radii (R); see Figure 6.8.

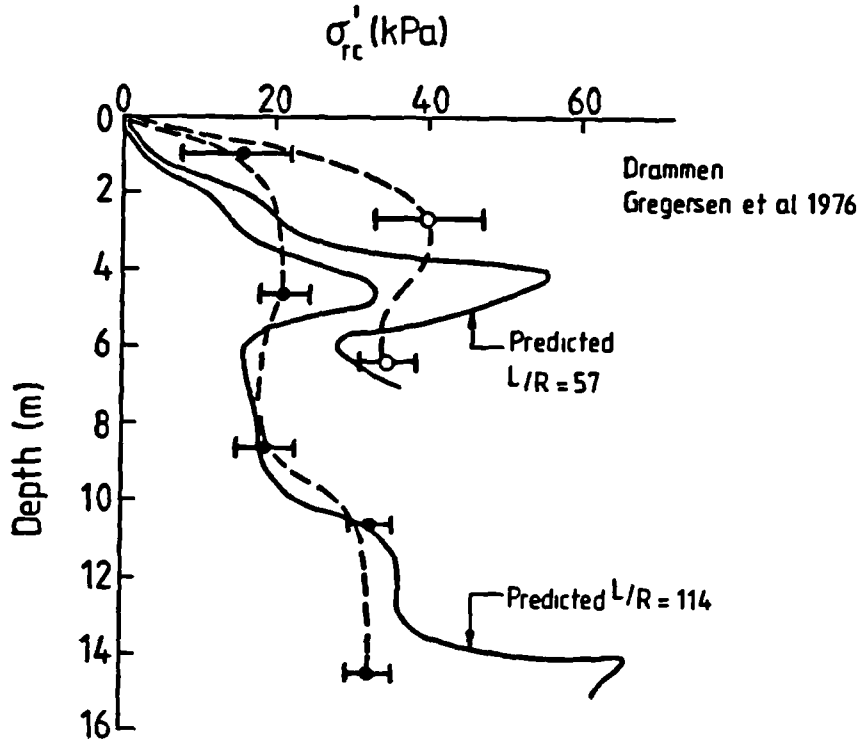

Figure 9.3 Predictions for σ'_{rc} data recorded at Drammen (using Eqn. 2)

The relative independence of τ_{av} on pile length for L ≥40R has been observed frequently in field and laboratory tests (see Sections 3.3 & 3.4), suggesting that, as at Labenne and Drammen, this phenomenon arises because the local radial effective stresses reduce with h/R. This h/R effect had not previously been appreciated for piles in sand (e.g. see comments of Olsen 1990 in Section 3.4.9).

In summary, the direct measurements of σ'_{rc} and general characteristics displayed by the average shear stresses mobilised on piles in sand

[1]Other un-instrumented piles at Drammen confirmed this trend.

support the general form of Eqn. 2. However, as is evident on Figures 9.2 & 9.3, this equation over-predicts σ'_{rc} values recorded very close to the pile tip ($h/R < 8$); no measurements of σ'_{rc} were obtained in the ICP tests at this location.

9.3.2 Relationship between σ'_{rc} and relative density

Most of the pile design methods discussed in Chapter 3 relate the shaft resistance to the initial relative density (D_r) of the sand. D_r is generally assessed from in-situ tests such as the Cone Penetration test (CPT), Standard Penetration test (SPT) or pressuremeter test. It is therefore of interest to express the correlations for σ'_{rc} in terms of D_r.

CPT q_c values may be converted to equivalent relative densities using the general equation proposed by Jamiolkowski et al (1988) for normally consolidated sands:

$$D_r = 1/A \log_e [q_c / B(\sigma'_{v0})^C], \quad \text{(A, B \& C are constants)} \qquad \text{Eqn. 3}$$

Jamiolkowski et al, and others, suggest that the variation of q_c with D_r in sands at all overconsolidation ratios is described more precisely by this equation if the mean effective stress (p'_0) is substituted in place of σ'_{v0}.

Cone research in calibration chambers has indicated that the constants A, B and C vary with sand type. Based on a review of tests in a range of *normally consolidated medium quartz* sands, Lunne & Christoffersen (1983) found a best fit to all the data for A=2.91, B=61 and C=0.69 (when stresses are in kPa). Using these constants, Eqn. 3 may be substituted into Eqn. 2 and re-arranged to obtain[1]:

$$K_c = \sigma'_{rc}/\sigma'_{v0} = 0.7\ (\sigma'_{v0})^{-0.11}\ e^{2.91 D_r}\ (h/R)^{-0.33} \qquad \text{Eqn. 4}$$

This equation predicts a relatively weak dependence of K_c on σ'_{v0} and for

[1]Noting that, at Labenne, $q_b \approx q_c$ and the sand was assessed as being only very lightly overconsolidated (OCR ≈1.5).

σ'_{v0} in the range 30kPa to 300kPa (equivalent to σ'_{v0} values between 3m and 30m depth for an offshore pile), K_c is given by:

$$K_c = (0.42 \pm 0.05)\ e^{2.91D_r}\ (h/R)^{-0.33} \qquad \text{Eqn. 5}$$

Mean values of K_c calculated using Eqn. 5 are given in Table 9.1. Correlations between q_c and D_r for overconsolidated sands (see Jamiolkowski et al 1988) suggest that K_c values at OCR=10 will be between 20% and 30% less than those listed in this table.

	D_r =20%	D_r =50%	D_r =80%
h/R=10	0.35	0.84	2.0
h/R=30	0.24	0.58	1.4
h/R=50	0.20	0.49	1.17
h/R=100	0.16	0.39	0.93

Table 9.1 Illustration of how K_c may vary with h/R and D_r in a normally consolidated sand.

Bearing in mind the assumptions used to establish Eqn. 5, a number of interesting trends emerge:

- There is a strong dependence of K_c on D_r; K_c values at D_r =20% are almost 6 times smaller than those at D_r =80%.
- Given that the undisturbed lateral stress coefficients (K_0) in normally consolidated sands varies between 0.4 and 0.5 (Jaky 1944), K_c is apparently less than K_0 at all h/R ratios in loose sand and at h/R > 50 in medium dense sand.
- The dependence of K_c on h/R incorporated in Eqn. 5 implies that the average K_c value (K_{av}) acting over a given pile of length L varies in proportion to $(L/R)^{-0.33}$ in a sand deposit of constant D_r and in which σ'_{v0} increases linearly with depth (Note that: $K_{av} = [2/(\gamma_{soil}L^2)]\int^L \sigma'_{rc}\, dz$).

If the vertical effective stresses adjacent to a displacement pile (σ'_z) are comparable to σ'_{v0} and if there is no arching of these stresses, then

the active pressure coefficient K_a [$\approx (1-\sin\phi')/(1+\sin\phi')$] may be a lower bound value for K_c. Given that $K_a \approx 0.3$ (for $\phi'=33°$), it is possible that the extremely low K_c values predicted in loose sand at large distances from the pile tip may not occur in practice.

9.4 CHANGES IN RADIAL EFFECTIVE STRESS DURING PILE LOADING

9.4.1 General characteristics

The experiments at Labenne showed that the radial effective stresses acting on the pile shaft changed from their initial equilibrium values (σ'_{rc}) during pile loading. The general pattern of the changes that took place is illustrated on Figure 9.4, which plots the average variations of the normalised shear stresses (τ_{rz}/σ'_{rc}) and radial effective stresses (σ'_r/σ'_{rc}) during first-time compression and tension tests.

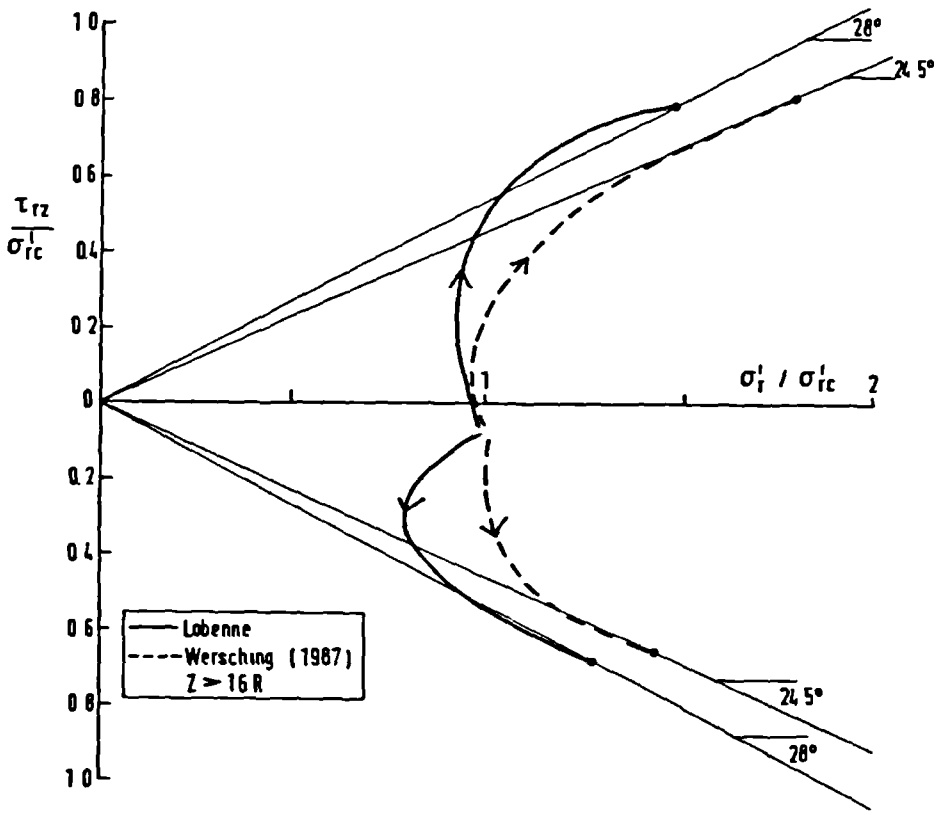

Figure 9.4 'Stress paths' followed during loading of the ICP at Labenne and the laboratory model piles of Wersching.

The compression 'stress path' exhibits an initial small reduction in σ'_r/σ'_{rc} followed by a large increase to a value at peak shear stress of ≈1.5. In contrast, σ'_r/σ'_{rc} reduced to ≈0.8 in tension tests, before increasing to a final value of ≈1.25. A peak obliquity (δ_p) of ≈30° is mobilised before peak shear stresses are attained at δ_f ≈28°.

The laboratory tests of Wersching (1987) are (to my knowledge) the only other case history which reports the variation of radial effective stresses with shear stresses for piles in sand. These variations are compared with the Labenne data on Figure 9.4. Although no initial reduction in σ'_r was measured, Wersching's data show comparable increases in σ'_r and lower final values of σ'_r/σ'_{rc} in tension tests.

It is noteworthy that similar variations of the normal effective stresses were measured in *constant volume* direct shear interface tests on Hostun sand (Boulon & Nova 1990).

9.4.2 Factors causing σ'_r changes

This section considers possible factors causing the radial effective stresses changes during pile loading. The reductions and increases in these stresses, referred to above, are discussed separately.

9.4.2.1 Reductions in σ'_r

The radial effective stresses (σ'_r) reduced during the early stages of pile loading at Labenne, before increasing dramatically as the pile approached failure. The magnitudes of the initial reductions in σ'_r at Labenne were greatest in first-time tension tests, which consequently gave lower shaft capacities than compression tests or tension re-tests. The first-time tension tests also exhibited a much softer load-displacement characteristic[1].

[1]The first-time tension tests were LB2/L1T and LB1/FEX (see Table 6.3). Note that the residual stresses in these piles would also contribute to (but not fully explain) their soft stiffness characteristic (see Section 6.5.2).

These features may be compared to the anisotropic response of the Labenne sand seen in K_0 consolidated undrained (CK_0U) triaxial compression and extension tests (see Sections 5.1.7 and 6.6). By drawing an analogy between these data and the pile tests, it may be surmised that the pile installation process created an anisotropic soil fabric adjacent to the shaft which was such that in first-time tension tests, where the piles were loaded in the opposite direction to the previous (installation) direction, the sand showed more contractant behaviour (as suggested by the larger initial reductions in σ'_r) and a low stiffness. A much stiffer response was measured in tension re-tests and no reductions in σ'_r were observed. These characteristics are consistent with laboratory observations of the effects of induced anisotropy and principal stress rotations on the response of sand to shear (e.g. Arthur et al 1977).

Symes (1983) has shown that anisotropic effects are less pronounced in denser sands. It may therefore be conjectured that, given that the increases in σ'_r after the initial reductions were similar in tension and compression tests at Labenne (see below), tension piles installed in loose sands will experience lower overall increases in σ'_r. This hypothesis is compatible with data presented by Briaud & Tucker (1984) which showed that differences between tensile and compressive shaft capacities were more significant in loose sands (see Section 3.4.3).

9.4.2.2 Increases in σ'_r

Shear box interface tests, discussed in Section 5.1.7 and Appendix D, showed that medium dense to dense samples of Labenne sand dilate when sheared against a rough steel interface ($R_i \geq 5\mu m$). Most of this dilation occurred after ≈80% of the peak stress obliquity (δ_p) had been mobilised and ceased when the interface friction angle (δ) reduced to its ultimate value (δ_{cv}). The increases in radial effective stress measured in the pile tests, summarised on Figure 9.4, correspond directly with this dilation pattern: σ'_r begins to increase at $\delta \approx 0.8\delta_p$ and stops increasing at $\delta = \delta_f$. It therefore appears that the radial displacement of the sand adjacent to the pile shaft caused the observed increases in σ'_r.

Uesugi & Kishida (1986) studied the mechanisms of sand-steel shear using

a simple shear interface apparatus which allowed the total movement of the sample to be distinguished from the movement due to interface slippage. They concluded that the dilation of the sample is associated with the re-orientation of a narrow band of soil close to the interface after the initiation of slippage. Under these conditions, the amount of dilation is likely to be independent of the pile radius (R).

The radial effective stress change ($\Delta\sigma'_r$) at the pile shaft resulting from a boundary displacement (δh) can be estimated (as suggested by Boulon & Foray 1986 and others) from cylindrical cavity expansion theory, which shows that for an elastic soil mass of shear stiffness G:

$$\Delta\sigma'_r = 2\ G\ \varepsilon_c, \qquad \text{where } \varepsilon_c = \text{cavity strain} = \delta h/R$$

or

$$\Delta\sigma'_r/\sqrt{\sigma'_{v0}} = 2\ \delta h\ (G/\sqrt{\sigma'_{v0}})/R \qquad \text{Eqn. 6}$$

Seed & Idriss (1970), amongst others, have shown that, at small strains and at a given OCR, G is proportional to $\sqrt{\sigma'_{v0}}$ and varies with relative density[1]. Eqn. 6 therefore implies that $\Delta\sigma'_r/\sqrt{\sigma'_{v0}}$ varies linearly with (a) the relative density (D_r), (b) the degree of dilation and (c) the inverse of the pile radius.

The applicability of Eqn. 6 was investigated for the Labenne experiments using the shear stiffness moduli measured in pressio-penetrometer tests during *initial* inflation of the pressuremeter bag (located at h/R=7). These values, which are plotted against cavity strain on Figure 5.5, are expected to provide a good estimate[2] of the radial soil stiffness at the leading instrument position (h/R=8) on the ICP.

The increase in radial effective stress ($\Delta\sigma'_r$) at h/R=8 measured during first-time load tests at Labenne (after reaching a minimum during the initial stages of loading) were 30kPa and 25 ±4kPa for pile penetrations

---

[1]At larger strains, the shear stiffness becomes more dependent (for a given strain) on σ'_{v0} (or more precisely on the mean effective stress level p'_0) e.g. see Tatsuoka & Shibuya (1991).

[2]As the pressio-penetrometer is jacked into the ground in a similar way to the ICP and also has a similar diameter (89mm).

of 1.8m and 6m respectively. These increases are compared in Table 9.2 with the predictions for $\Delta\sigma'_r$ made using Eqn. 6 for a δh value of 0.05mm and pressuremeter moduli (G_p) derived from Figure 5.5.

It is evident that the predicted $\Delta\sigma'_r$ values are about twice those measured. The resolution of the stiffness data does not permit evaluation of Eqn. 6 for cavity strains (ε_c) less than 0.1%, but a tentative extrapolation suggests that the observed increases in σ'_r could be explained by a radial displacement (δh) of as little as ≈0.02mm. This δh value is significantly smaller than the values of between 0.05mm and 0.15mm measured in shear box interface tests on medium dense and dense samples of Labenne sand (see Figure D16, Appendix D).

Test	Depth (m)	δh (mm)	ε_c (%)	G_p (MPa)	$\Delta\sigma'_r$ (kPa)
LB1/L1C & LB1/L1T	5.55	0.05	0.1	27	54
LB2/L1C	1.45	0.05	0.1	30	60

Table 9.2 Predictions for $\Delta\sigma'_r$ using Eqn. 6

The discrepancy between predicted and measured δh values may be because (i) the shear box tests were performed under conditions of constant normal stress, (ii) the increases in σ'_r due to dilation were greater than those interpreted because reductions in σ'_r were taking place simultaneously due to the rotations of the principal stress directions or (iii) the initial stresses and boundary conditions in the shear box tests did not match those in-situ.

The applicability of Eqn. 6 is discussed further in Section 9.4.4.

9.4.3 Empirical correlations for σ'_r changes

The increases in σ'_r during pile loading at Labenne had a significant effect on the magnitudes of the peak local shear stresses. This observation prompted a re-assessment of the results from other laboratory model pile tests, where these changes were measured directly or could be inferred.

The case histories considered have been discussed in Chapter 3 and are listed in Table 9.3. One additional series of experiments considered is that performed by Eissautier (1986), (also reported by Boulon & Nova 1986), who tested 32mm diameter piles within a chamber (D=300mm) filled with Hostun no. 2 sand. A special lateral boundary condition was imposed on the chamber using a pressurised rubber bag. As the sample changed in volume, the pressure within this bag was regulated in accordance with appropriate stiffness characteristics measured in pressuremeter tests on Hostun sand (Renoud-Lias 1978). The radial effective stresses acting on the piles at shaft failure (σ'_{rf}) in compression tests were inferred from the boundary stresses for vertical effective stresses (applied at the sand surface) of up to 800kPa. Most model pile experiments tests have been performed at low stress levels and therefore the great merit of Eissautier's tests is that they have shown, using appropriate boundary conditions, how σ'_{rf} may be expected to vary with the stress level.

Values of $\Delta\sigma'_r$, ($= \sigma'_{rf} - \sigma'_{rc}$), for each case history (including Labenne), are listed in Table 9.3. We note that $\Delta\sigma'_r$:

- increases with sand density (D_r)
- reduces with pile radius (R)
- increases with σ'_{v0}
- is never negative but may be zero in loose sands.

Material	Reference	D_{50} (mm)	R (mm)	σ'_{v0} (kPa)	$\Delta\sigma'_r$(kPa) Loose	Med.	Dense[1]
Hostun 2	Eissautier (86)	0.7	16	10	14	-	36
	(L, P, C)[2]		16	40	28	-	128
			16	100	27	-	250
			16	300	0	-	450
			16	500	0	-	520
			16	800	0	-	640
Leucate	Lebègue (64)[3]	0.5	25	5	2	7.5	18
	(L, P, T)		65	5	0	3.5	11
			112	5	0	3	7
Leighton B.	Wersching (87)	0.45	57	17	10.7	-	-
	(L, J, C)		57	22	6.8	-	-
			57	28	6.6	-	-
Hostun 2	Puech et al (82)	0.7	28	20	13	-	64
	(F, P, T)						
Silty sand	Puech et al (82)	≈0.1	137	55	4	-	-
	(F, J, T)						
Labenne	This thesis	0.32	51	29	-	24.5	-
	(F, J, C)		51	62	14.4	-	-
			51	73	-	28.2	-
			51	84	17.0	-	-

[1] Loose: D_r < 35%, Medium: 35% < D_r < 65%, Dense D_r >65%. D_r estimated from CPT q_c profiles for field tests.

[2] F: field test, L: laboratory test; P: sand poured around pile, J:pile jacked; T: tested in tension, C: tested in compression.

[3] Values of $\Delta\sigma'_r$ are inferred from shear stress measurements assuming δ=24°

Table 9.3 Measured radial stress increases ($\Delta\sigma'_r$) in sands during pile loading

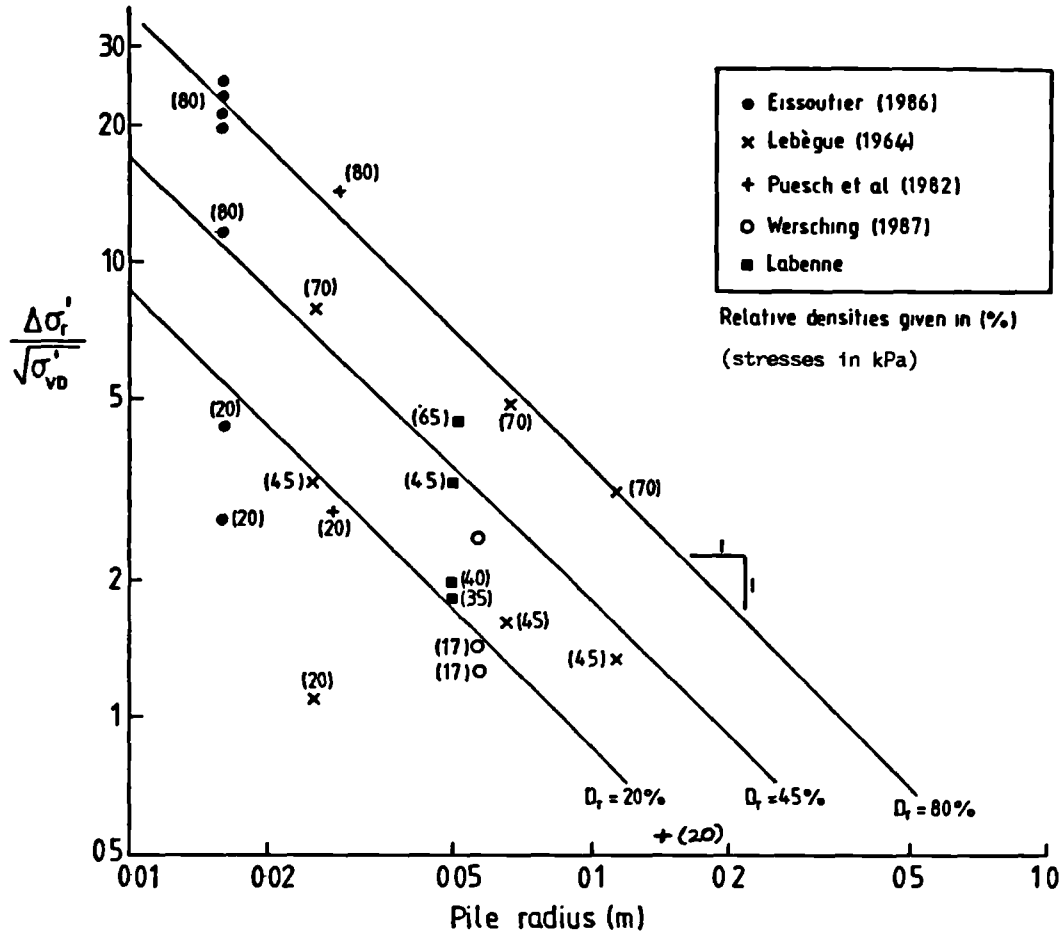

Figure 9.5 Measured variation of $\Delta\sigma'_r$ with R, D_r and $\sqrt{\sigma'_{v0}}$

These trends are broadly compatible with those predicted by Eqn. 6 and are investigated on Figure 9.5 by plotting the variation of $\Delta\sigma'_r/\sqrt{\sigma'_{v0}}$ with R, using logarithmic axes. It is evident that, for a constant relative density, the slope of the "$[\Delta\sigma'_r/\sqrt{\sigma'_{v0}}]$ v R" trend lines is ≈ -1. Regression analyses confirmed this dependence and gave the following best fit relationships (stresses in kPa):

$$\Delta\sigma'_r/\sqrt{\sigma'_{v0}} = (0.4 \pm 0.2)D_r/R, \text{ for all data} \qquad \text{Eqn. 7}$$

and $$\Delta\sigma'_r/\sqrt{\sigma'_{v0}} = 0.22\, D_r/R, \qquad \text{for the Labenne data only} \qquad \text{Eqn. 8}$$

Eqn. 7 provides an <u>upperbound</u> estimate of the value of $\Delta\sigma'_r$ for the cases

considered. This is because loose sand often showed no increases in radial effective stress and nor did denser sand at higher stress levels[1]. The value of $\Delta\sigma'_r$, for a given pile radius, therefore appears to depend on the dilatancy of the sand which is a function of both the relative density and the stress level. This dependence was deduced by Robertson (1982) from friction sleeve measurements made in Cone Penetration tests (see Figure 3.8). These measurements suggested (indirectly) that $\Delta\sigma'_r$ varied with the maximum angle of dilation of the sand (ν_{max}).

Been & Jeffries (1985) proposed that the dilatancy of the sand can best be described by the state parameter (ψ), defined as the difference between the void ratio of the sand (e) and critical state void ratio (e_{cs}) at the same stress level. Sand dilates under shear when $\psi < 0$ and contracts when $\psi > 0$. Re-interpreting Robertson's data on Figure 3.8 in terms of ψ values[2], suggests that for a pile of the same radius as a CPT tool (i.e. 18mm):

$$\Delta\sigma'_r/\sigma'_{rc} \approx [1.2\ e^{-9\psi} - 1]\ , \quad \text{for } \psi < 0 \text{ and } R = 18\text{mm} \qquad \text{Eqn. 9}$$

Correlations of this form[3], which also take the influence of pile radius into account, are likely to provide more consistent predictions for $\Delta\sigma'_r$ than Eqn. 7. However, the uncertainties involved in assessing ψ values for the sands in the data base precludes (at present) any further development of this approach.

9.4.4 General comments on relationships for $\Delta\sigma'_r$

Eqn. 6, $[\Delta\sigma'_r/\sqrt{\sigma'_{v0}} = 2\ \delta h\ (G/\sqrt{\sigma'_{v0}})/R\ ]$, was derived purely on theoretical considerations of the behaviour of sand in interface shear. It is encouraging that this equation predicts a similar trend to that

---

[1]In addition, $\Delta\sigma'_r$ values measured in compression tests were used, where possible, in preference to values measured in tension tests.

[2]using a correlation presented by Been & Jeffries (1985) between (ϕ'_p-ϕ'_{cv}) and ψ, and Bolton's (1986) relationship between (ϕ'_p -ϕ'_{cv}) and ν_{max}. A similar approach suggested that the in-situ ψ value of the Labenne sand varied between -0.15 and -0.05.

[3]The 'amplification factor' in dilatometer tests has been related to ψ in a similar way (see Jamiolkowski et al 1988).

backfigured from $\Delta\sigma'_r$ measurements i.e. Eqn. 7 : $\Delta\sigma'_r/\sqrt{\sigma'_{v0}} = (0.4 \pm 0.2)$ D_r /R. There are however a number of noteworthy inconsistencies between both equations:

(i) The inferred radial displacement of sand at the pile interface during the ICP tests ($\delta h \approx 0.02$mm) is at least three times smaller than δh values measured in shear box interface tests on the Labenne sand.

(ii) The value of δh is expected to be related to the mean particle size of the sand, D_{50}, (see Boulon & Nova 1990) and the interface roughness, R_t, (as verified by teflon shear box tests on Labenne sand, see Appendix D). However, although D_{50} varied significantly in the case histories listed in Table 9.3, the regression analyses used to develop Eqn. 7 showed no systematic dependence on D_{50}. (No information concerning the R_t values used in these tests is provided).

(iii) Shear box tests show that loose sands (or denser sands at higher stress levels) contract when sheared against an interface and consequently Eqn. 6 predicts that σ'_r at shaft failure (σ'_{rf}) will be significantly <u>less</u> than the pre-loading σ'_r value. The data summarised on Table 9.3 indicate that this does not occur in practice.

It is suggested that a systematic series of direct shear interface tests performed under conditions of constant normal stiffness, such as those reported for rock samples by Johnston et al (1987), may help to explain some of these anomalies. These tests should attempt to match the (estimated) conditions existing adjacent to a pile in sand.

9.5 INTERFACE FRICTION ANGLES

It has been shown in Chapter 6 that the interface friction angle at peak local shear stress (δ_f) is closely comparable to the *constant volume* interface friction angle (δ_{cv}) measured in shear box and ring shear interface tests. For this reason, additional research was initiated at Imperial College (Everton 1991) to examine the factors that control the magnitudes of δ_{cv} measured in shear box interface tests and hence give

further insight into the factors influencing shaft capacity. The tests were performed on a number of *dry uniform quartz sands*, having mean particle sizes ranging from 0.04mm to 1.5mm. The normal stress was varied between 25kPa and 200kPa and relative densities ranged from 30% to 80%.

These tests showed that the magnitude of δ_{cv} was independent of the initial relative density of the sample but varied significantly with the mean particle size (D_{50}). The measured variation of δ_{cv} with D_{50} is shown in Figure 9.6 for all tests that used a rough steel interface (centre line average roughness, R_1 = 8 ±2μm) and normal stresses (σ'_n) between 40kPa and 120kPa. Also included on this figure are the δ_{cv} values measured in equivalent tests on Labenne sand (as described in Section 5.1.7) and Leighton Buzzard sand (Lemos 1986); these tests also showed that δ_{cv} was independent of relative density.

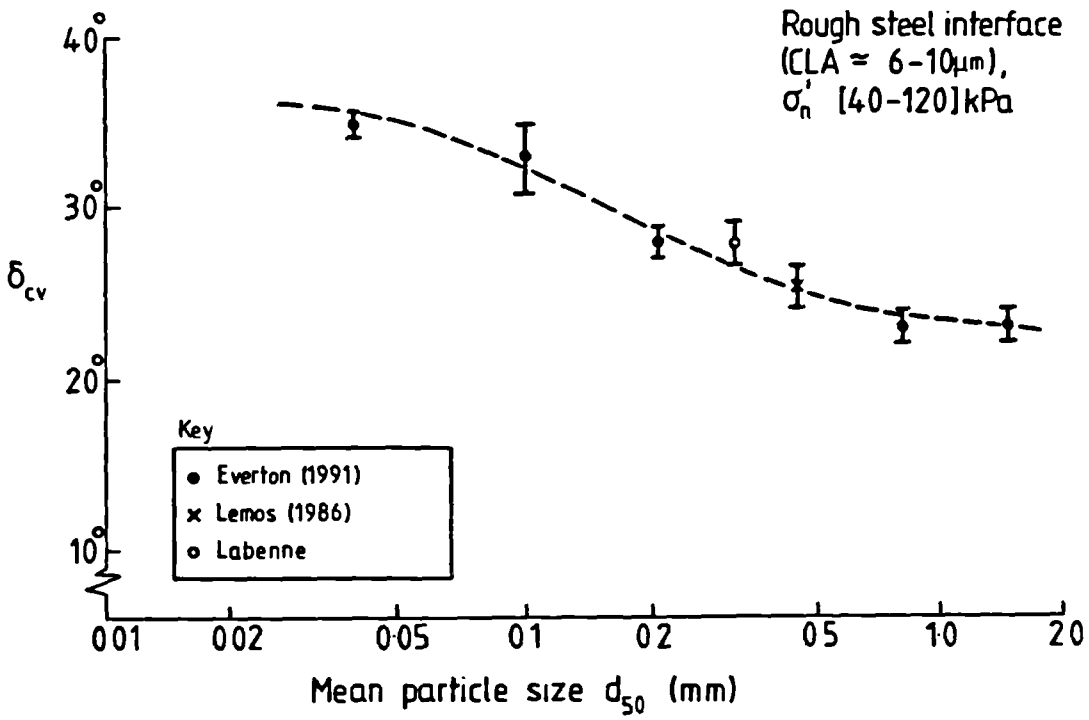

Figure 9.6 Variation of δ_{cv} with D_{50} for sand sheared against a 'rough' steel interface

The three data sets are compatible and display a marked reduction of δ_{cv} with D_{50}. This trend, if extrapolated to the field, suggests that, for the same values of σ'_{rf}, the shaft capacity of a steel pile in a fine sand (D_{50} ≈0.1mm) will be almost 50% higher than that of an equivalent pile in a coarse sand (D_{50} ≈1.0mm). It is noteworthy that the API (1989) guidelines imply that the capacity in fine sand will be ≈50% lower than in coarse sand and that the interface friction angle depends strongly on relative density.

Two other features emerged from the shear box tests:

- δ_{cv} values measured with concrete interfaces were comparable to the soil on soil ϕ'_{cv} values, suggesting that failure will not be initiated at the shaft of concrete piles.
- In the experiments performed by Everton (1991) and Lemos (1986), δ_{cv} reduced by between 5° and 10° when the normal effective stress (σ'_n) was increased from 30kPa to 200kPa. A smaller dependence on σ'_n was measured in the tests on Labenne sand (δ_{cv} reduced by 2° between σ'_n =40kPa and 120kPa).

Little dependence of δ_{cv} on stress level (σ'_n) was observed in interface tests performed using the simple shear apparatus (Uesugi & Kishida 1986), torsional shear apparatus (Yoshimi & Kishida 1981) and ring shear apparatus (Jardine & Ridley 1992). It is suggested that the trend measured in shear box tests may have arisen because of the difficulties associated with reducing (and correcting for) the friction developed between the top half of the shear box and the interface. Further research on the dependence of δ_{cv} on σ'_n is required, as it clearly has important implications for the design of piles.

The variation of δ_{cv} with D_{50}, shown on Figure 9.6, is consistent with the measurements made in the interface tests of Uesugi & Kishida at normal stress levels up to 1000kPa and the limited set of ring shear data reported by Jardine & Ridley. The tests of Uesugi & Kishida indicated that a more fundamental parameter controlling the magnitude of δ_{cv} was the interface roughness (measured over a gauge length equal to D_{50}) divided by D_{50}. However, this roughness value is not easily determined and it is

suggested that δ_{cv} for typical industrial steel piles (CLA roughness, $R_1 \approx 10\mu m$) may be approximated using Figure 9.6.

9.6 IMPLICATIONS OF CORRELATIONS FOR σ'_{rc} AND $\Delta\sigma'_r$

This section examines the implications of the correlations for σ'_{rc} and $\Delta\sigma'_{rc}$ (Eqns. 4 & 7) for the shaft capacities of displacement piles installed in *normally consolidated sand deposits of uniform relative density*. The precise magnitudes of the predictions should not be considered to be generally applicable because of the many assumptions and limited data on which these correlations are based.

The Labenne (and other) data suggested that σ'_{rc} and $\Delta\sigma'_{rc}$ for a displacement pile installed in a normally consolidated quartz sand may be estimated using the following expressions:

$$K_c = \sigma'_{rc}/\sigma'_{v0} = 0.7\ (\sigma'_{v0})^{-0.11}\ e^{2.91Dr}\ (h/R)^{-0.33} \qquad \text{(Eqn. 4)}$$

and

$$\Delta\sigma'_r/\sqrt{\sigma'_{v0}} = (0.4 \pm 0.2)D_r\ /R \qquad \text{(Eqn. 7)}$$

Given that the peak local shear stress (τ_f) is given by $\tau_f = (\sigma'_{rc} + \Delta\sigma'_r)\tan\delta_{cv}$, these expressions may be re-arranged to give the following relationship for the average shaft shear stress τ_{av} ($= \int^L \tau_f\ dz$) in a material of constant relative density (assuming that δ_{cv} is independent of the stress level):

$$\tau_{av} = 0.7 \tan\delta_{cv}\ e^{2.9\ Dr}\ R^{0.33} \int^L (\sigma'_{v0})^{+0.89}\ (L-z)^{-0.33}\ dz + 0.4 \tan\delta_{cv}\ D_r/R \int^L (\sigma'_{v0})^{+0.5}\ dz \qquad \text{Eqn. 10}$$

The variation with L/R of the average β value (β_{av}) = $\tau_{av}/\ (\sigma'_{v0})_{mean}$ predicted by Eqn. 10 (using numerical integration) is given on Figure 9.7 for D_r values of 50% and 80%, δ_{cv} =30° and σ'_{v0} =10z (kPa). Some important trends regarding the effects of pile radius and slenderness ratio (L/R) may be noted:

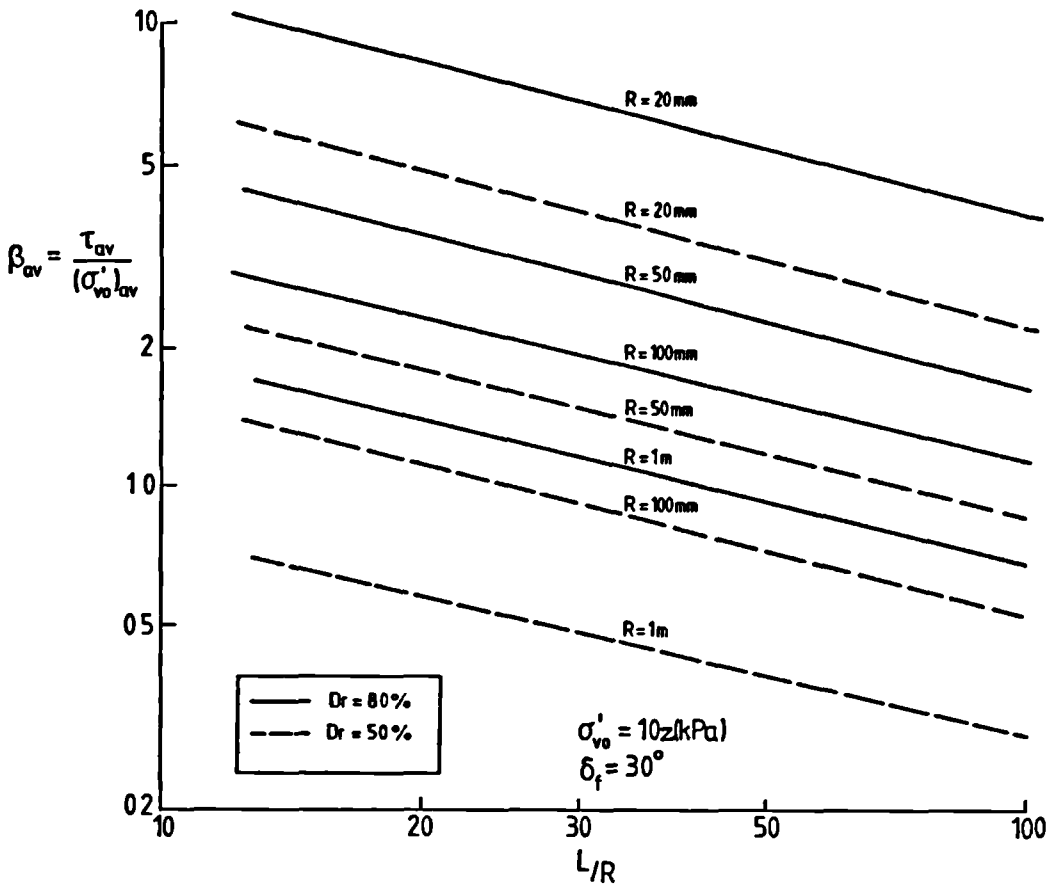

Figure 9.7 Predicted variation of β_{av} (Ktanδ) with D_r, R and L/R

(i) β_{av} values for a typical laboratory pile of radius =20mm are about <u>six</u> times those values predicted for a large offshore pile (R=1m).

(ii) The influence of pile radius on β_{av} values diminishes rapidly; for a given L/R value, β_{av} for R=1m is typically only 40% less than that predicted for R=100mm and only 10% less than the predictions for R=300mm.

(iii) β_{av} reduces with L/R and the rate of this reduction is similar for piles of all radii. This is an interesting result given the appreciable difference between the stress levels operating adjacent to large and small diameter piles at a given L/R ratio.

Following from (iii), it may be shown that the average shaft shear stress (τ_{av}) increases in proportion to $L^{(0.54 \pm 0.04)}$ for piles of all diameters. By comparison, conventional 'earth pressure' design methods (e.g. API 1989) assume that τ_{av} increases in proportion to L, and average shear stress approaches (e.g. Lings 1985) assume τ_{av} is independent of pile length (for L/R > 40).

Kérisel (1964) noted that the magnitudes of β_{av} values developed on the shafts of laboratory piles were not compatible with those mobilised by full scale piles. It is evident from the foregoing this is because of the much larger relative increases in radial effective stress which model piles experience during loading; the contribution of these increases to pile capacity are very significant (and dominant) for laboratory piles but are negligible for full scale piles (R ≥300mm). Such scale effects also have important implications for model pile tests performed in the centrifuge.

9.7 COMPARISONS WITH RESULTS FROM OTHER FIELD TESTS

The expressions developed in the preceding sections are based primarily on the observations made at Labenne. This section investigates their general applicability to full scale pile behaviour, using data from six well documented driven pile test sites. The details of the case histories are summarised in Tables 9.4 & 9.5 and the mean CPT q_c profiles (that have been reported) are shown on Figure 9.8. This data base covers sand deposits with relative densities between 20% & 95% and piles with a maximum length of 20m and maximum diameter of 508mm. All piles were closed-ended.

9.7.1 Shaft capacities in compression

Predictions for *compressive* shaft capacities (τ_{av}) are compared with measured τ_{av} values[1] in Table 9.4. These predictions assume (stresses in kPa):

[1]The data base of reliable measurements of τ_{av} in compression tests is extremely small because of the difficulties associated with measuring the residual loads in piles after installation (see Section 3.4.1).

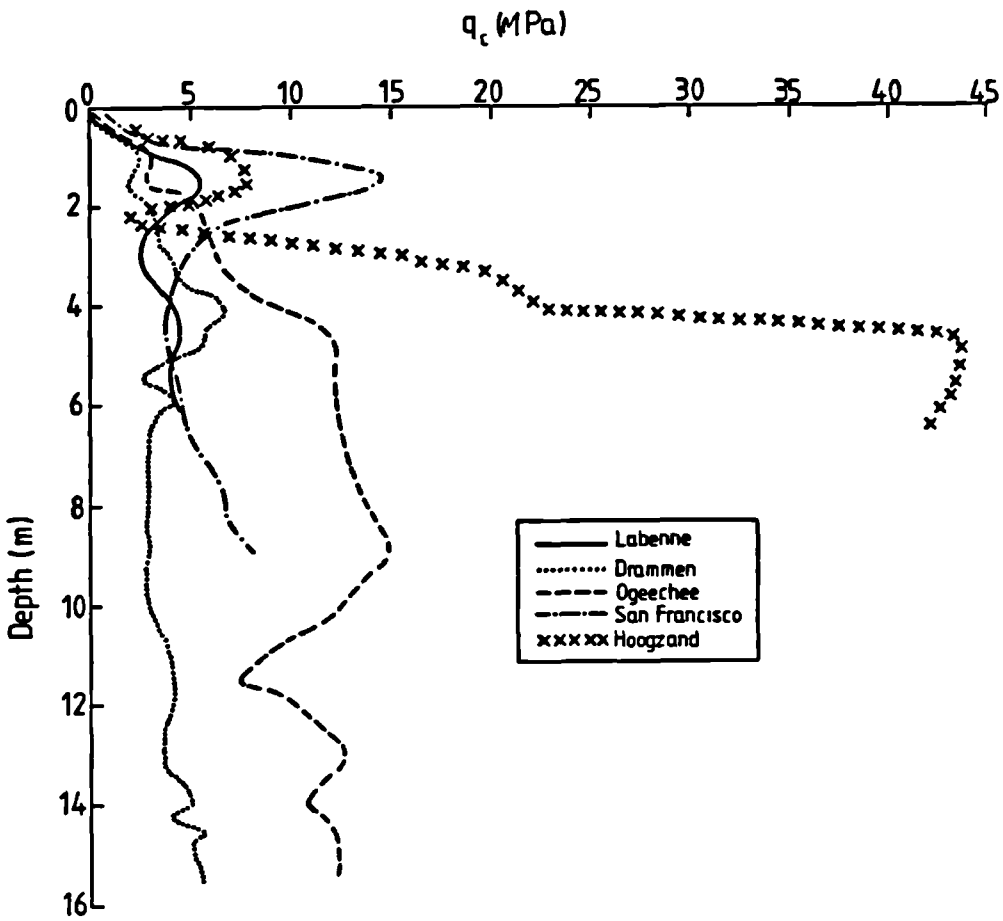

Figure 9.7 CPT q_c profiles at test sites

(i) $\sigma'_{rc} = 0.0114\ q_c\ (\sigma'_{v0})^{0.2}\ (h/R)^{-0.33}$ (Eqn. 2)

(ii) $\Delta\sigma'_r/\sqrt{\sigma'_{v0}} = 0.22\ D_r\ /R$ (Eqn. 8),
where $D_r = (1/2.91)\ \log_e\ [q_c\ /61(\sigma'_{v0})^{0.71}]$ (after Lunne & Christoffersen 1983 for normally consolidated sands)

(iii) δ_f is independent of σ'_r and varies with D_{50} as shown in Figure 9.6 (for steel piles)

(iv) τ_{av} is given by: $(1/L) \int^L \tau_f\ dz = (1/L)\tan\delta_f \int^L (\sigma'_{rc} + \Delta\sigma'_r)\ dz$.

The predictions for τ_{av} are seen to be within ≈10% of the capacities measured at Labenne and within ≈20% of capacities measured at the other sites, despite the wide differences between the q_c values and piles at these sites with those at Labenne. In addition, it may be observed that the equations predict the stabilisation of τ_{av} with pile depth observed at Labenne, Drammen and Ogeechee. This stabilisation is not due to:

- smaller increases in radial effective stresses at depth during pile loading[1]. At each site (except Labenne), Eqn. 8 predicts comparable (and insignificant) mean increases in σ'_r for all pile lengths (see Table 9.4)
- a similar type of q_c profile at each site. This is evident on examination of the ratios of the measured τ_{av} values to the *mean* q_c values; at Ogeechee, $\tau_{av}/(q_c)_{mean}$ reduced from 9.5 x10^{-3} to 6.9 x10^{-3} for an increase in pile length (L) from 6.2m to 15m, and at Drammen, $\tau_{av}/(q_c)_{mean}$ was 9.0 x10^{-3} for L=8m and 7.4 x10^{-3} for L=16m.

These observations suggest that the τ_{av} profiles at Drammen and Ogeechee arose because σ'_{rc} varied with h/R in a similar way to that measured at Labenne.

9.7.2 Shaft capacities in tension

It is assumed tentatively that, as at Labenne, σ'_r reduced by ≈20% during the initial stages of tension loading[2] and that σ'_{rf} at peak tensile capacity is given:

$$\sigma'_{rf} \approx 0.8\sigma'_{rc} + \Delta\sigma'_{rd}, \qquad \text{Eqn. 11}$$

where $\Delta\sigma'_{rd}$ is the increase in σ'_r due to dilation (Eqn. 8)

No q_c profiles were reported at Arkansas River or Low-Sill, where 8 tension tests were performed (see Table 9.5). Eqn. 4 was used to calculate σ'_{rc} values at these sites, assuming average relative densities (D_r) assessed by Toolan et al (1990) from Standard Penetration tests (Eqn. 4 relates σ'_{rc} to D_r).

The predictions for tensile shaft capacities are compared with measured capacities in Table 9.5. Most predictions fall within 20% of the measured values, apart from the 15m long pile at Ogeechee where the tensile capacity is under-predicted by ≈40% and at Drammen where the capacity of the shorter pile is over-predicted by 56%.

---

[1]because of reduced dilatancy at depth (as suggested by Toolan et al 1990; see Section 3.4.10).

[2]As discussed in Section 9.4.2.1, the initial reductions in σ'_r may be a function of relative density.

Site	D_{50} (mm)	D (mm)	L (m)	Mean σ'_{rc} (kPa)	Mean σ'_{rf} (kPa)	δ_f (°)	Pred. τ_{av} (kPa)	Meas. τ_{av} (kPa)	Pred./ meas. τ_{av}
Labenne	0.32	102							
		(LB1)	2.0	31.2	43.4	30[1]	25.1	24.8	1.01
			4.0	27.2	39.4	30	22.7	21.3	1.06
			5.5	28.5	41.6	30	24.0	27.0	0.89
		(LB2)	2.0	29.4	41.7	30	24.1	25.5	0.95
			4.0	29.9	42.6	30	24.6	22.0	1.12
			5.5	31.2	45.1	30	26.0	28.1	0.93
Drammen	0.20	280	8.0	34.3	38.8	34[2]	26.2	30.0	0.87
(Gregersen et al 1973)			16.0	30.0	34.5	34	23.3	27.0	0.86
Ogeechee	0.5	457	6.2	92.2	97.2	27	49.5	59.4	0.83
(Vesic 1970) & 0.1			8.9	115.0	119.5	27	60.9	59.6	1.02
			12.0	106.0	110.0	27	56.0	68.8	0.81
			15.0	110.0	115.5	27	58.9	67.4	0.87
Hoogzand	0.13	356	6.75	303.0	312.0	31	188	202	0.93
(Beringen et al 1979)									
San Fran.	0.5	273	9.15	52.0	58.0	25	27.0	22.0	1.23
(Briaud et al 1989)									

[1] Mobilised on pile casings during installation at Labenne

[2] Concrete piles

Table 9.4 Predictions for compressive shaft capacities

Site	D (mm)	L (m)	Mean σ'_{rc} (kPa)	Mean σ'_{rf} (kPa)	δ_f (°)	Pred. τ_{av} (kPa)	Meas. τ_{av} (kPa)	Pred./ meas. τ_{av}
Labenne[1]	102	5.92	32.2	39.7	30	22.9	26.5	0.86
Ogeechee[2]	457	15.0	110.0	93.5	27	47.6	71.4	0.67
Drammen[3]	280	8	34.3	32.4	34	21.8	14.0	1.56
	280	16	30.0	28.3	34	19.1	19.0	0.99
Hoogzand[4]	356	6.75	303	251	31	151	162	0.93
Arkansas[5]	324	16.2	91.3	80.5	26	39.3	43.0	0.91
	406	16.1	106.1	91.0	26	44.4	38.3	1.16
	508	16.2	108.1	91.3	26	44.5	37.8	1.18
	406	12.2	80.0	69.0	33	44.8	41.2	1.08
Low-Sill[6]	508	19.8	119	99.1	28.5	53.8	47.9	1.12
	406	20.1	106	89.7	28.5	48.7	61.2	0.80
	406	13.7	45	40.2	33	26.1	36.0	0.73
	457	19.8	115	96.3	28.5	52.3	51.9	1.01

[1]Test LB2/L1T

[2]Vesic (1970), see Table 9.4

[3]Gregersen et al (1973), see Table 9.4

[4]Beringen et al (1979), see Table 9.4

[5]Mansur & Hunter (1970), D_{50} = 0.4±0.2mm, D_r =63% from SPT's, precast concrete pile for L=12.2m.

[6]Mansur & Kaufman (1958), 15m of silt (D_r =55%) with δ_f=33° overlying dense (D_r =90%) medium sand with δ_f =27°

Table 9.5 Predictions for tensile shaft capacities

9.7.3 Comparison with existing pile design methods

Three popular design methods used to assess the shaft capacities of displacement piles in sand are:

(i) The API(1989) recommendations (see Table 3.1)

(ii) Relationships between τ_{av} and D_r. (The more recent of these correlations, proposed by Toolan et al (1990) *for tension piles*, is reviewed here; see Figure 3.5)

(iii) The Laboratoire des Ponts et Chaussées (LPC) cone method which relates the local ultimate shear stress to the CPT q_c value (after Bustamante & Gianeselli 1982; see Table 3.2).

The shaft capacities predicted by these methods and the "ICP method", for the pile tests listed in Tables 9.4 & 9.5, are compared with measured capacities in Table 9.6. It is evident that for piles in this data base:

- API(1989) is the most conservative of the methods and typically under-predicts capacities by ≈30%. The method only appears to give reasonable predictions for piles greater than ≈15m in length in medium dense sands.
- The LPC cone method shows the greatest scatter and would over-predict the capacities of longer piles.
- The method of Toolan et al gives good predictions as it recognises (unlike the two other methods) the tendency for τ_{av} to stabilise with pile length. However, it should be borne in mind that the method is based on a best fit trend line of measured τ_{av} values in only 24 tension tests *including* 12 of the tests listed in Table 9.5.

The "ICP method" is seen to give the best predictions. This is because the method:

- incorporates the feature which causes the apparent stabilisation of τ_{av} with depth i.e. the reduction in σ'_{rc} with distance from the pile tip (h/R).

- acknowledges that the variation in σ'_r during pile loading is different in first-time compression and tension tests and also varies with the pile diameter.
- allows for the dependence of the interface friction angles on the soil and pile type.

9.8 FINAL COMMENTS

The observations made in the Labenne experiments have been assimilated into a series of correlations which are in good agreement with the general trends shown by displacement piles in sand and limited data base of existing field measurements. The experiments have provided fresh insight into the factors controlling shaft capacities of piles in sand and demonstrated the great rewards that can be realised from using high quality instrumented piles.

It is clear, however, that there is considerable scope for improvement of the proposed correlations. Further high quality instrumented tests are urgently required. These should examine the critical dependence of unit shaft frictions on (a) the pile diameter, (b) the initial relative density and stress state of the sand, (c) the direction of loading and (d) the pile end condition.

Site	D (mm)	L (m)	Test	ICP method	API (89)	Toolan (90)	LPC (82)
Labenne	102	2.0	Comp.	0.98	0.31	-	0.79
		5.5	Comp.	0.91	0.57	-	0.85
		5.9	Tens.	0.86	0.62	0.87	0.85
Drammen	280	8.0	Comp.	0.87	0.51	-	1.53
		16.0	Comp.	0.86	0.95	-	1.68
		8.0	Tens.	1.56	1.10	1.43	1.53
		16.0	Tens.	0.99	1.35	0.89	1.68
Ogeechee	457	6.2	Comp.	0.83	0.37	-	0.53
		8.9	Comp.	1.02	0.47	-	0.70
		12.0	Comp.	0.81	0.55	-	0.68
		15.0	Comp.	0.87	0.65	-	0.72
		15.0	Tens.	0.67	0.61	0.67	0.68
Hoogzand	356	6.75	Comp.	0.93	0.16	-	0.58
		6.75	Tens.	0.93	0.20	0.68	0.58
San Fran.	273	9.15	Comp.	1.23	1.52	-	1.29
Arkansas	324	16.2	Tens.	0.91	0.95	0.88	-
	406	16.1	Tens.	1.16	1.06	0.99	-
	508	16.2	Tens.	1.18	1.08	1.01	-
	406	12.2	Tens.	1.08	0.75	0.90	-
Low-Sill	508	19.8	Tens.	1.12	0.89	1.31	-
	406	20.1	Tens.	0.80	0.72	1.05	-
	406	13.7	Tens.	0.73	0.57	0.89	-
	457	19.8	Tens.	1.01	0.79	1.15	-
No. of tests				23	23	13	15
Average				0.98	0.73	0.98	0.98
St. Deviation				0.18	0.34	0.21	0.41

Table 9.6 Ratios of predicted to measured shaft capacities for four methods

CHAPTER 10

SUMMARY OF ICP TESTS IN CLAY

CONTENTS OF CHAPTER 10

SUMMARY OF ICP TESTS IN CLAY

10.1 INTRODUCTION 372

10.2 PILE INSTALLATION 372

10.2.1 Radial and shear stresses 372

10.2.2 Pore pressure 375

10.2.3 Radial effective stress 377

10.3 EQUALISATION 378

10.3.1 Radial total stress 378

10.3.2 Pore pressure dissipation 379

10.3.2.1 Radial distribution after installation 380

10.3.2.2 Permeability 381

10.3.2.3 Coefficient of consolidation 382

10.3.3 Radial effective stress 385

10.3.3.1 Short term minimum 386

10.3.3.2 Set-up after full equalisation 387

10.3.4 Equalised radial effective stress 387

10.4 LOAD TESTING 390

10.4.1 Overall shaft displacement behaviour 390

10.4.2 Local shear stress variations 392

10.4.3 Loading effective stress paths 394

10.4.3.1 General 394

10.4.3.2 Stress path shapes 395

10.4.3.3 Angles of interface friction 397

10.5 THE 'h/R' EFFECT' 399

10.5.1 General observations 400

10.5.1.1 Radial total stress 400

10.5.1.2 Pore pressure 402

10.5.1.3 Equalised radial effective stress 403

10.5.2 Factors causing the 'h/R effect' 403

10.5.2.1 Instantaneous installation of a frictionless pile 403

10.5.2.2 The effects of time 405

10.5.2.3 The influence of cyclic loading 408

10.5.3 Summary 411

10.1 INTRODUCTION

This chapter reviews the trends that have become evident from the ICP tests in Cowden till and Bothkennar clay. The pile tests performed by Bond (1989) in the London clay (see Section B2, Appendix B) are also discussed so that a more complete picture of the characteristics of displacement piles, as shown by ICP tests, may be obtained.

The observations made during installation, equalisation and load testing are summarised and compared in Sections 10.2, 10.3 and 10.4 respectively. General patterns of behaviour are identified and these are synthesised in Chapter 11 with the full data base of measurements available from other instrumented pile test programmes in clays.

Section 10.5 examines in detail the trend seen in the ICP tests and other instrumented pile tests for stresses acting at fixed depths to reduce as the pile penetrates to deeper levels. This phenomenon has not been generally recognised, but has important implications for pile design.

10.2 PILE INSTALLATION

10.2.1 Radial and shear stresses

Four main features were shown by the radial total stresses (σ_{ri}) and shear stresses (τ_{rz}) recorded during installation of the ICP:

(i) At all three sites, the profiles with depth of σ_{ri} and τ_{rz} recorded at each instrument position (i.e. leading, following and trailing) reflected closely the profiles of the CPT end resistance (q_c), undrained shear strength (c_{u0}) and pressuremeter limit values (p_{lim}).

(ii) σ_{ri} and τ_{rz} measured in a given soil horizon reduced as the pile penetrated to deeper levels i.e. they fall with distance from the pile tip (h/R).

(iii) The shear stresses (τ_{rz}) mobilised in the tests in the Cowden till and London clay tests exhibited a strong dependence on the jacking velocity; τ_{rz} fell by over 40% when the jacking rate was reduced

from 500mm/min to 80mm/min.

(iv) Radial total stresses (σ_{r1}) showed no significant dependence on rate at any of the three sites.

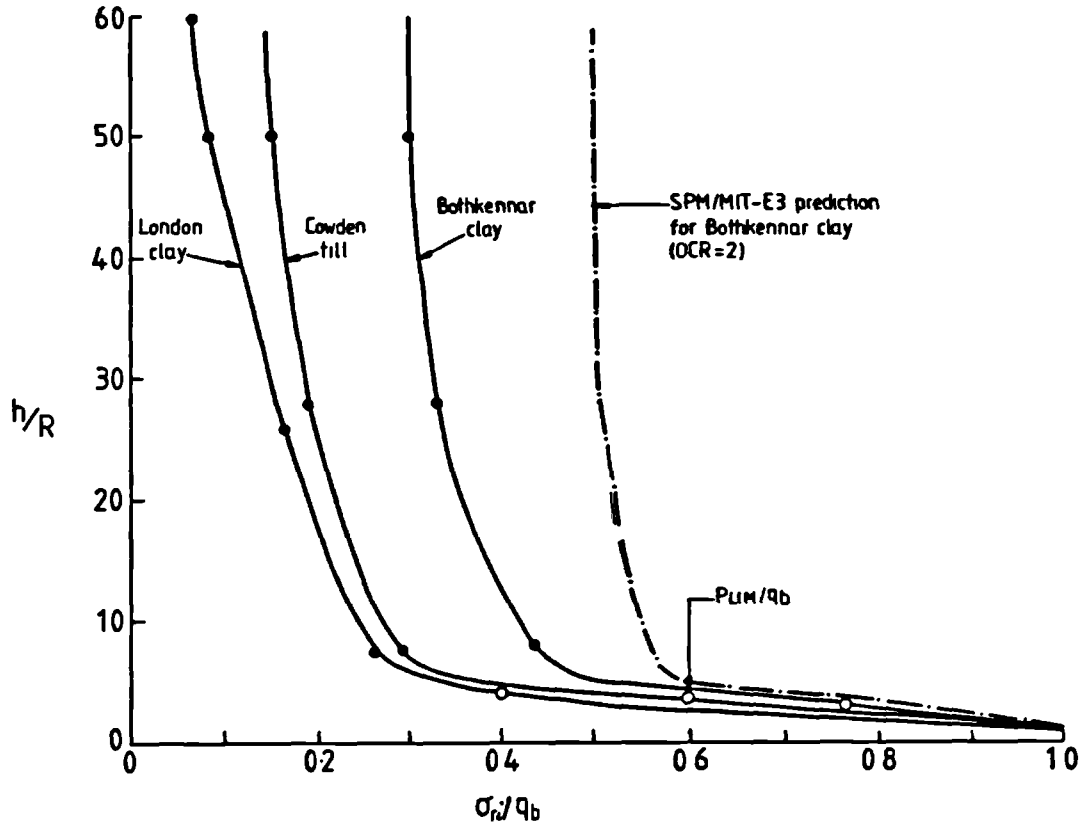

Figure 10.1 Mean variations of σ_{r1}/q_b with h/R

The combined effect of features (i) and (ii) is shown on Figure 10.1, which plots the mean ratios of the radial stress to the pile end bearing (σ_{r1}/q_b) against h/R for all depths penetrated by the piles[1]. This diagram illustrates the strong influence of h/R on the σ_{r1} distribution.

During steady (closed-ended) penetration, conditions at the pile tip are analogous to those of an expanding spherical cavity and, to a first approximation, $\sigma_{r1} \approx q_b$. As the tip advances, σ_{r1} reduces and is of similar

[1]No installation q_b values are reported for the ICP tests in the London clay and, for these tests, q_b is assumed equal to q_c.

magnitude to the pressuremeter limit pressure (p_{lim}) when h/R ≈3, so equalling the stress required to expand a cylindrical cavity. With increasing penetration, the focus of stress concentration near the tip moves further away and σ_{ri} continues to reduce so that, at h/R ≈50, σ_{ri} attains values that are between 3 and 10 times less than the maximum stress recorded (when h/R ≈0). The rate of stress reduction with h/R is not unique and varies with soil type; factors that may affect this rate are discussed in Section 10.5.

The two dimensional nature of pile installation, as shown by Figure 10.1, is clearly in conflict with the cylindrical Cavity Expansion Method (see Section 2.3.1), which assumes that the soil is strained monotonically in the radial direction only and that σ_{ri} is equivalent to p_{lim} over most of the shaft length. The Strain Path Method (SPM), which adopts a more realistic two dimensional model of the installation process (see Section 2.3.2), does predict that stresses reduce with increasing h/R but, as seen on Figure 10.1, the rate of this reduction is far less than that observed experimentally.

Log-log regression analyses of all the installation radial stress data gave the best fit power-law relationships listed in Table 10.1. These relationships showed no systematic variation with pile depth (L < 6.5m) and the quoted scatters are believed to reflect the inherent variability of the materials.

Cowden till	$\sigma_{ri}/q_b = 0.61\ (h/R)^{-0.36}$	Scatter: ±18%
Bothkennar clay	$\sigma_{ri}/q_b = 0.72\ (h/R)^{-0.24}$	Scatter: ±6%
London clay	$\sigma_{ri}/q_b = 0.95\ (h/R)^{-0.59}$	Scatter :±25%

Table 10.1 Correlations for σ_{ri} data ($8 \le h/R \le 50$)

10.2.2 Pore pressure

The pore pressures measured during installation showed two common features:

- Pressures decreased at the beginning of a jacking stage and remained at lower values (u_m) throughout the push.
- On the completion of a jacking stage, pressures rose rapidly to relatively steady large positive values (u_s).

The pore pressures measured during jacking stages (u_m) were generally more variable and showed less consistent patterns than the stationary pressures (u_s). It has been shown in Chapters 7 & 8 that, at both Cowden and Bothkennar, the values of u_m measured at pile velocities in excess of 1mm/min (e.g. during installation) were probably not representative of the pressures acting on the principal displacement shear. The pore pressures acting in this shear zone control the shaft's resistance to jacking and were assessed as falling between the recorded values of u_m and u_s (see Section 10.2.3) i.e. the pressures *at the pile shaft* during jacking appear to be lower than those acting on the principal displacement shear.

A better understanding of the complicated patterns of the pore pressure data can be obtained by recognising that the local (undrained) pressures are a combination of four components:

(a) The initial ambient (hydrostatic) profile (u_0)

(b) Positive pore pressure developed due to the increase in mean total stress (u_{ts}) caused by insertion of the pile in the ground

(c) Shear induced pressure (u_{sh}) as the penetration of the pile distorts the surrounding clay - this component may be negative or positive depending on whether the soil contracts or dilates when sheared.

(d) Positive cyclic pore pressure (u_{cyc}) induced by the many loading and re-loading cycles (i.e. each jacking stage) imparted to the soil during installation

i.e. $u = u_0 + u_{ts} + u_{sh} + u_{cyc}$

With these components in mind, further general observations concerning the pore pressure readings can be made.

(i) The reduction in pressure at the beginning of a jacking stage suggests that there is a tendency for the material adjacent to the pile shaft to dilate when sheared (i.e. $u_{sh} < 0$). A review of this phenomenon in Appendix A concludes that pressure reductions are related to the (dilatant) characteristics of the *partially equalised, pre-sheared soil*; no pressure reductions are measured by sensors that are continuously entering 'fresh' strata (such as in piezocone tests).

(ii) At Cowden, a direct correlation was observed between shear stresses falling and pore pressures (u_m) rising, when the jacking rate was slowed from 500mm/min to 80mm/min. The rate dependence of shear stresses therefore appeared to be due to a rate effect on the shear induced pressures (u_{sh}) and possible partial drainage effects[1]. It should be noted, however, that at velocities less than 10mm/min (during the plunging stages of load tests), u_{sh} seemed to be highly rate dependent at all sites, even though the corresponding shear stresses were practically unaffected by rate (see Figure A2, Appendix A).

(iii) Rapid pore pressure increases (from u_m to u_s) were seen at the end of jacking, suggesting that larger positive excess pore pressures exist further away from the shaft and water flows radially towards the pile when it comes to rest. A much slower increase in pressure was registered at the shaft in heavily overconsolidated clays (e.g. in the London clay and at shallow depths at Cowden), implying that a more extensive zone of negative shear induced excess pressures existed in these materials. This effect may have been exaggerated by a poor response time of the probes caused by cavitation of the probe fluid during installation in these materials.

---

[1]Although the ICP tests in the London clay showed a similar rate dependence of shear stresses, no corresponding pore pressure effect was observed. This may have been because the u_m values measured were at the cavitation limit of the probe fluid and that the real suctions in the material during jacking were lower than this limit.

(iv) The maximum excess pore pressures measured at fixed depths when the piles were stationary, Δu_{max} ($= u_s - u_0$), reduced at all sites with the distance from the pile tip (h/R) in sympathy with the observed reductions of σ_{r1} with h/R. Δu_{max} values also showed a similar dependence on soil consistency to the σ_{r1} measurements. It is suggested that, when shear induced pressures are not extensive, these maxima reflect increases in the mean total stresses associated with pile installation.

(v) Cyclic induced positive pore pressures (u_{cyc}) may complicate the pore pressure regime even further; these are likely to increase with h/R as the number of jacking cycles at any given depth increases.

10.2.3 Radial effective stress

The evaluation of the radial effective stresses mobilised on the principal displacement surface during fast installation is hindered by the anomalous pore pressures measured at the pile face. However, if the interface friction angle (δ) mobilised on the SST's during *slow* load tests is assumed to operate during installation, σ'_r values may be interpreted using the installation τ_{rz} values from: $\sigma'_r = \tau_{rz}/\tan\delta$. Values of $K_1 = (\sigma'_{r1}/\sigma'_{v0})$ calculated in this way, assuming $\delta = 20°$ and 30° at Cowden and Bothkennar respectively (see Section 10.4), are summarised in Table 10.2. These K_1 values correspond to installation pore pressures larger than u_m but smaller than u_s (see Table A4, Appendix A), suggesting that pore pressures do in fact reduce on the principal displacement surface during jacking, but that this reduction is over-recorded by sensors on the pile shaft.

z(m)	K_i (Cowden)			K_0	K_i (Bothkennar)			K_0
h/R	8	28	50		8	28	50	
1.5	20.0	13.0	-	2.6	0.65	0.50	0.50	0.95
2.5	16.5	-	-	2.6	0.50	0.42	0.40	0.62
3.5	7.0	3.5	2.5	1.9	0.47	0.38	0.33	0.57
4.5	4.7	3.5	-	1.4	0.43	0.35	-	0.55
5.5	5.0	-	-	1.3	0.42	-	-	0.53

Table 10.2 'Corrected' K_i values

The K_i values interpreted at Cowden vary from between 1.3 and 8 times the undisturbed lateral stress coefficient (K_0), whereas at Bothkennar, K_i values are always less than K_0. It appears that the large shear strains imposed during installation in the sensitive, contractant Bothkennar clay caused significant de-structuration of the material and a reduction in the mean effective stress. In contrast, the dilatant and insensitive Cowden till appears to experience an increase in mean effective stress.

10.3 EQUALISATION

10.3.1 Radial total stress (σ_r)

The radial total stress changes during equalisation at all instrument positions are summarised for each site on Figure 10.2, by plotting the mean variations of (H/H_i)[1] with time. This figure shows that radial stresses reduce with time in all materials, with greatest relative reductions taking place in Bothkennar clay.

If the material adjacent to the pile was linear-elastic (and isotropic) throughout the equalisation process, radial stresses would not change, leaving H/H_i at unity (Sills 1975). The measured reductions are

[1] $H/H_i = (\sigma_r - u_0)/(\sigma_{ri} - u_0)$. These coefficients showed variations of less than 0.1 from the mean values plotted on Figure 10.2. Note also that H/H_i values were greater than 1 in the 'disturbed' London Clay at $z < 4m$ ($h/R > 40$, for $L \approx 6m$).

attributed to a yielding zone close to the pile which interacts with the elastic (unyielding) high stiffness material remote from the shaft.

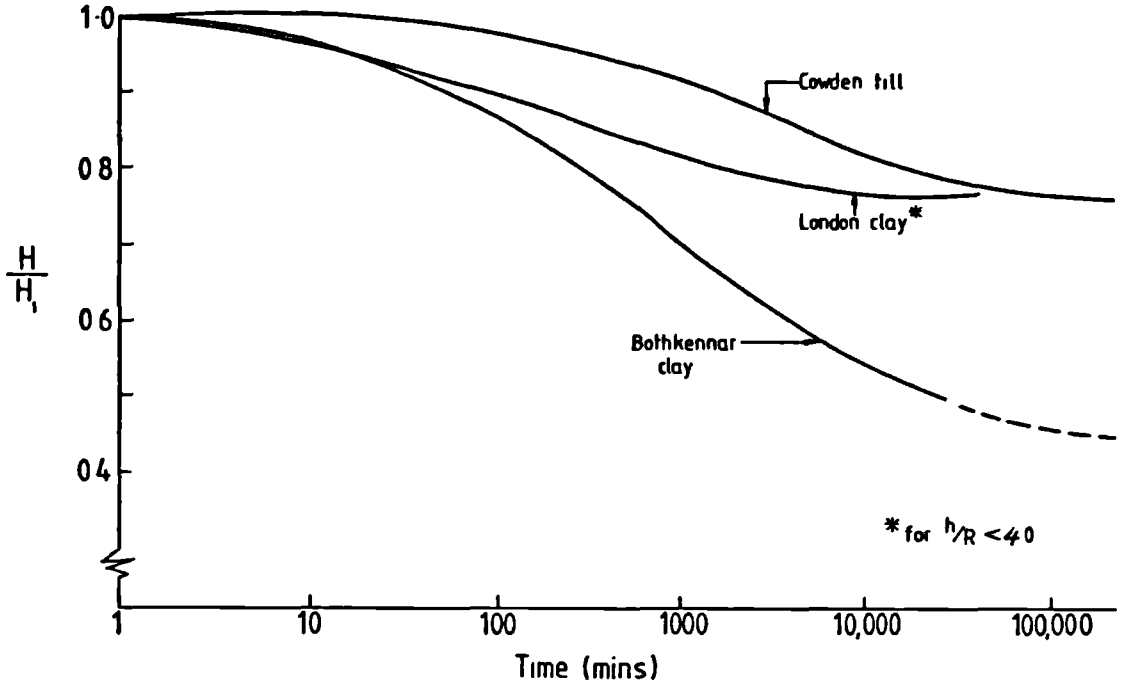

Figure 10.2 Relative changes in radial total stresses during equalisation

10.3.2 Pore pressure dissipation

Although no measurements were made remote from the ICP's, the pore pressure dissipation curves recorded during equalisation may be used to assess the likely radial distribution of pressures after installation and the approximate magnitudes of the permeabilities (k_h) and coefficients of consolidation (c_h) controlling consolidation.

The interpretations of the dissipation curves presented in this section ignore the initial rise in pressure that took place within ≈5mins of installation at Cowden and Bothkennar and was probably associated with lower pressures very close to the pile shaft. These lower pressures appeared to spread out to greater radial distances at large h/R ratios (h/R > 5) in the London clay (see Figure B2, Appendix B) and were such that the clay adjacent to the shaft swelled throughout most of the equalisation period.

10.3.2.1 Radial distribution after installation

The pore pressure variations during equalisation of the ICP at Bothkennar have been predicted using initial pressures calculated by SPM/MIT-E3 analyses of the installation process and a finite element coupled consolidation computer program that assumed radial drainage only (Whittle 1991; see Appendix C). It is shown in Appendix C that the 'Class C' predictions for pore pressure dissipation matched the measured variations (at h/R ≥30) almost precisely. It is therefore surmised that the initial distribution of excess pressures used as input to the equalisation analyses was similar to that which existed at the site after pile installation. This distribution is shown on Figure 10.3.

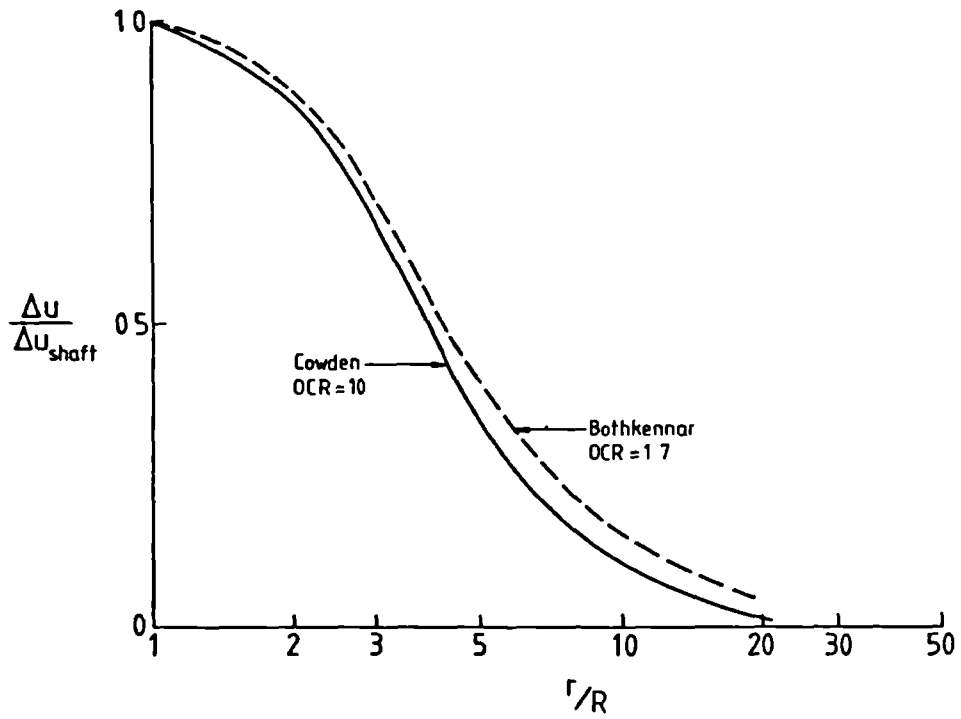

Figure 10.3 Estimated radial distribution of excess pore pressures induced by pile installation

SPM/MIT-E3 analyses predict that installation causes a larger radial extent of excess pore pressures in materials of high small strain stiffness and low OCR (see Figure 2.10, Chapter 2). Based on a parametric study of these analyses, the initial radial distribution of excess pore

pressures at Cowden, also shown on Figure 10.3, was deduced[1]. This (tentative) distribution is biased towards predictions made for Boston Blue Clay, which has similar small strain stiffness characteristics to Cowden till. A limited set of pore pressure measurements made in the soil mass adjacent to driven and jacked piles at Cowden (Ove Arup & Partners 1986 and Ponniah 1989) are in general agreement with this distribution.

The SPM/MIT-E3 analyses suggest that the higher stiffness and OCR of Cowden till lead to an initial distribution of excess pressure which is comparable to that at Bothkennar. A plateau extending to $r/R \approx 2$ is observed which is followed by a semi-logarithmic reduction with r/R to $r/R \approx 10$. Minor excess pressures ($\Delta u/\Delta u_{shaft} < 0.1$) extend to $r/R \approx 30$. These distributions are in sharp contrast to those inferred from dissipation data measured in the ICP tests in the London Clay (Bond & Jardine 1991), which suggest that initial excess pressures were very small at $r/R \geq 4$.

10.3.2.2 Permeability

The average clay permeability (k_h) operating during equalisation may be estimated from the dissipation curves using published solutions from *radial* coupled consolidation analyses. These analyses assumed that k_h remains constant throughout equalisation.

The average dissipation curves measured at Cowden and Bothkennar at h/R=53 and $z \approx 3.5$m (i.e. far from the pile tip) are shown on Figure 10.4. It is seen that, although the initial radial distributions of excess pressures at both sites were assessed to be similar, the dissipation rate at Cowden is slower over the latter stages of equalisation. This is attributed to the different stiffness and permeability characteristics of the materials.

SPM/MIT-E3 coupled consolidation analyses, assuming a k_h value of 1×10^{-9} m/s, predicted both the shape and magnitude of the Bothkennar dissipation curve on Figure 10.4 (see Figure C1, Appendix C). This k_h value is in

[1]For locations far from the pile tip. However, data reported by Roy et al (1981) suggest that these *normalised* distributions are independent of the location of the tip (see Figure B13, Appendix B).

good agreement with permeability range of [0.5-1.5] $x10^{-9}$ m/s assessed from self-boring permeameter and pushed piezometers tests at Bothkennar.

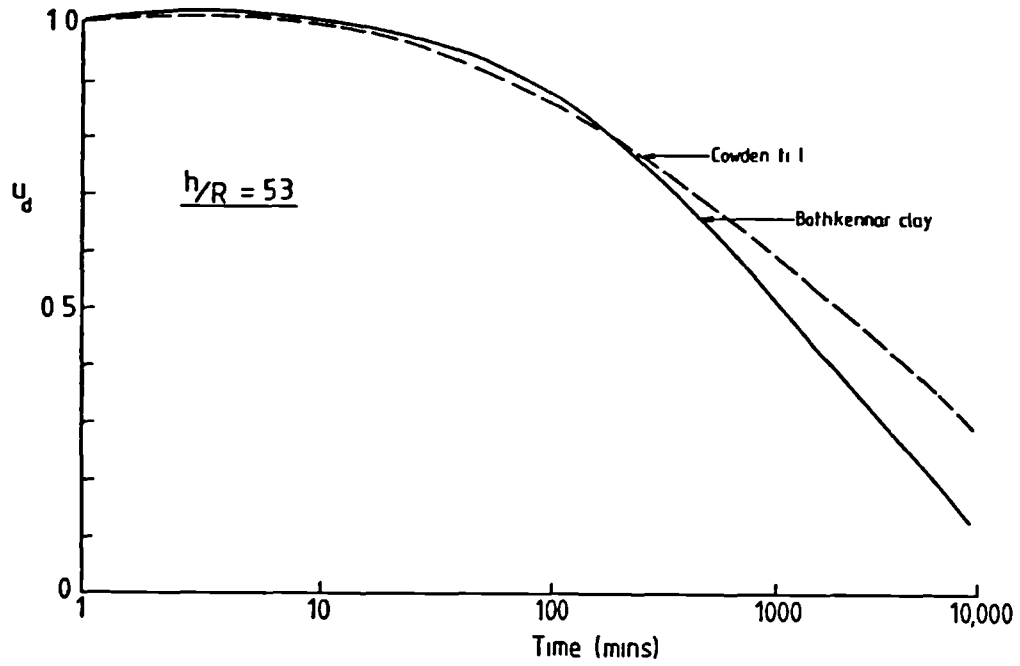

Figure 10.4 Pore pressure dissipation at h/R=53

No coupled consolidation analysis was performed for Cowden till. However, by assuming that its stiffness is similar to that of Boston Blue clay, a best fit to the dissipation curve on Figure 10.4 (h/R=53, OCR=10) was obtained for $k_h \approx 0.8 \times 10^{-10}$ m/s. This value is over <u>ten</u> times smaller than that assessed at Bothkennar, but falls within the range [0.1-2.2] $x10^{-10}$ m/s, proposed by Marsland & Powell (1985) for Cowden till.

10.3.2.3 Coefficient of consolidation

Linear uncoupled consolidation analyses may be used to assess the average horizontal coefficient of consolidation ($c_h = k_h/m_h\gamma_w$) controlling the dissipation process. These assume that both the permeability and compressibility remain constant throughout equalisation.

The dissipation curves measured close to the pile tip (h/R=5) for piles installed to ≈6m at Cowden, Bothkennar and Canons Park are shown on Figure 10.5. A comparison of this figure and the data recorded at h/R=53

(Figure 10.4) shows clearly that dissipation takes place more rapidly closer to the pile tip and is fastest in the London clay.

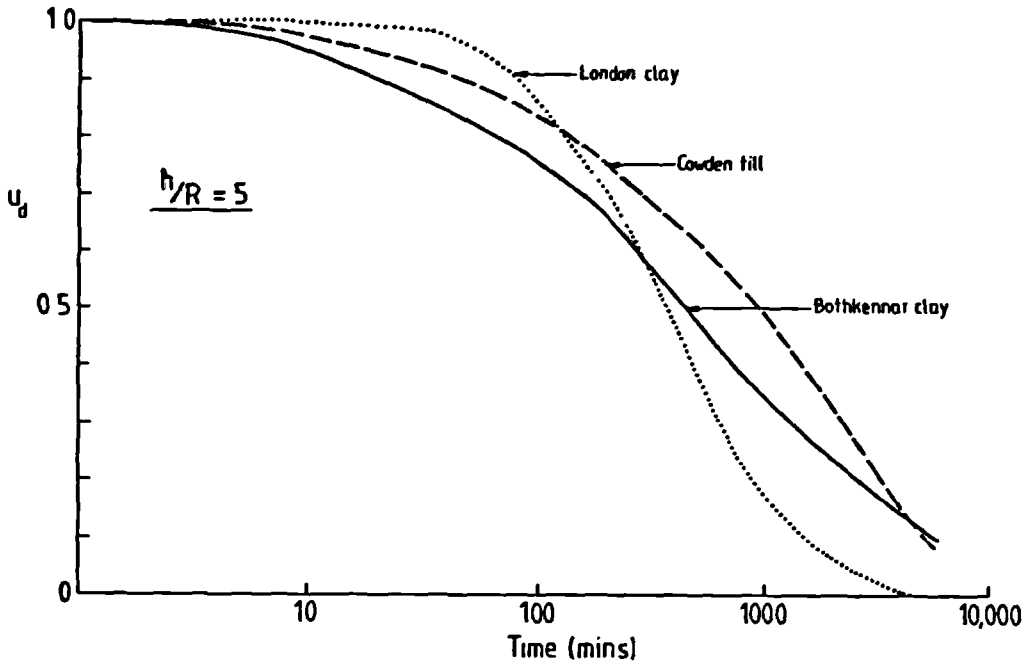

Figure 10.5 Pore pressure dissipation at h/R=5

Houlsby & Teh (1988) verified that the faster dissipation rates seen close to the pile tip are due to more three dimensional (spherical) nature of pore water flow at this location. They conducted a series of 2-D axisymmetric linear consolidation analyses, where the initial pressures were derived using the Strain Path Method and the clay was assumed to be an incompressible, elastic, perfectly-plastic material. Solutions are presented for the degree of pore pressure dissipation (U_d) at time factors $T = c_h\ t/\ [r^2\ (G/c_u)^{0.5}]$. A best fit between these solutions and the dissipation curves <u>at all h/R ratios</u> was found for G/c_u =100 and the following c_h values:

London clay:	1.35mm^2/s (43m^2/year)
Cowden till:	0.55mm^2/s (17m^2/year)
Bothkennar clay:	0.90mm^2/s (28m^2/year)

Similar average c_h values for Cowden till and Bothkennar clay were derived from solutions reported by Levadoux (1980), which assumed that

the installation pore pressures reduced semi-logarithmically with r/R to r/R≈40. This distribution is broadly compatible with that derived in SPM/MIT-E3 analyses (Figure 10.3).

It is interesting that the c_h values for Cowden till and Bothkennar clay differ by a factor of less than 2, although their respective permeabilities differ by a factor of 10. These c_h values are within the range of values measured in oedometer tests on overconsolidated clays, suggesting that consolidation takes place primarily in the recompression mode (as opposed to the virgin compression mode - when c_h values are typically two orders of magnitude smaller).

A number of comments may be made regarding 'the curve fitting exercises' employed to establish c_h values:

(i) The dissipation curves for London clay (at h/R=5) were compatible with a constant c_h. This trend is consistent with evidence presented by Bond & Jardine (1991) which suggested that the clay adjacent to the shaft remained in an overconsolidated state after full equalisation (see Section 2.4.5)

(ii) For Cowden and Bothkennar, the dissipation curves predicted using constant c_h values were generally within 10% of measurements for $1.0 \geq U_d \leq 0.4$. It may therefore be conjectured that, for this phase of the equalisation process, most of the soil in the vicinity of the pile shafts experienced relatively small strains

(iii) Larger deviations between predictions and measurements were observed towards the latter stages of consolidation at Cowden and Bothkennar ($U_d \leq 0.4$) and the dissipation process is modelled poorly by assuming a constant c_h value. Levadoux & Baligh (1986) attribute such deviations to soil yielding close to the shaft, which retards dissipation and reduces the average c_h value. These observations provide a rather indirect indication that the clay adjacent to the shaft may have tended to a normally consolidated stress state at these two sites.

10.3.3 Radial effective stress (σ'_r)

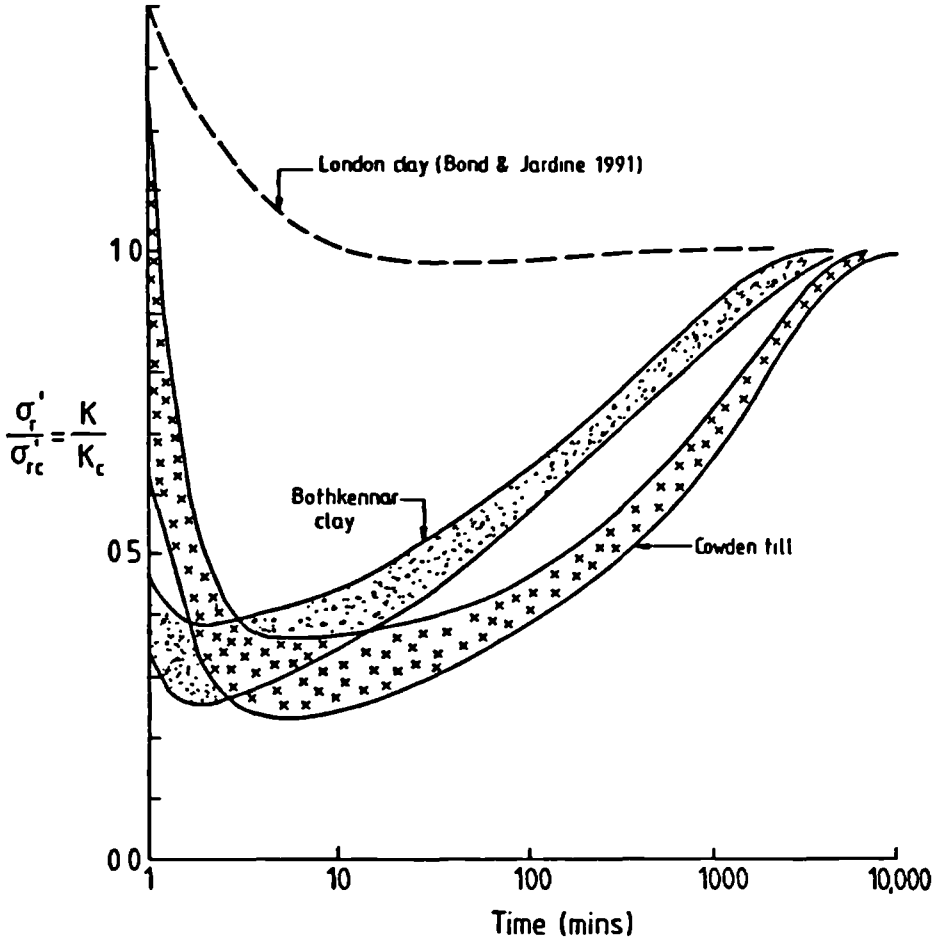

Figure 10.6 Radial effective stress variation during equalisation

The radial total stress and pore pressure changes during equalisation, discussed above, lead to the variations of the set-up coefficient K/K_c ($=\sigma'_r/\sigma'_{rc}$) with time, shown on Figure 10.6, where t=1 min corresponds to the time at the final stage of pile jacking. This figure shows the full range of these coefficients measured by all instruments on piles fast-jacked (at 500mm/min) to ≈6m depth. The installation values of σ'_r (plotted at t=1min) have been corrected for the apparently anomalous installation pore pressures, as outlined in Section 10.2.3, so that this plot may be considered as representative of σ'_r conditions on the

principal displacement shear (which control the pile capacity)[1]. The short term minimum in σ'_r and degree of set-up displayed by these data are discussed below.

10.3.3.1 Short term minimum

An interesting feature of the Cowden tests was that σ'_r reduced rapidly after pile installation and remained at relatively low values for ≈100 mins before rising and eventually reaching fully equalised values after ≈5 days. In contrast, σ'_r at Bothkennar, except for an initial slight reduction, increased throughout equalisation (albeit at a reducing rate).

Previous research with instrumented piles in clay (e.g. Coop 1987) has indicated short term minima in σ'_r and shown that these minima were most pronounced in dilatant clays. The phenomenon appears to arise because of the large negative shear induced excess pressures existing close to the shaft in these materials which, as discussed in Section 10.2.2, lead to a radial flow of water towards the pile after it comes to rest. It is encouraging to see that SPM/MIT-E3 analyses predict a similar trend (see Figure 2.12).

The load tests at Cowden showed that the minimum σ'_r also corresponded to a minimum in shaft capacity. The capacities did not, however, vary in direct proportion to σ'_r; a load test performed 2 hours after installation showed increases in σ'_r, whereas σ'_r reduced in load tests performed after equalisation (see Section 10.4.3). The increases in σ'_r in the short term test therefore partly offset its low pre-loading σ'_r values.

The occurrence of a short term minimum in capacity has important implications for large diameter piles, as equalisation proceeds at a much slower pace (in inverse proportion to the square of the diameter).

---

[1] σ'_r values calculated for h/R=8 have also accounted for the intense hydraulic gradients existing close to the pile tip shortly after installation. The pore pressures at h/R=8 were assessed from the pressures recorded at h/R=5 and h/R=30 using Figure 10.12.

10.3.3.2 Set-up after full equalisation

At Bothkennar, the fully equalised radial effective stresses (σ'_{rc}) were about *three* times the installation σ'_r values (σ'_{ri}) at all instrument positions, indicating a large positive set-up. In contrast, smaller and less consistent set-up effects were observed at Cowden, with σ'_{ri} being ≈20% *larger* than σ'_{rc} at h/R=8 but ≈30% *less* than σ'_{rc} at h/R=50. Values of $\sigma'_{rc}/\sigma'_{ri}$ at Cowden also depended on the rate of pile installation: the 'slow' jacked pile (at 80mm/min) mobilised σ'_{ri} values which were ≈25% less than σ'_{rc} values at all instrument positions. The ICP tests in the London Clay also showed variable trends for $\sigma'_{rc}/\sigma'_{ri}$.

10.3.4 Equalised radial effective stress

It was seen at Cowden and Bothkennar that the radial effective stresses were within 5% of fully equalised values after ≈85% of excess pore pressures generated by installation had dissipated. This situation arose because the dissipation of the remaining excess pore pressures (15%) was almost matched by equivalent reductions in radial total stress.

The equalised radial effective stresses (σ'_{rc}) showed a similar dependence on soil consistency and h/R to that shown by the installation radial total stress records (σ_{ri}). These similarities are not surprising given that the relaxation coefficients, K_c/H_i [= $\sigma'_{rc}/(\sigma_{ri} - u_0)$], measured at *all* instrument positions were practically constant at each site (0.75 ±0.1 at Cowden and 0.44 ±0.04 at Bothkennar). By applying these coefficients to the ($\sigma_{ri} - u_0$) values, it is possible to estimate the σ'_{rc} profiles for all pile lengths less than the final penetration depth[1].

For the average value of K_c/H_i at each site, regression analyses of the ($\sigma_{ri} - u_0$) data gave the best fit relationships listed in Table 10.3 (8 ≤ h/R ≤ 50 and L < 6.5m). These relationships are expected to be less accurate than those derived for σ_{ri} values (see Table 10.1) because of the added variability of the relaxation coefficients.

---

[1]At Labenne, equalisation was achieved in less than ≈1min and therefore ($\sigma_{ri} - u_0$) values recorded during installation pause periods were equivalent to σ'_{rc} values (see Section 6.4).

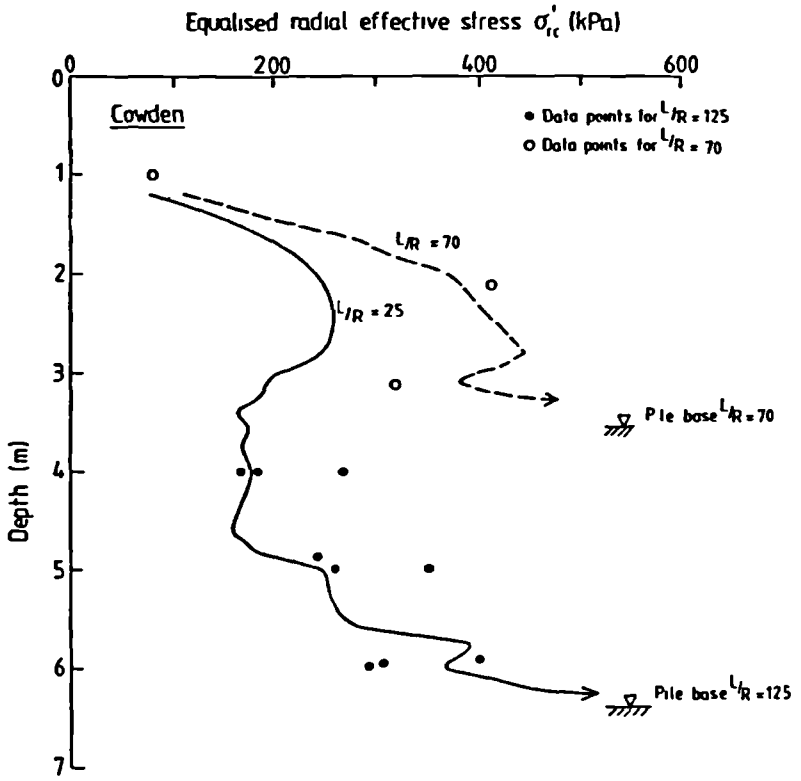

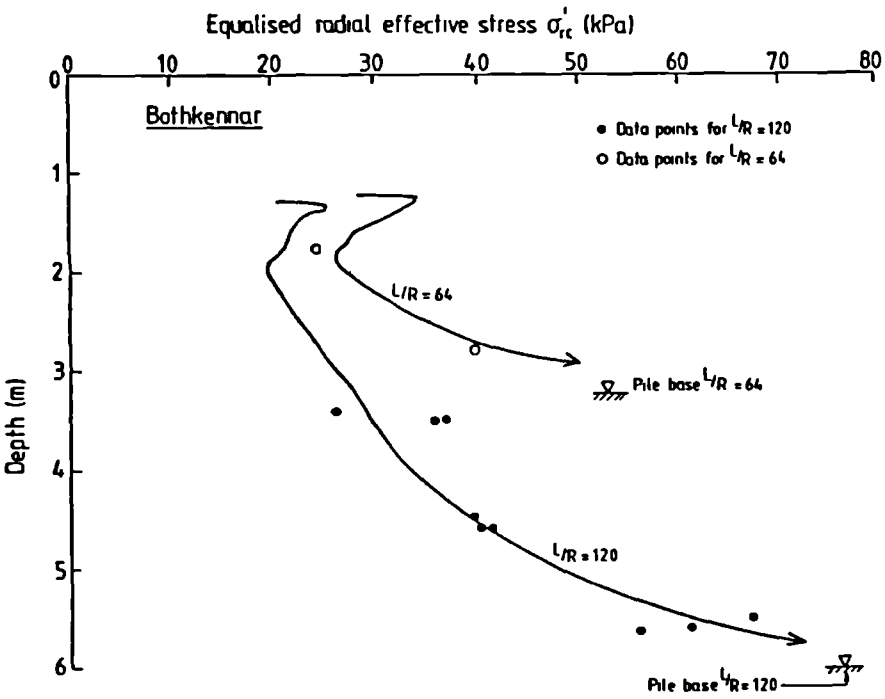

Figure 10.7 Predicted and measured σ'_{rc} profiles

Cowden till	$\sigma'_{rc}/q_b = 0.435\ (h/R)^{-0.365}$
Bothkennar clay	$\sigma'_{rc}/q_b = 0.277\ (h/R)^{-0.272}$
London clay	$\sigma'_{rc}/q_b = 0.740\ (h/R)^{-0.59}$
Labenne sand	$\sigma'_{rc}/q_b = 0.024\ (h/R)^{-0.33}$ (see Section 9.3)

Table 10.3 Approximate relationships for σ'_{rc} ($8 \le h/R \le 50$[1])

The variations of σ'_{rc} predicted by these expressions are compared on Figure 10.7 with the measured σ'_{rc} values at Cowden and Bothkennar. It is evident that the expressions agree very well with the measurements at Bothkennar, but are less accurate at Cowden, presumably because of the greater variability of Cowden till. This variability is reflected by the relatively wide scatter in the measured σ'_{rc} values and was also evident in the regression analyses (see Table 10.1). The calculated profiles of σ'_{rc} differ slightly from those assessed purely from the σ'_{rc} data in Figure 7.15 and 8.18. These differences highlight the problems associated with interpreting a profile from a limited data set.

Two implications of the expressions in Table 10.3 are:

- The σ'_{rc} values developed on piles in clays are a much higher proportion of the base resistance than those developed in the Labenne sand. This is a consequence of the more dramatic reduction in stress with h/R close to the pile tip in sand, possibly reflecting its free draining and particulate characteristics.

- For all sites, the *average* values of σ'_{rc} (as predicted by integrating the expressions in Table 10.3) vary with pile length in a similar way to the average shaft shear stresses (τ_{av}) mobilised during installation (see Figures 6.8, 7.4 and 8.3). It is therefore likely that τ_{av} values mobilised in load tests after equalisation would show a similar dependence on pile length.

[1]Except at h/R > 40 in the disturbed London clay where a 'relaxation' coefficient of greater than 1 was measured.

10.4 LOAD TESTING

This section first discusses the variations with displacement of the total shaft load and the local shaft frictions measured in load tests with the ICP and then compares the loading effective stress paths (τ v σ'_r) measured in each test programme.

10.4.1 Overall shaft displacement behaviour

The most striking feature of the Cowden and Bothkennar load displacement curves (as well as those measured at Labenne) was the distinctly softer stiffness characteristic shown by tension tests (see Figures 6.12, 7.17 & 8.20). It has been suggested in Chapters 6-8 that the dependence of stiffness on the loading direction was related to the anisotropy in the soil created by installation. This hypothesis is supported by the much reduced stiffness observed in compression tests that were preceded by a tension test and the stiffer response seen in tension re-tests. However, as the response to first-time tension and compression loading in the ICP tests in the London clay was similar, it appears that the anisotropic effects induced by installation are strongly dependent on the soil type.

A detailed study of the load displacement characteristics is only possible if the complete stress regime in the ground after equalisation is known and a realistic soil model is used which incorporates, amongst other things, the strong dependence of stiffness on strain level. However, Poulos (1989) indicated that reasonable first order estimates of average stiffness values controlling the overall load displacement behaviour could be obtained from simplified analyses which assume that (i) the soil is linear-elastic and of constant stiffness along the shaft length and (ii) a 'cut off' exists for the local shaft frictions.

Analyses of this type[1] were performed for load tests at Cowden and Bothkennar. These took account of the compressibility of the piles and

[1]The analyses were performed using the computer program (PILSET), which was developed and written by the author. Stiffness matrices for the soil were derived using integrated forms of Mindlin's equations (Vaziri et al 1982). Full details of the code are available from OASYS (1988).

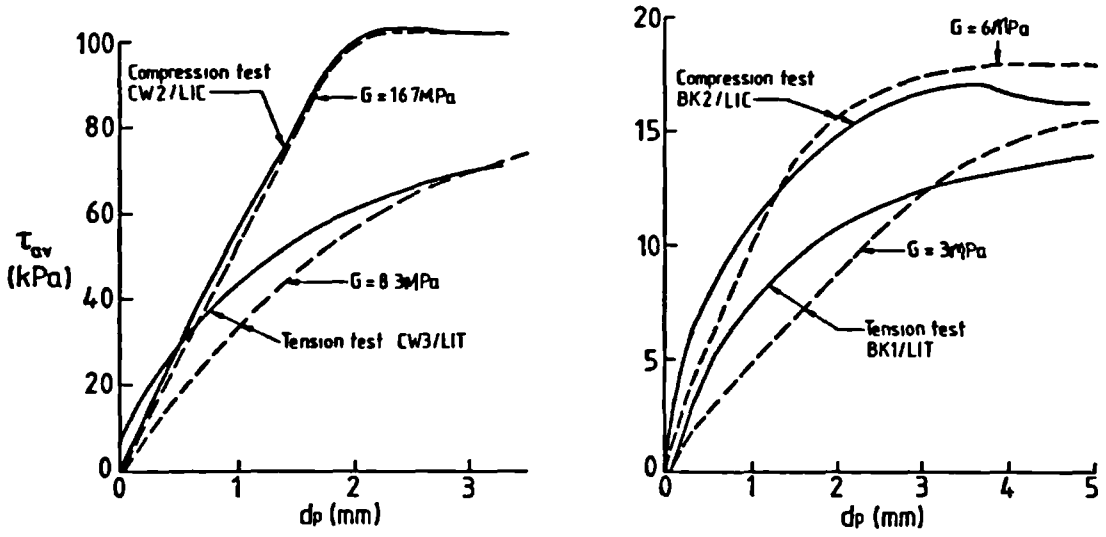

Figure 10.8 Predicted and measured τ_{rz} v d_p variations

assumed that the 'cut-off' values were equivalent to the peak local shaft frictions measured directly by the ICP. An iterative approach was required to match the predictions with the measured shaft load displacement curves. The best fit lines are compared with the data on Figure 10.8 and show:

- The assumption of a constant shear stiffness value (G) was far less appropriate for the tensions tests, which indicated highly non-linear behaviour at both sites.

- The average stiffness values in tension tests were only half of those interpreted for the compression tests.

- Comparable average ratios of G/p'_0 were computed at both sites, amounting to ≈200 in compression and ≈100 in tension[1].

[1]The pre-installation mean effective stress (p'_0) at the midpoint of the embedded shaft lengths was ≈80kPa at Cowden and ≈27kPa at Bothkennar.

10.4.2 Local shear stress variations

The variations of local shear stresses (τ_{rz}) with pile head displacement have been seen in Chapters 6-8 to depend on the local shear stiffness and the loading direction. The post-peak variations depend on the brittleness of the soil fabric set up during installation and are affected by the installation jacking rate and the pile's plunging rate at failure.

The pile head displacements (d_p) required to mobilise peak local shear stresses generally increased with depth because the piles failed progressively from the top down. Primarily, this reflects the way in which local shear stiffness values also increased with depth and in proportion to the pre-loading radial effective stress (σ'_{rl}). Note, for example, when σ'_{rl} was larger at shallower depths (e.g. Test BK4s/L1C; see Figure 8.22), the τ_{rz} v d_p variations showed a stiffer characteristic than at depth. The compressibility of the pile also added to the tendency for peak local stresses to develop earlier at shallow depths.

Typical variations of the normalised local shear stresses [$\tau_{rz}/(\tau_{rz})_{max}$] with pile head displacement (d_p) for fast-jacked piles tested in compression are given in Figure 10.9. The corresponding variations of $\tau_{rz}/(\tau_{rz})_{max}$ with local displacement (d) are also shown on Figure 10.9; these were assessed from the measured load distributions and estimates for the axial rigidity of the pile[1]. The main points to note are:

(i) The pre-peak relationship at Bothkennar is significantly more curved than at Cowden and Canons Park.

(ii) There is not a unique local value of displacement (d) at which shear stresses reach a peak value; displacements at peak varied from ≈1mm at Cowden to almost 4mm at Bothkennar.

(iii) A dramatic post-peak reduction in shear stress is observed in the London clay. Bond (1989) showed that this was because post-peak (slow) displacement creates a more highly ordered soil fabric to that which was induced by fast-jacking during installation. This led to a sharp reduction in the interface friction angle (δ).

---

[1]No account was taken of the possible additional compression at the joints between each segment of the ICP.

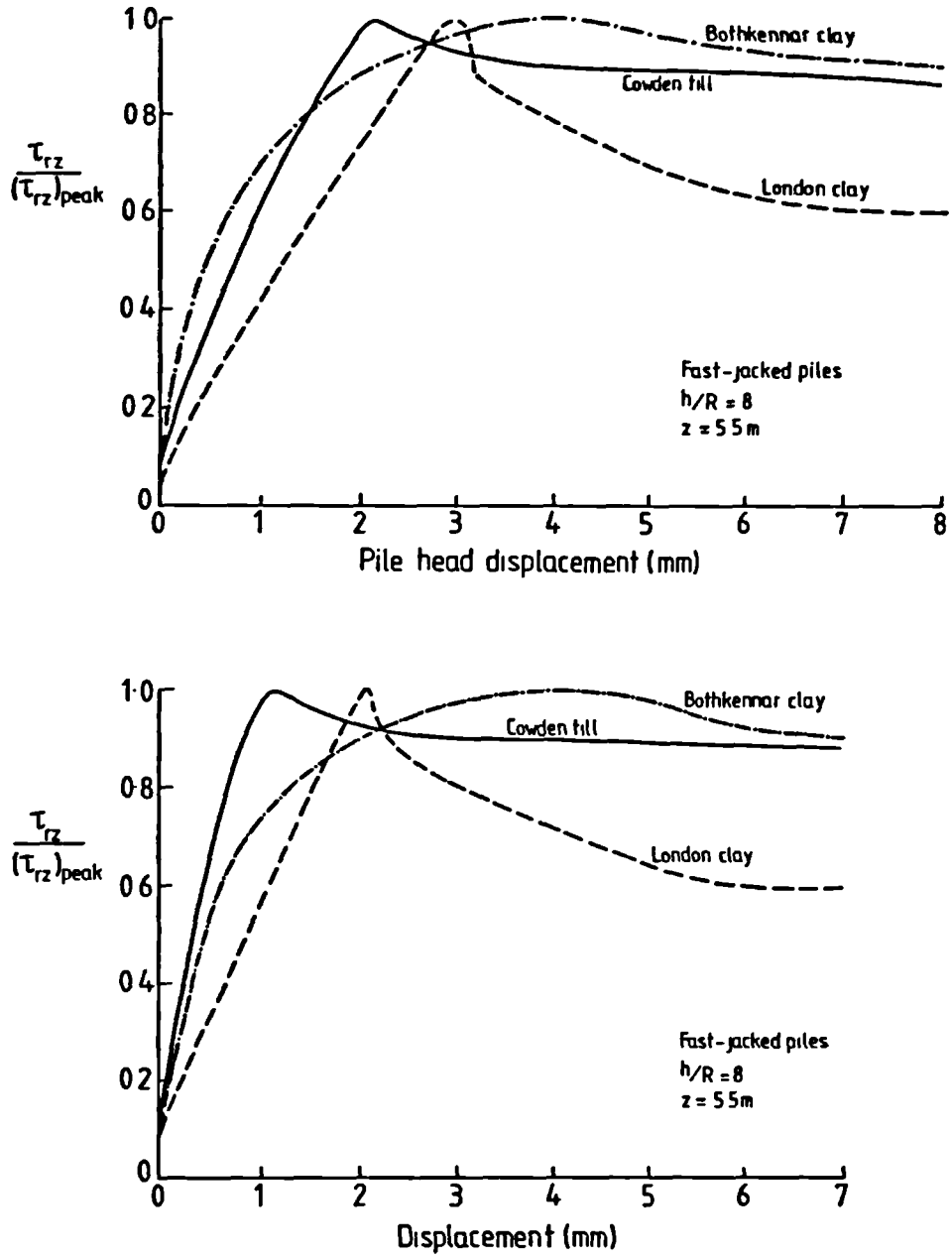

Figure 10.9 Variations of τ_{rz} with d_p & d at h/R=8 and z ≈5.5m

(iv) Post-peak brittleness amounts to ≈10% at Cowden and Bothkennar. At Cowden, this brittleness was due to a reduction in the δ value (as the pile re-ordered the soil fabric), whereas, at Bothkennar, post-peak reductions in shear stresses were caused (in some cases) by reductions in radial effective stress as well as a minor changes in δ.

It should be noted that most full scale pipe piles are more compressible than the ICP. Consequently, the shear stresses acting over most of their shaft lengths will have reduced to ultimate post-peak values when the peak pile capacity is mobilised (see Figure 2.2). The data on Figure 10.9 imply that the unit shaft capacity of a full scale pipe pile at maximum load in London clay will be only 60-70% of that measured in the ICP tests; the peak unit shaft capacities measured in the ICP tests at Cowden and Bothkennar are not expected to differ by more than 10% from those of equivalent full scale piles.

10.4.3 Loading effective stress paths

10.4.3.1 General

One of the most useful features of the ICP is its ability to record the effective stress paths (τ v σ'_r) followed by elements at the pile-soil interface during pile loading. These stress paths provide a concise way of characterising each test and combine in one plot the measurements of radial stress, shear stress and pore pressure.

The mean stress paths recorded by the ICP during first-time compression and tension tests that were performed *after equalisation of σ'_r on fast-jacked piles* in Cowden till, Bothkennar clay & London clay are given on Figure 10.10. These paths have been normalised by the pre-loading (equalised) radial effective stress (σ'_{rc}).

It is evident that, at each site, radial effective stresses reduce moderately during pile loading and are at a minimum value (σ'_{rf}) when the peak local shear stress (τ_f) is mobilised. Values of $\sigma'_{rf}/\sigma'_{rc}$ show only a minor dependence on the soil type and direction of loading and fall between 0.8 and 1.0 in all cases. However, the obliquities at peak shear stress (δ_p) show a far greater dependence on soil type, varying from between ≈12° for London clay to ≈29° for Bothkennar clay. Post-peak, σ'_r remains relatively constant or increases and the obliquities reduce by up to 4° to reach their ultimate values (δ_{ult}).

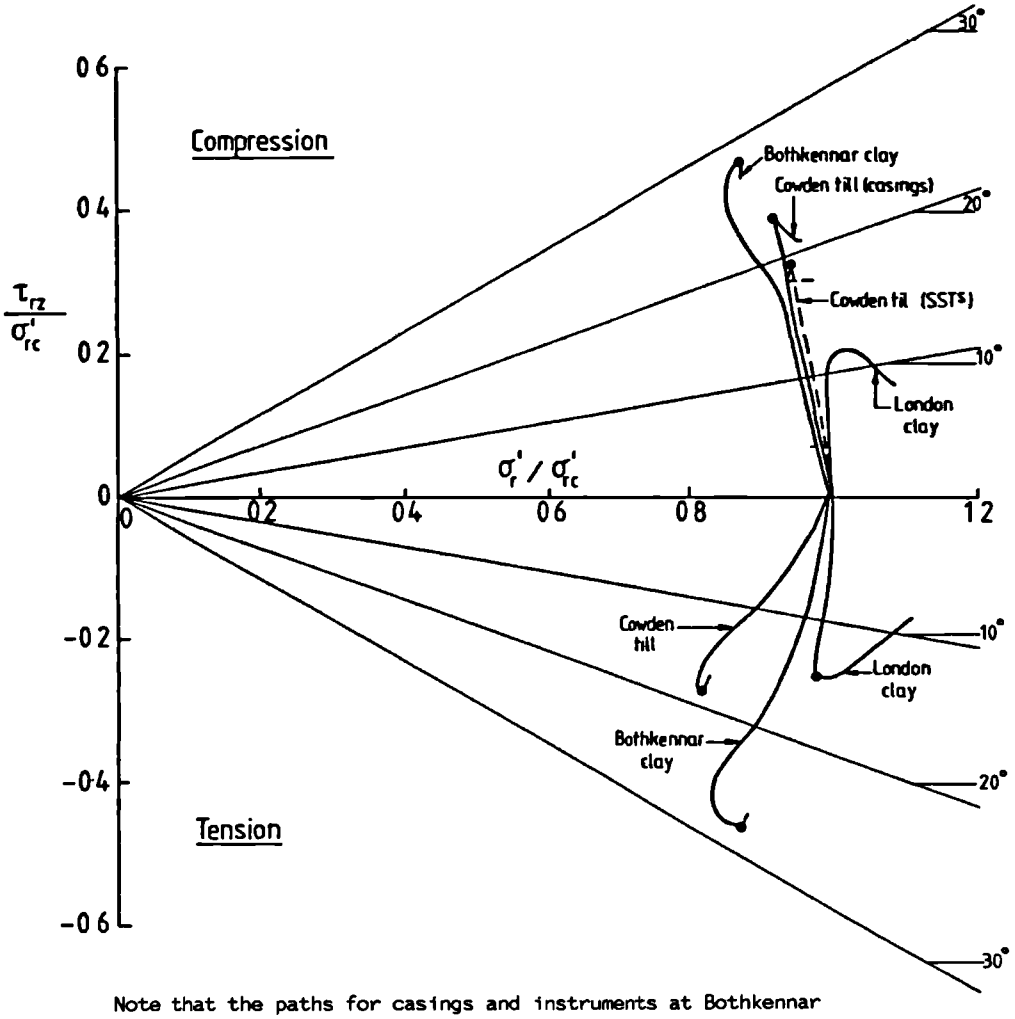

Note that the paths for casings and instruments at Bothkennar and Canons Park were identical (see Section A3, Appendix A).

Figure 10.10 Typical effective stress paths measured during load testing of fast-jacked piles after equalisation

10.4.3.2 Stress path shapes

As discussed in Section 2.3.6, Randolph & Wroth (1981) and Azzouz et al (1990) have suggested that the stress paths (τ_h/σ'_{nc} v σ'_n/σ'_{nc}) measured in constant volume direct simple shear (DSS) tests on normally consolidated or very lightly overconsolidated intact samples (OCR ≤1.3) should be similar to the paths shown on Figure 10.10. This premise was checked for the Bothkennar load tests in Section 8.4 and was shown to be unsatisfactory because (see Figure 8.26):

(i) Pre-peak pile loading stress paths (after equalisation of radial effective stresses) showed an overall reduction in σ'_r/σ'_{rc} which was considerably less than reductions in σ'_n/σ'_{nc} seen in DSS tests at OCR ≤1.3.

(ii) Post-peak, the pile loading stress paths were clearly incompatible with those measured in DSS tests. The latter show the normal effective stress reducing continuously while the obliquity increases to reach ϕ'_{cv}.

The ICP tests have also shown that the shape of the pile loading stress paths depends on the degree of equalisation of the clay surrounding the pile shaft. This dependency is illustrated in Table 10.4 which lists the values of $\sigma'_{rf}/\sigma'_{rl}$ recorded during compression load tests at Cowden and Bothkennar at five average degrees of pore pressure dissipation (U_d). (Note σ'_{rl} is the pre-loading radial effective stress and U_d =0.0 corresponds to full dissipation of excess pore pressures).

	U_d =1.0	U_d =0.88	U_d = 0.80	U_d=0.22	U_d=0.15
Cowden	1.75[1]	1.3	-	0.88	-
Bothkennar	1.40[1]	-	0.95	-	0.87

Table 10.4 Mean values of $\sigma'_{rf}/\sigma'_{rl}$

Although the values of $\sigma'_{rf}/\sigma'_{rl}$ measured at U_d =1.0 (i.e. during installation) may be influenced by the rate of pile loading, a clear trend for $\sigma'_{rf}/\sigma'_{rl}$ to reduce as equalisation progresses is evident. This response is consistent with the predictions of Levadoux & Baligh (1986) who show that the clay at the pile shaft will exhibit characteristics of overconsolidated (dilatant) clays for U_d ≥0.3. A similar inference was made from the pore pressure dissipation curves in Section 10.3.2.

Values of $\sigma'_{rf}/\sigma'_{rl}$ measured in load tests performed *after full equalisation* were typically ≈15% higher in re-tests than in first-time tests. This increase may be attributed to ageing effects and the plastic hardening induced by pre-shearing in the first-time test.

[1]Interpreted values for the principal displacement shear (see Section 10.2.3)

10.4.3.3 Angles of interface friction

The interface friction angles (δ_p & δ_{ult}) vary greatly between soil types and have a dominant influence on shaft capacity. The abrupt change in curvature of the stress paths at peak shear stress and the Canons Park fabric studies, described by Bond & Jardine (1991), suggest that these angles are controlled by the residual sliding characteristics of the soil-interface system. The ring shear apparatus provides the best means of assessing such characteristics (Lupini et al 1981) and therefore a series of 'pile-modelling' ring shear interface tests were performed for each material investigated with the ICP. In each case:

- The interfaces were of the same roughness and material (stainless steel, centre line average roughness ≈8.5μm) as those of the surface stress transducers (SST's) on the ICP's and the normal stresses applied were comparable to the radial effective stresses measured on the piles.
- Samples were subjected initially to a large relative displacement (greater than 1m) in a series of shearing pulses at ≈500mm/min. This stage modelled the rapid and large relative displacements which the soil adjacent to the pile shaft experiences during fast-jacking.

Table 10.5 compares the values of δ_p and δ_{ult} measured in these tests with the mean peak and ultimate obliquities observed in first-time pile load tests on fast-jacked piles (rate =500mm/min).

	Pile tests				Ring shear tests		
	δ_p°	δ_{ult}°	δ_p°	δ_{ult}°	δ_p°	δ_{ult}°	ϕ'_r°
	(comp.)		(tens.)				
Cowden till (casings)	24.5	21.0	17.5	17.5	-	-	25
(SST's)	19.5	19.0	18.5	18.5	27	23	25
Bothkennar clay	28.5	28.0	28.5	28.0	31	30	33
London clay	12.5	9.1	12.5	9.1	13	10	10

Table 10.5 Comparison of ring shear data with pile test results

The ring shear tests are seen to provide an excellent estimate of the magnitudes of both δ_p and δ_{ult} measured in the pile tests in Bothkennar and London clays, but over-predict δ values measured at Cowden. Lemos (1986) showed that δ values mobilised by Cowden till were highly sensitive to minor changes in its composition and to the properties of the interface. It is possible that the (one) ring shear interface experiment performed with this material did not match the conditions in-situ precisely.

The ring shear tests also:

- provided an indication of how shear stresses vary with the pile displacement rate. However, the specific rate dependence observed in the tests, particularly at velocities greater than 100mm/min, was not compatible with that observed in the field.
- showed how shear stresses may be expected to vary with displacement during installation jacking stages.
- predicted the dependence of the δ_p values developed in pile load tests on the installation rate.

Also listed in Table 10.5 are the residual angles (ϕ'_r) measured in soil on soil ring shear tests[1]. These angles are the same or marginally higher than the δ_{ult} values measured in interface experiments, suggesting that the specific type of interface used did not represent a significant plane of weakness and failure probably occurred within the soil at a short distance from the interface. It therefore appears that, by comparison with the field measurements of δ_{ult}, shaft failure may have occurred on the surfaces located within the soil mass in all ICP tests, apart from at the locations of the SST's at Cowden.

The only major anomaly evident from Table 10.5 is that the ring shear tests failed to predict the large difference between δ values measured in compression and tension tests at Cowden. This incompatibility at first suggests that failure in tension tests occurred within the soil mass and

[1]Soil on soil ring shear tests on Cowden till and London clay are reported in Lupini et al (1981) and Tika (1989). The Bothkennar soil on soil tests are discussed in Section 5.3.12.

not at the pile surface, or on a residual surface close to the pile. However, if this were the case, one might expect that σ'_r would continue to reduce post-peak as the obliquity increases to ϕ'_{cv} ≈26° (as in DSS tests). The unit shaft capacities and δ values mobilised in all tension tests (including tension re-tests) were lower than those measured in equivalent compression tests and therefore this anomaly cannot be explained by measurement error.

Lemos (1986) and Tika (1989) performed comparable 'pile-modelling' ring shear interface tests on a wide range of soils. Based on these tests, a tentative correlation between δ_p & δ_{ult} and the plasticity index (PI) of the clay is proposed in Figure D3, Appendix D. This correlation suggests that δ_{ult} reduces with PI and is ≈17° at a PI =19% (i.e. for Cowden till) and only ≈9° at a PI =50% (i.e. for Bothkennar clay below 4m depth). Although a better correlation may be arrived at by relating δ to the granular void ratio (e_g), it appears from a comparison of the data in Table 10.5 with Figure D3 that the only reliable way of estimating the field δ values is by direct measurement in appropriate interface tests. These tests are not difficult to perform and it is suggested that they should be carried out as a matter of routine when displacement piles are proposed for major projects.

10.5 THE 'h/R EFFECT'

In all experiments with the ICP, the stresses developed at fixed depths on the pile shaft reduced as the relative depth of the pile tip (h/R) increased. This feature is examined in detail in this section as it has important implications, but is ignored in almost all current pile design methods.

Any reduction of stress with h/R cannot, by definition, be identified in pile experiments where σ_r and u are measured at a single location on the shaft e.g. in the piezo-lateral stress cell investigations (Azzouz & Morrison 1988 and Azzouz & Lutz 1986). Where high quality measurements have been made with multiple instrument clusters (see Appendix B), it is often the case that only data recorded after installation are reported. No *direct* check of a dependence on h/R can be made in these instances.

Only the experiments of Coop (1987) with the Oxford University instrumented pile (referred to as the IMP) allow the dependence of radial stresses on h/R to be compared with that measured in ICP tests. More experimental observations are available (primarily from piezocone tests) concerning the dependence of pore pressures on h/R.

10.5.1 General observations

Before making some general observations concerning the h/R effect seen in the ICP tests and other instrumented pile tests, it is first worthy of mention that Poskitt (1992), and others, have suggested that the h/R dependence may be caused by pile bending or pile whip during installation. The ICP tests demonstrated that these are not major factors as, even though the orientation of *all* instruments with respect to a given direction (e.g. North-South) was different for each pile, virtually the same dependence of a given stress component on h/R was measured by all piles installed at a given site. This dependence was also independent of the pile depth and was similar for stresses recorded both during and after installation.

10.5.1.1 Radial total stress

The experiments with the 80mm diameter 'IMP', reported by Coop (1987), included measurements of radial stress at h/R=5.5 and h/R ≈22 in London Clay, Gault Clay and Huntspill Clay (see Appendix B). The installation radial total stress ratios (H_i) measured in these tests and in the ICP tests are plotted against h/R on Figure 10.11. These ratios are normalised by a reference value of $H_i = (H_i)_{ref}$, recorded at h/R=8 in the ICP tests and at h/R=5.5 in the IMP tests.

All experiments showed that H_i reduced with h/R. In particular, it is noted that:

- There is an approximately linear variation of log $[H_i/(H_i)_{ref}]$ with log (h/R) at Cowden and Bothkennar. These variations imply that H_i reduces in inverse proportion to $(h/R)^{0.36}$ at Cowden and in inverse proportion to $(h/R)^{0.27}$ at Bothkennar.

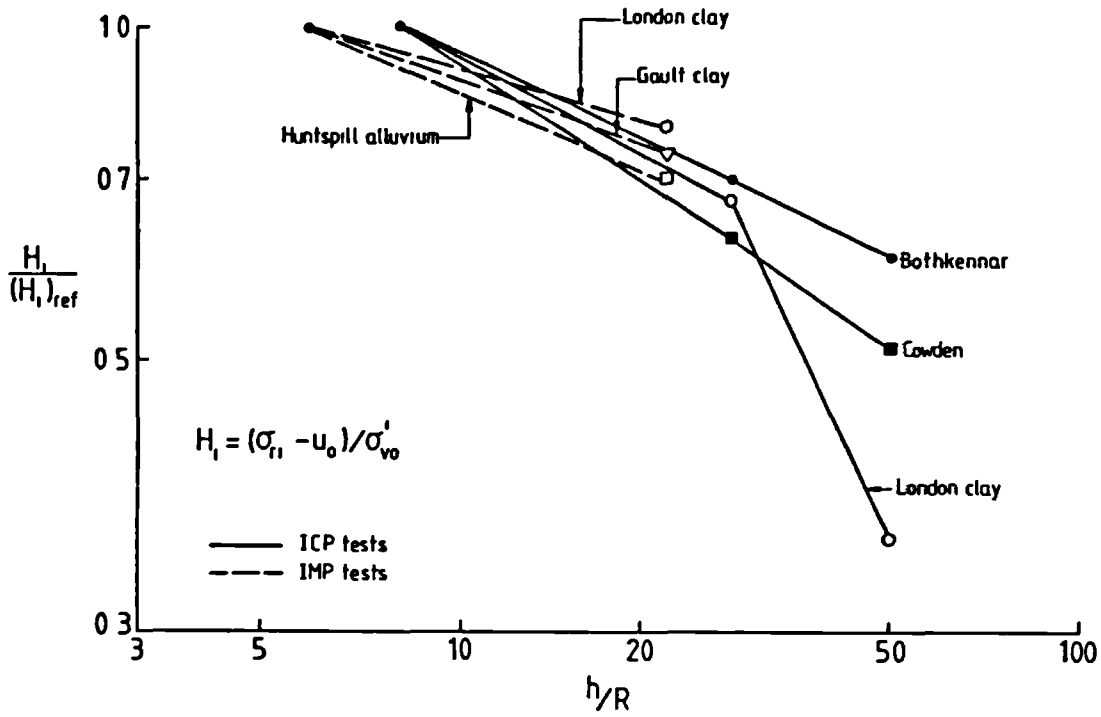

Figure 10.11 Dependence of H_1 on h/R

- All IMP tests show a comparable reduction of H_1 with h/R, despite wide difference between the soils investigated (e.g. Gault Clay at OCR ≥15 and Huntspill Clay at OCR ≈1.5).

- The reduction of H_1 with h/R measured in IMP tests is less pronounced than that observed in the ICP tests. For example, in the London clay at 5 < h/R < 28, H_1 reduces in inverse proportion to $(h/R)^{0.33}$ in the ICP tests, but only in inverse proportion to $h/R^{0.16}$ in IMP tests.

- Much larger reductions in stress are observed between h/R=28 and h/R =50 in the ICP tests in the London clay. These reductions were measured in the 'disturbed' London Clay between 2.5m and 4m at Canons Park (see Section B2, Appendix B).

10.5.1.2 Pore pressure

The variations with h/R of the maximum pore pressure ratios ($\Delta u_{max}/\sigma'_{v0}$) recorded during the pause periods in between jacking stages at Cowden and Bothkennar are shown (using logarithmic axes) on Figure 10.12. The equalisation data showed that these maxima are fully developed after ≈3 mins and are therefore equivalent to maxima that would have been recorded if pile installation was terminated at the end of any jacking stage.

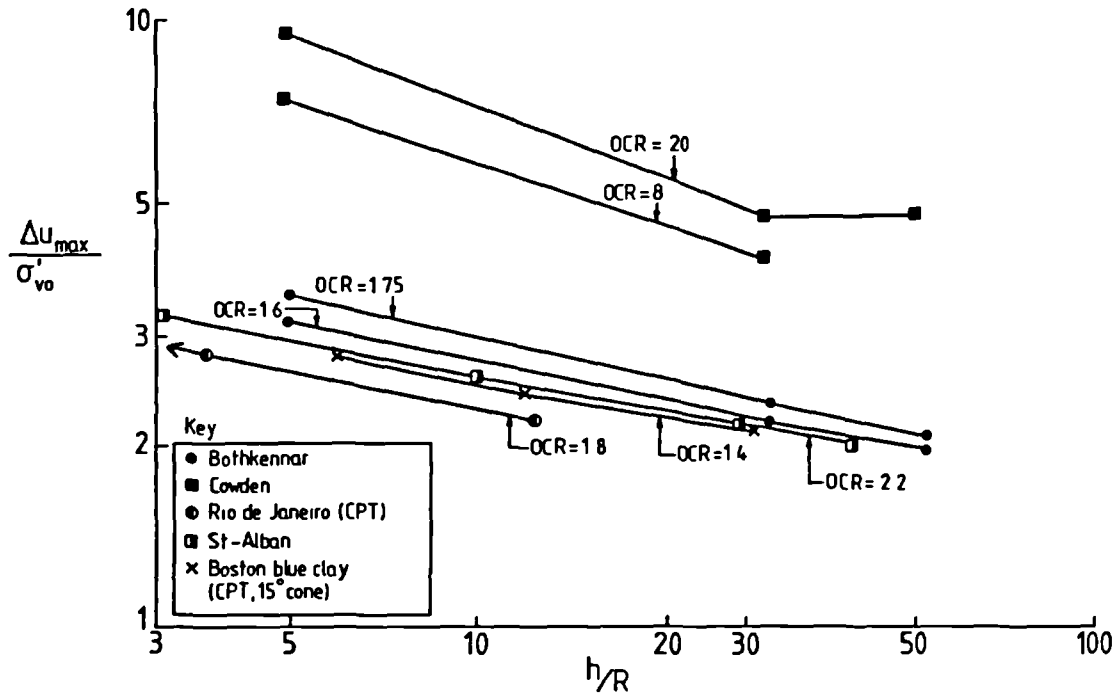

Figure 10.12 Dependence of $\Delta u_{max}/\sigma'_{v0}$ on h/R

Also included on Figure 10.12 are the maximum pore pressure ratios recorded after installation of 220mm diameter piles in St-Alban clay (Roy et al 1981) and during piezocone tests in Boston Blue and Rio de Janeiro soft clays (Baligh et al 1980, Sills et al 1988)[1]. We note:

[1]The pore pressures recorded by the IMP showed very inconsistent patterns and are not plotted on this figure. Bond & Jardine (1990) attributed this response to the poor saturation of the IMP probes and their inability to respond quickly from cavitation.

- Pore pressures ratios in lightly overconsolidated materials (including Bothkennar) reduce approximately in inverse proportion to $(h/R)^{0.2}$ over the h/R range considered. The magnitudes of these ratios vary by ±15% between sites.
- At h/R < 30, ratios in Cowden till show a slightly more pronounced reduction with h/R. An even steeper reduction was observed in the ICP tests in the London Clay where $\Delta u_{max}/\sigma'_{v0}$ reduced from a typical value of ≈8 at h/R =5 to values often less than 2 at h/R =30.

10.5.1.3 Equalised radial effective stresses

The results plotted on Figure 10.7 show that the equalised radial effective stress ratio ($K_c = \sigma'_{rc}/\sigma'_{v0}$) in ICP tests depends on h/R, but the precise form of this dependence is difficult to establish because K_c measurements were only obtained for two pile lengths. However, as discussed in Section 10.3.4, because the relaxation factors (K_c/H_1) at each site were independent of the instrument position, it may be assumed that K_c depends on h/R in a similar way to that shown by the (much more abundant) set of H_1 measurements.

10.5.2 Factors causing the 'h/R effect'

The data presented above show that, while stresses reduce with the relative depth of the pile tip (h/R), the magnitude of the relative reductions varies both with pile type and soil type. This section explores possible factors causing these variations by first examining the distribution of stresses that are predicted for the instantaneous installation of a frictionless pile and then reviewing aspects of real piles which may cause a deviation from these predictions.

10.5.2.1 Instantaneous installation of a frictionless pile.

Based on extensive laboratory investigations, Baligh (1975) postulated that the mechanics of undrained pile penetration are such that soil deformations are controlled by the geometry of the pile and are essentially independent of the shearing resistance of the soil. This is the basic assumption made by the Strain Path Method to model the

installation process (see Section 2.3).

The Strain Path Method (SPM) predicts that soil elements close to the pile tip experience very large strains but that these strains reduce significantly as the pile tip penetrates to deeper levels i.e. as the soil 'flows' in the direction of increasing h/R. Using these strain fields and an appropriate constitutive model for the soil, the method predicts that installation radial stresses (σ_{ri}) vary with h/R. This is illustrated in Figure 10.1 for Bothkennar and Boston Blue clays (at OCR≤4) where a clear reduction of σ_{ri} with h/R is observed. However, the rate of change of σ_{ri} with h/R is appreciably less than that measured in the ICP tests (and also IMP tests), particularly at large h/R ratios.

The discrepancy between the observations and predictions may be due to the (simplifying) assumptions made by the SPM (discussed in Section 2.3.2). In particular,

(i) It is generally found that, when stresses are calculated from the soil strain paths, the equations for vertical and radial equilibrium cannot be satisfied simultaneously. This inequilibrium, although usually only significant at the pile tip, arises because of errors in the predicted strain paths, which were established on the assumption that they were independent of the shearing resistance of the soil.

(ii) The SPM assumes implicitly that the pile is frictionless. For a rough pile (in a clay with shearing resistance), one can envisage that the streamlines of 'soil flow' would exhibit less ordered characteristics, such as seen within the boundary layers of turbulent fluid flow. The existence of friction may, for example, prevent streamlines from becoming tangential to the pile shaft at low h/R and therefore independent of the location of the tip (see Figure 2.8). This situation could arise if a layer of clay adhering to the (rough) pile surface thickens with increasing h/R, causing a progressive radial shift of the principal displacement shear from the pile shaft.

(iii) The SPM assumes that the pile is installed to its final depth instantaneously and does not account for the possible dependence

of the installation stresses on time and cyclic loading. These effects are examined in the next sections.

10.5.2.2 The effects of time

A typical ICP installation required ≈10 strokes of the jack to move the pile tip from 8 radii to 50 radii below a particular soil horizon. The average pause period between jacking stages was ≈6 mins (allowing for the time required to add extra pile casings to the pile head), implying that a period of typically 1 hour had elapsed between the time measurements were made at any fixed depth by the leading instruments (at h/R =8) and the trailing instruments (at h/R =50).

It is possible that the reduction in radial total stress with h/R is partly because the clay at further distances from the pile tip (and hence after longer elapsed periods) is at a more advanced state of equalisation. The relative reductions in radial total stress (H/H_1) with time during equalisation, shown on Figure 10.2, suggest that a time lag of 1 hour would cause a maximum difference of ≈10% between the radial stresses recorded at h/R =8 and h/R =50.

It has been seen in Section 10.3 that pore pressure dissipation is controlled by radial drainage remote from the pile tip but by spherical drainage closer to the tip. These different boundary conditions hamper a true assessment of the effect of a time lag on the pore pressure measurements as well as the σ_{r1} records. Nevertheless given that (a) the mean trend of H/H_1 with time was similar at *all* instrument positions at each site, (b) the normalised radial distribution of pore pressure at the end of installation does not vary significantly with h/R (proven, for example, in St-Alban clay; see Figure B13, Appendix B) and (c) the fully equalised stresses (σ'_{rc}) showed a comparable dependence on h/R to σ_{r1}, it is suggested that the effects of partial equalisation on the observed h/R effect are small.

The length of pause period preceding jacking stages was, however, seen to have a *permanent* effect on the response of the clay. A graphic example of the effect of this time dependence was evident in the experiments at

Bothkennar. The installation of pile BK4 was halted at 3.15m for 4 days, by which time 90% of excess pore pressures had dissipated and radial effective stresses had reached equilibrium values. Jacking was then re-commenced to a final pile tip penetration of ≈6m. The records obtained at z <3.5m during the re-jacking phase and subsequent equalisation and load testing are compared in Table 10.6 with equivalent measurements made by piles that were installed without any significant break in jacking.

	After a pause period of 4 days (pile BK4)	'Normal' installation (pause periods ≈6mins)
H_i	0.90	2.30
$\Delta u_i/\sigma'_{v0}$	0.4-0.8	1.5-2.25
$\Delta u_{max}/\sigma'_{v0}$	0.8	2.25
Time for u_{max}	500 mins	< 3 mins
U_d after 2500mins	0.7	0.3
Peak obliquity in load test (δ_p)	19.0°	28.5°

Table 10.6 The effect of pause periods at Bothkennar (z <3.5m, h/R ≥ 28)

This comparison reveals that:

(i) The radial total stresses and pore pressures recorded by instruments during re-jacking after the extended pause period were initially only ≈35% of those measured during 'normal' installation. These stresses became comparable to the stresses recorded during 'normal' installation at depths greater than ≈4.5m.

(ii) In contrast to the sharp increases in pore pressure observed after 'normal' installation, the pore pressure probes after the extended pause period indicated a sluggish response and took ≈500 mins to register their maximum pressures. The dissipation of these pressures was also slow and, as a consequence, the radial effective stresses appeared to reduce throughout most of the equalisation period (see Figure 8.17).

These observations illustrate (albeit for an extreme situation) the effect of a lengthy pause period between installation jacking stages. It appears from (i) that the reductions in stress which took place during equalisation of pile BK4 (at z <3.5m) affected the subsequent stress measurements permanently i.e. these reductions were irreversible.

Similar observations were made by Morrison (1984) during installation of the piezo-lateral stress (PLS) cell in Boston Blue Clay. The PLS cell measured stresses at 0.94m from its tip and was installed in 1.52m long jacking strokes (see Figure B5, Appendix B). Morrison classified the records obtained during the first 0.94m penetration as 'non-virgin' data, as the clay at these depths had been pre-sheared during the previous jacking stroke. He noted that:

- When pause periods between jacking stages were low (less than 200 secs[1]), *normalised* radial stresses and pore pressures recorded in 'non-virgin' strata were always ≈10% lower than those recorded during the last 0.56m of the jacking stroke i.e. in virgin strata.
- After longer pause periods, stresses and pore pressures remained low throughout the whole jacking stroke and only attained values similar to the 'virgin' data in the next jacking stage.
- Pore pressures initially increased during equalisation in 'non-virgin' material (also seen in ICP tests) but decreased monotonically with time in 'virgin' material.

The vast majority of soil adjacent to displacement piles (including the ICP) has been pre-sheared by a previous jacking stage and may be classified (using Morrison's term) as 'non-virgin' material. The PLS cell investigations have shown that the response of this material during installation differs significantly from that sheared for the first time ('virgin' material) and confirmed that the length of the pause period has an important influence on the measurements.

Morrison attributed the "unusual" measurements in non-virgin strata to the development of a densified "clay cake" on the pile shaft during pause

[1]Equivalent to ≈20 mins on ICP (in terms of times for radial consolidation).

periods and argued that this 'cake' did not allow instruments to record stresses that were representative of those acting on the principal displacement shear (considered to be at a short distance from the pile). This view is compatible with the unusual equalisation data and value of δ_p measured at z <3.5m by pile BK4 (see Table 10.6), but does not explain the high consistency of δ_p values measured at <u>all</u> instrument positions on the ICP in both first-time and reload tests, performed after a large range of equalisation periods. These δ_p values were also in good agreement with the results from drained ring shear interface experiments.

Three main conclusions may be made from the foregoing:

(i) The reductions in stresses with h/R during installation do not appear to be due to *temporary* partial equalisation effects.

(ii) A jacking stage preceded by a pause period of short duration has a *permanent* effect on all subsequent measurements made at any given depth and leads to a stress reduction with h/R. This reduction arises because of the dependence of the characteristics of the clay adjacent to the shaft on the pre-shearing history and degree of equalisation.

(iii) Pause periods, that are sufficient for significant equalisation to take place, may result in the formation of a clay cake on the pile shaft and anomalous measurements at fast rates of displacement.

10.5.2.3 <u>The influence of cyclic loading</u>

The ICP installation procedure subjects soil elements adjacent to the pile to a series load-unload excursions during each jacking stage. As the material at the trailing instrument position (h/R=50) experiences ≈12 cycles compared with 2 cycles at the leading instrument position (h/R =8), it is possible that part of the observed h/R effect may be due to a systematic relationship between 'h' and the number of cycles experienced by each soil horizon.

Typical variations of shear stress (τ_{rz}) with radial effective stresses (σ'_r) recorded during jacking cycles at Cowden and Bothkennar are shown on Figure 10.13.

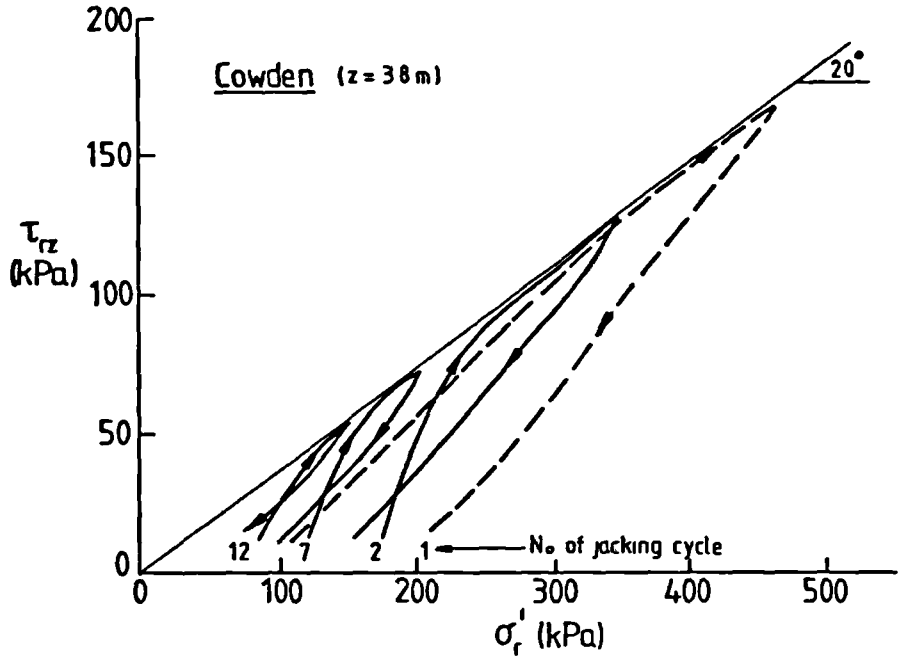

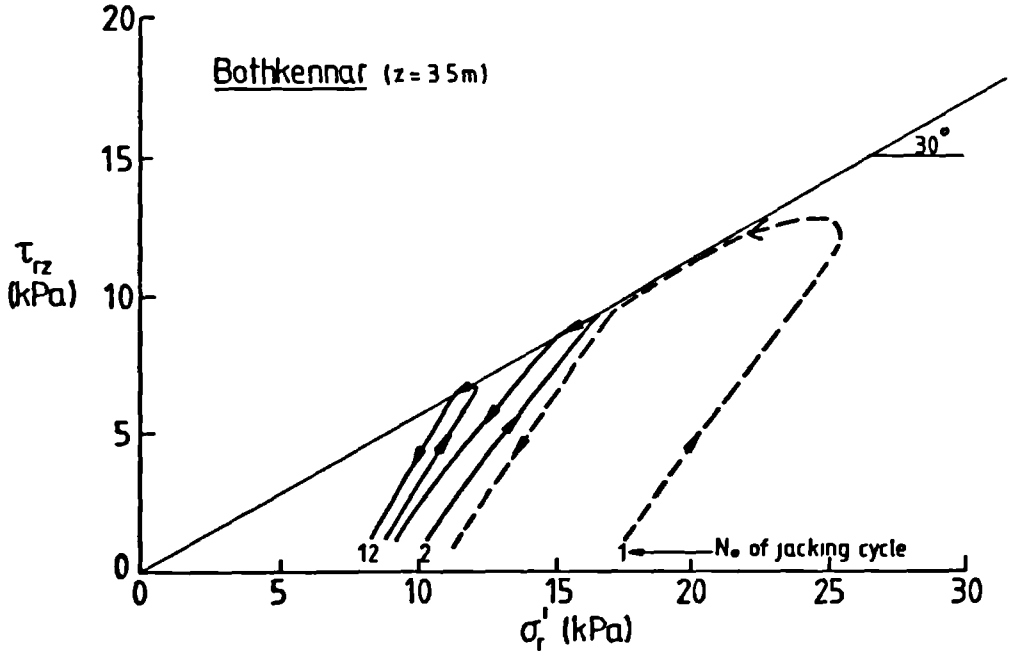

Figure 10.13 Typical τ_{rz} v σ'_r paths followed during installation

The σ'_r data plotted on this figure have been corrected for the anomalous pore pressures recorded at fast rates of displacement in accordance with

the procedure outlined in Section 10.2.3 and are therefore considered to be representative of those acting on the principal displacement shear.

Points to note include:

- At both sites, σ'_r increases at the beginning of a pile push. Such increases were also measured during load tests performed at the very early stages of equalisation (see Section 10.4.3).
- During penetration, τ_{rz} shows slight increases at Cowden and reductions at Bothkennar.
- As τ_{rz} returns to near zero values at the completion of a jacking stage, σ'_r reduces to a value *lower* than its pre-loading value, even though the pile had advanced to a deeper level.
- The effects of further cycles is to reduce both the stationary and moving values of σ'_r.

Laboratory experience indicates that undrained, large strain load cycling reduces both the mean effective stress (p') and the undrained shear strength (c_u). Reductions in σ'_r with h/R possibly result from this phenomenon. There is, however, no means of checking this hypothesis, as:

- p' cannot be calculated because the ICP instrumentation measures only two of the four stress components required to define the stress conditions adjacent to the shaft.
- Investigations into the cyclic characteristics of soils have not (to my knowledge) been performed under conditions analogous to those adjacent to a pile i.e. where the sample is *failed* in each shearing cycle and the mean total stress is allowed to vary from cycle to cycle.

It is noteworthy that the ICP subjected soil elements at a fixed depth to almost twice the number of jacking cycles that were applied in experiments of Coop (1987). Cyclic loading effects therefore offer a plausible explanation for why Coop measured a smaller dependence of stresses on h/R to that measured in ICP tests (see Figure 10.11).

10.5.3 Summary

No clear evidence exists to prove conclusively which factors affect the observed reduction in stresses with the distance from the pile tip. A review of existing data suggests that this reduction depends on the soil type, pile type and installation method and arises from a combination of the strain paths imposed on the soil by monotonic pile installation and the effects of discrete shearing cycles of the soil in a partially equalised state.

Chapter 11 examines the existing data base of measurements made by high quality instrumented displacement piles in clay and proposes correlations for σ_{r1}, $\Delta u_{max}/\sigma'_{v0}$ and σ'_{rc}. Before these correlations were derived it was necessary to decide on whether stresses reduced with the normalised distance from the pile tip (h/R), the absolute distance from the pile tip (h) or the number of jacking cycles (h/J, where J is the stroke length of the jack). More consistent correlations were derived when h/R was used in preference to 'h' or 'h/J' and it was tentatively assumed that the normalised distance (i.e. h/R) was more generally applicable. It is clear, however, that further research specifically investigating the 'h/R effect' is required.

CHAPTER 11

CORRELATIONS FOR DISPLACEMENT PILES IN CLAY

CONTENTS OF CHAPTER 11

CORRELATIONS FOR DISPLACEMENT PILES IN CLAYS

11.1 INTRODUCTION 416

11.2 THE DATA BASE 416

11.2.1 Clay types 416

11.2.2 Pile configurations 419

11.3 INSTALLATION 420

11.3.1 Radial total stress 420

11.3.2 Pore pressure 423

11.3.3 Radial effective stress 424

11.4 EQUALISATION 425

11.4.1 Relaxation of radial total stress 425

11.4.1.1 Analytical predictions 426

11.4.1.2 Empirical correlation for K_c/H_1 427

11.4.2 Pore pressure dissipation 429

11.4.3 Equalised radial effective stress 430

11.5 ULTIMATE LOCAL SHAFT FRICTION 433

11.6 IMPLICATIONS OF EFFECTIVE STRESS APPROACH FOR EXISTING DESIGN METHODS 434

11.6.1 The α method 434

11.6.2 The β method 438

11.7 CONCLUSIONS 439

11.1 INTRODUCTION

It has been shown that the shaft capacity of a displacement pile is controlled by a complex series of stress changes in the soil during installation, equalisation and load testing. These changes may be viewed separately by expressing the peak local shear stress (τ_f) as follows:

$$\tau_f = \sigma'_{rf} \tan \delta_p$$

$$= [H_1]\ [H_c/H_1]\ [K_f/K_c]\ \sigma'_{v0} \tan \delta_p$$

The four key parameters in this expression are:

H_1: the normalised radial total stress ratio mobilised during *installation* = $[(\sigma_{ri}-u_0)/\sigma'_{v0}]$

H_c/H_1: the radial total stress relaxation coefficient during *equalisation* = $[(\sigma_{rc}-u_0)/(\sigma_{ri}-u_0)] = K_c/H_1$

K_f/K_c: the ratio of σ'_r at peak local shear stress (σ'_{rf}) during pile *loading* after equalisation to the initial pre-loading (equalised) σ'_r value (σ'_{rc}).

δ_p: the obliquity at peak local shear stress

A review of the literature (Section 2.4) identified 10 programmes of instrumented displacement pile tests in clay where reliable measurements of the effective stresses acting on the pile shafts were obtained. Appendix B collates these measurements and expresses the data in terms of the four parameters given above. The overall patterns obtained from these data and the ICP tests are investigated in this Chapter and an attempt is made to develop a general expression for τ_f which is based on the physical measurements made in instrumented pile tests.

11.2 THE DATA BASE

11.2.1 Clay types

Twelve clay types (including Cowden till and Bothkennar clay) have been investigated using high quality instrumented displacement piles. The

average index properties, apparent OCR (derived from oedometer tests, where possible) and UU triaxial compression strength (c_{u0}) of these materials within the depths penetrated by the respective piles are summarised in Table 11.1. The specific variations with depth of these and other parameters, such as K_0 and the CPT end resistance (q_c), are listed in Tables B5-B16 in Appendix B.

Tests have been performed in a relatively wide range of clay types. These include clays with plasticity indices (PI) between 15% and 60%, liquidity indices (LI) between -0.2 and +3.2 and OCR's of up to 50.

Clay	PI (%)	LL (%)	LI (%)	App. OCR	c_{u0} (kPa)	L_{max} (m)	D mm	Reference used
Cowden	19	38	-0.2	10	110	6.4	102	This thesis
Bothkennar	40	65	0.7	1.7	17	6.0	102	This thesis
London clay	45	75	0.0	30	100	6.0	102	Bond (1989)
Boston Blue	22	43	1.0	1.5	45	40	38	Morrison (1984)
Empire	52	80	0.3	1.6	80	75	38	Azzouz & Lutz (1986)
Gault	48	75	0.0	20	135	9	80	Coop (1987)
Huntspill	35	65	1.0	1.6	30	9	80	Coop (1987)
Gt Yarmouth[1]	28	51	1.0	1.7	25	9	80	Coop (1987)
St. Alban[1]	18	42	3.2	2.2	25	7.6	219	Roy et al (1981)
Haga	15	40	1.0	5	65	5.2	153	Karlsrud & Haugen (1985)
Tokyo	55	100	1.0	6	30	5.6	300	Koizumi & Ito (1967)
Rio de Jan.	60	125	1.6	1.8	8	6.7	220	Soares & Dias (1990)

Table 11.1 Average parameters at test sites

[1]Only pore pressure measurements were obtained at St-Alban and no stresses after installation are reported in Gt. Yarmouth clay.

Burland (1990) proposed the use of the void index (I_v) to describe the state of compactness of a given sediment. I_v is given by:

$$I_v = (e - e^*_{100}) / C_c^*, \text{ where}$$

e is the in-situ void ratio, e^*_{100} is the void ratio of the intrinsic (normally consolidated, reconstituted) material[1] at σ'_{v0} =100kPa and C_c^* is the compressibility of the intrinsic material. In-situ I_v values were estimated at the depths where stress measurements were obtained in each pile test programme using Burland's correlations between the void ratio at the liquid limit (e_L) and the values of e^*_{100} and C_c^*:

$$e^*_{100} = 0.109 + 0.679\, e_L - 0.089\, e_L^2 + 0.016 e_L^3$$
$$C_c^* = 0.256\, e_L - 0.04$$

Typical *average* I_v values for each test programme are plotted against $\log(\sigma'_{v0})$ on Figure 11.1 which also plots the variation of I_v with $\log(\sigma'_{v0})$ for normally consolidated reconstituted material i.e. the intrinsic compression line (ICL). By comparing each I_v value with the corresponding I_v value at the same stress level on the ICL and noting the average in-situ OCR's of each material (given in Table 11.1), Burland's research suggests that the clays in the data base can be categorised as follows:

(i) insensitive clay with a high OCR (Cowden, London & Gault)
(ii) insensitive clay with low OCR (Empire)
(iii) sensitive clay with moderate OCR's (Haga and Tokyo)
(iv) sensitive clay with low OCR (Bothkennar, Huntspill, Boston blue and Rio de Janeiro)

Although the same classification of soil types could be made simply on inspection of the liquidity indices and OCR's, I_v values have been evaluated to allow trends to be established in Section 11.4. I_v is considered to be a more reliable measure of the in-situ condition of the

[1]defined as a material which has been reconstituted at a water content 25% to 50% higher than its liquid limit and then consolidated under one dimensional conditions.

clay than the liquidity index as it is defined in terms of directly measured *mechanical* properties (C_c^* and e^*_{100}).

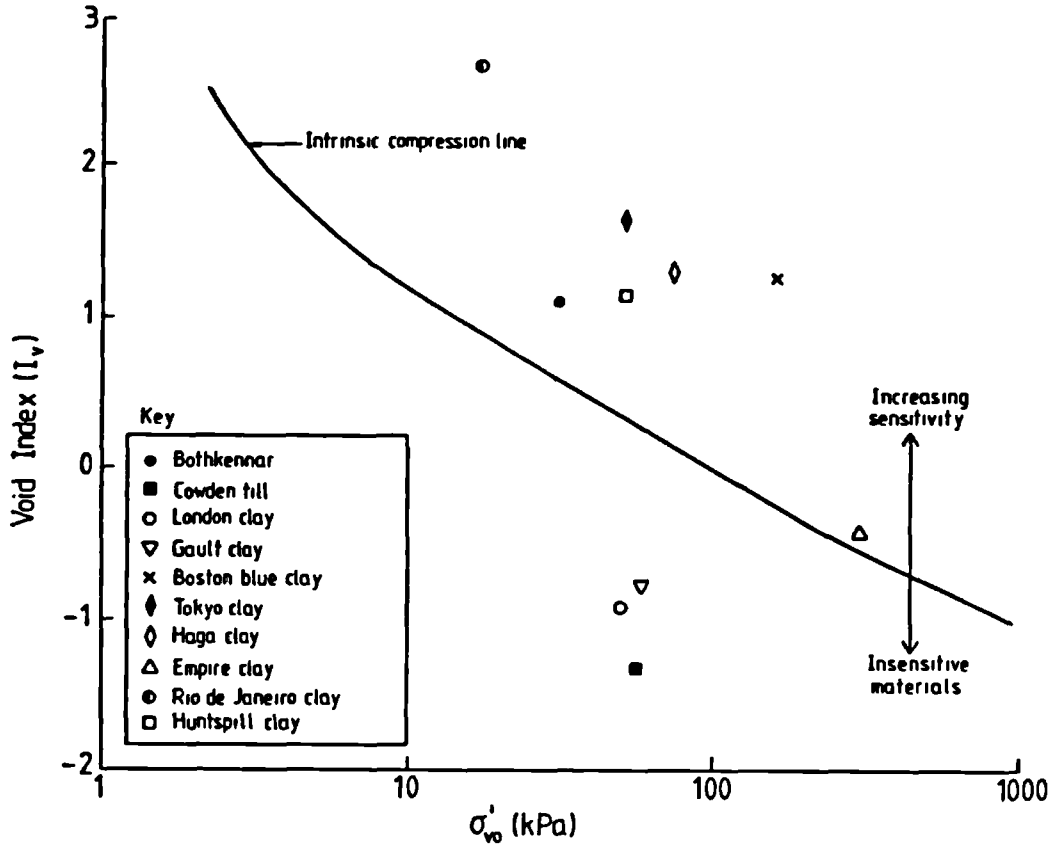

Figure 11.1 In-situ void indices for materials in case histories

11.2.2 Pile configurations

The diameters of the piles in the data base ranged from between 38mm (the piezo-lateral stress (PLS) cell experiments in Boston Blue Clay and Empire Clay) to 300mm (at Tokyo). All piles were jacked to final penetration depths of less than 10m (except for the PLS tests). Stresses were measured at between 1 and 5 locations on the pile shafts and the sensors were generally positioned within 55 pile radii of the pile tips i.e. $h/R < 55$.

11.3 INSTALLATION

11.3.1 Radial total stress

The most abundant and reliable set of records in the data base are those of the radial total stresses measured during installation (σ_{ri}). A detailed examination of these data revealed that, as was evident in the ICP tests, σ_{ri} depended on the soil consistency (as expressed by the values of OCR, c_{u0} or q_c) and reduced with the distance from the pile tip (h).

A number of regression analyses on the data base were performed to investigate if a general trend existed between σ_{ri}, h and either OCR, q_c or c_{u0}. It was assumed tentatively that the measurements could be unified if the distance from the tip of each pile (h) was normalised by its pile radius (R) i.e. h/R (see Section 10.5). These analyses showed:

- The most consistent trend was found when $(\sigma_{ri}-u_0)/\sigma'_{v0}$ (i.e. H_i) was related to the apparent OCR's of the clay strata. This may partly be because the assessment of OCR is less sensitive to different sampling procedures (which have a significant effect on measured c_{u0} values) and the resolution of q_c measurements in very soft materials is often poor.

- the reduction of σ_{ri} with h/R (or h) was not unique (see Section 10.5), but the rate of this reduction was, in most cases, relatively small for h/R ≥20.

The H_i ratios measured in all case histories at h/R ≥20 are plotted against apparent OCR on Figure 11.2 using logarithmic axes. It is evident that log (H_i) increases approximately linearly with log (OCR). The relationship :$H_i = 1.9\ OCR^{0.4}$ provides reasonable predictions for most of these data. Better predictions are obtained if the dependence of H_i on h/R is accounted for and the following best fit relationship for <u>all</u> data (3 ≤ h/R ≤95) was deduced:

$$H_i = 3.92\ OCR^{0.41}\ (h/R)^{-0.2} \qquad \text{Eqn. 1}$$

(correlation coefficient r^2 =0.86 for 110 data points)

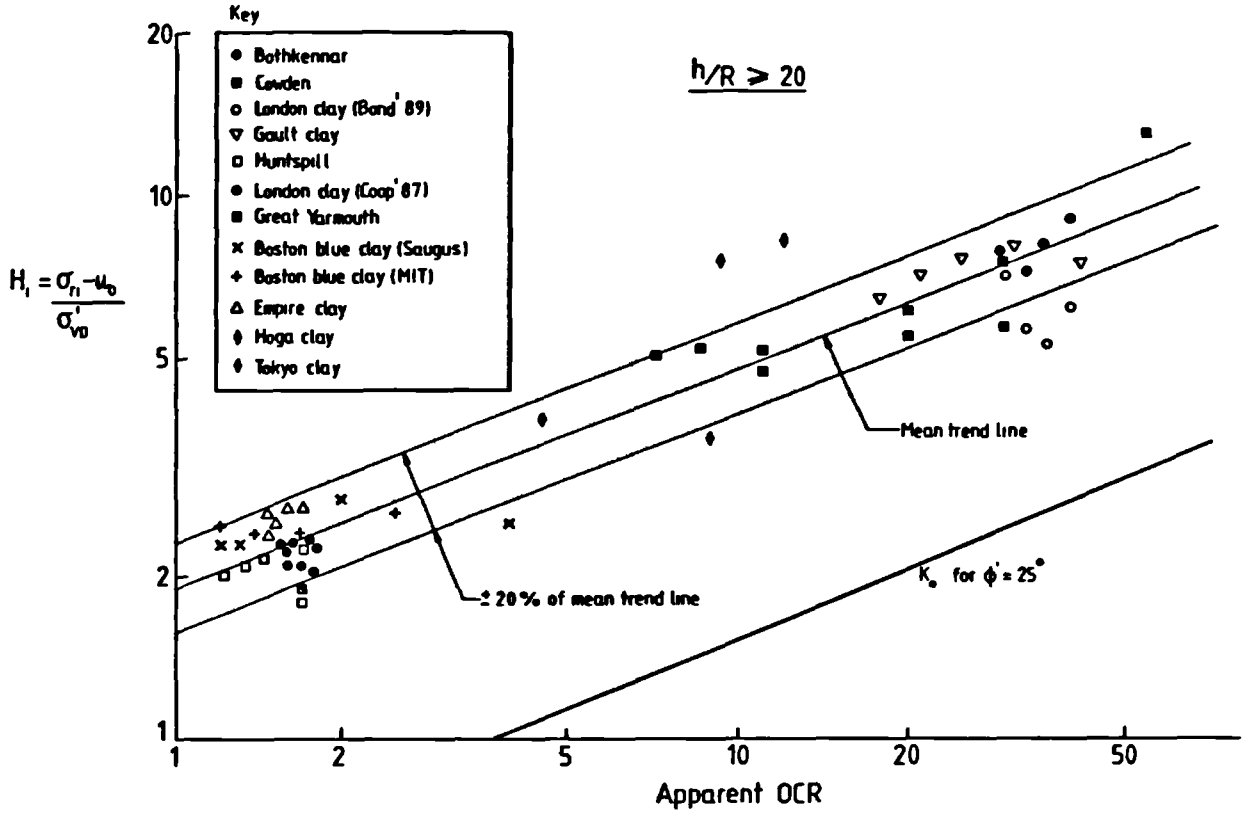

Figure 11.2 H_1 variation with apparent OCR for h/R ≥20

Eqn. 1 generally predicts measured H_1 values to an accuracy of ±20%. Notable exceptions were the under-predictions (by ≈30%) at h/R=95 in the Empire clay and at all h/R ratios in the Tokyo clay and the over-predictions (by ≈30%) at h/R≥50 in the 'disturbed' London clay and at h/R=22 in the Huntspill and Gt. Yarmouth clays.

Some implications of Eqn. 1 are listed below:

(i) If H_1 is considered to depend only on OCR and h/R, then the average reduction of H_1 with h/R for all the data base is less than that measured in the ICP tests which showed that H_1 varied with $h/R^{-0.3\pm0.05}$. This may be because most of the other piles were installed in larger jacking strokes (thereby subjecting the soil at a given depth to a lower number of load cycles) and had a smoother surface finish than that of the ICP (see Section 10.5).

(ii) A parametric study of reported SPM/MIT-E3 analyses (presented in Section 2.3) suggested that these analyses also predict that H_1 is almost a unique function of OCR and h/R and the relationship $H_1 = 1.3\ OCR^{0.55}$ provided a good fit to the predictions for h/R ≥15 (see Figure 2.11). This relationship under-estimates measured H_1 values by ≈25% for OCR <4.

(iii) For the simple process of mechanical loading followed by unloading with no subsequent reloading, $K_0 \approx 0.58\ OCR^{0.42}$, for a typical ϕ' value of 25° (Mayne & Kulhawy 1982). The ratio of H_1 to K_0 is then given approximately by:

$$H_1/K_0 = (\sigma_{r1} - u_0)/(\sigma_{h0} - u_0) \approx 6.75\ (h/R)^{-0.2} \qquad \text{Eqn. 2}$$

This ratio therefore appears to be virtually independent of the clay consistency (or OCR) and varies from ≈ 5 at h/R=5 to between 3 and 3.5 for h/R ≥20.

(iv) The increase in radial stress due to the expansion of an infinitely long cavity in an elastic perfectly-plastic material is given by Hill (1950) as $\Delta\sigma_r = c_u\ [1 + \ln\ (G/c_u)]$, where c_u is the undrained shear strength in plane strain. As the plane strain undrained shear strength is comparable to the peak undrained strength in triaxial compression (Hight et al 1987), $c_u/\sigma'_{v0} \approx 0.3\ OCR^{0.8}$; see Section 2.2.2. Therefore for a typical G/c_u value of 100 (see Bond 1989), Hill's expression may be re-written as:

$$(H_1)_{cav.\ exp.} \approx 1.7\ OCR^{0.8} + K_0$$
$$\approx 1.7\ OCR^{0.8} + 0.58\ OCR^{0.42}$$

This equation is in reasonable agreement with the trends projected for very small h/R values, but over-predicts measurements made at h/R ≥4 for all OCR's. The over-prediction becomes progressively larger with increasing OCR and h/R. It is therefore clear that the Cavity Expansion Method (see Section 2.3.1) does not provide a realistic description of the pile installation process.

11.3.2 Pore pressure

The Cowden and Bothkennar tests (as well as other case histories) have indicated that only pore pressures recorded at low pile velocities (less than 1mm/min) can be considered representative of those acting on the principal displacement shear. For this reason, attention is focused on the more reliable measurements made when the piles came to rest after installation.

In most cases, pore pressure maxima (u_{max}) were recorded shortly after installation, indicating that higher pressures exist at a short distance from the shaft while the pile is moving (see Section 10.2.2). The maximum excess pore pressures ratios ($\Delta u_{max}/\sigma'_{v0}$) measured in all case histories (including data from piezocone tests shown on Figure 10.12) are plotted against the apparent OCR on Figure 11.3.

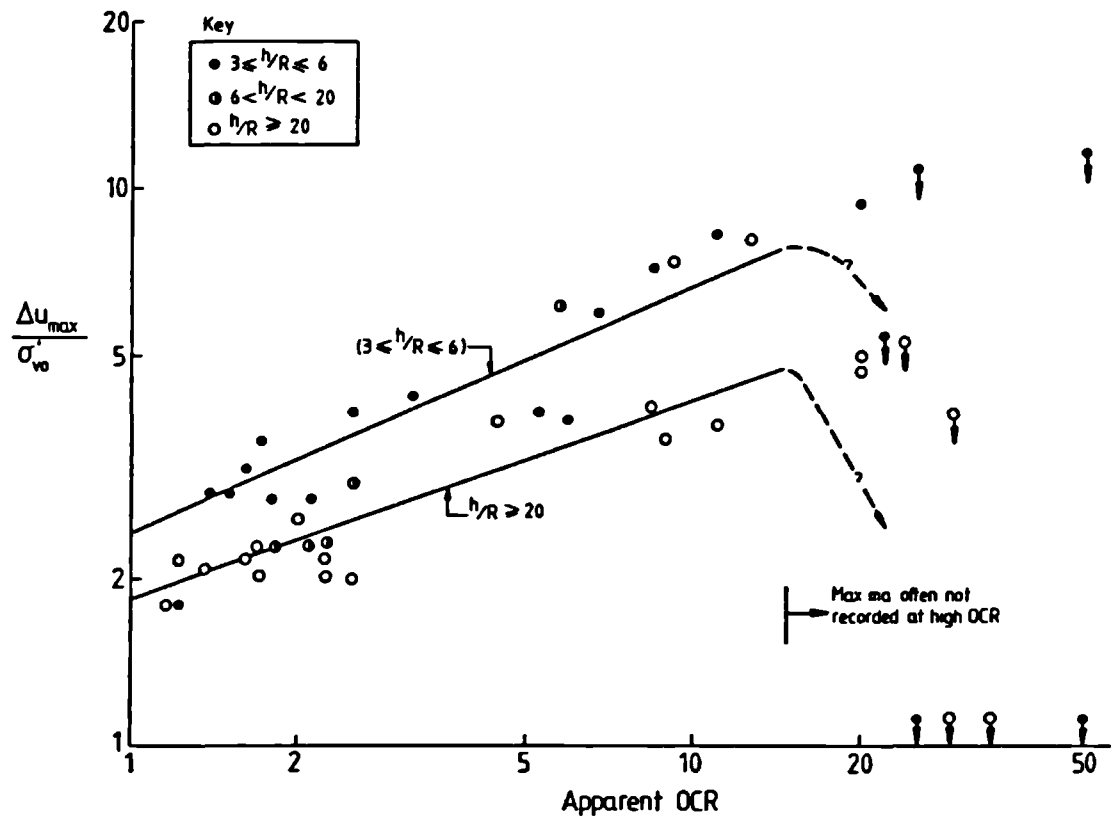

Figure 11.3 $\Delta u_{max}/\sigma'_{v0}$ variation with apparent OCR

It is evident that the values of $\Delta u_{max}/\sigma'_{v0}$ are controlled most strongly by the OCR and h/R values. Regression analyses for *OCR ≤10* gave the following best fit relationships (h/R ≥3)

$$\Delta u_{max}/\sigma'_{v0} = 3.1\ OCR^{0.5}\ (h/R)^{-0.2} \quad \text{or} \qquad \textbf{Eqn. 3}$$

$$\Delta u_{max}/\sigma'_{v0} = 1.8\ OCR^{0.36} \quad \text{for } h/R \geq 20 \qquad \textbf{Eqn. 4}$$

It is noteworthy that Eqn. 3 has a correlation coefficient of only 0.73 compared to the corresponding coefficient of 0.86 obtained for the H_1 relationship (Eqn. 1). This less systematic pattern is compatible with SPM/MIT-E3 predictions which show that $\Delta u_{max}/\sigma'_{v0}$ ($=\Delta u_1/\sigma'_{v0}$) also depends significantly on other soil properties, such as the sensitivity and small strain stiffness (see Figure 2.11).

In low OCR and sensitive materials, the maximum pore pressure (u_{max}) always occurred within 5 mins of the completion of installation. However, in higher OCR, insensitive materials, the pressures recorded during installation were low (and often negative) and u_{max} took a longer period to develop (e.g. over 1 day at h/R ≥5 in the London clay). This is probably because of (a) the more extensive region that experiences negative (shear induced) pore pressures in these materials and (b) a less satisfactory response of the pore pressure probes due to cavitation of their saturation fluid during installation. These two factors contribute to the scatter shown on Figure 11.3 at OCR > 10.

In summary, it appears that no simple empirical relationship exists that can predict the magnitude of $\Delta u_{max}/\sigma'_{v0}$ to an acceptable accuracy.

11.3.3 Radial effective stress

Radial effective stress (σ'_r) measurements made during pile installation show complicated and inconsistent trends because reliable pore pressures are not measured at fast rates of displacement or after the fluid of pore pressure probes has cavitated. In addition, radial stresses and pore pressures in low OCR and sensitive materials are similar in magnitude and minor errors in either of these measurements can lead to disproportionate errors in the calculated σ'_r values. Given (a) these

measurement difficulties, (b) the fact that pore pressures are more sensitive than radial stresses to the full range of soil properties and (c) the small size of the data base, it is suggested that any correlation for installation σ'_r values would be unreliable.

The lateral stress coefficients, $K_i = (\sigma'_r/\sigma'_{v0})$, *measured immediately after installation*[1], do however show one notable general characteristic: K_i is generally less than the undisturbed coefficient (K_0) in low OCR and sensitive materials and greater than K_0 in high OCR, insensitive materials. In general, the ratio K_i/K_0 appears to decrease with increasing sensitivity and reducing OCR.

11.4 EQUALISATION

11.4.1 Relaxation of radial total stress

Following the logic set out in Section 11.1, the derivation of a general expression for τ_f requires the development of a correlation that can satisfactorily predict the overall stress changes that took place during equalisation in each of the case histories. It would be preferable to develop such a correlation in terms of the radial *effective* stress lateral stress coefficients K_i and K_c. However, for the reasons given in Section 11.3.3, the measurements of K_i are considered unreliable in both contractant and dilatant materials, and therefore any dependable correlation must be expressed in terms of radial total stresses.

This section attempts to derive an empirical expression for the relative change in radial *total* stresses during equalisation that is compatible with the measurements in the data base and reflects the underlying processes controlling equalisation. This change is expressed in terms of the relaxation coefficient, H_c/H_i, defined as:

$$H_c/H_i = [(\sigma_{rc}-u_0)/(\sigma_{ri}-u_0)] = \sigma'_{rc}/(\sigma_{ri} - u_0) = K_c/H_i$$

[1]These coefficients do not suffer from pore pressure measurement difficulties at high velocities, but is should be noted that their values are generally less than the K ratios mobilised during installation (see Section 10.2.3 and Figure 10.6).

Analytical predictions for K_c/H_i are briefly discussed first to provide a basis for the proposed correlation.

11.4.1.1 Analytical predictions

Trial pits excavated adjacent to the piles installed in London clay and Haga clay (see Section 2.4.5) have shown that the magnitude of K_c/H_i can be related to the degree of contraction that the material close to the pile shaft undergoes during equalisation. Therefore, if it is assumed that the equalisation process can be idealised to a one dimensional axially symmetric situation where an annulus of material close to the pile of width (ΔR) consolidates (i.e. contracts) along a curve parallel to the intrinsic compression line, under an applied stress of σ'_r, and the surrounding soil mass remains elastic (of shear stiffness G), then the change in radial total stress ($\Delta\sigma_r$) during equalisation is given *approximately* by:

$$\Delta\sigma_r = (K_c - H_i)\ \sigma'_{v0} \approx -2G\ (\Delta R/R)\ C_c^*\ \log\ (K_c/K_i)$$

If the radial extent of the yielding zone (ΔR) is proportional to R (as predicted by the Strain Path Method) and H_i/K_0 is a constant (Eqn. 2), then the relaxation coefficient (K_c/H_i) is given by:

$$K_c/H_i \approx 1 - A\ [G/\sigma'_{h0}]\ [C_c^*\ \log\ (K_c/K_i)], \qquad \text{Eqn. 5}$$

where A is a constant

Eqn. 5 suggests that:

- K_c/H_i is less than 1 when σ'_r increases during equalisation (i.e. in contractant materials) and greater than 1 when σ'_r decreases during equalisation (i.e. in strongly dilatant materials).
- As K_i reduces with increasing sensitivity and decreasing OCR (Section 11.3.3), K_c/H_i values will be lower in more sensitive clays and less overconsolidated clays.
- There is not a simple dependence of K_c/H_i on the plasticity index (PI) of the clay as G/σ'_{h0} reduces with PI (e.g. see Smith 1992) but C_c^* generally increases with PI (for deposits lying a similar distance above the 'A-line' on the soil plasticity chart).

SPM/MIT-E3 analyses of the equalisation process have shown that the continual interaction of the yielding zone and outer zone and the non-linearity of the materials affect the value of the relaxation coefficient significantly. SPM/MIT-E3 equalisation analyses, reported to date, (discussed in Section 2.3) predict that K_c/H_1 is always less than 1. However, these analyses also predict that, as suggested by Eqn. 5, K_c/H_1 decreases with increasing sensitivity and reducing OCR and shows no systematic variation with the clay plasticity (see Figure 2.13).

11.4.1.3 Empirical correlation for K_c/H_1

It is evident from the foregoing that a correlation for K_c/H_1 must account for the effects of the initial sensitivity and OCR of the clay.

The sensitivity S_t of a lightly overconsolidated clay (providing swelling volume changes are small) is given approximately by $S_t \approx OCR\ \sigma'_{v0}/\sigma'_{ve}$, where σ'_{ve} is the σ'_v value on the intrinsic compression line at the in-situ void ratio. Therefore, the difference between the void index of the in-situ material (I_v) and the void index of the intrinsic material $(I_v)_{ICL}$ at the same stress level, defined as I_v^*, provides a measure of the sensitivity and OCR of the clay i.e.

$$I_v^* = I_v - (I_v)_{ICL} = [e - (e)_{ICL}]/C_c^* \approx \log(S_t/OCR)$$

Burland (1990) suggests that I_v^* for heavily overconsolidated materials can be considered as an approximate measure of OCR i.e. for more negative I_v^* values, the clay is likely to be in a more heavily consolidated stress state.

Based on the foregoing, it was considered that K_c/H_1 may be related empirically to I_v^*. This relationship is investigated in Figure 11.4 which plots the mean K_c/H_1 ratios in the data base[1] against the I_v^* values at the depths where these ratios were recorded. (The symbols used for each site are the same as those used in previous figures).

[1]Excluding the K_c measurements made in the 'disturbed' London clay which gave K_c/H_1 values of greater than 1.0 (see Table B5, Appendix B).

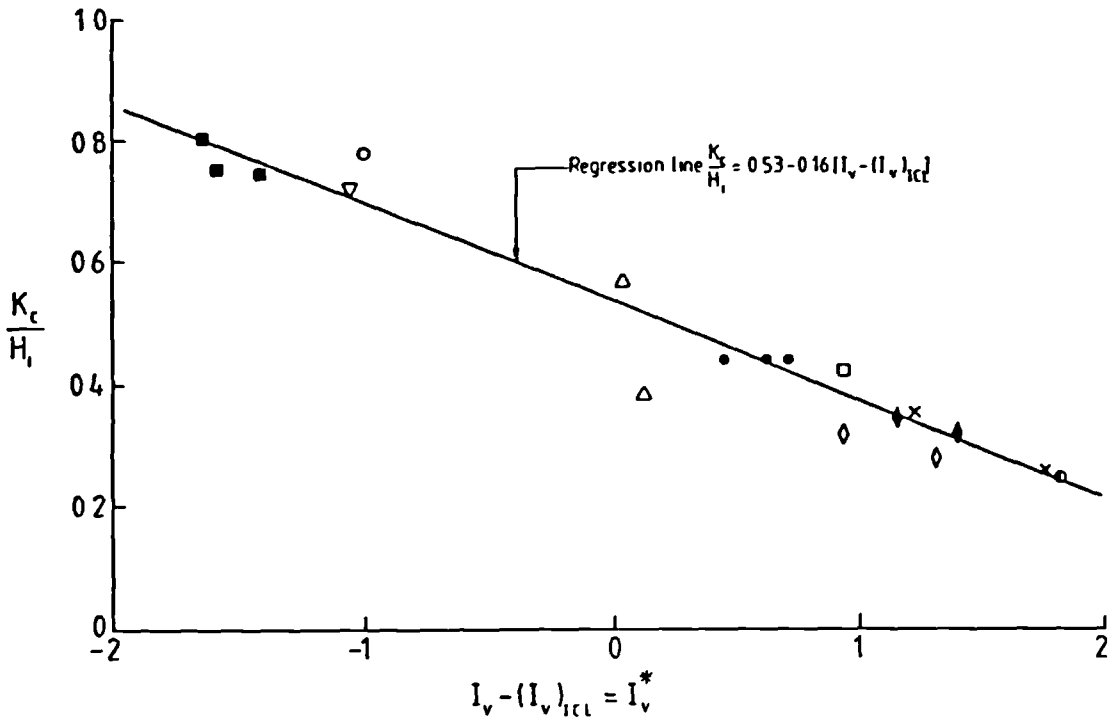

Figure 11.4 K_c/H_1 variation with I_v^*

A definite trend for K_c/H_1 to reduce with I_v^* is observed and the following best fit regression line predicts the measured K_c/H_1 values to within 20%.

$$K_c/H_1 = 0.53 - 0.16\ I_v^* \qquad \text{Eqn. 6}$$

While it is probable that other factors (such as stiffness and strength) affect the magnitude of K_c/H_1, the sparsity of the data base precludes the refinement of Eqn. 6.

As K_c/H_1 appears to be most strongly dependent on sensitivity and OCR (or I_v^*), it follows that empirical correlations for K_c must also account for this dependence. Previous correlations proposed for K_c, which were derived from instrumented pile test data (e.g. Bond 1989 & Azzouz et al 1990), have not accounted for the influence of sensitivity. For these

relationships (see Section 2.2.4), Bond found a poor fit for "unrepresentative cases" such as Haga and Tokyo clays and Azzouz et al considered the measurements in Empire clay anomalous. These apparent inconsistencies can be explained by the effects of clay sensitivity.

11.4.2 Pore pressure dissipation

The ICP tests have shown that dissipation of excess pore pressures after pile installation can be approximated using linear consolidation theory and a recompression value of the horizontal coefficient of consolidation (c_h) of the clay. This finding is investigated for the full data base by plotting (on logarithmic axes) the pile diameter (D) against the time required for 90% of excess pore pressures to dissipate (t_{90}). Only data at h/R ≥12 are considered because of the proven strong three dimensional effect on the consolidation characteristics closer to the pile tip.

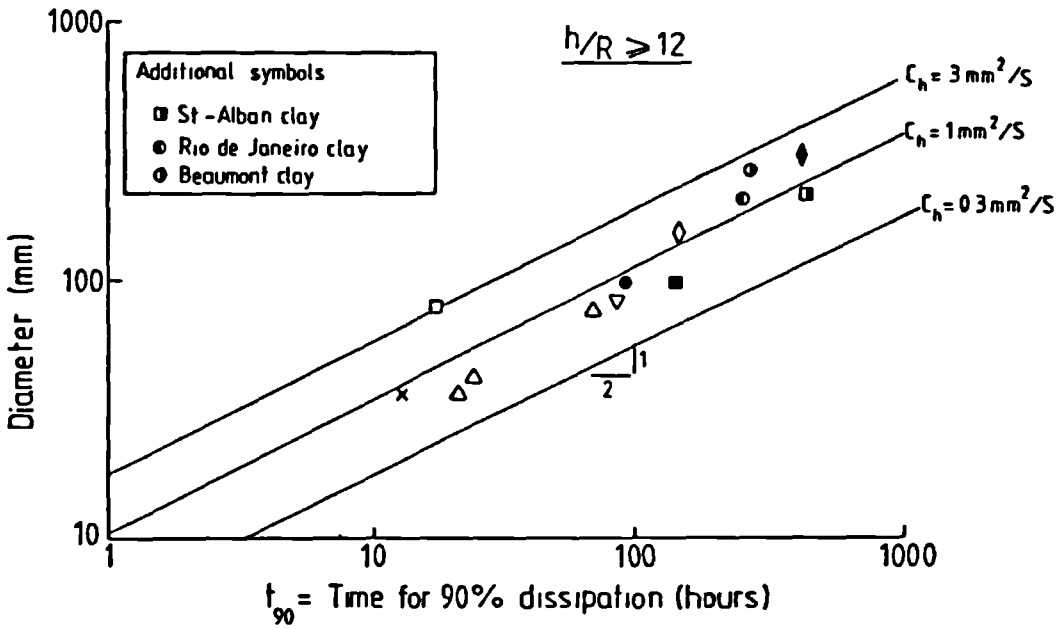

Figure 11.5 Dependence of t_{90} on pile diameter (symbols as before)

Despite the wide range in clay and pile types, an approximately linear increase in log (t_{90}) with log (D) is observed. This linear increase is consistent with a constant time factor T (= $4c_h\ t/D^2$) at t_{90} and the

assumption that only radial drainage takes place. Based on predictions made by Levadoux & Baligh (1980) and Houlsby & Teh (1988)[1], a time factor at t_{90} of 130 has been selected to construct lines of constant c_h on Figure 11.5.

All data lie within the c_h range of $0.3mm^2/s$ and $3.0mm^2/s$. This relatively narrow range is surprising given that c_h is a combination of the soil permeability and compressibility, both of which vary greatly among the materials included in the data base.

These observations suggest that a very simple estimate may be made of the time required for consolidation around a full scale industrial (closed-ended) displacement pile. For example, a 1m diameter pile in a typical clay soil ($c_h \approx 1mm^2/s$) may be expected to reach t_{90} in $[130 \times 1000^2 /4]$ secs $\approx$1 year.

11.4.3 Equalised radial effective stress

The equalised lateral stress coefficients K_c ($=\sigma'_{rc}/\sigma'_{v0}$) recorded at h/R $\geq$ 20 are plotted against apparent OCR on Figure 11.6[2]. It is evident from a comparison of this plot with the equivalent plot of the H_1 data on Figure 11.2 that (i) far fewer measurements of K_c have been made and (ii) the variation with OCR is less consistent. For example, at OCR $\approx$1.5, K_c values in Boston blue clay are up to 60% less than those measured in Empire clay, whereas the H_1 values in these materials differed by less than 10%. This has been seen in Section 11.4.1 to be due to the dependence of the reduction of σ_r during equalisation on the sensitivity of the clay.

Also shown on Figure 11.6 are the mean trend lines for K_c deduced from the H_1 data recorded at h/R $\geq$ 20 (where $H_1 \approx 1.9\ OCR^{0.4}$) and the variation of the relaxation coefficient with I_v^* (Eqn. 6) i.e.

$$K_c = H_1\ [K_c/H_1] = 1.9\ OCR^{0.4}\ [0.53 - 0.16\ I_v^*] \qquad (h/R \geq 20)$$

---

[1]Linear consolidation analyses, using initial pressures derived in SPM analyses.

[2]Discounting the data recorded in the 'disturbed' London Clay.

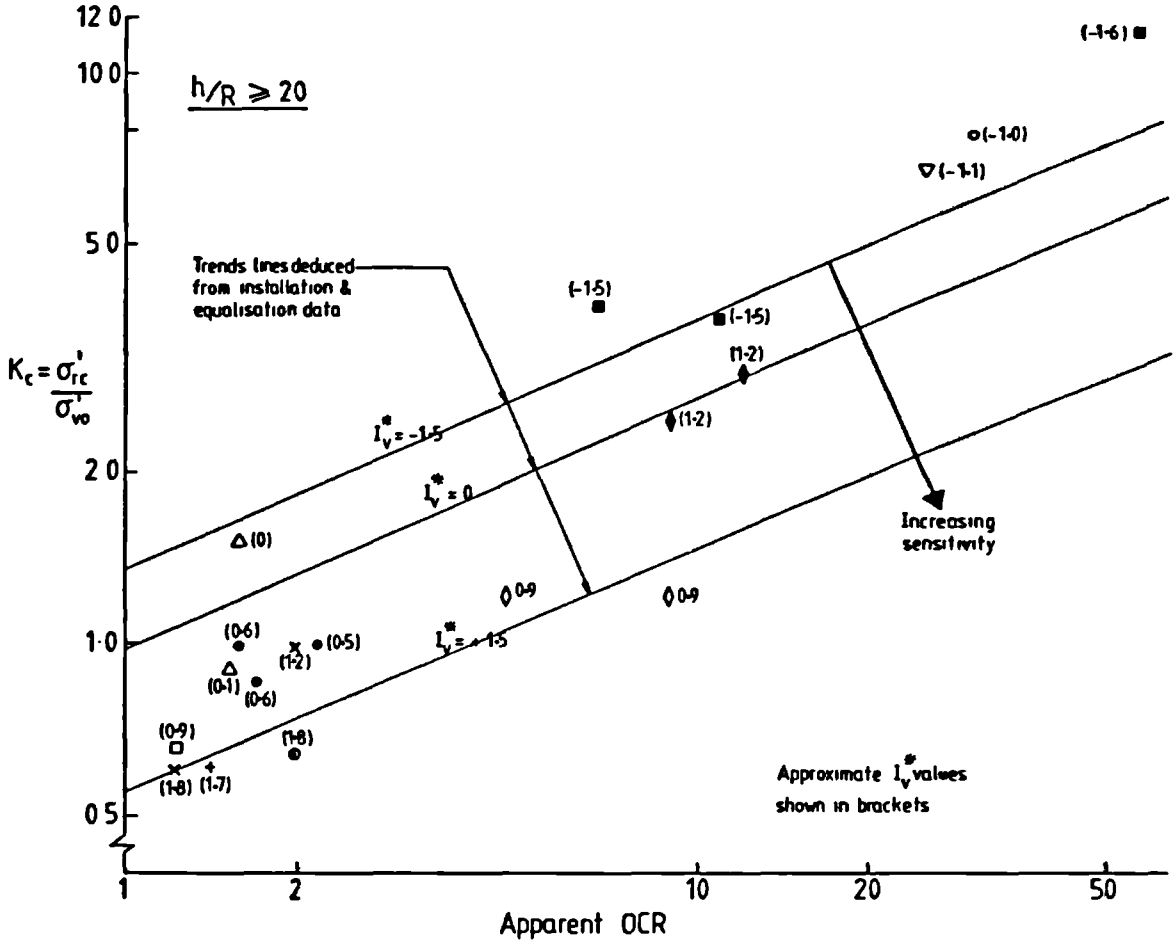

Figure 11.6 K_c variation with apparent OCR and I_v^*

These K_c lines are shown for I_v^* values of -1.5, 0 and +1.5 and are seen to reduce the apparent scatter in the data significantly. It is noteworthy that, if the observed dependence of K_c on sensitivity is not taken into consideration, a significantly different dependence of K_c on OCR is deduced which has higher correlation coefficient (i.e. $K_c = 0.58\ OCR^{0.72}$). This dependence is erroneous and demonstrates the difficulties in establishing correlations from a small data base without knowledge of the all the major factors affecting the measurements.

K_c/H_1 showed no systematic dependence on the relative depth of the pile tip (h/R). Therefore, using the relationship derived for all the H_1 data,

K_c is given by:

$$K_c = H_1 \; [K_c/H_1] = 3.9 \; OCR^{0.41} \; (h/R)^{-0.2} \; [0.53 - 0.16 \; I_v^*] \qquad \text{Eqn. 7}$$
$$(3 < h/R < 95)$$

Predictions for K_c using Eqn. 7 are accurate to ±20% for 27 out of the 32 measured K_c values (including 11 values measured in ICP tests). The five exceptions were the over-predictions by 60% at h/R=42 at Haga and by 35% at h/R= 5.5 in the Gault & Huntspill clays and the under-predictions by 35% at h/R=8 in the London clay and by 26% at h/R=25 in Tokyo clay.

Two further comments may be made concerning the suggested expression for K_c (i.e. Eqn. 7):

- A slightly different relationship between K_c, OCR, I_v^* and h/R is obtained if only the measured K_c data is used in the regression analyses[1]. However, Eqn. 7 is believed to be more representative because it is based on the far more abundant set of H_1 data (110 data points).

- Ideally, a relationship for K_c should separate the effects of sensitivity (S_t) and OCR and be expressed in terms of three functions (f_1, f_2 and f_3) i.e. $K_c = f_1 \; [OCR] \; f_2 \; [\log (S_t)] \; f_3 \; [h/R]$. This will be possible when more K_c data become available.

In summary, Eqn. 7 appears to provide a good first order estimate of the equalised radial effective stresses developed on closed-ended displacement piles in clay. Other factors such as soil stiffness and strength may have secondary influences, but is believed that the primary reason for the observed scatter is the variable dependence of the stresses on h/R (such as seen in the ICP tests). This limitation should be borne in mind when examining the implications for the proposed expression for τ_f given below.

---

[1] $K_c = 3.7 \; OCR^{0.48} \; [0.53 - 0.16 \; I_v^*] \; [h/R]^{-0.2}$

11.5 PREDICTION OF SHAFT CAPACITIES

Given an estimate of K_c ($=\sigma'_{rc}/\sigma'_{v0}$), the prediction of the peak local shaft friction that can be mobilised on pile loading after equalisation (τ_f) requires an assessment of two other variables:

(i) the obliquity at peak shear stress, $\delta_f = \tan^{-1}(\tau_f/\sigma'_{rf})$

(ii) the load test coefficient, defined as $K_f/K_c = \sigma'_{rf}/\sigma'_{rc}$

(i) Obliquity at peak shear stress (δ_f)

The ICP tests have shown that, for all but one case (the tension tests at Cowden), values of δ_f can be estimated with high precision from measurements made in ring shear interface tests which (a) simulate the displacement history of soil elements adjacent to a pile and (b) use interfaces with comparable properties to those of the pile. These tests showed that δ_f can vary from ≈8° to ≈30° for steel interfaces with a roughness typical of industrial piles. It is suggested that a reliable estimate of δ_f for any given pile design can only be obtained from a specific set of appropriate ring shear tests using the in-situ material. In the absence of this information, δ_f may be (cautiously) estimated from the correlation with clay plasticity shown on Figure D3 in Appendix D.

(ii) Load test coefficient (K_f/K_c)

The load test coefficient measured in first-time undrained load tests with the ICP, performed after equalisation, typically varied between ≈0.8 and ≈1.0. It is interesting that similar coefficients were measured during drained and undrained pile loading at Bothkennar.

Unfortunately, load test data from other instrumented pile tests were not of the same quality as the ICP tests and only approximate values of K_f/K_c are reported. These varied from 0.5 in Boston Blue clay (BBC) to 0.8 ± 0.1 in Haga clay and 1.0 in Gault and Huntspill clays. The very low values measured in BBC are not considered to be reliable (see Section B3.4, Appendix B).

These data suggest that a K_f/K_c value of 0.8 would provide a realistic lower bound value for design purposes and using Eqn. 7, the following expression for τ_f is obtained:

$$\tau_f = (K_f/K_c)\ K_c\ \sigma'_{v0} \tan \delta_f$$

$$\tau_f = 3.1\ \sigma'_{v0}\ OCR^{0.41}\ (h/R)^{-0.2}\ [0.53 - 0.16\ I_v^*]\ \tan \delta_f \qquad \text{Eqn. 8}$$

When estimating the total shaft capacity from Eqn. 8 ($Q_{shaft} = 2\pi R \int^L \tau_f dz$) the effects of progressive failure should be accounted for by adjusting values of δ_f at various levels along the shaft in accordance with their dependence on post-peak relative displacement assessed from ring shear interface tests. As (a) the ultimate residual angle (δ_{ult}) will operate over most of the shaft length of conventional pipe piles (see Section 10.4.2) and (b) σ'_r in the ICP tests generally remained constant or increased marginally post-peak, it is proposed that assuming $\delta_f = \delta_{ult}$ in Eqn. 8 will lead to a safe estimate of the local shaft frictions at pile failure.

11.6 IMPLICATIONS OF EFFECTIVE STRESS APPROACH FOR EXISTING DESIGN METHODS

Although the ICP tests have demonstrated clearly that the effective stresses acting on the pile shaft control shaft capacity, it is worthwhile to examine the correspondence between the effective stress expression (Eqn. 8) and the trends predicted by the two most popular design approaches for piles in clay: the α and β methods.

11.6.1 The α method

The shaft capacity of offshore displacement piles in clay are generally assessed using the API(1989) 'α method', described in Section 2.2. This method relates the ultimate shaft shear stress (τ_{av}) to the average UU triaxial shear strength of the clay (c_{u0}) by an adhesion factor α which is given by:

$$\alpha = 0.5\ (c_{u0}/\sigma'_{v0})^{-0.5} \qquad \text{for } c_{u0}/\sigma'_{v0} \le 1$$
$$= 0.5\ (c_{u0}/\sigma'_{v0})^{-0.25} \qquad \text{for } c_{u0}/\sigma'_{v0} > 1$$

Data reported by Ladd et al (1977) and Hight et al (1987) indicate that, for most clay soils, the undrained strength ratio for peak shear strengths measured in triaxial compression (c_{u0}/σ'_{v0}) may be approximated by the expression:

$$c_{u0}/\sigma'_{v0} = (0.3\pm0.05)\ OCR^{0.8\pm0.05} \qquad \text{Eqn. 9}$$

It should be noted that this type of relationship is not valid for materials, such as London clay[1], which fail in triaxial tests before critical state conditions are reached (due to the formation of shear bands). With this point in mind, the API expressions for α may be re-written using Eqn. 9 as:

$$\alpha \approx 0.91\ OCR^{-0.4} \qquad \text{for } OCR \le 4.5$$
$$\approx 0.68\ OCR^{-0.2} \qquad \text{for } OCR > 4.5 \qquad \text{Eqn. 10}$$

Using the same approximation for c_{u0}/σ'_{v0}, Eqn. 8 may be re-expressed as:

$$\tau_f = \alpha_L\ c_{u0} \qquad (\alpha_L \text{ is the local adhesion factor})$$

$$\tau_f \approx \{\ 10.3\ OCR^{-0.4}\ (h/R)^{-0.2}\ [0.53 - 0.16\ I_v^*]\ \tan\delta_f\ \}\ c_{u0} \qquad \text{Eqn. 11}$$

In a deposit where the OCR, δ_f & I_v^* values are constant, the *average local adhesion factor* developed along a pile shaft of length L is then given by:

$$(\alpha_L)_{av} = (1/L) \int^L (\tau_f/c_{u0})\ dz$$

$$\approx 12.9\ OCR^{-0.4}\ (L/R)^{-0.2}\ [0.53 - 0.16\ I_v^*]\ \tan\delta_f \qquad \text{Eqn. 12}$$

Values of α are usually backfigured from load tests by dividing the measured ultimate shaft shear stress by the average c_{u0} value along the pile length. In a soil deposit where c_{u0} increases linearly with depth[2] (and OCR, δ_f and I_v^* are constant), the value of α implied by Eqn. 11 is:

---

[1]The OCR implied by Eqn. 9 for the London clay at Canons Park is ≈10 (for 3m < z < 6m), whereas the corresponding OCR measured in high pressure oedometer tests and inferred from the geological history is ≈40.

[2]from zero at the surface.

$$\alpha = \tau_{av}/(c_{u0})_{av}$$

$$= [1/(L(c_{u0})_{av})] \int^{L} \tau_f \, dz$$

$$\approx 14.3 \, OCR^{-0.4} \, (L/R)^{-0.2} \, [0.53 - 0.16 \, I_v^*] \tan \delta_f \qquad \text{Eqn. 13}$$

Eqn. 13 predicts α values that are ≈10% higher than Eqn. 12. Although this difference is not very significant, it can be appreciated that with other types of c_{u0} profiles, the α values backfigured from load tests might bear little resemblance to the true average local α value, $(\alpha_L)_{av}$, mobilised along the pile shaft. However, most engineers (by necessity) need to assume that the values of α given by Eqn. 10 are *local* values as, in practice, the OCR varies significantly in most soil deposits.

The values of $(\alpha_L)_{av}$ predicted by Eqn. 12 for a typical offshore pile (L/R=75) with a δ_f value[1] of 25° are compared on Figure 11.7 with values of α recommended by API. The agreement between the predicted trend with OCR and the API recommendations is encouraging. It may be surmised from this comparison that the variation proposed by API is biased towards piles of moderate length in low OCR, sensitive materials and high OCR, insensitive materials.

By varying one of the parameters in Eqns. 12 and 13 (i.e. OCR, L/R, δ_f or I_v^*), it is evident that $(\alpha_L)_{av}$ and α reduce by a factor of:

- ≈3.3 for an increase in OCR from 1.5 to 30
- ≈2.6 for a reduction in δ from 25° (typical angle for a low plasticity clay) to 10° (for a high plasticity clay)
- ≈1.8 for an increase in I_v^* from 0.0 to +1.5 (i.e. a significant increase in clay sensitivity)
- ≈1.4 for an increase in L/R from 20 to 100

[1]Used for illustration purposes only; δ_f varied between 8° and 30° in the ICP tests alone.

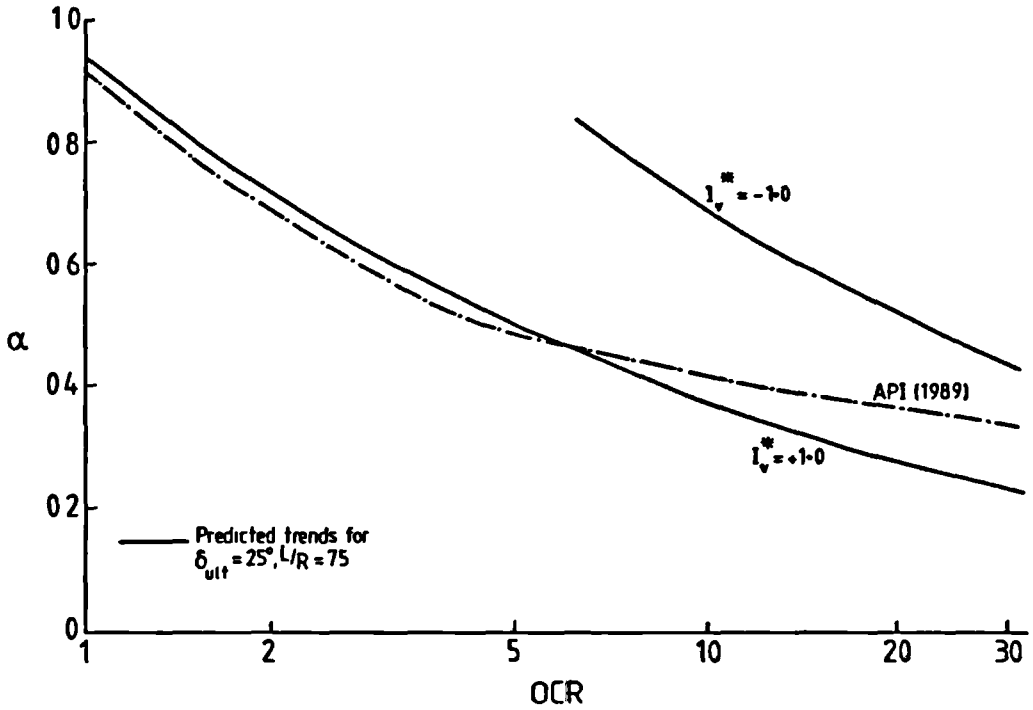

Figure 11.7 Comparison of predicted 'α v OCR' variation with API (1989) recommendations

As expected, good agreement between the α values measured in the ICP tests in Cowden till and Bothkennar clay is found using the appropriate parameters in Eqns. 12 & 13[1]. However, the α value mobilised in the ICP tests in the London clay is under-predicted by a factor of more than 2. This is primarily because the relationship assumed between c_{u0}/σ'_{v0} and OCR (Eqn. 9) is not valid for London clay. α values backfigured from pile tests in the materials such as London Clay will clearly be incompatible with those derived in other materials with a similar c_{u0}/σ'_{v0} value, thereby adding to the difficulties associated with using the α method for pile design.

In summary, although the dependence of α on OCR predicted by Eqns. 12 & 13 is in general agreement with the relationship between α and OCR

[1]Although a 'perfect' match is only obtained if the specific dependence of stresses on h/R measured at these sites is adopted.

deduced by API (Eqn. 10), it is evident that this relationship is not unique because of the predicted strong dependence of α on other factors such as the interface shearing characteristics of the materials, the clay sensitivity and the pile slenderness ratio (L/R). Further limitations of the α method are detailed in Section 2.2.

11.6.2 The β method

Although the α method is used most often for pile design in clays, the β method, described in Section 2.2.3, is often employed to check the design in lightly and moderately overconsolidated clays. Two of the more popular expressions for β are listed below:

$$\beta = \tau_{av}/(\sigma'_{v0})_{mean}$$

$$= (0.4 \pm 0.13)\ OCR^{0.5} \quad , \text{ for } \phi'_{cv} = 25° \qquad \text{(Meyerhof 1976)}$$

$$= (0.4 \pm 0.1)\ \frac{(L(m)+20)}{(2L(m)+20)}\ OCR^{0.5} \qquad \text{(Flaate \& Selnes 1977)}$$

Noting that average radius of the piles used in the data base of Flaate & Selnes[1] was ≈0.125m and slenderness ratios (L/R) ranged from 20 to 160, their expression for β may be re-written (approximately) as follows:

$$\beta \approx (0.58 \pm 0.14)\ OCR^{0.5}\ (L/R)^{(-0.15 \pm 0.03)}$$

In a material of constant OCR, I_v^* & δ_f and when σ'_{v0} increases linearly with depth, the average value of β implied by the expression derived for τ_f (i.e. Eqn. 8) is given by:

$$\beta = 4.3\ OCR^{0.41}\ (L/R)^{-0.2}\ [0.53 - 0.16\ I_v^*]\ \tan \delta_f \qquad \text{Eqn. 14}$$

I_v^* is typically between +1.2 and -0.8 in low OCR, sensitive materials and if δ_f varies between 20° and 25°, Eqn. 14 implies:

$$\beta = (0.65 \pm 0.08)\ OCR^{0.41}\ (L/R)^{-0.2}, \text{ or}$$

---

[1]Excluding about half of the piles in the data base which were tapered.

$$\beta = (0.29 \pm 0.08)\ OCR^{0.41}\ ,\quad \text{for } L/R \text{ between 50 and 100}$$

The similarity between these equations for β and those deduced empirically is quite striking and supports the general form of the expression for τ_f (Eqn. 8). However, as with the α method, predicted β values depend critically on δ_f, I_v^* and L/R as well as OCR.

11.7 CONCLUSIONS

A general expression for the local ultimate shaft shear stress (τ_f) that can be mobilised on *closed-ended* displacement piles in clay has been proposed which is based on the available data base of measurements of local effective stresses made in high quality instrumented pile tests. This expression is in general agreement with (a) the trends predicted by SPM/MIT-E3 analyses for pile installation and equalisation and (b) with general trends backfigured from the ultimate shaft capacities mobilised by displacement piles.

The α and β design methods are used most often to estimate the shaft capacities of displacement piles in clay. While the influence of OCR on capacities is acknowledged by these methods, it has become evident that their neglect of the following (very influential) parameters has contributed to their poor reliability (see Briaud & Tucker 1988):

(i) The coefficient of friction ($\mu = \tan \delta_f$); this coefficient can vary by at least a factor of 4 between clay types.

(ii) The clay sensitivity; if other parameters are held constant, a pile in insensitive clay may mobilise over twice the shaft friction of a pile in sensitive clay.

(iii) The pile slenderness ratio; the ICP tests have shown that because of the dependence of local stresses on h/R, the unit shaft capacity of a pile with L/R=20 can be almost twice that of a pile with L/R =100. The differences in the unit capacities will be even larger if the effects of progressive failure are not taken into account.

The proposed expression for τ_f takes these three factors into account and, in addition, allows the shaft capacities of piles installed in soil

deposits with non-uniform distributions of OCR (as is more common) to be evaluated.

Further instrumented pile test data are required to refine and extend the correlations developed in this Chapter. Specific aspects which need to be addressed include (i) the dependence of τ_f on L/R (given that the ICP tests showed a more pronounced dependence on h/R to other piles in the data base), (ii) the effect of the pile end condition (this Thesis considered closed-ended piles only) and (iii) the influence of the pile diameter (the maximum diameter in the data base was only 300mm)[1].

[1]Tests on large diameter instrumented piles, which were sponsored by BP International Ltd., are due to be published in June 1992.

CHAPTER 12

CONCLUSIONS

CONTENTS OF CHAPTER 12

CONCLUSIONS

12.0 OUTLINE 444

12.1 PRINCIPAL CHARACTERISTICS OF DISPLACEMENT PILES 444

12.1.1 Jacked pile installation 444

12.1.2 Equalisation 446

12.1.3 Load testing 448

12.2 PROPOSED DESIGN METHODS 450

12.3 THEORETICAL PREDICTIONS 451

12.4 SUGGESTIONS FOR FURTHER RESEARCH 453

12.0 OUTLINE

This Chapter provides a short summary of the main conclusions drawn in this Thesis.

There are four main sections. The first section lists the principal characteristics of closed-ended instrumented displacement piles, as shown by the tests reported or reviewed in this Thesis. This is followed by a summary of the (tentative) pile design methods that have been proposed and an outline of some of the shortcomings of existing design methods. Some views regarding the potential of theoretical approaches for piles in clay are given in third section, whilst suggestions for further research are offered in the final section.

12.1 PRINCIPAL CHARACTERISTICS OF DISPLACEMENT PILES

12.1.1 Jacked pile installation

Measurements made by piles, as they were jacked into the ground in a series of pushes (equivalent to the stroke of the jack), revealed the following characteristics:

1. The radial total stresses (σ_{ri}) and shear stresses (τ_{rz}) developed on the pile shaft (at fixed distances from the tip) follow a similar trend with depth to the CPT end resistance (q_c), the undrained shear strength (in clays) & the pressuremeter limit pressure (p_{lim}), and therefore reflect directly the initial consistency of the soil.

2. σ_{ri} and τ_{rz} values acting *at fixed depths* reduce as the pile penetrates to deeper levels i.e. they fall with distance from the pile tip (h). The rate of stress reduction diminishes as h increases.

3. In clays, radial total stresses are typically between two and five times the initial undisturbed horizontal stresses (σ_{h0}), but are comparable or less than σ_{h0} in loose and medium dense sands.

4. σ_{r1} can be described as a function of q_c and h/R, but this function varies with soil type. For clays, H_1 $[=(\sigma_{r1}-u_0)/\sigma'_{v0}]$ correlates well with apparent OCR and h/R.

5. The shaft shear stresses mobilised during installation are strongly dependent on the pile jacking rate in some materials (e.g. Cowden till and London clay), but only show a minor rate dependence in other materials (e.g. Labenne sand and Bothkennar clay). Ring shear interface tests may be used to assess the particular rate dependence of a given soil.

6. Pile installation in uniform fine to medium Labenne sand (at jacking rates $\leq$ 500mm/min) was essentially a drained process.

7. Excess pore pressures are developed in clay and persist for some time after installation. The pressures reduce at the beginning of a jacking stage and remain at low values until the completion of the pile push. These reductions are related to the (dilatant) characteristics of the partially equalised, pre-sheared soil.

8. The measured reduction in pore pressure during jacking in clays is strongly rate dependent and is larger than would be anticipated from the measured interface shear stresses. It has been suggested that pore pressures recorded at rates in excess of $\approx$1mm/min are not representative of those acting on the principal displacement shear, which may exist at a short distance from the shaft.

9. Pore pressures (in clays) generally increase to large positive values shortly after completion of a jacking stage, suggesting that steep pore pressure gradients exist between the pile surface and the surrounding soil mass during jacking. The slower increases in pressures observed in heavily overconsolidated clays may imply that more extensive volumes of soil experience negative shear induced pressures in these materials.

10. The excess pore pressure ratios recorded in between jacking stages ($\Delta u_s/\sigma'_{v0}$) in low OCR and sensitive clays show a similar dependence on OCR and h/R to the H_1 values; this trend is far less systematic in high OCR clays.

11. In ICP tests, radial effective stresses (σ'_r) on the principal displacement shear increased by ≈50% at the beginning of a jacking stage in both sands and clays; these stresses returned (approximately) to their initial pre-loading values on completion of the pile push.

12. In low OCR and sensitive clays, the radial effective stresses (σ'_r) existing immediately after installation are less than the initial undisturbed horizontal effective stresses (σ'_{h0}); in high OCR, insensitive clays, σ'_r is usually greater than σ'_{h0}.

13. In the ICP tests, the parameters H_1, $\Delta u_s/\sigma'_{v0}$ (in clays) and τ_{rz}, measured at fixed depths in the soil profile varied in inverse proportion to $(h/R)^{0.3\pm0.05}$. Other instrumented pile test data generally showed a milder dependence on h/R.

14. The specific 'h/R effect' depends on the soil type, pile type and installation method and may arise from a combination of (i) the strain paths imposed on the soil by monotonic pile installation (ii) the shearing cycles imposed by jacking or driving and (iii) arching effects.

12.1.2 Equalisation

After installation, the soil mass surrounding the pile equilibrates with its new environment. The measured characteristics of this process in sands and clays are summarised below.

Sands

1. Full equalisation (i.e. σ'_r remained constant with time) was attained in Labenne sand within just one minute of the completion of installation.

2. The equalised radial effective stresses (σ'_{rc}) developed on piles in sand can be described as functions of either (a) q_c and h/R, or (b) relative density, σ'_{v0} and h/R.

Clays

1. Pore pressures generally reach a maximum value shortly after installation and then reduce monotonically to ambient values. The pore pressure dissipation process can be modelled approximately using linear consolidation theory, assuming an average coefficient of consolidation (c_h) for the soil mass of between 0.3mm^2/s and 3.0mm^2/s. Dissipation is controlled by radial drainage over most of the pile shaft but, close to the tip, spherical drainage takes place and dissipation proceeds at a faster pace.

2. Radial total stresses generally reduce throughout equalisation and only attain a constant value (σ_{rc}) after all excess pore pressures have dissipated. The radial total stress relaxation coefficient, defined as: $[(\sigma_{rc}-u_0)/(\sigma_{ri}-u_0)]$, decreases with increasing clay sensitivity and reducing OCR and typically varies from between 0.2 and 0.8. This coefficient is independent of h/R.

3. The radial effective stresses (σ'_r) reach minimum values after installation (as pore pressures rise initially). These minima are more pronounced in high OCR, insensitive clays and lead to a short term minimum in pile capacity.

4. After reaching its (short term) minimum, σ'_r increases and attains a constant, fully equalised value (σ'_{rc}) when ≈85% of the excess pore pressures have dissipated. σ'_{rc} values in contractant clays are considerably larger than the σ'_r values existing immediately after installation and there is a strong positive set-up. σ'_r may, however, experience a net reduction in strongly dilatant clays.

5. $\sigma'_{rc}/\sigma'_{v0}$ ($=K_c$) depends most strongly on the apparent OCR, the relative depth of the pile tip (h/R) and the clay's sensitivity.

12.1.3 Load testing

Load testing of the ICP provided interesting data concerning the effects of the installation process and progressive failure on the shaft load - displacement characteristics. However, the most revealing data were obtained from the plots of the effective stress paths (τ_{rz} v σ'_r) followed by elements at the pile-soil interface during loading. These paths showed clearly that, in all cases, the peak local shear stress (τ_f) may be described by the simple Coulomb failure criterion : $\tau_f = \sigma'_{rf} \tan \delta_p$, where σ'_{rf} = radial effective stress at peak local shear stress and δ_p is the obliquity at peak shear stress (or interface friction angle).

The general characteristics shown by these 'stress paths' are summarised below. Pile loading in clays, apart from in one test at Bothkennar, was essentially undrained; the load tests in the Labenne sand were drained.

Clays

1. After equalisation, radial effective stresses *reduce* during 'first-time' undrained loading and at peak shear stress are typically 0.85 ±0.10 of the pre-loading σ'_r value (σ'_{rc}); a drained load test at Bothkennar gave comparable pre-peak reductions in σ'_r. Smaller reductions in σ'_r are measured in reload tests.

2. σ'_r increases during load tests performed at the very early stages of equalisation (as it did during installation jacking stages).

3. Post-peak, σ'_r remains relatively constant, or increases marginally. The obliquity [$\tan^{-1}(\tau/\sigma'_r)$] reduces from its maximum at peak local shear stress (δ_p) to an ultimate value (δ_{ult}) which may be up to 5° less than δ_p, depending on the pile installation rate, the loading history and the clay's composition.

4. δ values vary significantly with clay type; the δ_{ult} value for Bothkennar Clay was ≈30°, but only amounted to ≈8° in the London Clay.

5. The values of δ_p and δ_{ult} can be estimated with high precision from

measurements made in ring shear interface tests which (a) simulate the displacement history of soil elements adjacent to a pile and (b) use interfaces with comparable properties to those of the shaft.

Sands

1. In 'first-time' load tests at Labenne, σ'_r reduced over the early stages of loading; these reductions amounted to ≈20% of σ'_{rc} in tension tests but were only ≈5% of σ'_{rc} in equivalent compression tests. This trend is believed to reflect anisotropy in the soil fabric created by pile installation.

2. σ'_r started to rise just before the peak obliquity (τ/σ'_r) was mobilised and continued to increase until the maximum value of the peak local shear stress (τ_f) was attained. These increases were similar in tension and compression tests and could be related to dilation of the sand at the pile-soil interface.

3. Simplified analyses and a review of the available data showed that the increases in σ'_r during loading vary in inverse proportion to the pile radius and depend primarily on the initial relative density (D_r) and stress state of the sand. These studies suggested that the increases make a negligible contribution to the shaft capacities of full scale piles ($D \geq 500$mm), but have an over-riding influence on capacities that are mobilised by most laboratory model piles.

4. The obliquity at peak shear stress is comparable to the *constant volume* friction angle (δ_{cv}) measured in direct shear soil-interface tests, for interfaces with similar surface properties to those of the pile.

5. The ICP field tests and the laboratory interface tests have indicated that δ_{cv} is independent of the initial relative density of the sand. Laboratory studies have also shown that, for a given interface, δ_{cv} reduces significantly with the mean particle size of the sand (D_{50}).

12.2 PROPOSED DESIGN METHODS

Tentative design methods for evaluating the shaft capacity of closed-ended displacement piles in sand and clay have been proposed. These methods describe the shaft capacity in terms of the simple Coulomb effective stress failure criterion ($\tau_f = \sigma'_{rf} \tan \delta$) and were derived using the trends and data recorded in the ICP tests and previous (high quality) instrumented pile test programmes. The method established for piles in clay also incorporates trends identified from SPM/MIT-E3 analyses (see Section 12.3).

Expressions are suggested for the local shear stresses acting on displacement piles at failure (τ_f); these account for the influence of the installation, equalisation and loading processes on capacity and allow the dependence of the interface friction angles on the soil and pile type to be specified.

In particular,

- for clays, the value of τ_f/σ'_{v0} is expressed as a function of the apparent in-situ OCR, the relative depth of the pile tip (h/R), the interface friction angle and the clay's sensitivity.

- for sands, τ_f is expressed as function of the CPT end resistance (q_c), the relative depth of the pile tip (h/R) and the interface friction angle. Corrections to this τ_f value are proposed to account for the influence of the pile diameter, the stress level and the direction of pile loading.

A limited comparison of the shaft capacities predicted by these methods with measured capacities was very encouraging. This comparison also revealed notable shortcomings of existing pile design methods. For example, the API (1989) guidelines, which are commonly used to design displacement piles, ignore (implicitly) the influence of the following parameters which were shown by this (and other) research to have a controlling influence on shaft capacities:

- Important material parameters, including the interface shearing characteristics of all soils and the sensitivity of clays
- The dependence of equalised radial effective stresses in all soils on the relative depth of the pile tip (h/R)
- The influence (on unit shaft capacities) of the pile diameter in sands
- The effects of pile compressibility
- The direction of pile loading (i.e. compression or tension)

While API (1989) recommends interface friction angles for sands, the specified dependence on D_r and D_{50} is not compatible with the measurements made in the ICP tests at Labenne and laboratory interface shear studies.

Bond (1989), Azzouz et al (1990) and Karlsrud & Nadim (1990) have also proposed design methods based on measurements made in instrumented pile tests in clays. However, these were based on a more limited data set and did not account for all of the major influential factors identified in this research.

12.3 THEORETICAL PREDICTIONS

The Strain Path Method (SPM), used in conjunction with the MIT-E3 soil model, is the most promising theoretical method available for predicting displacement pile behaviour in clays. The Cavity Expansion Method has been found to be a poor model that gives unrealistic predictions for the main parameters of interest.

A parametric study of predictions made by SPM/MIT-E3 analyses showed that the method predicted many of the trends seen in the ICP tests and in other instrumented pile tests, although the absolute magnitudes of the stresses calculated were usually in error. Some of the more important of these *trends* include:

- A strong (and almost unique) dependence of the installation radial total stress ratio (H_1) on OCR.
- The generation of negative shear induced pore pressures during pile installation in dilatant clays.

- The dependence of radial stresses and pore pressures on the relative depth of the pile tip (h/R).
- The reduction in radial total stresses during equalisation.
- The tendency for radial effective stresses to reduce shortly after installation in dilatant materials.
- The influence of clay sensitivity and OCR on the magnitudes of the equalised radial effective stresses.
- The reduction in radial effective stresses during undrained pile loading after equalisation.

Notable limitations of the method include:

- Predictions depend significantly on the laboratory tests selected to derive input parameters. A review of the predictions made for the ICP tests at Bothkennar suggested that pile behaviour is modelled more accurately using the properties of the *partially* destructured[1], less sensitive, material rather than the properties of the undisturbed intact material.
- The radial total stress and pore pressure changes induced by installation are generally under-estimated. Consequently, the predictions for equalisation and load testing are also in error.
- The measured dependence of stresses on h/R is greatly under-predicted.
- Predictions for pile loading made assuming a simple shear continuum failure are not realistic after peak local shear stresses are mobilised. This appears to be primarily because interface slippage and residual sliding are not modelled by the MIT-E3 soil model.

It is considered that the method (in its present form) cannot be used with confidence to predict pile capacities in clay. The ICP tests have suggested that the deviation between predictions and measurements is partly because the method does not model particular aspects of real pile installation such as (a) pause periods (b) friction on the pile shaft and (c) load cycling. The method has been seen, however, to be a very useful

---

[1] i.e. consolidated under K_0 conditions to 1.5-2.0 σ'_{vy} (not remoulded or reconstituted).

tool for identifying and understanding the parameters that control the behaviour of displacement piles in clay.

No theoretical method has been proposed for displacement piles in sands.

12.4 SUGGESTIONS FOR FURTHER RESEARCH

The research has demonstrated that each test on a pile equipped with high quality instrumentation adds further insight into the basic mechanics of pile behaviour. Furthermore, it has been seen that the effective stress measurements obtained can allow rational design methods to be developed that reflect the underlying processes controlling pile capacities.

It is clear that any additional high quality instrumented pile test data will help to refine and consequently generalise the findings of this Thesis. The phrase 'high quality' should not, however, be taken lightly: even with robust and apparently reliable instrumentation, careful (and often painful) attention to detail is required to obtain data of an acceptable accuracy. It is also essential to the interpretation of test results that the soil properties at a test site are investigated thoroughly.

While there is almost infinite scope for further research with instrumented piles (at least for those piles which measure the effective stresses developed at the shaft and base), it is possible that tests which investigated the following aspects would reap the most rewards:

- the difference between small scale and large scale field piles at a given site; this will be possible in the near future as the results from large scale instrumented tests at Pentre and Tilbrook Grange (both in England) will be made public.
- the 'h/R effect'; this could be achieved by varying the length of the jacking stroke, duration of the pause period, pile diameter and pile surface roughness systematically. An investigation of this

type would (i) answer many of the questions raised in this Thesis concerning the factors affecting the reduction in stresses with h/R and (ii) provide data that may allow the Strain Path Method to be extended to model aspects of real pile installation in clays.

- the differences between closed-ended and open-ended displacement piles for a range of pile diameters and soil types. (Correlations developed in this Thesis apply only to closed-ended piles and are unlikely to be valid for open-ended, unplugged piles).

There is an acute shortage of effective stress data for piles in sand and consequently the existing design methods have a very poor reliability. It is vital that future instrumented pile programmes are performed in sands.

APPENDIX A

INSTRUMENT PERFORMANCE

CONTENTS OF APPENDIX A

INSTRUMENT PERFORMANCE

A1.0 GENERAL 458

A1.1 Measurement range 458

A1.2 Instrument drift 459

A2.0 PORE PRESSURE PROBES 460

A2.1 General 460

A2.2 Long term performance 461

A2.2.1 Background 461

A2.2.2 Performance at Cowden 462

A2.2.3 Performance at Bothkennar 463

A2.2.4 Conclusion 465

A2.3 Measurements at high pile velocities in clays 466

A2.3.1 Trends during installation in ICP tests 466

A2.3.2 Trends during load tests in ICP tests 467

A2.3.3 Measurements in other pile tests 471

A2.3.4 Conclusion 473

A2.4 Influence of filter stone 473

A3.0 SURFACE STRESS TRANSDUCERS 476

A3.1 General 476

A3.2 Shear stress measurements 476

A3.2.1 General trends 476

A3.2.2 Factors affecting the τ_{rz} and f_s data 478

A3.3 Elastic cell action effects 482

A1.0 GENERAL

The instruments on the ICP were designed originally for use in the stiff overconsolidated London Clay at Canons Park. This Appendix examines their performance in the three soil types investigated for this research programme, each of which differed considerably from the London Clay.

A1.1 Measurement range

Table A1 compares the maximum and average ranges measured for each instrument with its design calibration range and the measurements made at Canons Park.

Instrument	SST		ALC	PPU
Measurement	σ_r (kPa)	τ_{rz} (kPa)	P (kN)	u (kPa)
Design range	0-870	±262	±209	[-50 to +1500]
Maxima measured				
Canons Park	1000	120	125	[-100 to +500]
Labenne	110	50	100	30
Cowden	800	250	250	[-100 to +600]
Bothkennar	190	25	30	200
Average measurement during load tests				
Canons Park	550	100	30	[-100 to +100]
Labenne	50	30	25	15
Cowden	400	60	30	[-50 to +75]
Bothkennar	60	18	10	40

Table A1 Range of loads measured by instruments on the ICP

While the measurements made at Cowden and Canons Park approached the design limits of the instruments, those at Labenne and Bothkennar were considerably smaller. This did not affect the overall success of these experiments as the instruments were shown to have a good linearity characteristics; data of high resolution could be obtained with careful attention to detail and comprehensive calibration procedures[1].

The pore pressures probes had been designed to recover quickly from cavitation and were therefore suited ideally to use at Cowden, where negative pore pressures were measured. Pore pressures were generally positive at Labenne and at Bothkennar.

A1.2 Instrument drift

Drift in the zero readings of instruments, through creep and hysteresis, is a well known problem in soil instrumentation.

A complete summary of the drifts of all instrument zero readings from before pile installation to after pile extraction is provided in Tables A5-A10 at the end of this Appendix. The average overall drift associated with each instrument type is summarised in Table A2; these data provide an indication of the performance of the instruments and the reliability of the measurements.

Instrument	Labenne	Cowden	Bothkennar
Axial load cell (kN)	± 0.6	± 0.5	± 0.7
Pore pressure probe (kPa)	± 3.5	± 4.0	± 3.0
Radial stress sensor (kPa)	± 3.0	± 4.0	± 4.0
Shear stress sensor (kPa)	± 0.4	± 1.0	± 0.8

Table A2 Average zero drifts of instruments

[1]Each instrument was calibrated prior to each use on site and the calibration range adopted was varied to suit the range of measurements that were expected. However, in all cases (when instruments had not been damaged or over-stressed), calibration coefficients varied by less than 2% from one set of calibrations to the next.

A comparison between these drift values and the ranges of measurements summarised on Table A1, shows that they are well within acceptable limits. In a few individual cases, as noted in Tables A5-A10, unacceptable drifts did occur, but these could be tolerated because of the in built redundancy in both the instrumentation and pile test programmes.

It is not known if the drifts occurred uniformly with time, or were associated with particular events, such as pile installation or extraction, and judgements had to be made when applying drift corrections. The initial instrument zero readings were used for pile installation and equalisation (usually covering a period of 4 days) and a correction of half of the overall drift of each instrument was applied to the initial calibration zero for records made during load tests and pile extraction. In this way, it was hoped that the measurement error at any stage would be limited to about half of the overall drift value.

The signals from *all* instruments at Bothkennar experienced occasional and *identical* large shifts in their output voltages. These excursions occurred about every three hours and lasted for about one hour. The effect could not be reproduced in the laboratory and was considered to be due to problems associated with the earthing of the power supply on site. The problem could not be rectified, despite numerous efforts by IC technicians and electricians. Fortunately, the jumps were easily discernible from the records and could be corrected for. However, to be certain of their magnitudes, a 'dummy' instrument was connected into the measuring system for each test. This could be used to correct the signals for all the other instruments. The output from the temperature sensor in each SST provided a further check on the magnitudes of the signal jumps.

A2.0 PORE PRESSURE PROBES

A2.1 General

When the piles were stationary or moving at a slow rate (as in load tests), the pore pressure probes gave consistent and repeatable measurements of pore pressure. Pore pressures registered by the two probes in the same instrument cluster were in very good agreement with

each other and with equivalent measurements made on other piles. These pressures, coupled with the radial and shear stress measurements, led to consistent and realistic angles of interface friction (δ).

This section discusses two problematic aspects of the measurements, which became evident through extensive use of the probes:

(i) The tendency for measurements to become erratic after the probes were in the ground for a long period.
(ii) The 'unexpected' measurements obtained when the pile is moving quickly in clay soils.

A2.2 Long term performance of the pore pressure probes

A2.2.1 Background

The first set of ICP tests in the London Clay at Canons Park had shown that negative pore pressures were developed at the pile shaft during installation. The pore pressure probe was designed specifically to (a) cope with the measurement of these negative pressures and (b) be fast-acting to allow reliable records to be made when the pile is moving quickly.

The probe design (see Figure 4.2) uses:

- silicone oil as its saturation fluid; this fluid can recover quickly from cavitation (see Lunne et al 1986).
- a small internal volume, ensuring minimum compliance and a high response time.
- a very thorough saturation procedure in the laboratory with no loss of saturation between the laboratory and the field. (Inadequate saturation in a probe with such a small internal volume would be affect response times severely).

This design performed very well in short term tests at Canons Park. Despite measuring negative pore pressures during pile jacking (which probably caused cavitation of the silicone oil), rapid increases in pore pressure were observed at the completion of a jacking stage, indicating

that the probes remained 'alive'. However, the probes' signals exhibited large and random fluctuations 4 to 8 days after pile installation and the readings were deemed unreliable. This response initially gave cause for concern for the probe performance at Cowden and Bothkennar, where piles would be monitored over long periods.

Bond (1989) attributed the long term instabilities to the diffusion of small amounts of air/gas into the probes and identified three possible sources of air:

- If the silicone oil is not completely de-aired, the suctions measured during pile installation cause air to come out of solution.
- Even if the silicone oil is completely de-aired, vapour will form within the probe's cavity at high suctions. This may eventually be replaced by water/air.
- Galvanic cells involving the two steels (stainless & molybdenum) which make up the pile may be formed on the pile surface and generate gases.

Diffusion of air from the outside into the probe is an irreversible process which will continue until all the silicone oil has been replaced by air. When this happens, the measured pressure will start to increase as the air pressure equilibrates with that in the soil (Vaughan 1991).

A2.2.2 Long term probe performance at Cowden

Because of the problems experienced at Canons Park, it was decided to use ceramic filter stones in place of the 'standard' stainless steel discs in three of the six probes mounted on one of the piles installed during the first phase of tests at Cowden (i.e. pile CW2). The ceramic stones had an air 'blow-through pressure' six times higher than the

stainless steel discs[1] and were intended to slow down potential diffusion of air into the probes and hence improve their long term performance.

Pile CW2 was monitored for 3 months and the pore pressure variations for this period are shown on Figure A1. The individual performance of each probe in this test is described in Table A8 and is summarised below:

- Two of the six probes (P12C and P14) measured small (30kPa maximum) unexplainable jumps in pressure but recovered subsequently. (Permanent jumps of greater than 100kPa were often observed in the London Clay).
- The values of pore pressure recorded at the end of the monitoring period, when allowance is made for transducer related drift, were within 10kPa of the nominal hydrostatic values.
- There was no discernible difference between the long term performance of the probes with stainless steel discs and those with ceramic stones.

The subsequent response of the probes during the final load test on this pile (Test CW2/L3C) did not indicate any deterioration in their performance.

A2.2.3 Long term probe performance at Bothkennar

Pile BK2 was left in the ground for 32 days after its initial load test, which was performed 4 days after installation. As mentioned in Chapter 4, no records were obtained during most of this period as the logger was switched off by a power cut on site. The long term performance of the probes can, however, be assessed from the pore pressure records made when the site team returned to site to carry out the second load test on this pile.

---

[1]but were ≈600 times less permeable to silicone oil than the stainless steel discs. This was evident during saturation in the laboratory, where it was observed that the passage of 100ml of silicone oil through the ceramic stones under a pressure difference of 600kPa took ≈2 hours compared with ≈30 secs for a similar passage of oil under a pressure difference of 300kPa through the stainless steel discs.

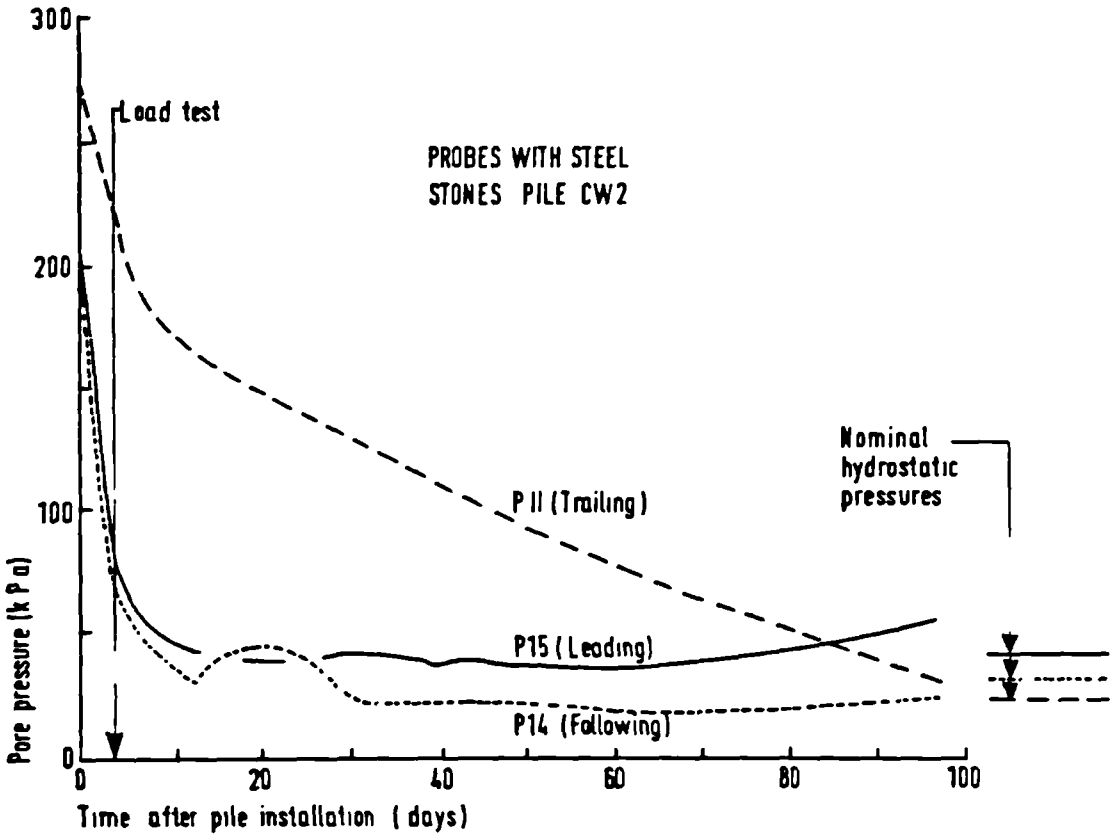

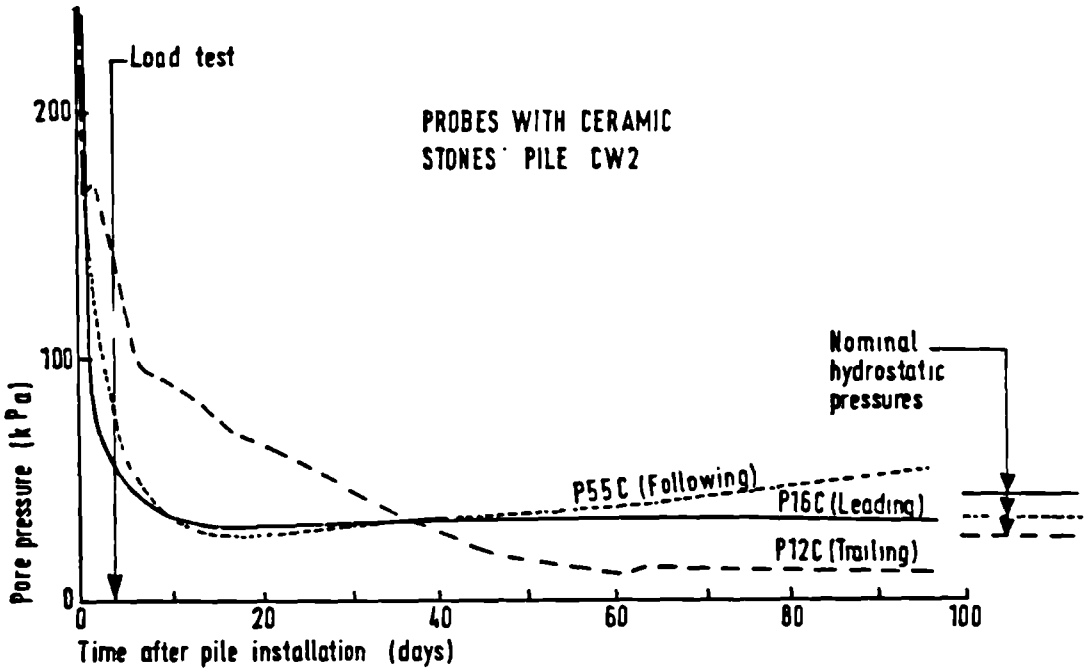

Figure A1 Long term monitoring of pore pressures at Cowden

Table A3 compares the pore pressure measurements made after 4 days (u_4) and 36 days (u_{36}) with the nominal hydrostatic pressures (u_0).

Probe	u_4 (kPa)	u_{36} (kPa)	u_{36}[1] (kPa)	u_0 (kPa
P16	63.4	53.3	53.0	45.8
P22	74.5	70.4	55.4	45.8
P51	51.1	38.4	38.8	33.6
P54	50.9	61.9	59.9	33.6
P13	35.2	37.9	33.3	21.8
P52	35.2	24.7	18.7	21.8

Table A3 Long term pore pressures at Bothkennar

Discounting the increase in pressure recorded by P54, it can be deduced that the average excess pore pressures reduced from ≈18kPa to ≈7kPa in the period from 4 days to 36 days. An excess pressure of ≈7kPa remaining after 36 days is consistent with the Bothkennar consolidation analyses performed by Whittle (1991) (see Appendix C), which predicted that full dissipation of excess pressures may take up to 100 days.

A2.2.4 Conclusion

The long term performance of the standard probe design at Cowden and Bothkennar was generally satisfactory and it was not necessary to use the 'large volume', de-airable probes that were required to measure long term pore pressures at Canons Park.

It is possible (but by no means certain) that the problems encountered at Canons Park were associated with the sulphate rich, acidic conditions at this site. These conditions are conducive to the formation of galvanic cells involving the two steels on the piles which may produce gases that diffuse into the probes. Di Biaggio (1977) also attributed the long term

[1]corrected for transducer related drift.

drift of pore pressure readings to the formation of galvanic cells between dissimilar metals. Diffusion of air into the probes may also have been accentuated by the large suctions measured during installation and load testing, which caused cavitation of the probe fluid. Pore pressures were higher at Cowden than at Canons Park and were always positive at Bothkennar.

A2.3 Measurements at high pile velocities in clays

This section examines the trends of the pore pressure measurements made at high pile velocities in the ICP tests and in other pile tests. Some conclusions are drawn in Section A2.3.4.

A2.3.1 Trends during installation in ICP tests

Compression load tests at Cowden and Bothkennar mobilised mean ultimate interface friction angles (δ_{ult}) at the location of the SST's of ≈20° and ≈30° respectively. If these δ_{ult} values also applied at the rates operating during installation, then the pore pressures implied by the installation radial and shear stress records are given by:

$$u = \sigma_{ri} - \tau_{rz}/\tan \delta_{ult}.$$

These 'expected' u values are listed in Table A4 and are seen to fall *between* the pressures measured during jacking (u_m) and those recorded when the pile was stationary in between jacking stages (u_s). It thus appears that a reduction in pore pressure must occur during jacking if the values of δ_{ult} at fast and slow rates of displacement are comparable. However, the magnitude of this reduction is too large to be consistent with the observed shaft resistance.

While the magnitudes of u_m values appear to be incompatible with the anticipated δ_{ult} angles, it is noteworthy that they reflect changes in the shaft resistance. At Cowden, for example, a reduction in the installation rate from 500mm/min to 80mm/min did not alter the radial total stresses, but caused a reduction of ≈40% in the shaft resistance and a corresponding increase in u_m of ≈40%. Subsequent slow tests performed

after full equalisation proved that the rate dependence is related to transient phenomena, such as changes in pore pressure, rather than permanent changes in the soil fabric (i.e. changes in δ_{ult}).

	z(m)	h/R	Expected pore pressure (kPa)	u_m (kPa)	u_s (kPa)
Cowden	3	5	126	0	375
	4	5	214	0	444
	5	5	225	0	431
	6	5	100	0	307
	3	30	110	95	260
	4	30	115	60	260
	5	30	200	100	300
	3.5	53	190	165	275
Bothkennar	3	5	106	93	134
	4	5	129	100	152
	5	5	150	109	171
	3	30	83	94	71
	4	30	102	84	113
	3	53	82	72	92

Table A4 Pore pressures during installation in ICP tests (jacking rate =500mm/min)

A2.3.2 Trends during load tests in ICP tests

The influence of rate on *post-peak* pore pressures was investigated in a specially designed experiment at Bothkennar, performed after completion of the second load test on pile BK2. The shear stresses (τ_{rz}) and pore pressures (u) measured in this test for a range of post-peak displacement rates are shown on Figure A2. Radial total stresses (σ_r) remained constant after the initial peak resistance was mobilised.

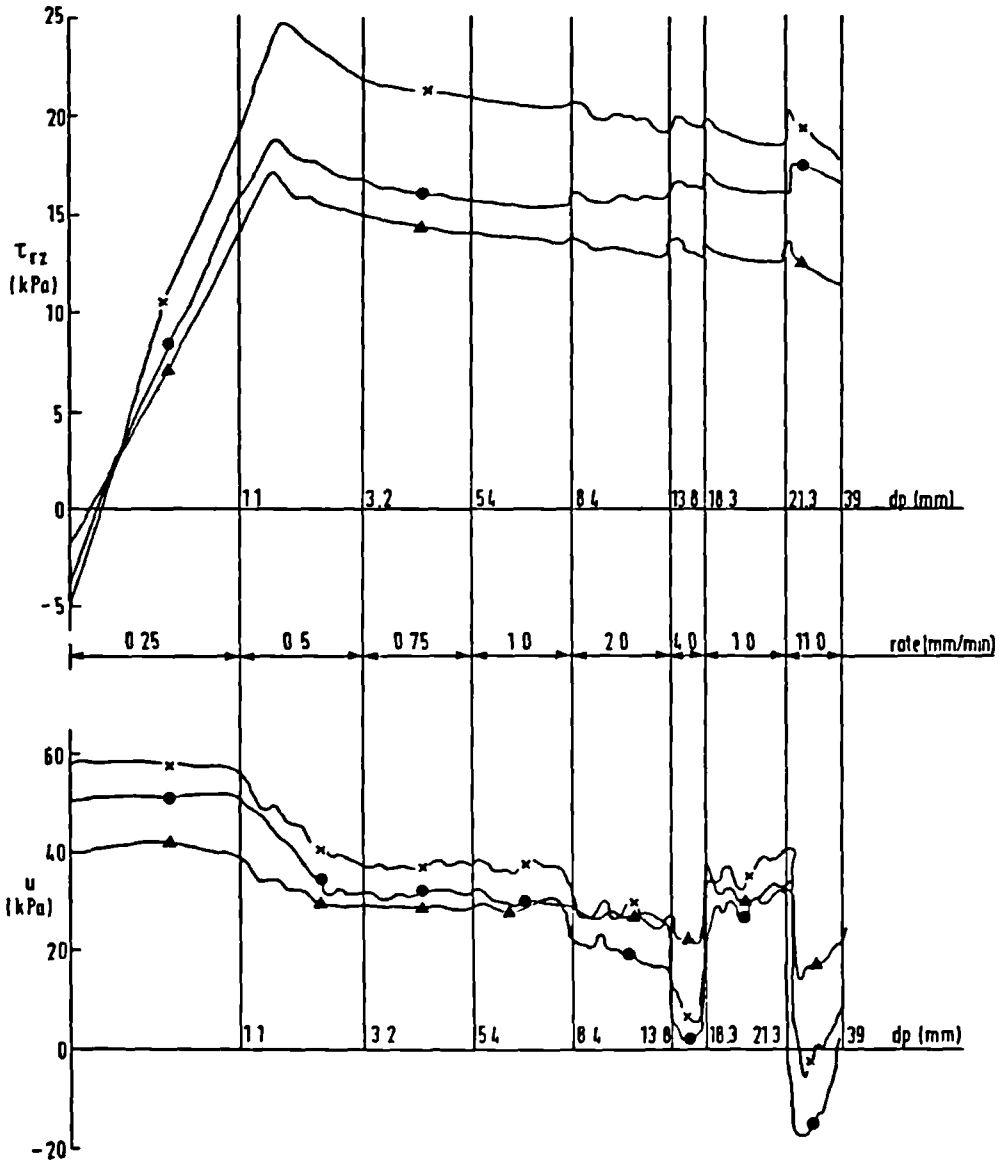

Figure A2 Data recorded during the 'rate experiment' at Bothkennar

Peak shear stresses increased by about 6% when the pile displacement rate was increased from 1mm/min to 11mm/min. This relatively small rate effect is comparable to that observed in ring shear tests over the same velocity intervals (see Figure 5.31). However, the pore pressure records show a more marked dependence on displacement rate. Lower pore pressures (or larger pressure reductions) are measured at faster displacement rates and it appears, from the data recorded during the repeat loading stage at

1mm/min, that there is a one-to-one relationship between the pore pressure and the pile velocity which is independent of the shearing resistance of the soil.

All 'undrained' load tests at Bothkennar showed large pore pressure reductions immediately after (brittle) failure, whilst the shear and radial total stresses remained almost constant. The observations summarised on Figure A2 suggest these reductions were related primarily to the rate at which the pile plunged. The reduction in pressure from that at peak to that after a further displacement of ≥4mm, referred to as Δu_{rate}, is plotted on Figure A3 against the post-peak pile displacement rate for all load tests performed at Bothkennar. Δu_{rate} is seen to amount to ≈60kPa at 20mm/min close to the pile tip (at h/R=5), whilst smaller values were measured further from the pile tip (h/R =30 and 53).

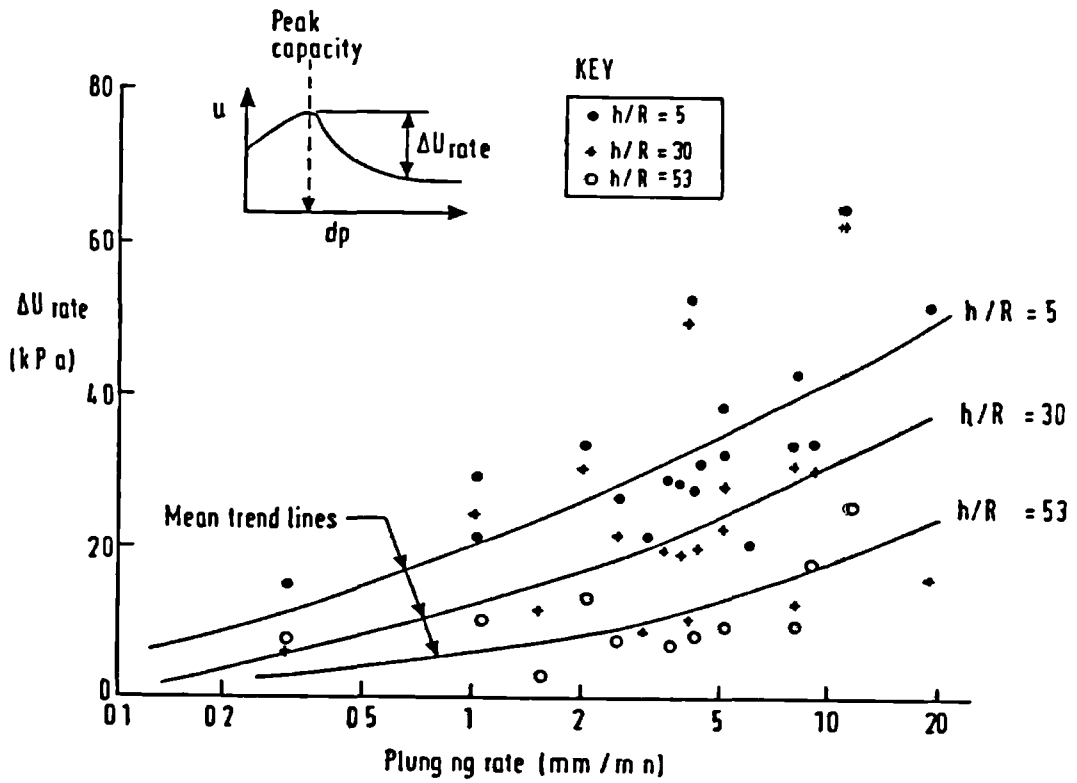

Figure A3 Rate dependence of pore pressure reductions in load tests at Bothkennar

The post-peak pore pressure reductions imply proportionate drops in the interface friction angles, δ [$= \tau_{rz}/(\sigma_r - u)$], as σ_r and τ_{rz} remain practically unchanged. This is demonstrated in Figure A4, where the values of δ_{ult} calculated at *all* instrument positions for the load tests (and during installation) at Bothkennar are plotted against pile displacement rate. It is evident that, at pile velocities in excess of ≈1mm/min, the apparent δ_{ult} value starts to fall below that measured during slow tests (≈30°) and tends to a relatively constant angle of ≈15° at velocities greater than ≈5mm/min.

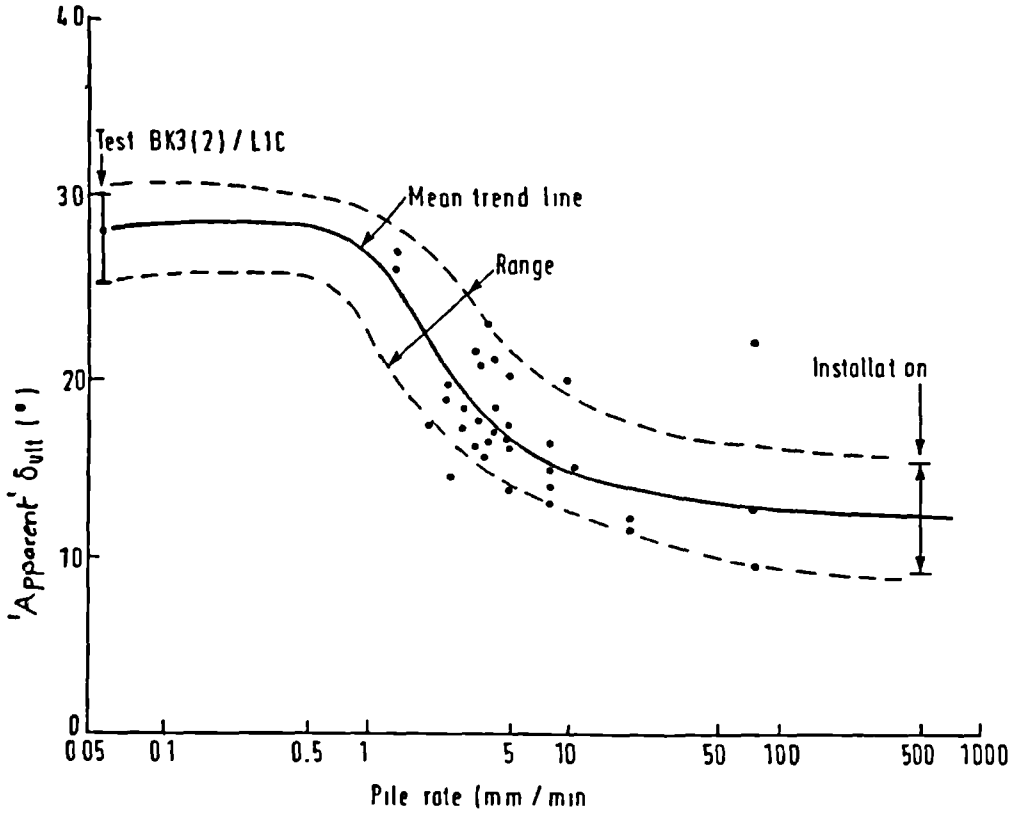

Figure A4 Apparent dependence of δ_{ult} on rate at Bothkennar

Large post-peak reductions in pore pressure were also observed in load tests at Cowden. These also led to a dependence of the calculated δ_{ult} values on pile rate, as shown on Figure A5. However, only a limited amount of data can be plotted as, in most cases, post-peak pore pressures were close to the cavitation pressure of the pore pressure fluid (i.e. below a suction of 50kPa) and therefore cannot be quoted with confidence.

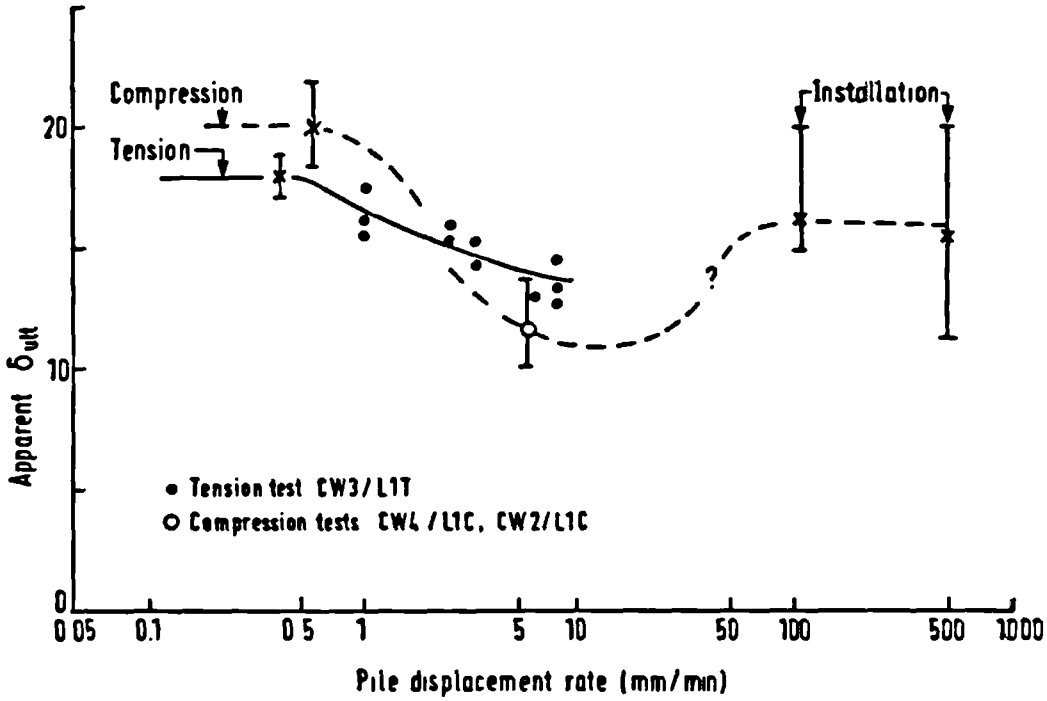

Figure A5 Apparent dependence of δ_{ult} on rate at Cowden

Data from pile reload tests reported in Chapters 7 & 8 indicate that the low δ_{ult} values measured at fast rates *are not associated with a low strength residual fabric* and are purely a consequence of the large rate dependence of the measured pore pressures. It has been concluded that the pore pressures recorded at fast rates are probably not representative of those acting on the principal displacement shear and the δ_{ult} values that they imply should not be accepted as true failure parameters for the pile-soil system.

A2.3.3 Measurements in other pile tests

Measurements made during fast shear in other instrumemted pile and penetrometer test programmes (see Appendix B) showed the following trends:

(i) Pore pressures decreased during fast shear in pile tests in the normally consolidated clays at Huntspill & Gt. Yarmouth and in the heavily overconsolidated clays at Madingley & Canons Park (Coop

1987, Bond 1989) and gave 'fast shear' δ_{ult} values which were less than those measured during slow shear. A smaller discrepancy between slow and fast δ_{ult} values was evident in the high OCR materials. This may have been because in these materials (a) the pore pressure reductions that would have occurred were restricted by the cavitation pressure of the probe fluid and (b) pore pressures are a smaller proportion of radial total stresses.

(ii) In pile experiments carried out in the normally consolidated soft clay at Harvey, Louisiana, Bogard & Matlock (1990) noted that:

"As one or more slip surfaces develop, dilation tends to occur with a very localized but marked reduction of pore pressure at the slip surface. After the end of plastic slip, the depressed pore pressures return to a value which is somewhat higher than the pre-slip pressure, generally in a period less than 5 minutes."

(iii) In experiments with the piezo-lateral stress (PLS) cell in lightly overconsolidated materials (see Section B5), it was observed that on completion of a jacking stroke during installation, pore pressures decreased monotonically in 'virgin ground' but increased initially in 'non-virgin' ground[1]. It was noted by Morrison (1984) that "even when the delay times for rod (addition) were small, the pore pressures during non-virgin penetration are always less than (equivalent) pressures measured during virgin penetration" ; these observations are discussed in more detail in Section 10.5.2.

(iv) Pore pressure sensors on standard piezocones are located on the cone or at the cone shoulder and these tests do not in general show a reduction in pressure at the beginning of each jacking stroke. The measurements with the PLS cell suggest that the pore pressure reductions noted during fast shear only occur in pre-sheared soil. (It should be noted that the vast majority of the soil adjacent to displacement piles is pre-sheared soil).

---

[1]Morrison defines 'non-virgin' ground as that which had been sheared by the pile in the previous jacking stroke.

A2.3.4 Conclusion

The foregoing observations have shown that at fast pile displacement rates, pore pressures reduce within the failure zone of both (initially) contractant and dilatant clays when these clays are in a pre-sheared, partially equalised condition. However, much of the pressure reductions recorded *at the pile shaft* occur with no corresponding change in radial total stress or shear stress and appear to increase in magnitude with increasing rate and stress level. These measurements lead to an unrealistic (although relatively consistent) dependence of δ_{ult} on pile rate.

It is evident that the anomalous pore pressures recorded at fast rates at Cowden and Bothkennar are not unique to these sites or to the instrumentation on the ICP and appear to be a feature of all measurements made by pore pressure sensors mounted on piles. Two possible hypotheses are proposed for the observed phenomenon:

(i) As the pile moves through the soil rapidly, irregularities on the pile surface may set up 'eddies' and un-uniform pore pressures in the 'stream flow' of soil past the pile. Such areas of low pressure near the probe positions are not representative of those acting on the principal displacement shear which may exist at a short distance from the pile.

(ii) Pore pressure is by definition a *static* concept and measurements made at fast rates of displacement in a material which is not free draining may not be appropriate for use with the principal of effective stress (Vaughan 1991).

It is clear that further research into the effective stresses developed on interfaces at fast rates of displacement is required.

A2.4 Influence of filter stone

For the reasons described in Section A2.2.2, ceramic filter stones were used in place of the standard stainless steel filters in three of the six probes mounted on pile CW2 at Cowden. This section briefly describes the

short term performance of these probes.

The records of P14 (stainless steel disc) and P55C (ceramic stone) during installation and load testing are shown on Figure A6.

It is evident that:

- During installation jacking stages (at 500mm/min), the pore pressures recorded by P55C are ≈200kPa higher than those recorded by P14. During the pause periods in between jacking (which were of at least 3 mins duration), the two probes register similar pressures.
- The pressures recorded by both probes during the load test are very similar. It can be seen, however, that as the pile failed and started plunging at a rate of about 2mm/min, the trace for P55C lags slightly behind that of P14.

A comparison of all the records from the two sets of probes suggested that the ceramic filters retarded the response time. This was probably because the saturation procedure adopted for these filters was not adequate to cope with their very low permeability to silicone oil (see Section A2.2.2)[1].

It is interesting that, in contrast to the pore pressures measured by the probes with stainless steel discs, pressures recorded by probes with ceramic stones (particularly those with noticeably poor response times) led to values of δ_{ult} during fast-jacking which were more comparable to the slow shear δ_{ult} value. It is possible that the low response time of these probes effectively averaged the rapidly fluctuating pressures close to the probe positions and, in so doing, recorded a more appropriate measure of pore pressure.

---

[1]The overall compliance of a probe containing even small amounts of undissolved air is increased considerably. Gibson's (1963) time lag theory shows that the response time of the probes is reduced at least 200 fold for 0.01% inclusion of air. (Note that, even if the filters were fully saturated, a longer response time for the ceramic filter is expected as some movement of the silicone oil must take place as the membrane of the transducer responds to a change in pressure).

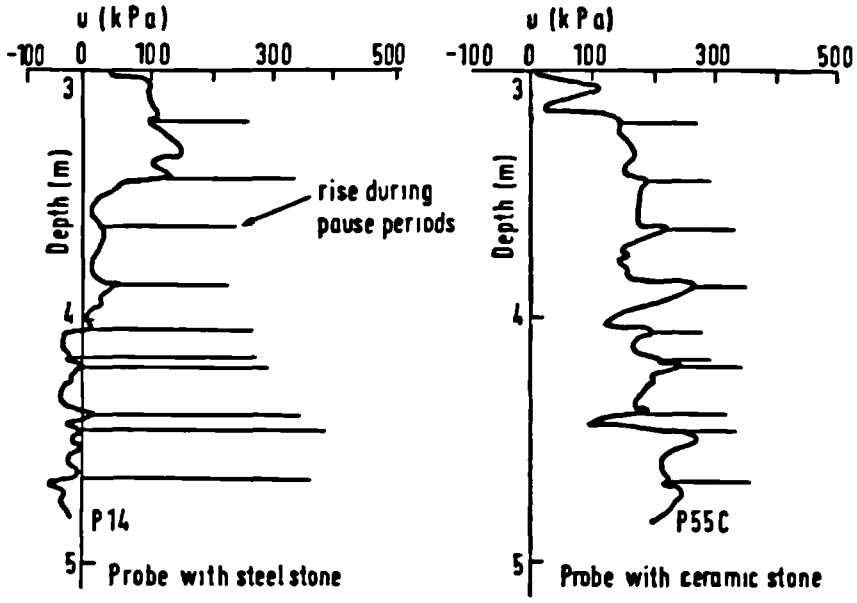

Installation CW2 : Following probes

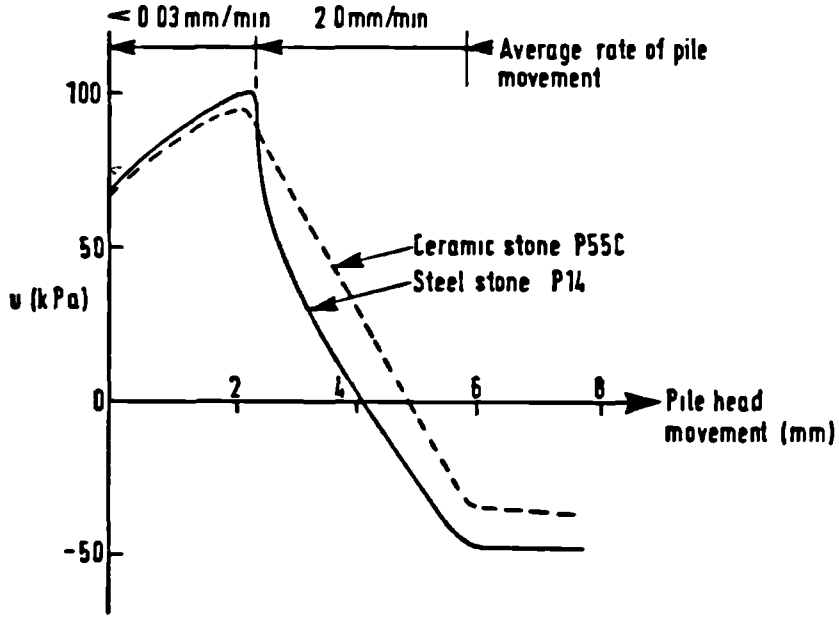

Load test CW2/LIC : Following probes

Figure A6 Pore pressures recorded during installation and load testing by probes with stainless steel and ceramic filters

A3.0 SURFACE STRESS TRANSDUCERS

A3.1 General

The surface stress transducers (SST's) performed entirely satisfactorily at all sites. Measurements were highly repeatable and in good agreement with data from other instrumented pile test programmes. Two specific problems are discussed in this Appendix:

- The discrepancy, noted in some instances, between the local shear stresses measured by the SST (τ_{rz}) and the shear stresses derived from the axial load cell data (f_s).
- The degree of under-registration of shear and radial stresses due to the compliance of the instrument.

A3.2 Shear stress measurements

A3.2.1 General trends

The shear stresses measured by the ICP can be checked by comparing the two independent sets of shear stress measurements i.e. those measured directly by the SST's (τ_{rz}) and those derived from the axial load cell data (f_s). The f_s data are considered more reliable because of the simplicity of the ALC design and the insensitivity of the f_s measurements to cell action effects (discussed in Section A3.3) or surface roughness variations.

Figure A7 compares the values of τ_{rz} and f_s recorded during installation of two piles at Cowden by plotting the ratio of the average of the values of τ_{rz} measured by adjacent instrument clusters to the values of f_s derived from the same clusters. The SST's are seen to apparently under-register shear stresses by between 15% and 30%. The degree of under-registration is virtually independent of pile depth but appears to be more pronounced at greater distances from the pile tip. In contrast, the f_s and τ_{rz} data sets were in very good agreement in the tests in London

and Bothkennar clays; τ_{rz} values measured during installation at Labenne were typically ≈12% less than those inferred from the f_s data.

The τ_{rz} and f_s data recorded during load tests at Cowden are compared in Figure A8. A similar degree of under-registration to that recorded during installation is evident in the compression load test (Test CW2/L2C), but the τ_{rz} and f_s variations are in good agreement in the tension test (Test CW3/L1T). At all other sites, the τ_{rz} and f_s variations during load tests were in excellent agreement. The data at Labenne did, however, exhibit a similar 'apparent' degree of under-registration of τ_{rz} to that measured during installation (≈12%) during the post-peak stages of load tests on piles that failed in a brittle manner.

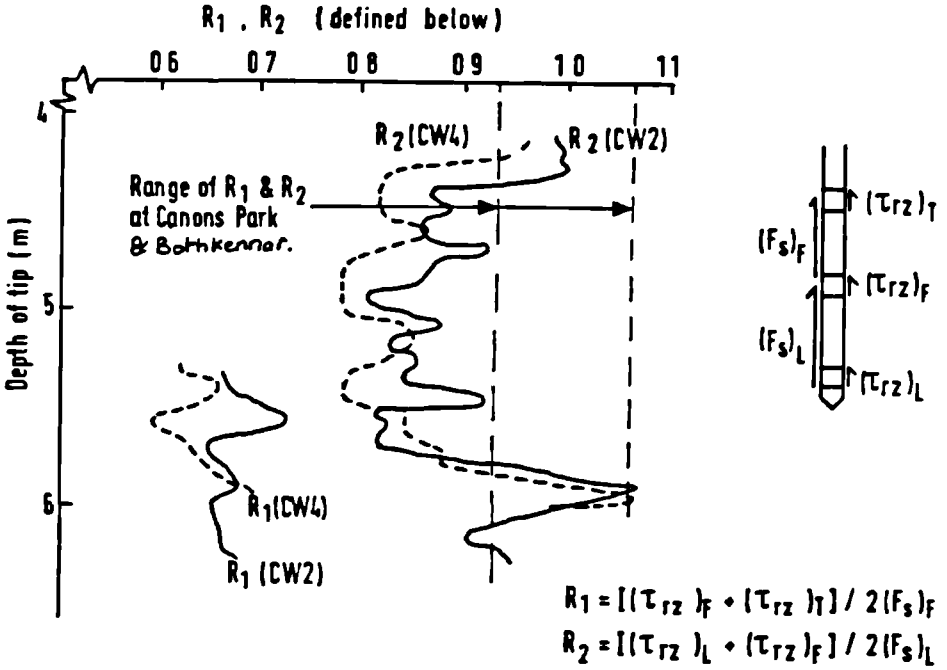

Figure A7 Comparison of installation τ_{rz} and f_s data at Cowden

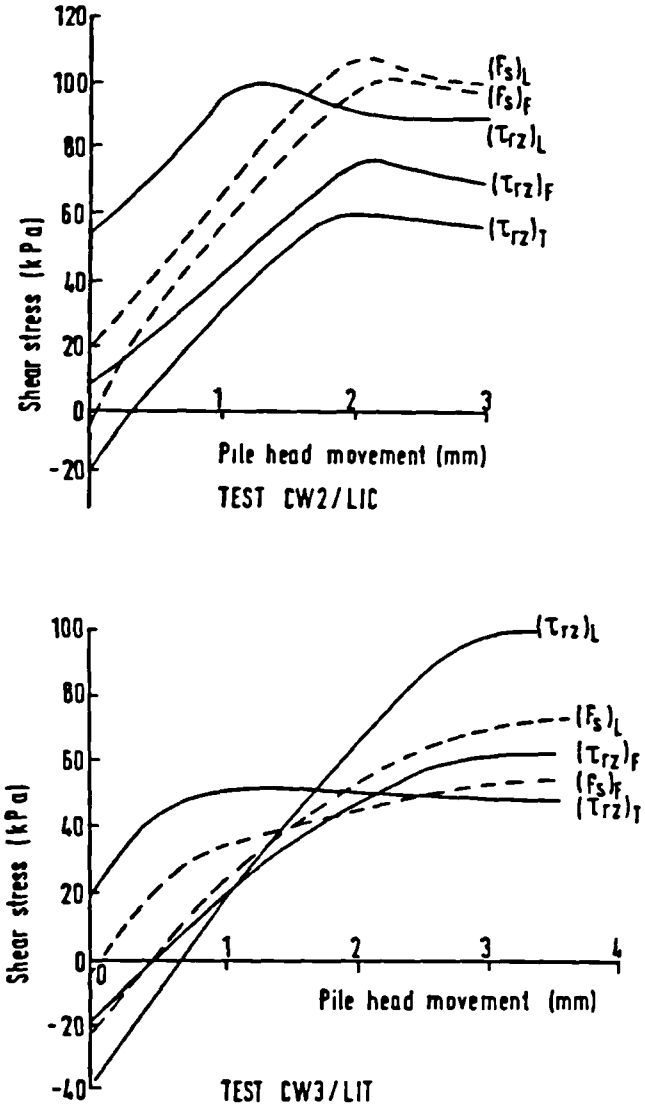

Figure A8 Typical τ_{rz} and f_s variations in load tests at Cowden

A3.2.2 <u>Factors affecting the τ_{rz} and f_s data</u>

Possible reasons for the discrepancies observed between τ_{rz} and f_s in compression loading at Cowden and at fast rates of displacement at Labenne include:

(i) <u>Errors in the assumed load transfer to the SST in the area of the rubber bonding surrounding its window pane</u>: A comparison of the two

calibration procedures used for radial stress (see Section 4.2.1) showed that the 'effective area' of the loading platen should include half the area of the rubber bonding surrounding the window pane (see Figure 4.4). However, it is possible that, as the rubber bonding is slightly recessed with respect to the window pane, more than half of the load in this area will be transmitted to the housing of the instrument. This would lead to a maximum under-prediction of the shear stresses and radial soil stresses of 7.2% and 6% respectively.

(ii) Elastic cell action effects: The compliance of the SST leads to under-registration of stresses; this effect will be more pronounced in stiff soils.

(iii) Un-measured erratic variations in radial effective stresses between instrument clusters: It is unlikely that these variations would lead to a consistent 'apparent' under-registration of τ_{rz}, but their effect should be borne in mind when examining the data.

(iv) Differences between the surface properties of the window panes of the SST's and the interconnecting casings: These differences may be such that the coefficient of friction for soil sheared against the SST's is less than that when sheared against the casings.

The combined effects of (i) and (ii) (see Section A3.3) do not provide a full explanation for the trends of the τ_{rz} and f_s measurements at Cowden, nor do they explain the compatibility of these data at Canons Park and Bothkennar. The influence of (iv) is examined below for each ICP site and is shown to be the most likely explanation for the observed phenomenon.

Cowden data

Figure A9 compares the effective stress paths (τ v σ'_r) measured using the τ_{rz} and f_s data during compression and tension tests at Cowden (see Section 7.4.4).

It is apparent that the maximum interface friction angle mobilised on the

window panes of the SST's in the compression test is ≈5° less than that mobilised on the remainder of the pile shaft. This angle (≈19°) is greater than the peak angle shown by both the τ_{rz} and f_s data in the tension test (≈18°), where these measurements were in good agreement (see Figure A8). It thus appears that the surface properties of the window panes of the SST's do not allow an interface friction angle of greater than ≈19° to be developed. For a pile tested in compression, this restriction leads to values of τ_{rz} that are about 25% less than equivalent f_s values.

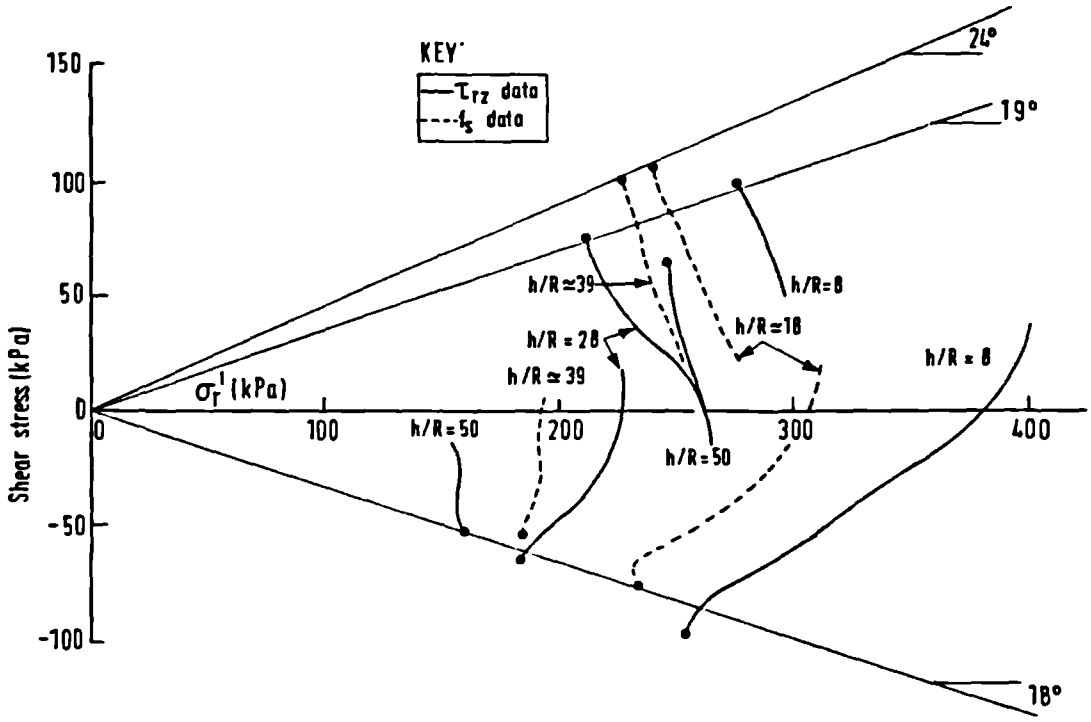

Figure A9 Typical effective stress paths followed during load tests at Cowden

The discrepancy between τ_{rz} and f_s values at Cowden was noted after the first phase of tests (piles CW1 and CW2). To investigate if the smoother surface finish of the SST's in these tests (centre line average (CLA) roughness 6 ± 1μm) had contributed to the discrepancy, the window panes of the SST's on piles CW3 and CW4, used in Phase 2, were shot blasted to a roughness comparable to that of the pile casings (CLA roughness ≈9μm).

However, as seen on Figure A7, provision of a more uniform overall pile roughness, did not improve the agreement between τ_{rz} and f_s during installation pile CW4.

Other factors, besides roughness, must therefore affect the interface shearing resistance. Bowden & Tabor (1967) showed that the hardness and texture can have a significant effect on metallic friction and Lemos (1986) demonstrated that this also applies to interface shear for low plasticity materials such as Cowden till and Labenne sand. The differences in hardness and surface texture of the stainless steel SST's and molybdenum steel casings may therefore offer a possible explanation for why higher interface friction angles could be mobilised on the casings. It should be noted that while the two steels may have a similar roughness, they will have different textures because of differences in their hardness values.

Bothkennar and London clay data

The agreement between the τ_{rz} and f_s records in the London and Bothkennar clays could be anticipated from ring shear interface tests with these materials, which showed that a steel interface with a roughness comparable to that of the ICP does not represent a plane of weakness and that the shearing plane was probably located within the soil at a short distance from the interface.

Labenne data

Discrepancies between the τ_{rz} and f_s measurements were only in evidence at Labenne during installation and plunging failures in load tests. Data obtained from ring shear tests on Labenne sand (Section 5.1.7) suggest that the 'dynamic' interface friction angle (at 500mm/min) may be up to 3° less than the 'static' angle (i.e. at rates less than ≈1mm/min). It is therefore possible that the different post-peak characteristics of the τ_{rz} and f_s data at fast rates of displacement may be related to differences between the static and dynamic frictional characteristics of the sand when sheared against the SST's and casings.

A3.3 Elastic cell action effects

To register a load, the loading platen/window pane of the SST must deflect by a finite amount and by so doing the earth pressure acting on the cell is reduced. This is a well known problem in the design of earth pressure cells for stiff soils, where a balance must be struck between the sensitivity and compliance of the instrument (Carder & Krawczyk 1975).

Approximate estimates of the cell action errors were derived using integrated forms of Mindlin's equations (Vaziri et al 1982) which assume that the soil is a homogeneous elastic half space[1]. The percentage under-registration of radial and shear stress ($\varepsilon_{\sigma r}$, ε_{τ}) predicted by this means can be shown to be:

$$\varepsilon_{\sigma r} \approx 100\ f_{\sigma r}\ G$$
$$\varepsilon_{\tau} \approx 52\ f_{\tau}\ G\ ,$$

where $f_{\sigma r}$ is the radial compliance of the SST = 2.3×10^{-8} m/kPa, f_{τ} is the shear compliance of the SST = 7.6×10^{-8} m/KPa and G is the shear stiffness (kPa).

This analysis indicates that the under-registration of the shear stress is likely to be almost double that applying to the radial stress. However, selecting appropriate values of G to evaluate the above expressions is difficult because soil stiffness depends strongly on the strain level, the stress history and the stress level, all of which are unknown.

Cell action effects will be most severe in stiff soils at small strains. The mean triaxial compression shear stiffness of the intact materials at a depth of 4.5m and an axial strain of 0.01% are listed below to provide an indication of the relative importance of under-registration at each site.

---

[1]The calculations were performed using the computer programme MINDLIN, which was written by the author. Full details of its assumptions are provided in OASYS (1988).

Site	G (MPa)
Labenne	60
Cowden	40
Canons Park	30
Bothkennar	12

When substituted into the above expressions for ε_{or} and ε_{τ}, these G values lead to very large predictions of under-registration. For example, the equations predict that at a strain of 0.01%, the shear stresses at Labenne are under-registered by ≈24%. However, a number of observations from the field tests suggest that such large under-registrations did not occur:

(i) The shear stresses that were measured by the SST's (τ_{rz}) at Canons Park and Bothkennar, both when the pile was stationary and during installation and load testing, are in close agreement with the average measurements derived from the axial load distribution (f_s), which is not affected by cell action effects.

(ii) Whilst the failure values of τ_{rz} were often less than equivalent f_s values at Cowden (and to a lesser extent at Labenne), the pre-failure changes in shear stress measured by the SST's during pile loading <u>and</u> unloading were in close agreement with the corresponding changes in shear stress measured by the axial load cells.

(iii) The discrepancy between τ_{rz} and f_s values measured at Cowden was similar during installation (when the stiffness is low) and during load testing after equalisation (when the stiffness is higher).

(iv) Measurements of radial stress during pile installation at Canons Park by Coop (1987) with an instrument, which was 20 times more compliant[1], and therefore more susceptible to under-registration than the SST, showed good agreement with the measurements made by the SST's (see Section B4, Appendix B).

(v) Under-registration should increase significantly with depth as stiffness increases. This was not apparent in any test.

While cell action effects should be borne in mind when examining data, it appears from the foregoing that these effects were not significant in the field tests with the ICP.

[1]As indicated by its optimisation factor, defined as the instrument compliance divided by the radius of the loading platen.

Instrument layout at Labenne

Cluster	Pile LB1	Pile LB2	h/R
Leading	SST4R	SST8R	8
	A44	A4	3
	P55, P56	P14, P15	5
Following	SST3R	SST2R	≈28
	A43	A3	≈32
	P13, P54	P53, P16	≈30
Trailing	SST2L	SST3L	50
	A42	A2	55
	P51, P52	P11, P12	53

Axial load cells at Labenne : Zero drifts (kN)

Instrument	Pile LB1	Pile LB2
A2	-	0.0
A3	-	-0.1
A4	-	+0.8
A42	+0.7	-
A43	+0.3	-
A44	-2.0	-

Surface stress transducers at Labenne : Zero drifts (kPa)

Instrument		Pile LB1	Pile LB2
SST2L	(comp circuit)	+2.0	-
	(shear circuit)	+0.0	-
SST2R	(comp circuit)	-	-3.5
	(shear circuit)	-	+1.0
SST3L	(comp circuit)	-	+5.0
	(shear circuit)	-	-0.5
SST3R	(comp circuit)	+0.2	-
	(shear circuit)	+0.1	-
SST4R	(comp circuit)	+0.5[1]	-
	(shear circuit)	-5.6[1]	-
SST8R	(comp circuit)	-	+7.0
	(shear circuit)	-	-0.3

1. This instrument suffered a leak through the rubber bonding surrounding the window pane which rendered one compression circuit unstable.

Table A5 Instrument layout and zero drifts at Labenne

Pore pressure probes (Labenne) : Approximate[1] zero drifts (kPa)

Instrument	Pile LB1	Pile LB2
P11	-	-5.0[2]
P12	-	+0.7
P13	-3.1	-
P14	-	-4.0[2]
P15	-	-8.4[2]
P16	-	+1.0
P51	-4.6[2]	-
P52	-10.0[2]	-
P53	-	+2.0[2]
P54	+2.3	-
P55	-0.5	-
P56	-3.0	-

1. Difference between zero in brass chamber prior to test and on pile after extraction.
2. These 'apparent' drifts appear to be related to an error in the assumed initial zero.

Instrument layout : Cowden

Cluster	Pile CW1	Pile CW2	Pile CW3	Pile CW4	h/R
Leading	SST8R	SST4R	SST8R	SST4R	8
	A4	A44	A4	A44	3
	P51,P56	P16,P15C	P13,P16	P51,P56	5
Following	SST2R	SST3R	SST2R	SST3R	≈28
	A3	A43	A3	A43	≈32
	P52,P54	P14,P55C	P14,P54	P16,P52	≈30
Trailing	SST3L	SST2L	SST3L	SST2L	50
	A2	A42	A2	A2	55
	P13,P53	P11,P12C	P11,P15	P53,P55C	53
Lagging	A42	A2	A42	A42	77

Table A6 Zero drifts of pore pressure probes at Labenne and instrument layout at Cowden

Axial load cells at Cowden : Zero drifts (kN)

Instrument	Pile CH1	Pile CH2	Pile CH3	Pile CH4
A2	+6.3[1]	-6.2	-0.7	+0.7
A3	+0.9	-	+0.4	-
A4	-0.2	-	-0.1	-
A42	+0.2	+1.2	-1.6	0.0
A43	-	+0.2	-	+0.2
A44	-	+0.4	-	-0.1

1. Caused by overload to 250kN (nominal capacity = 209kN)

Surface stress transducers at Cowden : Zero drifts (kPa)

Instrument		Pile CH1	Pile CH2	Pile CH3	Pile CH4
SST2L	(comp circuit)	-	-12.7	-	-2.0
	(shear circuit)	-	-1.0	-	+0.4
SST2R	(comp circuit)	+5.0	-	+8.6	-
	(shear circuit)	-1.8	-	+1.4	-
SST3L	(comp circuit)	-12.0	-	-4.6	-
	(shear circuit)	+0.6	-	-0.4	-
SST3R	(comp circuit)	-	-20.4[1]	-	-1.6
	(shear circuit)	-	-3.6	-	-0.2
SST4R	(comp circuit)	-	-0.4	-	+1.6
	(shear circuit)	-	-1.4	-	+1.5
SST8R	(comp circuit)	-1.3	-	+4.5	-
	(shear circuit)	-0.6	-	-1.6	-

1. This is the first test in which this instrument was used after it was fitted with a new Cambridge load cell.

Table A7 Instrument zero drifts at Cowden

Pore pressure probes at Cowden: Approximate[1] zero drifts (kPa)

Instrument	Pile CW1	Pile CW2	Pile CW3	Pile CW4
P11	-	-6.0	-6.0	-
P12	-	-98.0[2]	-	-
P13	NP[3]	-	+9.7	-
P14	-	-1.3	+4.3	-
P15	-	+17.5[4]	+5.2	-
P16	-	-0.9	-6.7	-1.4
P51	-0.1	-	-	-4.2
P52	NP	-	-	+1.7
P53	-0.3	-	-	-3.0
P54	NP	-	+3.8	-
P55	-	+16.0[4]	-	+4.8
P56	+0.7	-	-	-1.0

1. Difference in zero between zero in brass chamber prior to test and zero on pile after extraction
2. This value is adjudged to be erroneous as the probe was measuring reasonable values of pore pressure immediately prior to extraction.
3. No probe readings due to faulty plug connections.
4. See below

Long term performance of probes at Cowden : Pile CW2

Probe	Type/position	Performance
P11	Stainless steel (Trailing)	Very slow reduction in pore pressure with time and slow response during installation and load testing- probable cause: inadequate saturation in the laboratory.
P12	Ceramic (Trailing)	30-50kPa jump in signal 1 day after installation, but recovered subsequently.
P14	Stainless steel (Following)	20kPa jump in signal 12-20days after installation, recovered subsequently.
P55	Ceramic (Following)	Slow positive drift upwards after 20 days. Total drift of ≈20kPa is transducer related.
P15	Stainless steel (Leading)	Erratic jumps in signal throughout entire period; possible cause: faulty plug connection.
P16	Ceramic (leading)	No unusual behaviour

Table A8 Pore pressure probe performance at Cowden

Instrument layout at Bothkennar

Cluster	Pile BK1	Pile BK2	Pile BK3	Pile BK4	h/R
Leading	SST8R	SST4R	SST8R	SST4R	8
	A4	A44	A4	A44	3
	P14,P21	P16,P22	P14,P54	P16,P21	5
Following	SST2R	SST3R	SST2R	SST3R	≈28
	A3	A43	A3	A43	≈32
	P13,P15	P51,P54	P52,P56	P11,P15	≈30
Trailing	SST3L	SST2L	SST3L	SST2L	50
	A2	A2	A2	A2	55
	P11,P56	P13,P52	P13,P16	P22,P51	53
Lagging	A42	A42	A42	A42	77

Axial load cells at Bothkennar: Zero drifts (kN)

Instrument	Pile BK1	Pile BK2	Pile BK3	Pile BK4
A2	+1.2	+0.1	+0.1	-0.3
A3	NM[1]	-	-0.0	-
A4	NM	-	+1.3	-
A42	+0.4	+2.6[2]	+0.7	+0.5
A43	-	+0.8	-	-0.5
A44	-	+0.5	-	0.0

1. Not measured (no final zero readings obtained due to pile leak).
2. This drift could be corrected for noticeable (but unexplainable jump) in signal.

Table A9 Instrument layout and axial load cell zero drifts at Bothkennar

Surface stress transducers at Bothkennar: Zero drifts (kPa)

Instrument		Pile BK1	Pile BK2	Pile BK3	Pile BK4
SST2L	(comp circuit)	-	NM[1]	-	+6.0[2]
	(shear circuit)	-	-0.5	-	-1.5
SST2R	(comp circuit)	+8.0[2]	-	+0.8	-
	(shear circuit)	-1.3	-	-0.5	-
SST3L	(comp circuit)	+2.7	-	-1.2	-
	(shear circuit)	NM	-	-0.7	-
SST3R	(comp circuit)	-	+0.3	-	-6.0[2]
	(shear circuit)	-	+0.9	-	-0.3
SST4R	(comp circuit)	-	+6.0[2]	-	-2.0
	(shear circuit)	-	-0.5	-	+0.0
SST8R	(comp circuit)	NM	-	+5.2[2]	-
	(shear circuit)	NM	-	-1.5	-

1. Not measured (no final zero readings obtained due to pile leak).
2. Drifts of σ_r in range [5-8]kPa but no discernible jump in signals. For these instruments, σ_r can only be considered accurate to ≈5kPa.

Pore pressure probes at Bothkennar: Approximate[1] zero drifts (kPa)

Instrument	Pile BK1	Pile BK2	Pile BK3	Pile BK4
P11	-1.9	-	-	-2.5
P13	-0.9	-4.6	+0.6	-
P14	NM[2]	-	+1.3	-
P15	+1.5	-	-	+4.9
P16	-	+0.3	+0.8	-4.0
P21	NM	-	-	+7.0
P22	-	+15.0	-	+3.4
P51	-	-0.4	-	-1.1
P52	-	+6.0	-3.8	-
P54	-	+2.0	-4.2	-
P56[3]	-6.2	-	-22.2	-

1. Difference between zero in brass chamber prior to test and on pile after extraction.
2. Not measured (no final zero readings obtained due to pile leak).
3. Possibly developed after end of tests as probe gave sensible readings in field.

Table A10 Instrument zero drifts at Bothkennar

APPENDIX B

INSTRUMENTED DISPLACEMENT PILES IN CLAY

CONTENTS OF APPENDIX B

INSTRUMENTED DISPLACEMENT PILE TESTS IN CLAY

B1.0 INTRODUCTION 494

B2.0 EXPERIMENTS BY BOND (1989) 494

- B2.1 Soil conditions 494
- B2.2 Installation 497
- B2.3 Equalisation 498
- B2.4 Load testing 498
- B2.5 Trial pit investigations 501
- B2.6 Quality of data 502

B3.0 EXPERIMENTS WITH THE PIEZO-LATERAL STRESS CELL 503

- B3.1 Instrumentation 503
- B3.2 Soil profiles 503
- B3.3 Installation and equalisation 504
- B3.4 Load testing 506

B4.0 EXPERIMENTS BY COOP (1987) 507

- B4.1 Operation and instrumentation 508
- B4.2 Installation 510
- B4.3 Equalisation 512
- B4.4 Load testing 512

B5.0 EXPERIMENTS BY NGI 515

- B5.1 Site properties 515
- B5.2 Instrumentation 515
- B5.3 Installation and equalisation 517
- B5.4 Load testing 517
- B5.5 Trial pit investigations 518

B6.0 FIELD TESTS AT ST-ALBAN 518

- B6.1 Instrumentation 518
- B6.2 Installation 519
- B6.3 Equalisation 521
- B6.4 Load testing 522
- B6.5 Trial pit investigations 522

B7.0 EXPERIMENTS IN TOKYO CLAY 523

B8.0 EXPERIMENTS BY BOGARD & MATLOCK (1990) 523

B9.0 EXPERIMENTS AT COWDEN 525

B10.0 LABORATORY TESTS BY FRANCESCON (1983) 525

B11.0 OTHER PILE TESTS 526

B1.0 INTRODUCTION

This Appendix reviews the relatively small number of previous test programmes that successfully obtained measurements of the effective stresses developed on the shafts of displacement piles in clay. These programmes are listed in Tables 2.3 & 2.4 in Chapter 2.

The following aspects of each test series are presented. (Greater detail is provided for tests where high quality data was obtained; see Table 2.3).

- the soil profile at each site
- the instruments employed
- the trends observed during pile installation, equalisation and load testing

All measurements are summarised on Tables B5-B16 (at the end of this Appendix) in terms of the normalised parameters defined in Section 2.1, Chapter 2. This data base is compared with measurements made with the ICP at Cowden and Bothkennar in Chapter 11.

B2.0 EXPERIMENTS BY BOND (1989)

Bond (1989) performed five tests with the Imperial College Instrumented Pile (ICP) in the London Clay at Canons Park, North London. The piles were installed to a depth of ≈6m and similar installation and load testing procedures to those described in Chapter 4 were adopted. These tests are also reported by Bond & Jardine (1990, 1991).

B2.1 Soil conditions

The London clay is an aged stiff fissured silty clay that was deposited around 40 million years ago. A review of the geology of the Canons Park area suggested that the clay had been mechanically overconsolidated by the erosion of between 75 and 150m of overlying material.

The site has been investigated thoroughly using a large variety of in-situ and laboratory tests. These investigations allowed the soil profile

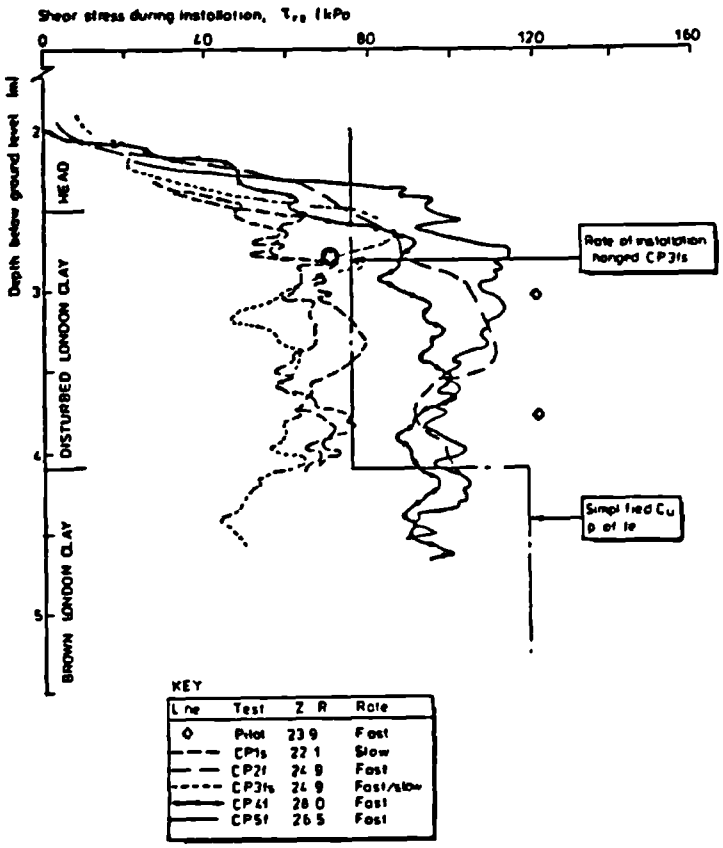

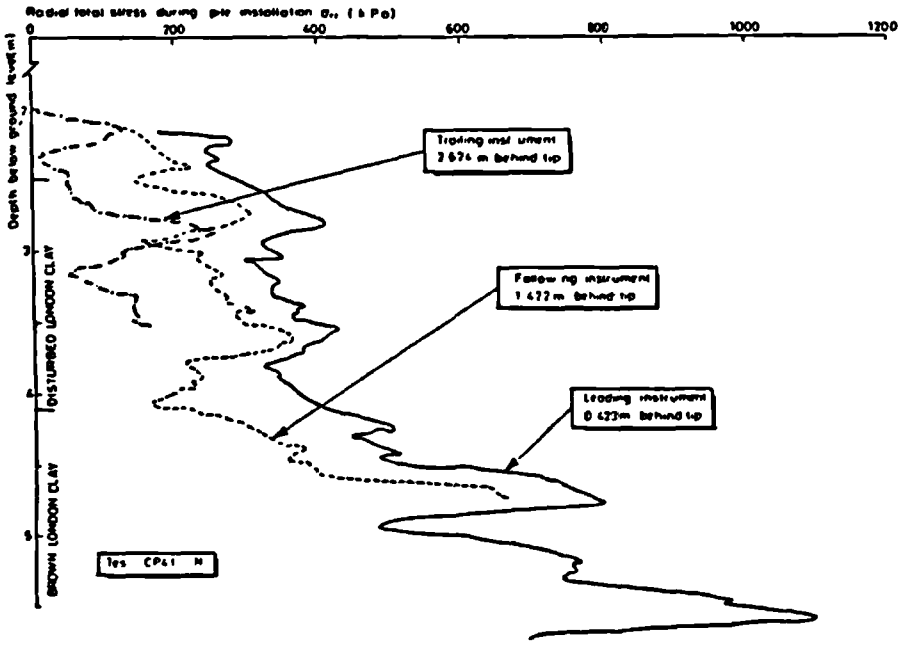

Figure B1 Installation radial (total) and shear stresses in London clay

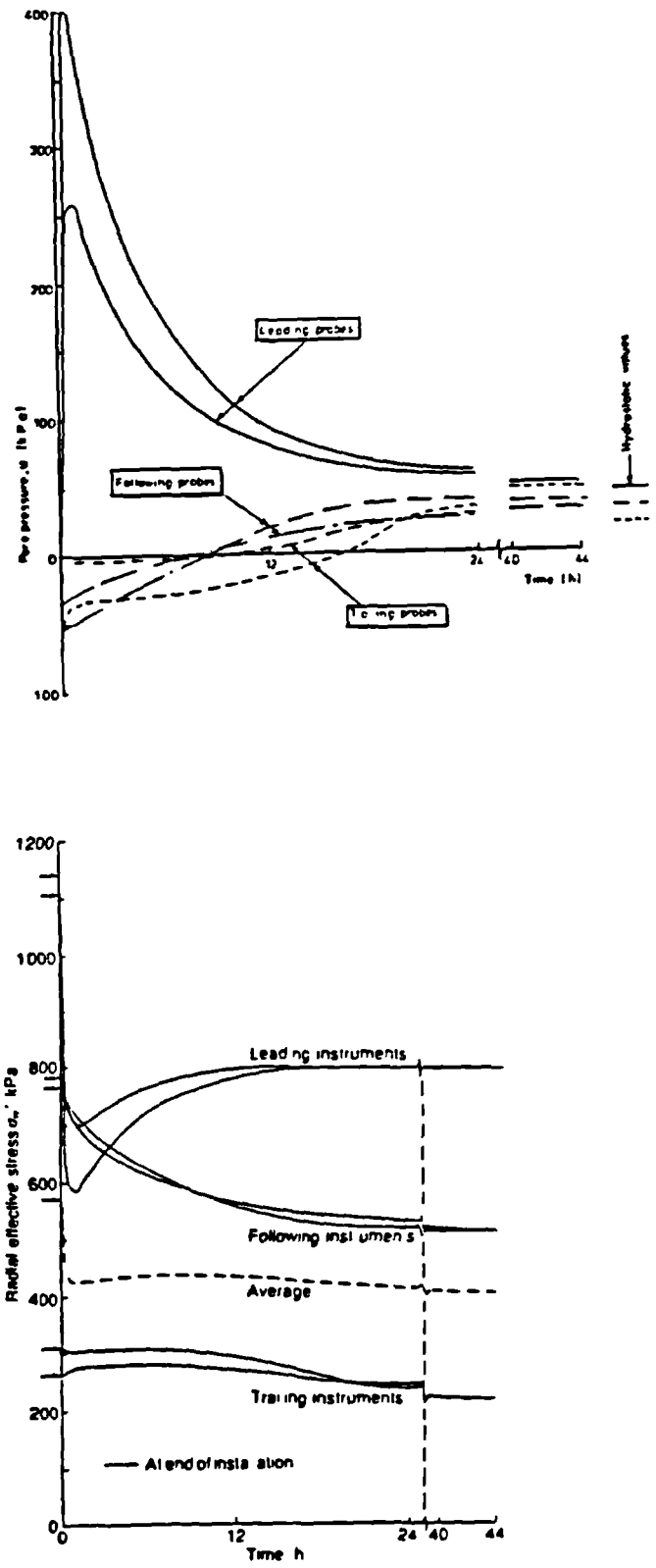

Figure B2 Equalisation data in London Clay

within the depths penetrated by the ICP to be established with reasonable precision (see Table B5). Two main points regarding the mechanical properties of intact London clay are worthy of note:

- Under triaxial conditions, intact samples fail before reaching critical state conditions (ϕ'_{cv} ≈22.5°). This is believed to result from shear band formation involving softening through both water content changes and fabric re-orientation.
- London clay has a 'sliding tending towards transitional' mode of shearing in direct shear (at large relative displacements). In this shearing mode, clay particles align in the direction of shearing and form a low strength residual surface.

B2.2 Installation

Examples of the radial and shear stresses (σ_{rf} & τ_{rz}) recorded during installation at Canons Park are shown on Figure B1. The complete set of installation data showed the following trends:

- Radial stresses increased with depth and depended on the consistency of the strata through which the pile was installed. In addition, stresses recorded in a given soil horizon reduced with the distance from the pile tip (h/R). For example, σ_{rf} recorded at depth of 3.5m by the trailing instrument (located at h/R ≈50) was only ≈40% of that recorded at the same depth by the leading instrument (located at h/R=8). All measurements fell between the pressuremeter limit pressure (p_{lim}) and the initial undisturbed horizontal stress (σ_{h0}).
- Shear stresses (τ_{rz}) did not reflect the stronger consistency of the brown London Clay, but showed a pronounced dependence on the pile rate; τ_{rz} values recorded at ≈80mm/min were ≈40% less than those recorded at the 'standard' rate of 500mm/min.
- Although not apparent from Figure B1, which only shows τ_{rz} records at one instrument position, τ_{rz} values reduced with distance from the pile tip (h/R). The reduction was not, however, as pronounced as that seen for the σ_{rf} records: τ_{rz} values at h/R=50 were typically ≈70% of those recorded at h/R=8.

- *Negative* pore pressures were measured at all instrument positions during pile jacking, suggesting that the clay adjacent to the shaft dilates strongly during shear. Pressures increased to small positive values on the completion of a jacking stage.
- The interface friction angle, δ, [$=\tan^{-1}(\tau_{rz}/\sigma'_{r1})$] mobilised during installation was typically $\approx 8°$, but in some cases was only $\approx 5°$.

B2.3 Equalisation

The main features of the data recorded during pile equalisation are summarised on Figure B2. It is noted that:

- Pore pressures rose sharply after installation at the leading instrument position and reached a maximum within 30 mins. Higher pressures were recorded by probes that required less time to attain this maximum. Consequently, much smaller pore pressure maxima were observed at the following and trailing instrument positions as these took between 2 and 20 hours to be realised.
- Pore pressures decreased, subsequently and, in all cases, were within 15kPa of nominal hydrostatic pressures in less than 1 day.
- Radial total stresses reduced by about 20% during equalisation at the leading and following instrument positions, but increased by a similar amount at the trailing instrument position (which was located in the disturbed London Clay; see Table B5)
- The pore pressure response measured at the leading instrument position caused an apparent *short term minimum* in its σ'_r value. At other instrument positions, σ'_r reduced throughout equalisation.

B2.4 Load testing

Piles were loaded to failure in $\approx$ 2 hours. Examples of the variations with pile head displacement (d_p) of the shear stress (τ_{rz}), pore pressure (u) and radial stress (σ_r) for a fast-jacked pile (rate =500mm/min) and a slow-jacked pile (rate =80mm/min) are shown on Figure B3. The general trends observed in all load tests were:

- Pre-peak, relatively minor changes in both σ_r and u were recorded.

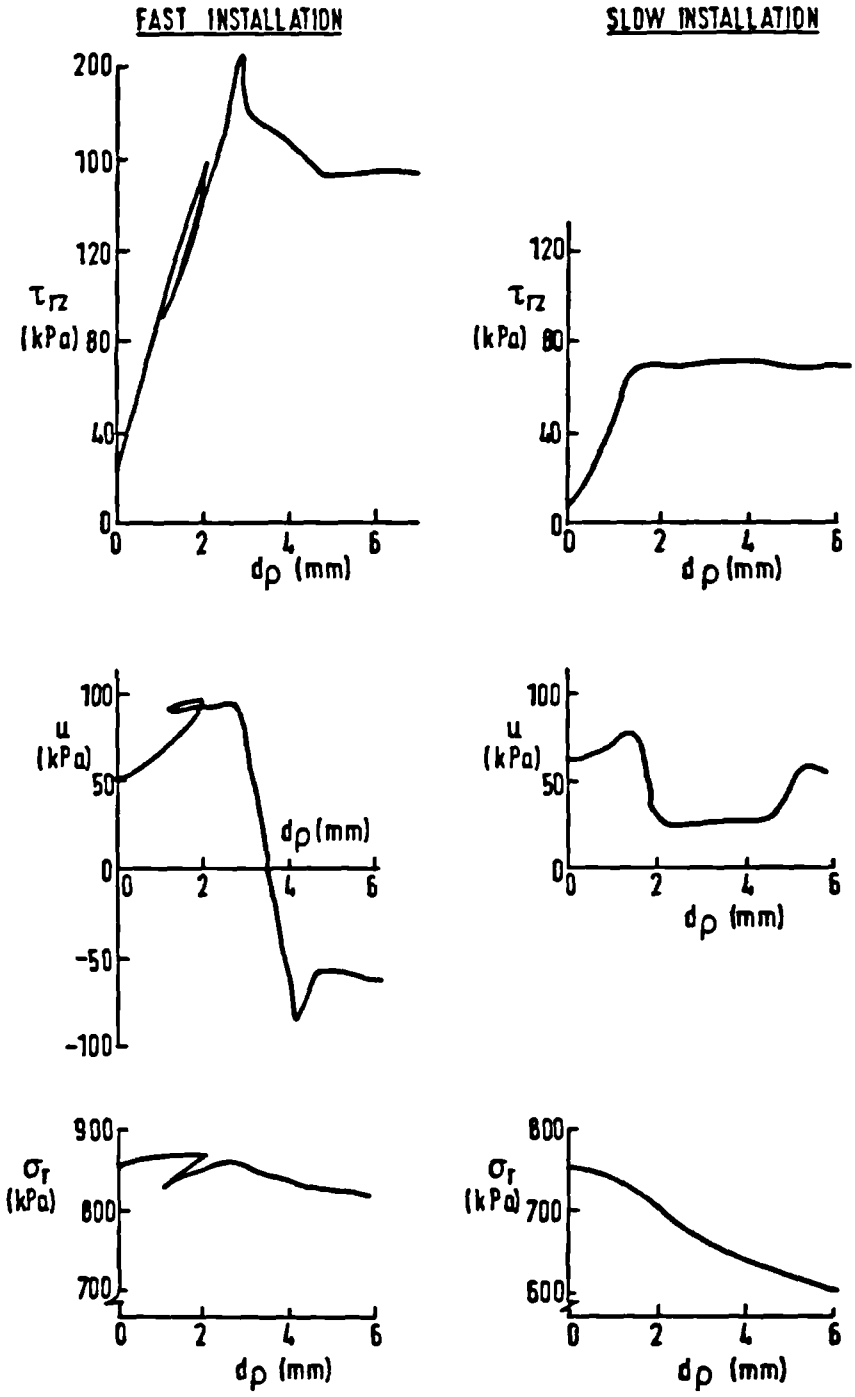

Figure B3 Local stress variation with d_p in load tests in London Clay

- Fast-jacked piles failed in a brittle manner in first-time load tests and gave a peak α value of ≈0.9, whilst slow-jacked piles and reload tests (in the same loading direction) on fast-jacked piles failed in a ductile manner and mobilised an α value only ≈0.55.

- Post-peak, pore pressures reduced and σ_r remained relatively constant. The reductions in pore pressure were more pronounced in piles that failed in a brittle manner and led to large increases in σ'_r.
- The capacity of piles (after full equalisation) was less than the load required to complete the last jacking stage at installation. This could be anticipated from Figure B2, which shows that the average equalised radial effective stress (σ'_{rc}) was less than the average radial effective stress recorded during installation.
- Tension capacities were similar to the compressive capacities of fast-jacked piles, but were higher than the compressive capacities of slow-jacked piles. Equivalent (un-instrumented) driven piles at Canons Park had capacities similar to fast-jacked piles.

The stress paths (τ_{rz} v σ'_r) recorded during a tension test on a fast-jacked pile (CP5f/L1T) and a compression test on a slow-jacked pile (CP3fs/L1C) are plotted on Figure B4 and summarised in Table B1, which also compares the interface friction angles, δ [$=\tan^{-1}(\tau_{rz}/\sigma'_r)$], with peak drained angles measured in ring shear interface (RSI) tests. These tests simulated the displacement history of soil elements adjacent to the piles (see Appendix D).

	CP5f/L1T	CP3fs/L1C
K_f/K_c	1.08	0.88
Peak δ (δ_p)	13.0°	8.0°
Post-peak increase in σ'_r	+95kPa	-34kPa
Ultimate δ (δ_{ult})	9.1°	8.5°
RSI peak δ	12.6°	9.6°

Table B1 Load test parameters measured in London clay

The lower capacity of the slow-jacked pile is clearly due its lower δ_p value. This was predicted by RSI tests which showed that a slow installation rate (less than 100mm/min) would lead to the formation of a low strength residual surface of well aligned clay particles (with a δ value of ≈9.6°). Higher rates of installation evidently created a stronger residual surface comprising more randomly oriented clay

particles (with $\delta \approx 12.6°$). Subsequent slow shearing in the same direction led to a residual surface of similar strength to that induced by slow pile installation.

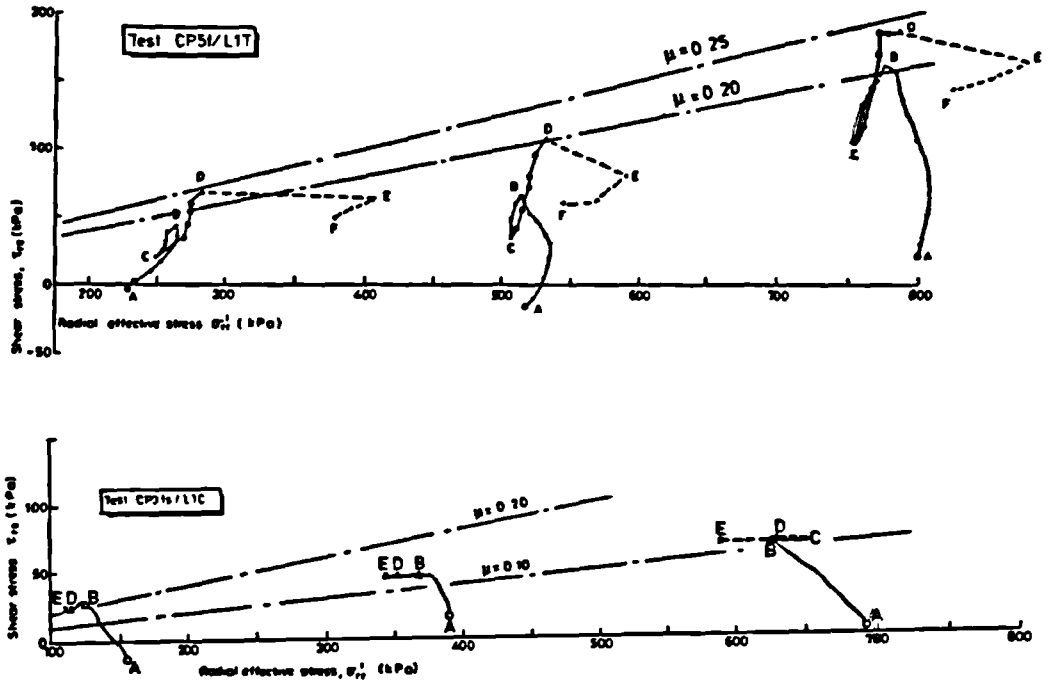

Figure B4 τ_{rz} v σ'_r paths during load tests in London Clay

B2.5 Trial pit investigations

Trial pits were excavated adjacent to a slow-jacked pile and a driven (un-instrumented) pile after load testing. Samples taken from these pits allowed examination of the clay fabric adjacent to the piles as well as measurement of the radial variation of water content, shear strength and mean effective stress. Four main conclusions were drawn from these investigations:

(i) The process of installation did not remould the clay adjacent to the piles: instead there was a systematic distortion of the soil which diminishes with radial distance. The extent of the disturbance was limited to within 4 radii of the pile.

(ii) Slow pile installation led to highly polished slip surface at a distance of ≈1mm from the pile shaft. In contrast, the fabric close

to the driven pile was less even and consisted of frequent, but discontinuous, shear surfaces. These observations are consistent with the measured dependence of shaft capacity on the installation rate.

(iii) The mean effective stress at the pile shaft (estimated from suction measurements) was about four times the initial mean effective stress (p'_0) but only 30-40% of that expected at the critical state, indicating that the London clay was in an *overconsolidated* state at the end of equalisation (Bond & Jardine 1991)

(iv) Mean effective stresses reduced with distance from the pile shaft to initial in-situ values (p'_0) at a distance of 4 radii from the pile. However, no radial variation of water content or shear strength (as measured with a pocket penetrometer) was observed.

B2.6 Quality of data

The measurements made in all tests at Canons Park were repeatable and in close agreement with measurements made by Coop (1987) at Canons Park using another instrumented pile (see Section B4). The high quality of data measured is evident from the compatibility of δ values to results from direct shear interface tests and studies of the clay fabric developed adjacent to the piles. The data proved conclusively that the pile capacity is controlled by the effective stresses acting at the pile soil-interface.

However, the following particular features of the measurements should be noted:

- Pore pressures were generally below -50kPa during installation and therefore the fluid in the probes was likely to have cavitated. σ'_r calculated in these instances may have been in error.
- δ values measured during fast shearing (e.g. during installation) were often as low as 5°. This angle is considerably less than drained residual angle of the material (see Section A2.3.2).
- No oedometer tests have been performed on the <u>disturbed</u> London clay. The OCR assumed for this material may be in error as the proposed OCR profile was based on the removal of overburden at the

site and oedometer tests on the underlying brown London clay.

- Values of σ_{r1} (and q_c) increase significantly between 4.1m and 4.6m as the instruments moved from the disturbed London Clay to the brown London Clay. Measurements made in this 'transition' zone should be treated with caution.

B3.0 EXPERIMENTS WITH THE PIEZO-LATERAL STRESS CELL

The piezo-lateral stress (PLS) cell was designed at the Massachusetts Institute of Technology (MIT) to investigate fundamental aspects of pile behaviour in soft materials. Extensive investigations with the instrument have been made in Boston Blue Clay and Empire clay (e.g. see Azzouz & Morrison 1988, Azzouz & Lutz 1986). These tests were highly successful and are considered in detail in this section to highlight features of pile behaviour in soft clays.

B3.1 Instrumentation

The PLS cell (diameter=38.4mm) measures the radial total stress, pore pressure and axial load developed at either ≈54 or 95 radii from its conical tip (Figure B5). Boreholes were drilled through superficial deposits at all sites before jacking the instrument at a steady rate of 1200mm/min to penetrations of up to ≈80m.

Radial stresses acting on the instrument apply pressure to a thin film of water, which is trapped between the cell's (thin) outer membrane and a solid steel stem. The water pressure is measured by a transducer housed within the stem and is almost exactly equivalent to the applied radial stress. The compliance of the instrument is negligible if the water is completely de-aired. Another transducer, to measure pore pressure, is linked to a stainless steel porous disc which is located at the base of the radial stress sensor.

B3.2 Soil profiles

PLS cell measurements have been made in the Boston Blue Clay at Saugus and the MIT Campus and in the Empire clay at Empire, Louisiana. These

sites had thick deposits of lightly overconsolidated material of varying plasticity and sensitivity. The soil profile at each site is summarised at typical depths in Table B6.

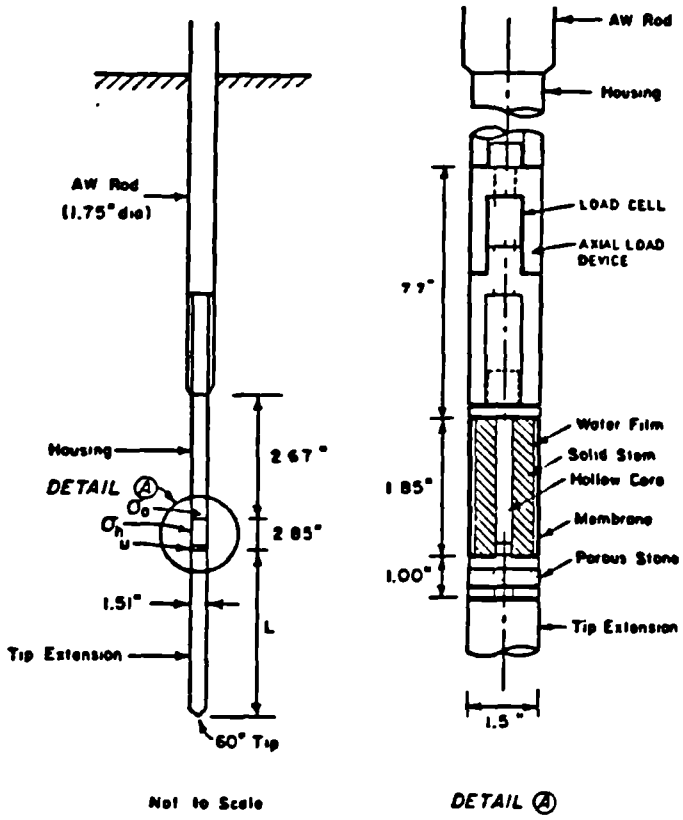

Figure B5 Configuration of the PLS cell

B3.3 Installation and equalisation

Typical stress measurements made during installation of the PLS cell are shown on Figure B6(a). Radial stresses increase linearly with depth in a similar way to the q_c and c_{u0} profiles and are typically over twice the free field vertical effective stress (σ'_{v0}). Pore pressures are *positive* and also increase linearly with depth, but are of a similar magnitude to the radial stresses, so that calculated σ'_r values are very low and less than the initial undisturbed horizontal effective stresses (σ'_{h0}).

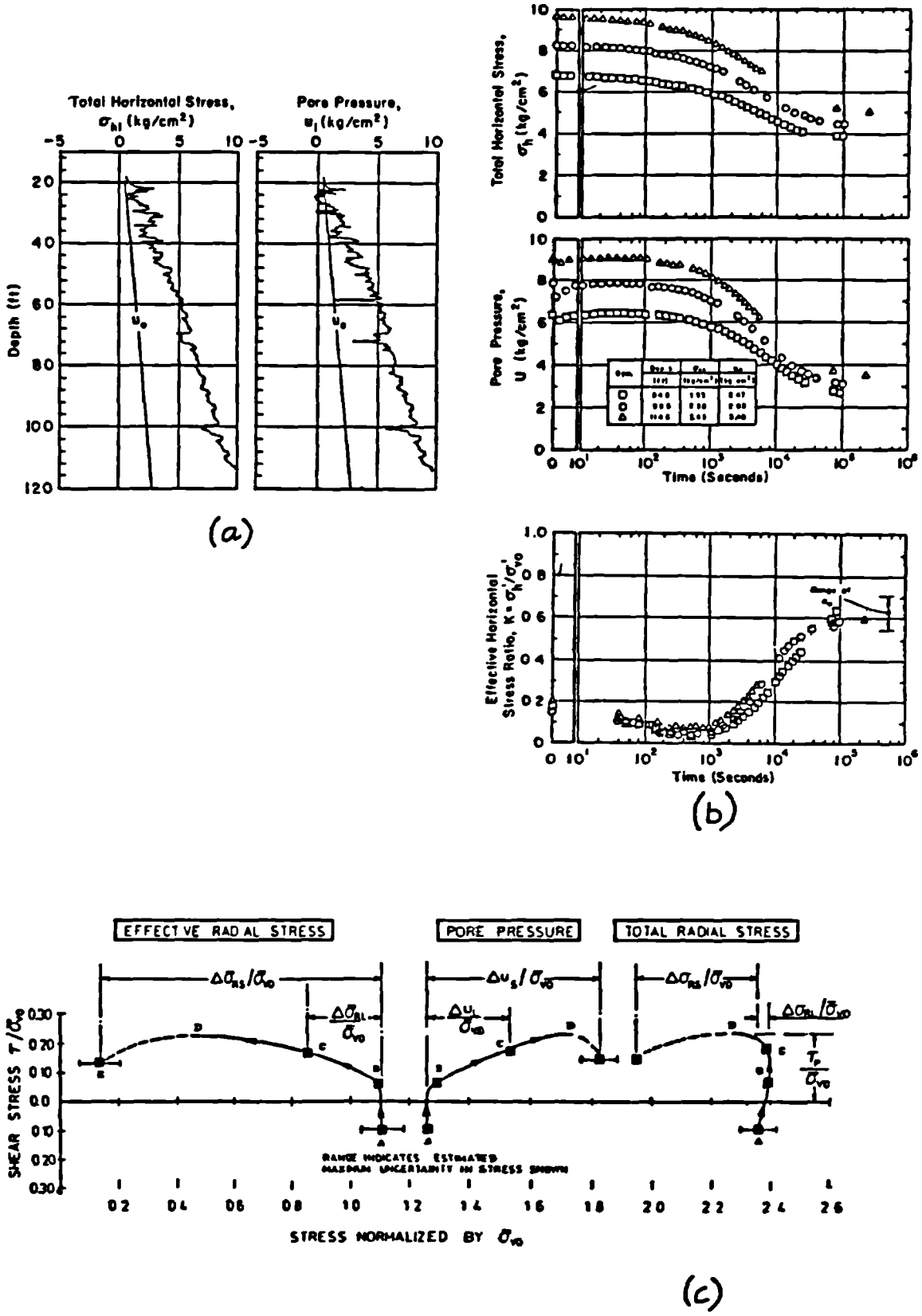

Figure B6 Typical data recorded by the PLS cell during installation (top left), equalisation (top right) and load tests (bottom)

Stress variations measured after installation of the PLS cell to three different depths at Saugus are shown on Figure B6(b). It is evident that:

- Radial total stresses reduce by almost 50% during equalisation. This reduction is considerably larger than observed in the heavily overconsolidated London Clay.
- Radial effective stresses appear to reduce initially in the first 10 mins after installation (as pore pressures increased marginally over this period) and thereafter increase, reaching equilibrium values (σ'_{rc}) when all excess pore pressures have dissipated.
- Measurements at different depths are in good agreement when normalised by σ'_{v0}.

The installation and equalisation data at the three sites are summarised on Table B7 and indicate:

- Similar values of H_1 and $\Delta u_1/\sigma'_{v0}$ for all depths at the three sites.
- An appreciably higher relaxation coefficient (K_c/H_1) in Empire clay, which leads to higher values of K_c.
- K_c values almost six times greater than K_1 ($= H_1 - \Delta u_1/\sigma'_{v0}$) i.e. there is a strong positive set-up.

B3.4 Load testing

Attempts were made with the PLS cell to measure the variation of shear stress with radial effective stress during pile loading. These 'stress paths' are the only such paths previously reported in the literature for piles installed in soft clay. Typical measurements during a compression load test at Saugus are shown on Figure B6(c). It can be seen that significant reductions in σ'_r occur as the peak shear stress is approached (path B-C-D). This reduction is caused by a large increase in pore pressure and is indicative of a contractant response of the clay at the pile-soil interface. Morrison (1984) noted the similarity of these stress paths with those measured in constant volume direct simple shear (DSS) tests.

The stress paths, reported by Morrison, must (as he insists) be viewed

as approximate, as the displacement control of the tests was too crude to obtain precise measurements of τ_{rz} and σ'_r at peak load. In particular,

- Pore pressures recorded at peak load were "unsteady" and the pressure assumed for point D on Figure B6(c) was that measured ≈10secs after relaxation of the load to ≈90% of the peak load.
- Point E does not represent a point on the failure stress path as the device at this stage was not at failure.
- The shear stress is calculated from the difference between the axial stress measured at the end of the 'AW rod' (Figure B5) and an assumed end bearing value. The observations with the ICP in the London clay suggest that this shear stress will be larger than the *local* shear stress acting on the shaft at the instrument position.
- The surface finish of the PLS cell is far smoother than that of the porous stone and of conventional piles.

The load test results were quoted in terms of the parameter $\rho = \tau_f / \sigma'_{rc}$, and average ρ values are summarised Table B2. These compare reasonably well with the peak shear stress divided by the initial vertical effective stress (c_{uss}/σ'_{v0}) measured in DSS tests on *normally consolidated* samples of the clays.

Site	PI (%)	OCR	ρ	c_{uss}/σ'_{v0}
Saugus	24	2-4	0.27 ±0.06	0.22
Saugus	21	1.2	0.23 ±0.10	0.22
Empire	59	1.7	0.25	0.26
Empire	48	1.5	0.27	0.25

Table B2 PLS cell load test results

B4.0 EXPERIMENTS BY COOP (1987)

Experiments with an instrumented model pile (IMP) were performed by Coop in two heavily overconsolidated clays and two lightly overconsolidated clays (Coop 1987, Coop & Wroth 1989). General properties of these clays are outlined in Table B3; complete site profiles are summarised in Tables B8-B10.

Site	Soil type	OCR	PI (%)	c_{u0} (kPa)
Madingley[1]	Gault clay	15-30	48	120-150
Canons Park	London clay	23-40	≈45	75-120
Huntspill[2]	Soft alluvium	1.1-2.3	35	20-40
Gt Yarmouth	Soft alluvium	1.6-1.8	28	20-30

Table B3 Soil types investigated by Coop (1987)

B4.1 Operation and instrumentation

The instrumented section of the IMP is 80mm in diameter and 1135mm long and comprises two concentric cylinders attached to a common pile head. Earth and pore pressure cells are mounted on the outer cylinder. The inner cylinder connects the pile head with the tip assembly, so that end bearing forces are transmitted directly to the pile head and are not measured. Shear stresses are derived from a number of axial load cells, which are connected to the outer cylinder. The IMP houses a plunger within the inner cylinder which may be held fixed or free to allow both closed-ended and open-ended installation. Most of the experiments were carried out closed-ended and the pile was jacked into the ground at a rate of ≈230mm/min (jack stroke length ≈350mm). Pause periods between jacking stages were typically only ≈ 30 secs, but were up to 10 mins when a new drill rod was added after every 1m penetration.

The configuration of the instruments on the pile is shown on Figure B7. A typical instrument cluster has two radial stress sensors, 2 pore pressure probes and 2 axial load cells. Details of the radial stress and pore pressure sensors are also shown on Figure B7. The design of the

[1]The Gault Clay at Madingley, Cambridgeshire, is a stiff fissured silty clay. The clay bears many similarities to the London clay, most notable of which is its tendency to form low strength residual surfaces.

[2]The ground conditions at Huntspill (Somerset) and Great Yarmouth (East Anglia) consist of a wide variety of lightly overconsolidated, geologically recent, estuarine sediments. Conditions at Great Yarmouth are more variable than at Huntspill and the precise conditions at the IMP sounding at this site are not certain.

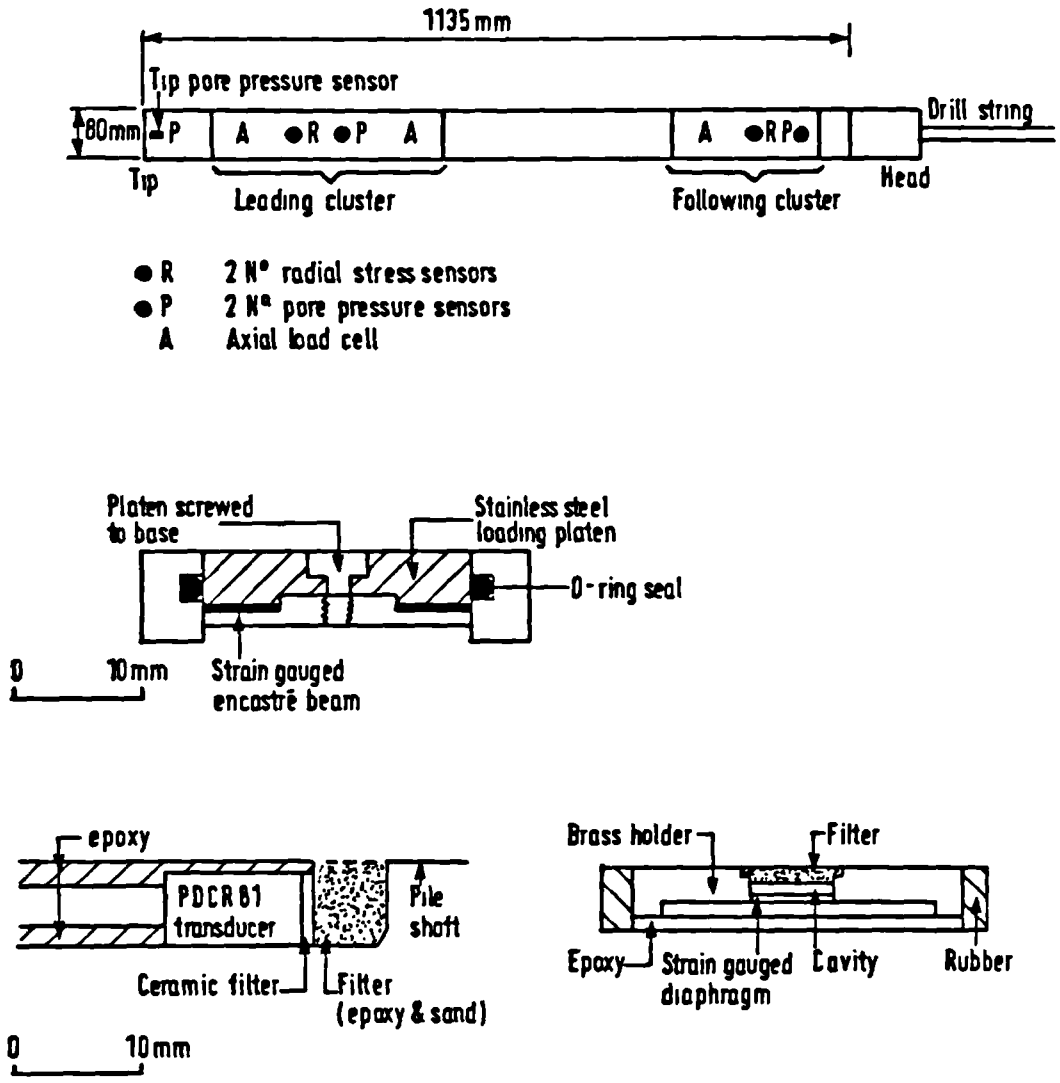

Figure B7 Configuration and instrumentation on the IMP

radial stress sensors is similar in principle to the SST's mounted on the ICP except that radial stresses acting on the loading platen cause the strain-gauged beam to bend rather than compress. Pore pressures were measured using either a Druck semi-conductor transducer or a strain gauged diaphragm. Filter stones were made from an epoxy-sand mixture or porous plastic and were saturated with a mixture of glycerine and water.

While these designs generally performed well in the field, some particular features should be noted:

- The outer cylinder of the IMP is made from brass with a roughness and hardness appreciably less than that of a typical industrial steel pile.
- The radial stress sensor has a smaller area and higher radial compliance than that of the SST's mounted on the ICP. These features make it more susceptible to local soil variations and cell action effects[1] (see Section A3.3, Appendix A).
- During installation at Canons Park, the IMP pore pressure probes showed a less jagged profile with depth than the profile measured with the ICP. Bond & Jardine (1990) attribute this response to the inability of the IMP probe design to recover quickly from cavitation.

B4.2 Installation

The radial stress measurements at Madingley and Huntspill are shown on Figure B8 for closed-ended installations[2]. Both profiles increase approximately linearly with depth in a similar way to c_{u0} profiles at each site (see Tables B8-B9). Although not clear from this figure, a detailed examination of the data reveals that, as in the tests of Bond (1989), stresses recorded at a given depth depend on the relative depth of the pile tip (h/R). When this h/R effect is taken into account, the σ_{r1} measurements made at Canons Park with the IMP and ICP are in reasonable agreement with each other.

Pore pressures reduced at the beginning of each pile push and were generally *negative* during pile pushes at Madingley and Canons Park and *positive* at Huntspill and Great Yarmouth. However, all the pore pressure data show considerable variability; measurements made by separate sensors in the same instrument cluster registered pressures which often differed by over 100kPa.

---

[1]Coop recognised that these effects were a potential problem in stiff soils and used a back pressure to restrain the loading platen from moving. This procedure was, however, only used after pile installation.

[2]Radial total stresses measured at h/R=5.5 during the initial stages of open-ended penetration were ≈30% <u>less</u> than these stresses, supporting the view that lower radial stresses are developed adjacent to un-plugged, open-ended displacement piles.

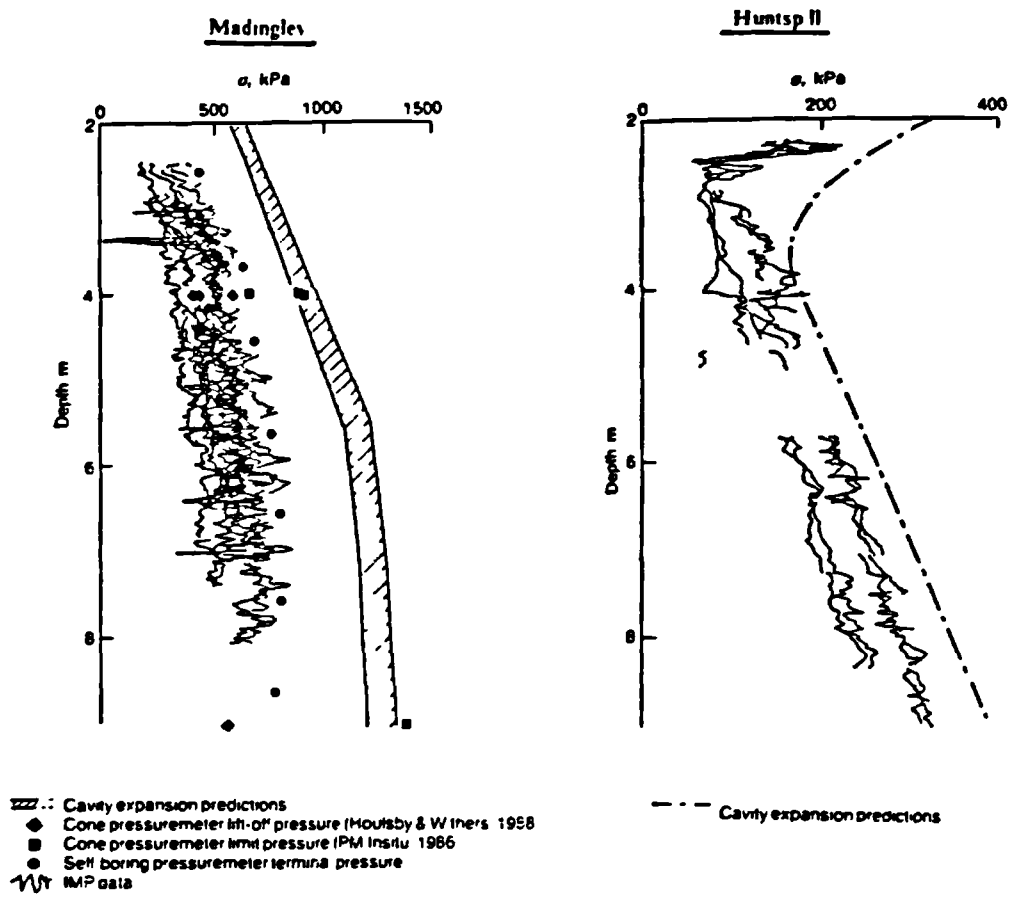

Figure B8 Radial total stresses recorded by the IMP during installation

Radial effective stresses (σ'_{r1}) may be calculated with more confidence in the lightly overconsolidated materials at Huntspill and Gt. Yarmouth, as cavitation of the fluid of the pore pressure probes was unlikely. However, at these sites, τ/σ'_{r1} ratios were considerably less than the drained residual ratios measured in ring shear interface tests. For example, ratios of between 0.05 and 0.15 were recorded during installation at Huntspill, whereas the drained residual ratio measured in ring shear interface tests varied between 0.28 and 0.36 (see Section A2.3, Appendix A).

B4.3 Equalisation

The IMP was monitored at Madingley and Huntspill, with its tip at ≈5.5m, until radial effective stresses had reached equilibrium values. The data recorded are shown on Figure B9 and show comparable features at both sites:

- Pore pressures initially rise after installation and reach a maximum after ≈15 mins.
- Radial total stresses decrease monotonically.
- Radial effective stresses (σ'_r) show a short term minimum as a consequence of the initial rise in pore pressure.
- After reaching this minimum, σ'_r increases at a reducing rate to a constant equalised value (σ'_{rc}). Full equalisation was achieved more rapidly in the more permeable clay at Huntspill.

Coop & Wroth (1989) attribute the initial pore pressure rise to a pore pressure maximum "which is radially remote from the shaft". The ensuing minimum in σ'_r was shown to be a real effect by a load test performed at Huntspill at the time this minimum occurred. This test gave a shaft capacity which was 34% less than that measured during installation.

B4.4 Load testing

The IMP was loaded to failure in ≈90 secs after full equalisation at Madingley and Huntspill. The data recorded are given on Figure B10 and show that:

- No significant pre-peak changes in radial total stress (σ_r) or pore pressure (u) are measured i.e. σ'_r remains constant.
- Peak capacity was mobilised at a stress ratio (τ/σ'_r) of ≈0.17 at Madingley and ≈0.25 at Huntspill. These ratios are in reasonable agreement with ratios measured in appropriate drained ring shear interface tests.
- Pore pressures dropped dramatically post-peak when the pile plunged at a rate of ≈150mm/min.

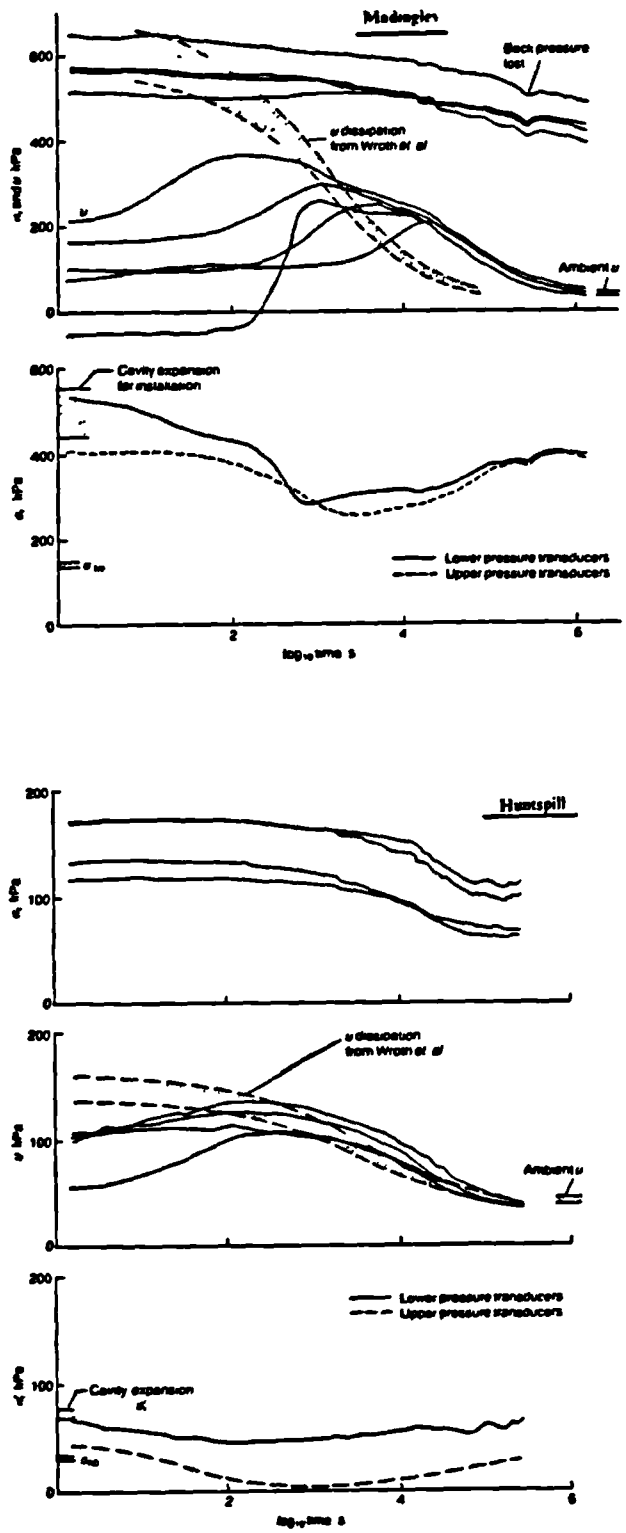

Figure B9 Equalisation data recorded by the IMP

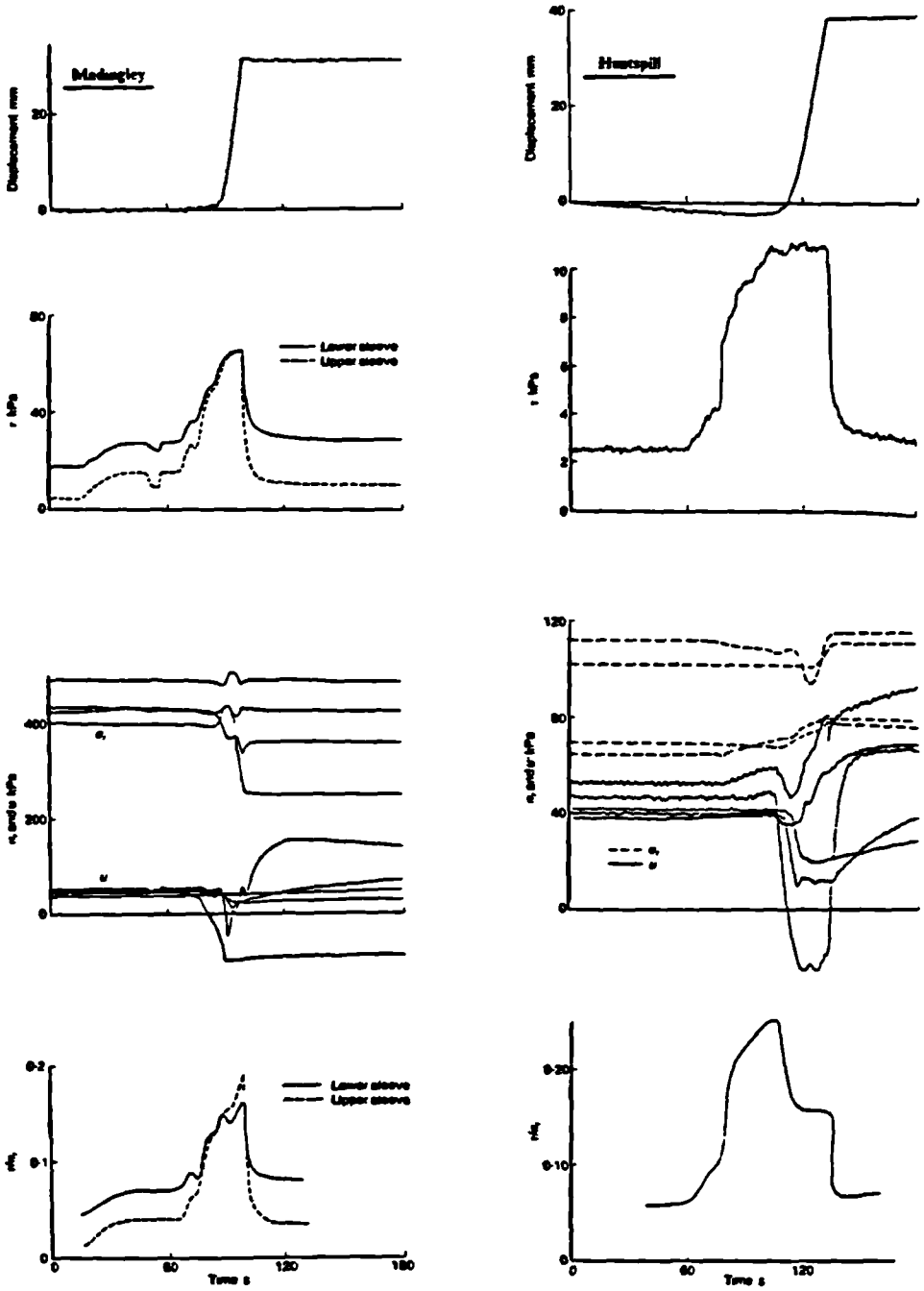

Figure B10 Data recorded by the IMP during load tests

- At Huntspill, the radial effective stresses at shaft failure (σ'_{rf}) were *less* than the σ'_r values recorded during installation and yet the load test capacities were ≈1.6 times *greater* than installation capacities.

The lower than expected values of τ/σ'_r measured during pile installation and the incompatibility of the σ'_r values with installation and load test capacities suggest that σ'_r was over-recorded during installation. Coop & Wroth (1989) attribute the apparently confusing measurements to "the stresses measured at the IMP shaft (being) unrepresentative of those on the failure plane which may be at a small distance from the shaft".

B5.0 EXPERIMENTS BY NGI

The Norwegian Geotechnical Institute (NGI) have carried out extensive tests with instrumented piles at Haga, Onsøy and Lierstranda in Norway and at Pentre in England. Unfortunately, only the results from Haga have been published to date as the data from the other three sites are currently confidential to NGI's sponsors (These data are due to be published in June 1992).

B5.1 Site properties

The material at Haga is described as a firm sensitive clay. The OCR of the deposit reduces from ≈ 17 at 1m depth to ≈3 at 5m depth (see Table B11). This overconsolidation was caused by the combination of leaching, chemical weathering and the removal of 6m of overburden at the test site area. Despite being overconsolidated, the material shows many of the characteristics of low OCR materials e.g. a high liquidity index and a contractant response when sheared.

B5.2 Instrumentation

Sixteen, 153mm diameter, closed-ended instrumented piles were jacked to a depth of ≈5m. The instrument configuration and a detail of a typical instrument cluster are shown on Figure B11.

A typical instrument cluster comprised a pore pressure and radial stress transducer, both of which worked on the vibrating wire principle[1]. The loading platen of the radial stress sensor was made from a hard rubber disc (≈40mm in diameter) which was glued to the membrane. The pore pressure transducer was almost identical except that an epoxy filter, which was saturated in water, was fitted in place of the rubber disc. Internal strain gauges were used to monitor the axial pile load.

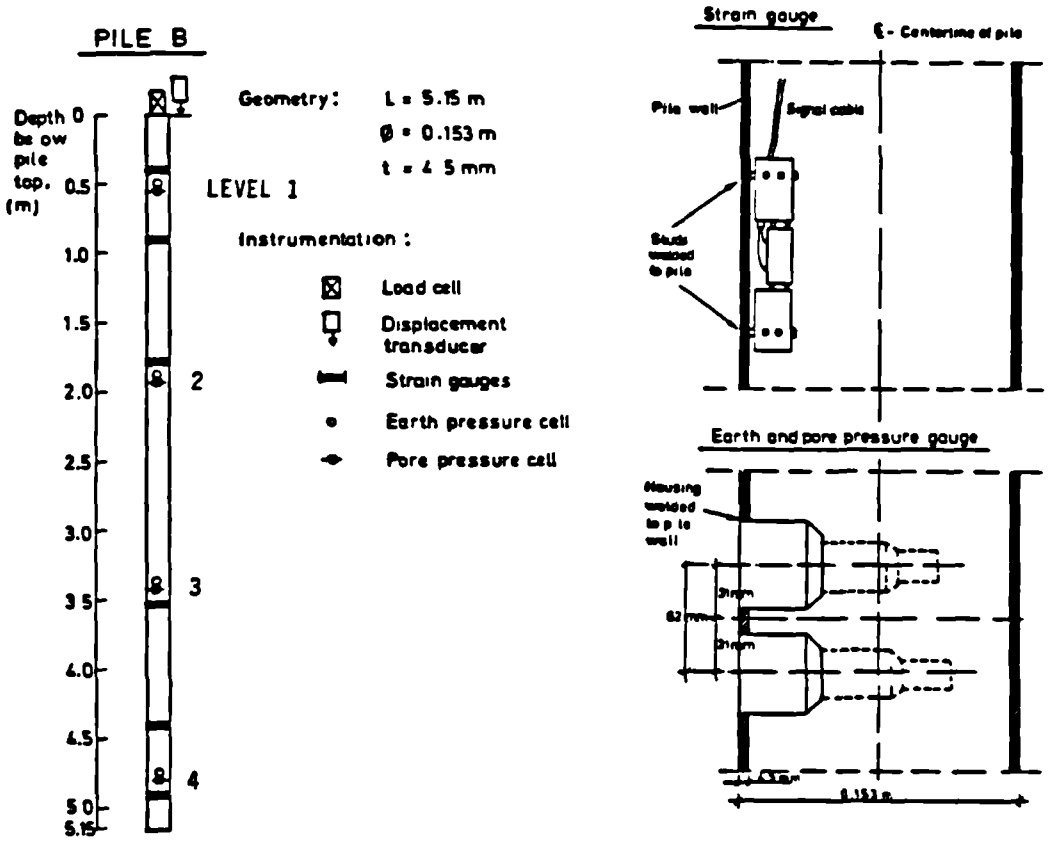

Figure B11 Pile configuration and instrumentation at Haga

[1]Each instrument contains a steel wire which is suspended between two supports and maintained in continuous vibration by an exciter magnet. A pressure or force applied to the device causes the transducer diaphragm to bend and thus change the natural frequency of the vibrating wire. This change of frequency is calibrated with the applied pressure.

B5.3 Installation and equalisation

The results from Haga were typical of those obtained in contractant materials (e.g. with the PLS cell). In particular, it was observed that:

- Radial stresses and pore pressures were of similar magnitude during installation and calculated radial effective stresses immediately after installation were approximately zero (and sometimes less than zero !)
- Radial total stresses reduced significantly during equalisation, giving a relaxation coefficient (K_c/H_1) of ≈0.3

B5.4 Load testing

Over thirty load tests were performed at Haga; the main findings are outlined below:

- Radial effective stresses reduced by an average of ≈20% up to peak load in first-time load tests (K_f/K_c ≈0.8 ± 0.1). Peak angles of interface friction were ≈26° but showed a large scatter[1].
- Piles tested in compression and tension failed in a ductile manner and had comparable shaft capacities.
- Shaft capacities increased with time *after* full equalisation (at t_{eq} =7 days). This increase amounted to ≈6% per week (for 1 week < t_{eq} < 4 weeks) and was attributed by Karlsrud & Haugen (1985) to "bonding of clay minerals" .
- Piles that were *reloaded* to failure after a period to allow for reconsolidation showed a marked increase in capacity[2]. This increase was caused by higher values of δ_p (≈30°) and smaller reductions in σ'_r during pile loading.
- Multiple load tests to failure increased shaft capacities to over 1.5 times the initial capacities. This pre-shearing effect was attributed to changes in the characteristics (e.g. "more

---

[1] δ_p =26 ±8°; this large range is attributed to instrumentation inaccuracies.

[2] This behaviour may be contrasted to that of fast-jacked piles in London Clay, where reload capacities were lower than initial capacities.

dilatancy") of the "remoulded" material next to the pile shaft.

B5.5 Trial pit investigations

Karlsrud & Haugen (1985) identified 3 zones adjacent to the piles from investigations made in trial pits. The extent and properties of these zones are given in Table B4.

Zone	Extent	Properties
A	r/R <1.2	"Completely remoulded" denser fabric (low water content (w), high shear strength)
B	1.2 <r/R <2.6	Zone of pure shear distortion (increasing w and reducing shear strength with radius)
C	r/R >2.6	As intact material

Table B4 Zones adjacent to piles at Haga

B6.0 FIELD TESTS AT SAINT-ALBAN

A very comprehensive set of pore pressure measurements was obtained adjacent to piles installed in the Champlain clay at St-Alban, 80km south of Québec. These data and other investigations at St-Alban have been reported extensively e.g. Roy et al. 1981, Roy & Lemieux (1986) and Konrad & Roy (1987). The clay is a very sensitive soft clayey silt and silty clay with average OCR of ≈2.3 (see Table B12).

B6.1 Instrumentation

Six 219mm diameter, closed-ended steel piles were equipped with pairs of pneumatic pore pressure probes at four levels along the pile shafts. An extensive arrangement of Geonor 'vibrating wire' piezometers were jacked to various depths and radial distances from these piles about three weeks before the beginning of pile installation[1]. A total pressure cell, of the

[1]Some of the Geonor pore pressure probes were installed to within 2 radii of a pile (i.e. r/R=3) and consequently may have affected the consolidation characteristics of the pile-soil system.

same diameter as the pile, was located at the pile base to measure the pile end bearing. No other measurements of total stresses were made.

B6.2 Installation

The piles were jacked from the base of a 1m deep pre-bored hole at a rate of between 10mm/min and 70mm/min to a final penetration of ≈7.6m. Jacking was not continuous due to the need to add additional pile segments as installation progressed.

Average pore pressure ratios ($\Delta u_i/\sigma'_{v0}$) measured by the probes mounted on the piles during installation are summarised in Table B12. It is evident that $\Delta u_i/\sigma'_{v0}$ (as measured in a given soil horizon) reduces from a typical value of ≈4.2 near the pile tip to ≈2.0 when the pile penetrates to deeper levels to give a h/R value of 41. This latter ratio is comparable to the ratio measured by the PLS cell (at h/R ≥50) in lightly overconsolidated clays. $\Delta u_i/\sigma'_{v0}$ appears to be relatively independent of h/R for h/R≥30.

A comprehensive (and unique) set of pore pressure measurements remote from the pile shaft was obtained. These data[1] have been re-plotted in a different form on Figure B12 to show the variation of the pore pressure ratio with both h/R and r/R. The two dimensional nature of the pile installation is clearly evident and it is noted that:

- Large hydraulic gradients exist around the pile tip, but these diminish rapidly with the distance from the pile tip.
- Significant excess pore pressures extend to r/R >20.
- Pore pressure ratios are at a maximum at all radii near the level of the pile tip.

[1]The data shown on this figure comprise over 400 pore pressure measurements at different depths and h/R ratios. Contours of $\Delta u_i/\sigma'_{v0}$ could therefore be estimated with confidence.

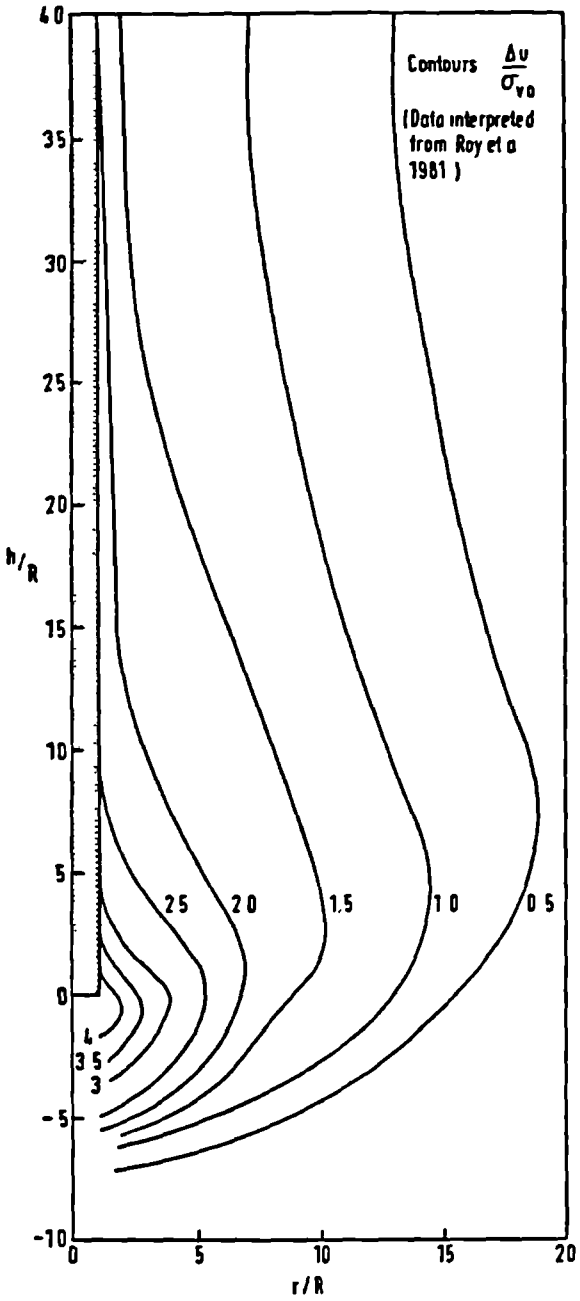

Figure B12 Contours of excess pore pressure ratios at St-Alban

It is encouraging to see that the pore pressure ratio contours show the same general pattern as those predicted by the Strain Path Method (SPM). A comparison between measurements and SPM predictions (c.f. Figure 2.9, Chapter 2) reveals two main differences (aside from the magnitudes of $\Delta u_1/\sigma'_{v0}$):

(a) The contours predicted by the SPM in the vicinity of pile tip are more rounded than those surrounding the pile tips at St-Alban. This may be due to the different tip geometries of the piles.

(b) The SPM predicts a less pronounced dependence of the pore pressure ratio on h/R.

The excess pore pressures remote from the pile normalised by the excess pressures at the pile shaft ($\Delta u/\Delta u_{shaft}$) are plotted against r/R on Figure B13. It is evident that, at <u>all</u> h/R values, excess pore pressures decrease approximately semi-logarithmically with r/R and extend to r/R≈30. If drainage took place during installation, then different distributions at each h/R value would be expected. It can therefore be concluded that *the decrease in the pore pressure ratio with h/R is not associated with partial drainage during installation.*

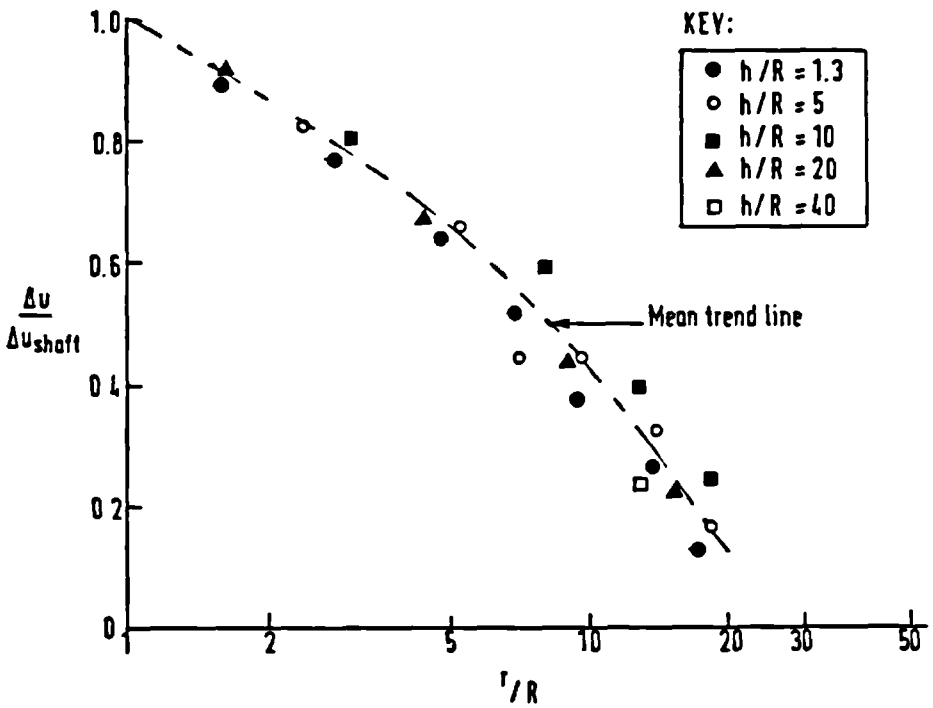

Figure B13 Normalised radial distributions of pore pressure at St-Alban

B6.3 <u>Equalisation</u>

The variations of pore pressures at the pile shaft during equalisation showed similar trends to those measured with the PLS cell (Figure B6(b)).

One notable feature of the measurements made remote from the shaft was that pore pressures at radial distances greater than r/R ≈6 *increased* over the early stages of equalisation. This is an expected feature of radial consolidation.

B6.4 Load testing

The load test data at St-Alban showed:

- Load test capacities after full equalisation were almost eight times the installation capacity i.e. there was very significant positive set-up.
- Installation and load test capacities could be correlated directly with the pore pressures measured at the pile shaft. These pressures remained constant throughout the load tests (piles were loaded to failure in ≈3 hours).

B6.5 Trial pit investigations

In-situ tests and tests on samples taken from trial pits excavated adjacent to the piles after equalisation showed that the properties of the material close to the pile shaft (r/R≤4) differed from those at larger radial distances in the following ways:

(a) Field vane strengths were ≈20% lower. These strengths did not vary after equalisation had been achieved.
(b) Peak undrained triaxial compression strengths and cone penetration resistances showed no systematic trend.
(c) Water contents for r/R < 2 were lower.
(d) The ratio of the compression index to the swelling index (C_c/C_s) and the rigidity (G_{sec}/c_{u0}) were lower.
(e) Preconsolidation pressures were similar.

Roy & Lemieux (1986) concluded from these observations that:

- The material close to the pile shaft experienced large shear strains which caused a collapse of the sensitive fabric of the

intact clay. The patterns of C_c/C_s measurements suggested that this "destructuration" was not as severe as complete remoulding.

- The densification of the clay caused by pile installation was minimal and detectable only at $r/R \leq 2$ (observation c).
- Ageing and thixotropy did not increase the shear strength of the clay (observation (a)).
- It follows from (b) and (e) that the strengths of the destructured clay were a function of the stress field prevailing around the pile after equalisation. The inconsistent trends of the c_u data suggest that this stress field varied with depth.

B7.0 EXPERIMENTS IN TOKYO CLAY

The pile tests reported by Koizumi & Ito (1967) in Tokyo Clay were among the first tests where effective stresses acting on full displacement piles were measured. The test piles (300mm in diameter) were equipped with a number of 'vibrating wire' earth and pore pressure cells. The level of the site was lowered by 1.5m prior to the beginning of the test programme and piles were installed at a rate of ≈100mm/min to a final penetration of 5.55m.

Although the Tokyo Clay has a high plasticity index, it is similar in many other respects to the Haga Clay e.g. high sensitivity, liquidity index and high OCR (in range 4-20, due presumably to chemical weathering). The measurements obtained (see Table B13) also show similarities with Haga:

- Radial effective stresses which are almost zero during installation.
- Large reductions in radial total stress during equalisation leading to an average relaxation coefficient (K_c/H_1) of ≈0.32

B8.0 EXPERIMENTS BY BOGARD & MATLOCK (1990)

A series of tests with an instrumented probe, which is similar in design to the PLS cell, were performed in lightly overconsolidated clays at Harvey and Empire, Louisiana. The data showed similar trends to

measurements with the PLS cell (see Table B14), although the results did not appear to be as consistent. Additional features to those observed with the PLS cell were:

- Consolidation times for probes of 44mm and 76mm diameter were (as expected from radial consolidation theory) proportional to the square of the diameter (Figure B14).
- Consolidation proceeded at a faster pace for open-ended piles.
- As the piles plunged post-peak in load tests, large reductions in pore pressure were observed. This was attributed to local "dilation" at the pile-soil interface.
- Shearing resistance increased by between 5% and 15% per log cycle increase in probe displacement rate.
- Radial total stresses mobilised adjacent to open-ended probes during installation and after equalisation were *up to 40% less* than those measured on closed-ended probes.

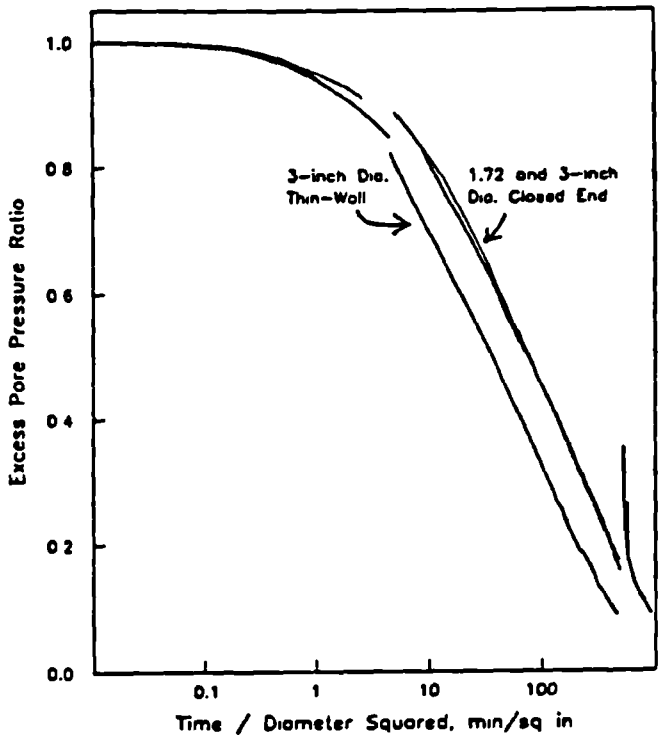

Figure B14 Pore pressure dissipation curves measured by Bogard & Matlock (1990)

B9.0 EXPERIMENTS AT COWDEN

Only four of the twenty or so piles installed in the glacial till at Cowden achieved moderate success with instrumentation. Comparisons between the trends shown by all the piles and the ICP tests at Cowden are made in Chapter 7.

The 'successfully' instrumented piles (reported by Ponniah 1989 and Mc Anoy et al 1982) were open-ended and equipped with three levels of earth and pore pressure cells; these were mounted on cover plates welded to the sides of the shafts. The piles (193mm diameter) were jacked at an average rate of 10mm/min, using a stroke length of 100mm, to a depth of 9.9m. Only those cells positioned at h/R=5 and h/R=70 performed satisfactorily during installation and *all* earth pressure cells became unstable shortly after installation. Ponniah (1989) estimated that the piles were fully plugged (i.e. acted as closed-ended pile) between 0-3m, 5-6.5m and 9-9.9m. The data recorded are summarised in Table B15.

B10.0 LABORATORY TESTS BY FRANCESCON (1983)

19mm diameter cone-ended piles were jacked into a pressurised chamber (diameter ≈200mm) containing kaolin at different overconsolidation ratios. The instrument cluster, positioned at h/R ≈15, was similar to that employed on the IMP (Section B4).

Two test series were performed: 'series A' used a chamber with a rigid boundary and 'series B' adopted a stress controlled flexible boundary. Because of likely boundary effects and other scale effects, these results may not be applicable to full scale piles. They do, however, highlight the major influence of OCR on the magnitudes of the radial stresses developed during installation and after equalisation (see Table B14). It is interesting that the relaxation of radial total stress during equalisation in 'series A' (with the rigid boundary) is appreciably less than measured in 'series B' and in field tests. This observation suggests that the 'elastic' stiffness of the material remote from the pile shaft plays an important part in controlling the reduction in σ_r during equalisation.

B11.0 OTHER PILE TESTS

Three other pile test programmes which merited close examination were in:

- Very soft sensitive plastic Rio de Janeiro soft clay (1x220mm diameter pile; Soares & Dias 1990)
- San Francisco Bay mud (1x152mm diameter pile; Reese and Seed 1955)
- Stiff moderately overconsolidated clays at Beaumont (pile group of 9x273mm diameter piles and 1 single pile; O'Neill et al 1982)

The data measured in these tests, which are summarised in Table B16, show general agreement with trends observed in similar materials, discussed above.

SITE PROPERTIES: CANONS PARK

Stiff fissured silty clay from 2.5 -6.0m (London Clay - LC)

z (m)	u_0 (kPa)	σ'_{v0} (kPa)	c_{u0} (kPa)	q_c (MPa)	p_{lim} (MPa)	K_0[1]	OCR[2]	
2.5	14	34	76	1.60	0.37	2.30	46	Disturbed LC
3.0	19	39	76	1.68	0.51	2.41	40	LL= 85% PL =30%
3.5	23	44	76	1.70	0.58	2.39	36	PI = 55%
4.0	27	49	76	1.73	0.60	2.37	33	
4.5	32	55	119	2.16	0.99	2.33	30	Brown LC
5.0	36	60	119	2.59	1.36	2.28	27	LL= 66% PL=30%
5.5	40	66	119	2.89	1.32	2.24	25	PI =36%
6.0	44	71	119	3.11	1.28	2.19	23	

1 derived from measurements of σ_{h0} from self boring pressuremeter tests

2 based on an assessment of the amount of overburden removed and high pressure oedometer tests in the brown LC

INSTALLATION NORMALISED RADIAL TOTAL STRESS (H_1)

z(m)	h/R=8	h/R=28	h/R=50	
3	8.9	6.3	2.8	
3.5	8.2	5.4	3.3	
4.0	8.1	5.8		
4.5	10.5	7 - 14		
5.0	11.1			
5.5	14.6			(u_1 < 0)

EQUALISATION DATA

	z(m)	H_1	$(\Delta u_{max}/\sigma'_{v0})$	K_c	K_c/H_1
h/R=8	≈5.5	14.7	[5.5,11]	12.3	0.83
h/R≈27	≈4.5	10.7	[0.2-4.0]	8.0	0.75
h/R≈50	≈3.4	[2.5-5.2]	≈0.35	5.6	1.20
h/R=61	≈2.8	2.55	?	4.6	1.8

TABLE B5 Pile tests in London Clay (Bond 1989)

PROPERTIES AT SITES OF PLS CELL MEASUREMENTS

Lightly overconsolidated soft silty clays

Site	z (m)	u_0 (kPa)	σ'_{v0} (kPa)	q_c (MPa)	c_{u0} (kPa)	K_0	OCR	Index props.
S	12.2	112	92	0.61	47	0.90	4	PI≈23%, LL≈44
S	18.3	171	137	0.82	45	0.72	2	LI ≈0.9
S	24.4	234	184	0.76	43	0.62	1.3	PI≈21%, LL≈42
S	30.5	295	230	1.00	50	0.60	1.2	LI ≈1.0
MIT	19.1	154	200	1.88	58	0.80	2.5	PI≈21%, LL≈43
MIT	22.9	191	230	1.86	42	0.68	1.7	LI ≈1.0
MIT	25.9	221	254	1.76	24	0.63	1.4	
MIT	29.0	251	278	2.01	24	0.60	1.2	
E	36.6	425	167	1.41	45	0.76	1.7	PI ≈59%, LL≈87%
E	42.7	486	205	1.67	50	0.75	1.6	LI ≈0.3
E	48.8	547	249	1.90	60	0.74	1.5	
E	67.1	737	398	2.74	83	0.72	1.5	PI ≈48%, LL≈71%
E	73.2	798	438	2.92	88	0.72	1.5	LI ≈0.27

Table B6 Soil properties at PLS sites; Saugus (S), MIT and Empire (E)

INSTALLATION AND EQUALISATION DATA SUMMARY (PLS CELL)

Site	z(m)	h/R	H_1	$\Delta u_1/\sigma'_{v0}$	K_c	K_c/H_1
S	12.2	54	2.5	2.35	0.9	0.36
S	18.3	54	2.7	2.55	1.0	0.37
S	24.4	54	2.3	2.2	0.60	0.26
S	30.5	54	2.3	2.2	0.60	0.26
MIT	19.1	54	2.6	2.5	0.65	0.25
MIT	22.9	54	2.4	2.0	0.77	0.32
MIT	25.9	54	2.4	1.9	0.62	0.26
MIT	29.0	54	2.5	2.2	0.59	0.24
E	36.6	95	2.7	2.2	1.54	0.57
E	42.7	95	2.7	2.2	1.54	0.57
E	48.8	95	2.7	2.2	1.54	0.57
E	67.1	95	2.4	2.1	0.90	0.38
E	73.2	95	2.4	2.1	0.90	0.38

Table B7 PLS cell data recorded at Saugus (S), MIT and Empire (E)

SITE PROPERTIES: MADINGLEY

Stiff fissured silty clay (Gault Clay): PI≈48%, LL≈75%, PL≈27%

z (m)	u_0 (kPa)	σ'_{v0} (kPa)	c_{u0} (kPa)	q_c (MPa)	K_0[1]	OCR[2]
3	20	36	107	1.50	3.15	42
4	29	46	124	1.75	2.78	31
5	38	57	144	2.00	2.55	25
6	46	67	152	2.30	2.37	21
7	54	77	152	2.65	2.23	18
8	64	87	152	3.10	2.14	16
9	72	98	152	3.60	2.06	15

[1] assessed from σ_{h0} measurements made in self-boring pressuremeter tests

[2] Based on OCR measurements from two high pressure oedometer tests and the trend of K_0 values (for ϕ = 24°, OCR = $[K_0/0.59]^{2.43}$, Mayne and Kulhawy 1982)

INSTALLATION NORMALISED RADIAL TOTAL STRESS (H_i)

z(m)	h/R=5.5	h/R=22
3	11.0	7.6
4	10.9	8.1
5	10.1	7.6
6	9.3	7.1
7	8.3	6.5
8	7.3	

u_i varied randomly from -50kPa to 200kPa

EQUALISATION DATA

	z(m)	H_i	$(\Delta u/\sigma'_{v0})_{max}$	$K_c(\approx H_c)$	K_c/H_i
h/R=5.5	5.6	9.1	up to ≈5.5	6.22	0.68
h/R=22	4.9	9.1	up to ≈5.5	6.79	0.75

Table B8 Pile tests at Madingley (Coop 1987)

SITE PROPERTIES :HUNTSPILL

Soft silty clay from 2-9m, PI≈35%, LL≈65%, PL≈30%

z (m)	u_0 (kPa)	σ'_{v0} (kPa)	c_{u0}[1] (kPa)	q_c (MPa)	K_0[2]	OCR[3]
3	27	32	20	0.38	0.77	2.3
4	37	40	19	0.36	0.67	1.7
5	45	49	23	0.44	0.65	1.5
6	52	59	27	0.51	0.63	1.4
7	60	69	30	0.58	0.61	1.3
8	67	78	34	0.66	0.60	1.2
9	75	88	38	0.73	0.58	1.1

[1] derived from the q_c profile at IMP location, using an N_k factor of 15, which was backfigured from c_{u0} data for the complete site

[2] Derived from OCR variation, assuming $K_0 = (1-\sin\phi')\,OCR^{\sin\phi'}$, with $\phi' = 27.5°$

[3] Based on oedometer tests and data reported by Coop for Somerset alluvium

INSTALLATION NORMALISED RADIAL TOTAL STRESS (H_1)

z(m)	h/R=5.5	h/R=22
3	2.3	1.6
4	2.7	1.8
5	2.9	2.1
6	2.9	2.2
7	2.9	2.1
8	2.9	2.0

$\Delta u_i/\sigma_{v0} = 1.5 \pm 0.5$ for $h/R \geq 5.5$ Higher ratios were recorded closer the pile tip

EQUALISATION DATA

	z(m)	H_1	$(\Delta u_{max}/\sigma'_{v0})$	Kc	K_c/H_1
h/R=5.5	8.1	2.4	1.2-1.7	1.20	0.50
h/R=22	7.4	1.8	1.2-1.7	0.66	0.37

Table B9 Pile tests at Huntspill (Coop 1987)

SITE PROPERTIES: GREAT YARMOUTH

z (m)	u_0 (kPa)	σ'_{v0} (kPa)	c_{u0} (kPa)	K_0[1]	OCR[2]	
3	28	22	-	0.69	2.1	Sandy SILT (PI≈14%
4	38	29	-	0.67	1.9	LL≈27%)
5	48	37	20	0.64	1.8	Clayey SILT
6	58	44	23	0.63	1.7	(PI≈28%,LL≈51%)
7	68	51	26	0.62	1.7	
8	78	58	30	0.61	1.6	
9	87	66	33	0.61	1.6	

[1] assessed from σ_{h0} measurements made in self-boring pressuremeter tests.

[2] Based on K_0 va ues and c_{u0}/σ'_{v0} ratios with ϕ =32°

INSTALLATION NORMALISED RADIAL TOTAL STRESS (H_1) :GREAT YARMOUTH

z(m)	h/R=5.5	h/R=22	
3	2.1	1.7	
4	1.8	1.1	
5	4.0	3.4	
6	2.6	1.9	
7	2.6	1.5	
8	2.1	0.9	
9	1.9		($\Delta u_1/\sigma'_{v0}$ ≈1.0)

INSTALLATION NORMALISED RADIAL TOTAL STRESS (H_1) :CANONS PARK

z(m)	h/R=5.5	h/R=22
3	11.2	9.3
3.5	9.8	8.2
4.0	8.7	7.3
4.5	9.2 ± 2	8 ± 1.5
5.0	10.9	

Table B10 Pile tests at Great Yarmouth and Canons Park (Coop 1987)

SITE PROPERTIES: HAGA

Firm, sensitive, leached CLAY, LI ≈0.8-1.0

z (m)	u_0[1] (kPa)	σ'_{v0} (kPa)	c_{u0} (kPa)	K_0[2]	OCR[2]	
1	0	18	55.0	1.70	17	(PI≈15%, LL≈40%, PL≈25%)
2	0	36	62.5	1.20	9	
3	0	54	62.5	0.95	5	
4	0	72	62.5	0.90	4	
5	0	89	66.0	0.80	3	(PI ≈37%, LL≈63%, PL≈26%) -from 4.5m-5.5m
6	0	106	62.5	0.75	2.3	(as between 0-4.5m)

[1] Average values u_0 varied by ≈20kPa with time, depth and location.

[2] From oedometer tests (quoted values)

INSTALLATION AND EQUALISATION DATA

z(m)	h/R	H_1	$(\Delta u_{max}/\sigma'_{v0})$	K_c	K_c/H_1
0.5	61	3.3	3.3	0.92	0.28
1.9	42	3.6	3.6	1.24	0.34
3.4	23	3.9	3.9	1.25	0.32
4.8	5	3.95	4.3	1.10	0.28

Table B11 Pile tests at Haga (Karlsrud & Haugen 1985)

SITE PROPERTIES: SAINT-ALBAN (CHAMPLAIN) CLAY

Soft lightly overconsolidated silty clay and clayey silt.
PI =18 ± 8%, LL≈42%, PL≈24%, LI ≈3
Silt layer between 4.3-5.1m with PI≈10%, LL≈30%

z (m)	u_0 (kPa)	σ'_{v0} (kPa)	q_c (kPa)	c_{u0} (kPa)	OCR[1]
3	22	20	180	17	2.3
4	32	27	225	21	2.2
5	42	32	270	26	2.2
6	52	36	320	29	2.3
7	62	41	380	34	2.4

[1] Derived from oedometer tests

INSTALLATION PORE PRESSURE RATIOS ($\Delta u_i/\sigma'_{v0}$)

z(m)	h/R≈1	h/R=14	h/R=27	h/R=41
3	4.0	2.3	2.2	2.0
4	4.1	2.3	2.1	-
5	4.2	2.3	-	-
6	4.6	2.5-3.0	-	-
7	4.4	-	-	-

Table B12 Pile tests at St-Alban (Roy et al 1981)

SITE PROPERTIES: TOKYO

Firm very sensitive[1] silty CLAY, LI ≈0.8-1.0
Liquid and plastic limits increase with depth, PI [40-75]%

z (m)	u_0 (kPa)	σ'_{v0} (kPa)	c_{u0}[2] (kPa)	K_0[3]	OCR[4]	
1	10	6	23	1.90	20	(PI≈40%, LL≈80%, PL≈40%)
2	20	11	23	1.52	11	
3	30	17	29	1.32	7.5	
4	39	22	34	1.17	5.5	
5	49	28	27	1.13	5.0	
6	59	33	25	1.08	4.4	(PI≈70%, LL≈120%, PL≈50%)

[1] Remoulded samples failed under their own weight

[2] Values prior to 1 5m excavation at site

[3] Derived from OCR values assuming ϕ =22° (Mayne and Kulhawy 1982)

[4] From oedometer tests and accounting for excavation at site

INSTALLATION AND EQUALISATION DATA

z(m)	h/R	H_1	K_c	K_c/H_1
1.2	29	11.6	≈5	0.43
1.8	25	8.6	≈3	0.35
2.4	21	7.9	2.5	0.32
3.0	17	6.8	2.4	0.35
4.0	10	6.2	2.0	0.32
5.25	2	7.0	2.2	0.31

$\Delta u_{max}/\sigma'_{v0} \approx H_1$ during installation

Table B13 Pile tests at Tokyo (Koizumi & Ito 1967)

EXPERIMENTS WITH INSTRUMENTED PROBES (LOUISIANA)

Harvey, Lousiana: Soft normally consolidated silty CLAY (PI≈48%, LL≈77, LI ≈0.7)

Empire, Louisiana: Soft lightly overconsolidated silty CLAY (PI ≈59%, LL≈87%, LI ≈0.35)

z(m)	u_0	σ'_{v0}	c_{u0}	K_0	OCR	h/R	H_1	$\Delta u_1/\sigma'_{v0}$	K_c[1]	K_c/H_1
Harvey:										
14.6	140	86	25	0.58	1.0	75	2.67	2.28	≈1.25	0.47
Empire										
48.8	547	249	83	0.74	1.5	75	3.45	3.00	≈2.00	0.58
						≈40[2]	3.30	2.90	≈1.60	0.48

[1] Extrapolated values as radial effective stresses had not come to full equilibrium

[2] No h/R values are quoted (inferred from Bogard et al 1985)

LABORATORY EXPERIMENTS IN KAOLIN

Kaolin with a PI≈31% and c_{u0} between 11 and 55kPa; measurements at h/R ≈15

Series	c_{u0}/σ'_{v0}	K_0	OCR	H_1	$\Delta u_1/\sigma'_{v0}$	K_c	K_c/H_1
A	0.21	0.7	1	1.03	1.05	0.86	0.83
	0.38	0.9	2	1.41	1.41	1.33	0.94
	0.62	1.2	4	1.91	1.79	1.85	0.97
	1.03	1.6	8	3.29	2.36	2.92	0.89
B	0.22	0.7	1	1.20	0.99	0.67	0.56
	0.37	0.9	2	2.08	1.80	1.10	0.53
	0.64	1.2	4.2	2.82	2.63	1.67	0.59
	1.05	1.6	8.3	3.89	3.78	2.42	0.62
	1.67	2.1	17	5.33	6.00	3.33	0.62
	3.80	3.8	50	9.50	9.88	6.84	0.72

Table B14 Pile tests at Louisiana (Bogard & Matlock 1990)
Laboratory pile tests in Kaolin (Francescon 1983)

SITE PROPERTIES: COWDEN

Stiff to hard glacial TILL (PI ≈19%, LL≈37%, PL≈18%, LI < 0.0)
(Full details provided in Section 5.2)

z (m)	u_0 (kPa)	σ'_{v0} (kPa)	c_{u0} (kPa)	q_c (MPa)	K_0	OCR
1	2	20	150	2.60	2.6	>50
2	12	32	205	3.85	2.6	50
3	21	43	175	3.24	2.5	30
4	29	56	98	1.77	1.6	11
5	36	70	98	1.75	1.3	7
6	44	83	105	1.85	1.2	5.5
7	51	99	107	1.86	1.1	4.5
8	59	111	110	1.90	1.0	3.7
9	59	132	107	1.82	0.95	3.3

INSTALLATION DATA[1]

	h/R=5		h/R=70	
z(m)	H_i	$\Delta u_i/\sigma'_{v0}$	H_i	$\Delta u_i/\sigma'_{v0}$
1.0	23.6	< 0	14.4	-
2.0	24.9	< 0	15.9	6.4
4.0	10.6	3.0		
6.0	7.8	1.9		
7.0	9.2	3.6		
8.0	8.8	3.5		
9.0	8.3	2.5		

[1] Radial stress sensors became unstable after pile insta ation

Table B15 Pile tests at Cowden (Ponniah 1989)

PILE TESTS IN RIO DE JANEIRO CLAY

Very soft plastic CLAY (LL≈ 125%, PI≈ 60%, LI≈1.55)

z(m)	h/R	σ'_{v0}	c_{u0}[1]	OCR	K_0	H_i[2]	$\Delta u_i/\sigma'_{v0}$	K_c[2]	K_c/H_i
4.0	25	12.6	6.5	2.0	0.65	3.1	2.9	0.78	0.25
5.2	14	16.6	7.8	1.8	0.61	2.8	2.7	0.70	0.25
6.6	1.0	21.1	9.5	1.7	0.60	-	5.2	-	-

[1] Peak vane shear strengths (kPa) but are probably comparable to UU strengths

[2] reported in the form $(\sigma_{ri} - u_0)/c_{u0} \approx 6$ and $\sigma'_{rc}/c_{u0} \approx 1.5$.

PILE TESTS IN SAN FRANCISCO BAY MUD

PI ≈18%, OCR ≈1-1.4, K_0 ≈0.55

z (m)	σ'_{v0} (kPa)	c_{u0}[1] (kPa)	h/R	H_i	$\Delta u_i/\sigma'_{v0}$
4.3	20	9	36	0.97	-
4.9	32	10	28	1.52	-
5.5	43	11.5	20	-	-
6.1	56	13	12	-	-
6.7	70	14	4	2.43	2.0

[1] Based on limited unconfined compression triaxial data

[K_c values are considered unreliable (ranged from 0.14-0.54)]

PILE TESTS IN BEAUMONT CLAY

Stiff insensitive clay which had been overconsolidated by desiccation

z (m)	σ'_{v0} (kPa)	c_{u0} (kPa)	K_0[1]	OCR[1]	h/R	K_c[2]	
5.8	79	85	1.3	6	54	3.5	(PI≈ 45%, LL≈68%)
10.4	127	160	1.0	4.5	21	2.0 ± 0.6	(PI ≈15%, LL≈30%)
12.5	148	160	0.9	4	5	2.2 ± 0.6	

[1] Based on oedometer and pressuremeter test results

[2] Values for single and group piles

Table B16 Pile tests in Rio De Janeiro, San Francisco & Beaumont clays.

APPENDIX C

SPM / MIT - E3 PREDICTIONS FOR THE ICP TESTS AT BOTHKENNAR

CONTENTS OF APPENDIX C

SPM/MIT-E3 PREDICTIONS FOR THE ICP TESTS AT BOTHKENNAR

C1.0 INTRODUCTION 542

C2.0 MIT-E3 PARAMETER SELECTION 542

C3.0 COMPARISON OF MEASUREMENTS WITH PREDICTIONS 545

- C3.1 General 545
- C3.2 Predictions for installation & equalisation 546
- C3.3 Predictions for load testing 549
- C3.4 Discussion 550

C4.0 CONCLUSION 551

C1.0 INTRODUCTION

This Appendix considers the potential of the Strain Path Method (SPM), used in conjunction with the MIT-E3 soil model, as an analytical tool for predicting the behaviour of displacement piles in low OCR clays. Comparisons are presented between the predictions made with this method and the field data obtained in the ICP tests at Bothkennar.

Two sets of SPM/MIT-E3 analyses were performed by Prof. Andrew Whittle at the Massachusetts Institute of Technology (MIT), (Whittle 1991):

(i) The first set were carried out prior to the pile tests at Bothkennar and are referred to as 'Class A' predictions. These were based on site investigation data provided by Imperial College (IC) and the Geotechnical Consulting Group (GCG) to Prof. Whittle, although his interpretation of the data differed from that suggested by IC/GCG.

(ii) Following an initial (and unfavourable) comparison between the 'Class A' predictions and the field measurements, it was suggested that the parameter selection might not have been appropriate. The basis for a new analysis was agreed at a meeting with Prof. Whittle at IC and an updated set of 'Class C' predictions were made. The revised input parameters were closer to those suggested originally and also made use of laboratory data that was not available for the 'Class A' analysis.

Full details of the principles, assumptions and limitations of SPM/MIT-E3 analyses are provided in Section 2.3. The properties of Bothkennar clay are described in Section 5.3 and the results from the ICP tests are presented in Chapter 8.

C2.0 MIT-E3 PARAMETER SELECTION

The input parameters used by the MIT-E3 soil model in the Class A and Class C predictions are given in Table C1, which also provides a

description of each parameter. Over half of these variables (C, n, h, c, s_t, ω, γ, ψ_0) were determined using special computer aided techniques, developed at MIT, which effectively curve fit laboratory test data.

Test Type	Parameter/ Symbol	Physical contribution/ meaning	Boston Blue Clay	Bothkennar Clay January 1991	Bothkennar Clay November 1991
1-D Consolidation (Oedometer CRS, RF etc.)	e_0	Void ratio at reference stress on virgin consolidation line	1.12	1.75	1.55
	λ	Compressibility of virgin normally consolidated clay	0.184	0.483	0.365
	C	Non-linear volumetric swelling behaviour	22.0	2.4	10.0
	n		1 6	3.0	1.75
	h	Irrecoverable plastic strain	0.2	2.5	1.0
K_0-oedometer or K_0-triaxial	K_{0nc}	K_0 for virgin normally consolidated clay	0 48	0.52	0.52
	2G/K	Ratio of elastic shear to bulk modulus (Poisson's ratio for intial unload)	1.05	0.92	0.92
Undrained Triaxial Shear Tests:	ϕ'_{TC}	Critical state friction angles in triaxial compression and extension (large strain failure criterion)	33.4^0	42.0^0	35.0^0
	ϕ'_{TE}		45.9^0	42.0^0	38.0^0
OCR=1; CK_0UC	c	Undrained shear strength (geometry of bounding surface)	0.86	1.00	1.1
OCR=1; CK_0UE	s_t	Amount of post-peak strain softening in undrained triaxial compression	4.5	10.0	4.2
OCR=2; CK_0UC	ω	Non-linearity at small strains in undrained shear	0.07	0.5	0.1
	γ	Shear induced pore pressure for OC clay	0.5	0.2	0.4
Resonant Column*	κ_0	Small strain compressibility at load reversal	0.001	0.002	0.005
Drained Triaxial	ψ_0	Rate of evolution of anisotropy (rotation of bounding surface)	100 0	100.0	100.0

* Alternatively use field data from cross-hole shear wave velocity type tests.

Table C1 MIT-E3 input parameters for Bothkennar clay

Bothkennar clay was deposited in a low energy sedimentary environment before being aged and weakly cemented. This specific history gave the undisturbed clay properties which are different to those observed after large strain shearing disturbance, or consolidation beyond yield. The extensive studies reported by Smith (1992) and Smith et al (1992) show

that the clay's behaviour is not normalisable in terms of stress and water content over the stress range applying to the Bothkennar ICP tests. Therefore, a decision had to be made as to whether the input parameters should reflect the characteristics shown in laboratory tests on the undisturbed clay or those shown in SHANSEP type tests (see Ladd & Foott 1974), where samples were consolidated under K_0 conditions to stresses higher than those acting in situ.

The Class A predictions were made on the basis of the undisturbed properties, whilst the Class C analysis used parameters (principally) from the SHANSEP type tests. The laboratory tests used to derive the input parameters (Table C1) are listed in Table C2.

Parameters	Class A	Class C
e_0, λ , h	restricted flow (RF) oedometer tests	standard (incremental load) oedometer tests
ϕ'_{tc}, ϕ'_{te} s_t, c, ω, γ	CK_0U triax. tests on intact Sherbrooke block samples	CK_0U triax. SHANSEP tests (i.e. OCR =1)
C, n	RF oedometer tests	Isotropic swelling of intact samples

Table C2 Laboratory tests used for parameter selection

The basis for the selection of parameters for the revised 'Class C' predictions was agreed at a meeting at IC with Prof. Whittle and was prompted by:

- the availability of more extensive laboratory test data which helped both with improving our understanding of the material and the derivation of parameters.

- agreement that the RF oedometer test is difficult to interpret and that the data from the more consistent maintained load oedometer

tests should be used.

- acknowledgement that the (haematite) cementation, which makes a very important contribution to the sensitivity, compressibility and peak strength of the intact clay, will not have a significant influence on the characteristics of the material adjacent to the pile as it will be destroyed by the process of installation.

These factors had the effect of assigning the Class C material a (i) significantly lower sensitivity, (ii) lower value of ϕ'_{tc}, (iii) lower virgin compressibility, (iv) more linear variation of stiffness with strain and (v) higher small strain stiffness.

C3.0 COMPARISON OF MEASUREMENTS WITH PREDICTIONS

C3.1 General

The notation used to compare the field measurements with the predictions is given in Table C3. Subscripts i, c and f are used to denote values of these parameters at the completion of installation, after full equalisation and at peak capacity in load tests respectively.

Normalised radial total stress	H	$= (\sigma_r - u_0)/\sigma'_{v0}$
Excess pore pressure ratio	$\Delta u/\sigma'_{v0}$	$= (u - u_0)/\sigma'_{v0}$
Lateral stress coefficient	K	$= \sigma'_r/\sigma'_{v0}$
Peak obliquity	δ_p	$= [\tan^{-1}(\tau_{rz}/\sigma'_r)]_{max}$
Skin friction ratio	ρ	$= (K_f/K_c) \tan \delta_p$

Table C3 Notation

The following points regarding the comparison should be noted:

- The pile test programmes performed with the ICP at three clay sites, including Bothkennar, have shown that the stresses developed on the pile shaft are influenced strongly both by the initial OCR

of the material and the relative depth of the pile tip (h/R). SPM analyses also predict a strong dependence on OCR but suggest that the stresses are relatively independent of h/R for h/R ≥15 (see Figure 10.1). The four ICP's installed to 6m depth at Bothkennar provided measurements of σ_r, u and τ_{rz} at h/R ≈8, 28 and 50. Data recorded at h/R ≥ 28 (z ≤ 4.6m for L=6m) were found to be practically independent of the relative depth of the pile tip and it is these data that are compared with the SPM/MIT-E3 predictions.

- The average OCR at Bothkennar at the relevant soil depths (3-4.5m) is 1.7 ± 0.2. Comparisons are made with the mean value predicted by the analyses, which were performed for OCR's of 1.5 and 2.0.

- SPM/MIT-E3 radial coupled consolidation analyses present data during equalisation (at time 't' after installation) in terms of the time factor T_p defined as : $[p'_0\ k_h\ t]/[\gamma_w\ R^2]$. A mean initial effective stress (p'_0) of 25kPa and a permeability (k_h) of 1 x 10^{-9} m/s were selected for comparison purposes. The p'_0 value corresponds to that at the trailing instrument position (h/R=50) at a depth of 3.5m and the k_h value was assessed from pushed piezometers and self-boring permeameter tests at the depths of interest (GCG 1990).

C3.2 Predictions for pile installation and equalisation

Table C4 compares predictions and measurements for installation and equalisation using the normalised parameters defined in Table C3. The factors r_a and r_c represent the ratios of the predicted to measured values for Class A and Class C analyses respectively.

Parameter	Measured (h/R ≥30)	Class A	Class C	r_a	r_c
H_1	2.30	1.88	1.93	0.82	0.84
$\Delta u_1/\sigma'_{v0}$	2.10[1]	1.80	1.62	0.80	0.72
K_1	-	0.08	0.31	-	-
t_{50} (hrs)[2]	16.7	6.9	14.6	0.36	0.86
K_c	1.00	0.40	0.97	0.40	0.97
K_c/K_1	-	5.0	3.12	-	-
$K_c(=H_c)/H_1$	0.44	0.21	0.50	0.48	1.14

Table C4 Pile installation and equalisation results

It is evident that:

- The Class A analysis under-estimates installation H_1 and $\Delta u_1/\sigma'_{v0}$ values and over-estimates the reduction in radial total stresses during equalisation. These effects lead to a K_c value which is only 40% of that measured.

- The Class C analysis under-estimates the installation stresses by ≈20%, but predicts a higher than measured relaxation coefficient (K_c/H_1). The net result is that the calculated value of K_c is almost identical to the mean value measured at h/R ≥30.

The predicted variations of the pore pressure factor ($\Delta u/\Delta u_1$) and the radial total stresses (as described by H/H_1) during equalisation are compared with measured variations on Figure C1.

[1]Recorded 1 min after installation. Ratios of $\Delta u_1/\sigma'_{v0}$ of ≈1.6 were recorded whilst jacking was in progress but these may be misleading because of a rate effect on the pore pressure measurements at high pile velocities (see Chapter 8 and Appendix A).

[2]t_{50} = time for dissipation of 50% of excess pore pressures.

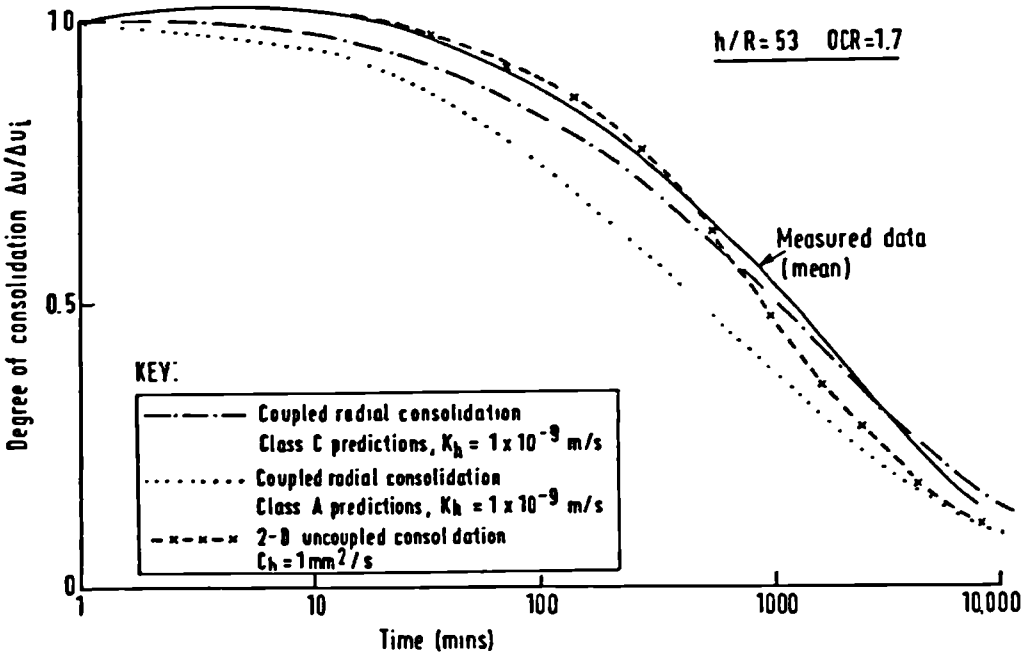

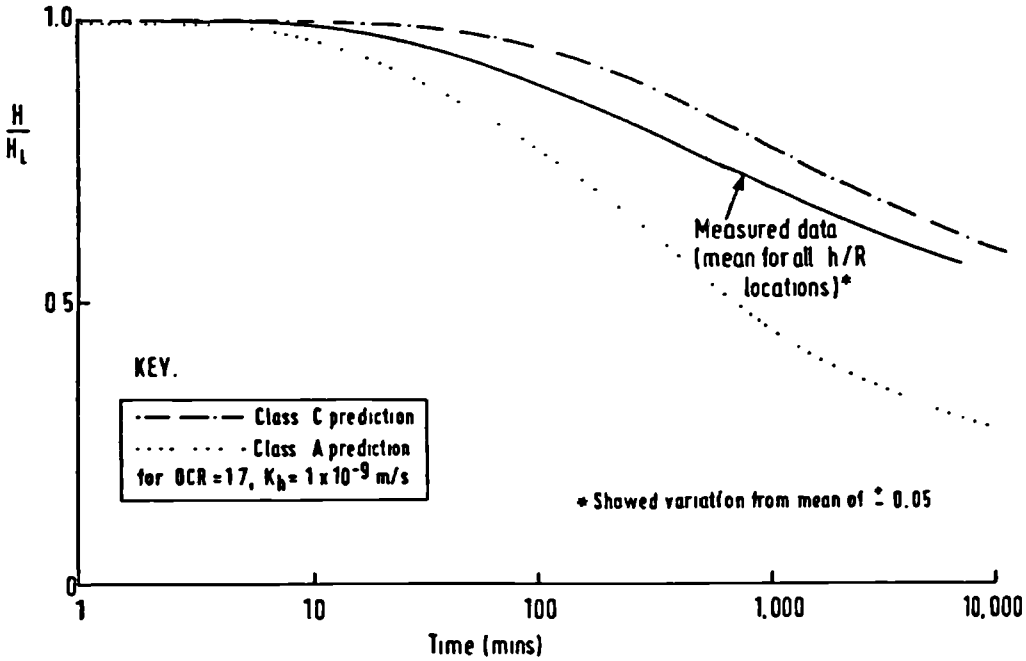

Figure C1 Predicted and measured trends during equalisation

It is clear that the predictions for equalisation made by the Class C analysis are in close agreement with the measurements and therefore its accurate assessment of K_c cannot be considered as fortuitous. It is also evident that the coupled consolidation analysis (in which the total stresses and coefficient of consolidation (c_h) vary with radius and time) describes the form of the dissipation curves more precisely than the uncoupled analysis, where c_h is assumed constant throughout equalisation[1].

C3.3 Predictions for load testing

Predictions of the key parameters for undrained compression pile loading to failure are compared with the measured values in Table C5. The associated 'effective stress paths' are compared in Figure C2.

Parameter	Measured	Class A	Class C	r_a	r_c
δ_p(°)	28.5	24.8	23.7	0.87	0.83
K_f/K_c	0.87	0.74	0.7	0.85	0.80
ρ	0.47	0.35	0.31	0.74	0.66

Table C5 Failure parameters in load tests

It is apparent that both Class A and Class C analyses over-predict the reduction in radial effective stress that takes place during loading (i.e. K_f/K_c) and under-predict δ_p. These effects lead to an under-prediction of ≈30% in the skin friction ratio (ρ).

The deviation from the measured behaviour is most pronounced post-peak, where the analyses indicate behaviour analogous to that observed in DSS tests (i.e. normal effective stresses continuing to decrease while the obliquity increases). The post-peak measurements are in fact more compatible with the development of a principal displacement shear close

[1]A 2-D uncoupled analysis indicated that, at h/R ≥15, the consolidation process was governed by radial consolidation only. Dissipation rates were considerably faster closer to the pile tip where both vertical and radial drainage occurred.

to the shaft and a departure from continuum behaviour.

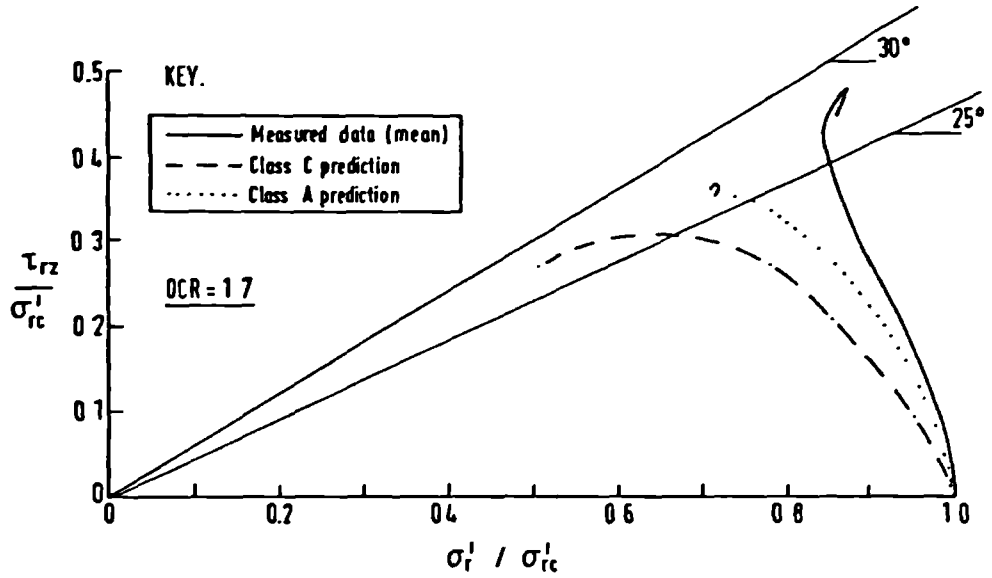

Figure C2 Predicted and measured trends for undrained pile load tests (after equalisation)

C3.4 Discussion

It is clear from the foregoing that, for a given material, the SPM/MIT-E3 predictions are very sensitive to the choice of soil parameters. However, because of the inter-dependent nature of these parameters, it is difficult to determine those which have most influence on the predictions.

Some insight into the method was obtained in Section 2.3 by comparing the results of the predictions for Bothkennar Clay with SPM/MIT-E3 predictions reported for other clay types (Boston Blue Clay, Empire Clay, Haga Clay and London Clay). This parametric study revealed:

- The radial total stress parameter, H_1, is most strongly dependent

on OCR. Despite wide differences between the soil types, over 90% of the predictions fall within 10% of the relationship $H_1 = 1.3\ OCR^{0.55}$ (see Figure 2.11).

- The relaxation coefficient (H_c/H_1) decreases with the sensitivity of the clay and increases with OCR. The predicted K_c ($=H_c$) values, which are critical to the evaluation of shaft capacities, are therefore primarily functions of sensitivity and OCR (see Figure 2.13). Although other parameters, such as λ, κ_0 and ϕ', are undoubtedly important to predictions, it appears that, in the analyses performed to date, these values have been specified so as to compensate for the prescribed sensitivity.

The Class A analysis derived key input parameters from tests on intact block samples. These samples exhibited greater sensitivity and compressibility than the partially destructured samples (i.e. as measured in SHANSEP tests), the properties of which were used to derive parameters for the Class C analysis. The parametric study therefore explains how these two means of determining input parameters gave the wide differences between the Class A and Class C predictions. The high accuracy of the Class C analysis suggests that pile behaviour is modelled more accurately using the properties of the *partially destructured*, less sensitive, material.

C4.0 CONCLUSION

The main conclusions arising from this study are:

(i) SPM/MIT-E3 predictions depend significantly on the choice of laboratory tests to derive input parameters.

(ii) The Class C analysis used parameters derived from tests on partially destructured clay. The predictions for $h/R \geq 30$ matched both the magnitudes and trends of the field measurements made during installation and equalisation with a high degree of accuracy.

(iii) The Class C analysis did not predict the extent to which the measured stresses increased with reducing h/R.

(iv) The Class A analysis was based on input parameters derived from laboratory tests on undisturbed intact clay behaviour. Here, the predicted stresses were in poor agreement with the measurements at all h/R's.

(v) The numerical predictions for pile loading were not particularly realistic. This may partly be because (a) the MIT-E3 does not model interface slippage or sliding on a residual surface and (b) the predictions for the equalised vertical and circumferential effective stresses after equalisation are in error.

Despite these points of quantitative detail, it can be concluded that the method offers significant promise as a tool for identifying and understanding the parameters that control the behaviour of displacement piles in low OCR clays.

APPENDIX D

DIRECT SHEAR INTERFACE TESTS

CONTENTS OF APPENDIX D

DIRECT SHEAR INTERFACE TESTS

D1.0 INTRODUCTION 556

D2.0 RESEARCH USING THE RING SHEAR APPARATUS..... 557

D2.1 The ring shear apparatus 557

D2.2 Shearing modes 558

D2.3 Research by Lemos & Tika 559

D3.0 TEST PROCEDURES 562

D3.1 Sample preparation 562

D3.2 Interfaces 563

D3.3 Ring shear procedures 563

D4.0 RING SHEAR INTERFACE TESTS ON LABENNE SAND 564

D5.0 RING SHEAR INTERFACE TESTS ON COWDEN TILL 567

D5.1 Slow shearing steps 567

D5.2 Fast shearing steps 567

D5.3 Sample inspection 569

D6.0 RING SHEAR TESTS ON BOTHKENNAR CLAY 570

D6.1 Slow shearing steps 570

D6.2 Fast shearing steps 573

D7.0 SHEAR BOX TESTS ON LABENNE SAND 575

D7.1 Soil-interface tests 575

D7.2 Soil on soil tests 577

D1.0 INTRODUCTION

An important aspect of my research was to compare the coefficients of friction mobilised on the shaft of the ICP with coefficients measured in laboratory direct shear interface tests. To this end, a number of 'pile modelling' ring shear interface tests were performed with Labenne sand, Cowden till and Bothkennar clay. These tests are described in full in this Appendix and compared with the ICP test results in Chapters 9 and 10.

During installation, soil elements adjacent to a displacement pile undergo large relative displacements at very fast shearing rates. The Imperial College (IC) ring shear apparatus was developed to study the behaviour of soils after large shear displacements and is therefore suited ideally to assessing the coefficients of friction appropriate to displacement piles. Tika-Vassilikos (1991) and Bond (1989) found good agreement between the friction angles measured in ICP tests in the London Clay and those measured in ring shear interface (RSI) tests, but only when these tests modelled the correct (a) displacement history (b) normal stress level and (c) properties of the interface; these three parameters were modelled in the RSI tests described in this Appendix.

The procedures followed in all the RSI tests are outlined in Section D3 and the results from the tests on Labenne sand, Cowden till and Bothkennar clay are presented in Sections D4, D5, and D6 respectively. Previous research with the ring shear apparatus at IC is briefly summarised in Section D2.

Two further sets of direct shear tests, which were performed to assist interpretation of the ICP tests, are also described:

- Ring shear soil on soil tests on Bothkennar clay (Section D6)
- Shear box soil on soil and soil-interface tests on Labenne sand (Section D7)

All experimental data are presented in Tables D1-D5 and Figures D10-D17 at the end of this Appendix. Summary plots are included within the text.

D2.0 RESEARCH USING THE RING SHEAR APPARATUS

D2.1 The ring shear apparatus

The design and principles of the ring shear apparatus (RSA) have been described by Bishop et al (1971), Lupini (1981) and others. A simplified section through the apparatus is shown on Figure D1.

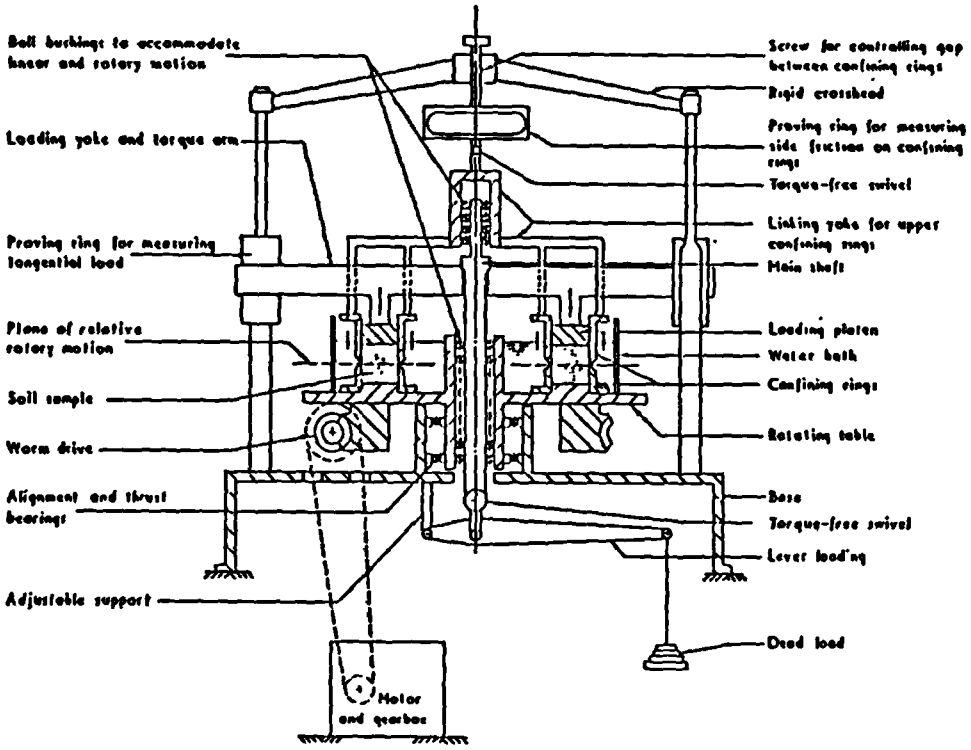

Figure D1 The Imperial College ring shear apparatus

An annular shaped sample (external diameter =152mm, internal diameter =102mm) is sheared on a plane of relative rotary motion at mid-height of the sample, while being confined laterally and subjected to a constant normal stress. The lower half of the sample (or a replacement interface) rotates, whilst the upper half remains fixed and reacts, through a torque arm, against a pair of load cells at each end of the arm; these load cell measure the torque applied to the sample. Side friction between the sample and the upper confining ring is measured by another load cell, so

that the normal force acting on the shearing plane is known precisely. All data are recorded automatically by a data logger.

D2.2 Shearing modes

The research with the RSA at IC has shown that soils in direct shear exhibit one of four shearing modes (Lupini et al 1981):

(a) *Sliding*

This mode is dominant in high plasticity clays with a high clay content. A low strength shear surface of strongly orientated platy particles is formed and shearing is by sliding of clay minerals over each other. The shear surface of aligned clay minerals, once formed, is not affected significantly by subsequent shearing.

(b) *Turbulent*

This mode is dominant in materials with a low clay content and possessing a high proportion of rotund particles. Shearing is by rotation of the large fraction of silt and sand particles and interference between these particles prevents the clay minerals from adopting a preferred orientation in the shear zone. The resistance of a given shear surface may be modified by subsequent shearing which can change the porosity in the shear zone.

(c) *Transitional*

This mode involves both turbulent and sliding behaviour in different parts of the shear zone and occurs in materials of intermediate plasticity and clay content. The shearing characteristics are *very* sensitive to small changes in clay content.

(d) *Interface sliding*

Materials that exhibit a turbulent or 'transitional tending towards turbulent' shearing mode in soil on soil shear may exhibit a sliding characteristic if sheared against an interface. This can occur as a flat interface may prevent the interference of massive particles and allow clay particles to align.

Lupini et al. (1981) suggest that the best index for the assessment of the shearing mode and residual friction angle is the granular void ratio of the material (e_g)[1] and produced the plot shown on Figure D2, which sets limits for the residual stress ratio (τ/σ'_{nc}) for each shearing mode and value of e_g.

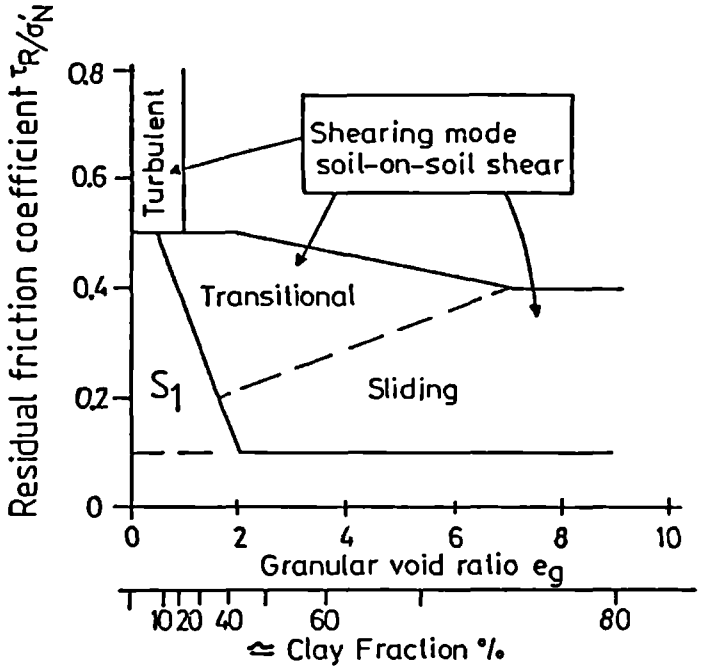

S_1 Possible sliding shear when soil is failed against a smooth interface.

Figure D2 Dependence of residual stress ratio on e_g

D2.3 Research by Lemos and Tika

Further research in a wide range of clay soils by Lemos (1986) and Tika (1989) quantified the importance of various parameters which contribute to the wide ranges on Figure D2. These parameters include soil mineralogy, fabric & grading, history of relative displacement, normal stress level and interface roughness & hardness.

[1]This ratio relates the volume of platy clay particles to the volume of remaining particles.

Friction angles (δ) of clay soils measured by Lemos and Tika in drained stages of ring shear 'pile-modelling' *interface* tests are plotted on Figure D3[1]. In each case, drained shearing was preceded by a fast shearing stage, which subjected samples to a relative displacement of ≥200mm at velocities between 100 and 1000mm/min. This pre-shearing step modelled the displacement history of soil elements adjacent to a jacked pile during installation. Figure D3 shows that for the specific range of materials, pre-shearing rates, normal stresses and interfaces considered:

- Both the peak and post-peak friction angles (δ_p, δ_{ult}) reduce by a factor of about 2 for an increase in plasticity index from 10% to 45%.
- the fast pre-shearing stage induces an initial peak angle (δ_p) which is typically ≈2.5° larger than the post-peak ultimate value (δ_{ult}).

These observations are by no means general to all the data measured by Lemos and Tika. For example, the residual angle for an interface with a CLA roughness of 0.005μm may be only half of the equivalent value plotted on Figure L3 and this angle can depend significantly on the previous displacement of the sample. Glass interfaces generally tend to give higher residual angles than steel interfaces of equal roughness and the angles appear to be moderately dependent on the normal stress level for σ'_{nc} <200kPa. While Figure D3 may provide an approximate estimate of the likely friction angles operating during slow shear adjacent to typical industrial piles, the research has shown that an accurate assessment of these angles, for a given soil under certain conditions, can only be made by direct measurement.

[1]The soils tested included Lower Cromer & Magnus till, London clay and a range of siltstones. Note also that δ is defined as: $\tan^{-1}(\tau/\sigma_{nc})$, where τ= applied shear stress and σ'_{nc} = normal effective (consolidation) stress.

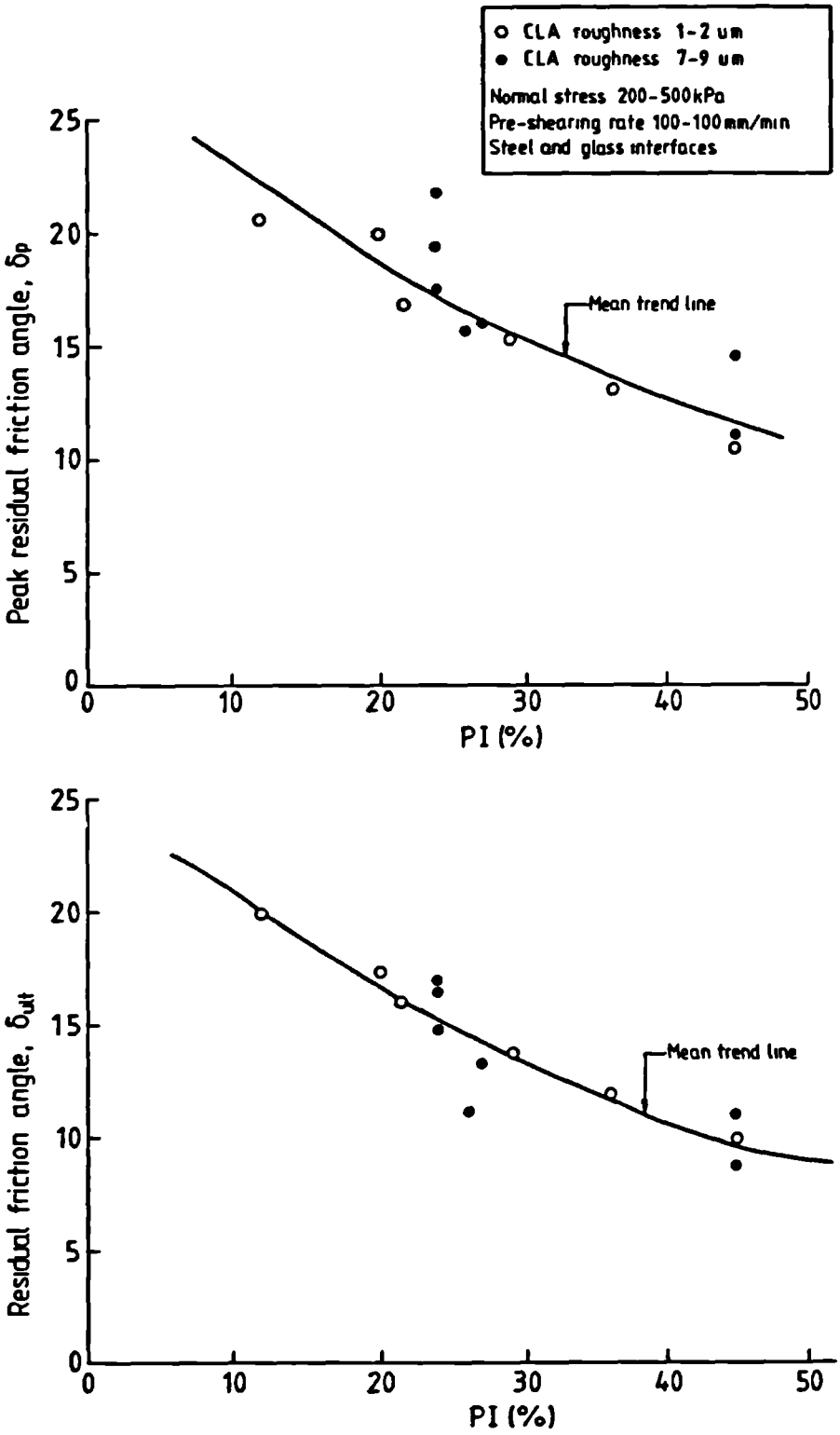

Figure D3 Correlation between δ_p & δ_{ult} and PI for displacement piles

The ring shear tests described in this Appendix and additional ring shear tests reported by Jardine & Ridley (1992) confirmed the approximate nature of the correlation on Figure D3 and, in particular, showed that:

(i) The δ_{ult} value of Bothkennar clay with a PI value of 48% is 31°±2° (for a steel interface with a CLA roughness ≈8.5μm). This angle is over 20° higher than that suggested by Figure D3 (see Section D6).

(ii) A wide range of δ values can be mobilised by clays of low to medium plasticity (PI <25%) because of their high sensitivity to the properties of the interface.

D3.0 TEST PROCEDURES

D3.1 Sample preparation

Labenne sand: A large range of relative densities were investigated in the tests on the Labenne sand (mostly in shear box interface tests) and the following methods of placing the sand in the apparati were used:

(i) Dropping dry sand from a height of 40mm through a funnel with a tip diameter of 8mm. This method gave relative densities in the range 45% to 60%.

(ii) Tamping moist sand in 3 layers with ≈200 tamps per layer. Relative densities of up to 80% could be achieved by this means.

These densities were varied by altering the funnel diameter or drop height when using method (i) and by varying the compactive effort when using method (ii). Samples were also vibrated to alter their densities.

Cowden till: The till (LL=40%, PI=20%) was first dried to allow the fraction greater than 0.6mm to be removed by sieving and then remoulded at a water content of 22% before placement in the apparatus. Subsequent consolidation of the sample reduced the water content to 19.5%, which is comparable to that of the in-situ material.

Bothkennar clay : The sample used for the test series on Bothkennar clay was a Laval piston sample from 5.0m depth with a LL=80%, PI=48% and organic content of 3.4%. The material was remoulded by hand and placed in the RSA. The remoulding process reduced the water content from the in-situ value of 71% to a value of 64% prior to consolidation.

D3.2 Interfaces

The ring shear interfaces were made from stainless steel annuli and were shotblasted, prior to each use, to a centreline average (CLA) roughness of 8-9μm. This roughness is comparable to that of the surface stress transducers on the ICP and is also typical of industrial steel piles (Tika-Vassilikos 1991).

The interfaces used in shear box tests on Labenne sand were made from mild steel and varied in CLA roughness from ≈5.5μm to 9.5μm. A teflon interface (CLA ≈2μm) was also used to add further insight into parameters affecting the interface shear behaviour of sand.

D3.3 Ring shear procedures

Samples were consolidated under normal stresses (σ'_{nc}) comparable to the radial effective stresses developed on the ICP. The 'gap' between the upper confining ring and interface/lower confining ring was then opened to ≈0.3mm, and about 2 hours later, samples were subjected to a relative displacement in excess of 1.2m by a series of shearing pulses performed at a rate of ≈500mm/min. Each pulse was preceded by a pause period of ≈4 mins[1]. This stage simulated the displacement history imposed on soil elements adjacent to the shaft by pile jacking and was considered to be sufficient to ensure that residual conditions pertained in the shear zone.

---

[1]During pause periods, the 'gap' was opened and closed several times to reduce the friction between the sample and the upper confining ring. Despite adopting this procedure, the friction in some cases amounted to as much as 20% of the applied stress. Values of σ'_{nc} quoted herein have been corrected for side friction.

The samples were allowed consolidate for 24 hours before shearing at a slow (drained) rate, thereby simulating the load testing stage of the piles. The 'slow' rates were selected to ensure at least 95% dissipation of excess pore pressure over 1mm displacement. No difference in shearing resistance was observed when the rates were increased or reduced by a factor of 4, verifying the assumption of full drainage. Subsequent shearing steps varied the displacement rate and the normal stress, allowing periods for consolidation where appropriate.

It should be noted that pore pressures are not measured in routine RSA tests and, at fast rates of displacement, the effective stresses are unknown. At these rates, the normal effective stress is not necessarily equal to the consolidation stress (σ'_{nc}) and only information on the total stresses can be obtained.

A further feature of ring shear testing, which became apparent, was the inconsistent trends shown by the vertical movements of samples during shear. For example, in some situations where the shearing characteristics suggested that the sample dilated, the transducers measuring vertical movement indicated that the sample had contracted. This was because the tendency of sample to contract or dilate during shear was often masked by its settlement due to soil loss through the 'gap'.

Full descriptions of the techniques employed in ring shear testing are given by Lupini (1981), Lemos (1986) and Tika (1989).

D4.0 RING SHEAR INTERFACE TESTS ON LABENNE SAND

The two ring shear interface tests (Nos. 1 & 2) on Labenne sand were performed by Dr. T. Tika at IC; details of the shearing programme are provided in Table D1. The initial relative density of the samples (D_r) and CLA roughness of the interfaces (R_1) were 56% & 9.5μm in Test 1 and 80% & 7μm in Test 2.

The variations of the friction angle, δ [$=\tan^{-1}(\tau/\sigma'_{nc})$], with displacement during all shearing steps of the experiments are shown on Figure D4 and are summarised as follows:

- The shearing resistances mobilised in both experiments were closely comparable, despite the differences in the initial D_r and R_1 values[1].
- Slow shearing steps (at 0.042mm/min) mobilised a peak interface friction angle (δ_p) of 30.8° ±0.5° (see Table D3). Post-peak, this angle reduced by ≈2.5° and the samples exhibited a stick-slip shearing characteristic with δ varying by ±1.5° from a mean value of ≈28.5°. This mean value is 5° less than the constant volume angle (ϕ'_{cv}) of the sand in direct shear (see Section D7), indicating that the interface properties controlled the shearing resistance.
- A peak resistance was observed at the beginning of each fast shearing step (rate ≈530mm/min); this dropped very quickly to give a *total stress* δ value of 27° ±2.0°. All steps (except for the very first step in each experiment) showed comparable behaviour and there was not a systematic dependence of resistance on displacement.

The mean values of δ recorded in the fast and slow shearing stages are comparable, suggesting that, even at a rate of 530mm/min, conditions in the shear zone are essentially drained[2]. The slightly lower shearing resistance at high velocities may have been associated with (a) the generation of very small positive pore pressures or (b) a change to a 'dynamic' shearing mode which required less energy than the shearing mode at slower rates of displacement.

Inspection of the interfaces at the end of the experiments showed that their roughness had reduced by 2-3μm from the initial R_1 values (9.5μm and 7μm).

---

[1]Note that the density of the samples was likely to have changed during the course of the experiments due to loss of soil through the gap between the upper confining ring and the interface as well as due to contraction/dilation under shear.

[2]This was proved by the pore pressure measurements made during jacking (at 500mm/min) of the ICP at Labenne (see Figure 6.3).

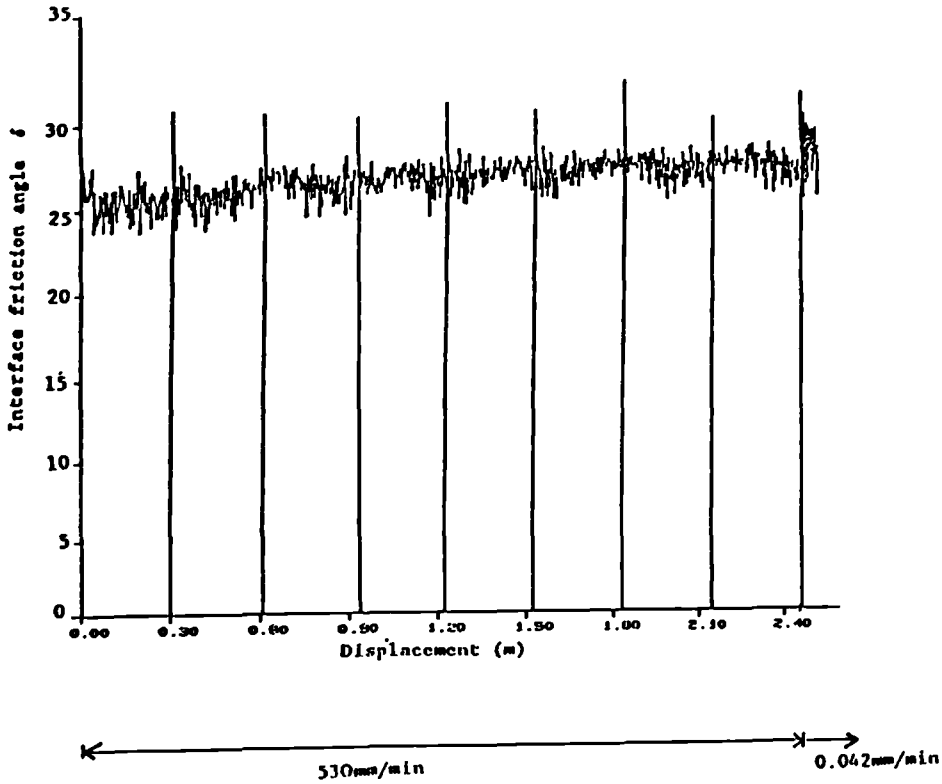

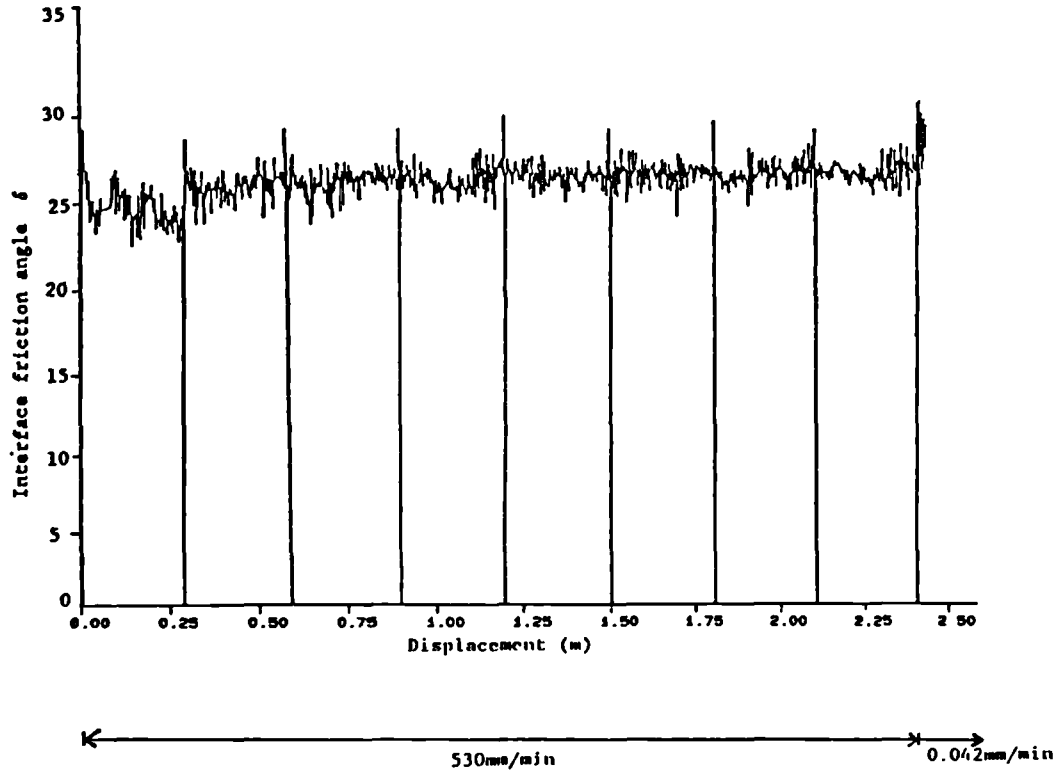

Figure D4 Ring shear interface tests on Labenne sand; Test 1 (top) and Test 2 (bottom); see Tables D1 & D3 for further details

D5.0 RING SHEAR INTERFACE TESTS ON COWDEN TILL

The results from the ring shear interface experiment conducted on Cowden till are given in Tables D1 & D3 and Figures D10-D12; trends observed during slow (drained) and fast shearing steps are described below.

D5.1 Slow shearing steps

Peak interface friction angles (δ_p) mobilised in slow (drained) tests after fast pre-shearing varied between 24° and 28° and were developed after relative displacements of ≈0.5mm. δ reduced subsequently and tended towards a relatively constant residual value (δ_{ult}) of 23° ± 1° after ≈2mm displacement. These angles are plotted against the pre-shearing rate on Figure D5(b), which suggests that the fast pre-shearing stage created a slightly disordered shear zone; continued slow shearing apparently overcame this disturbance. These characteristics are indicative of a *transitional tending towards turbulent* mode of shearing (see Section D2).

The δ_{ult} angles are slightly smaller than the soil on soil residual value of 25°, quoted by Lupini at al (1981), but are higher than the range of 13° to 20°, measured by Lemos (1986), for Cowden till sheared against a *smooth* glass interface.

D5.2 Fast shearing steps

It is apparent from Figures D10-D12 that during most fast shearing steps, a relatively large displacement (of between 50 and 300mm) is required before the stress ratio (τ/σ'_{nc}) achieves a steady maximum value. This effect may be due to the generation of (un-observed) negative excess pore pressures. Lemos (1986) observed a similar effect in interface tests with tills of low to medium plasticity and attributed the increase in resistance to the influence of abraded steel particles which force the shear zone to move progressively away from the interface and become embedded within the soil. This hypothesis does not, however, explain the general agreement between all fast shearing pulses measured at a given rate.

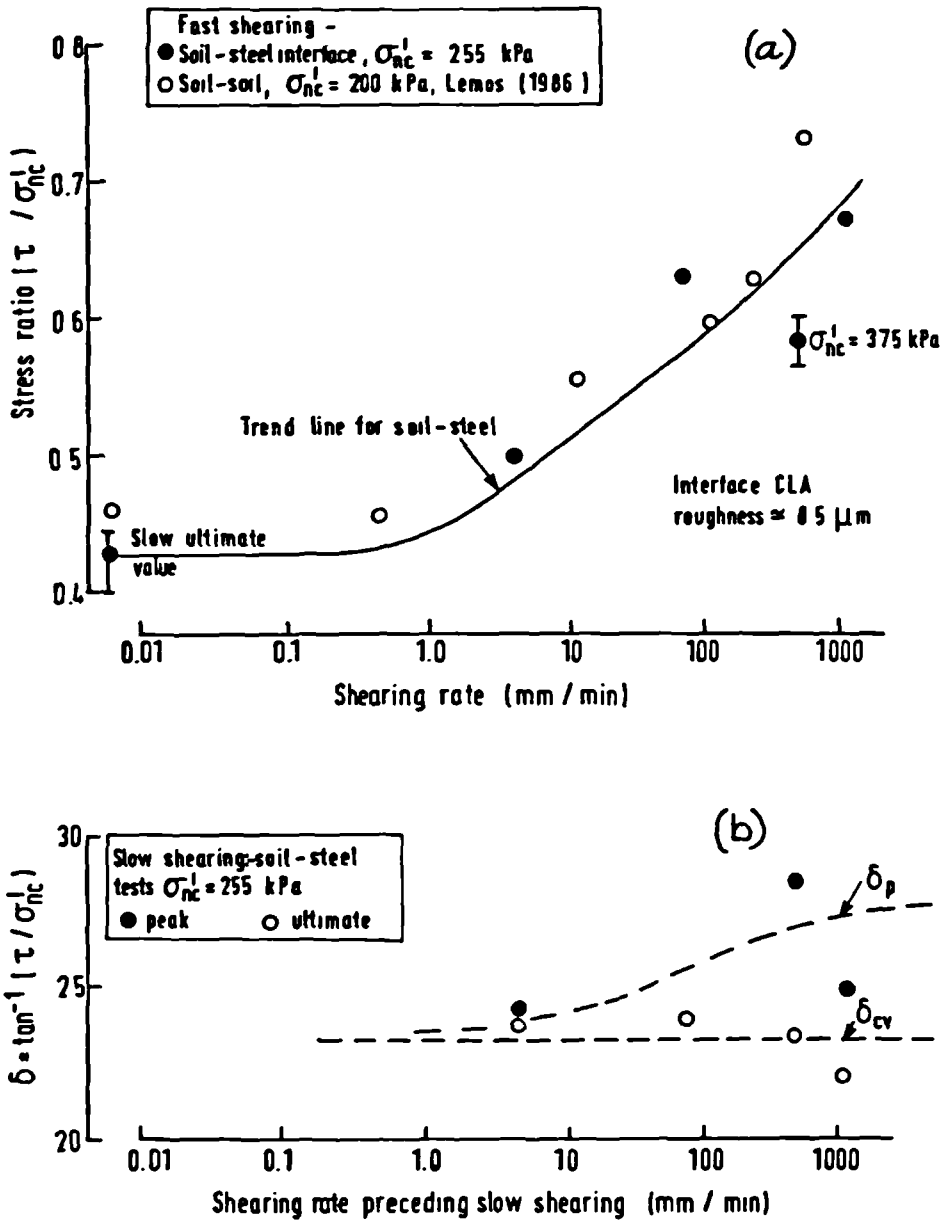

Figure D5 Trends shown by Cowden till in soil-steel interface shear

Figure D5(a) plots the *maximum* total stress ratios measured in each fast shearing step against displacement rate. A steep rate effect is observed for rates in excess of 1mm/min: increasing the velocity from 1mm/min to 1000mm/min increases the shearing resistance by ≈55%; soil on soil tests on Cowden till, performed by Lemos, showed a comparable trend.

The relatively constant ultimate friction angles (δ_{ult}) measured in subsequent slow shearing steps show that these rate effects are related primarily to transient phenomena such as the development of pore water suctions and viscosity. The data on Figure D5(b) suggest that there is also a small structural effect.

D5.3 Sample inspection

Inspection of the sample after the completion of the experiment showed that the soil surface in contact with the interface had not been polished and was discoloured by small particles abraded from the steel interface. The sample adhered to the interface and, when pulled away from it, tended to separate within the soil. These observations and the similarity between the shearing resistances measured in this test to those measured in soil on soil tests suggest that failure probably took place within the soil close to the interface.

The CLA surface roughness of the interface reduced from an initial value of 8.5μm prior to testing to 5.5μm at the end of the experiment. It is suspected that most of this change took place during the first fast shearing step, when the material was initially sorted at the interface. As seen on Figure D10, this step exhibited trends less characteristic of those recorded in all subsequent steps.

D6.0 RING SHEAR TESTS ON BOTHKENNAR CLAY

Extensive investigations into the properties of Bothkennar clay at the UK soft clay test bed site have been carried out (e.g. Hawkins et al 1989 and Hight et al 1992). However, no data on its residual strength characteristics have been reported.

The unusual composition of Bothkennar clay made the prediction of its behaviour in direct shear from the ring shear data base difficult. For material between 3.5m and 7m, the plasticity index (≈50%) and clay fraction (25-40%) hint that the sliding mechanism would predominate. However, two features of its composition suggest that a transitional/ turbulent shearing mode may be expected (see Paul et al 1991):

- The clay fraction is composed primarily of rock flour and kaolinite and contains a smaller percentage of platy particles than many other clay soils. In addition, the silt and fine sand particles are angular rather than rounded in shape.
- The clay's high plasticity index is strongly related to its organic content. When the organic matter is removed, the liquid limit falls to give a plasticity index of between 20% and 25%.

This uncertainty prompted a comprehensive series of both soil on soil and soil-interface ring shear tests on the Bothkennar clay, with the primary aim of assisting the interpretation of the ICP tests. The tests are also summarised by Lehane & Jardine (1992).

Three experiments were performed (two interface tests: nos. 2 and 3) and details of each shearing step and the measurements made are given in Tables D1-D4 and Figures D13-D15. The data obtained during slow (drained) and fast shearing steps are discussed separately below.

D6.1 Slow shearing steps

All slow shearing steps mobilised the peak friction angles shown on Figure D6(a) after a displacement of between 1mm and 5mm. The measurements are remarkably consistent, given that the data points

represent behaviour over a range of normal stresses and pre-shearing rates. The peak angles fall within 33° ± 1.0° and 31° ± 2.0° in soil on soil and soil-interface shear respectively.

Three of the eleven slow shearing stages exhibited post-peak brittleness, whilst no loss of strength was observed in the remaining eight[1]. This inconsistency gave the relatively large range in ultimate residual angles of 25-32° shown on Figure D6(b). In the cases where brittleness was observed, subsequent slow shearing stages, performed after a change in σ'_{nc} or intervals of faster shearing, indicated ultimate angles which were closer to the peak values shown on Figure D6(a). It thus appears that the degree of particle sorting that may be inferred from the lower ultimate residual angles was not a permanent feature controlling subsequent shearing behaviour and could be destroyed by fast shearing or variations in σ'_{nc}.

The close agreement between the soil on soil and soil-interface resistances indicates that the interface did not represent a plane of weakness. This was confirmed on inspection of the samples after the experiments which showed no evidence of interface slippage or change in interface roughness; the clay adhered firmly to the interface and tended to separate within the soil when pulled away from it.

The insensitivity of the peak and ultimate residual angles to the displacement history (after an initial displacement of ≥1200mm) suggests that Bothkennar clay has a *turbulent* shearing mode in both soil on soil and soil-steel shear (see Section D2).

---

[1]A more clay dominated fabric may have existed in the brittle steps. This is possible as the material within the shear zone of the RSA can change as soil is lost through the gap between the upper and lower halves of the apparatus. It was noted that by the end of the three tests, samples had reduced in thickness by ≈3mm due to loss of soil only.

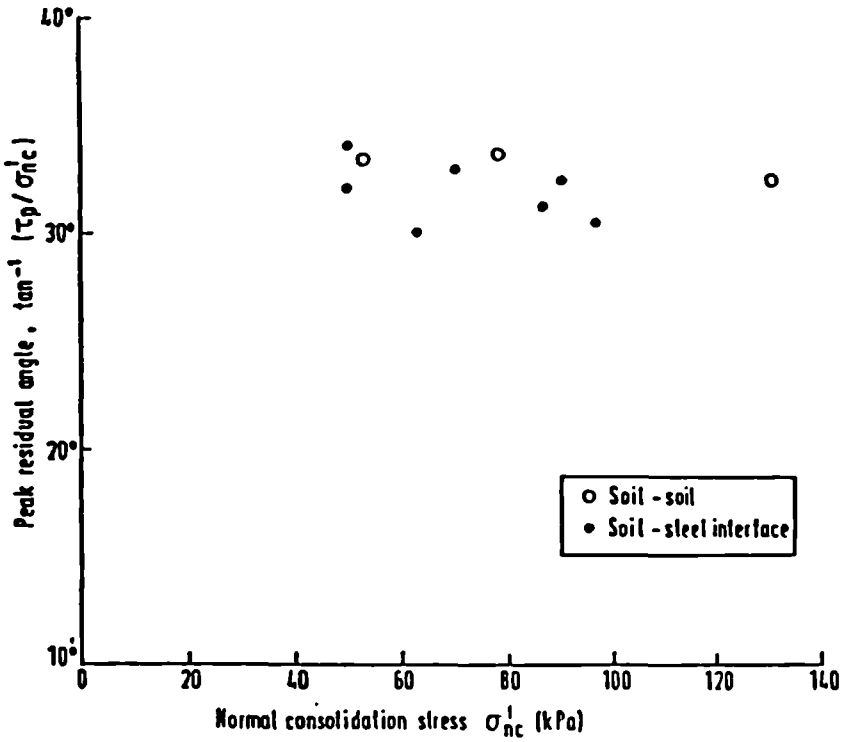

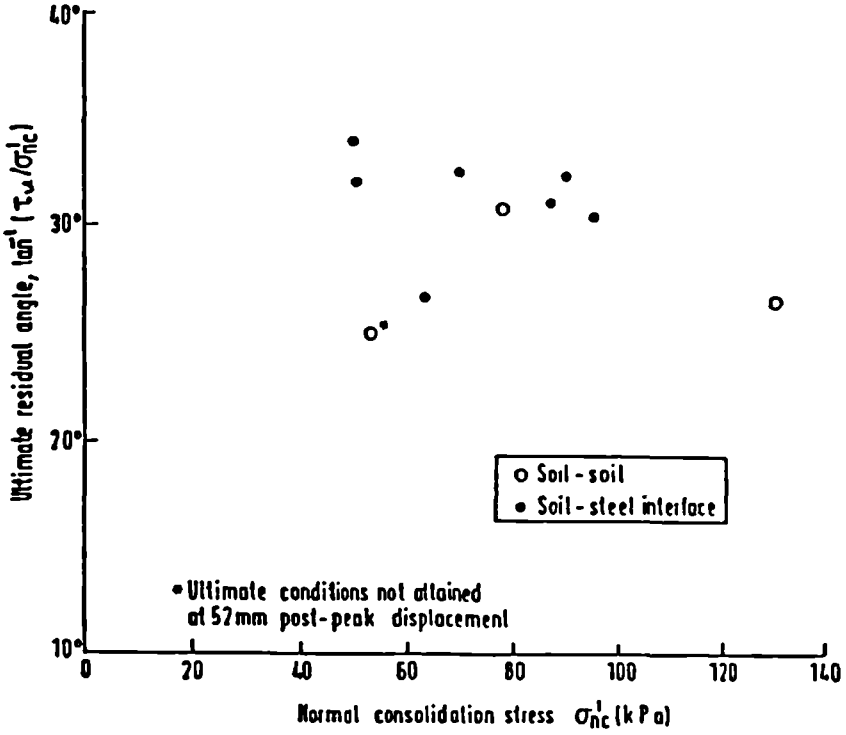

Figure D6 Peak and residual angles measured in ring shear soil-soil and soil-steel interface tests on Bothkennar clay

D6.2 Fast shearing steps

Samples were subjected to fast shearing at rates of between 2mm/min and 500mm/min prior to slow shearing steps. The fast steps were characterised by an initial peak in shearing resistance followed by a reduction to a constant ultimate resistance after a displacement of between 20 and 100mm. Although showing the same trends, the measured resistances show considerable variability between tests e.g. average ultimate total stress ratios (τ/σ'_{nc}) at the displacement rate of 500mm/min were 0.23, 0.30 and 0.39 in tests 1-3 respectively. Vaughan (1991) commented that such a large range is not untypical of measurements made during fast shear in the RSA and stated that the poor repeatability of the data recorded during fast shear in the apparatus is an anomaly which requires further research.

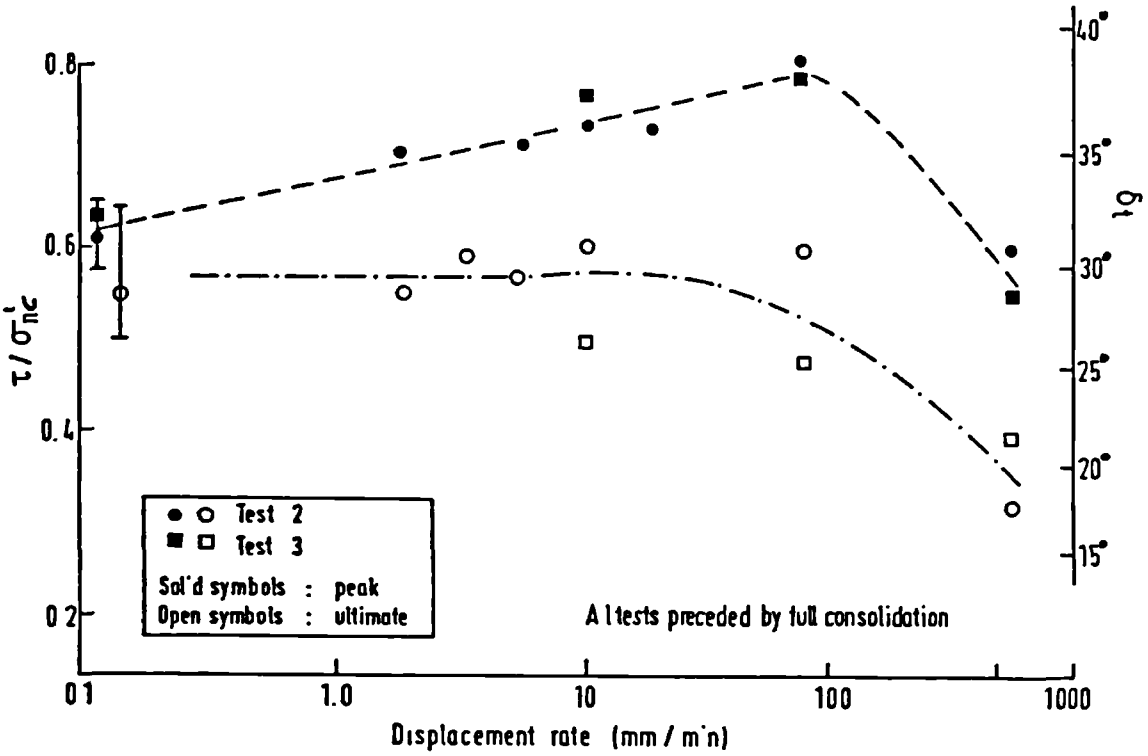

Figure D7 Rate dependence of Bothkennar clay in soil-steel ring shear interface tests

In spite of the poor degree of repeatability, a consistent trend, as shown on Figure D7, emerges when the peak and ultimate resistances (normalised by σ'_{nc}) are plotted against the displacement rate adopted in each shearing stage[1]. It is evident that:

- for velocities less than ≈100mm/min, resistances increase by ≈6% per log cycle increase in rate.

- Above a rate of ≈100mm/min, peak resistances drop with increasing rate and are less than the drained peak resistance at a rate of 500mm/min.

- Ultimate resistances show no significant rate effect at rates less than 100mm/min, but also reduce dramatically at faster rates.

The initial increase in peak resistances (or '*positive*' rate effect) has been measured for many soils and is attributed to viscous phenomena combined with variable degrees of particle sorting within the shear zone (Lemos 1986, Tika 1989). The '*negative*' rate effect at faster rates of displacement at first suggests that large excess pore pressures are generated at these rates. However, evidence presented by Lemos (1986) and Tika (1989)[2] indicate that the phenomenon may in fact be related to a transition from turbulent shearing mode to a dynamic mode, which dissipates less energy and involves the creation of a particularly high void ratio in the shear zone.

---

[1]For those shearing stages that were preceded, where necessary, by a period to allow for full consolidation.

[2]A limited series of ring shear tests were performed by Lemos (1986) and Tika (1989), where attempts were made to measure pore pressures at the interface in the RSA. Although these tests met with little success, the available data suggested that excess pore pressures were not generated during fast shear.

D7.0 SHEAR BOX TESTS ON LABENNE SAND

D7.1 Soil-interface tests

The arrangement used for the shear box interface tests on Labenne sand is shown on Figure D8. In total, 15 soil-interface tests were carried out using two mild steel interfaces and one teflon interface. The investigations sought to determine the influence of the initial sand relative density (D_r) and the roughness of the interface (R_i) on the magnitudes of the interface friction angles. The normal stresses used covered the range of radial effective stresses developed on the ICP at Labenne (40-120kPa)[1].

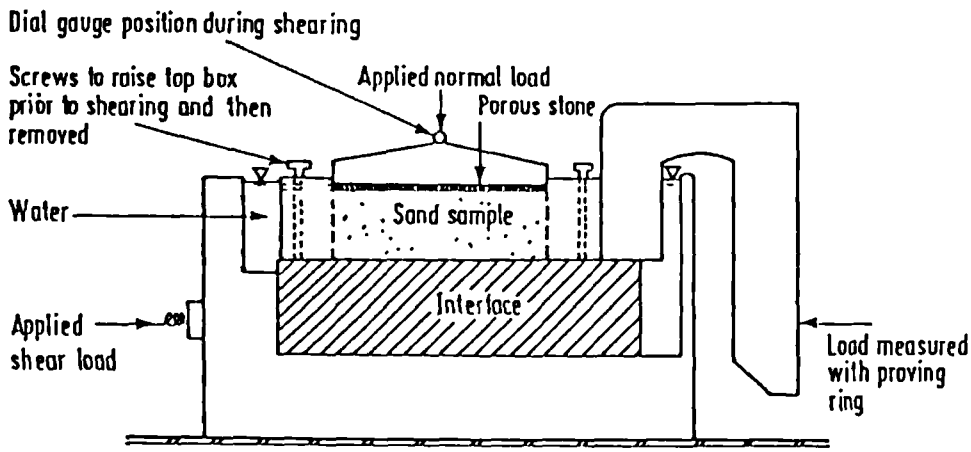

Figure D8 Shear box arrangement for interface tests

The results from the tests are su marised in Table D5; variations of the shear stress (τ) & vertical displacement (δh) with the displacement on the plane of shearing (δl) are plotted on Figure D16.

[1]The interface friction angles appeared to show a small dependence on the stress level, reducing typically be ≈2° when σ'_n was increased from ≈40kPa to ≈120kPa (see Section 9.5).

Points to note include:

- A peak value of shear stress does not occur for samples with an initial void ratio (e_i) of greater than 0.6 (D_r <60%) and the sand *contracts* (δh is negative) during shear.
- For e_i <0.6 (D_r >60%), peak values of shear stress are observed and the sand *dilates* during shear. Less brittleness is apparent for smoother interfaces.
- Shear stresses attain constant ultimate values when the samples cease dilating or contracting i.e. remain at constant volume.
- The characteristics measured in tests with the teflon interface are significantly different to those observed using steel interfaces, illustrating the importance of the relative hardness and texture of the interface.

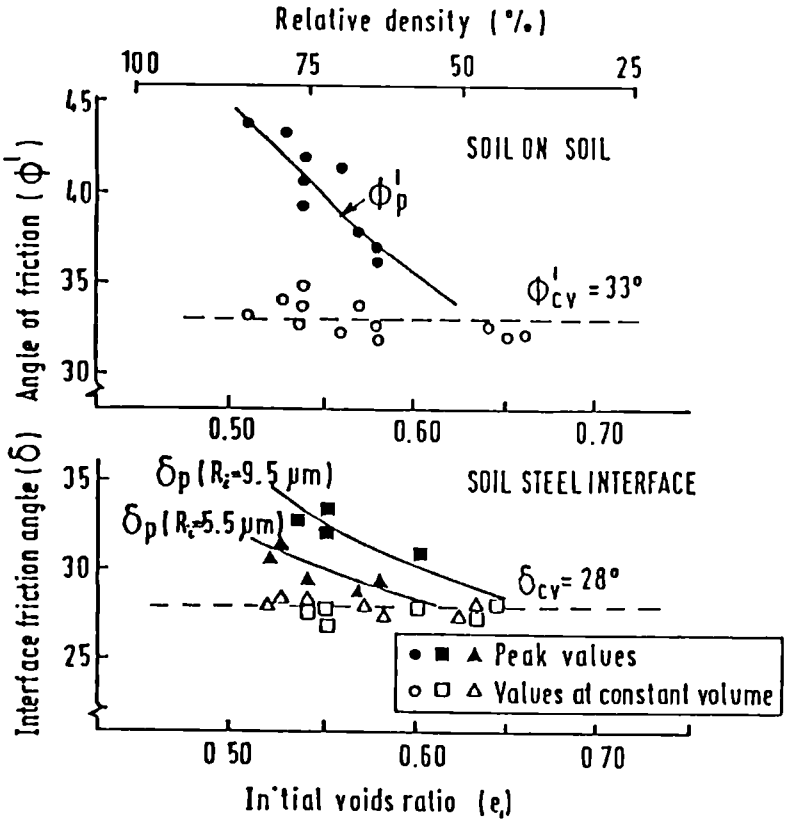

Figure D9 Friction angles measured in soil-soil and soil-steel shear box tests on Labenne sand

The values of δ [$=\tan^{-1}(\tau/\sigma'_n)$] derived from Figure D16 at maximum shear stress (δ_p) and when constant volume conditions were reached (δ_{cv}) are plotted on Figure D9 against the initial void ratio of the samples. It is evident that, while δ_p is moderately dependent on sand density and interface roughness, the ultimate, constant volume angle (δ_{cv}) appears to be independent of both of these parameters[1].

D7.2 Soil on soil tests

The shear box was also used to estimate the angle of friction (ϕ') of the Labenne sand for a range of initial densities. 12 tests were carried out and the measured variations of τ with δh and δl are shown on Figure D17. The measured peak and constant volume friction angles (ϕ'_p and ϕ'_{cv}) are listed on Table D5 and plotted on Figure D9 against e_i.

The data show trends typical of sub-rounded quartz sand (e.g. see Bolton 1986 and Cornforth 1973) and indicate that the direct shear constant volume angle (ϕ'_{cv}) is close to the static angle of repose of the sand and the angle measured during the final stages of triaxial tests (see Section 5.1.7.1). These data are compared with the results from soil-interface tests in Section 5.1.7.3

[1]but δ_{cv} for tests using a teflon interface ($R_i \approx 2\mu m$) was only 20.5° ± 0.6°.

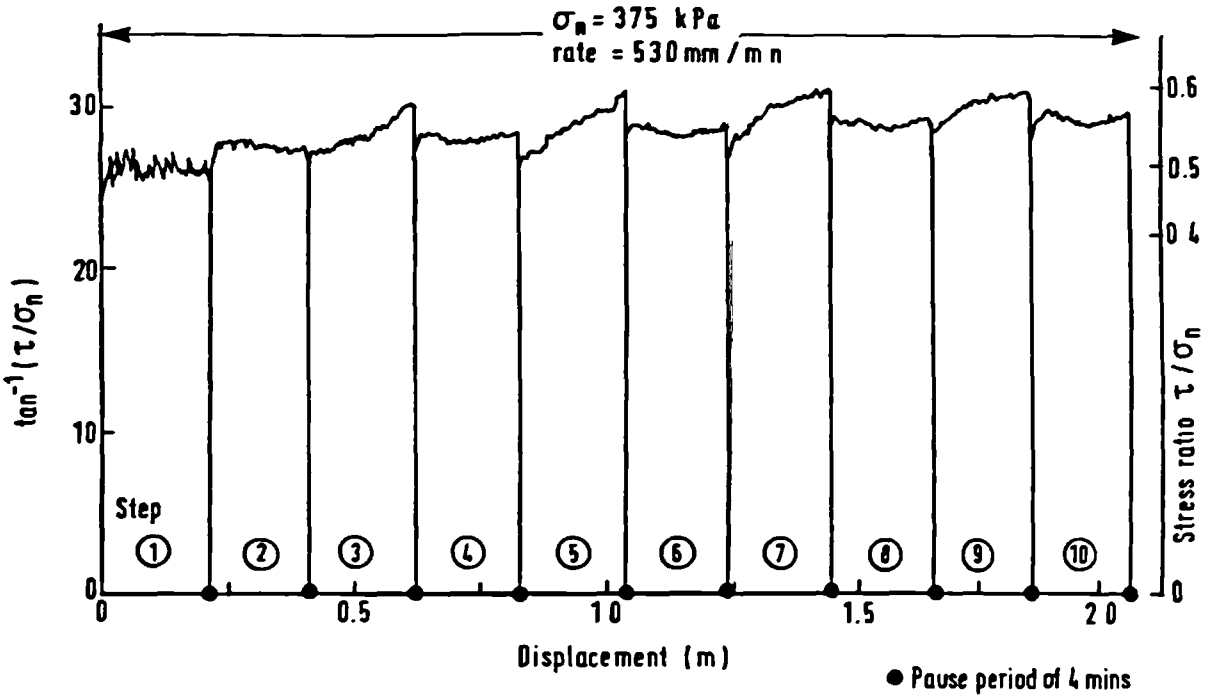

STAGE B

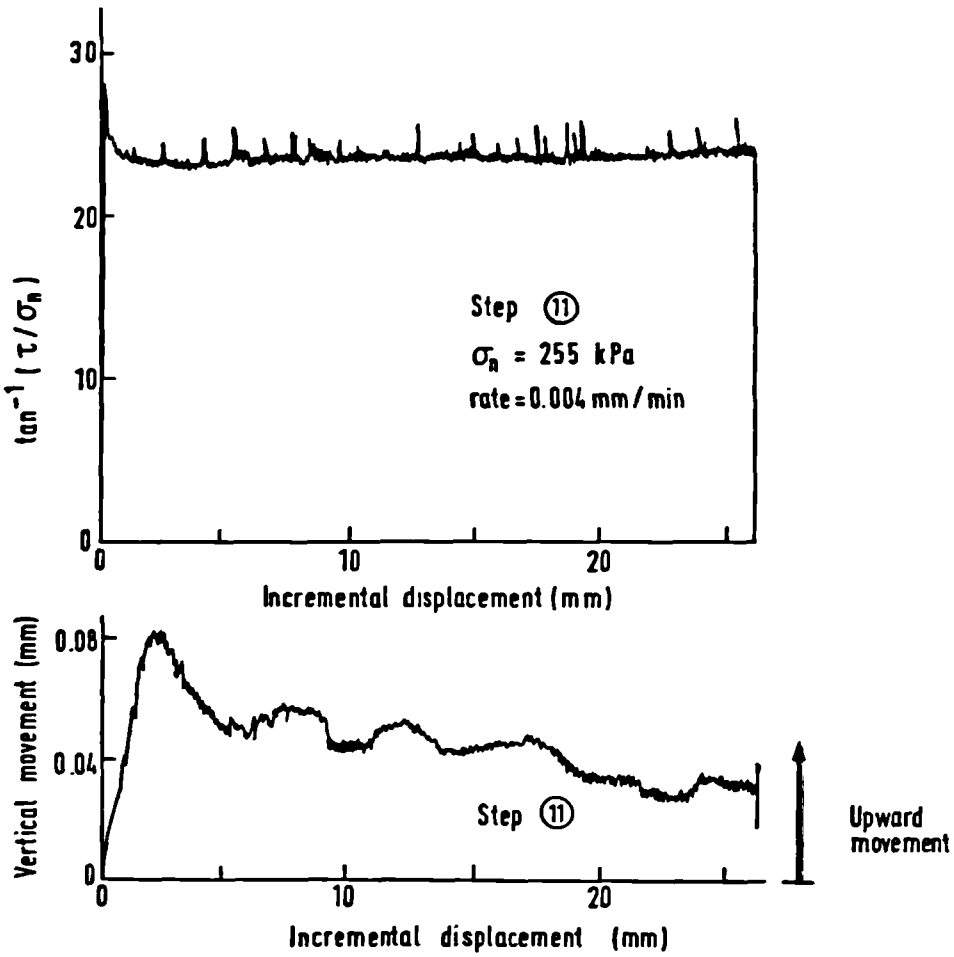

STAGE C

Figure D10 RSI test on Cowden till, Steps 1 to 11

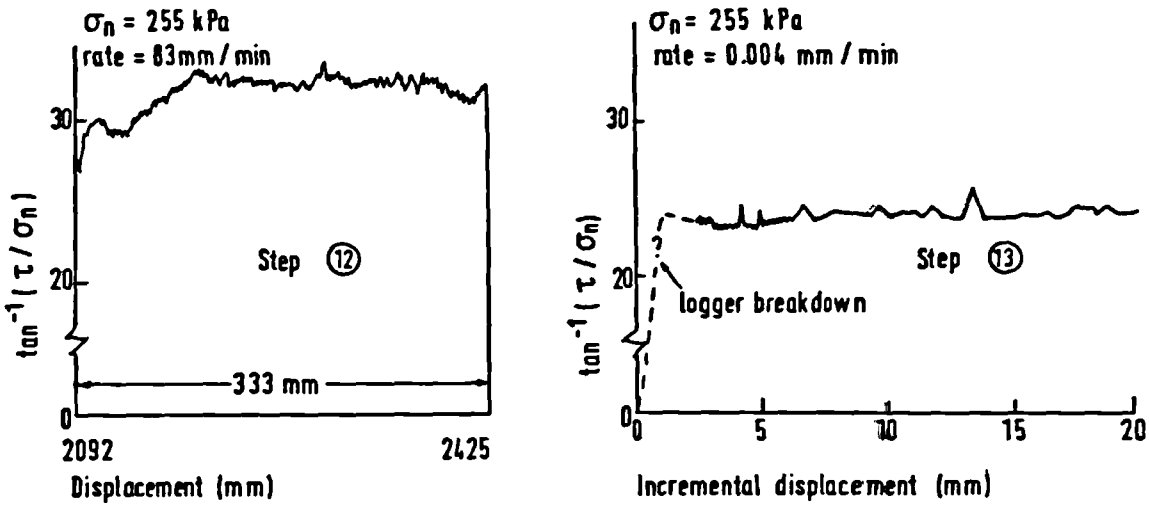

STAGE D

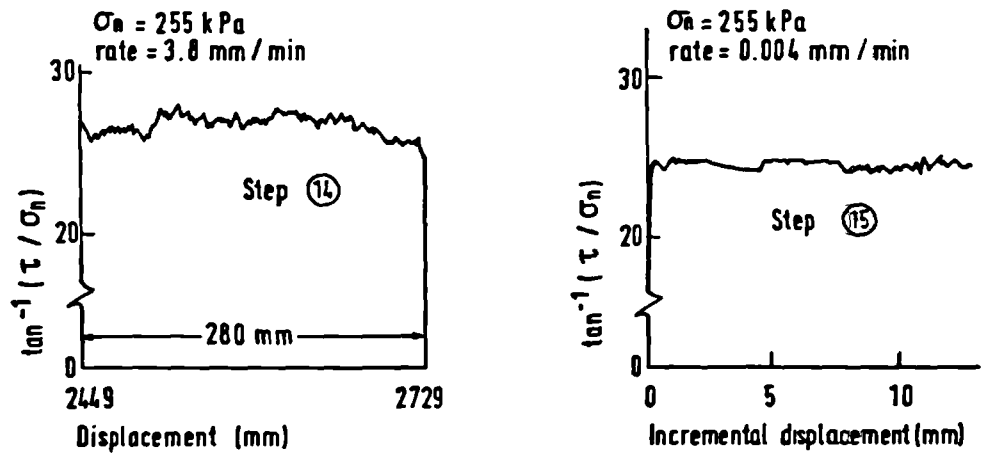

STAGE E

Figure D11 RSI test on Cowden till, Steps 12-15

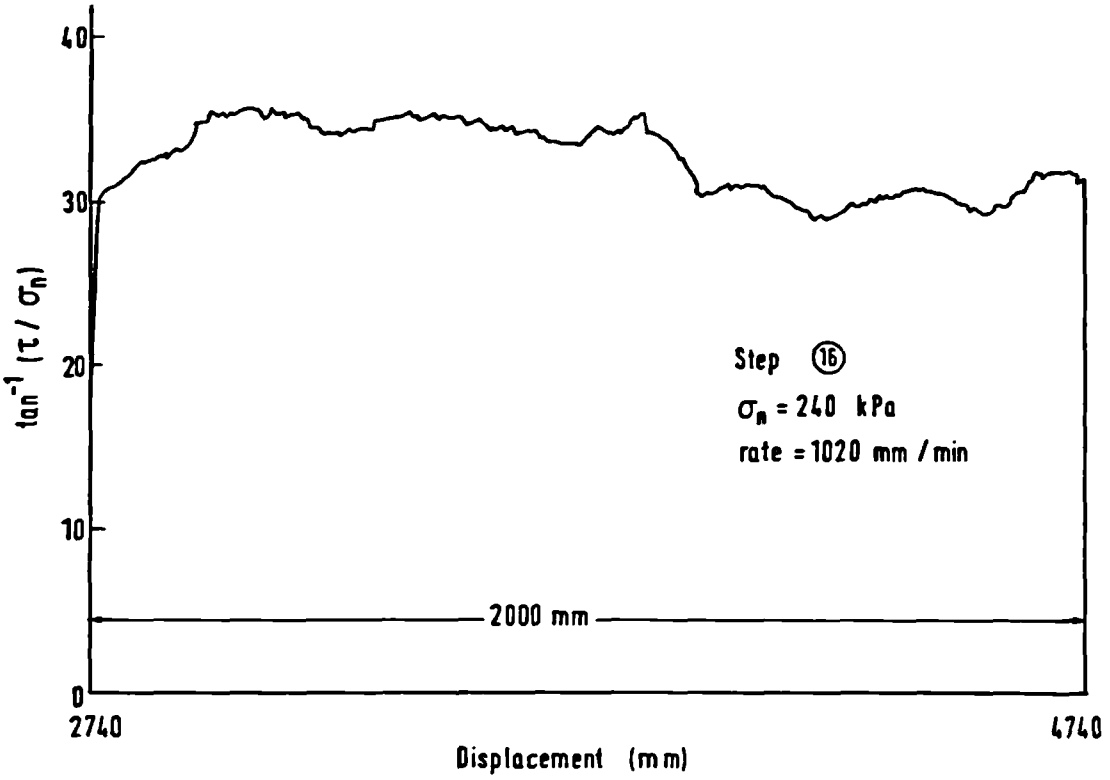

STAGE F

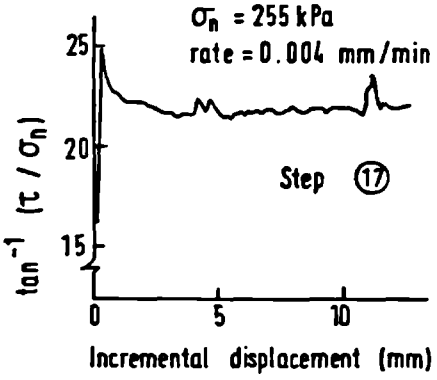

Figure D12 RSI test on Cowden till, Steps 16 & 17

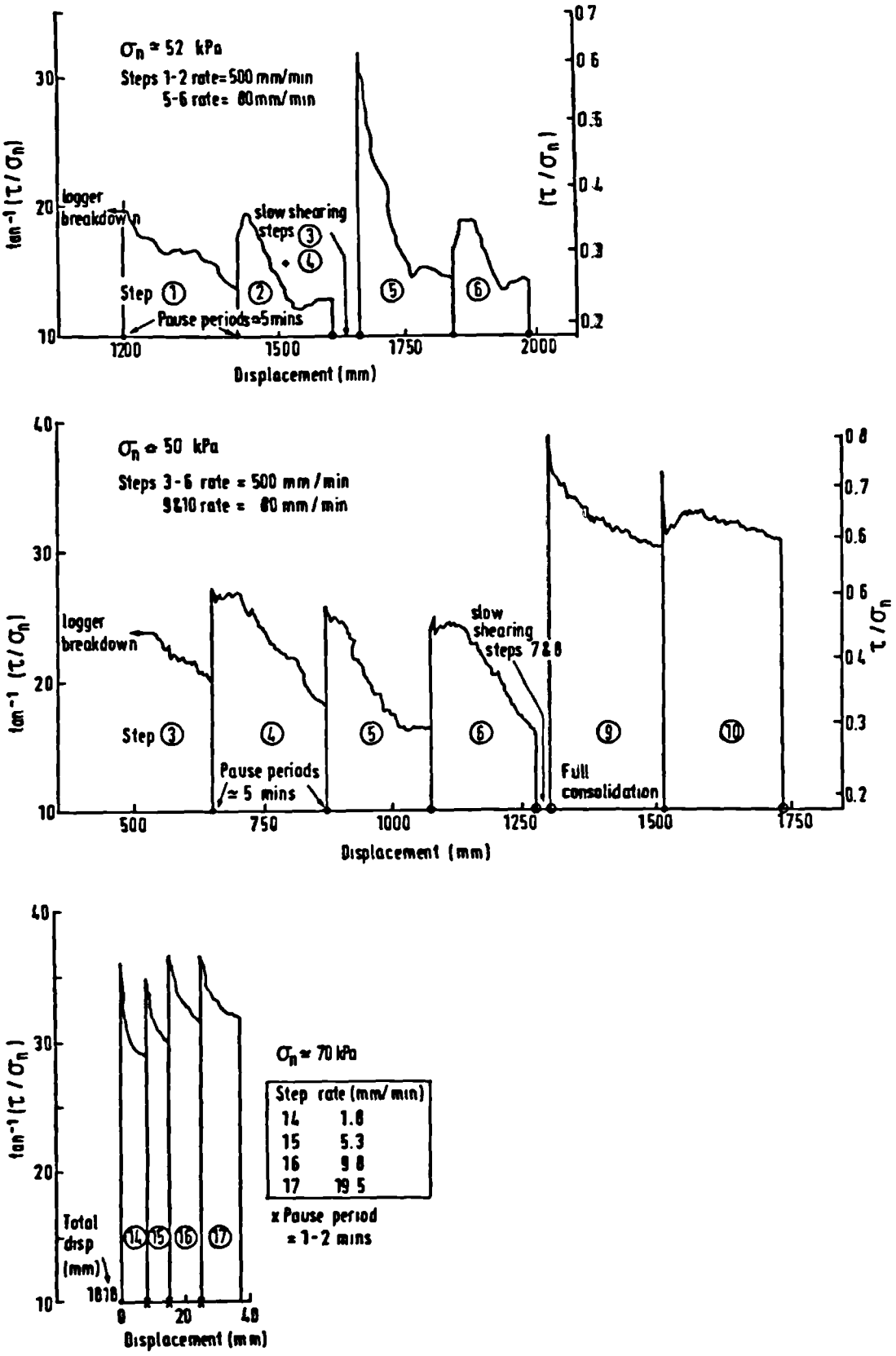

Figure D13 RS fast shearing steps on Bothkennar clay, Test 1 (top) and Test 2 (bottom)

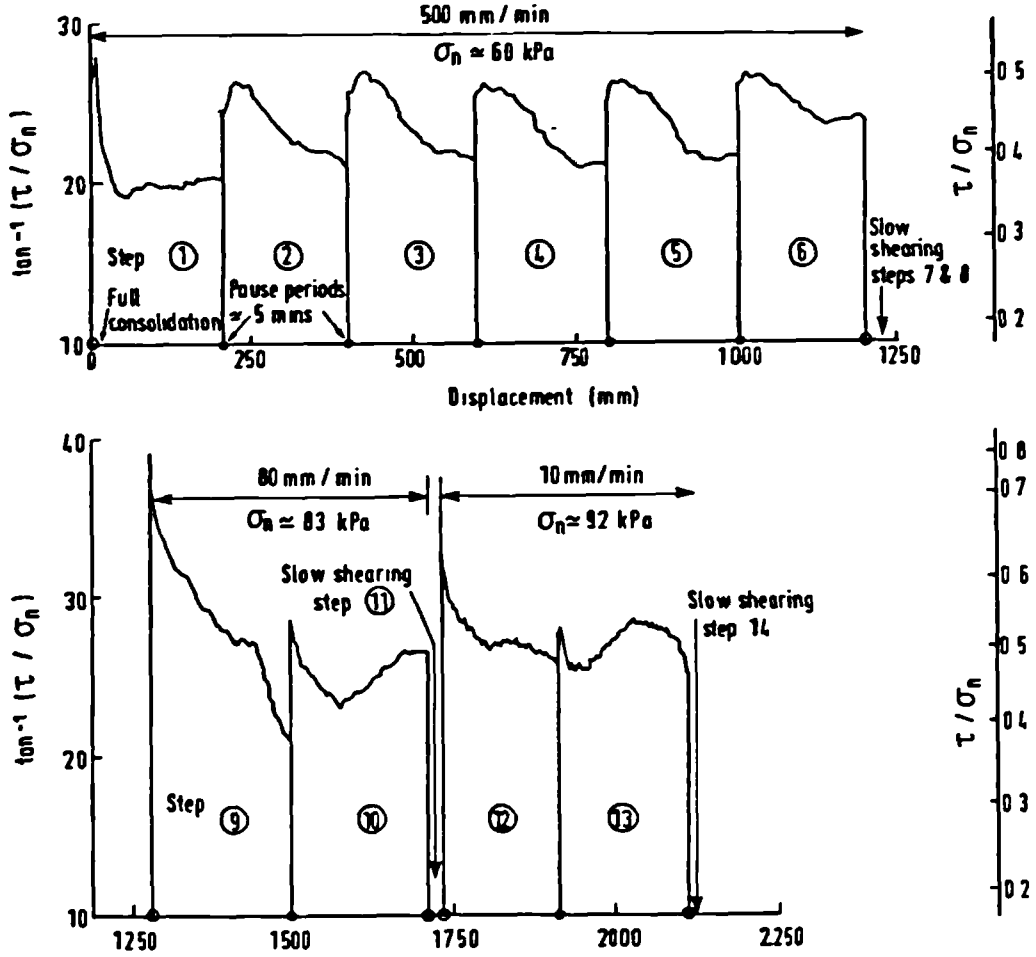

Figure D14 RS fast shearing steps on Bothkennar clay, Test 3

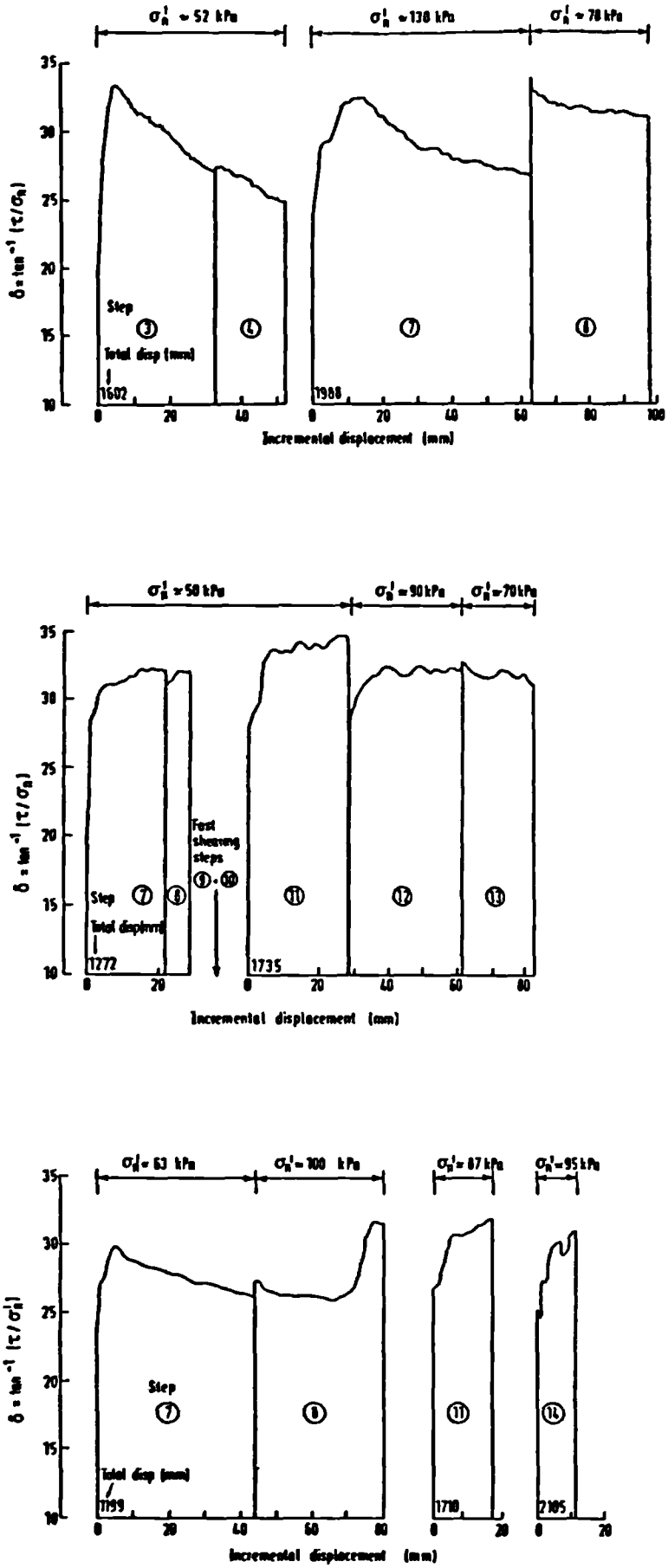

Figure D15 RS slow shearing steps on Bothkennar clay, Test 1 (top), Test 2 (middle) and Test 3 (bottom)

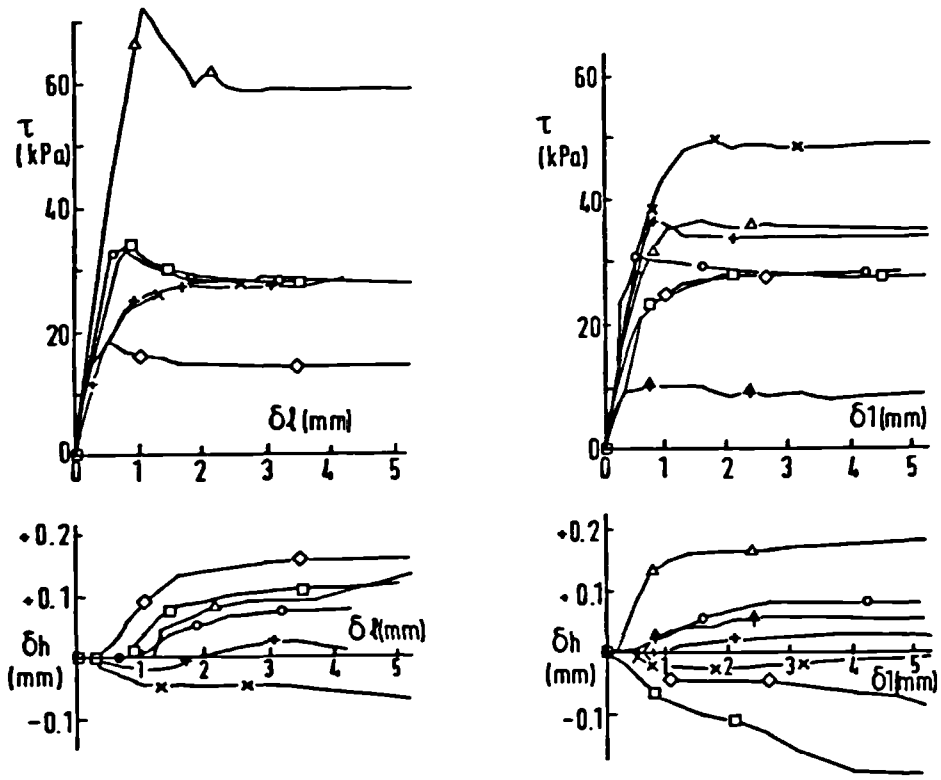

Interface $R_i \simeq 9.5 \mu m$

Test Nº	σ_n (kPa)	e_i
□ 1	52.6	0.55
○ 2	52.6	0.54
△ 9	115.3	0.55
+ 12	52.6	0.64
× 13	52.6	0.64
◇ 14	27.9	0.55

Interface $R_i \simeq 5.5 \mu m$

Test Nº	σ_n (kPa)	e_i
□ 4	52.6	0.63
○ 3	52.6	0.52
△ 5	65.0	0.54
+ 6	65.0	0.58
× 7	89.8	0.57
◇ 8	52.6	0.62
♦ 15	15.5	0.58

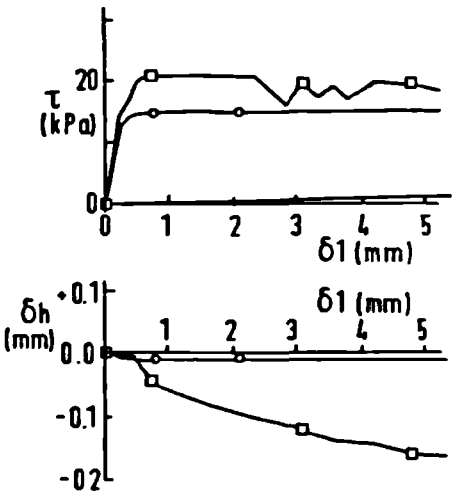

Teflon interface $R \simeq 2 \mu m$

Test Nº	σ_n (kPa)	e_i
□ 10	52.6	0.55
○ 11	40.2	0.60

Figure D16 Shear box interface tests on Labenne sand, steel interfaces (top) and teflon interface (bottom)

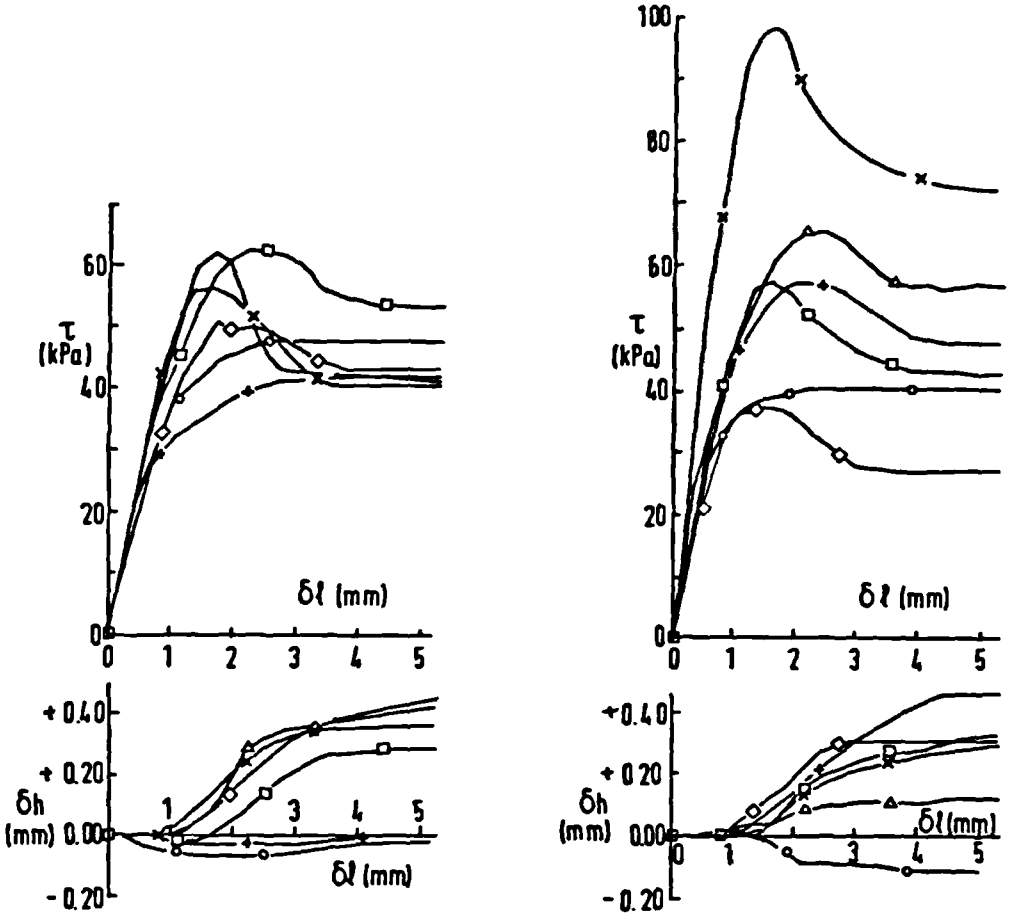

Test Nº	σ_n (kPa)	e_L
□ A	77.4	0.54
○ B	77.4	0.65
△ C	65.0	0.51
◆ D	65.0	0.64
× E	65.0	0.56
◇ F	65.0	0.57

Test Nº	σ_n (kPa)	e_L
□ G	65.0	0.54
● H	65.0	0.66
▲ I	89.8	0.58
◆ J	77.4	0.58
× K	115.0	0.54
◇ L	40.0	0.53

Figure D17 Shear box tests on Labenne sand (soil on soil)

Step	σ'_{nc} (kPa)	Disp rate (mm/min)	Disp (mm)	Pause period prior to step
Soil-interface : Test 1 (Labenne sand, D_r =56%)				
1-8	73	530	8x307	5 mins between each pulse
9	73	0.042	61	1 day
Soil-interface : Test 2 (Labenne sand, D_r =80%)				
1-8	73	530	8x301	5 mins between each pulse
9	73	0.042	31	1 day
Soil-interface : Test 1 (Cowden till)				
1-10	375	530	10x210	5 mins between each pulse
11	245	0.004	27	1 day
12	245	83	333	5 mins
13	245	0.004	20	1 day
14	245	3.8	280	5 mins
15	245	0.004	13	1 day
16	240	1020	2000	5 mins
17	250	0.004	13	1 day
Soil on soil : Test 1 (Bothkennar clay)				
1-2[1]	52	500	2x200	5 mins between each pulse
3	52	0.008	33	1 day
4	52	0.008	19	5 mins
5	52	80	165	5 mins
6	52	80	165	5mins
7	130	0.008	63	1 day
8	78	0.008	45	1 day

[1] preceded by 1200mm disp at 500mm/min

Table D1 Ring shear testing programme (1)

Step	σ'_{nc} (kPa)	Disp rate (mm/min)	Disp (mm)	Pause period prior to step
Soil-interface : Test 2 (Bothkennar clay)				
3-6[1]	50	500	4x212	5 mins between each pulse
7	50	0.008	22	1 day
8	50	0.008	7	2 mins
9	50	80	215	10 mins
10	50	80	220	5 mins
11	50	0.008	28	1 day
12	90	0.008	34	1 day
13	70	0.008	22	1 day
14	70	1.8	7	5 mins
15	70	5.3	7	2 mins
16	70	9.8	10	1 min
17	70	19.5	13	1 min
Soil-Interface: Test 3 (Bothkennar clay)				
1-6	60	500	6x200	5 mins between each pulse
7	63	0.008	44	1 day
8	100	0.004	36	1 day
9	83	80	210	1 day
10	83	80	218	5 mins
11	87	0.001	17	1 day
12	92	10	220	1 day
13	92	10	220	5 mins
14	95	0.008	12	1 day

[1] preceded by 424mm disp at 500mm/min

Table D2 Ring shear testing programme (2)

Test	Step	σ'_{nc} (kPa)	Preceded by	δ_p	δ_{ult}	Disp for δ_{ult} (mm)
Soil-interface tests : Labenne sand						
1	9	73	2000mm disp at 530mm/min	31.2	28.5 ±1.5	1.5
2	9	73	2000mm disp at 530mm/min	30.5	28.5 ±1.5	1.6
Soil-interface test : Cowden till						
2	11	245	2100mm disp at 530mm/min	28.0	23.5	1.5
2	13	245	333mm disp at 83mm/min	N/A[1]	24.0	N/A[1]
2	15	245	280mm disp at 3.8mm/min	24.0	24.0	0.6
2	17	250	2000mm disp at 1020mm/min	25.0	22.0	0.5
Soil-interface test : Bothkennar clay						
2	7	50	1270mm disp at 500mm/min	32.0	32.0	15
2	11	50	435mm disp at 80mm/min	34.0	34.0	15
2	12	90	Step 11	32.5	32.5	10
2	13	70	Step 12	33.0	32.5	20

[1] no data available due to data logger fault

Table D3 Ring shear test results (1)

Test	Step	σ'_{nc} (kPa)	Preceded by	δ_p	δ_{ult}	Disp for δ_{ult} (mm)
Soil-interface test : Bothkennar clay						
3	7	63	1200mm disp at 500mm/min	30.0	26.5	40
3	8	100	Step 7	27.5	26.5-32	40
3	11	87	428mm disp at 80mm/min	31.2	31.2	15
3	12	95	440mm disp at 10mm/min	30.5	30.5	11
Soil on soil test : Bothkennar clay						
				ϕ'_{pres}	ϕ'_{res}	Disp for ϕ'_{res} (mm)
1	3	52	1600mm disp at 500mm/min	33.4	25	52
1	7	130	330mm disp at 80mm/min	32.5	26.8	63
1	8	78	Step 7	33.8	31.0	35

Table D4 Ring shear test results (2)

Soil on soil shear box tests

Test No.	σ'_{nc} (kPa)	Placing method[1] of sample	e_i	$\phi_p°$	$\phi_{cv}°$
A	77.4	(ii)	0.54	39.0	34.5
B	77.4	(i)	0.65	32.0	32.0
C	65.0	(ii)	0.51	43.8	32.7
D	65.0	(i)	0.64	32.3	32.3
E	65.0	(ii)	0.56	41.0	32.0
F	65.0	(i)	0.57	37.5	33.5
G	65.0	(ii)	0.54	41.5	33.8
H	65.0	(i)	0.66	32.0	32.0
I	89.8	(i)	0.58	36.0	32.4
J	77.4	(i)	0.58	36.6	32.0
K	115.0	(ii)	0.54	40.4	32.5
L	40.2	(ii)	0.53	42.8	33.8

Soil-interface shear box tests

Test No.	σ'_{nc} (kPa)	Placing method[1] of sample	e_i	Interface roughness (μm)	$\delta_p°$	$\delta_{cv}°$
1	52.6	(ii)	0.55	9.5	33.0	27.8
2	52.6	(ii)	0.54	9.5	32.5	28.0
3	52.6	(ii)	0.52	5.5	30.8	28.2
4	52.6	(i)	0.63	5.5	27.9	27.9
5	65.0	(ii)	0.54	5.5	29.5	28.0
6	65.0	(i)	0.58	5.5	29.3	27.5
7	89.8	(i)	0.57	5.5	28.9	28.0
8	52.6	(i)	0.62	5.5	27.4	27.4
9	115.0	(ii)	0.55	9.5	32.3	27.0
10	52.6	(ii)	0.55	2.0 (Teflon)	21.2	18.0
11	40.2	(i)	0.60	2.0 (Teflon)	19.9	19.2
12	52.6	(i)	0.63	9.5	27.5	27.5
13	52.6	(i)	0.64	9.5	28.0	28.0
14	27.9	(ii)	0.55	9.5	33.8	27.1
15	15.5	(i)	0.58	5.5	33.8	29.4

[1] (see text)

Table D5 Shear box tests on Labenne sand

REFERENCES

Airey D.W. and Wood D.M. (1987), 'An evaluation of direct simple shear tests on clay', Geotechnique 37(1), pp25-35

Allersma H.G.N. (1988), 'Optical analysis of stress and strain surrounding the tip of a penetrating probe', Proc. 1st Int. Symp. on Penetration Testing, ISOPT-1, 2, pp615-620

Amar S., Baguelin F. and Jézéquel (1982), 'Pressio-penetrometer for geotechnical surveys on land and offshore', Proc. 2nd Eur. Symp. on Penetration Testing, Amsterdam, 2, pp419-423

American Petroleum Institute (API), (1989), RP2A: 'Recommended practice of planning, designing and constructing fixed offshore platforms', 18th edition, Washington

Arthur J.R.F., Chua K.S. and Dunstan T. (1977), 'Induced anisotropy in sand', Geotechnique, 27(1), pp13-30

Azzouz A.S. and Lutz D.G. (1986), 'Shaft behaviour of a model pile in plastic Empire clays', J. Geotech. Eng., ASCE, 112(4), pp389-406

Azzouz A.S. and Morrison M.J. (1988), 'Field measurements on model pile in two clay deposits', J. Geotech. Eng., ASCE, 114(1), pp104-121

Azzouz A.S., Baligh M.M. and Whittle A.J. (1990), 'Shaft resistance of piles in clay', J. Geotech. Eng. Div., ASCE, 116(2), pp205-221

Baguelin F., Bustamante M. and Frank R. (1986), 'The pressuremeter for foundations: French experience', Proc. Special Conf. on In-Situ Tests in Geotech. Practice, Blacksburg, Virginia, pp31-46

Baguelin F., Jézéquel J.F. and Shields D.H. (1978), 'The pressuremeter and foundation engineering', Book 4 in Trans. Tech. Publ., Series on Rock and Soil mechanics.

Baligh M.M. (1975), 'Theory of deep static cone penetration resistance', Research report No. R75-56, Order No. 517, Dept. of Civil Eng., Massachusetts Institute of Technology

Baligh M.M. (1984), 'The simple-pile approach to pile installation in clays', in 'Analysis and design of pile foundations', Proc. Symp. on Codes and Standards, ASCE National Conv., San Francisco, pp310-330

Baligh M.M. (1985), 'Strain Path Method', J. Geotech. Eng., ASCE 111(9), pp1108-1136

Baligh M.M. (1986), 'Undrained deep penetration: II. Pore pressures', Geotechnique, 36(4), pp487-501

Baligh M.M., Vivatrat V. and Ladd C.C. (1980), 'Cone penetration in soil profiling', J. Geotech. Eng., ASCE, 106(GT4), pp447-461

Been K. and Jeffries M.G. (1985), 'A state parameter for sands', Geotechnique, 35(2), pp99-112

Been K., Jeffries M.G. and Hachey J. (1991), 'The critical state of sands', Geotechnique, 41(3), pp365-381

Berezantsev V.G. (1961), 'Load-bearing capacity and deformation of piled foundations', Proc. of 5th Int. Conf. on Soil Mech., Paris, 2, pp11-12

Beringen F.L., Windle D. and Van Hooydonk W.R. (1979), 'Results of loading tests on driven piles in sand', Recent developments in the design and construction of piles, ICE, London, pp213-225

Bishop A.W., Green G.E., Garga V.K., Andresen A. and Brown J.D. (1971), 'A new ring shear apparatus and its application to the measurement of residual strength', Geotechnique, 21(4), pp273-328

Bogard J.D and Matlock H. (1990), 'In-situ segment model experiments at Empire, Louisiana', Proc. Offshore Tech. Conf., Houston, 2, pp459-467

Bogard J.D and Matlock H. (1990), 'In-situ segment model experiments at Harvey, Louisiana', Proc. Offshore Tech. Conf., Houston, 2, pp469-477

Bogard J.D., Matlock H., Audibert J.M.E. and Mamford S.R. (1985), 'Three years experience with model pile segments', Proc. Offshore Tech. Conf., Houston, 1, pp65-72

Bolton M.D. (1986), 'The strength and dilatancy of sands', Geotechnique 36(1), pp65-78

Bond A.J.(1989), 'Behaviour of displacement piles in overconsolidated clays', PhD Thesis, Univ. of London (Imperial College)

Bond A.J. (1990), 'Theoretical predictions of pile behaviour in a heavily overconsolidated clay', Internal report, Dept. of Civil Eng., Univ. of London (Imperial College)

Bond A.J. and Jardine R.J. (1990), Discussion on 'Field studies of an instrumented model pile in clay' by Coop M.R. and Wroth C.P. (1989), Geotechnique 40(4), pp669-672

Bond A.J. and Jardine R.J. (1990), 'Research on the behaviour of displacement piles in an overconsolidated clay, UK Dept. of Energy OTH Report, OTH89 296, HMSO, London

Bond A.J., Jardine R.J. and Dalton J.C.P. (1991), 'The design and performance of the Imperial College instrumented pile', Am. Soc. for testing materials, Geotech. Testing J., 14(4), pp413-424

Bond A.J. and Jardine R.J. (1991), 'Effects of installing displacement piles in high OCR clay', Geotechnique 41(3), pp341-363

Boulon M. and Nova R. (1990), 'Modelling of soil-structure interface behaviour, a comparison between elastoplastic and rate type laws', Computers and Geomechanics, 9, pp21-46

Boulon M. and Foray P. (1986), 'Physical and numerical simulation of lateral shaft friction along offshore piles in sand', Proc. 3rd Int. Conf. on numerical methods in offshore piling, Nantes, France, pp127-147

Bowden F.P. and Tabor A. (1967), 'Friction and lubrication', Revised Reprint, London, Methuen; see Lemos (1986)

Briaud J.L. and Audibert J.M.E. (1990), 'Some thoughts on API RP2A for vertically loaded piles', Proc. 22nd Offshore Tech. Conf., Houston, 4, pp9-16

Briaud J.L. and Tucker L.M. (1984), 'Piles in sand: a method including residual stresses', J. of Geotech. Eng. Div., ASCE, 110(11), pp119-137

Briaud J.L and Tucker L.M. (1988), 'Measured and predicted axial response of 98 piles', J. of Geotech. Eng. Div., ASCE, 114(9), pp984-1001

Briaud J.L., Tucker L.M. and Ng E. (1989), 'Axially loaded 5 pile group and single pile in sand', Int. Conf. on Soil Mech. and Fdn. Eng., Balkema, Rotterdam, pp1121-1124

BS 1377 (1975), 'Methods of test for soils for civil engineering purposes', British Standards Institution, London

Building Research Establishment (BRE) (1986), 'The behaviour of piles as anchorages fro buoyant structures', Dept. of Energy, Offshore Tech. Report, OTH 86 222

Burland J.B. (1973), 'Shaft friction of piles in clay - a simple fundamental approach', Ground Eng., 6(3), pp30-42

Burland J.B. (1990), 'On the compressibility and shear strength of natural clays', 30th Rankine lecture, Geotechnique, 40(3), pp327-378

Bustamante M. (1982), 'The pile loading test', in "Foundation Eng., Vol. 1 - Foundation design and construction", Editor: G. Pilot, Presse de l'école nationale des Ponts et Chaussées, pp263-273

Bustamante M. and Gianeselli L. (1982), 'Pile bearing capacity by means of static penetrometer CPT', Proc. 2nd Eur. Symp. on penetration testing, Amsterdam, pp493-499

Bustamante M., Frank R. and Christoulas S. (1991), 'Evaluation de quelques methodes de calcul de pieux forces', Revue Francaise de Geotechnique (in press); see Jardine & Christoulas (1991)

Butterfield R. (1979), 'A natural compression law for soils (an advance on e-log p' ', Geotechnique, 29(4), pp469-480

Butterfield R. and Bannerjee P.K. (1970), 'The effect of porewater pressures on the ultimate bearing capacity of driven piles', Proc. 2nd Southeast Asian Conf. Soil Mech. & Fdn. Eng., Singapore, pp385-394

Butterfield R. and Johnston I.W. (1973), 'The stress acting on a continuously penetrating pile', Proc. 8th Int. Conf. Soil Mech. & Fdn. Eng., Moscow, 2.1, pp39-45

Canadian Geotechnical Society (1985), Canadian Fdn. Eng. manual, 2nd edition, Canadian Geotech. Soc., Vancouver

Carder D.R. and Krawczyk J.V. (1975), 'Performance of cells designed to measure soil pressure on earth retaining structures', TRRL Lab. Report 689, Dept. of Environment, TRRL, Crowthorne, England; see Bond (1989)

Chandler R.J. and Martins J.P. (1982), 'An experimental study of skin friction around piles in clay', Geotechnique 32(2), pp119-132

Chong F. (1988), 'Density changes of sand on cone penetration resistance', Proc. of 1st Int. Symp. on Penetration Testing, ISOPT-1, Balkema, Rotterdam, 2, pp707-714

Coop M.R. (1987), 'The axial capacity of driven piles in clay', DPhil Thesis, Univ. of Oxford

Coop M.R. and Wroth C.P. (1989), 'Field studies of an instrumented model pile in clay', Geotechnique, 39(4), pp679-696

Cornforth D. (1973), 'Prediction of drained strength of sands from relative density measurements', paper in 'Evaluation of relative density and its role in geotechnical projects involving cohesionless soils', ASTM STP 523, pp281-303

Coyle H.M. and Castello R.R. (1981), 'New design correlations for piles in sand', J. of Geotech. Eng. Div., ASCE, 107 (GT7), pp965-986

Davidson J.L., Mortensen R.A. and Barreiro D. (1981), 'Deformations in sand around a cone penetrometer tip,' Proc. 10th Int. Conf. on Soil Mech. and Fdn. Eng, Stockholm, 2, pp467-470

De Beer E.E. (1977), 'Static sounding in clay and loam', Proc. Fugro 15-years Symp., Utrecht, Fugro BV, Leidschemdam (Netherlands), pp43-68

De Campos T.M.P. (1984), 'Two low plasticity clays under cyclic and transient loading', PhD Thesis, Univ. of London (Imperial College)

Dennis N.D. and Olsen R.R. (1983), 'Axial capacity of steel pipe piles in clay', Proc. Conf. on Geotech. Practice on Offshore Eng., Austin, Texas, pp370-388

Derbyshire E. and Love M.A. (1981), 'Fabric and sedimentological properties of selected glacial clays', Research report, Dept. of Geology, Univ. of Keele; see Marsland (1985)

Di Biaggio E. (1977), 'Field instrumentation - a geotechnical tool', Proc. 1st Baltic Conf. on Soil Mech. and Fdn. Eng., Gdansk, 1, pp29-40

Eissautier M. (1986), 'Frottement latéral des pieux en milieu pulvérulent, essais en chambre de calibration', Thèse de 3ème cycle, Univ. of Grenoble; see Boulon & Foray (1986)

Everton S. (1991), 'Behaviour of sands in shear box interface tests', MSc Diss, Univ. of London (Imperial College)

Famechon C. (1973), 'Les sable des Landes', Bull. Liaison Laboratoire des Ponts et Chaussées, No. 66 (1222), pp105-118

Flaate K. and Selnes P. (1977), 'Side friction of piles in clay', Proc. 9th Int. Conf. Soil Mech. & Fdn. Eng., Tokyo, 1, pp517-522

Fleming W.G.K., Weltman A.J., Randolph M.F. and Elson W.K. (1985), 'Piling Engineering', Surrey Univ. Press, John Wiley & Sons, New York

Focht J.A. and O'Neill M.W. (1985), 'Piles and other deep foundations', Theme Lecture No. 4, Proc 11th Int. Conf. Soil Mech. & Fdn. Eng., San Francisco, 1, pp187-209

Francescon M. (1983), 'Model pile tests in clay. Stresses and displacements due to installation and axial loading', PhD Thesis, Univ. of Cambridge

Gallagher K.A. and St John H.D. (1980), 'Field scale model studies of piles as anchorages for buoyant platforms', Proc. Eur. Offshore Petroleum Conf. and Exhibition, London, Paper EUR 135

Gens A. (1982), 'Stress-strain and strength characteristics of a low plasticity clay', PhD Thesis, Univ. of London (Imperial College)

Gens A. and Hight D.W. (1979), 'The laboratory measurement of design parameters for a glacial till', Proc. 7th Eur. Conf. on Soil Mech. and Fdn. Eng., Brighton, 2, pp57-65

Georgiannou V.N. (1988), 'The behaviour of clayey sands under monotonic and cyclic loading', PhD Thesis, Univ. of London (Imperial College)

Geotechnical Consultancy Group (GCG) (1990), 'Input parameters for Strain Path Analyses for the Bothkennar pile tests', report submitted to Dept. of Civ. Eng., Univ. of London (Imperial College)

Geotechnical Consultancy group (GCG) (1991), 'Soil properties at the SERC soft clay test bed site at Bothkennar', London SW7

Geotechnique Symposium in print (1992), Geotechnique, 42(2), (in press)

Gibbs H. J. and Holtz W.G. (1957), 'Research on determining the density of sands by spoon penetration test', Proc. 4th Int. Conf. on Soil Mech., London, 1, pp35-39

Gibson R.E. (1963), 'An analysis of system flexibility and its effect on time-lag in pore-water pressure measurements', Geotechnique, 13 (1), pp1-11

Gostelow T.P. and Browne M.A. (1986), 'Engineering geology of the upper Forth estuary', British Geological Survey report No. 16-8

Gregersen O.S., Aas G. and Dibiagio E. (1973), 'Load tests on friction piles in loose sand', Proc. 8th Int. Conf. on Soil Mech. and Fdn. Eng, Moscow, 2, pp109-117

Hanna T.H. and Tan R.H.S. (1973), 'The behaviour of long piles under compressive loads in sand', Can. Geotech. J., 10(3), pp311-340

Hawkins A.B., Larnach W.J., Lloyd I.M. and Nash D.F.T. (1989), 'Selecting the location, and initial investigation of the SERC soft clay test bed site, Quarterly J. of Eng. Geology, 22, pp281-316

Heijnen W. (1974), 'Penetration testing in the Netherlands:state of the art report', Proc. 1st Eur. Symp. on Penetration Testing, 1, pp79-83

Hettler A. (1982), 'Approximation formulae for piles under tension', IUTAM Conf. on Defm. and failure of granular materials, Delft, pp603-608

Hight D.W., Bond A.J. and Legge J.D. (1992), 'Geotechnical characterisation of the Bothkennar clay', Geotechnique, 42(2), (in press)

Hight D.W., Gens A. and Jardine R.J. (1985), 'Evaluation of geotechnical parameters from triaxial tests on Offshore Clay,' Proc. Int. Conf. on Offshore Site Investigation, Society for Underwater Tech., London, pp253-268

Hight D.W., Jardine R.J. and Gens A. (1987), 'The behaviour of soft clays', Spec. publ. on 'Embankments on soft clay', Bull. of publ. works research centre, Athens, pp33-158

Hight D.W. and Lawrence D. (1992), 'The end resistance of pipe piles in sand', Geotech. Consultancy Group, London SW7, Int. report

Hill R. (1950), 'The mathematical theory of plasticity', Oxford Univ. Press, London, pp356; see Bond (1989)

Hird C.C., Powell J.J.M. and Yung P.C.Y. (1991), 'Investigations of the stiffness of a glacial clay till, Proc. 10th Eur. Conf. on Soil Mech. and Fdn. Eng., Florence 1991, 1, pp107-110

Houlsby G.T. and Teh C.I. (1988), 'Analysis of the piezocone in clay', Proc. of 1st Int. Symp. on Penetration Testing, ISOPT-1, Balkema, Rotterdam, 2, pp777-783

Hughes J.M.O. and Robertson P.K. (1985), 'Full-displacement pressuremeter testing in sand', Can. Geotech. J., 22, pp298-307

Hunter A.H. and Davisson P. (1969), 'Measurements of pile load transfer', Performance of Deep Fdns., ASTM spec. publ. 444, pp106-117

Huntsman S.R. (1985), 'Determination of in-situ lateral pressure coefficients of cohesionless soils by static cone penetrometer', PhD Thesis, Univ. of California, Berkeley, USA; see Jamiolkowski et al (1988)

Jaky J. (1944), 'The coefficient of earth pressure at rest', J. of union of Hungarian Engineers and Architects', 22, pp355-358; see Mayne & Kulhawy (1982)

Jamiolkowski M., Ghionna V.N., Lancellotta R. and Pasqualini E. (1988), 'New correlations of penetration tests for design practice', Penetration testing ISOPT-1, Rotterdam, 2, pp263-296

Jardine R.J. (1985), 'Investigations of pile-soil behaviour, with special reference to the foundations of offshore structures', PhD Thesis, Univ. of London (Imperial College)

Jardine R.J. (1992), 'Non-linear stiffness parameters from undrained pressuremeter tests', Can. Geotech. J., June 1992, (in press)

Jardine R.J. and Bond A.J. (1989), 'Behaviour of displacement piles in a heavily overconsolidated clay', Proc. 12th Int. Conf. on Soil Mech. and Fdn. Eng., Rio de Janeiro, 1, pp1147-1152

Jardine R.J. and Christoulas S. (1991), 'Recent developments in defining and measuring static piling parameters', Proc. Int. Conf. on Deep Foundations, Paris, Presse de l'Ecole Nationale des Ponts et Chaussées, pp713-745.

Jardine R.J., Lehane B.M., Smith P.R., Gildea P. (1993), 'Instrumented footing tests in soft clay', Proc. Conf. on Case Histories in Geotech. Eng., Missouri-Rolla, U.S., June 1993, (in preparation)

Jardine R.J. and Potts D.M. (1988), 'Hutton tension leg platform foundations: prediction of driven pile behaviour', Geotechnique, 38(2), pp231-252

Jardine R.J. and Ridley A.M. (1992), 'Ring shear interface tests on North Sea clays', Int. Report, Dept. of Civ. Eng., Univ. of London (Imperial College)

Jardine R.J. and Smith P.R. (1991), 'Evaluating design parameters for multi-stage construction', Proc. Int. Conf. Geotech. Eng. for Coastal Development, Yokohama, pp197-202

Jardine R.J., St. John H.D., Hight D.W. and Potts D.M. (1991), 'Some practical implications of a non-linear ground model', Proc. of 10th Eur. Conf. on Soil Mech. and Fdn. Eng., Florence, 1, pp223-228

Jelgersma S. (1966), 'Sea level changes during the last 10,000 years', Proc. of Int. Symp. Royal Meteorological society, pp54-71

Johnston I.W. (1972), 'Electro-osmosis and porewater pressures: their effect on the stresses acting on driven piles', PhD Thesis, Southampton Univ.; see Bond (1989)

Johnston I.W., Lam T.S.K. and Williams A.F. (1987), 'Constant normal stiffness direct shear testing for socketed pile design in weak rock', Geotechnique, 37(1), p83-89

Jolly J.P. (1963), 'The effects of varying the means of application of energy to a model pile driven in cohesionless soil', M.A.Sc. Thesis, Dept. of Civil Eng., Univ. of Toronto; see Robinsky et al (1964)

Karlsrud K. and Haugen T. (1985), 'Axial static capacity of steel model piles in overconsolidated clay', Proc. 11th Conf. Soil Mech. & Fdn. Eng., San Francisco, 3, pp1401-1406

Karlsrud K. and Nadim F. (1990), 'Axial capacity of offshore piles in clay', Proc. 22nd Offshore Tech. Conf., Houston, 1, pp405-416

Kavvadas M. (1982), 'Non-linear consolidation around driven piles in clay', PhD Thesis, Massachusetts Institute of Technology

Kenney T.C. (1959), Discussion on 'Geotechnical properties of glacial lake clays', J. Soil Mechs. Div., ASCE, 85(SM3), pp67-79; see Smith (1992)

Kenney T.C. (1967), 'Field measurements of in situ stresses in quick clays', Proc. Geotech. Conf. on Shear Strength Properties of Natural Soils and Rocks, Oslo, 1, pp45-55

Kérisel J. (1964), 'Deep foundations - basic experimental facts', Conference on deep foundations, Mexico, 1, pp5-44

Kérisel J. (1985), 'The history of geotechnical engineering up until 1700', Proc. 11th Int. Conf. on Soil Mech. and Fdn. Eng., Golden Jubilee Vol., San Francisco, pp3-94

Kiousis P.D., Voyiadjis G.Z. and Tumay M.T (1988), 'A large strain theory and its application in the analysis of the cone penetration mechanism', Int. J. Num. & Anal. Methods in Geomechanics, 12, pp45-60

Kirby R.C. and Roussel G.R. (1980), 'Evaluation of prediction methods, field model pile tests, Hamilton Airforce base, Novato, California', Woodward Clyde Consultants report on ESACC project, prepared for Amoco Prod. Co.; see Coop (1987)

Kishida H. and Uesugi M. (1987), 'Tests of the interface between sand and steel in the simple shear apparatus', Geotechnique, 37(1), pp45-52

Koizumi Y. and Ito K. (1967), 'Field tests with regard to pile driving and bearing capacity of piled foundations', Soils and Foundations, 7(3), pp30-53

Konrad J.M. and Roy M. (1987), 'Bearing capacity of friction piles in marine clay', Geotechnique, 37(2), pp163-175

Kraft L.M. (1991), 'Performance of axially loaded pipe piles in sand', J. of Geotech. Eng. Div., ASCE, 117(2), pp272-296

Kraft L.M., Focht J.A. and Amerasinghe S.F. (1981), 'Friction capacity of piles driven into clay', J. Geotech. Eng. Div., ASCE 107(GT11), pp1152-1541

Kulhawy F.H. (1984), 'Limiting tip and side resistance: fact or fallacy?', Proc. Analysis and Design of Pile Fdns., ASCE, pp80-98

La Rochelle P., Sarrailh J., Tavenas F., Roy M. and Leroueil S. (1981), 'Causes of sampling disturbance and design of a new sampler for sensitive soils', Can. Geotech. J., 18(1), pp52-66

Ladd C.C. and Edgers L. (1972), 'Consolidated, undrained direct simple shear tests on saturated clays', Research report R72-82, No. 284, Dept. of Civ. Eng., Massachusetts Institute of Technology; see Ladd et al (1977)

Ladd C.C. and Foott R. (1974), 'New design procedure for stability of soft clays', J. Geotech. Eng., ASCE 100(GT7), pp763-786

Ladd C.C., Foott R., Ishihara K., Schlosser F. and Poulos H.G. (1977), 'Stress-deformation and strength characteristics', State-of-the-art Report, Proc. 9th Int. Conf. Soil Mech. Fdn. Eng., Tokyo, 2, pp421-494

Lebègue M.Y. (1964), 'Etude expérimental des efforts d'arrachage et de frottement négatif sur les pieux en milieu pulvérulent', Annales de l'institute du bâtiment et de travaux publics, Serie soils et fondations 17, Nos 199-200, pp808-822

Ledoux J.L., Menard J. and Soulard P. (1982), 'The penetro-gammadensimeter', Proc. 2nd Eur. Symp. on penetration testing, Amsterdam, 2, pp419-423

Lefebvre G. and Poulin C. (1979), 'A new method of sampling in sensitive clay', Can. Geotech. J., 16(1), pp226-233

Lehane B.M. and Jardine R.J. (1992), 'The residual strength of Bothkennar clay', Geotechnique, 42(2), (in press)

Lehane B.M. and Jardine R.J. (1992), 'The behaviour of displacement piles in glacial till', Proc. Conf. on the Behaviour of Offshore Structures', BOSS' 92, London, (in press)

Lehane B.M. and Jardine R.J. (1992), 'The behaviour of a displacement pile in Bothkennar clay', Wroth Mem. Symp., Oxford, (in press)

Lehane B.M., Jardine R.J., Bond A.J. and Frank R. (1992), 'Mechanisms of shaft friction in sand from instrumented pile tests', J. Geotech. Eng., ASCE, (in press)

Lemos L.J.L. (1986), The effect of rate of shear on residual strength of soil', PhD Thesis, Univ. of London (Imperial College)

Lemos L.J.L. and Vaughan P.R. (1992), 'Clay interface shear resistance', Research report, Dept. of Civ. Eng., Univ. of London (Imperial College), submitted to Geotechnique.

Levadoux J.N. (1980), 'Pore pressures in clays due to cone penetration', PhD Thesis, Massachusetts Institute of Technology

Levadoux J.N. and Baligh M.M (1980), 'Pore pressures during cone penetration in clays', Massachusetts Institute of Technology research report, Dept. of Civ. Eng., No. R80-15, Order no. 666

Levadoux J.N. and Baligh M.M. (1986), 'Consolidation after undrained piezocone penetration I : Prediction', J. Geotech. Eng., 112(7), pp707-726

Lings M. (1985), 'The skin friction of driven piles in sand', MSc Dissertation, University of London (Imperial College)

Lunne T. and Christoffersen H.P. (1983), 'Interpretation of cone penetrometer data for offshore sands', Offshore Tech. Conf., OTC 4464, Houston, pp181-192

Lunne T., Powell J.J.M., Quarterman R.S. and Eidsmoen T.E. (1986), 'Piezocone testing in overconsolidated clays', Proc. 39th Can. Geotech. Conf. on 'In-situ Testing and Field Behaviour', Carlton Univ., Ottawa, Canada, pp209-218

Lupini J.F. (1981), 'The residual strength of soils', PhD Thesis, Univ. of London (Imperial College)

Lupini J.F., Skinner A.E. and Vaughan P.R. (1981), 'The drained residual strength of cohesive soils', Geotechnique, 31 (2), pp181-213

Madgett P.A. and Catt J.A. (1978), 'Petrography stratigraphy and weathering of late Pleistocene tills in East Yorkshire, Lincolnshire and North Norfolk', Proc. Yorks. Geol. Soc., 42(5), pp55-108; see Marsland & Powell (1985)

Mair R.J. and Wood D.M. (1987), 'Pressuremeter testing: Methods and interpretation', CIRIA Ground Eng. Report: In-situ testing, Butterworths, London

Mansur C.I. and Hunter A.H. (1970), 'Pile tests - Arkansas River project', J. Soil Mech. Fdn Div., ASCE, 96(SM5), pp1545-1582

Mansur C.I. and Kaufman R.I. (1958), 'Pile tests, Low-Sill structure, Old River, Louisiana', Transactions ASCE, Vol. 123, pp715-743

Marcusson W. and Franklin A. (1979), 'State of the art of undisturbed sampling of cohesionless soils', Proc. Int. Symp. on soil sampling, Singapore, pp57-71

Marsland A. (1985), 'The influences of geological processes and test procedures on measured and evaluated parameters', Proc. Int. Conf. on Offshore Site Investigation, Soc. for Underwater Tech., London, pp231-254

Marsland A. and Powell J.J.M. (1985), 'Field and laboratory investigations of the clay tills at the Building Research Establishment test site at Cowden, Holderness', Proc. Int. Conf. on Construction in Glacial Tills and Boulder Clays', Edinburgh, pp147-168

Mayne P.W. and Kulhawy F.H. (1982), 'K_0-OCR relationships in soils', J. Geotech. Eng. Div., ASCE, 108 (GT6), pp851-872

McAnoy R.P., Cashman A.C. and Purvis D. (1982), 'Cyclic tensile testing of a pile in glacial till', Proc. 2nd Int. Conf. on Num. Methods in Offshore Piling, Austin, Texas, pp257-291

Meyerhof G.G. (1951), 'The ultimate bearing capacity of foundations', Geotechnique, 2, pp301-332

Meyerhof G.G. (1976), 'Bearing capacity and settlement of pile foundations', The 11th Terzaghi Lecture, J. Geotech. Eng. Div., ASCE, 102(GT3), pp197-228

Meyerhof G.G. (1983), 'Scale effects of ultimate pile capacity', J. Geotech. Eng. Div., ASCE, 109 (GT6), pp797-806

Morrison M.J. (1984), 'In-situ measurements on a model pile in clay', PhD Thesis, Dept. of Civ. Eng., Massachusetts Institute of Technology

Nauroy J.F., Brucy F. and Le Tirant P. (1985), 'Pieux battus sollicités en tension', Proc. 11th Int. Conf. Soil Mech. & Fdn. Eng., San Francisco, 3, pp1607-1610

Nader S.Rad and Lunne T. (1988), 'Direct correlations between piezocone test results and undrained shear strength of clay', Proc. of 1st Int. Symp. on Penetration Testing, ISOPT-1, Balkema, Rotterdam, 2, pp911-917

Nordlund R. L. (1963), 'Bearing capacity of piles in cohesionless soils', J. of Soil Mech. and Fdns. Div., ASCE, 89 (SM3), pp1-35

O' Neill M.W., Hawkins R.A. and Audibert J.M.E. (1982), 'Installation of pile group in overconsolidated clay', J. Geotech. Eng. Div., ASCE, 108 (GT11), pp1136-1386

OASYS (1988), 'Geotechnical computer program users manual', OASYS Ltd., London W1P 6BQ

Olsen R.E. (1990), 'Axial load capacity of steel pipe piles in sand', Proc. 22nd Offshore Tech. Conf., Houston, 4, pp17-24

Ove Arup and Partners (1986), 'Research on the behaviour of piles as anchors for buoyant structures', Dept. of Energy, Offshore Technology Report, OTH 86 215.

Paul M.A., Peacock J.D. and Wood B.F. (1991), 'The engineering geology of the soft clay at the national soft clay research site Bothkennar', Research report, Dept. of Civil Eng., Heriot Watt Univ., Edinburgh

Ponniah D.A. (1991), Personal communication

Ponniah D.A. (1989), 'Instrumentation of a jacked in pile', Proc. of ICE conf. on instrumentation in geotechnical engineering, Nottingham, paper 27, pp207-220

Poskitt A. (1992), Personal Communication

Potts D.M. and Martins J.P. (1982), 'The shaft resistance of axially loaded piles in clay', Geotechnique, 32(4), pp369-386

Potyondy J.G. (1961), 'Skin friction between various soils and construction materials', Geotechnique, 2(4), pp339-353

Poulos H.G. (1989), 'Pile behaviour - theory and application', Rankine Lecture, Geotechnique, 39(3), pp365-415

Powell J.J.M. (1992), Personal communication

Powell J.J.M. and Quarterman R.S. (1988), 'The interpretation of cone penetration tests in clays, with particular reference to rate effects', ISOPT-1, 2, pp903-909

Powell J.J.M. and Uglow I.M. (1985), 'A comparison of three pressuremeters of different types in a glacial till clay', Proc. Int. Conf. on Offshore Site Investigation, Society for Underwater Tech., London, pp201-218

Powers M.C. (1953), J. of Sedimentary Petrology, 23(2), pp117-119; see Youd (1973)

Puech A.A. (1982), 'Basic data for the design of tension piles in silty soils', BOSS '82, pp141-157

Puech A., Boulon M. and Meimon Y. (1982), 'Behaviour of tension piles: field data and numerical modelling', 2nd Int. Conf. on Numerical Methods in Offshore Piling, Austin, USA, pp293-312

Randolph M.F. (1983), 'Design considerations for offshore piles', Proc. Conf. on Geotech. Practice in Offshore Eng., Austin, Texas, pp422-439

Randolph M.F. and Murphy B.J. (1985), 'Shaft capacity of driven piles in clay', Proc. 17th Offshore Tech. Conf., Houston, Texas, 1, pp371-378

Randolph M.F., Carter J.P. and Wroth C.P. (1979), 'Stress and pore pressure changes around a driven pile', Int. J. Num. & Anal. Methods in Geomechanics, 3, pp217-229

Randolph M.F. and Wroth C.P. (1979), 'An analytical solution for the consolidation around a driven pile', Int. J. Num. & Anal. Methods in Geomechanics, 3, pp217-229

Randolph M.F. and Wroth C.P. (1981), 'Application of the failure state in undrained simple shear to the shaft capacity of driven piles', Geotechnique, 31(1), pp143-157

Renoud-Lias B. (1978), 'Etude du pressiomètre en milieu pulvérulent', PhD Thesis, Univ. of Grenoble; see Boulon & Foray (1986)

Robertson P.K. (1982), 'In situ testing of soil with emphasis on its application to liquefaction assessment', PhD Thesis, Univ. of British Columbia, Vancouver, Canada; see Hughes & Robertson (1985)

Robinsky E.I. and Morrison C.F. (1964), 'Sand displacement and compaction around model friction piles', Can. Geotech. J.,1(2), pp81-93

Robinsky E.I., Sagar W.L. and Morrison C.F. (1964), 'Effect of shape and volume on the capacity of model piles in sand', Can. Geotech. J., 1(4), pp180-204

Robson R.J. (1988), 'Review of laboratory and field data from the Cowden test site, Holderness', MSc diss., Univ. of London (Imperial College)

Roy M., Blanchet R., Tavenas F. and La Rochelle P. (1981), 'Behaviour of a sensitive clay during pile driving', Can. Geotech. J., 18(1), pp67-85

Roy M. and Lemieux M. (1986), 'Long-term behaviour of reconsolidated clay around a driven pile', Can. Geotech. J., 23(1), pp23-29

Reese L.C. and Seed H.B. (1955), 'Pressure distribution along friction piles', Proc. ASTM, 55, pp1156-1182

Schmertmann J. (1978), 'Guidelines for cone penetration test:performance and design', US Dept. of Transp., Offices of Research and Development, Washington (DC), Report FHWA-TS-78-209

Searle L.W. (1979), 'The interpretation of Begemann friction jacket cone results to give soil types and design parameters', Proc. 7th Eur. Conf. on Soil Mech. and Fdn. Eng., Brighton, 2, pp265-270

Seed H.B. and Idriss I.M. (1970), 'Soil moduli and damping factors fro dynamic response analyses', EERC Report No. 70-10, Berkeley, Calif., U.S.

Semple R.M. and Ridgen W.J. (1984), 'Shaft capacity of driven pipe piles in clay', Proc. Symp. on Codes and Standards, ASCE National Conv., San Francisco

Skempton A.W. (1951), 'The bearing capacity of clays', Building Research Congress, London, 1, pp180-189

Skempton A.W., Yassin A.A. and Gibson R.E. (1953), 'Théorie de la force portante des pieux dans le sable', Annales de l'Institute Technique Bâtiment, Vol. 6, pp285-290; see Tomlinson (1963)

Skinner A.E. (1969), 'A note on the influence of interparticle friction on the shearing strength of a random assembly of spherical particles', Geotechnique, 19(1), pp150-157

Soares M.M. and Dias C.R.R. (1990), 'Behaviour of an instrumented pile in the Rio de Janeiro clay, Proc. 12th Int. Conf. on Soil Mech. and Fdn. Eng., Rio de Janeiro, 1, pp319-322

Sills G.C. (1975), 'Some conditions under which Biot's equations of consolidation reduce to Terzaghi's equation', Geotechnique, 25(1), pp129-132

Sills G.C., Almeida M.S.S. and Danziger F.A.B. (1988), 'Coefficient of consolidation from piezocone dissipation tests in a very soft clay', Proc. of 1st Int. Symp. on Penetration Testing, ISOPT-1, Balkema, Rotterdam, Vol. 2, pp967-974

Smith P.R. (1992), 'Properties of high compressibility clays with reference to construction on soft ground', PhD Thesis, Univ. of London (Imperial College)

Smith P.R., Jardine R.J. and Hight D.W. (1992), ' On the yielding of Bothkennar clay, Geotechnique Symposium in Print, 42(2), (in press)

Symes M.J. (1983), 'Rotation of principal stresses in sand', PhD Thesis, Univ. of London (Imperial College)

Tatsuoka F. and Shibuya S. (1991), 'Deformation characteristics of soils and rocks from field and laboratory tests', Keynote lecture, 9th Asian Conf. Soil Mech. Fdn. Eng., Bangkok

Tavenas F.A. (1971), 'Load test results on friction piles in sand', Can. Geotech. J., 8(1), pp7-22

Tavenas F.A. and Audy R. (1972), 'Limitations of the driving formulas for predicting bearing capacities of piles in sand', Can. Geotech. J., 9(1), pp47-62

Tang W.H. (1988), 'Offshore axial pile design reliability', Research report for Phase 1 of project PRAC 86-298, Dept. of Civ. Eng., Univ. of Illinois; see Karlsrud & Nadim (1990)

Terzaghi K. (1936), 'The shearing resistance of saturated soils and the angle between the planes of shear', Proc. 1st Int. Conf. Soil Mech. & Fdn. Eng., Cambridge, 1, pp161-165

Terzaghi K. and Peck R. (1967), 'Soil mechanics in engineering practice', 2nd Edition, New York, Publ. by John Wiley

Thorburn S. (1963), 'Tentative correction chart for the standard penetration test in non-cohesive soil', Civ. Eng. Public Wks Review, 58, pp752-753; see Tomlinson (1963)

Tika T. (1989), 'The effect of fast shearing on the residual strength of soils', PhD Thesis, Univ. of London (Imperial College)

Tika-Vassilikos T. (1991), 'Clay-on-steel ring shear tests and their implications for displacement piles', Geotech. Test. J., ASTM, 14(4), pp457-463

Tomlinson M.J. (1957), 'The adhesion of piles driven in clay soils', Proc. 4th Int. Conf. Soil Mech. & Fdn. Eng., London, 2, pp66-71

Tomlinson M.J. (1963), 'Foundation Design and Construction', Pitman Publ., London WC2B

Toolan F.E and Ims B.W. (1988), 'Impact of recent changes to API recommended practice for offshore piles in sand', J. of Underwater Tech., 14, No. 1

Toolan F.E., Lings M.L. and Mirza U.A. (1990), 'An appraisal of API RP2A recommendations for determining skin friction of piles in sand', Proc. 22nd Offshore Tech. Conf., Houston, U.S., 4, pp33-42

Vaughan P.R. (1991), Personal Communication

Uesugi M. and Kishida H. (1986), 'Influential factors of friction between steel and dry sands', Soils and Foundations, 26(2), pp33-46

Uesugi M. and Kishida H. (1986), 'Frictional resistance at yield between dry sand and mild steel', Soils and Foundations, 26(4), pp139-149

Vaziri H., Simpson B., Pappin J.W. and Simpson L. (1982), 'Integrated forms of Mindlin's equations', Geotechnique, 32(3), pp275-278

Vesic A.S. (1967), 'A study of bearing capacity of deep foundations', Final Report: Project B-189, Georgia Inst. of Tech., Atlanta

Vesic A.S. (1964), 'Investigations of bearing capacity of piles in sand', Duke Univ. Soil Mech. Laboratory Publ. No. 3

Vesic A.S. (1970), 'Tests on instrumented piles, Ogeechee river site', J. of Soil Mech. and Fdns. Div., ASCE, 96(SM2), pp561-584

Vesic A.S. (1977), 'Design of pile foundations', NCHRP synthesis of highway practice No. 42, Transp. research board, USA; see Kraft (1991)

Vijayvergiya V.N. and Focht J.A. (1977), 'A new way to predict capacity of piles in clay', Proc. Offshore Tech. Conf, Dallas, Texas, 2, pp865-871

Weltman A.J. and Healy P.R. (1978), 'Piling in boulder clay and other glacial tills', Dept. of Energy/CIRIA report PG5, London

Wersching S.N. (1987),' The development of shaft friction and end bearing for piles in homogeneous and layered soils', PhD Thesis, Polytechnic of South Wales

Whittle A.J. (1987), 'A constitutive model for overconsolidated clays with application to the cyclic loading of friction piles', PhD Thesis, Massachusetts Institute of Technology.

Whittle A.J. (1991), 'Predictions of instrumented pile behaviour at the Bothkennar site', Report submitted to Dept. of Civ. Eng., Univ. of London (Imperial College)

Whittle A.J. (1991), 'Interpretation of pile load tests at the Haga site', Proc. 10th Int. Conf. on Offshore Mech. and Arctic Eng., pp267-274

Whittle A.J. and Aubeny C.P. (1990), 'Pore pressure fields around piezocone penetrometers installed in clays', 7th Conf. of Int. Ass. for computer methods and advances in geomechanics, Cairns, Australia

Whittle A.J. and Baligh M.M. (1988), 'The behaviour of piles supporting tension leg platforms', Final report phase III to sponsors, Massachusetts Institute of Technology.

Whittle A.J., Baligh M.M., Azzouz A.S. and Malek A.M. (1988), 'A model for predicting the performance of TLP piles in clay', Proc. Conf. on Behaviour of Offshore Structures, Tapir, Trondheim, 3, pp97-112

Wong R.K.S. and Arthur J.R.F. (1986), 'Sand sheared by stresses with cyclic variations in direction', Geotechnique 36(2), pp215-226

Yoshimi Y. and Kishida T. (1981), 'A ring torsion apparatus for evaluating friction between soil and metal surfaces', Geotech. Test. J., ASCE, 4(4), p145-152

Youd T. (1973), 'Factors controlling maximum and minimum densities of sands', paper in 'Evaluation of relative density and its role in geotechnical projects involving cohesionless soils', ASTM STP 523, pp98-112